



Universitat de Girona

# BIOINSPIRED NON-HEME IRON CATALYSTS FOR CHALLENGING OXIDATIVE TRANSFORMATIONS: MECHANISTIC STUDIES AND CATALYTIC APPLICATIONS ON SELECTIVE ALKANE HYDROXYLATION AND ALKENE CIS-DIHYDROXYLATION

**Irene PRAT CASELLAS**

**Dipòsit legal: Gi. 1056-2013**

<http://hdl.handle.net/10803/117778>

**ADVERTIMENT.** L'accés als continguts d'aquesta tesi doctoral i la seva utilització ha de respectar els drets de la persona autora. Pot ser utilitzada per a consulta o estudi personal, així com en activitats o materials d'investigació i docència en els termes establerts a l'art. 32 del Text Refós de la Llei de Propietat Intel·lectual (RDL 1/1996). Per altres utilitzacions es requereix l'autorització prèvia i expressa de la persona autora. En qualsevol cas, en la utilització dels seus continguts caldrà indicar de forma clara el nom i cognoms de la persona autora i el títol de la tesi doctoral. No s'autoritza la seva reproducció o altres formes d'explotació efectuades amb finalitats de lucre ni la seva comunicació pública des d'un lloc aliè al servei TDX. Tampoc s'autoritza la presentació del seu contingut en una finestra o marc aliè a TDX (framing). Aquesta reserva de drets afecta tant als continguts de la tesi com als seus resums i índexs.

**ADVERTENCIA.** El acceso a los contenidos de esta tesis doctoral y su utilización debe respetar los derechos de la persona autora. Puede ser utilizada para consulta o estudio personal, así como en actividades o materiales de investigación y docencia en los términos establecidos en el art. 32 del Texto Refundido de la Ley de Propiedad Intelectual (RDL 1/1996). Para otros usos se requiere la autorización previa y expresa de la persona autora. En cualquier caso, en la utilización de sus contenidos se deberá indicar de forma clara el nombre y apellidos de la persona autora y el título de la tesis doctoral. No se autoriza su reproducción u otras formas de explotación efectuadas con fines lucrativos ni su comunicación pública desde un sitio ajeno al servicio TDR. Tampoco se autoriza la presentación de su contenido en una ventana o marco ajeno a TDR (framing). Esta reserva de derechos afecta tanto al contenido de la tesis como a sus resúmenes e índices.

**WARNING.** Access to the contents of this doctoral thesis and its use must respect the rights of the author. It can be used for reference or private study, as well as research and learning activities or materials in the terms established by the 32nd article of the Spanish Consolidated Copyright Act (RDL 1/1996). Express and previous authorization of the author is required for any other uses. In any case, when using its content, full name of the author and title of the thesis must be clearly indicated. Reproduction or other forms of for profit use or public communication from outside TDX service is not allowed. Presentation of its content in a window or frame external to TDX (framing) is not authorized either. These rights affect both the content of the thesis and its abstracts and indexes.



Universitat de Girona

Doctoral Dissertation

---

**Bioinspired Non-Heme Iron Catalysts for Challenging  
Oxidative Transformations: Mechanistic Studies and  
Catalytic Applications on Selective Alkane Hydroxylation  
and Alkene *cis*-Dihydroxylation**

---

IRENE PRAT CASELLAS

April 2013

Programa de Doctorat en Ciències Experimentals i Sostenibilitat

Directed by:

Dr. Miquel Costas Salgueiro

Dr. Xavi Ribas Salamaña

Memòria presentada per a optar al títol de **Doctora** per la  
**Universitat de Girona.**



Els sotasignants Dr. **Miquel Costas Salgueiro**, Professor Titular del Departament de Química de la Universitat de Girona i Dr. **Xavi Ribas Salamaña**, Professor Agregat del Departament de Química de la Universitat de Girona,

CERTIFIQUEN que la memòria que porta per títol “Bioinspired Non-Heme Iron Catalysts for Challenging Oxidative Transformations: Mechanistic Studies and Catalytic Applications on Selective Alkane Hydroxylation and Alkene *cis*-Dihydroxylation” que presenta la Irene Prat Casellas per a l’obtenció del títol de doctora, ha estat realitzat sota la seva direcció i que compleix els requeriments per poder optar a Menció Internacional.

I, perquè així consti i tingui els efectes oportuns, signen aquest document.

Dr. Miquel Costas Salgueiro

Dr. Xavi Ribas Salamaña

Girona, 22 d’abril del 2013.





A la meva família i a en Lluís

---



## AGRAÏMENTS

M'és difícil pensar que ja han passat més de quatre anys des de que vaig començar el doctorat, mirant enrere em venen un munt de records a la memòria i tots ells són fantàstics. S'acaba una etapa que sé de segur que no oblidaré i recordaré sempre amb un gran somriure, moltes persones han format part d'ella i han contribuït a la realització d'aquesta tesi. Amb aquestes quatre ratlles m'agradaria agrair a tothom que ho ha fet possible.

No puc començar d'altra manera que donant les gràcies als meus directors de tesi, en Miquel i en Xavi, per donar-me l'oportunitat de formar part del seu grup de recerca, per introduir-me en el món de la investigació i per totes les hores que m'han dedicat. En Miquel per la seva passió per la química que és inesgotable, per tenir sempre l'esperança que els resultats es poden millorar i per treure el màxim fruit de tots els meus treballs. En Xavi per fer-nos tocar de peus a terra quan ha estat necessari, per solucionar tots els problemes logístics i per estar en tot moment pendent de tot.

A tothom que forma i ha format part del Qbis: l'Anna per tota la seva ajuda, tan en els inicis de la tesi com ara per acabar d'enllestir alguns treballs. En Julio que sempre té una resposta a totes les preguntes i l'hi desitjo tota la sort del món amb l'starting grant. A la Laura que juntament amb l'Anna han sigut la meua referència en l'oxidació d'alcans i alquens. L'Alicia i l'Isaac que se'ls troba molt a faltar i els hi desitjo molta sort amb la seva recerca. La Mercè amb la qual he compartit més estones durant el doctorat, tan en el laboratori com en congressos i ara fins i tot en classes d'anglès, molta sort. En Zoel i l'Olaf que fan que les hores de despatx siguin més entretingudes, explicant bajanades i fent-nos passar una bona estona. En Ferran que a vegades sembla que no hi és però sempre té l'orella connectada per dir-hi la seva.

Els del coure que és van independitzar,... a la Cristina que habitualment comentem que sense ella s'està més tranquil, però també trobem a faltar el seu punt de vista femení. En Marc, bon company tant de carrera com de doctorat, tot i que de tant en tant difama falses històries sobre mi. En Joan i els seus gens nòrdics, que és capaç d'anar en màniga curta tot l'hivern. L'Imma amb les seves super ofertes, un gran fitxatge sens dubte. La Mireia que té la capacitat d'encomanar la seva felicitat allà on va. No em puc oblidar dels del 13, Arnau els dinars serien molt avorrits sense les teves històries. Gerard, sempre amunt i avall. En David, que no ha aconseguit encomanar-me la seva passió per les columnes, però crec que n'he après força i la Raquel que ha d'estar carregada de paciència per aguantar aquests 3 homes.

Finalment, a tots els que esteu fent el màster i els que començareu el doctorat aquest any molta sort amb la recerca futura: Teresa, Carlota, Oriol, Carla, Mònica, Jordi, Isma, Ming i la Clàudia. A tots els becaris de química, tant de la facultat com del parc, pels sopars i els bons moments junts.

Al professor Josep Maria Luis, la Dra. Mireia Güell i la Verònica Postils per la seva col·laboració amb els estudis computacionals.

També vull agrair a tots els directors d'estada que han estat molt atents amb mi i m'han donat un cop de mà amb la recerca quan ho he necessitat. El professor Leroy Cronin de l'University of Glasgow per donar-me l'oportunitat de formar part del seu grup i la Dra. Jennifer Mathieson per totes les hores treballant conjuntament per tal de que sortissin els experiments. El professor Matthias Beller i a la Dra. Kathrin Junge per l'estada al Leibniz-Institut für Katalyse i pels seus savis consells que van fer que el treball arribés a bon port. Finalment, el professor Martin Albrecht de l'University College of Dublin per l'entrega en la meva recerca i a tots els membres del seu grup que hem van acollir molt bé i hem van portar a nombrosos pubs Irlandesos.

Fora de l'àmbit de química voldria agrair a tota la meva colla, que tot i que els sopars i festes de dissabte a la nit s'han convertit en sopars-berenars de diumenge, la vostra companyia és la mateixa de sempre. A les cinc nenes més precioses de Bordils (jo inclosa) que tot i que cada cop costa més trobar dies per trobar-nos, sé que sempre hi sou. El Club Handbol Bordils i en especial a l'equip del meu germà que m'heu fet vibrar en incomptables partits d'handbol. A totes les nenes de volei, les que formeu part de l'equip i les que hi heu anat passant durant tots aquests anys, que sou més que simples companyes i que espero que els sopars i festes no s'acabin. A l'equip, molta força per afrontar la recta final de la temporada i poder aconseguir la permanència tant preuada, com ja sabem som un equip de primera! En Jordi de la Laia per donar el toc artístic a la portada de la tesi, moltes gràcies.

Finalment agrair a la meva família que sempre tenen una estona per escoltar les meves preocupacions i neguits i per les seves paraules càlides i reconfortants. Al meu germà, tot i que es fa difícil de veure sempre té un somriure i una abraçada per mi, i li desitjo molta sort amb el projecte final de carrera. En Lluís, el meu company de viatge que aguanta totes les meves rabietes i mals humors sense queixar-se, no em cansaré mai de donar-te les gràcies per tot el que fas per mi.

Moltes gràcies a tots,

Irene

# GRAPHICAL ABSTRACT

Summary (p. 1).

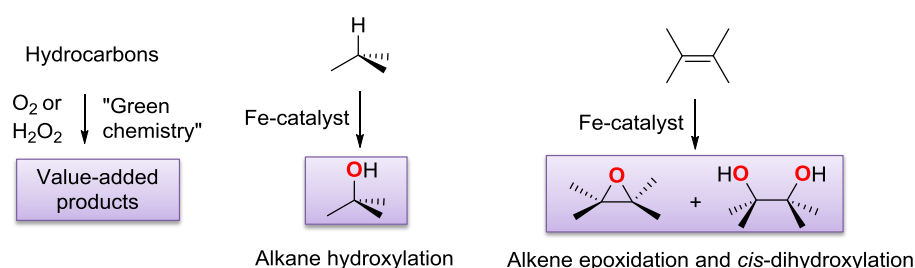
Full List of Publications (p. 4).

Glossary of Abbreviations (p. 6).

Full List of Figures, Tables and Schemes (p. 8).

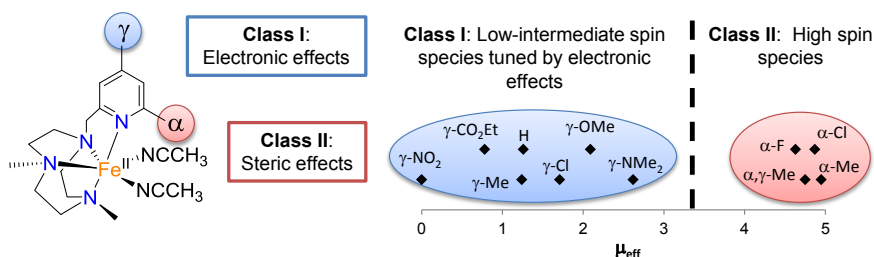
Acknowledgements (p. 13).

**Chapter I. General Introduction (p. 15).**

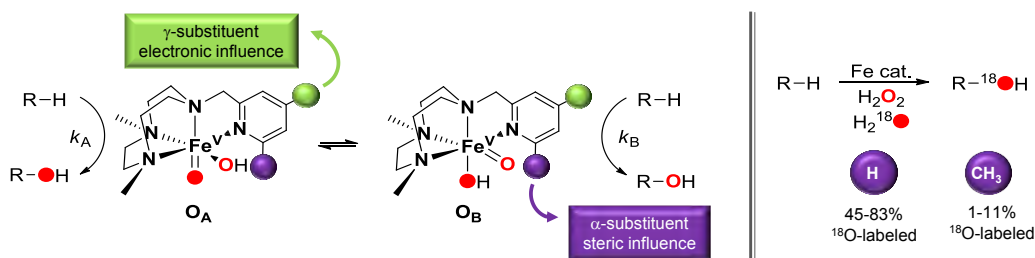


**Chapter II. Main Objectives (p. 67).**

**Chapter III. Assessing the impact of electronic tuning of the ligand in the spin state and catalytic oxidation ability of the Fe(Pytacn) family of complexes (p. 71).**

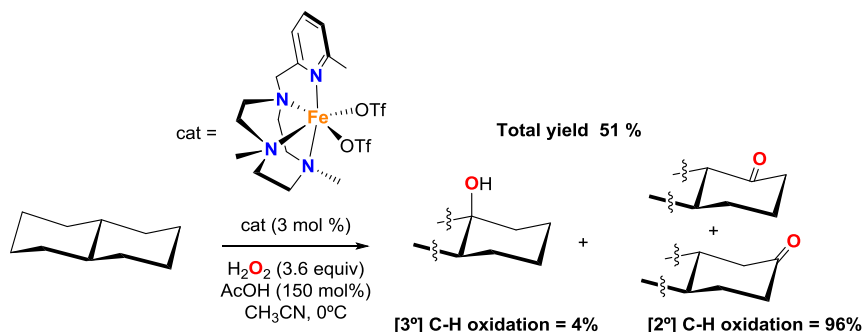


**Chapter IV. The mechanism of stereospecific C-H oxidation by Fe(Pytacn) complexes. Bioinspired non-heme iron catalysts containing *cis*-labile exchangeable sites (p. 95).**



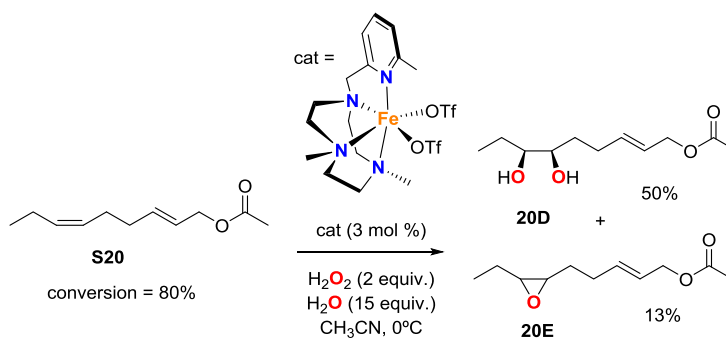
---

**Chapter V.** An iron catalyst for oxidation of alkyl C-H bonds showing enhanced selectivity for methylenic sites (p. 113).



---

**Chapter VI.** Fe(Pytacn)-catalyzed *cis*-dihydroxylation of olefins with hydrogen peroxide (p. 121).



---

**Chapter VII.** Observation of Fe(V)=O using variable-temperature mass spectrometry and its enzyme-like C-H and C=C oxidation reactions (p. 133).



---

**Chapter VIII.** Results and Discussion (p. 141).

---

**Chapter IX.** General Conclusions (p. 175).

---

**ANNEX** (p. 181).

---

# TABLE OF CONTENTS

Summary .....	1
Resum.....	2
Resumen.....	3
Ful List of Publications.....	4
Glossary of Abbreviations .....	6
List of Figures .....	8
List of Tables.....	9
List of Schemes.....	10
Acknowledgements.....	13
<b>CHAPTER I. GENERAL INTRODUCTION .....</b>	<b>15</b>
I.1. Advances in alkane and alkene oxidation reactions .....	17
I.1.1. Alkane oxidations .....	17
I.1.2. Alkene oxidations .....	18
I.1.3. Metalloenzymes and model compounds.....	19
I.2. Biological role of iron enzymes .....	20
I.2.1. Iron proteins involved in oxygen activation.....	21
I.2.1.1. Cytochrome P450.....	22
I.2.1.2. Rieske Oxygenases .....	24
I.2.2. High-valent iron-oxo species detected in biological systems .....	27
I.3. Catalytic applications by bioinspired non-heme iron complexes .....	28
I.3.1. Alkane oxidation.....	28
I.3.1.1. Hydroxylation .....	28
I.3.1.2. Desaturation.....	36
I.3.2. Alkene oxidation.....	37
I.3.2.1. Epoxidation.....	37
I.3.2.2. <i>cis</i> -Dihydroxylation.....	42
I.3.2.2.1. Iron(II) complexes based on N <sub>4</sub> ligands.....	42



I.3.2.2.2. Iron(II) complexes based on N,N,O ligands .....	46
I.4. Mechanistic aspects in catalytic oxidations reactions mediated by bioinspired non-heme iron complexes .....	47
I.4.1. Mechanistic probes .....	48
I.4.2. Intermediates on catalytic oxidations reactions .....	50
I.4.2.1. High-valent iron-oxo species involved in catalytic cycles of oxidation .....	50
I.4.2.1.1. High-valent iron-oxo intermediates for olefin oxidation .....	52
I.4.2.1.2. High-valent iron-oxo intermediates for alkane oxidation .....	56
I.4.2.2. Spectroscopic evidence of high-valent iron-oxo species .....	58
I.5. References.....	61
<b>CHAPTER II. MAIN OBJECTIVES .....</b>	<b>67</b>
<b>CHAPTER III. ASSESSING THE IMPACT OF ELECTRONIC TUNING OF THE LIGAND IN THE SPIN STATE AND CATALYTIC OXIDATION ABILITY OF THE Fe(PYTACN) FAMILY OF COMPLEXES. ....</b>	<b>71</b>
<b>CHAPTER IV. THE MECHANISM OF STEREOSPECIFIC C-H OXIDATION BY Fe(PYTACN) COMPLEXES. BIOINSPIRED NON-HEME IRON CATALYSTS CONTAINING CIS-LABILE EXCHANGEABLE SITES .....</b>	<b>95</b>
<b>CHAPTER V. AN IRON CATALYST FOR OXIDATION OF ALKYL C-H BONDS SHOWING ENHANCED SELECTIVITY FOR METHYLENIC SITES.....</b>	<b>113</b>
<b>CHAPTER VI. Fe(PYTACN)-CATALYZED CIS-DIHYDROXYLATION OF OLEFINS WITH HYDROGEN PEROXIDE. ....</b>	<b>121</b>
<b>CHAPTER VII. OBSERVATION OF Fe(V)=O USING VARIABLE-TEMPERATURE MASS SPECTROMETRY AND ITS ENZYME-LIKE C-H AND C=C OXIDATION REACTIONS .....</b>	<b>133</b>
<b>CHAPTER VIII. RESULTS AND DISCUSSION .....</b>	<b>141</b>
VIII. 1. Assessing the impact of electronic tuning of the ligand in the spin state and catalytic oxidation ability of the Fe(Pytacn) family of complexes .....	144

VIII.1.1. Structure-dependent electronic and magnetic properties.....	145
VIII.1.2. Performance in catalysis .....	149
VIII.2. The mechanism of stereospecific C-H oxidation by Fe(Pytacn) complexes. Bioinspired non-heme iron centers containing <i>cis</i> -labile exchangeable sites .....	152
VIII.3. An iron catalyst for oxidation of alkyl C-H bonds showing enhanced selectivity for methylenic sites .....	158
VIII.4. Fe(Pytacn)-catalyzed <i>cis</i> -dihydroxylation of olefins with hydrogen peroxide.....	163
VIII.4.1. Substrate scope.....	165
VIII.4.2. <i>cis</i> -Dihydroxylation mechanism .....	168
VIII.5. Observation of Fe(V)=O using variable-temperature mass spectrometry and its enzyme-like C–H and C=C oxidation reactions .....	169
VIII.6. References .....	174
<b>CHAPTER IX. GENERAL CONCLUSIONS .....</b>	<b>175</b>
<b>ANNEX .....</b>	<b>181</b>
A.1. Supporting Information Chapter III.....	183
A.2. Supporting Information Chapter IV .....	205
A.3. Supporting Information Chapter V .....	211
A.4. Supporting Information Chapter VI .....	223
A.5. Supporting Information Chapter VII .....	241
<b>SUPPLEMENTARY DIGITAL INFORMATION</b>	
• pdf file of the manuscript	
• cif files for each crystal structure presented in this thesis	



## SUMMARY

Discovery of systems that could catalyze the efficient and selective oxidation of hydrocarbons under mild conditions is still a challenge for organic chemistry. Some natural metalloenzymes can perform this oxidative chemistry with a high regio- and stereoselectivity; one of the most versatile families of enzymes is Rieske oxygenases, which contain a non-heme iron center and can catalyze the hydroxylation of alkanes and the *cis*-dihydroxylation of arenes, among others. In this thesis we focus on the synthesis of low molecular weight iron complexes mainly as functional models of the active center of these enzymes.

In the first place, we describe a family of iron complexes based on a tetradentate ligand containing a triazacyclononane macrocycle covalently attached to a methylpyridine arm. In a systematic manner, different electronic and steric substituents have been introduced in  $\alpha$  and  $\gamma$  positions of the pyridine ring. All complexes are spectroscopically and structurally characterized, showing different electronic properties in the iron center depending on the pyridine substituents. Moreover, the whole family of complexes catalyzes the hydroxylation of alkanes and the epoxidation and *cis*-dihydroxylation of alkenes using hydrogen peroxide as oxidant.

Oxidation of alkanes and alkenes mediated by this family of complexes are studied by means of isotopic labeling experiments and product analysis in order to determine the oxidation mechanism by which these complexes operate. These experiments, in combination with DFT calculations, point towards a  $\text{Fe}^{\text{V}}(\text{O})(\text{OH})$  as the active species for both oxidation reactions.

Preliminary oxidation results indicated that the catalyst with a methyl group in the  $\alpha$  position of the pyridine is the most efficient for catalyzing both reactions, alkane hydroxylation and alkene *cis*-dihydroxylation, in a preparative scale. In order to demonstrate its potential as a synthetic tool, a wide range of substrates incorporating several functional groups are oxidized.

In the final part of this thesis, we employ variable temperature mass spectrometry to identify key intermediates involved in the catalytic cycle of these oxidation reactions. By mixing the complex with hydrogen peroxide at  $-40\text{ }^{\circ}\text{C}$  we observe the generation of  $\text{Fe}^{\text{V}}(\text{O})(\text{OH})$  species. Isotopic labeling experiments shows that in the  $\text{Fe}^{\text{V}}(\text{O})(\text{OH})$  species one oxygen atom comes from water and the other from hydrogen peroxide. Also, the reaction of this species with an olefin proves that it is a catalytic intermediate. This is the first time such highly reactive intermediate has been observed under catalytic conditions.

## RESUM

Descobrir uns sistemes que siguin capaços de catalitzar l'oxidació d'hidrocarburs de manera eficaç, selectiva i en condicions suaus és encara un repte per la química orgànica. Alguns metal·loenzims naturals poden dur a terme aquesta química oxidativa amb una alta regio- i estereoselectivitat; una de les famílies d'enzims més versàtils són les oxigenases de Rieske, les quals contenen un centre de ferro no-hemo i poden catalitzar la hidroxilació d'alcans i la *cis*-dihidroxilació d'arens, entre d'altres. En aquesta tesi ens centrarem en la síntesis de complexos de baix pes molecular que imitin aspectes estructurals i funcionals del centre actiu d'aquests enzims.

En primer lloc, descrivim una família de complexos de ferro basats en uns lligands tetradentats que contenen el macrocicle de triazaciclononà enllaçat covalentment a un braç de piridina. De manera sistemàtica, s'introdueixen substituents amb diferents propietats electròniques i estèriques en les posicions  $\alpha$  i  $\gamma$  de l'anell de piridina. Tots els complexos es caracteritzen estructuralment i espectroscòpicament, indicant que les propietats electròniques del centre metàl·lic depenen dels substituents de la piridina. A més, tots els complexos són capaços de catalitzar la hidroxilació d'alcans i l'epoxidació i *cis*-dihidroxilació d'alquens utilitzant peròxid d'hidrogen com a oxidant.

L'oxidació d'alcans i alquens duta a terme per aquesta família de complexos s'estudia mitjançant experiments de marcatge isotòpic i anàlisis de productes per tal de determinar el mecanisme d'oxidació pel qual actuen. Aquest experiments conjuntament amb càlculs de DFT indiquen que la espècie activa capaç de catalitzar les dos reaccions d'oxidació és un  $\text{Fe}^{\text{V}}(\text{O})(\text{OH})$ .

Els resultats preliminars d'oxidació indiquen que el catalitzador amb un metil a la posició  $\alpha$  de la piridina és el millor per catalitzar les dos reaccions, tant la hidroxilació d'alcans com la *cis*-dihidroxilació d'alquens en escala sintètica. Per tal de demostrar els seu potencial a nivell sintètic s'ha dut a terme l'oxidació d'una gran quantitat de substrats, els quals incorporen diferents grups funcionals.

En la part final de la tesi, utilitzem l'espectrometria de masses a temperatura variable per tal de identificar intermedis involucrats en el cicle catalític d'oxidació. Mesclant el complex amb peròxid d'hidrogen a  $-40$  °C s'observa la formació de l'espècie  $\text{Fe}^{\text{V}}(\text{O})(\text{OH})$ . Experiments de marcatge isotòpic mostren que en l'espècie  $\text{Fe}^{\text{V}}(\text{O})(\text{OH})$  un àtom d'oxigen prové de l'aigua i l'altre del peròxid d'hidrogen. A part, la reacció d'aquesta espècie amb una olefina indica que es tracte d'un intermedi catalític. Aquest és el primer cop que s'han observat intermedis tant reactius utilitzant condicions catalítiques.

## RESUMEN

Descubrir unos sistemas capaces de catalizar la oxidación de hidrocarburos de forma eficaz, selectiva y utilizando condiciones suaves es aún un reto para la química orgánica. Algunos metaloenzimas naturales pueden realizar esta química oxidativa con una alta regio- i estereoselectividad; una de las familias de enzimas más versátiles es las oxigenasas de Rieske, que contienen un centro de hierro no-hemo y pueden catalizar la hidroxilación de alcanos y la *cis*-dihidroxiación de alquenos. En esta tesis nos centraremos en la síntesis de complejos de hierro de bajo peso molecular que imiten la estructura i la función del centro activo de estos enzimas.

En primer lugar, describimos la síntesis de una familia de complejos de hierro basados en un ligando tetradentado que contiene un macrociclo de triazaciclononano covalentemente enlazado a una piridina. De manera sistemática, se introducen sustituyentes con distintas propiedades electrónicas y estéricas en la posición  $\alpha$  y  $\gamma$  del anillo de piridina. Todos los complejos se caracterizan estructuralmente i espectroscópicamente, indicando que las propiedades electrónicas del centro metálico dependen de los sustituyentes del anillo de piridina. Además, todos los complejos son capaces de catalizar la hidroxilación de alcanos i la epoxidación i *cis*-dihidroxiación de alquenos utilizando peróxido de hidrogeno como oxidante.

La oxidación de alcanos i alquenos mediante esta familia de complejos se estudia utilizando experimentos de marcaje isotópico i análisis de productos con el fin de determinar el mecanismo de oxidación. Estos experimentos conjuntamente con cálculos de DFT indican que la especie activa capaz de catalizar ambas oxidaciones es un  $\text{Fe}^{\text{V}}(\text{O})(\text{OH})$ .

Los resultados preliminares de oxidación indican que el catalizador con un metilo en la posición  $\alpha$  de la piridina es el mejor para catalizar las dos reacciones, la hidroxilación de alcanos y la *cis*-dihidroxiación de alquenos en escala sintética. Con el fin de demostrar su potencial a nivel sintético se ha estudiado la oxidación de una gran variedad de sustratos, los cuales incorporan distintos grupos funcionales.

En la parte final de la tesis, utilizamos la espectrometría de masas a temperatura variable con el fin de identificar intermedios involucrados en el ciclo catalítico de oxidación. Mezclando el complejo con peróxido de hidrogeno a  $-40\text{ }^{\circ}\text{C}$  se observa la formación de la especie  $\text{Fe}^{\text{V}}(\text{O})(\text{OH})$ . Experimentos de marcaje isotópico muestran que la especie  $\text{Fe}^{\text{V}}(\text{O})(\text{OH})$  contiene un átomo de oxígeno que proviene del agua y el otro del peróxido de hidrogeno. Además, la reacción de esta especie con una olefina indica que se trata de un intermedio catalítico. Esta es la primera vez que se observa un intermedio tan reactivo utilizando condiciones catalíticas.

# FULL LIST OF PUBLICATIONS

This thesis is based on a compendium of the followed publications:

## Chapter III

1. Assessing the Impact of Electronic Tuning of the Ligand in the Spin State and Catalytic Oxidation Ability of the Fe<sup>II</sup>(Pytacn) family of complexes. Prat, I.; Company, A.; Corona, T.; Ribas, X.; Costas, M. Submitted to *Inorganic Chemistry* in **2013**.

## Chapter IV

2. The Mechanism of Stereospecific C-H Oxidation by Fe(Pytacn) Complexes. Bioinspired Non-Heme Iron Catalysts Containing *cis*-Labile Exchangeable Sites. Prat, I.; Company, A.; Postils, V.; Ribas, X.; Que, L. Jr.; Luis, J. M.; Costas, M. Accepted in *Chemistry a European Journal* in **2013**. DOI: 0.1002/chem.201300110.

## Chapter V

3. An Iron Catalyst for Oxidation of Alkyl C-H Bonds Showing Enhanced Selectivity for Methylenic Sites. Prat, I.; Gómez, L.; Canta, M.; Ribas, X.; Costas, M. *Chemistry a European Journal* **2013**, *19*(6), 1908-1913.

## Chapter VI

4. Fe(Pytacn)-Catalyzed *cis*-Dihydroxylation of Olefins with Hydrogen Peroxide. Prat, I.; Font, D.; Company, A.; Junge, K.; Ribas, X.; Beller, M.; Costas, M. *Advanced Synthesis and Catalysis* **2013**, *355*, 947-956.

## Chapter VII

5. Observation of Fe(V)=O using variable-temperature mass spectrometry and its enzyme-like C-H and C=C oxidation reactions. Prat, I.; Mathieson, J. S. ; Güell, M.; Ribas, X.; Luis, J. M.; Cronin, L.; Costas, M. *Nature Chemistry* **2011**, *3*, 788-793.

All these papers have been published, accepted to be published or submitted to journals that belong to the first quartile according to JCR.

Contributions in other publications not included in this thesis:

6. Modeling the *cis*-Oxo-Labile Binding Site Motif of Non-Heme Iron Oxygenases: Water Exchange and Oxidation Reactivity of a Non-Heme Iron(IV)-Oxo Compound Bearing a Tripodal Tetradentate Ligand. Company, A.; Prat, I.; Frisch, J. R.; Mas Ballesté R.; Güell M.; Juhász, G.; Ribas, X.; Münck, E.; M. Luis, J.; Que Jr. L.; Costas, M. *Chemistry a European Journal* **2011**, *17*, 1622-1634.
7. Iron Catalyzed C-H Hydroxylation and Olefin *cis*-Dihydroxylation with a Single Electron Oxidant and Water as Oxygen Atom Source. Garcia-Bosch, I.; Codolà, Z.; Prat, I.; Ribas, X.; Lloret-Fillol, J.; Costas, M. *Chemistry a European Journal* **2012**, *18*, 13269 – 13273.
8. EPR Detection of Fe(V)=O Active Species in Nonheme Iron-Catalyzed Oxidations. Lyakin, O.; Prat, I.; Bryliakov, KP.; Costas, M.; Talsi, EP. *Catalysis Communications*, **2012**, *29*, 105-108.
9. Regioselective oxidation of non activated alkyl C-H bonds with structurally elaborated non heme iron catalyst. Gómez, L.; Canta, M.; Font, D.; Prat, I.; Ribas, X.; Costas, M. *Journal of Organic Chemistry*. **2013**, *78*, 1421–1433.
10. Electronic Effects on Single Site Iron Catalysts for Water Oxidation. Codolà, Z.; Garcia-Bosch, I.; Acuña, F.; Prat, I.; Luis, J.M.; Costas, M.; Lloret-Fillol, J. Accepted in *Chemistry a European Journal* in **2013**. DOI: 10.1002/chem.201301112.



## GLOSSARY OF ABBREVIATIONS

- 2°: Secondary.
- 3°: Tertiary.
- A/K: Alcohol/Ketone ratio.
- AcOEt: Ethyl acetate.
- AcOH: Acetic acid.
- AcOOH: Peracetic acid.
- Asp: Asparagine.
- BBP: 2,6-bis(*N*-methylbenzimidazol-2-yl)pyridine.
- Bn-tpen: *N*-benzyl-*N,N',N'*-tris(2-pyridylmethyl)-1,2-diaminoethane.
- bpmcn: *N,N'*-dimethyl-*N,N'*-bis(2-pyridylmethyl)cyclohexane-trans-1,2-diamine.
- bpmen: *N,N'*-dimethyl-*N,N'*-bis(2-pyridylmethyl)ethane-1,2-diamine.
- Bpka: 3-(dipyridin-2-yl-methyl)-1,5,7-trimethyl-2,4-dioxo-3-azabicyclo[3.3.1]nonane-7-carboxylic acid.
- bqen: bis(quinolyl)-diamine.
- <sup>t</sup>Bu: *tert*-butyl.
- C<sub>6</sub>H<sub>12</sub>: Cyclohexane.
- C<sub>6</sub>D<sub>12</sub>: Cyclohexane-D<sub>12</sub>.
- Cat.: Catalyst.
- CF<sub>3</sub>SO<sub>3</sub>: OTf : Trifluoromethanesulfonate anion.
- CH<sub>3</sub>CN: Acetonitrile.
- cis*-1,2-DMCH: *cis*-1,2-dimethylcyclohexane.
- Cpd I: Compound I, active species for the cytochrome P450.
- Conv.: Conversion.
- CSI-MS: Cold-spray-ionization mass spectrometry.
- CV: Cyclic voltammetry.
- cyclam: 1,4,8,11-tetraazacyclotetradecane.
- Cyt P450: Cytochrome P450.
- D/E: *syn*-Diol/Epoxyde ratio.
- DFT: Density functional theory.
- dpaq: 2-[bis(pyridin-2-ylmethyl)]amino-*N*-quinolin-8-yl-acetamidate.
- syn*-diol: *cis*-dihydroxylation product in alkene oxidation.
- DMSO: Dimethyl sulfoxide.
- E<sub>1/2</sub>: Electrochemical potential.
- ee: Enantiomeric excess.
- Eq.: Equation.
- Equiv.: Equivalentents.
- EPR: Electron paramagnetic resonance.
- ESI-MS: Electro-spray-ionization mass spectrometry.
- GC: Gas chromatography.
- Glu: Glutamine.
- H<sub>2</sub>O<sub>2</sub>: Hydrogen peroxide.
- His: Histidine.
- HS: High spin.

Kcal: Kilocalorie.  
 KIE: Kinetic isotope effect.  
 L: Ligand.  
 L-N<sub>3</sub>(OCH<sub>3</sub>)<sub>2</sub>: (6-bis[1-(2-methylanisolylimino)ethyl]pyridine).  
 LS: Low spin.  
 mcpp: *N,N'*-dimethyl-*N,N'*-bis(((*R*)-4,5-pinenepyridin-2-yl)methyl)cyclohexane-1,2-diamine.  
 min: Minutes.  
 sMMO: soluble methane monooxygenase.  
 N4Py: *N,N*-bis(2-pyridylmethyl)-*N*-(bis-2-pyridylmethyl)amine.  
 NAD(P)H: Nicotinamide adenine dinucleotide (phosphate).  
 NaOCl: Sodium hypochlorite.  
 NDO: Naphthalene 1,2-dioxygenase.  
 NMR: Nuclear magnetic resonance.  
 N<sub>3</sub>O<sub>2</sub>-L: 1-carboxymethyl-4,7-dimethyl-1,4,7-triazacyclononane.  
 [Ox]: Oxidant.  
 P4H: Prolyl 4-hydroxylase.  
 pdp: *N,N'*-bis(2-pyridylmethyl)2,2'-bipyridine.  
 Ph-DPAH: di-(2-pyridyl)methyl)benzamide.  
 PhIO: Iodosylbenzene.  
 PhSMe: Thioanisole.  
 PPh<sub>3</sub>: Triphenylphosphine.  
 PrL1: 3,3-bis(1-methylimidazol-2-yl)propionate.  
 py: Pyridine.  
 c-Py<sub>2</sub>NMe<sub>2</sub>: *N,N'*-dimethyl-2,11-diaza[3.3](2,6)pyridinophane.  
 PyMAC: 2,7,12-trimethyl-3,7,11,17-tetra-azabicyclo[11.3.1] heptadeca-1(17),13,15-triene.  
 Py(ProPh<sub>2</sub>OH)<sub>2</sub>: 2,6-Bis[[*S*]-2-(diphenylhydroxymethyl)-1-pyrrolidinyl]methyl]pyridine.  
 Pytacn: 1-(2'-pyridylmethyl)-4,7-dimethyl-1,4,7-triazacyclononane.  
 RC: Retention of configuration in the oxidation of the tertiary C-H bonds of *cis*-1,2-dimethylcyclohexane.  
 r.t.: Room temperature.  
 SCE: Saturated calomel electrode.  
 Tacn: 1,4,7-triazacyclononane.  
 TauD: Taurine/ $\alpha$ -ketoglutarate dioxygenase.  
 TBHP: *tert*-butyl hydroperoxide.  
 THF: Tetrahydrofuran.  
 TN: Turnover number.  
 TMC: 1,4,8,11-tetramethyl-1,4,8,11-tetraazacyclotetradecane  
 tpa: tris(2-pyridylmethyl)amine.  
 tpoen = *N*-(2-pyridylmethoxyethyl)-*N,N*-bis(2-pyridylmethyl)amine.  
 Triflate: Trifluoromethanesulfonate.  
 TyrH: Tyrosine hydroxylase.  
 UV-Vis: Ultraviolet-Visible.  
 VT-MS: Variable-temperature mass spectrometry.  
 $\mu_{\text{eff}}$ : Effective magnetic moment.

## LIST OF FIGURES

<b>Figure I.1.</b> Bioinspired approach from metal active site of enzymes to designed functional models. The depicted functional model is inspired in the active site of Rieske Oxygenase enzymes.....	20
<b>Figure I.2.</b> The active site of cytochrome P450-camphor from <i>Pseudomonas putida</i> . The C-H bond ready for cleavage is highlighted in green.....	22
<b>Figure I.3.</b> Active center of Naphthalene Dioxygenase. The only crystallographically characterized O <sub>2</sub> complex of a mononuclear non-heme iron enzyme containing a 2-His-1-carboxylate facial triad. <sup>43</sup> .....	25
<b>Figure I.4.</b> Some of the iron(IV)-oxo complexes synthesized. ....	58
<b>Figure I.5.</b> Schematic representation of H <sub>4</sub> -TAML ligand (left). Geometry-optimized structure of [Fe <sup>V</sup> (O)(H <sub>4</sub> -TAML)] <sup>-</sup> as obtained from DFT calculations (right). ....	59
<b>Figure I.6.</b> Iron(II) complexes studied by EPR spectroscopy after mixing with oxidant agents. ....	60
<b>Figure I.7.</b> a) ESI-MS detection of an iron(V) bis-oxo. b) CSI-MS analysis to detect an iron(V)-oxo with a pentadentate ligand. ....	60
<b>Figure II.1.</b> Iron complexes employed in this thesis .....	70
<b>Figure VIII.1.</b> Schematic representation of complex [Fe <sup>II</sup> (CF <sub>3</sub> SO <sub>3</sub> ) <sub>2</sub> (pdp)] and Λ-[Fe <sup>II</sup> (CF <sub>3</sub> SO <sub>3</sub> ) <sub>2</sub> (mcpp)]...	159
<b>Figure VIII.2.</b> Ball and stick diagram of the X-ray structures of [Fe <sup>II</sup> (CF <sub>3</sub> SO <sub>3</sub> ) <sub>2</sub> (pdp)] (left), and <sup>Me,H</sup> <b>1</b> (right). Triflate and water ligands have been omitted, leaving only the oxygen atom attached to the iron centre. Colour code; iron (orange), oxygen (red), nitrogen (blue), carbon (gray) and hydrogen (white).....	162
<b>Figure VIII.3.</b> Full mass spectra after mixing catalyst <sup>H,H</sup> <b>1</b> with 100 equiv. of H <sub>2</sub> O <sub>2</sub> . ....	170
<b>Figure VIII.4.</b> Graph showing the decomposition of P/O species (486.1 <i>m/z</i> ) when the temperature is increased from -40°C to 20°C.....	170
<b>Figure VIII.5.</b> Full mass spectra after mixing catalyst <sup>H,H</sup> <b>1</b> with 10 equiv. of H <sub>2</sub> O <sub>2</sub> and adding 100 equiv. of <i>cis</i> -cyclooctene.....	172
<b>Figure VIII.6.</b> DFT Gibbs energy profile of the reaction between the iron(V)-oxo-hydroxo species O with <i>trans</i> -2-butene to form the hydroxyglycolate species H. TS = transition state.....	173

## LIST OF TABLES

<b>Table I.1.</b> Iron proteins involved in oxidative reactions. <sup>8, 17, 23</sup> .....	21
<b>Table I.2.</b> Oxidation of alkanes by tetradentate iron(II) complexes, ligands represented in Scheme I.9. .	31
<b>Table VIII.1.</b> Selected physical data for <sup>R,R'</sup> <b>2</b> .....	148
<b>Table VIII.2.</b> Oxidation of cyclohexane and <i>cis</i> -cyclooctene with H <sub>2</sub> O <sub>2</sub> using complexes [Fe <sup>II</sup> (CF <sub>3</sub> SO <sub>3</sub> ) <sub>2</sub> ( <sup>R,R'</sup> Pytacn)] ( <sup>R,R'</sup> <b>1</b> ) as catalysts. <sup>[a]</sup> Results for <sup>H,H</sup> <b>1</b> and <sup>Me,H</sup> <b>1</b> have been previously reported. <sup>6, 13</sup> .....	150
<b>Table VIII. 3.</b> Alkane hydroxylation reactions catalyzed by <sup>R,R'</sup> <b>1</b> . Results for <sup>H,H</sup> <b>1</b> and <sup>Me,H</sup> <b>1</b> have been previously reported. <sup>6, 14</sup> .....	153
<b>Table VIII.4.</b> Oxidation of <i>cis</i> -4-methylcyclohexyl pivalate by the family of complexes <sup>R,R'</sup> <b>1</b> .....	159
<b>Table VIII.5.</b> Oxidation of <i>cis</i> -4-methylcyclohexyl pivalate by different catalysts. <sup>[a]</sup> .....	160
<b>Table VIII.6.</b> Oxidation of <i>cis</i> -cyclooctene with the optimization conditions for the catalysts <sup>R,R'</sup> <b>1</b> .....	164
<b>Table VIII.7.</b> Substrate scope using the optimized conditions and <sup>Me,H</sup> <b>1</b> as catalyst. <sup>[a]</sup> .....	165
<b>Table VIII.8.</b> Catalysis using two iterative catalytic oxidations.....	168

## LIST OF SCHEMES

<b>Scheme I.1.</b> Important oxidation reactions. ....	17
<b>Scheme I.2.</b> Oxidation reactions catalyzed by Cyt P450. ....	22
<b>Scheme I.3.</b> Proposed catalytic mechanism for alkane hydroxylation performed by Cyt P450. ....	23
<b>Scheme I.4.</b> Postulated “oxygen rebound” mechanism for alkane hydroxylation in Cyt P450. ....	24
<b>Scheme I.5.</b> a) Schematic representation of the 2-His-1-carboxylate facial triad in the active center of the superfamily Rieske Oxygenases. b) Active center of 1,2-naphthalene dioxygenase (NDO) enzyme and its oxidative reaction towards naphthalene. ....	25
<b>Scheme I.6.</b> Catalytic cycle proposed for Rieske Oxygenases, showing the <i>cis</i> -dihydroxylation of naphthalene. ....	26
<b>Scheme I.7.</b> Structures of high-valent intermediates detected in natural enzymes. ....	27
<b>Scheme I.8.</b> Cyclohexane oxidation catalyzed by Reedijk system. <sup>75</sup> ....	29
<b>Scheme I.9.</b> Schematic representation of the most important tetradentate ligands used to prepare mononuclear iron(II) complexes that could perform the oxidation of alkanes. ....	30
<b>Scheme I.10.</b> Alkane hydroxylation catalyzed by $[\text{Fe}^{\text{II}}(\text{CF}_3\text{SO}_3)_2(\text{Me,RPytacn})]$ complexes. Catalyst:H <sub>2</sub> O <sub>2</sub> :cyclohexane = 1:100:1000. ....	32
<b>Scheme I.11.</b> Alkane hydroxylation using $[\text{Fe}^{\text{II}}(\text{pdp})(\text{CH}_3\text{CN})_2](\text{SbF}_6)_2$ . A: Substrate electronic effects on site selectivity in hydroxylation of multiple 3°C–H bonds. B: Selective hydroxylation based on steric effects. ....	33
<b>Scheme I.12.</b> Directed hydroxylation of C–H bonds by acid group and subsequently lactonization catalyzed by $[\text{Fe}^{\text{II}}(\text{pdp})(\text{CH}_3\text{CN})_2](\text{SbF}_6)_2$ . ....	33
<b>Scheme I.13.</b> Selective hydroxylation of (+)-artemisin by $[\text{Fe}^{\text{II}}(\text{pdp})(\text{CH}_3\text{CN})_2](\text{SbF}_6)_2$ . By recycling the starting material twice the diastereometrically pure product was afforded in 54% yield. ....	34
<b>Scheme I.14.</b> The combination of steric and electronic effects allows the selective oxidation of methylene group by the $[\text{Fe}^{\text{II}}(\text{pdp})(\text{CH}_3\text{CN})_2](\text{SbF}_6)_2$ . ....	34
<b>Scheme I.15.</b> $[\text{Fe}^{\text{II}}(\text{CF}_3\text{SO}_3)_2((S,S,R)\text{-mcpp})]$ complex described by Gomez and co-workers, and results in catalytic C–H oxidation reactions. ....	35
<b>Scheme I.16.</b> Selective oxidation of <i>cis</i> -4-methylcyclohexyl-1-pivalate by $[\text{Fe}^{\text{III}}(\text{dpaq})(\text{H}_2\text{O})]^{2+}$ complex. ....	36
<b>Scheme I.17.</b> Proposed mechanism for both, hydroxylation and dehydrogenation catalyst by complex $[\text{Fe}^{\text{II}}(\text{pdp})(\text{CH}_3\text{CN})_2](\text{SbF}_6)_2$ . ....	37
<b>Scheme I.18.</b> Catalysts structures identified from the combinatorial screening by studying the epoxidation activity in front of <i>trans</i> - $\beta$ -methylstyrene. Grey balls stand for the polystyrene support. ....	38
<b>Scheme I.19.</b> Epoxidation of 1-decene catalyzed by $[\text{Fe}^{\text{II}}(\text{bpmen})(\text{CH}_3\text{CN})_2](\text{SbF}_6)_2$ complex. ....	38
<b>Scheme I.20.</b> Schematic representation of some relevant iron catalysts for olefin oxidation. a) Dimeric phenanthroline based complex reported by Stack. b) Chiral dimeric complex reported by Menage. c) Chiral iron sexipyridine reported by Kwong. d) Iron(II) <i>bis</i> -terpyridine complex described by Che. ....	39
<b>Scheme I.21.</b> <i>In situ</i> generated asymmetric catalyst for stereoselective olefin epoxidation. ....	40
<b>Scheme I.22.</b> <i>In situ</i> generated catalyst which performs epoxidation of a high rang of olefins. ....	40
<b>Scheme I.23.</b> Best results obtained in the epoxidation of <i>trans</i> -stilbene using 5-chloro-1-methylimidazole ligand. ....	41
<b>Scheme I.24.</b> Iron(II) complexes employed for the enantioselective epoxidation of $\alpha,\beta$ -enones by Sun. ....	41
<b>Scheme I.25.</b> Bipyrrolidine base iron(II) complex catalyze the asymmetric epoxidation of various olefins in the presence of a carboxylic acid. ....	42

<b>Scheme I.26.</b> Representation of ligands used to prepared mononuclear iron(II) complexes to perform olefin oxidation along with the coordination they adopt around the metal center. Oxidation of <i>cis</i> -cyclooctene with H <sub>2</sub> O <sub>2</sub> catalyzed by the different iron(II) complexes. Catalytic conditions, catalyst:H <sub>2</sub> O <sub>2</sub> : <i>cis</i> -cyclooctene = 1:10:1000. E+D = Turnover number (TN, mols of product / mols of catalyst), E = epoxide, D = <i>syn</i> -diol. D/E = (mols of D / mols of E) [a] 50 equiv of H <sub>2</sub> O <sub>2</sub> instead of 10. [b] 1-octene was used as a substrate instated of <i>cis</i> -cyclooctene. [c] 500 equiv of <i>cis</i> -cyclooctene were used.....	43
<b>Scheme I.27.</b> Asymmetric <i>cis</i> -dihydroxylation using $\alpha$ -[Fe <sup>II</sup> (CF <sub>3</sub> SO <sub>3</sub> ) <sub>2</sub> (6Me <sub>2</sub> -pdp)] complex, obtaining <i>syn</i> -diol product in 97% ee. ....	44
<b>Scheme I.28.</b> Catalysts capable of performing oxidation of alkenes with high ratio diol/epoxide. ....	45
<b>Scheme I.29.</b> Large-scale catalysis performed by [Fe <sup>III</sup> (Cl) <sub>2</sub> (c-Py <sub>2</sub> NMe <sub>2</sub> ) <sup>+</sup> .....	46
<b>Scheme I.30.</b> A: Active site of a Rieske Oxygenases, naphthalene 1,2-dioxygenase B: Complex with Ph-DPAH ligand described by Que, and used as a mimic of Rieske Oxygenase active center. C: Complex with Bpka ligand.....	47
<b>Scheme I.31.</b> Competition between protio- and deuterioalkanes. ....	48
<b>Scheme I.32.</b> Oxidation of adamantane. ....	48
<b>Scheme I.33.</b> Radical reaction giving equimolar amounts of alcohol and ketone. ....	49
<b>Scheme I.34.</b> Isomers obtained in the tertiary alcohol oxidation of <i>cis</i> -1,2-dimethylcyclohexane. ....	49
<b>Scheme I.35.</b> "Oxo-hydroxo tautomerism". This process mediates the incorporation of oxygen from labeled water into the oxidized products. ....	50
<b>Scheme I.36.</b> Proposed formation of the iron(III)-hydroperoxo species and its possible evolution to more powerful high-valent iron-oxo species.....	52
<b>Scheme I.37.</b> Proposed formation of mononuclear high-valent iron-oxo intermediates via O-O heterolytic cleavage. ....	52
<b>Scheme I.38.</b> Examples of class A and Class B catalysts.....	53
<b>Scheme I.39.</b> Proposed mechanisms for olefin epoxidation and <i>cis</i> -dihydroxylation by class A and class B catalysts. ....	54
<b>Scheme I.40.</b> A) Olefine oxidation mechanism, the same Fe <sup>V</sup> (O)(OH) species is capable of catalyzing the epoxidation and the <i>cis</i> -dihydroxylation. B) Proposed mechanisms for iron-catalyzed oxidation in presence of carboxylic acid. ....	54
<b>Scheme I.41.</b> Proposed mechanism for the oxidation of olefins.....	55
<b>Scheme I.42.</b> Fe <sup>II</sup> /Fe <sup>IV</sup> mechanism postulated for alkene oxidation reactions catalyzed by iron bispidine complexes. ....	56
<b>Scheme I.43.</b> Mechanism of alkane hydroxylation by Fe <sup>V</sup> (O)(OH) via oxo-hydroxo tautomerism. Percentage of water incorporation depends on which tautomer catalyzes the oxidation reaction.....	57
<b>Scheme I.44.</b> Proposed rebound mechanism for alkane hydroxylation by [Fe <sup>II</sup> (CF <sub>3</sub> SO <sub>3</sub> ) <sub>2</sub> ( <sup>Me,H</sup> Pytacn)]. ....	58
<b>Scheme VIII.1.</b> Ligands and complexes employed in this thesis.....	144
<b>Scheme VIII.2.</b> Table: Spin state and $\mu_{\text{eff}}$ of <sup>R,R'</sup> 2 complexes at 298K in acetonitrile. Graphic: Representation of the effective magnetic moment of <sup>H,H'</sup> 2 in front of the Hammett constants ( $\sigma_p$ ). [a] Compounds <sup>R,R'</sup> 2 were prepared by dissolving the bis-triflate complexes <sup>R,R'</sup> 1 in CH <sub>3</sub> CN or CD <sub>3</sub> CN. ....	146
<b>Scheme VIII.3.</b> a) Representation of the effective magnetic moment of <sup>H,H</sup> 2, <sup>F,H</sup> 2, <sup>H,NO2</sup> 2 and <sup>H,NMe2</sup> 2 as a function of temperature. The effective magnetic moment was measured in a CD <sub>3</sub> CN solution using the Evans' method. b) X-Ray structure of <sup>Me,H</sup> 2SbF <sub>6</sub> at 100K. The table shows the Fe-N <sub>pyr</sub> , the average Fe-N <sub>tacn</sub> and the average Fe-N <sub>acn</sub> bond lengths for each of the three molecules (A, B and C) that form the unit cell at a given temperature (100 K, 150 K, 170 K and 300 K). Hydrogen atoms have been omitted for clarity. ....	147

<b>Scheme VIII.4.</b> Water assisted mechanism to explain the oxidation of olefins by mononuclear non-heme iron catalysts. ....	151
<b>Scheme VIII.5.</b> Proposed mechanism for alkene oxidation, where the fast equilibrium between the two tautomers is represented.....	152
<b>Scheme VIII.6.</b> Origen of oxygen atoms in the oxidation of cyclohexane. Blue: Percentage of oxygen incorporated from water, measured for all catalysts <sup>R,R'</sup> <b>1</b> . Red: Percentage of oxygen incorporated from hydrogen peroxide, measured for catalysts, <sup>H,H</sup> <b>1</b> , <sup>H,Me</sup> <b>1</b> , <sup>Me,H</sup> <b>1</b> , <sup>Me,Me</sup> <b>1</b> and <sup>F,H</sup> <b>1</b> . ....	153
<b>Scheme VIII.7.</b> Percentage of oxygen from water incorporation into alcohol products obtained in the oxidation of alkanes catalyzed by complexes <sup>R,R'</sup> <b>1</b> in presence of 1000 equiv. of H <sub>2</sub> <sup>18</sup> O.....	154
<b>Scheme VIII.8.</b> Schematic representation of complexes [Fe <sup>II</sup> (tpa)(CH <sub>3</sub> CN) <sub>2</sub> ] <sup>2+</sup> and [Fe <sup>II</sup> (bpmen)(CH <sub>3</sub> CN) <sub>2</sub> ] <sup>2+</sup> . ....	155
<b>Scheme VIII.9.</b> A common iron(V)-oxo-hydroxo species as the active species in C-H hydroxylation and C=C <i>cis</i> -dihydroxylation as postulated for [Fe <sup>II</sup> (tpa)(CH <sub>3</sub> CN) <sub>2</sub> ] <sup>2+</sup> and [Fe <sup>II</sup> (bpmen)(CH <sub>3</sub> CN) <sub>2</sub> ] <sup>2+</sup> catalysts. ....	155
<b>Scheme VIII.10.</b> Mechanism of cyclohexane hydroxylation that arises from DFT calculations considering the different isomers of catalyst <sup>H,H</sup> <b>1</b> (left) and <sup>Me,H</sup> <b>1</b> (right). ....	156
<b>Scheme VIII.11.</b> Concerted process mechanisms for the hydroxylation of cyclohexane by O.....	156
<b>Scheme VIII.12.</b> Space filling diagrams for complexes <sup>H,H</sup> <b>1</b> and <sup>Me,H</sup> <b>1</b> showing the steric protection of the bulky group in the α position of the pyridine ring. Triflate groups have been omitted for clarity. ....	158
<b>Scheme VIII.13.</b> Oxidation of different substrates by complex <sup>Me,H</sup> <b>1</b> (yields measured by GC). ....	161
<b>Scheme VIII.14.</b> Oxidation of <i>trans</i> -dimethylcyclohexane and <i>trans</i> -decalin by complex <sup>Me,H</sup> <b>1</b> ( yields measured by GC). ....	162
<b>Scheme VIII.15.</b> Regioselective C-H oxidation reactions catalyzed by [Fe <sup>II</sup> (CF <sub>3</sub> SO <sub>3</sub> ) <sub>2</sub> (pdp)], Λ-[Fe <sup>II</sup> (CF <sub>3</sub> SO <sub>3</sub> ) <sub>2</sub> (mcpp)] and <sup>Me,H</sup> <b>1</b> . [a] Cat:H <sub>2</sub> O <sub>2</sub> :substrate:AcOH 3:360:100:150. [b] Cat:H <sub>2</sub> O <sub>2</sub> :substrate:AcOH 3:200:100:150. [c] GC yield.....	163
<b>Scheme VIII.16.</b> Catalytic oxidation of 3-pentenoic acid by catalyst <sup>Me,H</sup> <b>1</b> . [a] Isolated yield. ....	166
<b>Scheme VIII.17.</b> Catalytic oxidation of <i>trans-trans-cis</i> -1,5,9-cyclododecatriene. [a] Isolated yield. ....	166
<b>Scheme VIII.18.</b> Catalytic oxidation of (2 <i>E</i> ,6 <i>Z</i> )-nona-2,6-dienyl acetate. ....	167
<b>Scheme VIII.19.</b> Catalytic oxidation of the natural product <i>cis</i> -jasmone.....	167
<b>Scheme VIII.20.</b> Mechanisms and shift of mass spectral peaks when the corresponding combination of H <sub>2</sub> <sup>18</sup> O or H <sub>2</sub> <sup>18</sup> O <sub>2</sub> are used to form the Fe <sup>V</sup> (O)(OH) species.....	171
<b>Scheme VIII.21.</b> Mechanisms and shift of mass spectral peaks when H <sub>2</sub> <sup>18</sup> O and H <sub>2</sub> <sup>18</sup> O <sub>2</sub> are used to give the hydrogenglycolates H and the glycolates G. ....	172

## ACKNOWLEDGEMENTS

This work would not have been possible without the following collaborations:

- Serveis Tècnics de Recerca from Universitat de Girona for technical support.
- Dr. Josep M<sup>a</sup> Luis, Dra. Mireia Güell and Verònica Postils from Institut de Química Computacional i Catàlisis of Universitat de Girona for DFT calculations.
- Prof. Dr. Leroy Cronin and Dra. Jennifer Mathieson from University of Glasgow for hosting a scientific visit and the collaborative work in development of variable-temperature mass spectrometry experiments.
- Prof. Dr. Mathias Beller and Dr. Kathrin Junge from Leibniz-Institut für Katalyse e. V. for hosting a scientific visit and the collaborative work in development of iron(II) catalysts to perform *cis*-dihydroxylation reactions.
- COST Action D40 for financial support of the short stay in the University of Glasgow.
- MEC of Spain for financial support through project CTQ2009-08464/BQU and for the PhD Grant AP2008-01626. Generalitat de Catalunya for project 2009 SGR-637. European Research Foundation for ERC-2009-Starting Grant 239910.





---

---

## **CHAPTER I.**

### **GENERAL INTRODUCTION**

---

---

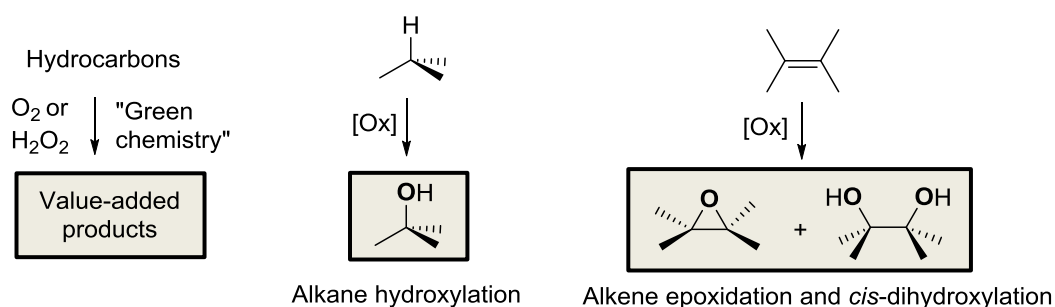


## I. GENERAL INTRODUCTION

### I.1. Advances in alkane and alkene oxidation reactions

The development of sustainable chemical methods for the selective oxidation of alkanes and alkenes is an important scientific goal with technological significance. The hydroxylation of alkanes and the *cis*-dihydroxylation and epoxidation of alkenes are important reactions because they allow the transformation of simple hydrocarbons into useful products for chemical synthesis (Scheme I.1).<sup>1-3</sup> Despite the large amount of research in this field over the last century, the development of systems that could perform this chemistry with high levels of activity, selectivity and efficiency are still a challenge.

An additional objective of these novel methodologies is that they must be environmentally friendly, preferentially relying on non-toxic reagents and catalytic methods with large atom economy, operating under mild conditions. Regarding oxidation reactions, the use of dioxygen and hydrogen peroxide as oxidants is preferred for their atom-economy and lack of toxicity.<sup>4</sup>



**Scheme I.1.** Important oxidation reactions.

#### I.1.1. Alkane oxidations

The functionalization of hydrocarbons in a sustainable manner is one of the main challenges for chemists. Their abundance in nature as natural gas or crude oil makes them the most convenient chemical feedstock. The oxidation of hydrocarbons is one of the most interesting reactions, first, because the introduction of an oxygen atom introduces functionality in these molecules, increasing their value as reagents for further chemical transformation. In second place, because oxidized alkane moieties are ubiquitous constituents of organic molecules with biological interest, and thus are chemical structures that are interesting *per se*. However, these reactions are fundamentally difficult due to the low reactivity of alkyl C-H bonds, and therefore, they are often disregarded as synthetic tools.<sup>5</sup>

Currently available methodologies involve highly reactive-oxidizing reagents, high temperatures and long-time reactions in order to overcome this lack of reactivity.<sup>6</sup> These harsh conditions introduce drawbacks in terms of chemo- and regioselectivity, essential to produce synthetically valuable products. Moreover, since most functional groups do not tolerate these harsh oxidative conditions,<sup>7</sup> selective oxidation often requires the use of protection-deprotection strategies, giving large amounts of waste.

An important step forward is the development of one-step oxidation methodologies, allowing the oxidation of C-H bonds in the later stage of the synthetic sequences in the presence of different functional groups and with high regio- and stereoselectivity. Natural systems, such as iron enzymes, are capable of perform this chemistry with high selectivity and efficiency. The design of metal based catalysts that mimic the natural enzymes is a challenging strategy that may allow for performing the selective oxidation of C-H bond in a predictive way and with short reaction times.<sup>8</sup>

### **I.1.2. Alkene oxidations**

Olefins are one of the most versatile starting materials and their oxidation leads to various value-added products such as epoxides, *syn*-diols, alcohols, aldehydes or ketones. All of these products are important building blocks for the production of bulk and fine chemicals. Epoxides are high useful intermediates to elaborate more complex products in organic synthesis. Current industrial epoxidation methods include the *chlorohydrin* process (for the preparation of ethylene and propylene oxide) and peracids as the most common reagents employed in fine chemistry. For economical and environmental reasons, molecular oxygen or hydrogen peroxide are the preferred oxidants.<sup>3</sup>

Another important class of product obtained in the oxidation of olefins are *syn*-diols. *syn*-Diols have a wide range of applications, for example, ethylene and propylene glycol are produced in large scale, due to their importance as polyesters monomers and as antifreeze agents. Moreover, chiral 1,2-*syn*-diol products are used as reaction intermediates in the synthesis of pharmaceuticals.<sup>9</sup>

Currently, diols are synthesized by a two-step sequence consisting of the epoxidation of an alkene with a peracid, hydroperoxide, or oxygen followed by hydrolysis of the resulting epoxide. The dihydroxylation process comprises a more atom-efficient and shorter route to the desired product. Typically these reactions are performed using high valent osmium, ruthenium or manganese catalysts. Over the last century, numerous synthetic approaches based mainly on osmium-catalysis have been described, and nowadays these systems are the

most reliable and efficient approach for the synthesis of *syn*-1,2-diol.<sup>10, 11</sup> Furthermore, the discovery by Sharpless of catalytic systems that can perform asymmetric dihydroxylation expanded the synthetic applications of osmium-catalysis.<sup>12, 13</sup> However, osmium reagents have some important drawbacks, in particular their cost and toxicity.

In response, several alternative methods for alkene oxidation have been investigated. Of those, the combination of hydrogen peroxide with non-toxic and inexpensive metal catalysts constitutes an ideal system for these oxidation reactions.<sup>14</sup>

### **1.1.3. Metalloenzymes and model compounds**

The problem of selectivity in the oxidation of non-activated C-H bonds and C=C under mild conditions had been solved successfully by Nature in the course of evolution through the use of metalloenzymes.

Metalloenzymes, utilize metals as the cofactors to catalyze a diverse array of biochemical reactions. Even though metal ions only account for less than 1% of the total protein weight, they are essential for the enzyme activity. Moreover, the metal ions have the ability to exist in multiple oxidation states and different geometries, and these characteristics are vital to promote complex biochemical transformations and participate in highly specialized biological functions such as oxygen activation.<sup>15</sup>

Metal ions in metalloproteins are usually coordinated by nitrogen, oxygen or sulfur atoms belonging to amino acids in the polypeptide chain of the protein. The nature of the metal and of the amino acid residues, the coordination geometry of the metal center, the relative disposition of the metal in the case of polymetallic systems and the three-dimensional configuration are crucial properties for the reactivity of the metalloprotein. All these factors determine the ability of the metal ion to stabilize different reaction intermediates, sometimes with distinct oxidation states, and they can also alter the shape of the active site that controls the accessibility, and the trajectories of the substrate approaching to the metal active center.

One of the interests in bioinorganic chemistry is the structural and spectroscopic characterization of the metalloproteins active site, and the study of their reactivity. Only very few successful examples of enzyme redesign in order to modify the active center have been reported recently, showing the possibility of changing the inherent catalytic activity of the enzyme.<sup>16</sup> However, due to the time-consuming and inherent difficulty of working with proteins, because of its high molecular weight and the complicated process of purification, synthetic model chemistry (bioinspired studies) constitutes an attractive approach for gaining knowledge about the protein chemistry. The aim of these systems is to mimic the reactivity of

the natural enzyme in catalyzed transformations by using synthetic low-molecular weight compounds, and provide mechanistic, structural and spectroscopic data for comparison with the biological system (Figure I.1).<sup>17</sup> The model chemistry is based in the design of suitable ligands to generate functional models with first row metal capable of achieving the same catalytic reactivity of the enzyme.

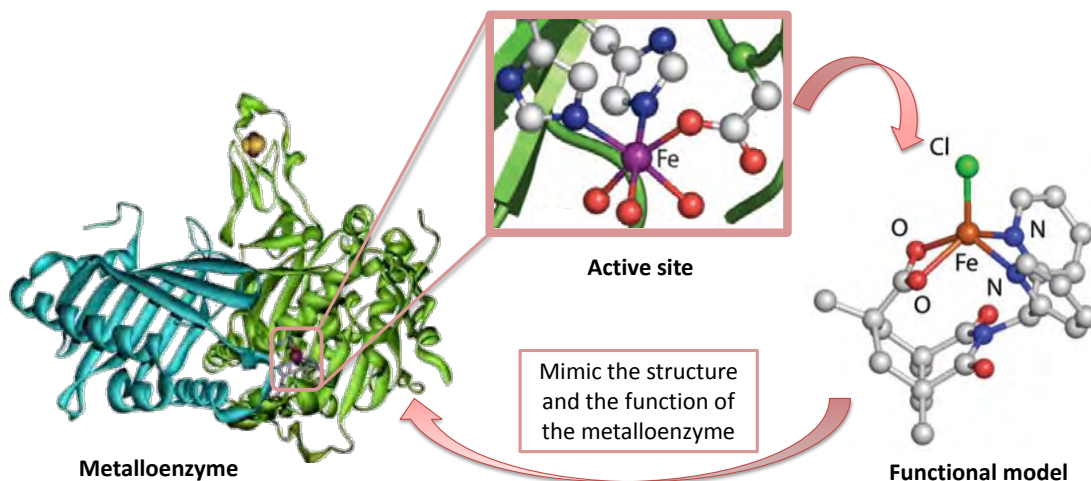


**Figure I.1.** Bioinspired approach from metal active site of enzymes to designed functional models. The depicted functional model is inspired in the active site of Rieske Oxygenase enzymes.

In this thesis, we use simple synthetic model complexes to reproduce the basic aspects of the oxidation reactivity of Rieske Oxygenase enzymes. With these models we study the mechanism of catalytic oxidation reactions of alkanes and alkenes, and specifically, we developed catalysts for the hydroxylation of alkanes and the *cis*-dihydroxylation of alkenes under preparative scale conditions.

## I.2. Biological role of iron enzymes

Iron is the element of choice for many essential biological transformations, because of its abundance in the earth, its inherent electronic properties and its accessible redox potentials. Iron-containing enzymes participate in biological oxidations and in oxygen transport, among others. For instance, it can be found in the active center of oxidases, hydrogenases, reductases, dehydrogenases and oxygenases.<sup>18</sup>

Iron is the fourth most common element in the earth's crust, and can exist in a wide range of oxidation states, although the most common are Fe<sup>II</sup> and Fe<sup>III</sup>. In order to explain some enzymatic process taking place in biological systems, higher and lower oxidation states, such as Fe<sup>IV</sup>, Fe<sup>V</sup> and Fe<sup>I</sup> have been postulated.<sup>17</sup> Indeed, recently Fe<sup>IV</sup>=O intermediate species in

natural systems have been characterized and described as catalytic intermediates in oxidative processes.<sup>19-22</sup>

Due to its versatility, iron is present in a wide range of metalloenzymes in different configurations such as heme systems with porphyrin ligands, iron-sulfur clusters and non-heme systems (with mononuclear and dinuclear centers).

### I.2.1. Iron proteins involved in oxygen activation

In Nature, a large amount of iron proteins are implicated in oxidation processes via O<sub>2</sub> activation. They can be classified in three different groups depending on their active site: heme oxygenases, mononuclear non-heme, and dinuclear non-heme oxygenases. The most representative iron proteins that take part in oxidative processes and the reactions they catalyze are showed in Table I.1.

In this introduction, only two systems will be explained in detail, the cytochrome P450 and Rieske Oxygenases. Both constitute relevant and paradigmatic examples of heme and mononuclear non-heme iron enzymes and moreover they are directly related to the work presented in this thesis.

**Table I.1.** Iron proteins involved in oxidative reactions.<sup>8, 17, 23</sup>

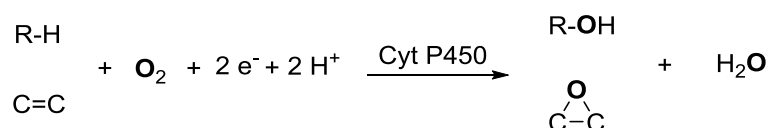
IRON-CONTAINING PROTEINS	CATALYTIC REACTION
<b>Heme proteins</b>	
Cytochrome P450	$\text{C-H or C=C} \xrightarrow[2 e^-, 2H^+]{O_2} \text{R-OH or } \begin{array}{c} \text{O} \\ \diagup \quad \diagdown \\ \text{C}-\text{C} \end{array} + \text{H}_2\text{O}$
<b>Mononuclear non-heme center</b>	
- <i>Iron(III) dioxygenases</i>	
Intradiol-cleaving catechol dioxygenases	
- <i>Iron enzymes that contain 2-His-1-carboxylate facial triad motif</i>	
Extradiol-cleaving catechol dioxygenases	
$\alpha$ -ketoglutarate dependent hydroxylases	$\text{R-H} + \text{R}'\text{COCO}_2\text{H} + \text{O}_2 \rightarrow \text{R-OH} + \text{R}'\text{CO}_2\text{H} + \text{CO}_2$
Rieske dioxygenases	
<b>Dinuclear non-heme center</b>	
soluble-Methane Monooxygenase (sMMO)	$\text{CH}_4 + \text{O}_2 + 2 \text{H}^+ + 2 e^- \rightarrow \text{CH}_3\text{OH} + \text{H}_2\text{O}$



### I.2.1.1. Cytochrome P450

Cytochrome P450 (Cyt P450) enzymes constitute a large family of heme proteins, which are present in all forms of life; plants, bacterial and mammals.<sup>24-26</sup> These enzymes take part in a large variety of vital processes, like drug metabolism, biosynthesis of steroids, and detoxification of xenobiotic substances. They are one of the most studied and best known oxidation metalloenzymes.

Cyt P450 carries out the oxidation of non-activated organic substrates, such as hydroxylation of aliphatic C-H bonds, and the epoxidation of C=C bonds with high regioselectivity and stereoselectivity. They can also catalyze N-, S- and O-dealkylation, N-oxidation, sulfoxidation and dehalogenation reactions, indicating that these families of enzymes are highly efficient and versatile. For these oxidations, P450 enzymes use molecular O<sub>2</sub> as oxidant and oxygen source and they act as monooxygenases. They insert one oxygen atom into a wide variety of biologic substrates, concomitantly with a two-electron reduction of the other oxygen atom to form a water molecule (Scheme I.2).<sup>15</sup>



**Scheme I.2.** Oxidation reactions catalyzed by Cyt P450.

In the last two decades, mechanistic information was obtained from several X-ray crystal structures, for instance the water-soluble Cyt P450-camphor adduct (Figure I.2).<sup>27</sup> The active site consists of an iron porphyrin (heme group) attached to the protein through coordination of a cysteine residue at one of the axial positions of the metal. The other axial position is occupied by a water molecule.

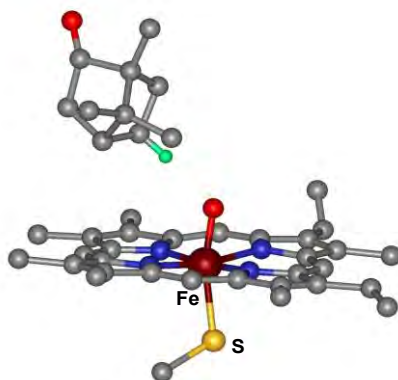
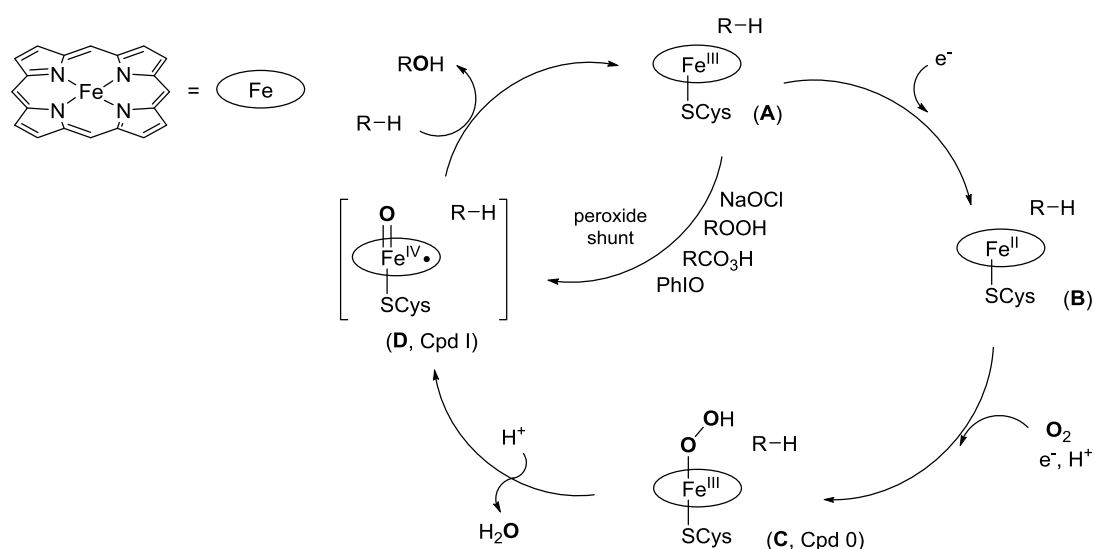


**Figure I.2.** The active site of Cyt P450-camphor from *Pseudomonas putida*. The C-H bond ready for cleavage is highlighted in green.

The oxygen activation mechanism of Cyt P450 family is considered the paradigm for  $O_2$ -activation at a mononuclear iron center. Nowadays, the principal features of the catalytic cycle of Cyt P450 are well-established.<sup>26, 27</sup> As shown in Scheme I.3, the initial step consists in the binding of the substrate at the active site, causing extrusion of the water ligand. The five coordinate iron site changes its spin state and increases the  $Fe^{III}/Fe^{II}$  oxidation potential, triggering injection of one electron from an electronic transport chain, causing the one-electron reduction of the iron center (**B**). The binding of molecular oxygen to the  $Fe^{II}$  center generates a ferric-superoxide complex, which rapidly traps one electron and one proton to afford the iron(III)-hydroperoxo complex (**C**, Cpd 0). This species undergoes proton assisted O-O heterolytic bond cleavage to generate a high-valent oxo- $Fe^{IV}$ -porphyrin radical cation (Cpd I) and a water molecule (**D**). In C-H oxidation reactions, the oxygen atom is transferred to the nearby substrate by a two-step process known as the "oxygen rebound".<sup>28</sup> For a given alkene, the oxo ligand is transferred in a nearly concerted manner to the olefin, thus stereospecifically forming epoxides. Finally, dissociation of the product completes the catalytic cycle. Direct cycling between the resting state (**A**) and the high-valent oxidant species (**D**) can be performed by using oxidants such as hydro and alkylperoxides, NaOCl, PhIO or peracids. This shortcut is known as the "peroxide shunt" (Scheme I.3) and it receives use in catalysis.<sup>29</sup> The intermediate species is postulated to be an iron(IV)-oxo porphyrin radical cation.<sup>30</sup>

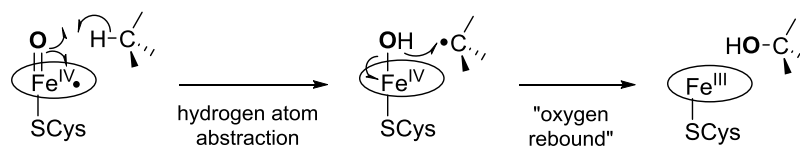
Model studies using synthetic porphyrin analogs provide evidences for the identification of the active species in the catalytic cycle and new strategies for elucidating the oxidation mechanism of biological processes.<sup>31-34</sup>



**Scheme I.3.** Proposed catalytic mechanism for alkane hydroxylation performed by Cyt P450.

The mechanism by which C-H bonds are oxidized by Cpd I of P450 is known as the "oxygen rebound" mechanism. This consists in a hydrogen-atom abstraction from the substrate by the iron-oxo species to give an iron(IV)-hydroxo and a alkyl radical, followed by the "rebound" to form a new C-O bond and recovering the iron(III) resting state (Scheme I.4).<sup>35,</sup>

36



**Scheme I.4.** Postulated "oxygen rebound" mechanism for alkane hydroxylation in Cyt P450.

It is important to consider that although a carbon centered radical is formed in these reactions, radical traps do not affect the reaction so it is thought as a very short-lived intermediate that does not leave the radical cage. Since this carbon centered radical does not freely diffuse into solution, its stereochemistry is retained.

### I.2.1.2. Rieske Oxygenases

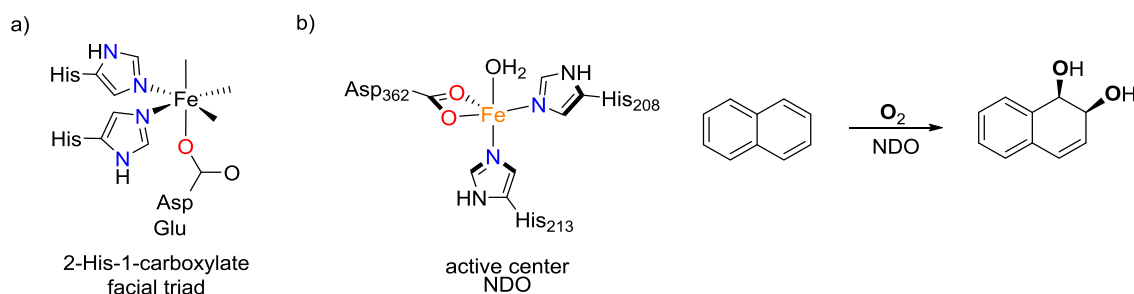
Great advances have been made in the last 20 years in the study of mononuclear non-heme iron enzymes due to the large number of crystal structures now available, and also the development of sophisticated spectroscopic techniques to study paramagnetic metal ions.<sup>8</sup>

Rieske Oxygenases are specially efficient and versatile iron enzymes, their biotechnological interest resides on their capacity to catalyze stereo- and enantioselective *cis*-dihydroxylation of arenes and olefins.<sup>37-39</sup> This novel transformation is not observed in any other enzymatic system, and also remains a challenge for synthetic organic chemistry.<sup>40, 41</sup> In natural processes, these enzymes are important because the *cis*-dihydroxylation of arenes constitutes the first step in the biodegradation of persistent pollutants such as aromatic molecules and leads the formation of catechols which are further degraded by intradiol- and extradiol-cleaving catechol dioxygenases.<sup>42</sup>

Moreover, these enzymes can also catalyze benzylic hydroxylation, desaturation, sulfoxidation, and O- and N-dealkylation.<sup>37</sup> The capacity to catalyze this wide range of oxidative transformations indicates that Rieske Oxygenases may be even more versatile than the P450 superfamily.

A common structural motif is found in the superfamily of Rieske Oxygenases, which consists of an active site with an iron center coordinated to three protein residues, two Histidines (His) and one Aspartate (Asp) or Glutamate (Glu). This structural motif is known as

the 2-His-1-carboxylate facial triad (Scheme I.5, a).<sup>43</sup> The protein residues occupy one face of an octahedron, leaving three free sites on the opposite face for the coordination of substrate, O<sub>2</sub> or water molecules.



**Scheme I.5.** a) Schematic representation of the 2-His-1-carboxylate facial triad in the active center of the superfamily Rieske Oxygenases. b) Active center of 1,2-naphthalene dioxygenase (NDO) enzyme and its oxidative reaction towards naphthalene.

One of the most studied Rieske Oxygenase enzyme is naphthalene 1,2-dioxygenase (NDO) from the bacteria *Pseudomonas putida* (Scheme I.5, b), which was crystallographically characterized in 1998.<sup>44</sup> The crystallographically determined structure shows that the enzyme contains two metal centers; an oxygenase component that consists in a mononuclear iron center where O<sub>2</sub> activation and substrate *cis*-dihydroxylation takes place, and a reductase component that consists in a Rieske-type Fe<sub>2</sub>S<sub>2</sub> cluster, and delivers electrons from NAD(P)H to the oxygenase center in a controlled way (Figure I.3). The structure of the active center is representative of other *cis*-dihydroxylation enzymes, such as benzoate 1,2-dioxygenase,<sup>45</sup> toluene 2,3-dioxygenase,<sup>46</sup> benzene dioxygenase<sup>47</sup> and phthalate dioxygenase.<sup>48</sup>

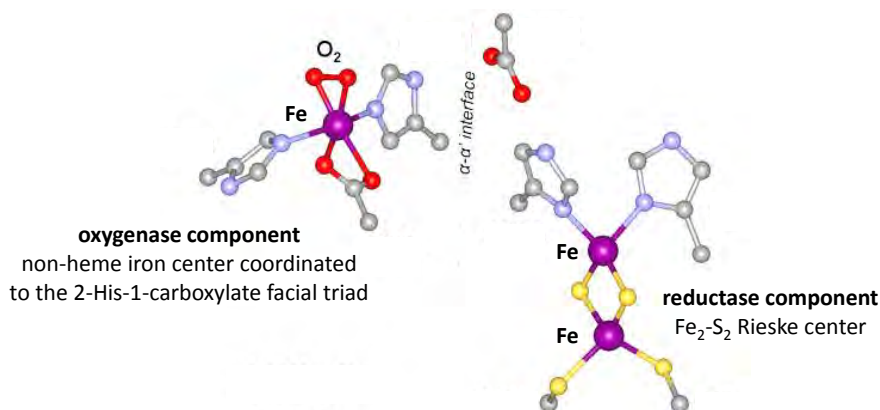
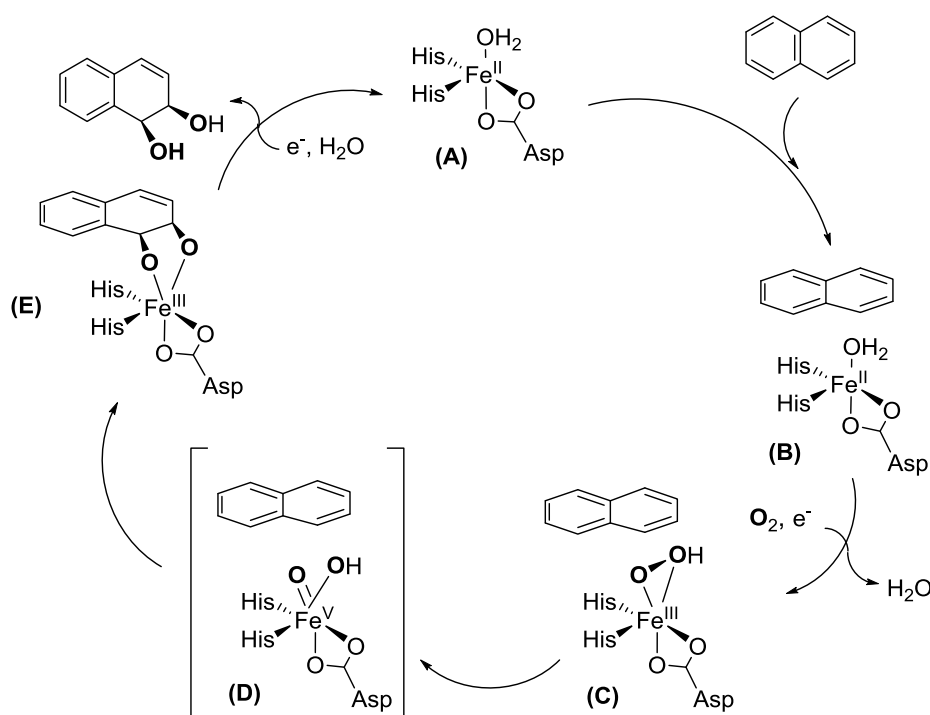


**Figure I.3.** Active center of Naphthalene Dioxygenase. The only crystallographically characterized O<sub>2</sub> complex of a mononuclear non-heme iron enzyme containing a 2-His-1-carboxylate facial triad.<sup>43</sup>

Mechanistic studies on enzymes belonging to the Rieske Oxygenase family have been made in order to propose a catalytic cycle for these enzymes (Scheme I.6). The cycle starts when the iron center, in its reduced state (**A**) binds the arene substrate (**B**). The enzyme readily reacts with  $O_2$  followed by electron transfer from the reductase component to generate the iron(III)-peroxo complex (**C**). This intermediate (**C**) has been trapped, and characterized by time-resolved cryo-crystallographic studies on frozen crystals on NDO exposed to  $O_2$ . These studies indicate that the peroxo ligand binds in a side-on configuration (Figure I.3).<sup>43, 49</sup> At this stage, two possible paths can take place: a) the direct interaction of the peroxide species with the substrate to generate the species (**E**) or b) O-O bond cleavage to generate the  $Fe^V=O$  complex (**D**), prior to substrate attack. Some labeling experiments have been undertaken in order to know which is the oxidant species; since peroxide type of species do not exchange their O-atoms with water, the observation that oxygen atoms from  $H_2^{18}O$  can be incorporated into the *syn*-diol product (3-10%)<sup>45</sup> constitutes a strong argument that the reaction species is an iron-oxo intermediate.



**Scheme I.6.** Catalytic cycle proposed for Rieske Oxygenases, showing the *cis*-dihydroxylation of naphthalene.

NDO enzymes can perform the catalytic oxidation when  $H_2O_2$  is used as oxidant in the same way as the “peroxide shunt” found in Cyt P450.<sup>50</sup> In general, the evidence suggests that a common mechanism is operating in Cyt P450 and Rieske Oxygenase enzymes and indicate that high-valent iron-oxo species are the responsible of the oxidation reaction.

Finally, experiments with radical clock substrates have shown that oxidation of norcarane with NDO enzyme occurs through the intermediacy of a short-lived carbon-centered radical,<sup>51</sup> strongly suggesting that a rebound like mechanism as P450 is operative.

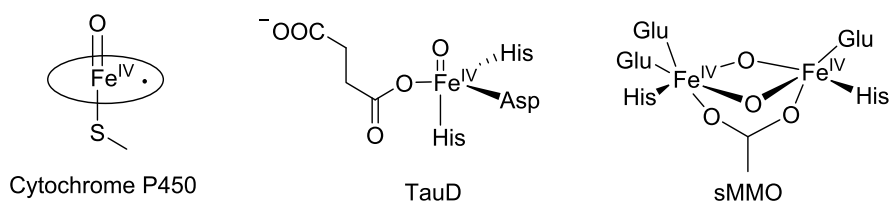
## 1.2.2. High-valent iron-oxo species detected in biological systems

There are a large number of iron proteins that can activate O<sub>2</sub> and catalyze the oxidation of different substrates. For a number of these enzymes the mechanism of O<sub>2</sub> activation is believed to entail the formation of high-valent iron-oxo intermediates. In the past ten years characterization of such intermediates has been accomplished in some specific natural systems.

In the oxidative processes catalyzed by P450, it has been proposed for decades the participation of an iron(IV)-oxo porphyrin  $\pi$ -radical as the active species capable of transferring the oxygen atom to the substrate. However, the isolation and characterization of the P450 iron(IV)-oxo species has not been reported until very recently (Scheme I.7).<sup>27, 52</sup>

In the case of non-heme mononuclear iron enzymes, high-valent iron-oxo species have been identified in the last decade. The first direct characterization of such intermediates has been provided by several  $\alpha$ KG-dependent oxygenases that catalyze either hydroxylation or halogenation of substrates. Some examples of these enzymes are taurine/ $\alpha$ -ketoglutarate dioxygenase (TauD),<sup>19, 53</sup> prolyl 4-hydroxylase (P4H)<sup>20</sup> and halogenase CytC3.<sup>22</sup> These high-valent species have also been detected in tyrosine hydroxylase (TyrH)<sup>21</sup> enzymes, that belongs to the family of aromatic amino acid hydroxylases. In all cases, an iron(IV)-oxo center in the high-spin state (S=2) has been identified (Scheme I.7).

Moreover, high-valent oxidation states are also detected and characterized for dinuclear non-heme iron proteins. For example a Fe<sup>III</sup>-O-Fe<sup>IV</sup> unit is known to operate in ribonucleotide reductase<sup>54, 55</sup> and a Fe<sup>IV</sup>-O-Fe<sup>IV</sup> core<sup>56</sup> has been identified as the oxidizing species in the case of the soluble form of methane monooxygenase (sMMO, Scheme I.7).



**Scheme I.7.** Structures of high-valent intermediates detected in natural enzymes.

## I.3. Catalytic applications by bioinspired non-heme iron complexes

The bioinspired approach consists in reproducing specific structural features of the reactive center of natural enzymes with synthetic compounds, with the aim of creating new and simpler systems that can perform the same catalytic transformation as the natural enzyme. This section focused on the description of synthetic models of mononuclear non-heme iron enzymes. Several non-heme iron complexes are able to catalyze the oxidation of alkanes and alkene *cis*-dihydroxylation or epoxidation giving high chemo- and stereoselectivities. The use of a first row transition metal and aqueous H<sub>2</sub>O<sub>2</sub> as terminal oxidant makes this process environmentally friendly.<sup>57, 58</sup> Moreover, N-coordinating ligands have revealed as very promising scaffolds for generating functional models of Rieske Oxygenases. On the other hand, the design of ligands combining N- and COO- coordinating groups has been also successfully described as biomimetic structural and functional models of natural enzymes.

### I.3.1. Alkane oxidation

#### I.3.1.1. Hydroxylation

The chemo- and stereospecific functionalization of aliphatic C-H bonds is an important and challenging goal for organic synthesis. The most remarkable results obtained up to date in Fe-catalyzed C-H oxidation are based in selected iron complexes containing tetradentate N-based ligands, which can catalyze selective H<sub>2</sub>O<sub>2</sub> oxidation of alkanes, and have raised broad interest. However, different approaches have been made before discovering these iron complexes, and are worthy described below.

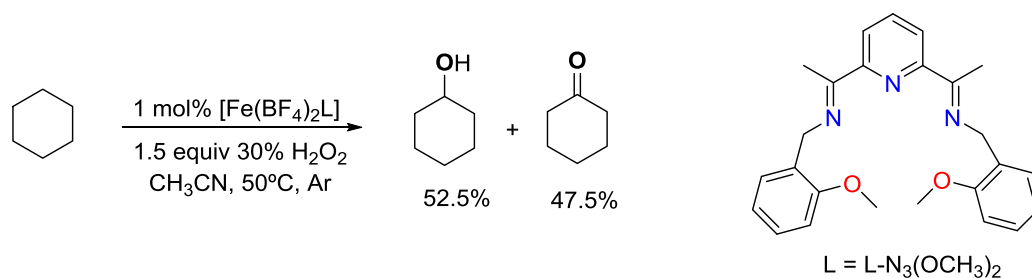
One of the pioneering examples in the oxidation of organic compounds combines first row transition metals, especially Fe<sup>II</sup> but also Cu<sup>I</sup>, Mn<sup>II</sup> and Co<sup>II</sup>, with peroxides under highly acidic conditions.<sup>59</sup> These oxidations are known as Fenton reactions, produce non selective reactions, and current studies indicate that this chemistry is based on free-diffusing oxygen radicals.<sup>59-61</sup> These reactions are characteristic for giving low product yields and also poor selectivities, which discards their use as synthetic tools.<sup>62</sup>

Gif chemistry is a more elaborated system that involves the combination of metallic iron, acetic acid, a reducing agent, oxygen as oxidant and pyridine as solvent, to generate chemical species that could oxidize organic substrates.<sup>6, 63</sup> The use of iron salts and hydrogen

peroxide in the presence of acetic acid is also effective for the same reactions.<sup>64,65</sup> Although the mechanistic picture behind these reactions remains complex and not completely understood, some recent mechanistic studies show that this kind of reactions generates hydroxyl radicals that are responsible for oxidative reactions.<sup>64</sup>

Polynuclear iron complexes with an oxo or carboxylate bridge have been traditionally explored as structural models of hydroxylases such as methane or alkane monooxygenase, and are described as good candidates for oxidation of strong C-H bonds.<sup>66-68</sup> The most efficient dinuclear Fe<sup>III</sup> complex is [Fe<sup>III</sup><sub>2</sub>(μ-O)(NO<sub>3</sub>)<sub>2</sub>(BBP)<sub>2</sub>(CH<sub>3</sub>OH)<sub>2</sub>](NO<sub>3</sub>)<sub>2</sub> which can oxidize cyclohexane with *tert*-butyl hydroperoxide (TBHP), giving an equimolar mixture of cyclohexanol and cyclohexanone (BBP = 2,6-bis(N-methylbenzimidazol-2-yl)pyridine). That is indicative of long-lived cyclohexyl radicals operating in the catalytic reaction.<sup>69</sup> Furthermore, polynuclear Fe<sup>III</sup> systems have been described, the tetranuclear [Fe<sup>III</sup><sub>4</sub>(N<sub>3</sub>O<sub>2</sub>-L)<sub>4</sub>(μ-O)]<sup>+4</sup> based on a triazacyclononane ring with a carboxylate arm (N<sub>3</sub>O<sub>2</sub>-L = 1-carboxymethyl-4,7-dimethyl-1,4,7-triazacyclononane)<sup>70</sup> and a hexanuclear iron [Fe<sup>III</sup><sub>6</sub>(μ<sub>3</sub>-O)(μ<sub>2</sub>-OH)(*p*-NO<sub>2</sub>C<sub>6</sub>H<sub>4</sub>CO<sub>2</sub>)<sub>11</sub>(DMF)<sub>4</sub>] with unusual core [Fe<sup>III</sup><sub>6</sub>(μ<sub>3</sub>-O)(μ<sub>2</sub>-OH)]<sup>+11</sup>.<sup>71</sup> Both of them can perform the efficient oxidation of cyclohexane to a mixture of alcohol and ketone.

Some pentadentate iron(II) complexes have been recently described and tested as alkane oxidation catalyst: [Fe<sup>II</sup>(CH<sub>3</sub>CN)<sub>2</sub>(N4Py)]<sup>2+</sup> (N4Py = N,N-bis(2-pyridylmethyl)-N-(bis-2-pyridylmethyl)amine),<sup>72</sup> [Fe<sup>II</sup>(Cl)(tpoen)]<sup>+</sup> (tpoen = N-(2-pyridylmethoxyethyl)-N,N-bis(2-pyridylmethyl)amine)<sup>73</sup> and [Fe<sup>II</sup>(CH<sub>3</sub>CN)<sub>2</sub>(BpdL<sub>2</sub>)]<sup>2+</sup> (BpdL<sub>2</sub> = bispidine derivatives)<sup>74</sup>. Using an excess of substrate and H<sub>2</sub>O<sub>2</sub> as oxidant, moderate to good yields were obtained in the oxidation of cyclohexane. Low ratios Alcohol/Ketone (A/K) were observed indicating that these transformations presumably work via Fenton-type of reactivity. A particular efficient example described by Reedijk was the pentadentate iron(II) complex with the ligand L-N<sub>3</sub>(OCH<sub>3</sub>)<sub>2</sub> (6-bis[1-(2-methylanisolylimino)ethyl]pyridine), which can quantitatively convert cyclohexane to a mixture of cyclohexanol and cyclohexanone (Scheme I.8), using 1% of catalyst and H<sub>2</sub>O<sub>2</sub> as oxidant.<sup>75</sup> The low ratio A/K is indicative of free cyclohexyl radicals diffusing in solution.

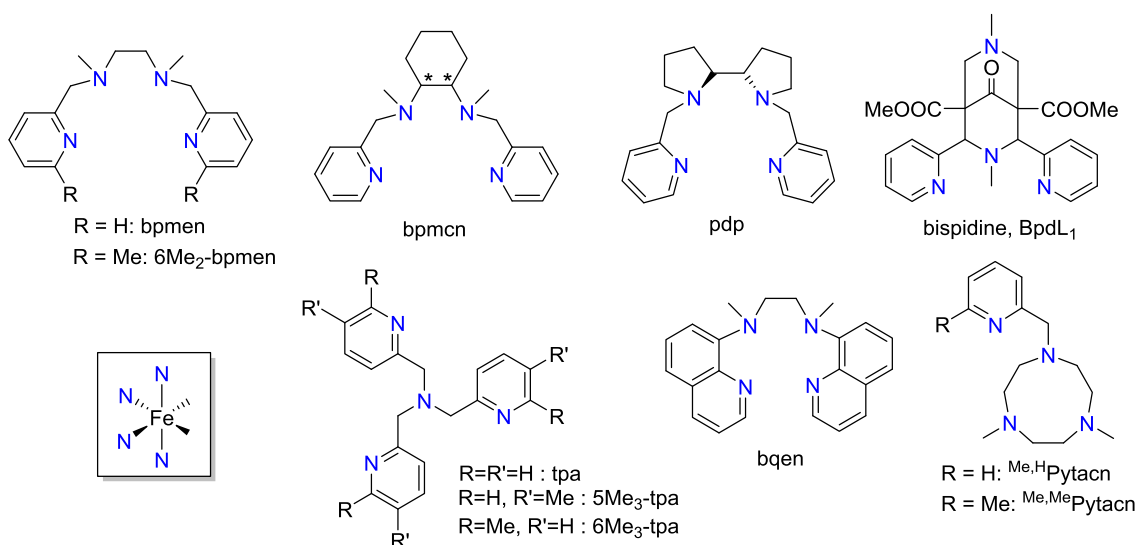


**Scheme I.8.** Cyclohexane oxidation catalyzed by Reedijk system.<sup>75</sup>



Mononuclear iron(II) complexes containing tetradentate N-based ligands have been largely investigated during the last decade due to their efficiency and versatility in performing oxidation reactions. A particularly relevant aspect of these systems is that allowed to perform the stereospecific hydroxylation of alkanes. However, the catalytic activity of these complexes is dramatically dependent on the ligand structure and small changes in its architecture could result in radical changes in the catalytic activity. Therefore, despite the wide variety of ligand structures described, only a few examples give high efficiencies and selectivities when H<sub>2</sub>O<sub>2</sub> is used as oxidant, showing a catalytic activity centered in the metal and avoiding radical formation.<sup>76</sup>

The first iron system that catalyze the stereospecific hydroxylation of C-H bonds was [Fe<sup>II</sup>(tpa)(CH<sub>3</sub>CN)<sub>2</sub>]<sup>2+</sup> described by Que and co-workers (tpa = tris(2-pyridylmethyl)amine) (Scheme I.9).<sup>77</sup> The catalytic reaction was performed using H<sub>2</sub>O<sub>2</sub> as the limiting reagent (10 equiv.) and cyclohexane as a substrate (1000 equiv.), moderate efficient conversion of H<sub>2</sub>O<sub>2</sub> into oxidation products was obtained. In addition, a high A/K ratio was found, indicative that the reaction involved a metal centered C-H hydroxylation process. Also, the stereospecific hydroxylation of *cis*-1,2-dimethylcyclohexane prove that the reaction occurs without stereoscrumbling, thus excluding the implication of long lived carbon centered radicals or cations.<sup>78, 79</sup> Isotopic labeling experiments also showed that atmospheric O<sub>2</sub> is not incorporated into oxidation products. Since then, different iron complexes that perform the stereospecific hydroxylation of alkanes have been described and are represented in Scheme I.9 and catalytic results are reported in Table I.2.



**Scheme I.9.** Schematic representation of the most important tetradentate ligands used to prepare mononuclear iron(II) complexes that could perform the oxidation of alkanes.

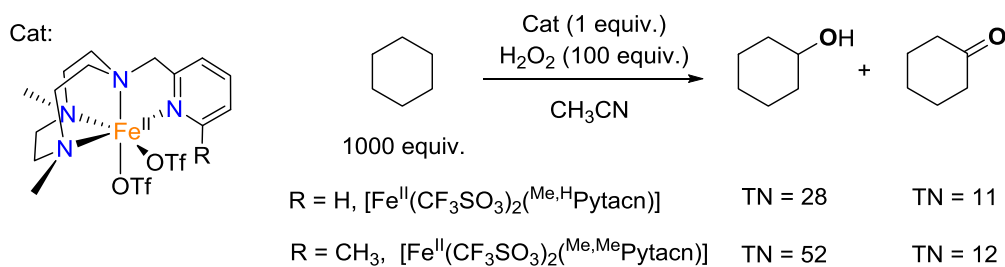
Another particularly relevant family of iron(II) complexes were those containing a linear bis-pyridine-bis-aliphatic amine ligand, such as bpmen (*N,N'*-dimethyl-*N,N'*-bis(2-pyridylmethyl)ethane-1,2-diamine), bpmcn (*N,N'*-dimethyl-*N,N'*-bis(2-pyridylmethyl)cyclohexane-*trans*-1,2-diamine), pdp (*N,N'*-bis(2-pyridylmethyl)2,2'-bipyridine) and bqen (bis(quinolyl)-diamine).  $[\text{Fe}^{\text{II}}(\text{bpmen})(\text{CH}_3\text{CN})_2]^{2+}$  and  $[\text{Fe}^{\text{II}}(\text{tpa})(\text{CH}_3\text{CN})_2]^{2+}$  families include a series of derivatives where aliphatic amine units and pyridine substitutions are altered with the aim of tuning the catalytic applications (Scheme I.9).<sup>78, 80, 81</sup>

**Table I.2.** Oxidation of alkanes by tetradentate iron(II) complexes, ligands represented in Scheme I.9.

catalyst	Cyclohexane		<i>cis</i> -1,2-DMCH	adamantane	Ref
	A + K (A/K) <sup>[a]</sup>	KIE	RC (%) <sup>[b]</sup>	3 <sup>o</sup> /2 <sup>o</sup> <sup>[c]</sup>	
$[\text{Fe}^{\text{II}}(\text{tpa})(\text{CH}_3\text{CN})_2]^{2+}$	3.2 (6)	3.5	100	17	78
$[\text{Fe}^{\text{II}}(5\text{Me}_3\text{-tpa})(\text{CH}_3\text{CN})_2]^{2+}$	4.0 (5)	3.8	100	21	78
$[\text{Fe}^{\text{II}}(6\text{Me}_3\text{-tpa})(\text{CH}_3\text{CN})_2]^{2+}$	2.9 (2)	3.3	54	15	78
$[\text{Fe}^{\text{II}}(\text{bpmen})(\text{CH}_3\text{CN})_2]^{2+}$	6.3 (5)	3.2	96	15	78
$[\text{Fe}^{\text{II}}(\text{bqen})(\text{CH}_3\text{CN})_2]^{2+}$	5.1 (5)	-	-	-	82
$[\text{Fe}^{\text{II}}(\alpha\text{-bpmcn})(\text{CH}_3\text{CN})_2]^{2+}$	5.9 (9)	3.2	>99	15	83
$[\text{Fe}^{\text{II}}(\beta\text{-bpmcn})(\text{CH}_3\text{CN})_2]^{2+}$	1.9 (0.9)	4.0	68	17	83
$[\text{Fe}^{\text{II}}(\text{CF}_3\text{SO}_3)_2(\text{H}^{\text{H}}\text{Pytacn})]$	6.5 (12)	4.3	93	30	84
$[\text{Fe}^{\text{II}}(\text{CF}_3\text{SO}_3)_2(\text{Me}^{\text{Me}}\text{Pytacn})]$	7.6 (10)	3.4	94	20	84

Catalyst:H<sub>2</sub>O<sub>2</sub>:alkane = 1:10:1000. [a] Turnover number (TN, mols of product / mols of catalyst), A = cyclohexanol, K = cyclohexanone. A/K = (mols A / mols K). [b] Retention of configuration in the oxidation of *cis*-1,2-dimethylcyclohexane. [c] 3<sup>o</sup>/2<sup>o</sup> = 3x(1-adamantanol)/(2-adamantanol+2-adamantanona).

More recently an innovative family of iron complexes containing tetradentate ligands based on the 1,4,7-triazacyclononane ring,  $[\text{Fe}^{\text{II}}(\text{CF}_3\text{SO}_3)_2(\text{Me}^{\text{R}}\text{Pytacn})]$  (Pytacn = 1-(2'-pyridylmethyl)-4,7-dimethyl-1,4,7-triazacyclononane) (Scheme I.9, Scheme I.10 and Table I.2) are described as powerful C-H oxidation catalysts. This system shows a remarkable efficiency in stereospecific alkane hydroxylation reactions using H<sub>2</sub>O<sub>2</sub> as oxidant agent, and also mechanistic studies prove that the oxidation occurs by a metal-based oxidant.<sup>84, 85</sup> Moreover, these systems allow increasing the concentration of H<sub>2</sub>O<sub>2</sub> to 100 equiv. maintaining the yields and selectivities. The most interesting numbers are found with  $[\text{Fe}^{\text{II}}(\text{CF}_3\text{SO}_3)_2(\text{Me}^{\text{Me}}\text{Pytacn})]$  which give a high ratio A/K (4.3) and good yields (64%). These catalytic results make this system promising for future synthetic application.

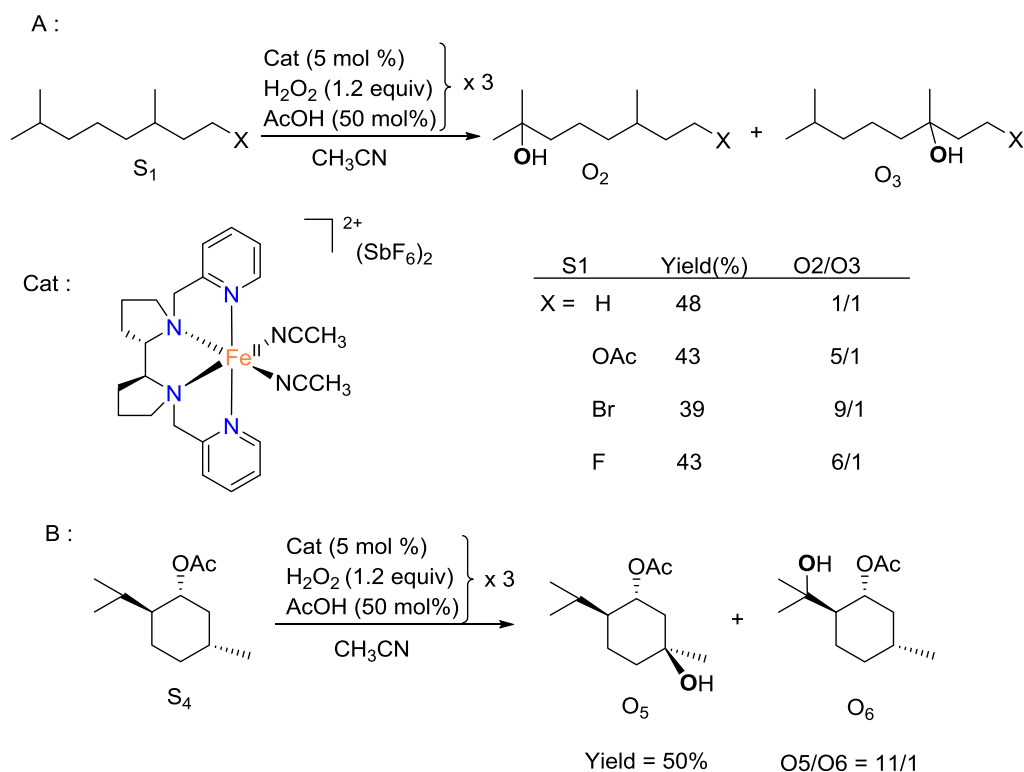


**Scheme I.10.** Alkane hydroxylation catalyzed by  $[\text{Fe}^{\text{II}}(\text{CF}_3\text{SO}_3)_2(\text{Me,R-PyTacn})]$  complexes.

Catalyst:H<sub>2</sub>O<sub>2</sub>:cyclohexane = 1:100:1000.

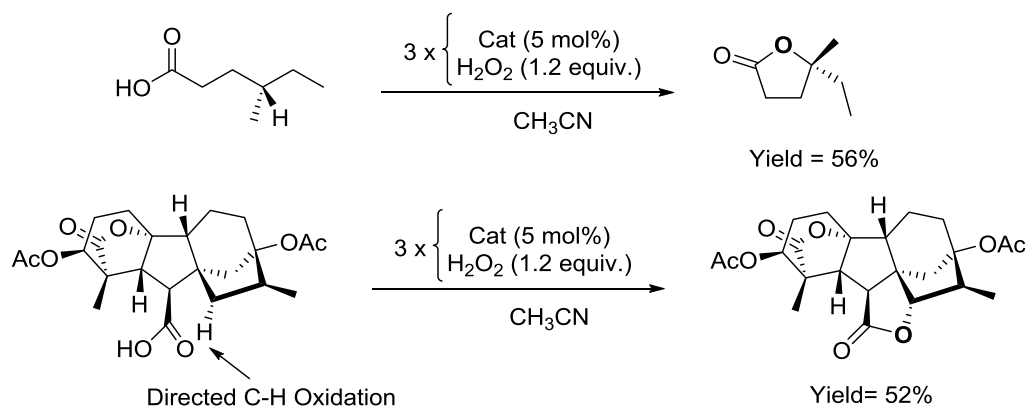
Despite their structural differences, all these complexes share tetradentate N-donor ligands and two *cis*-labile sites available for coordination with exogenous ligands, such as oxidant or substrate, and therefore these factors are thought to be essential to perform metal based oxidation. Studies from Menage and co-workers conclude that labile acetonitrile or triflate ligands are required for metal based pathways. Instead more strongly binding ligands such as chloride, lead to Fenton type reactions.<sup>86</sup>

The main problem of these systems is the use of a large excess of substrate relative to the oxidant, which was necessary to avoid overoxidation reactions. This limitation prevents the use of these catalysts as a synthetic tool for selective functionalization of C-H bonds.<sup>87</sup> In contrast, in a seminal piece of work, Che and White reported the Fe-catalyzed hydroxylation of unactivated tertiary C-H bonds achieving both synthetically useful yields and predictable selectivities.<sup>88</sup> The catalyst is a mononuclear iron complex,  $[\text{Fe}^{\text{II}}(\text{pdp})(\text{CH}_3\text{CN})_2](\text{SbF}_6)_2$ , and uses hydrogen peroxide in combination with acetic acid, as additive, to oxidize a range of substrates with diverse functionalities, including esters, amides, halides and epoxides. The authors show that the system exhibits selective oxidation in complex molecules with multiple tertiary C-H sites, on the basis of the electronic, and steric properties of C-H bonds (Scheme I.11). The authors demonstrate that the catalyst oxidizes preferentially the most electron-rich and the least sterically hindered tertiary C-H bond.



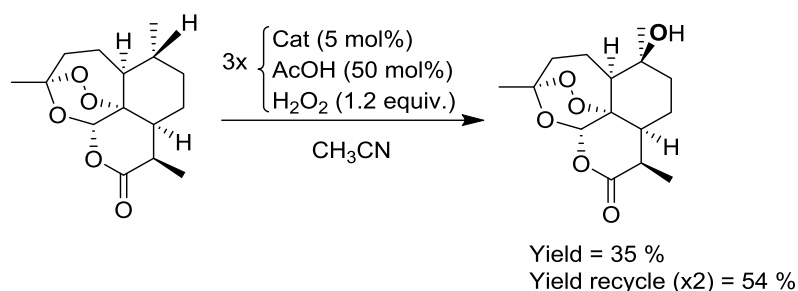
**Scheme I.11.** Alkane hydroxylation using  $[\text{Fe}^{\text{II}}(\text{pdp})(\text{CH}_3\text{CN})_2](\text{SbF}_6)_2$ . A: Substrate electronic effects on site selectivity in hydroxylation of multiple  $3^\circ\text{C-H}$  bonds. B: Selective hydroxylation based on steric effects.

The introduction of a carboxylate group in the substrate allows site-directed C-H oxidation, presumably via binding to the iron catalyst. The mechanistic studies show that rapid lactonization proceeds after the C-H hydroxylation.<sup>89</sup> This methodology could be applied in complex organic molecules such as tetrahydrogibberellic acid, where in this case the lactone product was obtained in 52% yield (Scheme I.12).



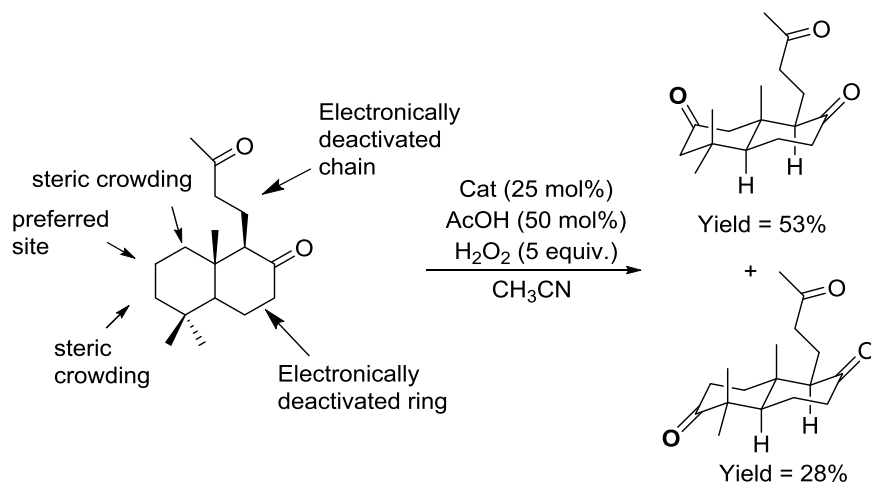
**Scheme I.12.** Directed hydroxylation of C-H bonds by acid group and subsequently lactonization catalyzed by  $[\text{Fe}^{\text{II}}(\text{pdp})(\text{CH}_3\text{CN})_2](\text{SbF}_6)_2$ .

Most important, complex natural products with multiple C-H bonds was selectively hydroxylated employing the same methodology (Scheme I.13).<sup>88</sup> Oxidation takes place at the most electron-rich and the least sterically hindered tertiary C-H bond.



**Scheme I.13.** Selective hydroxylation of (+)-artemisin by  $[\text{Fe}^{\text{II}}(\text{pdp})(\text{CH}_3\text{CN})_2](\text{SbF}_6)_2$ . By recycling the starting material twice the diastereometrically pure product was afforded in 54% yield.

In subsequent work, selective functionalization of methylene sites was also explored with this catalyst (Scheme I.14).<sup>90</sup> Again, steric and electronic effects were rapidly recognized as dictating elements of C-H bond selectivity. In addition, stereoelectronic and inductive factors were also recognized to dictate site selectivity. Modest selectivities were observed in simple substrate molecules, where only one of the directive factors is involved. However, in complex organic molecules, where multiple factors are involved, remarkable site selectivities could be achieved. In the following example, selective oxidation of a secondary C-H bonds take place in presence of tertiary C-H bonds.



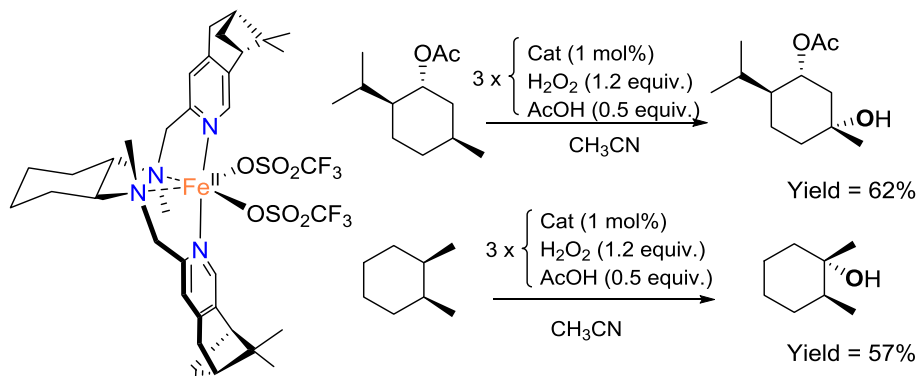
**Scheme I.14.** The combination of steric and electronic effects allows the selective oxidation of methylene group by the  $[\text{Fe}^{\text{II}}(\text{pdp})(\text{CH}_3\text{CN})_2](\text{SbF}_6)_2$ .

White and Chen developed a system that uses a 15% of catalyst loadings, an elaborated synthetic protocol via iterative additions of the reagents, and in some cases substrate recycling.<sup>91</sup> The system was highly efficient and the study established the factors that

determine C-H site selectivity by this oxidation catalyst. Considering the innate properties of C-H bonds, bond strength is usually a major factor that directs the reactivity in oxidation reactions, following the order  $3^\circ \text{C-H} > 2^\circ \text{C-H} > 1^\circ \text{C-H}$ . However, the order should be inverted on the basis steric effects, as  $3^\circ \text{C-H}$  bonds are sterically less accessible than secondary ones. Another factor is the presence of electronwithdrawing groups such as carbonyl moieties, which disfavors oxidation at proximal positions, because the oxidant has an electrophilic nature.

Furthermore, other factors have to be taken into account, in the case of oxidation of cyclohexane skeletons, equatorial C-H bonds are more efficiently oxidized than axial ones, because in the transition state breakage of the equatorial C-H bond liberates tension strain and minimize 1,3-diaxial interactions.<sup>92</sup>

With the aim of providing iron catalysts more resistant to bimolecular decomposition pathways, Gómez and co-workers designed an iron catalyst which contained pinene groups fused at positions 4 and 5 of the pyridine rings,  $[\text{Fe}^{\text{II}}(\text{CF}_3\text{SO}_3)_2((S,S,R)\text{-mcpp})]$  (mcpp = *N,N'*-dimethyl-*N,N'*-bis(((*R*)-4,5-pinenepyridin-2-yl)methyl)cyclohexane-1,2-diamine). The strategy consisted in tuning the structure of an effective catalyst, such as  $[\text{Fe}^{\text{II}}(\text{CF}_3\text{SO}_3)_2(\text{bpmen})]$  and  $[\text{Fe}^{\text{II}}(\text{pdp})(\text{CH}_3\text{CN})_2](\text{SbF}_6)_2$ , by introducing bulky groups to isolate the metal center generating a robust cavity that prevents self-decomposition pathways (Scheme I.15). This catalyst shows a high efficiency in C-H hydroxylation, giving yields comparable to  $[\text{Fe}^{\text{II}}(\text{pdp})(\text{CH}_3\text{CN})_2](\text{SbF}_6)_2$ , although using much lower catalyst loadings (3 mol%).<sup>93</sup>

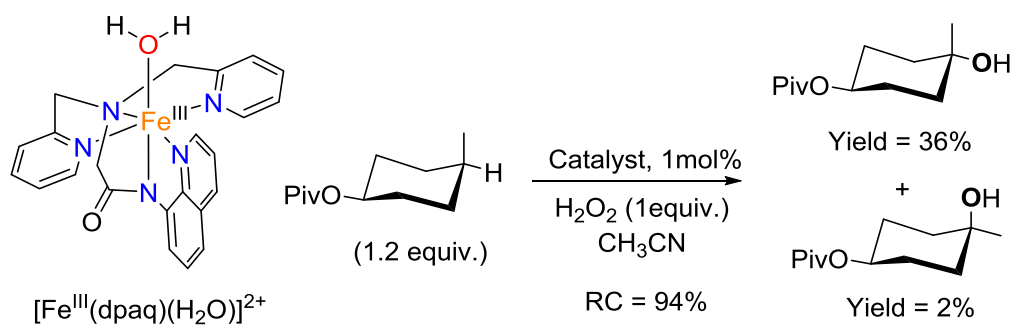


**Scheme I.15.**  $[\text{Fe}^{\text{II}}(\text{CF}_3\text{SO}_3)_2((S,S,R)\text{-mcpp})]$  complex described by Gómez and co-workers, and results in catalytic C-H oxidation reactions.

In a recent work, Kodera and co-workers reported a  $\text{N}_5$ -pentadentate ligand, dpaq = 2 - [bis(pyridin-2-ylmethyl)]amino-*N*-quinolin-8-yl-acetamidate, with the peculiarity that a nitrogen atom is part of an amidate moiety (see Scheme I.16). The complex  $[\text{Fe}^{\text{III}}(\text{dpaq})(\text{H}_2\text{O})]^{2+}$  can oxidize C-H bonds with selectivities and efficiencies similar of the ones described for the

best tetradentate iron(II) complexes. In the oxidation of cyclohexane, this catalyst gives high ratios of A/K (around 12) indicative that Fenton reactions are not involved. Moreover this fact is largely confirmed by obtaining a KIE of 3.9, indicative of an oxidant that responds sensitively to the strength of the C-H bond.<sup>94</sup>

The use of 1% of catalyst, 1 equiv. of H<sub>2</sub>O<sub>2</sub> and 1.2 equiv. of *cis*-4-methylcyclohexyl-1-pivalate in acetonitrile afforded the tertiary alcohol product with a 38% yield and 94% of stereoretention (Scheme I.16).



**Scheme I.16.** Selective oxidation of *cis*-4-methylcyclohexyl-1-pivalate by [Fe<sup>III</sup>(dpaq)(H<sub>2</sub>O)]<sup>2+</sup> complex.

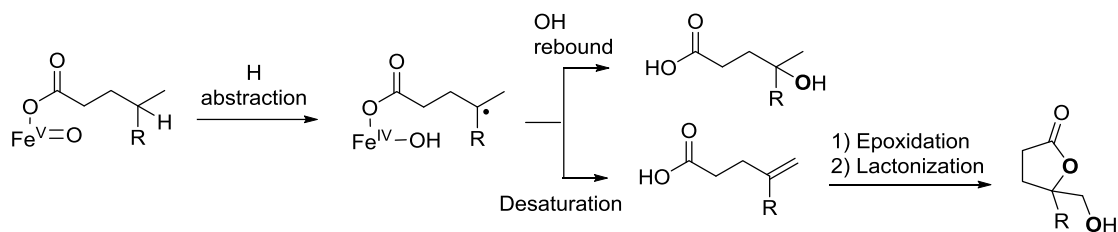
The authors postulate that the amide ligand is essential to afford these results with pentadentate ligands. It seems that this ligand facilitates the heterolysis of the O-O bond, which affords an iron(V)-oxo species responsible for the C-H bond oxidation reaction. In contrast, a neutral pentadentate ligand such as N4Py does not facilitate the O-O cleavage.<sup>95</sup>

Cold-spray-ionization mass spectroscopy (CSI-MS) was used to trap catalytic intermediates. The mixture of [Fe<sup>III</sup>(dpaq)(H<sub>2</sub>O)]<sup>2+</sup> and 50 equiv. of H<sub>2</sub>O<sub>2</sub> shows two important peaks that corresponds to [Fe<sup>III</sup>(dpaq)(OOH)]<sup>+</sup> and [Fe<sup>V</sup>(dpaq)(O)](ClO<sub>4</sub>)<sup>+</sup>, both of which are recognized as important intermediates in the oxidative catalytic cycle.

### I.3.1.2. Desaturation

Very recently, White and co-workers reported another catalytic reaction performed by non-heme iron complexes, which involve the desaturation of inert aliphatic C-H bonds. [Fe<sup>II</sup>(pdp)(CH<sub>3</sub>CN)<sub>2</sub>](SbF<sub>6</sub>)<sub>2</sub> was shown capable of performing both, C-H hydroxylation and desaturation reactions. The authors propose a mechanistic scenario where a high-valent iron-oxo species initiates C-H oxidation by performing a hydrogen abstraction reaction, generating a carbon-centered radical intermediate. This intermediate can undergo either, hydroxyl ligand rebound to give hydroxylation products, or a second one-electron oxidation to provide the final olefin product, as well as Fe<sup>III</sup> and H<sub>2</sub>O. Carboxylic acid functionalities on the substrate are required for desaturase activity, and on these bases it was proposed that the interaction

between the iron center and the carboxylate ligand is critical to avoid the  $-OH$  rebound. Moreover, the carboxylic acid moiety has the ability to direct the site of oxidation assisting the formation of  $\gamma$ -butyrolactones (Scheme I.17).<sup>96</sup>



**Scheme I.17.** Proposed mechanism for both, hydroxylation and dehydrogenation catalyzed by complex  $[Fe^{II}(pdp)(CH_3CN)_2](SbF_6)_2$ .

### I.3.2. Alkene oxidation

The oxidation of alkenes into epoxides or *syn*-diols is important because these reactions allow valuable intermediates to be prepared which are amenable to a number of further organic transformations.

#### I.3.2.1. Epoxidation

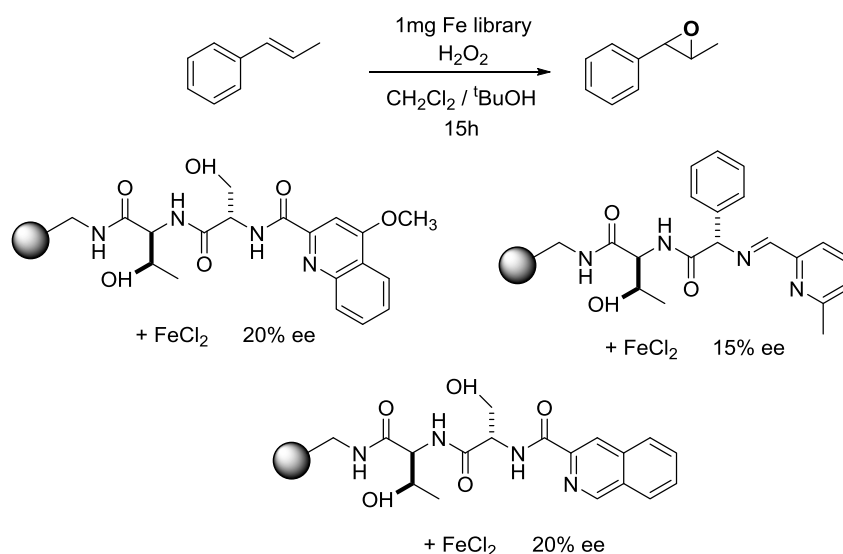
The combination of virtually any iron complex with peroxides generates oxidizing species that could eventually result in olefin epoxidation. Epoxides may result from metal centered oxidations but also from autooxidation radical chains. Not surprisingly, a number of reports have been published over the last decade where iron complexes catalyzed olefin epoxidation reactions. However, a limited number of examples have potential synthetic utility.

Valentine and co-workers reported one of the first non-heme iron catalyst,  $[Fe^{II}(CF_3SO_3)_2(cyclam)]$ , that could perform the selective epoxidation of alkenes using  $H_2O_2$  as oxidant (cyclam = 1,4,8,11-tetraazacyclotetradecane).<sup>97</sup> Cyclohexene was epoxidized in 40% yield by employing 2 mol% of catalyst.

In an original approach, Francis and Jacobsen described a combinatorial strategy for discovering novel catalysts for olefin epoxidation, using  $H_2O_2$  as oxidant. The authors screened 5,760 catalytic systems resulting from the combination of 192 polypeptide potential ligands, synthesized in a polystyrene resin, and 30 metal sources.<sup>98</sup> All the combinations were tested as potential epoxidation catalysts of *trans*- $\beta$ -methylstyrene, as a model substrate. The results showed that selected structures afford the epoxide product with high efficiencies in combination with  $FeCl_2$ , this combinatorial approach is represented in Scheme I.18. Moreover, these efficient catalytic epoxidation systems exhibited low yet significant enantioselectivity.

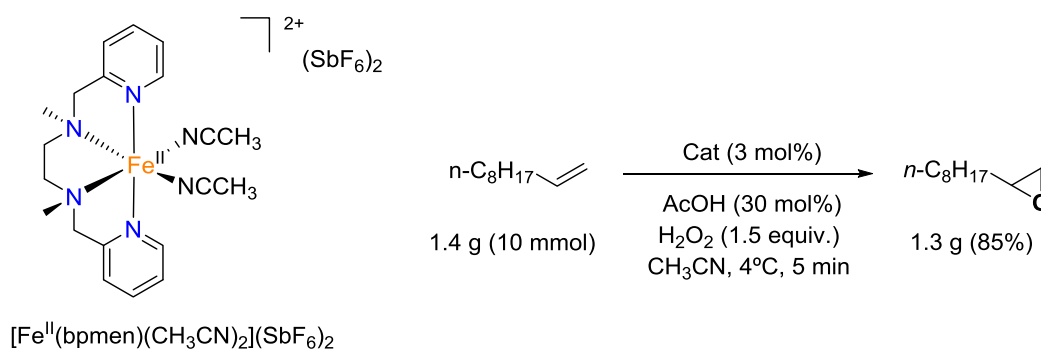


Under optimized reaction conditions, up to 78% epoxide yield and < 20 % ee was obtained by using 1.5 equivalents of H<sub>2</sub>O<sub>2</sub> and 5 mol% of the catalyst.



**Scheme I.18.** Catalysts structures identified from the combinatorial screening by studying the epoxidation activity in front of *trans*- $\beta$ -methylstyrene. Grey balls stand for the polystyrene support.

In a completely different approach, the Jacobsen group also described [Fe<sup>II</sup>(bpmen)(CH<sub>3</sub>CN)<sub>2</sub>](SbF<sub>6</sub>)<sub>2</sub>, as a very active catalyst for the epoxidation of aliphatic olefins. High epoxide yields (60-90%) were obtained by using 1.5 equiv. of H<sub>2</sub>O<sub>2</sub> and acetic acid as a key additive to ensure high product yields (Scheme I.19).<sup>99</sup>



**Scheme I.19.** Epoxidation of 1-decene catalyzed by [Fe<sup>II</sup>(bpmen)(CH<sub>3</sub>CN)<sub>2</sub>](SbF<sub>6</sub>)<sub>2</sub> complex.

Jacobsen report originally proposed that an in-situ generated oxo-carboxylate-bridged diiron(III) complex was the active catalyst. This structure is reminiscent to the active site of soluble oxidized methane monooxygenase (sMMO) enzyme. However, later work by Que and co-workers proved that this dimeric species was inactive and postulated a mononuclear iron(III) complex as the epoxidation agent, in this case the role of acetic acid in presence of

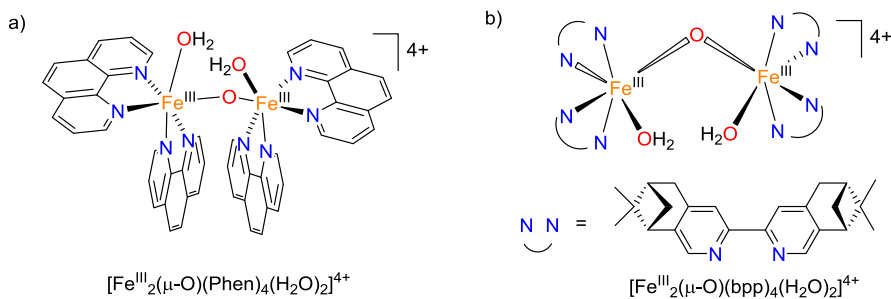
$\text{H}_2\text{O}_2$  was proposed to be the *in situ* generation of peracetic acid  $\text{AcOOH}$ , responsible for the olefin epoxidation.<sup>100</sup>

Dinuclear iron systems have also been described as potential catalysts for alkene epoxidation. Stack and co-workers report an  $\mu$ -oxoiron(III) dimer with phenanthroline ligands, that can epoxidize a wide range of alkenes, including terminal and electron-deficient ones, using peracetic acid as the oxidant. The *in situ* preparation of the catalyst from common reagents, the low catalyst loadings, the fast reaction times, and the high concentration of substrates converts this methodology into a synthetically efficient protocol for alkene epoxidation (Scheme I.20, a).<sup>101</sup>

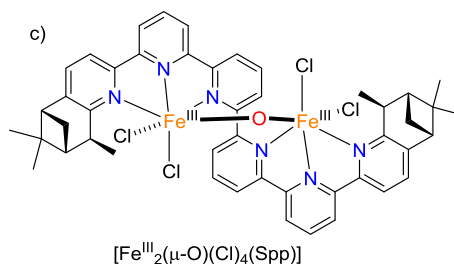
Regarding iron-based asymmetric epoxidation catalysis, Menage and co-workers have described a non-heme oxo-bridged diiron complex using chiral bipyridine ligands, that enantioselectivity catalyzes epoxidation of alkenes. The complex oxidizes olefins with high efficiencies, up to 850 TON, and moderate enantiomeric excesses (ee's) ranging from 9 to 63%. Best stereoselectivity results were obtained when electron-deficient substrates, such as chalcone, were used (Scheme I.20, b).<sup>102</sup>

In a recent work Kwong and co-workers reported a chiral sixpyridine iron complex as an efficient catalyst for the epoxidation of alkenes with  $\text{H}_2\text{O}_2$  in the presence of acetic acid, providing moderate enantiomeric excesses in the oxidation of aromatic olefins. Up to 43% ee was obtained in the oxidation of styrene (Scheme I.20, c).<sup>103</sup>

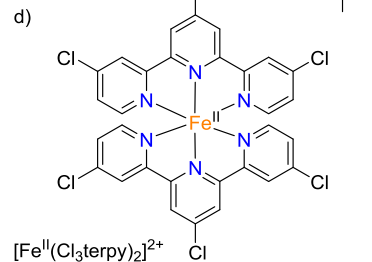
$\text{CH}_3\text{CO}_3\text{H}$  as oxidant:



$\text{H}_2\text{O}_2$  as oxidant:



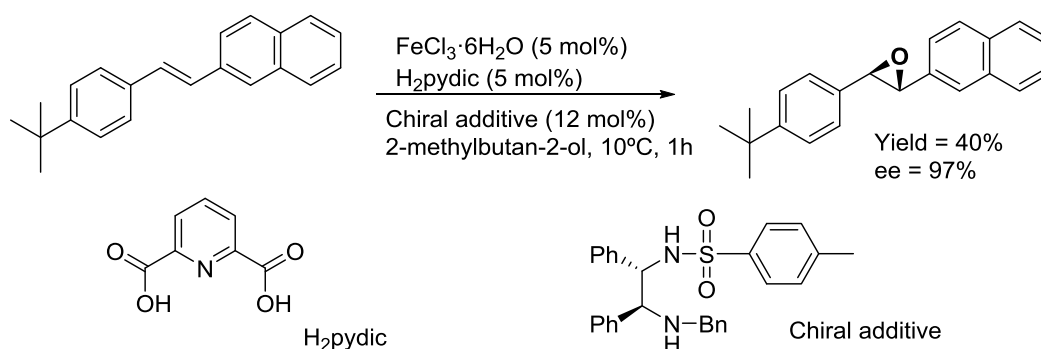
Oxone as oxidant:



**Scheme I.20.** Schematic representation of some relevant iron catalysts for olefin oxidation. a) Dimeric phenanthroline based complex reported by Stack. b) Chiral dimeric complex reported by Menage. c) Chiral iron sixpyridine reported by Kwong. d) Iron(II) bis-terpyridine complex described by Che.

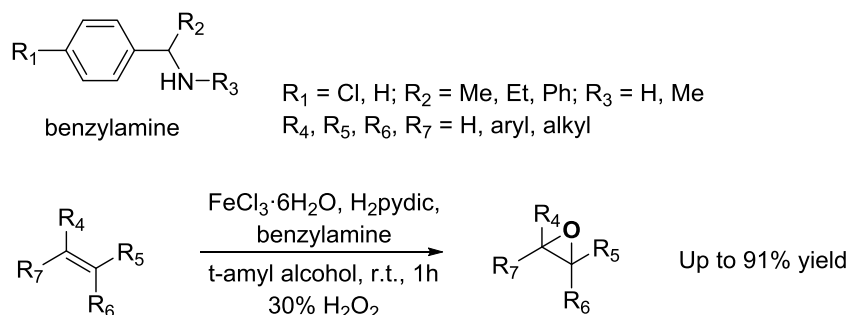
Che and co-workers reported an iron(II) *bis*-terpyridine complex that catalyzes the epoxidation of a diverse amount of alkenes, covering aliphatic, aromatic, terminal, electron-rich and electron-deficient olefins with good to excellent yields, up to 96% (Scheme I.20, d). Treatment of different alkenes and catalyst (5 mol %) with <sup>®</sup>Oxone at room temperature afforded the desired epoxide products. The ligand is robust and can be reused by the addition of a new batch of iron(II) salt. In addition, this catalysis conditions can be scaled up to gram scale.<sup>104</sup>

With the aim of developing a useful and convenient epoxidation system based on readily available components, Beller and co-workers developed a practical and efficient methodology to epoxidize olefins by using commercial available  $\text{FeCl}_3 \cdot 6\text{H}_2\text{O}$  in combination with pyridine-2,6-dicarboxylic acid and amines as ligands. Best stereoselective epoxidations mediated by iron was obtained by using chiral benzylamines as ligands. The catalytic system reached good yields and high enantiomeric excesses, up to 97% for *trans*-stilbene substrates (Scheme I.21).<sup>105, 106</sup>



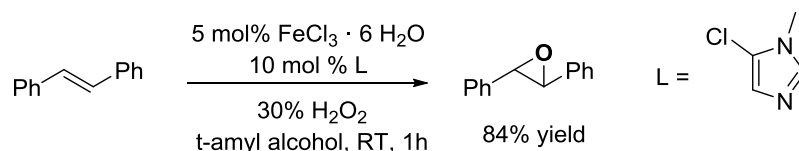
**Scheme I.21.** *In situ* generated asymmetric catalyst for stereoselective olefin epoxidation.

When pyrrolidine was used as a base, combination of  $\text{FeCl}_3 \cdot 6\text{H}_2\text{O}$  and pyridine-2,6-dicarboxylic acid at room temperature and under an aerobic atmosphere generated *in situ* the catalyst. The system shows excellent reactivity and selectivity towards aromatic olefins using  $\text{H}_2\text{O}_2$  as a terminal oxidant.<sup>107</sup> Change of the pyrrolidine amine by benzylamine derivatives allowed epoxidation of a high variety of aliphatic and aromatic olefins (Scheme I.22).<sup>108, 109</sup>



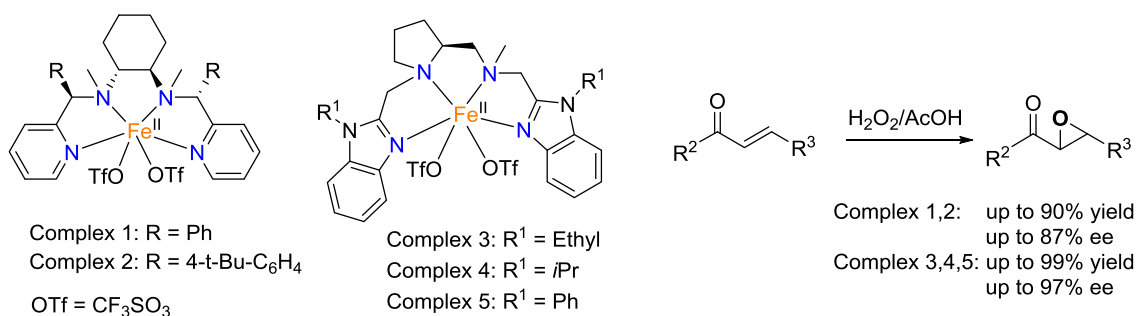
**Scheme I.22.** *In situ* generated catalyst which performs epoxidation of a high range of olefins.

In a subsequent evolution of the system, the addition of formamide ligands instead of amines allows epoxidation of styrenes and conjugated dienes in excellent yields.<sup>110</sup> The same group also reported a new selective epoxidation method, based on the combination of  $\text{FeCl}_3 \cdot 6\text{H}_2\text{O}$  and imidazole derivatives. This system epoxidizes aliphatic, aromatic olefins and conjugated dienes with moderate to excellent yields and high chemoselectivity.<sup>110-112</sup> The catalytic system was studied with a large variety of imidazoles, and the results show that a free 2-position of the imidazole ligand is essential for high catalytic activity. Moreover, the authors found that the 5-chloro-1-methylimidazole ligand provides the best results (Scheme I.23). Complex *trans*- $[\text{FeCl}_2(5\text{-Cl-1-Melm})_4]\text{Cl}$  was isolated, characterized and tested as a catalyst showing a catalytic activity similar to obtained from the *in situ* catalysis.<sup>112</sup>



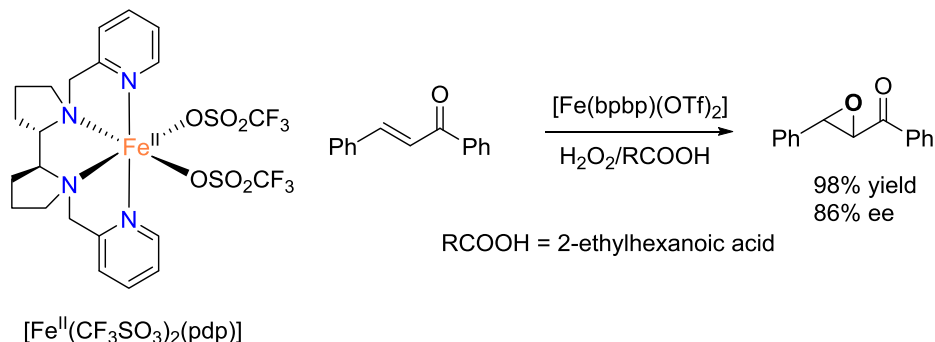
**Scheme I.23.** Best results obtained in the epoxidation of *trans*-stilbene using 5-chloro-1-methylimidazole ligand.

More recently, Wei Sun and co-workers reported a family of chiral iron(II) complexes based on  $\text{N}_4$ -ligands with a chiral cyclohexane diamine backbone that catalyze the enantioselective epoxidation of  $\alpha,\beta$ -enones. By using 2 mol% of catalyst, 5 equiv. of acetic acid (respect to the substrate) and the slow injection of 2 equiv. of  $\text{H}_2\text{O}_2$  afford the epoxidation of high number of  $\alpha,\beta$ -enones substrates with moderated to good yields (33-90%) and with enantiomeric excess up to 87% (Scheme I.24, complexes 1 and 2).<sup>113</sup> The same group reported a second catalyst based on a more rigid chiral diamine derived from *L*-proline and two benzimidazole donor groups. Using similar conditions as before and  $\alpha,\beta$ -enones as substrates, the authors could improve yields (up to 99%) and enantioselectivities (up to 97%) (Scheme I.24, complexes 3-5).<sup>114</sup>



**Scheme I.24.** Iron(II) complexes employed for the enantioselective epoxidation of  $\alpha,\beta$ -enones by Sun.

Finally, Talsi and co-workers reported the enantioselective epoxidation of a broad variety of alkenes by using 1 mol% of catalyst,  $[\text{Fe}^{\text{II}}(\text{CF}_3\text{SO}_3)_2(\text{pdp})]$ , and  $\text{H}_2\text{O}_2$  as oxidant. Using these simple conditions, without carboxylic acid addition, chalcone was epoxidized in 13% yield and 61% ee. The addition of carboxylic acid (1.1 equiv.) improves the efficiency and the enantioselectivity of this system giving yields up to 100%. The best results were obtained with 2-ethylhexanoic acid, giving the chalcone epoxide in 98% yield and 86% ee (Scheme I.25).<sup>115</sup>



**Scheme I.25.** Bipyrrrolidine base iron(II) complex catalyze the asymmetric epoxidation of various olefins in the presence of a carboxylic acid.

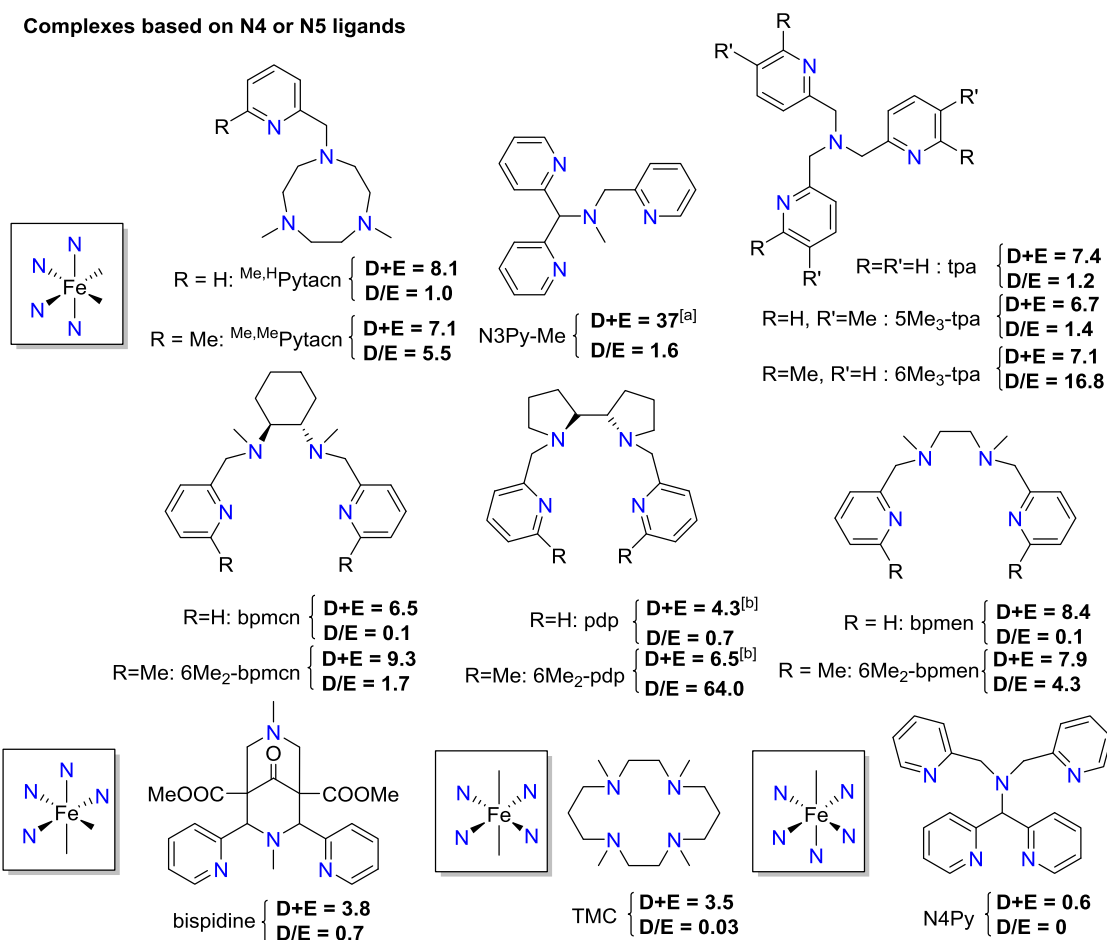
### I.3.2.2. *cis*-Dihydroxylation

Iron complexes have the ability to catalyze both epoxidation and *cis*-dihydroxylation of alkenes. The ones that are capable to mediate the *cis*-dihydroxylation of olefins constitute functional models of the Rieske Oxygenase family of enzymes.

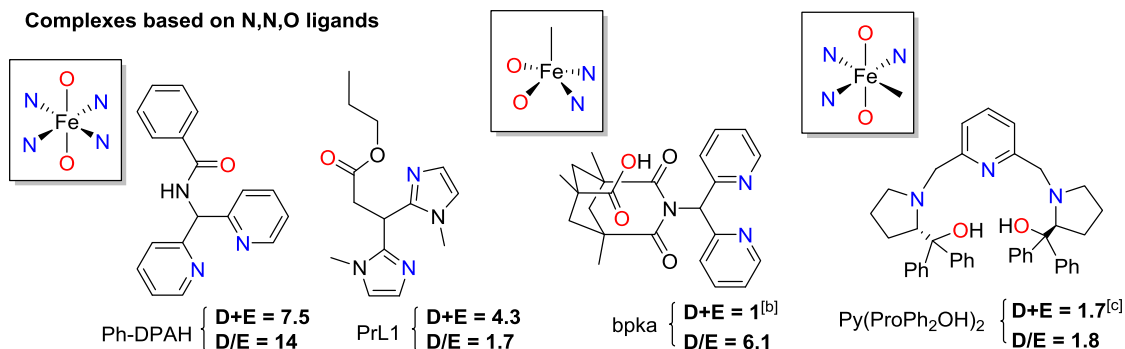
#### I.3.2.2.1. Iron(II) complexes based on $\text{N}_4$ ligands

The ability of iron complexes to catalyze olefin *cis*-dihydroxylation was first described for the  $[\text{Fe}^{\text{II}}(\text{tpa})]^{2+}$  family of complexes,<sup>116, 117</sup> and rapidly extended to a series of iron complexes containing N-based ligands, such as bpmen<sup>118, 119</sup>, bpmcn<sup>83</sup>, pdp<sup>120</sup>, bispidine<sup>121</sup>, N3Py-Me<sup>122</sup> (N-methyl-N-2-pyridylmethylbis(2-pyridyl)methylamine) and Pytacn<sup>84</sup> (Scheme I.26). The major drawback of these bioinspired catalysts is that they require the use of large excess of substrate, and provide very modest TN and substrate conversion. An important goal in the bioinspired oxidation catalysis field remains at designing novel catalysts for performing *cis*-dihydroxylation reactions in synthetically useful scale, ideally stereoselective, and that could constitute an alternative to Os-based technologies.<sup>11</sup>

## Complexes based on N4 or N5 ligands



## Complexes based on N,N,O ligands



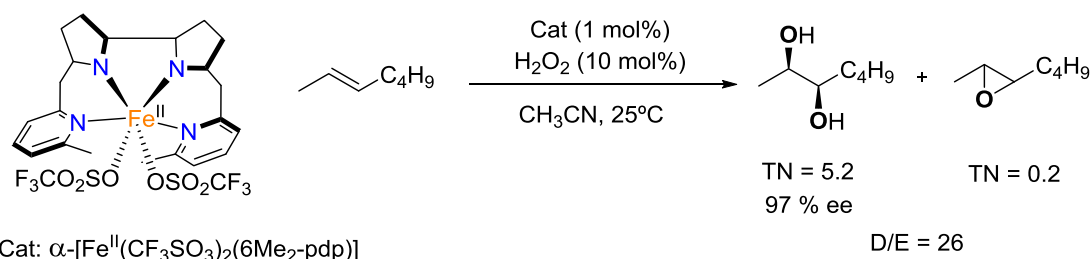
**Scheme I.26.** Representation of ligands used to prepared mononuclear iron(II) complexes to perform olefin oxidation along with the coordination they adopt around the metal center. Oxidation of *cis*-cyclooctene with H<sub>2</sub>O<sub>2</sub> catalyzed by the different iron(II) complexes. Catalytic conditions, catalyst:H<sub>2</sub>O<sub>2</sub>:*cis*-cyclooctene = 1:10:1000. D+E = Turnover number (TN, mols of products / mols of catalyst), E = epoxide, D = *syn*-diol. D/E = (mols of D / mols of E) [a] 50 equiv. of H<sub>2</sub>O<sub>2</sub> instead of 10. [b] 1-octene was used as a substrate instated of *cis*-cyclooctene. [c] 500 equiv. of *cis*-cyclooctene were used.

The results collected in Scheme I.26 show that non-heme iron complexes catalyze the oxidation of olefins into a mixture of epoxide and *syn*-diol, and can convert hydrogen peroxide into products giving yields up to 93% and ratios *syn*-diol/epoxide that range from 0.1 to 64. It

has been demonstrated that *syn*-diol and epoxide products are formed at the same time during the catalytic reaction, and the use of epoxide as a substrate in same reactions conditions does not afford the *syn*-diol, indicating that *syn*-diol does not derive from the epoxide ring opening. Moreover, the high retention of configuration that is observed in the oxidation of *cis*-2-heptene, together with the incorporation of oxygen from water into the oxidation products, by performing isotopic labeling experiments, indicates that these reactions are working via metal based oxidant and no free-radicals are involved.<sup>83, 117, 118</sup>

It is important to notice that ligand structure can modulate the *syn*-diol/epoxide ratio. A general feature is observed in the case of complexes with pyridine rings that contain tetradentate ligands, where the presence of methyl groups in  $\alpha$  position of the pyridine results in an increase in the *syn*-diol/epoxide ratio. Tetradentate ligands that adopt an equatorial coordination and leave two labile sites in a relative *trans* disposition, such as 1,4,8,11-tetramethyl-1,4,8,11-tetraazacyclotetradecane (TMC),<sup>123</sup> basically only affords the epoxide product. The same behavior is observed with pentadentate ligands with only one labile coordination site at the metal, such as N4Py,<sup>116</sup> although these systems are much less efficient. Based on these observations it seems that two labile sites in a *cis* configuration are essential to perform the *cis*-dihydroxylation of olefins.<sup>124</sup>

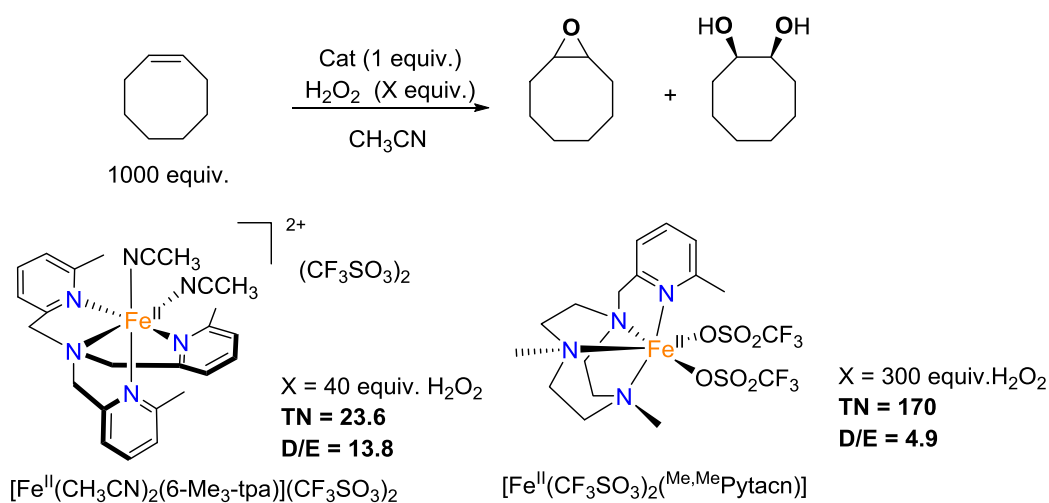
In a parallel way, the growing interest in obtaining chiral products has made particularly attractive the development of chiral iron-based *cis*-dihydroxylation catalysts. Good enantiomeric excesses in olefin *cis*-dihydroxylation reactions have been obtained with the two structurally related iron catalysts  $\alpha$ -[Fe<sup>II</sup>(CF<sub>3</sub>SO<sub>3</sub>)<sub>2</sub>(6Me<sub>2</sub>-pdp)] and  $\alpha$ -[Fe<sup>II</sup>(CF<sub>3</sub>SO<sub>3</sub>)<sub>2</sub>(6Me<sub>2</sub>-bpmcn)] (Scheme I.26).<sup>119, 120</sup> More effective asymmetric olefin *cis*-dihydroxylation was accomplished with  $\alpha$ -[Fe<sup>II</sup>(CF<sub>3</sub>SO<sub>3</sub>)<sub>2</sub>(6Me<sub>2</sub>-pdp)], which affords a moderate to high ratio *syn*-diol/epoxide, about 6 for cyclooctene oxidation and 60 or greater for 1-octene, and from modest to excellent enantiomeric excesses (11-97%) (Scheme I.27). Even though, the substrate conversion of this system is very poor (<5%).



**Scheme I.27.** Asymmetric *cis*-dihydroxylation using  $\alpha$ -[Fe<sup>II</sup>(CF<sub>3</sub>SO<sub>3</sub>)<sub>2</sub>(6Me<sub>2</sub>-pdp)] complex, obtaining *syn*-diol product in 97% ee.

As previously indicated, the key limitation of these systems is that a relatively low TN and substrate conversion are obtained. Large excess of substrate and small amounts of oxidant agents have been commonly employed. However, exceptional catalysts that overcome these limitations have started to appear.

A tpa-derivative ligand was used in complex  $[\text{Fe}^{\text{II}}(6\text{Me}_3\text{-tpa})(\text{CH}_3\text{CN})_2](\text{CF}_3\text{SO}_3)_2$  (Scheme I.28), which catalyzes the oxidation of aliphatic olefins with good yields and moderate selectivity towards *cis*-dihydroxylation in front of epoxidation products.<sup>125</sup> A triazacyclononane based catalyst,  $[\text{Fe}^{\text{II}}(\text{CF}_3\text{SO}_3)_2(\text{Me}_2\text{MePytacn})]$  has been described to perform cyclooctene oxidation affording large turnover numbers when 300 equivalents of  $\text{H}_2\text{O}_2$  are employed with a high ratio *syn*-diol/epoxide, 4.9 (141 TN of *syn*-diol versus 29 TN of epoxide).<sup>84</sup>



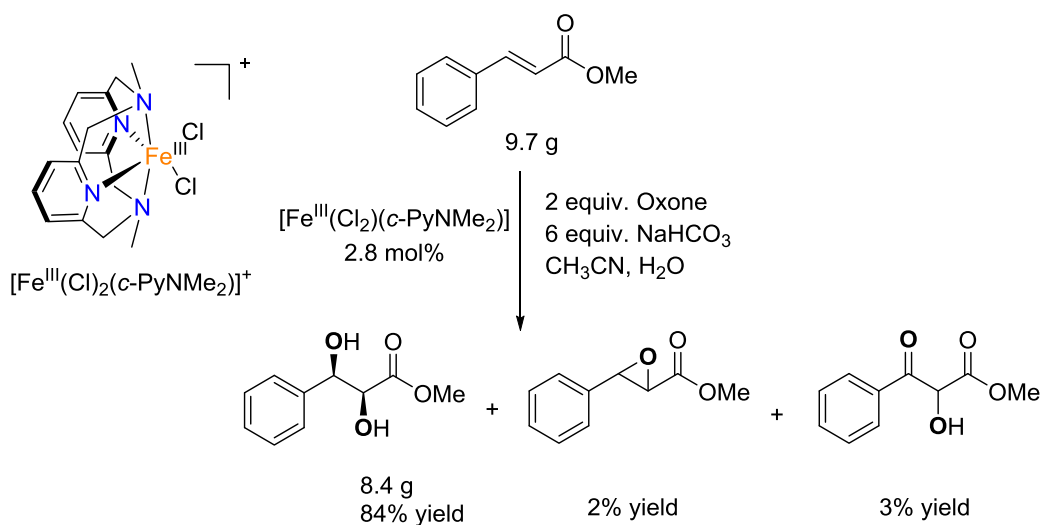
**Scheme I.28.** Catalysts capable of performing oxidation of alkenes with high ratio diol/epoxide.

Recently, Che and co-workers described a chemically robust iron complex  $[\text{Fe}^{\text{III}}(\text{Cl})_2(\text{c-Py}_2\text{NMe}_2)]^+$  ( $\text{c-Py}_2\text{NMe}_2 = N,N'$ -dimethyl-2,11-diaza[3.3](2,6)pyridinophane) as an efficient *cis*-dihydroxylation catalyst in combination with  $\text{Oxone}$  as oxidant, at room temperature. By using 0.7 to 3.5 mol% of catalyst loading, and limiting amounts of substrate, with 2 equivalents of  $\text{Oxone}$  a large range of alkenes could be oxidized. Best yields were obtained in the oxidation of electron-deficient olefins, from 56% to 99%, yielding high *syn*-diol/epoxide ratios (8.5-20.3). A particularly remarkable substrate is dimethyl fumarate, which is *cis*-dihydroxylated with a 99% selectivity. On the other hand, electron rich olefins are oxidized in moderate to good yields (16-64%) and low *syn*-diol/epoxide selectivities.

This method could be applied in large-scale, for example the *cis*-dihydroxylation of methyl cinnamate (9.7 g) with  $\text{Oxone}$  (2 equiv.) afforded the *syn*-diol product (8.4 g), in 84% yield (Scheme I.29). This reaction was performed by adding each of the substrate and the catalyst in two equal portions, and each portion was reacted with  $\text{Oxone}$ . The second



addition of the catalyst could be replaced by the iron salt,  $\text{Fe}(\text{ClO}_4)_2 \cdot 4\text{H}_2\text{O}_2$ , which allows the *in situ* regeneration of the catalyst obtaining the same results. Epoxides, hydroxycetones and ketones (or aldehydes) resulting from oxidative C-C cleavage are side products of the reaction.

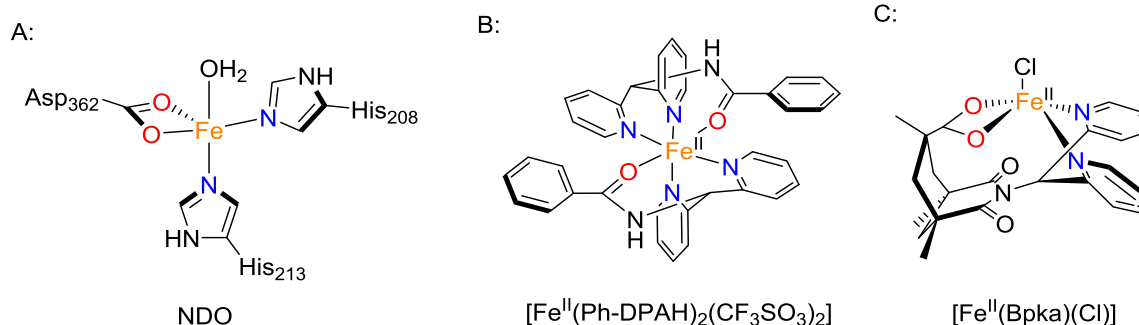


**Scheme I.29.** Large-scale catalysis performed by  $[\text{Fe}^{\text{III}}(\text{Cl})_2(\text{c-PyNMe}_2)]^+$ .

ESI-MS analyses at room temperature show the presence of a cluster ion that could be simulated as  $[\text{Fe}^{\text{V}}(\text{O})_2(\text{c-PyNMe}_2)]^+$ . On basis of ESI-MS studies and DFT analyses, the authors propose that this species is responsible for the *cis*-dihydroxylation of olefins.

#### **1.3.2.2.2. Iron(II) complexes based on N,N,O ligands**

Tetradentate N-donor ligands do not reflect the N,N,O ligand environment found at the active site of the Rieske Oxygenase family, which consists of a mononuclear iron coordinated to a 2-histidine-1-carboxylate motif (Scheme I.30, A). With the aim of modeling this facial triad, an iron(II) complex with a N,N,O-donor set ligand Ph-DPAH ((di-(2-pyridyl)methyl)benzamide) (Scheme I.30, B) was studied as a synthetic model. This catalyst performs the oxidation of a high range of olefins, with excellent selectivity towards *cis*-dihydroxylation<sup>126</sup> and yielding minimum amounts of epoxides. Along the same line, in a recent work, Klein Gebbink and co-workers reported a related complex that share the same facial N,N,O triad, PrL1 (3,3-bis(1-methylimidazol-2-yl)propionate)<sup>127</sup> and Py(ProPh<sub>2</sub>OH)<sub>2</sub> (2,6-Bis[[(S)-2-(diphenylhydroxymethyl)-1-pyrrolidinyl]methyl]pyridine)<sup>128</sup> showing epoxidation and *cis*-dihydroxylation activity (Scheme I.26).



**Scheme I.30.** A: Active site of a Rieske Oxygenases, naphthalene 1,2-dioxygenase B: Complex with Ph-DPAH ligand described by Que, and used as a mimic of Rieske Oxygenase active center. C: Complex with Bpka ligand.

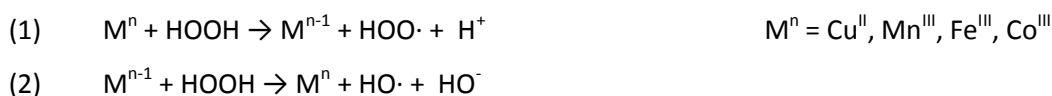
Que and co-workers, also, described a more accurate structure model of Naphthalene 1,2-Dioxygenase,  $[\text{Fe}^{\text{II}}(\text{Cl})(\text{Bpka})]$  (Bpka = 3-(dipyridin-2-yl-methyl)-1,5,7-trimethyl-2,4-dioxo-3-azabicyclo[3.3.1]nonane-7-carboxylic acid), which bears two pyridine N atoms and one carboxylate (Scheme I.30, C). The system acts as a functional model of the NDO enzyme. In the presence of  $\text{AgCF}_3\text{SO}_3$ , added in order to remove the chloride ligand, this complex could oxidize 1-octene substrate giving 0.67 TN of *syn*-diol and 0.11 TN of epoxide by using 10 equiv. of  $\text{H}_2\text{O}_2$ . However, the complex is only capable of performing a single turnover reaction.<sup>129</sup>

## I.4. Mechanistic aspects in catalytic oxidations reactions mediated by bioinspired non-heme iron complexes

The main advantages of the reactions catalyzed by enzymes are their selectivity and efficiency, but also that they work under mild conditions. For this reason, the development of biomimetic and bioinspired catalysts has been a major focus of attention for bioinorganic community. In addition, these biomimetic structures provide valuable information for understanding reaction mechanisms operating in the enzyme. The present work is directed towards the development of synthetic models of mononuclear non-heme iron enzymes such as Rieske Oxygenases, and the elucidation of their catalytic reaction mechanisms.<sup>8,57</sup>

In catalytic biomimetic studies, the reductive activation of  $\text{O}_2$  is replaced by the use of peroxides, which can be understood as a two electron reduced version of  $\text{O}_2$ . However, Fenton's reaction is associated to the combination of peroxides and red-ox active transition metals, such as  $\text{Fe}^{\text{II}}$ ,  $\text{Cu}^{\text{I}}$ ,  $\text{Mn}^{\text{II}}$  and  $\text{Co}^{\text{II}}$  (equations 1 and 2).<sup>62</sup> This chemistry generates freely-diffusing carbon and/or oxygen centered organic radicals. The challenge in the field consists on

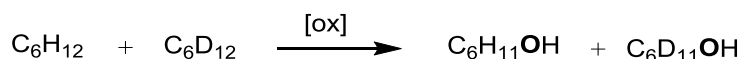
designing metal complexes that could avoid these reactions and that could engage in metal-centered oxidation reactions.<sup>4</sup>



### I.4.1. Mechanistic probes

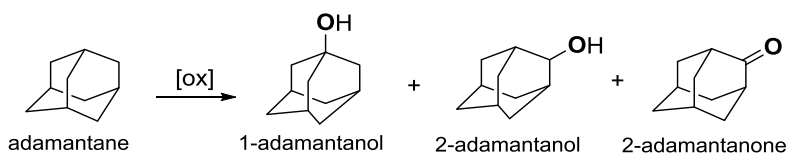
Different mechanistic probes have been used in order to identify the key oxidative species for substrate oxidation.<sup>57</sup> These probes give information about the presence of radicals in the catalytic solution and their lifetime. The absence of radicals is indicative of a metal based oxidant and selective oxidation will be expected in this case. Five different experiments that help elucidating the nature of the oxidant species are explained below.

**Kinetic isotope effects (KIE):** The KIE is the competition reaction between protio- and deuterioalkanes based on the difference of C-H/C-D bond strength (Scheme I.31). Radical oxidation reaction give low KIE values, between 1-2.<sup>130</sup> This is indicative of high powerful oxidants that do not discriminate between C-H and C-D bond strength. However, enzymatic reactions give higher KIE values, with a theoretical maximum of 7.<sup>131</sup> Surprisingly, some enzymes provide large KIE values, that can only be explained by tunneling effects; for example, KIE values > 11 for cytochrome P450<sup>29</sup> and 50–100 for methane monooxygenase.<sup>132</sup>



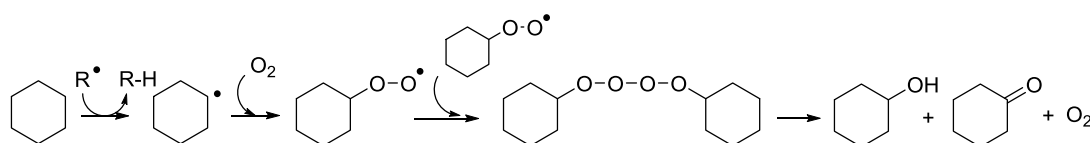
**Scheme I.31.** Competition between protio- and deuterioalkanes.

**Regioselectivity:** A case study is the regioselectivity competition in the oxidation of adamantane. This substrate contains 12 C-H bonds in secondary sites and 4 C-H bonds in tertiary sites (Scheme I.32). The regioselectivity is defined as a 3°/2° ratio (1-adamantanol / (2-adamantanol + 2-adamantanone)) and multiplied by 3 to normalize the ratio of secondary C-H bonds in front of tertiary). Low ratios of 3°/2° indicate no discrimination between the bond strength of tertiary C-H bonds and secondary ones, like in the case of hydroxyl radicals that give 3°/2° values near 2.<sup>133</sup> For enzymatic oxidation reactions, like cytochrome P450s, the adamantane regioselectivity can achieve 3°/2° ratios as high as 48.<sup>134</sup>



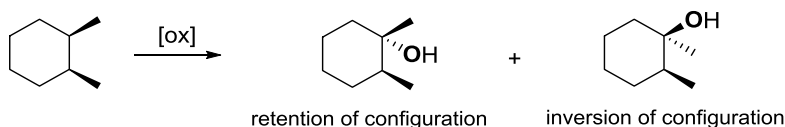
**Scheme I.32.** Oxidation of adamantane.

**Alcohol/ketone ratio (A/K):** This probe is indicative of the life time of the alkyl radical. In the oxidation of secondary alkanes (such as cyclohexane) if long-lived alkyl radicals are generated, they can trap  $O_2$  giving alkylperoxyl radicals (Scheme I.33),<sup>135</sup> the combination of two radicals result in a Russell-type termination giving equimolar amounts of alcohol and ketone.<sup>136</sup> In metal centered oxidations, the alkyl radicals formed have extremely short lifetimes, and rapidly react with the iron center to generate the alcohol product. For this system it would be expected the alcohol (2e- oxidation product) to be the unique product, although some ketone could be generated presumably due to further oxidation of the alcohol.



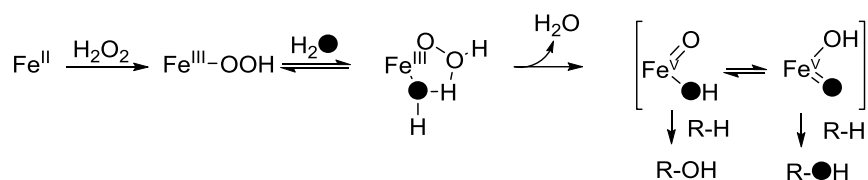
**Scheme I.33.** Radical reaction giving equimolar amounts of alcohol and ketone.

**Substrate-based probes of radical lifetime.** Another probe to quantify the life time of an alkyl radical is the oxidation of *cis* and *trans* isomers of 1,2-dimethylcyclohexane or decahydronaphthalene (decalin). The epimerization of the tertiary C-H bond will indicate the formation of long-lived alkyl radical intermediates giving *cis:trans* ratio of approximately 1 (Scheme I.34).<sup>137</sup> Instead, metal based systems afford tertiary alcohols with high retention of the configuration, due to the presence of short-lived alkyl radicals and the implication of concerted reaction pathways.



**Scheme I.34.** Isomers obtained in the tertiary alcohol oxidation of *cis*-1,2-dimethylcyclohexane.

**Labeling studies, oxo-hydroxo tautomerism:** Labeling studies have been used as a mechanistic tool to determine the origin of the oxygen that ends up into the oxidized product.<sup>78, 138</sup> If long-life radicals are present in the catalytic solution high levels of  $O_2$  incorporation would be found. On the other hand, metal based catalysts operating through metal-oxo species are capable of incorporating oxygen atoms from water into the oxidized products, which is explained by the generation of high valent metal-oxo species that can suffer an “oxo-hydroxo tautomerism”. This mechanism involves a rapid shift of two electrons and one proton from a hydroxo ligand to the oxo group leading to the transformation of the hydroxo ligand into an electrophilic oxo entity (Scheme I.35).



**Scheme I.35.** “Oxo-hydroxo tautomerism”. This process mediates the incorporation of oxygen from labeled water into the oxidized products.

The oxo-hydroxo tautomerism was first described for heme systems,<sup>138</sup> where the exchange takes place between two ligands in a relative *trans* configuration. Afterwards, the mechanism was extended to non-heme complexes; where the two groups implicated in the “oxo-hydroxo tautomerism” are mutually *cis*. In this case, a water-assisted pathway to form a high-valent oxo species is proposed, and this fact could explain the incorporation of oxygen from water into the oxidized products.<sup>78, 139</sup>

## I.4.2. Intermediates on catalytic oxidations reactions

In catalytic oxidation reactions,  $\text{H}_2\text{O}_2$  is commonly employed as oxidant, and iron(II) complexes are convenient precatalysts. Reaction of hydrogen peroxide with the ferrous complexes results in initial oxidation to form iron(III) complexes. These further react with hydrogen peroxide to form iron(III)-hydroperoxide species. These ferric-hydroperoxide ( $\text{Fe}^{\text{III}}\text{-OOH}$ ) species have been prepared, characterized and their reactivity have been studied showing only a sluggish oxidant capacity.<sup>140</sup> Because of that iron(IV)-oxo and iron(V)-oxo have been considered as the catalytic active species.

Recently different  $\text{Fe}^{\text{IV}}\text{=O}$  and  $\text{Fe}^{\text{V}}\text{=O}$  species have been prepared and characterized by different spectroscopic techniques, and in selected cases by X-Ray crystallography, and described to play a key role in the catalytic cycle of non-heme complexes in oxidation reactions. Some of this species are described in the following section.

### I.4.2.1. High-valent iron-oxo species involved in catalytic cycles of oxidation

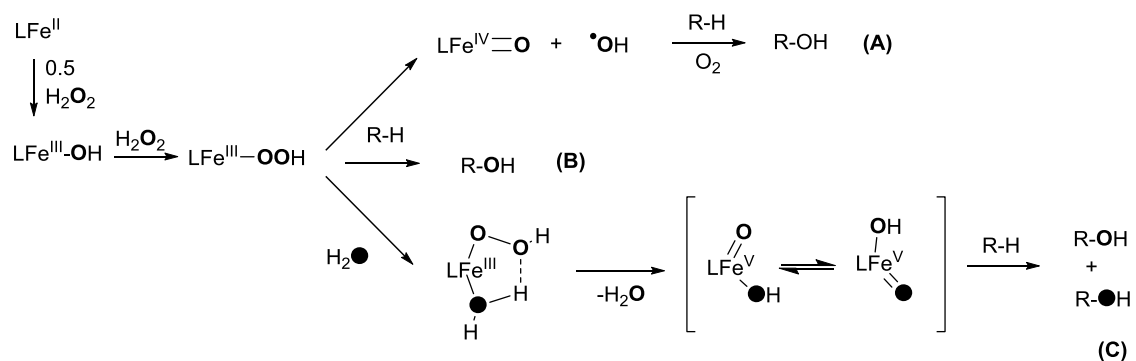
In the last twenty years great advances have been done in the identifications of key intermediates in oxidation reactions catalyzed by aminopyridine iron complexes, considered as bioinspired functional models of Rieske Oxygenase enzymes.

Initially different system had been proposed as the oxidant active species. The spectroscopically characterization of an iron(III)-hydroperoxide intermediate,  $[(\text{tpa})\text{Fe}^{\text{III}}(\text{OOH})]^{2+}$ , raised the question about the real oxidant.<sup>77, 141-144</sup> One proposal was that the hydroperoxide was the oxidant (Scheme I.36, B), but it was also considered that it can be a

precursor of a more powerful oxidant, either a  $\text{Fe}^{\text{V}}=\text{O}$  or  $\text{Fe}^{\text{IV}}=\text{O} + \cdot\text{OH}$  species (Scheme I.36, A and C). Different experiments have been performed with the aim of clarifying the real catalytic species. Study of the origin of the oxygen that ends up in the final oxidized product gives valuable information about this question. In the case that the iron(III)-hydroperoxide is the actual oxidant (Scheme I.36, B), the transferred oxygen atom must come from hydrogen peroxide. Instead, if this iron(III)-hydroperoxide undergoes O-O homolytic cleavage (Scheme I.36, A), to generate an iron(IV)-oxo and a hydroxyl radical, some oxygen from air must end up in the final product, because  $\text{O}_2$  traps carbon centered radicals at diffusion controlled rate, indicating that Fenton like radical reactions are taking place. Otherwise, if this iron(III)-hydroperoxide undergoes O-O heterolytic cleavage (Scheme I.36, C) by a water assisted process, some oxygen from water could end up at the final product, and no incorporation from  $\text{O}_2$  should be found in the oxidized products.

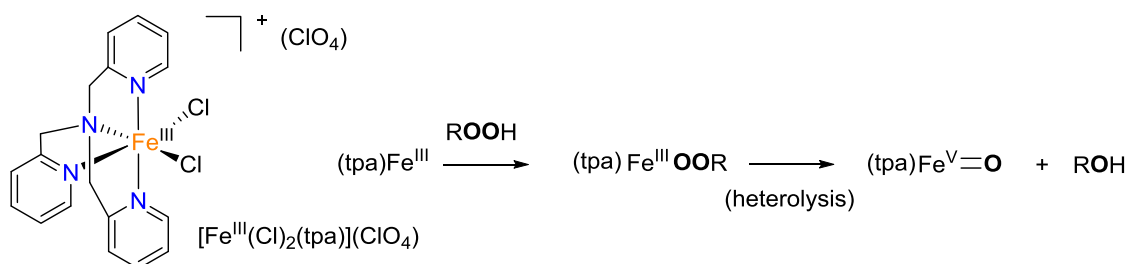
The possible role of the iron(III)-hydroperoxide species as the oxidant in alkane and alkene oxidation reactions has been discarded on the basis of a recent work of Nam and co-workers. The study shows that the decay rates of  $[\text{Fe}^{\text{III}}\text{-OOR(L)}]$  species ( $\text{R} = \text{H}, \text{}^t\text{Bu}$ ;  $\text{L} = \text{tpa}, \text{N4Py}$ ) in presence of organic substrate are very slow and quite similar to the decay rates observed in absence of substrates. Due to the high efficiency of these complexes under catalytic conditions, the kinetic experiments indicated that the hydroperoxide intermediate could not be considered as the catalytically active oxidant.<sup>140</sup> Furthermore, isotopic labeling experiments have shown a partial incorporation of oxygen from water into the oxidized products. In the case of  $[\text{Fe}^{\text{II}}(\text{tpa})(\text{CH}_3\text{CN})_2]^{2+}$  catalyst, the incorporation of water into the oxidized products is about 10% in olefin oxidation, and about 30% in the oxidation of alkanes.<sup>117, 145</sup> Similar labeling results have also been observed for other non-heme iron catalysts, such as  $[\text{Fe}^{\text{II}}(\text{bpmen})(\text{CH}_3\text{CN})_2]^{2+}$ <sup>118, 146</sup> and  $[\text{Fe}^{\text{II}}(\text{N3Py-Me})(\text{CH}_3\text{CN})_2]^{2+}$ .<sup>122</sup> Water incorporation into products is indicative of a water-assisted pathway that facilitates the heterolytic cleavage of the O-O bond to form the  $\text{Fe}^{\text{V}}(\text{O})(\text{OH})$  oxidant (Scheme I.36, C). Since iron(III)-hydroperoxide species could not exchange oxygen with water, water incorporation into products further confirms that this species cannot be the sole oxidant.

Iron(IV)-oxo intermediates were discarded for these kind of catalysis, because the formation of such species from the  $\text{Fe}^{\text{III}}\text{-OOH}$  intermediate would imply the generation of HO· radicals. Since these catalysts operate with high stereoretention in the oxidation of *cis*-1,2-dimethylcyclohexane, implication of free diffusing radicals can be also discarded (Scheme I.36, A).<sup>146</sup>



**Scheme I.36.** Proposed formation of the iron(III)-hydroperoxy species and its possible evolution to more powerful high-valent iron-oxo species.

Que and co-workers were the first to propose the formation of high-valent iron-oxo intermediates as catalytic active species for the oxidation of cyclohexane using *m*-chloroperoxybenzoic acid and *tert*-butyl hydroperoxide in acetonitrile. The complex used in the initial studies was  $[\text{Fe}^{\text{III}}(\text{Cl})_2(\text{tpa})](\text{ClO}_4)$ . The authors proposed that the basicity of the tpa ligand helped to stabilize a highly reactive  $\text{Fe}^{\text{V}}=\text{O}$  species, generated via heterolytic breakage of the O-O bond in a ferric alkylperoxide complex (Scheme I.37).<sup>147</sup>

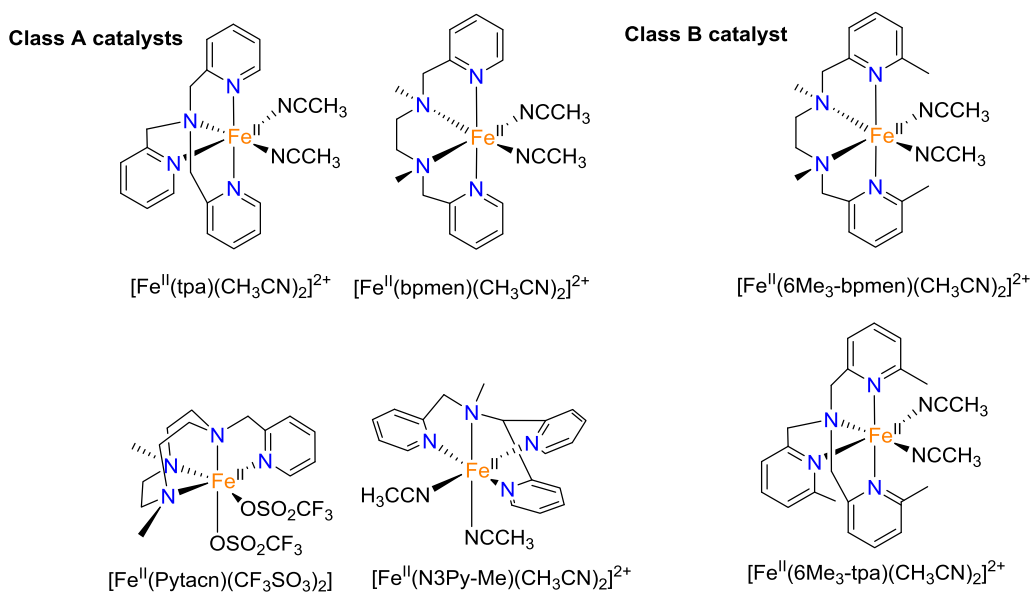


**Scheme I.37.** Proposed formation of mononuclear high-valent iron-oxo intermediates via O-O heterolytic cleavage.

#### I.4.2.1.1. High-valent iron-oxo intermediates for olefin oxidation

Isotopic labeling experiments in *cis*-dihydroxylation reactions are important because they indicate the origin of the oxygen atoms that end up into the oxidized product, and give information about the active species responsible for the oxidation. Que *et al.* defined two types of iron based catalysts on the basis of the origin of oxygen atoms that are transferred to the substrate in olefin oxidation results (Scheme I.38 and Scheme I.39): Class A were catalysts for which the *syn*-diol product contains one atom of oxygen that came from water and the other one that came from  $\text{H}_2\text{O}_2$ . Examples of this class of catalysts are  $[\text{Fe}^{\text{II}}(\text{tpa})(\text{CH}_3\text{CN})_2]^{2+}$ ,  $[\text{Fe}^{\text{II}}(\text{bpmen})(\text{CH}_3\text{CN})_2]^{2+}$ ,  $[\text{Fe}^{\text{II}}(\text{N3Py-Me})(\text{CH}_3\text{CN})_2]^{2+}$  and  $[\text{Fe}^{\text{II}}(\text{CF}_3\text{SO}_3)_2(\text{Pytacn})]$ ;<sup>83, 117</sup> Class B catalysts incorporate both oxygen atoms from a single  $\text{H}_2\text{O}_2$  into the *syn*-diol product, two examples are  $[\text{Fe}^{\text{II}}(6\text{Me}_3\text{-bpmen})(\text{CH}_3\text{CN})_2]^{2+}$  and  $[\text{Fe}^{\text{II}}(6\text{Me}_3\text{-tpa})(\text{CH}_3\text{CN})_2]^{2+}$ .<sup>83</sup>

The difference between the two classes has been studied by employing  $[\text{Fe}^{\text{II}}(\text{tpa})(\text{CH}_3\text{CN})_2]^{2+}$  and  $[\text{Fe}^{\text{II}}(6\text{Me}_3\text{-tpa})(\text{CH}_3\text{CN})_2]^{2+}$  as model catalysts for the class A and class B, respectively. Computational and vibrational analysis for mononuclear  $\text{LFe}^{\text{III}}\text{-OOH}$  species show clear differences in the O-O and Fe-O bond strength depending in the spin state of the complexes.<sup>145</sup> In class A catalysts, the complexes contain strong ligand-field ligands that favor low spin states. Spectroscopic analyses show a strong Fe-O bond and a weak O-O bond, which favors the O-O heterolysis of the hydroperoxo species via a water assisted process generating an  $\text{Fe}^{\text{V}}(\text{O})(\text{OH})$ , where one oxygen comes from water and the other one from hydrogen peroxide (Scheme I.39).<sup>118</sup>

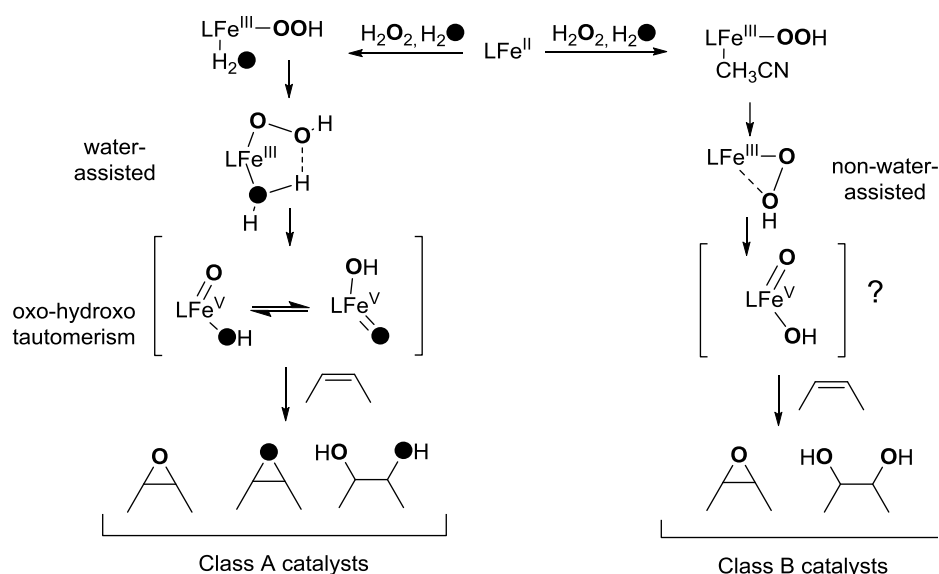


**Scheme I.38.** Examples of class A and Class B catalysts.

On the other hand, class B catalysts form a high-spin iron(III)-hydroperoxide with a strong O-O bond that disfavors its cleavage.<sup>148</sup> In this case the operating mechanism is not so clear; water is not incorporated into the oxidized products. Given the isotopic analysis, substrate oxidation could occur directly by the reaction of the iron(III)-hydroperoxo intermediate with the olefin, or via O-O lysis generating a high-valent iron-oxo intermediate, but without water assistance (Scheme I.39).<sup>83</sup>

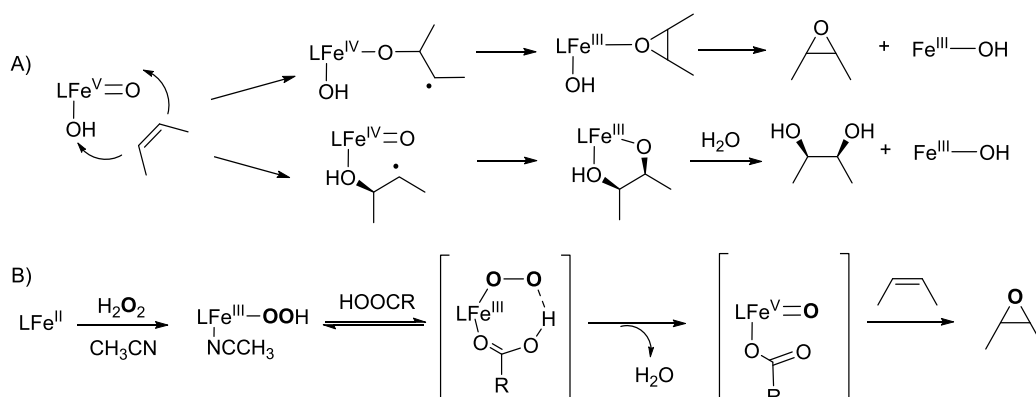
Furthermore, catalytic oxidation studies show a different behavior for the two classes of catalysts, while class B catalyst prefer to oxidize electron deficient olefins giving the *syn*-diol as a major product, class A favors the oxidation of electron rich alkenes giving mixtures of *syn*-diol and epoxide.





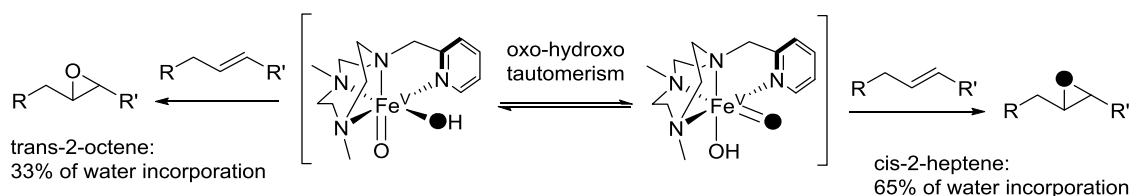
**Scheme I.39.** Proposed mechanisms for olefin epoxidation and *cis*-dihydroxylation by class A and class B catalysts.

DFT calculations employing  $[\text{Fe}^{\text{II}}(\text{tpa})(\text{CH}_3\text{CN})_2]^{2+}$  catalyst reveal that a common oxidant,  $\text{Fe}^{\text{V}}(\text{O})(\text{OH})$ , is responsible for the epoxidation and *cis*-dihydroxylation of olefins in class A catalysts. Each product originates from two different faces of  $\text{Fe}^{\text{V}}(\text{O})(\text{OH})$ , depending on the initial attack. When the attack over the olefin starts with the hydroxo group, the *syn*-diol is generated, while the direct insertion of the oxo group into the olefin produces the epoxide (Scheme I.40, A).<sup>122, 149, 150</sup> The presence of acetic acid in alkene oxidation reactions improves substantially the epoxidation efficiency, and inhibits the *cis*-dihydroxylation. It is proposed that acetic acid promotes the fast O-O cleavage in  $\text{Fe}^{\text{III}}\text{-OOH}$  generating and  $\text{Fe}^{\text{V}}(\text{O})(\text{OAc})$ , responsible for the epoxidation reaction (Scheme I.40, B).<sup>151</sup>



**Scheme I.40.** A) Olefin oxidation mechanism, the same  $\text{Fe}^{\text{V}}(\text{O})(\text{OH})$  species is capable of catalyzing the epoxidation and the *cis*-dihydroxylation. B) Proposed mechanisms for iron-catalyzed oxidation in presence of carboxylic acid.

Further complexities have been reported in a recent study based on epoxidation reactions catalyzed by  $[\text{Fe}^{\text{II}}(\text{CF}_3\text{SO}_3)_2(\text{Pytacn})]$ , showing that the percentage of water incorporation into the epoxide product depends on the nature of the olefin, and it ranges from 33% to 71%.<sup>84</sup> This fact is inconsistent with the formation of a single high-valent iron-oxo species and can be explained by an oxo-hydroxo tautomerism of the  $\text{Fe}^{\text{V}}(\text{O})(\text{OH})$  species. The two tautomers differ in the coordination position of the oxo and hydroxide ligand (Scheme I.41). The level of water incorporation into the epoxide product depends on the relative reactivity of the olefin with each of the two tautomeric species.



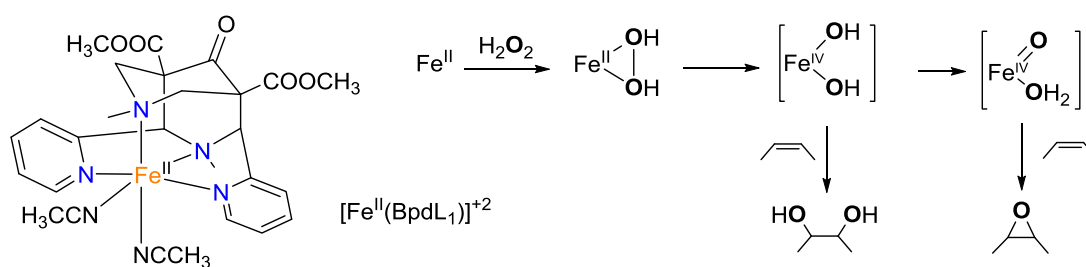
**Scheme I.41.** Proposed mechanism for the oxidation of olefins.

However, these considerations could not be extended to all non-heme iron systems. For instance, different reaction pathways have been assumed for  $\text{Fe}(\text{Ph-DPAH})$  (see Scheme I.26), which is selective for the *cis*-dihydroxylation of olefins. This system uses a facial tridentate ligand (N,N,O-ligand) inspired in the active site of Rieske dioxygenases. The main difference of this system and the ones described before is that they leave three sites available for exogenous ligands, leaving an extra site for water molecule binding.<sup>126</sup> Labeling experiments in the *syn*-diol formation indicate that the incorporation of one oxygen from water accounts for 33% of the *syn*-diol. This excludes a concerted attack of the peroxo moiety on the olefin double bond, and instead indicates that first the peroxo O-O bond must be cleaved generating a high-valent iron-oxo species.

Moreover, some authors demonstrated that iron(IV)-oxo species are also capable of performing the epoxidation of olefins stoichiometrically. The first ones who described this reaction were Que and co-workers, by mixing complex  $[\text{Fe}^{\text{II}}(\text{tpa})(\text{CH}_3\text{CN})_2]^{2+}$  and peracetic acid at  $-40\text{ }^\circ\text{C}$  to generate  $[\text{Fe}^{\text{IV}}(\text{O})(\text{tpa})]^{2+}$ . The latter species is capable of transferring the oxygen atom to the cyclooctene substrate in a 30% yield.<sup>152</sup> Since then, a large number of iron(II) complexes appeared that could perform the same chemistry. In addition, these systems can oxidize a large number of substrates, such as  $\text{PPh}_3$ , thioanisole ( $\text{PhSMe}$ ), DMSO or an olefin giving stoichiometric amounts of the oxidized product.<sup>152-156</sup> Moreover, it is important to highlight that  $[\text{Fe}^{\text{IV}}(\text{O})(\text{N4Py})]$ ,  $[\text{Fe}^{\text{IV}}(\text{O})(\text{Bn-tpen})]$  and  $[\text{Fe}^{\text{IV}}(\text{O})(\text{Pytacn})]$  complexes are also

competent for cleaving the strong C-H bond of aliphatic substrates (Bn-tpen = *N*-benzyl-*N,N',N'*-tris(2-pyridylmethyl)-1,2-diaminoethane).<sup>157, 158</sup>

More recently, Comba and co-workers reported a mononuclear iron complex based on a tetradentate bispidine ligand,  $[\text{Fe}^{\text{II}}(\text{BpdL}_1)]^{2+}$ , which can catalyze the epoxidation and *cis*-dihydroxylation of olefins by using  $\text{H}_2\text{O}_2$  as oxidant. The authors proposed that the species responsible for the olefin oxidation is a  $\text{Fe}^{\text{IV}}$  compound generated by the O-O homolysis of the short living  $\text{Fe}^{\text{II}}\text{-H}_2\text{O}_2$  precursor. DFT calculations predicted two novel high-valent isomers; an intermediate-spin  $\text{Fe}^{\text{IV}}(\text{OH})_2$  capable of performing olefin *cis*-dihydroxylation, and its tautomer  $\text{Fe}^{\text{IV}}(\text{O})(\text{H}_2\text{O})$  responsible of olefin epoxidation. Isotopic labeling experiments show that the origin of the oxygen that ends up at both products comes from hydrogen peroxide (Scheme I.42).<sup>121</sup> The mechanism proposed is an alternative to the one suggested for tetradentate  $[\text{Fe}^{\text{II}}(\text{tpa})(\text{CH}_3\text{CN})_2]^{2+}$  and  $[\text{Fe}^{\text{II}}(\text{bpmen})(\text{CH}_3\text{CN})_2]^{2+}$  catalysts, which implicates a  $\text{Fe}^{\text{V}}(\text{O})(\text{OH})$  oxidant.<sup>159</sup> This mechanism is also compatible with the results obtained for class B catalyst.



**Scheme I.42.**  $\text{Fe}^{\text{II}}/\text{Fe}^{\text{IV}}$  mechanism postulated for alkene oxidation reactions catalyzed by iron bispidine complexes.

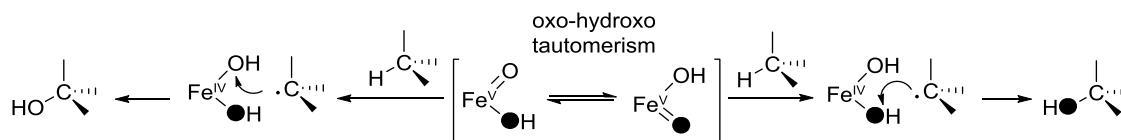
Finally, Rybak Akimova and co-workers reported an iron(II) complex with a pyridine-containing a macrocyclic ligand PyMAC (PyMAC = 2,7,12-trimethyl-3,7,11,17-tetraazabicyclo[11.3.1] heptadeca-1(17),13,15-triene) capable of oxidizing olefins via  $\text{Fe}^{\text{II}}/\text{Fe}^{\text{IV}}$  catalytic cycle using  $\text{H}_2\text{O}_2$  or isopropyl 2-iodoxybenzoate as oxidants. Low-temperature stopped-flow kinetic studies demonstrated the formation of an iron(IV)-oxo intermediate in the reaction of  $\text{Fe}^{\text{II}}$  complex with an oxidant. Furthermore, these studies show that iron(IV)-oxo species are competent intermediates for cyclooctene epoxidation with  $\text{H}_2\text{O}_2$  at room temperature.<sup>160, 161</sup>

#### I.4.2.1.2. High-valent iron-oxo intermediates for alkane oxidation

Most of complexes that can perform the selective hydroxylation of C-H belong to Class A family and are characterized for exhibiting a high kinetic isotopic effect, large normalized

$3^{\circ}/2^{\circ}$  C-H ratios and high stereoretention. Moreover, isotopic labeling experiments show a significant incorporation of water into the final oxidized product and a minimum percentage of  $O_2$  incorporation. All of these experiments demonstrate that the oxidation takes place at the metal center, via a high-valent iron-oxo species.<sup>78</sup> Class B catalysts can mediate the hydroxylation of alkanes but they exhibit a radical character, mechanistic probes show low percentages of the stereoretention in *cis*-1,2-DMCH oxidation.<sup>119, 151</sup>

The proposed mechanism for class A catalysts involve the same high-valent species postulated for olefin oxidation,  $Fe^V(O)(OH)$ . The incorporation of water into the final products is explained by a oxo-hydroxo tautomerism.<sup>138</sup> It is proposed that the oxidation of the C-H bond occurs via a rebound mechanism; the  $Fe^V(O)(OH)$  abstracts the hydrogen atom from the substrate generating a  $Fe^{IV}(OH)_2$  and the alkyl radical, which rapidly rebounds with the new hydroxo group. These mechanisms propose that the hydrogen-atom abstraction and the rebound take place at the same oxygen atom (Scheme I.43).



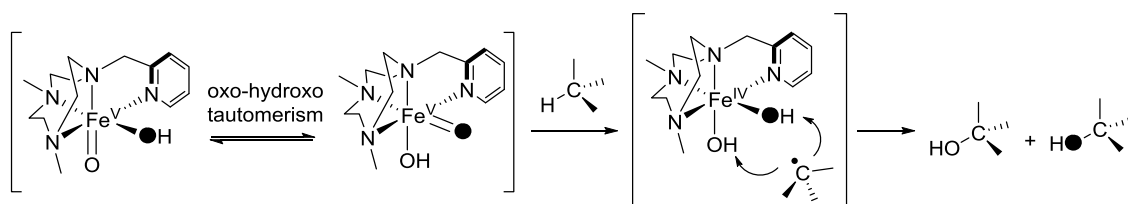
**Scheme I.43.** Mechanism of alkane hydroxylation by  $Fe^V(O)(OH)$  via oxo-hydroxo tautomerism.

Percentage of water incorporation depends on which tautomer catalyzes the oxidation reaction.

This mechanism suggests that there should be a competition between the oxo-hydroxo tautomerism and the oxidation of the substrate, such that slow reacting substrates should give more extent tautomerism and consequently, a larger incorporation of water into the oxidized product. Indeed, experiments performed with the  $[Fe^{II}(tpa)(CH_3CN)_2]^{2+}$  and the  $[Fe^{II}(bpmen)(CH_3CN)_2]^{2+}$  catalysts show that there is a correlation between the strength of the C-H bond and the level of water incorporation into the corresponding alcohol. Moreover, this model predicts that the maximum amount of water incorporation would be 50%, corresponding to an equivalent mixture of label and non-labeled oxo ligands.<sup>78</sup>

More recently, Company *et al.* have given further insights into the rebound mechanism by using the  $[Fe^{II}(CF_3SO_3)_2(^{Me,H}Pytacn)]$  catalyst. The authors showed unprecedented levels of water incorporation into the oxidized products and a high dependence of this water incorporation on the C-H bond strength. Secondary C-H bonds give levels of water incorporation up to 42%. Instead, for tertiary C-H bonds this percentage increases to 76%.<sup>85</sup> To explain these results, an alternative rebound mechanism was proposed: after hydrogen abstraction a common  $Fe^{IV}(OH)_2$  was generated, at this point the alkyl radical can rebound with any of the non-equivalent OH groups. The authors propose that secondary alkyl radicals do no

discriminate between the two OH groups, and therefore 50% of water incorporation is observed. On the other hand tertiary radicals favor the rebound with the OH group derived from water, explaining the unusual high levels of water incorporation (Scheme I.44).



**Scheme I.44.** Proposed rebound mechanism for alkane hydroxylation by  $[\text{Fe}^{\text{II}}(\text{CF}_3\text{SO}_3)_2(\text{Me,H})\text{Pytacn}]$ .

#### I.4.2.2. Spectroscopic evidence of high-valent iron-oxo species

High-valent iron-oxo species have been postulated as catalytic intermediates for numerous oxidation reactions. However, until 2000 no spectroscopic evidence had appeared for high-valent non-heme iron complexes. This fact is attributed to their high reactivity and the lack of convenient spectroscopic techniques. First iron(IV)-oxo species was detected by Wieghardt and co-workers, using a cyclam-acetate iron complex (Figure I.4).<sup>162</sup> Since then, numerous non-heme iron(IV) species began to appear, and the first crystal structures was obtained in 2003 by the reaction of  $[\text{Fe}^{\text{II}}(\text{CF}_3\text{SO}_3)_2(\text{TMC})]$  with PhIO affording the formation of  $[\text{Fe}^{\text{IV}}(\text{O})(\text{TMC})(\text{CH}_3\text{CN})](\text{CF}_3\text{SO}_3)_2$ , which was stable for a week at  $-40\text{ }^\circ\text{C}$ .<sup>153</sup>

Employing the same methodology several non-heme iron(IV)-oxo complexes has been synthesized; containing pentadentate  $\text{N}_5$  ligands such as N4Py,<sup>163</sup> R-tpen,<sup>157</sup> bispidine,<sup>164</sup> and tetradentate  $\text{N}_4$  as tpa<sup>152</sup> and  $\beta$ -bpmcn.<sup>165</sup> The results show that pentadentate and macrocyclic tetradentate ligands are the ones that confer more stability to the iron(IV)-oxo system (Figure I.4).<sup>57, 166</sup>

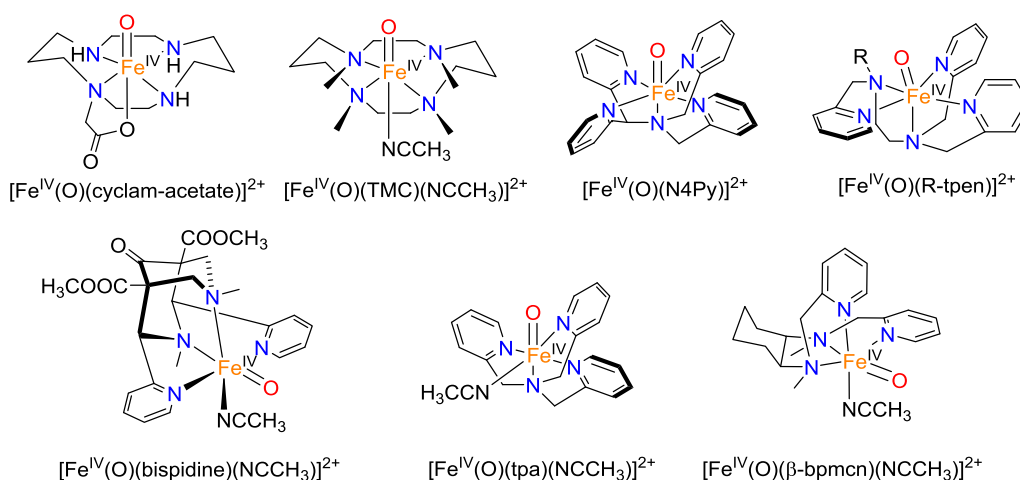


**Figure I.4.** Some of the iron(IV)-oxo complexes synthesized.

The first iron(V)-oxo species that could be prepared and characterized was reported in 2007 by Collins.<sup>167</sup> This species contains a tetraanionic tetraamino macrocyclic ligand (H<sub>4</sub>-TAML, Figure I.5), that was also used for stabilizing a variety of high-valent iron and manganese complexes.<sup>168</sup> Metastable species [Fe<sup>V</sup>(O)(H<sub>4</sub>-TAML)]<sup>-</sup> was characterized by UV-Vis, electron paramagnetic resonance (EPR), Mössbauer, X-ray absorption spectroscopy, electrospray ionization mass spectrometry (ESI-MS). Moreover, reactivity studies and density functional theory (DFT) calculations were also reported. The species was obtained by reaction of a Fe<sup>III</sup> precursor with *m*-chloroperbenzoic acid at low temperature (-60 °C).

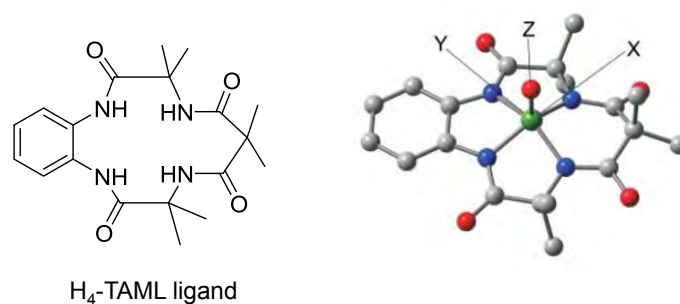


**Figure I.5.** Schematic representation of H<sub>4</sub>-TAML ligand (left). Geometry-optimized structure of [Fe<sup>V</sup>(O)(H<sub>4</sub>-TAML)]<sup>-</sup> as obtained from DFT calculations (right).

The system [Fe<sup>V</sup>=O(H<sub>4</sub>-TAML)]<sup>-</sup> exhibits relatively strong oxidation power, it oxidizes quantitatively Ph<sub>3</sub>P to Ph<sub>3</sub>P=O, PhSMe to the corresponding sulfoxide, and epoxidizes styrene and cyclooctene olefins.

In parallel, highly reactive iron(V)-oxo species have been trapped in catalytic olefin oxidation reactions by using EPR spectroscopic techniques. The high-valent species studied were generated through the oxidation of [Fe<sup>II</sup>(tpa)(CH<sub>3</sub>CN)<sub>2</sub>]<sup>2+</sup> and [Fe<sup>II</sup>(bpmen)(CH<sub>3</sub>CN)<sub>2</sub>]<sup>2+</sup> (Figure I.6). The EPR spectrum was acquired at -196 °C after the mixing of the Fe<sup>II</sup> complexes with *meta*-chloroperoxybenzoic acid or peracetic acid at -60 °C and storing at -70 °C for 26 min. The EPR spectra were characteristic of S = 1/2 species, that proved reactive with an alkene substrate. Since iron(III)-hydroperoxo species do not react with olefins, these spectroscopic features were associated with low-spin iron(V)-oxo intermediates.<sup>169</sup>

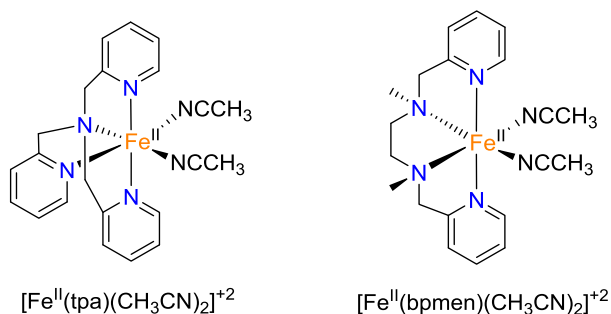


**Figure I.6.** Iron(II) complexes studied by EPR spectroscopy after mixing with oxidant agents.

More recently, mass spectrometry began to be an important technique to trap high reactive iron species. Che and co-workers detected the presence of a cluster ion that could be simulated as  $[\text{Fe}^{\text{V}}(\text{O})_2(\text{c-Py}_2\text{NMe}_2)]^+$ , by the reaction of  $[\text{Fe}^{\text{II}}(\text{Cl})_2(\text{c-Py}_2\text{NMe}_2)]$  with 8 equiv. of  $^{\circ}\text{Oxone}$ . Moreover, with the help of DFT analyses the authors propose that this species is the responsible for the *cis*-dihydroxylation of olefins (Figure I.7, a).<sup>170</sup>

Kodera and co-workers reported the use of cold-spray-ionization mass spectrometry (CSI-MS) to detect these oxidation intermediates. The complex  $[\text{Fe}^{\text{III}}(\text{dpaq})]^{3+}$ , with a pentadentate ligand, in presence of 50 equiv. of  $\text{H}_2\text{O}_2$  at  $-40\text{ }^{\circ}\text{C}$ , affords a peak with the  $m/z$  and the isotope distribution pattern consistent with the chemical formula  $[\text{Fe}^{\text{V}}(\text{dpaq})(\text{O})](\text{ClO}_4)^+$ . Isotopic labeling experiments using  $\text{H}_2^{18}\text{O}_2$  shift the mass signal in two units, indicating that the oxo comes from hydrogen peroxide (Figure I.7, b).<sup>94</sup>

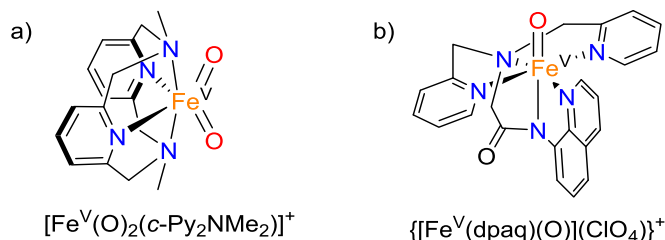


**Figure I.7.** a) ESI-MS detection of an iron(V) bis-oxo. b) CSI-MS analysis to detect an iron(V)-oxo with a pentadentate ligand.

Finally, Que and co-workers report the oxidation of the complex  $[\text{Fe}^{\text{IV}}(\text{O})(\text{TMC})(\text{CH}_3\text{CN})]^{2+}$  (Figure I.4) by using *t*-butyl hydroperoxide and strong base at a  $-44\text{ }^{\circ}\text{C}$ . The oxidation reaction generate a metastable specie  $S = \frac{1}{2}$  attributed to an  $[\text{Fe}^{\text{V}}(\text{O})(\text{TMC})(\text{NC}(\text{O})\text{CH}_3)]^+$ . The new iron(V) species has been characterized by UV-visible, resonance Raman, Mössbauer, and EPR methods. The spectroscopic data and DFT calculations support the formation of an iron(V) complex with an axial oxo and acetylrimido ligand.<sup>171</sup>

## I.5. References

1. Sheldon, R. A.; Kochi, J. A., *Metal-Catalyzed Oxidations of Organic Compounds*. Academic Press: New York, 1981.
2. Punniyamurthy, T.; Velusamy, S.; Iqbal, J., *Chem. Rev.* **2005**, *105*, 2329-2364.
3. Bäckvall, J. E., *Modern oxidation Methods*. Wiley-VCH: Weinheim, 2004.
4. Que Jr., L.; Tolman, W. B., *Nature* **2008**, *455*, 8.
5. Hashiguchi, B. G.; Bischof, S. M.; Konnick, M. M.; Periana, R. A., *Acc. Chem. Res.* **2012**, *45*, 885-898.
6. Barton, D. H. R.; Doller, D., *Acc. Chem. Res.* **1992**, *25*, 504-512.
7. Godula, K.; Sames, D., *Science* **2006**, *312*, 67-72.
8. Costas, M.; Mehn, M. P.; Jensen, M. P.; Que Jr., L., *Chem. Rev.* **2004**, *104*, 939-986.
9. Döbler, C.; Mehlretter, G. M.; Sundermeier, U.; Beller, M., *J. Org. Chem.* **2001**, *621*, 70-76.
10. Schröder, M., *Chem. Rev.* **1980**, *80*, 187-213.
11. Kolb, H. C.; VanNieuwenhze, M. S.; Sharpless, K. B., *Chem. Rev.* **1994**, *94*.
12. Hentges, S. G.; Sharpless, K. B., *J. Am. Chem. Soc.* **1980**, *102*, 4263-4265.
13. Sharpless, K. B.; Amberg, W.; Bennani, Y. L.; Crispino, G. A.; Hartung, J.; Jeong, K. S.; Kwong, H. L.; Morikawa, K.; Wang, Z. M., *J. Org. Chem.* **1992**, *57*, 2768-2771.
14. Bataille, C. J. R.; Donohoe, T. J., *Chem. Soc. Rev.* **2011**, *40*, 114-128.
15. Bertini, I.; Gray, H. B.; Stiefel, E. I.; Valentine, S. J., *Biological inorganic Chemistry: structure & reactivity*. University Science Books: Sausalito, California, 2007.
16. Coelho, P. S.; Brustad, E. M.; Kannan, A.; Arnold, F. H., *Science* **2013**, *339*, 307-310.
17. Kraatz, H. B.; Metzler-Nolte, N., *Concepts and Models in Bioinorganic Chemistry*. Wiley-VCH: Weinheim: 2006.
18. Cotton, F. A.; Wilkinson, G.; Murillo, C. A.; Bochmann, M., Copper: Group 11. In *Advanced Inorganic Chemistry*, 6th ed.; John Wiley & Sons: New York, 1999.
19. Price, J. C.; Barr, E. W.; Tirupati, B.; Bollinger, J. M. J.; Krebs, C., *Biochemistry* **2003**, *42*, 7497-7508.
20. Hoffart, L. M.; Barr, E. W.; Guyer, R. B.; Bollinger, J. M. J.; Krebs, C., *Proc. Natl. Acad. Sci. USA* **2006**, *103*, 14738-14743.
21. Eser, B. E.; Barr, E. W.; Frantom, P. A.; Saleh, L.; Bollinger, J. M. J.; Krebs, C.; Fitzpatrick, P. F., *J. Am. Chem. Soc.* **2007**, *129*, 11334-11335.
22. Galonic, D. P.; Barr, E. W.; Walsh, C. T.; Bollinger, J. M. J.; Krebs, C., *Nat. Chem. Biol.* **2007**, *3*, 113-116.
23. Wallar, B. J.; Lipscomb, J. D., *Chem. Rev.* **1996**, *96*, 2625-2658.
24. Montellano, P. O. d., *Cytochrome P450 : Structure, Mechanism, and Biochemistry*. 3rd ed.; Springer ed.: New York, 2005.
25. Meunier, B.; Bernadou, J., *Struct. Bonding* **2000**, *97*, 1-35.
26. Meunier, B.; de Visser, S. P.; Shaik, S., *Chem. Rev.* **2004**, *104*, 3947-3980.
27. Schlichting, I.; Berendzen, J.; Chu, K.; Stock, A. M.; Maves, S. A.; Benson, D. E.; Sweet, R. M.; Ringe, D.; Petsko, G. A.; Sligar, S. G., *Science* **2000**, *287*, 1615-1622.
28. Groves, J. T.; McCluskey, G. A., *J. Am. Chem. Soc.* **1976**, *98*, 859-861.
29. Sono, M.; Roach, M. P.; Coulter, E. D.; Dawson, J. H., *Chem. Rev.* **1996**, *96*, 2841-2887.
30. Rittle, J.; Green, M. T., *Science* **2010**, *330*, 933-937.
31. Ortiz de Montellano, P. R., *Chem. Rev.* **2010**, *110*, 932-948.
32. Shaik, S.; Lai, W.; Chen, H.; Wang, Y., *Acc. Chem. Res.* **2010**, *43*, 1154-1165.
33. Wang, X.; Peter, S.; Kinne, M.; Hofrichter, M.; Groves, J. T., *J. Am. Chem. Soc.* **2012**, *134*, 12897-12900.
34. Meunier, B.; Bernadou, J., *Topics in Catalysis* **2002**, *21*, 47-54.



35. Balahura, R. J.; Sorokin, A.; Bernadou, J.; Meunier, B., *Inorg. Chem.* **1997**, *36*, 3488-3492.
36. Costas, M., *Coord. Chem. Rev.* **2011**, *255*, 2912-2932.
37. Gibson, D. T.; Resnick, S. M.; Lee, K.; Brand, J. M.; Torok, D. S.; Wackett, L. P.; Schocken, M. J.; Haigler, B. E., *J. Bacteriol.* **1995**, *177*, 2615-2621.
38. Bruijninx, P. C. A.; van Koten, G.; Klein Gebbink, R. J. M., *Chem. Soc. Rev.* **2008**, *37*, 2716-2744.
39. Wolfe, M. D.; Parales, J. V.; Gibson, D. T.; Lipscomb, J. D., *J. Biol. Chem.* **2001**, *276*, 1945-1953.
40. Gibson, D. T.; Parales, R. E., *Curr. Opin. Biotechnol.* **2000**, *11*, 236-243.
41. Hudlicky, T.; Gonzalez, D.; Gibson, D. T., *Aldrichimica Acta* **1999**, *32*, 35-62.
42. Kovaleva, E. G.; Lipscomb, J. D., *Nat. Chem. Biol.* **2008**, *4*, 186-193.
43. Koehntop, K. D.; Emerson, J. P.; Que Jr., L., *J. Biol. Inorg. Chem.* **2005**, *10*, 87-93.
44. Kauppi, B.; Lee, K.; Carredano, E.; Parales, R. E.; Gibson, D. T.; Eklund, H.; Ramaswamy, S., *Structure* **1998**, *6*, 571-586.
45. Wolfe, M. D.; Altier, D. J.; Stubna, A.; Popescu, C. V.; Münck, E.; Lipscomb, J. D., *Biochemistry* **2002**, *41*, 9611-9626.
46. Gibson, D. T.; Yeh, W.-K.; Liu, T.-N.; Subramanian, V., *Oxygenases and Oxygen Metabolism*. In *Oxygenases and Oxygen Metabolism* Ed. Academic: New York, 1982; pp 51-62.
47. Crutcher, S. E.; Geary, P. J., *Biochem. J.* **1979**, *177*, 393-400.
48. Pavel, E. G.; Martins, L. J.; Ellis, W. R., Jr.; Solomon, E. I., *Chem. Biol.* **1994**, *1*, 173-183.
49. Karlsson, A.; Parales, J. V.; Parales, R. E.; Gibson, D. T.; Eklund, H.; Ramaswamy, S., *Science* **2003**, *299*, 1039-1042.
50. Wolfe, M. D.; Lipscomb, J. D., *J. Biol. Chem.* **2003**, *278*, 829-835.
51. Chakrabarty, S.; Austin, R. N.; Deng, D.; Groves, J. T.; Lipscomb, J. D., *J. Am. Chem. Soc.* **2007**, *129*, 3514-3515.
52. Markis, T. M.; von Koenig, K.; Schlichting, I.; Sligar, S. G., *J. Inorg. Biochem.* **2006**, *100*, 507-518.
53. Bollinger, J. M.; Price, J. C.; Hoffart, L. M.; Barr, E. W.; Krebs, C., *Eur. J. Inorg. Chem.* **2005**, *2005*, 4245-4254.
54. Sturgeon, B. E.; Burdi, D.; Chen, S.; Huynh, B.-H.; Edmondson, D. E.; Stubbe, J.; Hoffman, B. M., *J. Am. Chem. Soc.* **1996**, *118*, 7551-7557.
55. Riggs-Gelasco, P. J.; Shu, L.; Chen, S.; Burdi, D.; Huynh, B. H.; Que Jr., L.; Stubbe, J., *J. Am. Chem. Soc.* **1998**, *120*, 849-860.
56. Shu, L.; Nesheim, J. C.; Kauffmann, K.; Münck, E.; Lipscomb, J. D.; Que Jr., L., *Science* **1997**, *275*, 515-518.
57. Costas, M.; Chen, K.; Que Jr., L., *Coord. Chem. Rev.* **2000**, *200-202*, 517-544.
58. *Biomimetic Oxidations Catalyzed by Transition Metal Complexes*. Imperial College Press: London, 2000.
59. Walling, C., *Acc. Chem. Res.* **1975**, *8*, 125-131.
60. Sawyer, D. T.; Sobkowiak, A.; Matsushita, T., *Acc. Chem. Res.* **1996**, *29*, 409-416.
61. MacFaul, P. A.; Wayner, D. D. M.; Ingold, K. U., *Acc. Chem. Res.* **1998**, *31*, 159-162.
62. Walling, C., *Acc. Chem. Res.* **1998**, *31*, 155-157.
63. Barton, D. H. R., *Chem. Soc. Rev.* **1996**, 229.
64. Stavropoulos, P.; Celenligil-Cetin, R.; Tapper, A. E., *Acc. Chem. Res.* **2001**, *34*, 745-752.
65. Barton, D. H. R., *Tetrahedron* **1998**, *54*, 5805-5817.
66. Merckx, M.; Kopp, D. A.; Sazinsky, M. H.; Blazyk, J. L.; Müller, J.; Lippard, S. J., *Angew. Chem. Int. Ed.* **2001**, *40*, 2782-2807.
67. Friedle, S.; Reisner, E.; Lippard, S. J., *Chem. Soc. Rev.* **2010**, *39*, 2768-2779.
68. Siewert, I.; Limberg, C., *Chem. Eur. J.* **2009**, *15*, 10316-10328.

69. Wang, X.; Wang, S.; Li, L.; Sundberg, E. B.; Gacho, G. P., *Inorg. Chem.* **2003**, *42*, 7799-7808.
70. Romakh, V. B.; Therrien, B.; Süss-Fink, G.; Shul'pin, G. B., *Inorg. Chem.* **2007**, *46*, 3166-3175.
71. Trettenhahn, G.; Nagl, M.; Neuwirth, N.; Arion, V. B.; Jary, W.; Pöchlauer, P.; Schmid, W., *Angew. Chem. Int. Ed.* **2006**, *45*, 2794-2798.
72. Roelfes, G.; Lubben, M.; Chen, K.; Ho, R. Y. N.; Meetsma, A.; Genseberger, S.; Hermant, R. M.; Hage, R.; Mandal, S. K.; Young, V. G., Jr.; Zang, Y.; Kooijman, H.; Spek, A.; Que Jr., L.; Feringa, B. L., *Inorg. Chem.* **1999**, *38*, 1929-1936.
73. Li, F.; Wang, M.; Ma, C.; Gao, A.; Chen, H.; Sun, L., *Dalton Trans.* **2006**, 2427-2434.
74. Comba, P.; Maurer, M.; Vadivelu, P., *Inorg. Chem.* **2009**, *48*, 10389-10396.
75. Tang, J.; Gamez, P.; Reedijk, J., *Dalton Trans.* **2007**, *41*, 4644-4646.
76. Talsi, E. P.; Bryliakov, K. P., *Coord. Chem. Rev.* **2012**, *256*, 1418-1434.
77. Kim, C.; Chen, K.; Kim, J.; Que Jr., L., *J. Am. Chem. Soc.* **1997**, *119*, 5964-5965.
78. Chen, K.; Que Jr., L., *J. Am. Chem. Soc.* **2001**, *123*, 6327-6337.
79. Costas, M.; Rohde, J.-U.; Stubna, A.; Ho, R. Y. N.; Quaroni, L.; Münck, E.; Que Jr., L., *J. Am. Chem. Soc.* **2001**, *123*, 12931-12932.
80. Okuno, T.; Ito, S.; Ohba, S.; Nishida, Y., *J. Chem. Soc., Dalton Trans.* **1997**, 3547-3551.
81. Britovsek, G. J. P.; England, J.; White, A. J. P., *Inorg. Chem.* **2005**, *44*, 8125-8134.
82. England, J.; Britovsek, G. J. P.; Rabadia, N.; White, A. J. P., *Inorg. Chem.* **2007**, *46*, 3752-3767.
83. Costas, M.; Que Jr., L., *Angew. Chem. Int. Ed.* **2002**, *41*, 2179-2181.
84. Company, A.; Gómez, L.; Fontrodona, X.; Ribas, X.; Costas, M., *Chem. Eur. J.* **2008**, *14*, 5727-5731.
85. Company, A.; Gómez, L.; Güell, M.; Ribas, X.; Luis, J. M.; Que Jr., L.; Costas, M., *J. Am. Chem. Soc.* **2007**, *129*, 15766-15767.
86. Mekmouche, Y.; Ménage, S.; Pécaut, J.; Lebrun, C.; Reilly, L.; Schuenemann, V.; Trautwein, A.; Fontcave, M., *Eur. J. Inorg. Chem.* **2004**, *2004*, 3163-3171.
87. Enthaler, S.; Junge, K.; Beller, M., *Angew. Chem. Int. Ed.* **2008**, *47*, 3317-3321.
88. Chen, M. S.; White, M. C., *Science* **2007**, *318*, 783-787.
89. Bigi, M. A.; Reed, S. A.; White, M. C., *J. Am. Chem. Soc.* **2012**, *134*, 9721-9726.
90. Chen, M. S.; White, M. C., *Science* **2010**, *327*, 566-571.
91. Vermeulen, N. A.; Chen, M. S.; White, M. C., *Tetrahedron* **2009**, *65*, 3078-3084.
92. Newhouse, T.; Baran, P. S., *Angew. Chem. Int. Ed.* **2011**, *50*, 3362-3374.
93. Gomez, L.; Garcia-Bosch, I.; Company, A.; J., B.-B.; Polo, A.; Sala, X.; Ribas, X.; Costas, M., *Angew. Chem. Int. Ed. Engl.* **2009**, *48*, 5720-5723.
94. Hitomi, Y.; Arakawa, K.; Funabiki, T.; Kodera, M., *Angew. Chem. Int. Ed.* **2012**, *51*, 3448-3452.
95. Roelfes, G.; Lubben, M.; Hage, R.; Que Jr., L.; Feringa, B. L., *Chem. Eur. J.* **2000**, *6*, 2152-2159.
96. Bigi, M. A.; Reed, S. A.; White, M. C., *Nat. Chem.* **2011**, *3*, 216-222.
97. Nam, W.; Ho, R. Y. N.; Valentine, J. S., *J. Am. Chem. Soc.* **1991**, *113*, 7052-7054.
98. Francis, M. B.; Jacobsen, E. N., *Angew. Chem. Int. Ed.* **1999**, *38*, 937-941.
99. White, M. C.; Doyle, A. G.; Jacobsen, E. N., *J. Am. Chem. Soc.* **2001**, *123*, 7194-7195.
100. Fujita, M.; Que Jr., L., *Adv. Synth. Catal.* **2004**, *346*, 190-194.
101. Dubois, G.; Murphy, A.; Stack, T. D. P., *Org. Lett.* **2003**, *5*, 2469-2472.
102. Marchi-Delapierre, C.; Jorge-Robin, A.; Thibon, A.; Ménage, S., *Chem. Commun.* **2007**, 1166-1168.
103. Yeung, H.-L.; Sham, K.-C.; Tsang, C.-S.; Lau, T.-C.; Kwong, H.-L., *Chem. Commun.* **2008**, 3801-3803.
104. Liu, P.; Wong, E. L.; Yuen, A. W.; Che, C., *Org. Lett.* **2008**, *10*, 3275-3278.

105. Gelalcha, F. G.; Bitterlich, B.; Anilkumar, G.; Tse, M. K.; Beller, M., *Angew. Chem. Int. Ed.* **2007**, *46*, 7293-7296.
106. Gelalcha, F. G.; Anilkumar, G.; Tse, M. K.; Brückner, A.; Beller, M., *Chem. Eur. J.* **2008**, *14*, 7687-7698.
107. Anilkumar, G.; Bitterlich, B.; Gelalcha, F. G.; Tse, M. K.; Beller, M., *Chem. Commun.* **2007**, 289-291.
108. Bitterlich, B.; Anilkumar, G.; Gelalcha, F. G.; Spilker, B.; Grotevendt, A.; Jackstell, R.; Tse, M. K.; Beller, M., *Chem. As. J.* **2007**, *2*, 521-529.
109. Bitterlich, B.; Schröder, K.; Tse, M. K.; Beller, M., *Eur. J. Org. Chem.* **2008**, 4867-4870.
110. Schröder, K.; Enthaler, S.; Join, B.; Junge, K.; Beller, M., *Adv. Synth. Catal.* **2010**, 1771 – 1778.
111. Schröder, K.; Tong, X.; Bitterlich, B.; Tse, M. K.; Gelalcha, F. G.; Brückner, A.; Beller, M., *Tetrahedron Letters* **2007**, 6339–6342.
112. Schröder, K.; Enthaler, S.; Bitterlich, B.; Schulz, T.; Spannenberg, A.; Tse, M. K.; Junge, K.; Beller, M., *Chem. Eur. J.* **2009**, *15*, 5471-5481.
113. Wu, M.; Miao, C.-X.; Wang, S.; Hu, X.; Xia, C.; Kühn, F. E.; Sun, W., *Adv. Synth. Catal.* **2011**, *353*, 3014-3022.
114. Wang, B.; Wang, S.; Xia, C.; Sun, W., *Chem. Eur. J.* **2012**, *18*, 7332-7335.
115. Lyakin, O. Y.; Ottenbacher, R. V.; Bryliakov, K. P.; Talsi, E. P., *ACS Catalysis* **2012**, *2*, 1196-1202.
116. Chen, K.; Que Jr., L., *Angew. Chem. Int. Ed.* **1999**, *38*, 2227-2229.
117. Chen, K.; Costas, M.; Kim, J.; Tipton, A. K.; Que Jr., L., *J. Am. Chem. Soc.* **2002**, *124*, 3026-3035.
118. Quiñonero, D.; Morokuma, K.; Musaev, D. G.; Mas-Balleste, R.; Que Jr., L., *J. Am. Chem. Soc.* **2005**, *127*, 6548-6549.
119. Costas, M.; Tipton, A. K.; Chen, K.; Jo, D.-H.; Que Jr., L., *J. Am. Chem. Soc.* **2001**, *123*, 6722-6723.
120. Suzuki, K.; Oldenburg, P. D.; Que Jr., L., *Angew. Chem. Int. Ed.* **2008**, *47*, 1887-1889.
121. Bautz, J.; Comba, P.; Lopez de Laorden, C.; Menzel, M.; Rajaraman, G., *Angew. Chem. Int. Ed.* **2007**, *46*, 8067-8070.
122. Klopstra, M.; Roelfes, G.; Hage, R.; Kellogg, B. H.; Feringa, B. L., *Eur. J. Inorg. Chem.* **2004**, 846-856.
123. Mas-Balleste, R.; Costas, M.; Berg, T. v. d.; Que Jr., L., *Chem. Eur. J.* **2006**, *12*, 7489-7500.
124. Feng, Y.; England, J.; Que Jr., L., *ACS Catalysis* **2011**, *1*, 1035-1042.
125. Ryu, J. Y.; Kim, J.; Costas, M.; Chen, K.; Nam, W.; Que Jr., L., *Chem. Commun.* **2002**, *12*, 1288-1289.
126. Oldenburg, P. D.; Shteinman, A. A.; Que Jr., L., *J. Am. Chem. Soc.* **2005**, *127*, 15672-15673.
127. Bruijninx, P. C. A.; Buurmans, I. L. C.; Gosiewska, S.; Moelands, M. A. H.; Lutz, M.; Spek, A. L.; van Koten, G.; Klein Gebbink, R. J. M., *Chem. Eur. J.* **2008**, *14*, 1228-1237.
128. Gosiewska, S.; Lutz, M.; Spek, A. L.; Klein Gebbink, R. J. M., *Inorganica Chimica Acta* **2007**, *360*, 405-417.
129. Oldenburg, P. D.; Ke, C.-Y.; Tipton, A. A.; Shteinman, A. A.; Que Jr., L., *Angew. Chem. Int. Ed.* **2006**, *45*, 7975-7978.
130. Buxton, G. V.; Greenstock, C. L.; Helman, W. P.; Ross, A. B.; W., T., *J. Phys. Chem. Ref. Data* **1988**, *17*, 513-886.
131. Melander, L. C. S.; Saunders, W. H. J., *Reaction Rates of Isotopic Molecules*. Wiley: New York, 1980.
132. Nesheim, J. C.; Lipscomb, J. D., *Biochemistry* **1996**, *35*, 10240-10247.
133. Barton, D. H. R.; Beck, A. H.; Taylor, D. K., *Tetrahedron* **1995**, *51*, 5245-5254.
134. Groves, J. T.; Nemo, T. E., *J. Am. Chem. Soc.* **1983**, *105*, 6243-6248.

135. Ingold, K. U.; MacFaul, P. A., Distinguishing Biomimetic Oxidations from Oxidations Mediated by Freely Diffusing Radicals. In *Biomimetic Oxidations Catalyzed by Transition Metal Complexes*, Meunier, B., Ed. Imperial College Press: London, 2000; pp 45-89.
136. Russell, G. A., *J. Am. Chem. Soc.* **1957**, *79*, 3871-3877.
137. Miyajima, S.; Simamura, O., *Bull. Chem. Soc. Jpn.* **1975**, *48*, 526-530.
138. Bernadou, J.; Meunier, B., *Chem. Commun.* **1998**, 2167-2173.
139. Lee, K. A.; Nam, W., *J. Am. Chem. Soc.* **1997**, *119*, 1916-1922.
140. Park, M. J.; Lee, J.; Suh, Y.; Kim, J.; Nam, W., *J. Am. Chem. Soc.* **2006**, *128*, 2630.
141. Zang, Y.; Elgren, T. E.; Dong, Y.; Que Jr., L., *J. Am. Chem. Soc.* **1993**, *115*, 811-813.
142. Ho, R. Y. N.; Roelfes, G.; Feringa, B. L.; Que Jr., L., *J. Am. Chem. Soc.* **1999**, *121*, 264-265.
143. Lehnert, N.; Ho, R. Y. N.; Que Jr., L.; Solomon, E. I., *J. Am. Chem. Soc.* **2001**, *123*, 8271-8290.
144. Lehnert, N.; Ho, R. Y. N.; Que Jr., L.; Solomon, E. I., *J. Am. Chem. Soc.* **2001**, *123*, 12802-12816.
145. Fujita, M.; Costas, M.; Que Jr., L., *J. Am. Chem. Soc.* **2003**, *125*, 9912-9913.
146. Chen, K.; Que Jr., L., *Chem. Commun.* **1999**, 1375-1376.
147. Leising, R. A.; Norman, R. E.; Que Jr., L., *Inorg. Chem.* **1990**, *29*, 2553-2555.
148. Shan, X. P.; Que Jr., L., *J. Inorg. Biochem.* **2006**, *100*, 421-433.
149. Bassan, A.; Blomberg, R. A. M.; Siegbahn, E. M. P.; Que Jr., L., *Chem. Eur. J.* **2005**, *11*, 692-705.
150. Bassan, A.; Blomberg, R. A. M.; Siegbahn, E. M. P.; Que Jr., L., *Angew. Chem. Int. Ed.* **2005**, *44*, 2939-2941.
151. Mas-Ballesté, R.; Fujita, M.; Hemmila, C.; Que Jr., L., *Journal of Molecular Catalysis A: Chemical* **2006**, *251*, 49-53.
152. Lim, M. H.; Rohde, J.-H.; Stubna, A.; Bukowski, M. R.; Costas, M.; Ho, R. Y. N.; Münck, E.; Nam, W.; Que Jr., L., *Proc. Acad. Sci. USA* **2003**, *100*, 3665-3670.
153. Rohde, J.-U.; In, J.-H.; Lim, M.-H.; Brennessel, W. W.; Bukowski, M. R.; Stubna, A.; Münck, E.; Nam, W.; Que Jr., L., *Science* **2003**, *229*, 1037-1039.
154. Balland, V.; Charlot, M.-F.; Banse, F.; Girerd, J.-J.; Mattioli, T. A.; Bill, E.; Bartoli, J.-F.; Battioni, P.; Mansuy, D., *Eur. J. Inorg. Chem.* **2004**, 301-308.
155. Pestovsky, O.; Stoian, S.; Bominaar, E. L.; Shan, X.; Münck, E.; Que Jr., L.; Bakac, A., *Angew. Chem. Int. Ed.* **2005**, *44*, 6871-6874.
156. Ghosh, A.; Tiago de Oliveira, F.; Yano, T.; Nishioka, T.; Beach, E. S.; Kinoshita, I.; Münck, E.; Ryabov, A. D.; Horwitz, C. P.; Collins, T. J., *J. Am. Chem. Soc.* **2005**, *127*, 2505-2513.
157. Kaizer, J.; Klinker, E. J.; Oh, N. Y.; Rohde, J.-U.; Song, W. J.; Stubna, A.; Kim, J.; Münck, E.; Nam, W.; Que Jr., L., *J. Am. Chem. Soc.* **2004**, *126*, 472-473.
158. Company, A.; Prat, I.; Frisch, J. R.; Mas-Ballesté, D. R.; Güell, M.; Juhász, G.; Ribas, X.; Münck, D. E.; Luis, J. M.; Que Jr., L.; Costas, M., *Chem. Eur. J.* **2011**, *17*, 1622-1634.
159. Oldenburg, P. D.; Feng, Y.; Pryjomska-Ray, I.; Ness, D.; Que Jr., L., *J. Am. Chem. Soc.* **2010**, 17713-17723.
160. Ye, W.; Ho, D. M.; Friedle, S.; Palluccio, T. D.; Rybak-Akimova, E. V., *Inorg. Chem.* **2012**, *51*, 5006-5021.
161. Ye, W.; Staples, R. J.; Rybak-Akimova, E. V., *J. Inorg. Biochem.* **2012**, *115*, 1-12.
162. Grapperhaus, C. A.; Mienert, B.; Bill, E.; Weyhermüller, T.; Wieghardt, K., *Inorg. Chem.* **2000**, *39*, 5306-5317.
163. Klinker, E. J.; Kaizer, J.; Brennessel, W. W.; Woodrum, N. L.; Cramer, C. J.; Que Jr., L., *Angew. Chem. Int. Ed.* **2005**, *44*, 3690-3694.
164. Bautz, J.; Bukowski, M. R.; Kerscher, M.; Stubna, A.; Comba, P.; Lienke, A.; Münck, E.; Que Jr., L., *Angew. Chem. Int. Ed.* **2006**, *45*, 5681-5684.

165. Jensen, M. P.; Costas, M.; Ho, R. Y. N.; Kaizer, J.; Münck, E.; Que Jr., L.; Rohde, J.-U.; Stubna, A., *J. Am. Chem. Soc.* **2005**, *127*, 10512-10525.
166. Nam, W., *Acc. Chem. Res.* **2007**, *40*, 522-531.
167. de Oliveira, F. T.; Chanda, A.; Banerjee, D.; Shan, X.; Mondal, S.; Que Jr., L.; Bominaar, E. L.; Münck, E.; Collins, T. J., *Science* **2007**, *315*, 835-838.
168. Chanda, A.; Popescu, D.-L.; de Oliveira, F. T.; Bominaar, E. L.; Ryabov, A. D.; Münck, E.; Collins, J. T., *J. Inorg. Biochem.* **2006**, 606-619.
169. Lyakin, O. Y.; Bryliakov, K. P.; Britovsek, G. J. P.; Talsi, E. P., *J. Am. Chem. Soc.* **2009**, *131*, 10798-10799.
170. Chow, T. W.-S.; Wong, E. L.-M.; Guo, Z.; Liu, Y.; Huang, J.-S.; Che, C.-M., *J. Am. Chem. Soc.* **2010**, *132*, 13229-13239.
171. Van Heuvelen, K. M.; Fiedler, A. T.; Shan, X.; De Hont, R. F.; Meier, K. K.; Bominaar, E. L.; Münck, E.; Que, L., *Proceedings of the National Academy of Sciences* **2012**, *109*, 11933-11938.

---

---

## **CHAPTER II.**

### **MAIN OBJECTIVES**

---

---



## II. MAIN OBJECTIVES

Metalloenzymes can perform important oxidation reactions that have not a satisfactory solution in conventional organic synthesis. One of the branches of bioinorganic chemistry is concerned with the study of these biological systems to understand their operative mechanisms, and also to take advantage of this knowledge to generate small molecule catalysts, which could be used in technological applications to generate value-added products. Towards this end, model chemistry has been applied to prepare simple synthetic systems that reproduce structural aspects or/and the function of non-heme iron dependent oxygenases. These systems have also helped to improve the comprehension of the oxidative mechanisms by which these enzymes operate and moreover, in the last years have started to show promising results in the development of catalysts for the selective oxidation of organic compounds under preparative scale.

In this context, the aim of this thesis is to apply the model chemistry approach to design iron catalytic systems bioinspired in the family of Rieske Oxygenases enzymes. One of our targets is to understand the mechanism by which the hydroxylation of alkanes and the *cis*-dihydroxylation of alkenes take place at a non-heme iron center. Previous studies point towards a high-valent oxo-iron as the catalytic active species, but no evidence has been found so far under catalytic conditions. Furthermore, we are interested in finding new catalytic systems capable of performing the oxidation of alkanes and alkenes under preparative scale conditions.

In order to accomplish these objectives we have targeted the synthesis of a family of iron complexes based on the triazacyclononane ring, covalently appended with different pyridine derivatives, which confer distinctive electronic properties to the corresponding iron complexes. These ligands incorporated different groups in the pyridine ring; H, NMe<sub>2</sub>, OMe, Me, Cl, CO<sub>2</sub>Et, NO<sub>2</sub> in  $\gamma$  position and H, CH<sub>3</sub>, Cl, F in  $\alpha$  position. Our research group has previously demonstrated that this family of complexes is active for alkane and alkene oxidation (Figure 1), and that they can support and stabilize iron and manganese species with high oxidation states.<sup>1</sup> The latter feature constitutes a key aspect in our approach as the ability of these compounds to reach high oxidation states upon reaction with peroxides is considered to be crucial for eliciting metal-based oxidation chemistry, and also for avoiding Fenton-like free

<sup>1</sup> Company, A. Ph. D. Dissertation, Universitat de Girona, Girona, **2008**



diffusing radical processes. The former will lead to selective oxidative transformations, while the latter has limited synthetic value as produces indiscriminate non-selective oxidations.

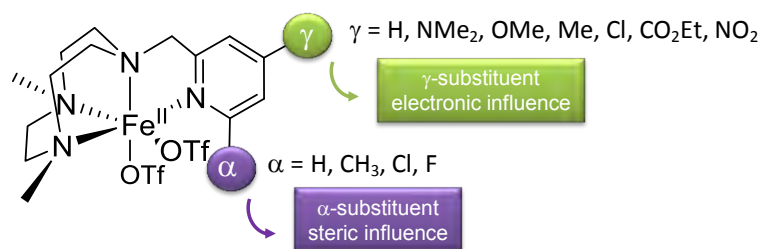


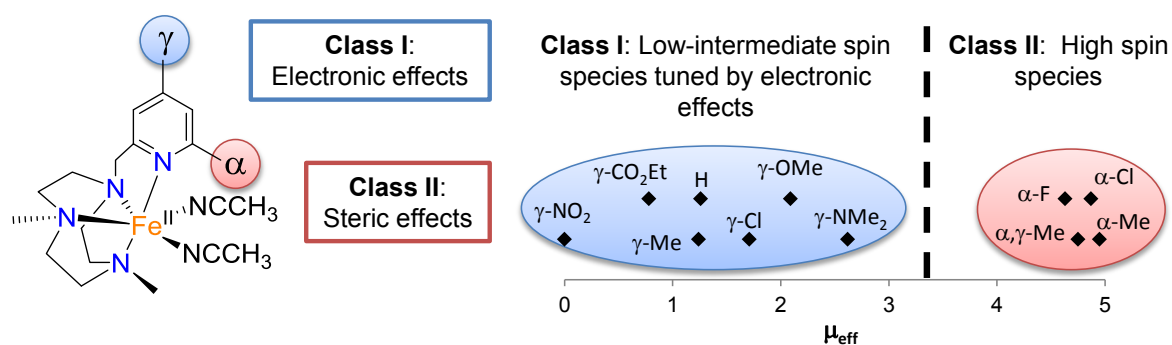
**Figure II.1.** Iron complexes employed in this thesis.

Considering these precedents the general objectives of this thesis are:

- To study the electronic properties of each complex by different spectroscopic techniques, such as UV-visible, X-ray diffraction,  $^1\text{H}$  NMR spectroscopy, magnetic susceptibility studies and measurement of the electrochemical potential ( $E_{1/2}$ ) of the  $\text{Fe}^{\text{III}}/\text{Fe}^{\text{II}}$  redox pair.
- To study their catalytic activity in the oxidations of alkanes and alkenes, using hydrogen peroxide as oxidant.
- To study the mechanisms aspects of the hydroxylation of alkanes by performing isotopic labeling experiments using  $\text{H}_2^{18}\text{O}$  and  $\text{H}_2^{18}\text{O}_2$ , product analysis and DFT calculations.
- To develop iron catalysts for alkane hydroxylation and alkene *cis*-dihydroxylation with possible application in preparative scale.
- To perform temperature controlled mass spectrometry (VT-MS) techniques in order to study metastable intermediates in the catalytic reaction, and to apply this technique to study catalytic oxidation reaction mediated by bioinspired non-heme iron complexes.

## CHAPTER III.

# ASSESSING THE IMPACT OF ELECTRONIC TUNING OF THE LIGAND IN THE SPIN STATE AND CATALYTIC OXIDATION ABILITY OF THE Fe(PYTACN) FAMILY OF COMPLEXES



This chapter corresponds to the following publications:

Irene Prat; Anna Company; Teresa Corona; Xavi Ribas; Miquel Costas. Submitted to *Inorganic Chemistry* in **2013**.

For this publication I. P. synthesis and characterize the iron(II) complexes. Besides I. P. study their catalytic activity as C-H and C=C oxidants. Finally I. P. was involved in the development of concepts and discussions, and wrote the manuscript together with M.C. and A. C. Contribution is approximately 70%.

# Assessing the Impact of Electronic Tuning of the Ligand in the Spin State and Catalytic Oxidation Ability of the Fe<sup>II</sup>(Pytacn) Family of Complexes

Irene Prat, Anna Company,\* Teresa Corona, Xavi Ribas, Miquel Costas\*

Departament de Química. Universitat de Girona. Campus Montilivi, E17071 Girona, Catalonia (Spain).

anna.company@udg.edu, miquel.costas@udg.edu

Received: ((will be filled in by the editorial staff))

**Abstract.** A family of iron complexes with general formula  $[\text{Fe}^{\text{II}}(\text{R,R}'\text{Pytacn})(\text{X})_2]^{n+}$  is described, where  $\text{R,R}'\text{Pytacn}$  is the tetradentate ligand 1-[(4-R'-6-R-2-pyridyl)methyl]-4,7-dimethyl-1,4,7-triazacyclononane, R (R = H, Me, F, Cl) refers to the group at the position  $\alpha$  of the pyridine, R' (R' = H, NMe<sub>2</sub>, OMe, Me, Cl, CO<sub>2</sub>Et, NO<sub>2</sub>) corresponds to the group at position  $\gamma$  and X denotes Cl, CH<sub>3</sub>CN or CF<sub>3</sub>SO<sub>3</sub> (OTf). Herein, we study the influence of the pyridine substituents R and R' in the electronic properties of the coordinated iron center, by a combination of structural, spectroscopic and electrochemical characterization using X-ray diffraction, <sup>1</sup>H NMR spectroscopy, UV-vis spectroscopy, cyclic voltammetry and magnetic susceptibility measurements (Evans' method). The electronic properties of the substituent in the  $\gamma$  position of the pyridine ring (R') finely tune the electronic richness of the metal center as ascertained by the  $E_{1/2}(\text{Fe}(\text{III})/\text{Fe}(\text{II}))$  redox potential and also modulate the strength of the ligand field, as shown by magnetic susceptibility measurements in CD<sub>3</sub>CN solution, which provide a direct indication of the population of the magnetically active high-spin S = 2 ferrous state. The series of complexes  $[\text{Fe}^{\text{II}}(\text{H,R}'\text{Pytacn})(\text{CD}_3\text{CN})_2]^{2+}$  exist in d<sub>3</sub>-acetonitrile solutions as mixtures of high-spin S = 2 and low-spin S = 0 complexes.

A direct correlation between the electron-releasing ability of R' and the effective magnetic moment is shown for this series of complexes, which is attributed to the tuning of the  $\pi$ -acceptor character of the pyridine ligand. On the other hand, the substitution of the hydrogen atom in the  $\alpha$  position of the pyridine by a methyl, chlorine or fluorine group influences the spin state of the iron center in favor of the high-spin S = 2 state. Crystallographic characterization of  $[\text{Fe}^{\text{II}}(\text{Me,H}\text{Pytacn})(\text{CH}_3\text{CN})_2](\text{SbF}_6)_2$  shows that the complex contains a low-spin iron center at 100 K but it becomes high-spin at 300 K. The whole family of complexes has been assayed in catalytic C-H and C=C oxidation reactions with H<sub>2</sub>O<sub>2</sub>, in order to evaluate how the electronic/steric properties of the ligand translate into their catalytic activity. These catalysts exhibit excellent efficiency in the stereospecific hydroxylation of alkanes and in the oxidation of olefins. Remarkably, R' substituents have little influence in the efficiency and chemoselectivity of the catalytic activity of the complexes, but the selectivity towards olefin *cis*-dihydroxylation is enhanced for complexes with R = Me, F or Cl. Isotopic labeling studies in the epoxidation and *cis*-dihydroxylation reactions show that R has a definitive role in dictating the origin of the oxygen atom that is transferred in the epoxidation reaction.

## Introduction

There is a growing interest in the development of transition metal complexes that can catalyze the selective oxidation of C-H and C=C bonds using green oxidants such as O<sub>2</sub> or peroxides with novel and better selectivities and efficiencies than traditional less sustainable methodologies.<sup>1</sup> In this regard, iron is a particularly attractive metal for catalyst development because of its high availability and lack of toxicity.<sup>2</sup> Since several highly selective oxygenases contain iron in their active site,<sup>3,4</sup> nature constitutes a

source of inspiration for the design of such iron oxidation catalysts.<sup>5,6</sup> For example, Rieske oxygenases are enzymes that bear a mononuclear non-heme iron center in its active center and they use O<sub>2</sub> to catalyze the hydroxylation of alkanes and the *cis*-dihydroxylation of arenes, in the first step of the degradation of persistent pollutants.<sup>7</sup>

Taking into consideration the ability of mononuclear iron sites to mediate oxidation reactions in a selective manner, several families of bioinspired mononuclear non-heme iron complexes have been developed and tested during the last decade in the challenging oxidation of C-H and C=C bonds,<sup>8-10</sup> and

selected families have proved to be capable of eliciting enzyme-like reactivity, meaning that they can mediate oxidations through metal-centered processes without a significant involvement of free diffusing radicals.<sup>5</sup> Such studies have shown that the activity of these complexes as oxidation catalysts depends in a very delicate manner on a number of aspects. Some of them are rather obvious such as metal nuclearity, ligand denticity, strength of metal binding, presence of available coordination sites, nature of the ligand donor set or the oxidatively robust nature of the ligand. However, other subtler aspects have been identified, which include ligand field and coordination topology.<sup>10,11-14</sup> Presumably, interconnections among multiple aspects exist and this complexity makes structure-activity correlations not straightforward.

Most iron complexes that carry out selective C-H and C=C oxidation reactions share some structural features that include i) exchangeable coordination sites that can engage in fast substitution reactions with the oxidant, and ii) ligand sets that can support iron centers in high oxidation states. Because of that, electronic factors that influence the lability of the complexes and the redox properties of the iron centers might have a significant impact on the catalytic activity. Electronic properties of the iron center can be modulated by the electron-donating ability of the ligand, but also by the strength of the ligand field, as this directly determines the spin state. Spin state is also at the basis of the lability of the complexes, since high-spin complexes are inherently faster than their low-spin analogues in substitution reactions.

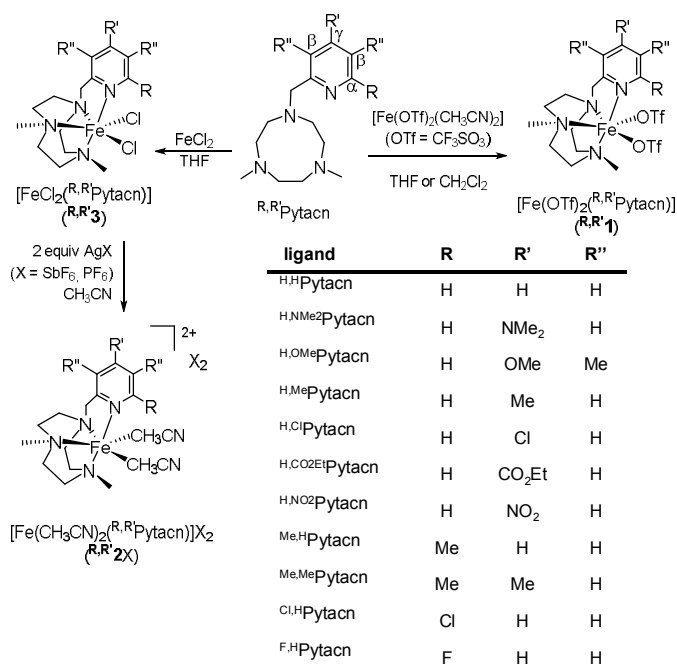
We have recently reported a family of iron complexes containing tetradentate ligands based on a 1,4,7-triazacyclononane ring derivatized with a methylpyridine ring. Complexes  $[\text{Fe}(\text{CF}_3\text{SO}_3)_2(\text{H,H-Pytacn})]$  (**H,H1**) and  $[\text{Fe}(\text{CF}_3\text{SO}_3)_2(\text{Me,H-Pytacn})]$  (**Me,H1**) (Scheme 1) exhibit efficient catalytic activity in the stereospecific hydroxylation of alkanes and the epoxidation and *cis*-dihydroxylation of alkenes using  $\text{H}_2\text{O}_2$  as oxidant.<sup>15</sup> As ascertained by several mechanistic probes, these oxidative transformations occur through the mediation of a high-valent iron-oxo species.<sup>15,16</sup> Moreover, compound **H,H1** is highly active in the oxidation of water to generate  $\text{O}_2$  using cerium as the sacrificial oxidizing reagent, in a process that mimics what occurs in photosystem II (PS II).<sup>17</sup>

In this work, the basic structure of **H,H1** has been modified by introducing a range of substituents in the  $\alpha$  and  $\gamma$  positions of the pyridine ring with different electronic and steric properties. We aim at evaluating the influence of these substituents in the electronic structure, as well as in the spectroscopic and structural features of the resulting iron(II) compounds by means of several spectroscopic techniques both in the solid state and in solution. Herein, we show how the straightforward substitution of the pyridine ring of the primary Pytacn structure leads to important modifications in the electronic properties of the iron(II) center, which in some cases is translated into

substantial changes in the spin crossover properties of the metal site. In order to evaluate how the substitution in the pyridine ring affects the catalytic activity of the resulting iron complexes, we have studied their catalytic performance in the oxidation of cyclohexane and cyclooctene, which constitute model substrates for C-H hydroxylation and C=C oxidation reactions, respectively.

## Results and Discussion

**Synthesis of ligands and complexes.** A family of tetradentate ligands ( $\text{R,R}'\text{Pytacn}$ , Scheme 1), which contains a triazacyclononane ring functionalized with different methylpyridine derivatives with distinctive electronic and steric properties, has been prepared. These ligands constitute an extension of the previously described  $\text{H,H-Pytacn}$  ligand, whose iron<sup>15,16,17</sup> and manganese<sup>18</sup> complexes were reported as robust and efficient oxidation catalysts. The introduction of several  $\text{R}'$  groups with different electronic properties in the  $\gamma$  position of the pyridine heterocycle ( $\text{R}' = \text{NMe}_2, \text{OMe}, \text{Me}, \text{H}, \text{Cl}, \text{CO}_2\text{Et}, \text{NO}_2$ ) is aimed at studying putative electronic effects without interference caused by steric effects. Instead, modification of the  $\alpha$  position of the pyridine ring ( $\text{R} = \text{H}, \text{Me}, \text{F}, \text{Cl}$ ) not only affects the electronic properties but also enables to tune the steric crowding around the iron metal site (Scheme 1).



**Scheme 1.** Ligands and complexes employed in this work.

Ligands  $\text{R,R}'\text{Pytacn}$  were prepared by alkylation of 1,4-dimethyl-1,4,7-triazacyclononane with the corresponding substituted picolyl chloride arm in acetonitrile, and they were obtained as pale yellow oils in good yields (67 – 73%) (see Supporting Information for a full description of the synthesis of ligands).

Reaction of the tetradentate  $^{R,R'}$ Pytacn ligands with  $[\text{Fe}(\text{OTf})_2(\text{CH}_3\text{CN})_2]$  ( $\text{OTf}^- =$  trifluoromethanesulfonate anion) in THF or  $\text{CH}_2\text{Cl}_2$  under anaerobic conditions afforded the desired bis-triflate complexes,  $[\text{Fe}(\text{OTf})_2(^{R,R'}\text{Pytacn})]$  ( $^{R,R'}\mathbf{1}$ ). Reaction in THF caused the direct precipitation of the compounds from the reaction solution. Slow diffusion of diethyl ether over saturated  $\text{CH}_2\text{Cl}_2$  solutions afforded  $^{R,R'}\mathbf{1}$  as crystalline materials in 63-73% yields (Scheme 1).  $[\text{FeCl}_2(^{R,R'}\text{Pytacn})]$  compounds ( $^{R,R'}\mathbf{3}$ ) were also prepared by reaction of  $\text{FeCl}_2$  and  $^{R,R'}$ Pytacn in THF giving analytically pure powders which were recrystallized from slow diethyl ether diffusion into saturated acetonitrile solutions. Following the synthetic procedure previously described for the preparation of  $[\text{Fe}(\text{CH}_3\text{CN})_2(^{H,H}\text{Pytacn})](\text{PF}_6)_2$  ( $^{H,H}\mathbf{2PF}_6$ )<sup>15</sup>,  $^{H,H}\mathbf{2SbF}_6$  and  $^{Me,H}\mathbf{2SbF}_6$  were synthesized by reaction of  $^{H,H}\mathbf{3}$  or  $^{Me,H}\mathbf{3}$  with 2 equiv  $\text{AgSbF}_6$  in acetonitrile. Subsequent removal of the precipitated  $\text{AgCl}$  and slow diethyl ether diffusion over the resulting solutions afforded the desired complexes as crystalline solids.

**Solid state characterization.** The solid state molecular structure of complexes  $^{R,R'}\mathbf{1}$  could be established by X-ray diffraction analysis. The crystal structures of  $^{H,H}\mathbf{1}$ ,  $[\text{Fe}^\text{II}(\text{H}_2\text{O})_2(^{Me,H}\text{Pytacn})](\text{OTf})_2$  and  $^{H,H}\mathbf{2PF}_6$  have been previously reported,<sup>15</sup> while the structures of  $^{H,NMe_2}\mathbf{1}$ ,  $^{H,OMe}\mathbf{1}$ ,  $^{H,Me}\mathbf{1}$ ,  $^{H,Cl}\mathbf{1}$ ,  $^{H,CO_2Et}\mathbf{1}$ ,  $^{H,NO_2}\mathbf{1}$ ,  $^{Me,Me}\mathbf{1}$ ,  $^{Cl,H}\mathbf{1}$  and  $^{F,H}\mathbf{1}$  are described for the first time in the present work. Compound  $^{Me,H}\mathbf{1}$  crystallizes out as very thin needles not suitable for X-ray diffraction. Instead, the corresponding bis-acetonitrile complex  $^{Me,H}\mathbf{2SbF}_6$  forms colorless rectangles which could be measured by X-ray diffraction at different temperatures (from 100K to 300K) showing a spin transition in the solid state (*vide infra*).

As representative examples of the bis-triflate complexes, the X-ray structures of complexes  $^{F,H}\mathbf{1}$ ,  $^{H,NO_2}\mathbf{1}$ ,  $^{H,NMe_2}\mathbf{1}$  and  $^{Me,Me}\mathbf{1}$  are depicted in Figure 1, experimental details of their crystal structure determination are collected in Table 1 and a list of selected bond can be found in Table 2. The structure of  $^{H,NMe_2}\mathbf{1}$  is of poor quality, precluding detailed discussion of its metrical parameters. The same information for  $^{Cl,H}\mathbf{1}$ ,  $^{H,Me}\mathbf{1}$ ,  $^{H,Cl}\mathbf{1}$ ,  $^{H,CO_2Et}\mathbf{1}$  and  $^{H,OMe}\mathbf{1}$  is found in the supporting information (Tables S1-S4 and Figures S1-S2). These complexes crystallize in the monoclinic or orthorhombic crystal system and they contain an iron(II) center in a distorted octahedral coordination geometry. Four coordination sites are occupied by the nitrogen atoms of the ligands, being the three N atoms of the triazacyclononane (tacn) macrocycle bound facially. That leaves two coordination sites in a relative *cis* configuration that are accessible for binding to triflate anions. The pyridine arm binds *trans* to one of the N-methyl groups of the ligand and the other two nitrogen atoms of the tacn ligand are *trans* to the triflate ligands. Average Fe-N bond distances for these complexes range between 2.1 and 2.2 Å, characteristic of high spin  $\text{Fe}^\text{II}$  complexes.<sup>19-23</sup>

Despite the similarities in the structure for the whole range of bis-triflate complexes  $^{R,R'}\mathbf{1}$ , some systematic differences arise when analyzed in more detail. The Fe-N<sub>py</sub> bond length changes systematically depending on the substitution in the  $\alpha$  position of the pyridine ring: this value is 2.21 Å in  $^{Me,Me}\mathbf{1}$  (one methyl group in the  $\alpha$  position of the pyridine), 2.26 Å in  $^{Cl,H}\mathbf{1}$  (a chlorine atom in the  $\alpha$  position), 2.20 Å in  $^{F,H}\mathbf{1}$  (a fluorine atom in the  $\alpha$  position) and decreases down to  $2.15 \pm 0.02$  Å in  $^{H,R'}\mathbf{1}$  (no substituent in the  $\alpha$  position of the pyridine ring).

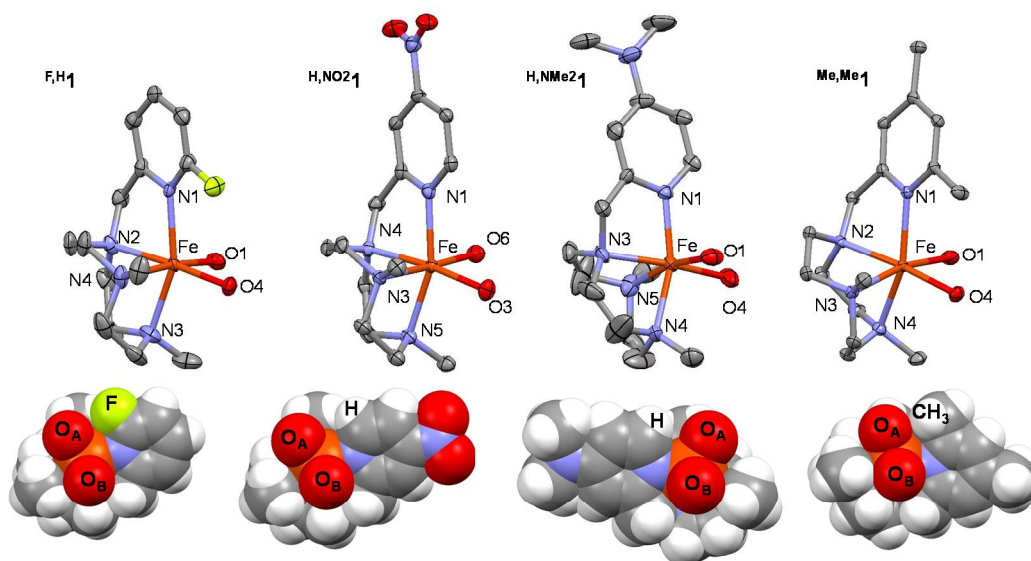


**Figure 1.** Top: X-Ray structures of  $^{F,H}\mathbf{1}$ ,  $^{H,NO_2}\mathbf{1}$ ,  $^{H,NMe_2}\mathbf{1}$  and  $^{Me,Me}\mathbf{1}$ . Hydrogen atoms and triflate groups have been omitted for clarity except for the oxygen atoms directly bound to the iron center, which are represented. Bottom: Space filling diagrams for complexes  $^{F,H}\mathbf{1}$ ,  $^{H,NO_2}\mathbf{1}$ ,  $^{H,NMe_2}\mathbf{1}$  and  $^{Me,Me}\mathbf{1}$ . Triflate groups have been omitted for clarity but the oxygen atoms directly bound to the iron center are represented.

This observation strongly suggests that the bulkiness of the substituent in the  $\alpha$  position of the pyridine ring has a significant and systematic influence on the Fe-N<sub>py</sub> distance, being longer for bulkier substituted pyridines. Substitution in the  $\gamma$  position of the pyridine only provides slight changes in the Fe-N<sub>py</sub> bond. For example, complexes with

electron-donating  $\gamma$  substituents (<sup>H,OMe</sup>**1**, and the same applies to <sup>H,NMe2</sup>**1** although in this case the quality of the structure requires caution) present a shortened Fe-N<sub>py</sub> bond around 2.14 Å, which contrasts with the longer bond of 2.17 Å found for complexes with electron-withdrawing groups (<sup>H,NO2</sup>**1** and <sup>H,CO2Et</sup>**1** with a nitro and an ester group respectively).

**Table 1.** Crystal data for <sup>F,H</sup>**1**, <sup>H,NO2</sup>**1**, <sup>H,NMe2</sup>**1** and <sup>Me,Me</sup>**1**.

	<sup>F,H</sup> <b>1</b>	<sup>H,NO2</sup> <b>1</b>	<sup>H,NMe2</sup> <b>1</b>	<sup>Me,Me</sup> <b>1</b>
Empirical formula	C <sub>16</sub> H <sub>23</sub> F <sub>7</sub> FeN <sub>4</sub> O <sub>6</sub> S <sub>2</sub>	C <sub>16</sub> H <sub>23</sub> F <sub>6</sub> FeN <sub>5</sub> O <sub>8</sub> S <sub>2</sub>	C <sub>18</sub> H <sub>29</sub> F <sub>6</sub> FeN <sub>5</sub> O <sub>6</sub> S <sub>2</sub>	C <sub>18</sub> H <sub>28</sub> F <sub>6</sub> FeN <sub>4</sub> O <sub>6</sub> S <sub>2</sub>
Formula weight	620.35	647.36	645.43	630.41
Temperature	100(2) K	100(2) K	300(2) K	100(2) K
Wavelength	0.71073 Å	0.71073 Å	0.71073 Å	0.71073 Å
Crystal system	Monoclinic	Monoclinic	Monoclinic	Orthorhombic
Space group	P 21/c	P 21/c	P 21/c	P2 <sub>1</sub> 2 <sub>1</sub> 2 <sub>1</sub>
Unit cell dimensions	a = 15.926 (4) Å $\alpha$ = 90° b = 9.434(2) Å $\beta$ = 115.519 (4)° c = 17.376(4) Å $\gamma$ = 90.00°	a = 9.431(11) Å $\alpha$ = 90° b = 14.173(18) Å $\beta$ = 95.27(2)° c = 17.400(2) Å $\gamma$ = 90.00°	a = 8.844(8) Å $\alpha$ = 90° b = 25.11(9) Å $\beta$ = 122.84(4)° c = 14.904(11) Å $\gamma$ = 90°	a = 8.8046(14) Å $\alpha$ = 90.00° b = 13.591(2) Å $\beta$ = 90.00° c = 21.920(3) Å $\gamma$ = 90.00°
Volume	2356.0(9) Å <sup>3</sup>	2407(5) Å <sup>3</sup>	2781(4) Å <sup>3</sup>	2622.9(7) Å <sup>3</sup>
Density (calculated)	1.749 g·cm <sup>-3</sup>	1.787 g·cm <sup>-3</sup>	1.542 g·cm <sup>-3</sup>	1.596 g·cm <sup>-3</sup>
Absorption coefficient	0.914 mm <sup>-1</sup>	0.901 mm <sup>-1</sup>	0.774 mm <sup>-1</sup>	0.818 mm <sup>-1</sup>
F(000)	1264	1320	1328	1296
Cell formula units_Z	4	4	4	4
Crystal size	0.6 x 0.1 x 0.07 mm	0.25 x 0.15 x 0.08 mm	0.3 x 0.3 x 0.25 mm	0.3 x 0.2 x 0.15 mm
$\Theta$ range for data collection	2.36 to 28.52°	2.25 to 28.68°	2.30 to 28.53°	2.39 to 28.34°
Limiting indices	-21<=h<=21 -12<=k<=12 -22<=l<=22	-12<=h<=11 -19<=k<=19 -23<=l<=22	-11<=h<=10, -31<=k<=33, -11<=l<=19	-11<=h<=11 -18<=k<=18 -29<=l<=29
Reflections collected	5817	25838	15558	40513
Independent reflections	34373 [R(int) = 0.0752]	5912 [R(int) = 0.0849]	6363 [R(int) = 0.3131]	6504 [R(int) = 0.0327]
Completeness to $\Theta$	97.1% ( $\Theta$ = 28.52°)	95.2% ( $\Theta$ = 28.68°)	90.1% ( $\Theta$ = 28.53°)	99.8% ( $\Theta$ = 28.34°)
Refinement method	Full-matrix least-squares on F <sup>2</sup>	Full-matrix least-squares on F <sup>2</sup>	Full-matrix least-squares on F <sup>2</sup>	Full-matrix least-squares on F <sup>2</sup>
Data/restraints/parameters	5817 / 0 / 327	5912 / 0 / 345	6363 / 4 / 331	6504 / 0 / 339
Goodness-of-fit on F <sup>2</sup>	1.024	1.072	0.895	1.034
Final R indices [I>2 $\sigma$ (I)]	R1 = 0.0591 wR2 = 0.1498	R1 = 0.0593 wR2 = 0.1467	R1 = 0.1328 wR2 = 0.3054	R1 = 0.0226 wR2 = 0.0554
R indices (all data)	R1 = 0.1133 wR2 = 0.1764	R1 = 0.0942 wR2 = 0.1603	R1 = 0.4161 wR2 = 0.4414	R1 = 0.0254 wR2 = 0.0565
Largest diff. peak and hole	1.750 and -0.701 e. Å <sup>-3</sup>	0.817 and -0.625 e. Å <sup>-3</sup>	0.603 and -0.546 e. Å <sup>-3</sup>	0.361 and -0.207 e. Å <sup>-3</sup>

**Table 2.** Selected bond lengths (Å) and angles (°) for  $\text{F}_2\text{H}_2$ ,  $\text{H}_2\text{NO}_2$ ,  $\text{H}_2\text{NMe}_2$  and  $\text{Me}_2\text{Me}_2$ .

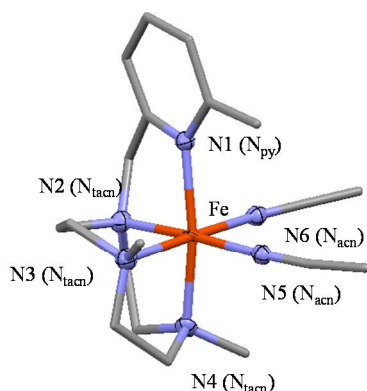
$\text{F}_2\text{H}_2$		$\text{H}_2\text{NO}_2$		$\text{H}_2\text{NMe}_2$		$\text{Me}_2\text{Me}_2$	
Fe-N1	2.196(4)	Fe1-N1	2.167(4)	Fe-N1	2.137(8)	Fe-N1	2.2112(13)
Fe-N2	2.201(4)	Fe1-N4	2.185(4)	Fe-N3	2.187(3)	Fe-N2	2.1720(13)
Fe-N3	2.218(4)	Fe1-N5	2.198(4)	Fe-N4	2.208(13)	Fe-N3	2.2419(13)
Fe-N4	2.211(4)	Fe1-N3	2.202(4)	Fe-N5	2.212(15)	Fe-N4	2.2247(13)
Fe-O2	2.043(3)	Fe1-O3	2.025(3)	Fe-O1	2.176(11)	Fe-O1	2.1910(12)
Fe-O4	2.149(3)	Fe1-O6	2.125(4)	Fe-O4	2.069(12)	Fe-O4	2.0513(11)
N1-Fe-N2	76.11(13)	N1-Fe1-N4	77.10(15)	N1-Fe-N3	78.7(4)	N1-Fe-N2	76.37(5)
N1-Fe-N4	92.43(15)	N4-Fe1-N5	80.70(16)	N1-Fe-N4	156.8(5)	N1-Fe-N3	107.38(5)
N1-Fe-O4	95.24(13)	N1-Fe1-O3	109.47(16)	N1-Fe-O4	98.4(5)	N1-Fe-O1	86.36(5)
N1-Fe-O1	106.49(13)	N1-Fe-O6	84.55(16)	N1-Fe-O1	88.6(4)	N1-Fe-O4	107.11(5)
N4-Fe-N2	79.99(14)	N4-Fe1-N3	81.04(14)	N5-Fe-N3	79.1(5)	N2-Fe-N4	80.28(5)
N4-Fe-N3	80.53(16)	N5-Fe1-N3	80.93(14)	N5-Fe-N4	82.2(6)	N3-Fe-N4	79.52(5)
N2-Fe-O4	92.66(14)	N4-Fe1-O6	93.44(15)	N5-Fe-O4	89.6(5)	N4-Fe-O1	86.81(5)
N4-Fe-O1	96.29(14)	N5-Fe1-O3	92.71(16)	N5-Fe-O1	168.7(6)	N4-Fe-O4	97.19(5)
N3-Fe-O1	96.35(15)	N5-Fe1-O6	97.84(14)	N3-Fe-O1	102.5(5)	N2-Fe-O1	100.62(5)
N2-Fe-N3	80.82(16)	N1-Fe1-N3	94.55(16)	N3-Fe-N4	80.0(5)	N2-Fe-N3	80.36(5)
N3-Fe-O4	88.74(14)	N3-Fe1-O3	96.75(15)	N4-Fe-O4	98.4(5)	N3-Fe-O4	93.84(5)
O4-Fe-O1	90.60(13)	O3-Fe1-O6	88.69(15)	O4-Fe-O1	88.6(5)	O1-Fe-O4	84.61(5)

**Table 3.** Crystal data for  $\text{Me}_2\text{H}_2\text{SbF}_6$  at 100K, 150K, 170K and 300K.

	$\text{Me}_2\text{H}_2\text{SbF}_6$ (100 K)	$\text{Me}_2\text{H}_2\text{SbF}_6$ (150 K)	$\text{Me}_2\text{H}_2\text{SbF}_6$ (170 K)	$\text{Me}_2\text{H}_2\text{SbF}_6$ (300 K)
Empirical formula	$\text{C}_{19}\text{H}_{32}\text{F}_{12}\text{FeN}_6\text{Sb}_2$	$\text{C}_{19}\text{H}_{32}\text{F}_{12}\text{FeN}_6\text{Sb}_2$	$\text{C}_{19}\text{H}_{32}\text{F}_{12}\text{FeN}_6\text{Sb}_2$	$\text{C}_{19}\text{H}_{32}\text{F}_{12}\text{FeN}_6\text{Sb}_2$
Formula weight	871.86	871.86	871.86	871.86
Temperature	100(2) K	150(2) K	170(2) K	300(2) K
Wavelength	0.71073 Å	0.71073 Å	0.71073 Å	0.71073 Å
Crystal system	Monoclinic	Monoclinic	Monoclinic	Monoclinic
Space group	Cc	Cc	Cc	Cc
Unit cell dimensions	a = 23.074(3) Å $\alpha = 90^\circ$ b = 31.986(3) Å $\beta = 134.383(5)^\circ$ c = 16.3798(15) Å $\gamma = 90^\circ$	a = 23.096(12) Å $\alpha = 90^\circ$ b = 32.049(17) Å $\beta = 134.519(7)^\circ$ c = 16.459(15) Å $\gamma = 90^\circ$	a = 23.436(18) Å $\alpha = 90^\circ$ b = 32.68(3) Å $\beta = 134.354(9)^\circ$ c = 16.695(13) Å $\gamma = 90^\circ$	a = 23.482(5) Å $\alpha = 90^\circ$ b = 32.849(7) Å $\beta = 133.833(3)^\circ$ c = 16.639(4) Å $\gamma = 90^\circ$
Volume	8639.7(14) Å <sup>3</sup>	8687(10) Å <sup>3</sup>	9142(12) Å <sup>3</sup>	9258 Å <sup>3</sup>
Density (calculated)	2.011 g·cm <sup>-3</sup>	2.000 g·cm <sup>-3</sup>	1.900 g·cm <sup>-3</sup>	1.876 g·cm <sup>-3</sup>
Absorption coefficient	2.459 mm <sup>-1</sup>	2.446 mm <sup>-1</sup>	2.324 mm <sup>-1</sup>	2.295 mm <sup>-1</sup>
F(000)	5088	5088	5088	5088
Cell formula units_Z	12	12	12	12
Crystal size	0.3 x 0.1 x 0.1 mm	0.3 x 0.1 x 0.1 mm	0.3 x 0.1 x 0.1 mm	0.3 x 0.1 x 0.1 mm
$\Theta$ range for data collection	2.16 to 28.28°	2.17 to 29.89°	2.11 to 28.31°	2.10 to 28.28°
Limiting indices	-27<=h<=27 -42<=k<=42 -7<=l<=7	-27<=h<=30 -43<=k<=42 -22<=l<=21	-31<=h<=30 -43<=k<=43 -22<=l<=22	-31<=h<=31 -43<=k<=43 -22<=l<=22
Reflections collected	31586	32066	52076	72488
Independent reflections	9426 [R(int) = 0.0262]	14887 [R(int) = 0.0659]	21952 [R(int) = 0.0862]	22556 [R(int) = 0.0412]
Completeness to $\Theta$	50 %	50 %	98.2 %	50%
Refinement method	Full-matrix least-squares on F <sup>2</sup>	Full-matrix least-squares on F <sup>2</sup>	Full-matrix least-squares on F <sup>2</sup>	Full-matrix least-squares on F <sup>2</sup>
Data/restraints/parameters	9426 / 344 / 1097	14887 / 2 / 1085	21952 / 2 / 1084	22556 / 2 / 1085
Goodness-of-fit on F <sup>2</sup>	1.074	1.036	0.990	1.016
Final R indices [I>2 $\sigma$ (I)]	R1 = 0.0337 wR2 = 0.0810	R1 = 0.0505 wR2 = 0.1272	R1 = 0.0629 wR2 = 0.1388	R1 = 0.0570 wR2 = 0.1488
R indices (all data)	R1 = 0.0345 wR2 = 0.350 (18)	R1 = 0.1407 wR2 = 0.1629	R1 = 0.0971 wR2 = 0.1597	R1 = 0.0766 wR2 = 0.1660
Largest diff. peak and hole	1.721 and -0.719 e. Å <sup>-3</sup>	3.864 and -3.292 e. Å <sup>-3</sup>	1.846 and -0.848 e. Å <sup>-3</sup>	1.710 and -0.586 e. Å <sup>-3</sup>

As previously reported,<sup>15</sup> the X-ray structure of the dark red compound  $\text{Me}_2\text{H}_2\text{PF}_6$  is characteristic of a low-spin (LS) iron(II) center as evidenced by the short Fe-N distances at around 2.0 Å.<sup>19-21,22-24</sup> The situation is different for the bis-acetonitrile complex  $\text{Me}_2\text{H}_2\text{SbF}_6$ , which structure was solved at 300 K, 170 K, 150 K and 100 K because an evident and reversible change in color from colorless to dark blue was observed upon cooling the crystal sample. Figure 2 shows a representation of the X-ray structure of  $\text{Me}_2\text{H}_2\text{SbF}_6$ , Table 3 collects the experimental details of the crystal structure determination and a list of selected bond distances can be found in Table 4. The unit cell of the structure contains three cationic  $[\text{Fe}(\text{Me}_2\text{H}_2\text{Pytacn})(\text{CH}_3\text{CN})_2]^{2+}$  molecules (A, B and C), slightly differing in their metrical parameters. The coordination geometry of this complex is the same as in the parent triflate analogues and it will not be described further. The X-ray structure at 300 K presents  $\text{Fe}^{\text{II}}$  centers with an average Fe-N distance of 2.20 Å, indicative of a high-spin (HS) electronic configuration (Figure 2).<sup>20,21,24</sup> A significant

contraction of the unit cell occurs upon cooling from 300 K to 100 K. It corresponds to a decrease of ~ 5% of the unit-cell volume (from 9258 Å<sup>3</sup> to 8640 Å<sup>3</sup>). This is accompanied by a contraction of the coordination sphere, so that the average Fe-N distance at 100K becomes 2.02 Å, a value typical of a low-spin (LS)  $\text{Fe}^{\text{II}}$  center (Table 4).<sup>20,21,24</sup> This contraction in bond distances is indicative of a spin transition in the solid state from high (300 K) to low-spin (100 K).<sup>25</sup> Interestingly, a close analysis of the structures at 150 K and 170 K shows that spin crossover is stepwise. This is best illustrated in the Fe-N<sub>acn</sub> distances (acn = acetonitrile); at 170 K the three complexes in the unit cell exhibit an average Fe-N<sub>acn</sub> distance of 2.13±0.04 Å, indicative of a HS configuration, but at 150 K two of the molecules exhibit a shorter Fe-N<sub>acn</sub> distance of 1.97±0.01 Å, characteristic of a LS configuration. Spin crossover of the third molecule occurs between 150 K and 100 K, and at the latter temperature the three molecules exhibit short Fe-N<sub>acn</sub> distances of 1.95 ± 0.02 Å.



T (K)	Structures	Fe-N <sub>py</sub>	Fe-N <sub>acn</sub>	Fe-N <sub>acn</sub>
100	A	2.060	2.039	1.944
	B	2.099	2.045	1.971
	C	2.028	2.032	1.946
150	A	2.127	2.072	1.981
	B	2.076	2.039	1.964
	C	2.125	2.139	2.084
170	A	2.194	2.182	2.133
	B	2.129	2.133	2.085
	C	2.201	2.221	2.165
300	A	2.251	2.213	2.191
	B	2.191	2.211	2.176
	C	2.175	2.201	2.178

**Figure 2.** X-Ray structure of  $\text{Me}_2\text{H}_2\text{SbF}_6$  at 100K. The table shows the Fe-N<sub>py</sub>, the average Fe-N<sub>acn</sub> and the average Fe-N<sub>acn</sub> bond lengths for each of the three molecules (A, B and C) that form the unit cell at a given temperature (100 K, 150 K, 170 K and 300 K). Hydrogen atoms have been omitted for clarity.

**Table 4.** Selected bond lengths (Å) for  $\text{Me}_2\text{H}_2\text{SbF}_6$  at 100K, 150K, 170K and 300K.

$\text{Me}_2\text{H}_2\text{SbF}_6$ (100 K)		$\text{Me}_2\text{H}_2\text{SbF}_6$ (150 K)		$\text{Me}_2\text{H}_2\text{SbF}_6$ (170 K)		$\text{Me}_2\text{H}_2\text{SbF}_6$ (300K)	
Fe(A)-N(1A)	2.060(9)	Fe(A)-N(1A)	2.127(10)	Fe(A)-N(1A)	2.194(8)	Fe(A)-N(1A)	2.251(6)
Fe(A)-N(2A)	2.000(7)	Fe(A)-N(2A)	2.028(9)	Fe(A)-N(2A)	2.161(8)	Fe(A)-N(2A)	2.179(6)
Fe(A)-N(3A)	2.058(8)	Fe(A)-N(3A)	2.097(9)	Fe(A)-N(3A)	2.175(8)	Fe(A)-N(3A)	2.213(6)
Fe(A)-N(4A)	2.060(9)	Fe(A)-N(4A)	2.090(10)	Fe(A)-N(4A)	2.210(8)	Fe(A)-N(4A)	2.248(6)
Fe(A)-N(5A)	1.948(9)	Fe(A)-N(5A)	1.984(9)	Fe(A)-N(5A)	2.119(9)	Fe(A)-N(5A)	2.188(6)
Fe(A)-N(6A)	1.940(7)	Fe(A)-N(6A)	1.977(10)	Fe(A)-N(6A)	2.146(9)	Fe(A)-N(6A)	2.194(6)
Fe(B)-N(1B)	2.099(9)	Fe(B)-N(1B)	2.076(8)	Fe(B)-N(1B)	2.129(8)	Fe(B)-N(1B)	2.191(6)
Fe(B)-N(2B)	1.991(8)	Fe(B)-N(2B)	1.999(8)	Fe(B)-N(2B)	2.094(8)	Fe(B)-N(2B)	2.182(7)
Fe(B)-N(3B)	2.076(7)	Fe(B)-N(3B)	2.056(9)	Fe(B)-N(3B)	2.163(8)	Fe(B)-N(3B)	2.218(6)
Fe(B)-N(4B)	2.069(8)	Fe(B)-N(4B)	2.061(10)	Fe(B)-N(4B)	2.143(9)	Fe(B)-N(4B)	2.234(6)
Fe(B)-N(5B)	1.979(8)	Fe(B)-N(5B)	1.961(9)	Fe(B)-N(5B)	2.069(10)	Fe(B)-N(5B)	2.167(7)
Fe(B)-N(6B)	1.962(8)	Fe(B)-N(6B)	1.967(8)	Fe(B)-N(6B)	2.101(9)	Fe(B)-N(6B)	2.184(6)
Fe(C)-N(1C)	2.028(9)	Fe(C)-N(1C)	2.125(6)	Fe(C)-N(1C)	2.201(5)	Fe(C)-N(1C)	2.175(4)
Fe(C)-N(2C)	2.005(7)	Fe(C)-N(2C)	2.121(9)	Fe(C)-N(2C)	2.201(7)	Fe(C)-N(2C)	2.181(6)
Fe(C)-N(3C)	2.035(8)	Fe(C)-N(3C)	2.147(9)	Fe(C)-N(3C)	2.228(7)	Fe(C)-N(3C)	2.221(6)
Fe(C)-N(4C)	2.056(8)	Fe(C)-N(4C)	2.150(11)	Fe(C)-N(4C)	2.233(9)	Fe(C)-N(4C)	2.231(7)
Fe(C)-N(5C)	1.934(8)	Fe(C)-N(5C)	2.090(9)	Fe(C)-N(5C)	2.162(8)	Fe(C)-N(5C)	2.184(7)
Fe(C)-N(6C)	1.958(8)	Fe(C)-N(6C)	2.078(10)	Fe(C)-N(6C)	2.168(8)	Fe(C)-N(6C)	2.172(7)



**<sup>1</sup>H-NMR spectroscopy.** As representative examples of the family of bis-triflate complexes, <sup>1</sup>H-NMR spectra of <sup>H,H</sup>**1**, <sup>Me,H</sup>**1**, <sup>H,NO<sub>2</sub></sup>**1** and <sup>H,NMe<sub>2</sub></sup>**1** in CD<sub>2</sub>Cl<sub>2</sub> are depicted in Figure 3. Figures S3 and S4 in the Supporting Information collect the <sup>1</sup>H-NMR spectra of all complexes (<sup>R,R'</sup>**1**). These complexes exhibit spectral windows that expand from -40 ppm to 200 ppm, which is indicative of octahedral t<sub>2g</sub><sup>4</sup>e<sub>g</sub><sup>2</sup> Fe<sup>II</sup> paramagnetic species. Spectra show mainly very broad signals because of the close proximity of the corresponding protons to the paramagnetic center. Along this line, in most of the cases the spectra are relatively simple, with a relatively small number of signals, suggesting that some protons give signals that are too broad to be effectively observed because of fast relaxation. Lowering the temperature causes a narrowing of the NMR signals as exemplified for complex <sup>Me,H</sup>**1** (Figure S5), which protons exhibit chemical shifts linearly dependent on 1/T, characteristic of a Curie behavior (Figure S6).

In spite of the width of the NMR signals at room temperature, it is possible to clearly identify β and γ protons of the pyridine, which appear as relatively sharp signals (Table 5). They can be assigned on the basis of their relative integration, by comparison of the spectra along the whole series of complexes and because polypyridyl Fe<sup>II</sup> complexes present typical NMR patterns.<sup>22,24,26</sup> This assignment explains the absence of a sharp signal at 15 - 20 ppm corresponding to the γ-proton for compounds <sup>H,R'</sup>**1** and <sup>Me,Me</sup>**1**, which bear a substituent in the *para* position of the pyridine ring, and the lack of the two sharp signals between 30 and 70 ppm in the <sup>1</sup>H-NMR spectrum of <sup>H,OMe</sup>**1**, for which the pyridine ring presents methyl groups in the two β positions.

Assignment of the α-methylpyridine group in <sup>Me,Me</sup>**1** and <sup>Me,H</sup>**1** can be also done because of the characteristic paramagnetic upfield shift of these protons arising from Fermi contact interactions between protons and the ferrous center, dominated by a spin polarization mechanism.<sup>24,27</sup> Resonances belonging to the N-CH<sub>3</sub> groups could be easily identified in the spectra of <sup>H,H</sup>**1**, and <sup>H,NMe<sub>2</sub></sup>**1**, as a very broad signal between 80-100 ppm, on the basis of their relative integration. The two N-CH<sub>3</sub> groups of each [Fe(Pytacn)] unit are chemically non equivalent, but they accidentally overlap in the spectra of <sup>H,H</sup>**1**. This situation is changed in the spectra of <sup>Me,H</sup>**1** and <sup>H,NO<sub>2</sub></sup>**1** where the two N-CH<sub>3</sub> groups appear as two different signals at 65/95 ppm and 95/110 ppm (Figure 3), and also in the spectra of <sup>R,H</sup>**1** (R = Me, Cl, F, Figure S4) and <sup>H,R'</sup>**1** (R' = OMe, Me, Cl and CO<sub>2</sub>Et, Figure S3) in CD<sub>2</sub>Cl<sub>2</sub>.

**Table 5.** <sup>1</sup>H-NMR chemical shifts (ppm) for β and γ protons of the pyridine ring of complexes <sup>R,R'</sup>**1** in CD<sub>2</sub>Cl<sub>2</sub>.

Complex	H <sub>β</sub>	H <sub>β</sub>	H <sub>γ</sub>
<sup>H,H</sup> <b>1</b>	49.2	36.3	17.7
<sup>H,NMe<sub>2</sub></sup> <b>1</b>	42.7	39.5	-
<sup>H,OMe</sup> <b>1</b>	-	-	-
<sup>H,Me</sup> <b>1</b>	47.7	35.6	-
<sup>H,Cl</sup> <b>1</b>	47.8	33.8	-
<sup>H,CO<sub>2</sub>Et</sup> <b>1</b>	49.7	34.9	-
<sup>H,NO<sub>2</sub></sup> <b>1</b>	47.8	33.2	-
<sup>Me,H</sup> <b>1</b>	53.1	38.8	16.5
<sup>Me,Me</sup> <b>1</b>	52.6	39.0	-
<sup>Cl,H</sup> <b>1</b>	60.3	32.4	18.6
<sup>F,H</sup> <b>1</b>	68.8	29.7	18.5

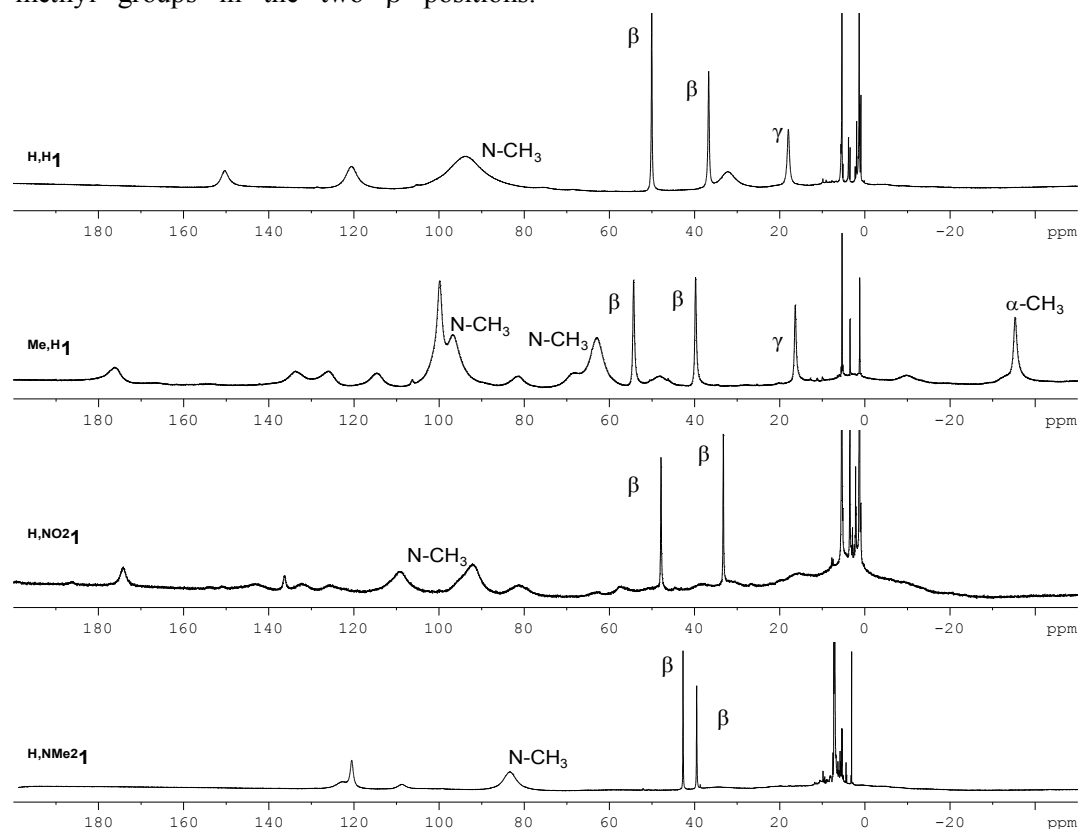
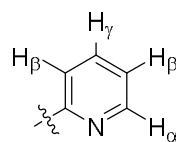


**Figure 3.** <sup>1</sup>H-NMR spectra of <sup>H,H</sup>**1**, <sup>Me,H</sup>**1**, <sup>H,NO<sub>2</sub></sup>**1** and <sup>H,NMe<sub>2</sub></sup>**1** in CD<sub>2</sub>Cl<sub>2</sub>.

$^1\text{H-NMR}$  spectra of  $^{\text{R,R}'}\mathbf{1}$  were also measured in  $\text{CD}_3\text{CN}$  (Figures 4-5 and S7-S10). Similarly to what is reported for other iron(II) complexes,<sup>20,28-30</sup> this solvent acts as a coordinating ligand and it displaces triflate groups to form solvato complexes  $[\text{Fe}^{\text{R,R}'}\text{Pytacn}(\text{CH}_3\text{CN})_2]^{2+}$  ( $^{\text{R,R}'}\mathbf{2}$ ) in which two acetonitrile molecules and the tetradentate  $^{\text{R,R}'}$ Pytacn ligand constitute the coordination sphere of the iron(II) center. This phenomenon was confirmed by comparing the  $^1\text{H-NMR}$  spectra of  $^{\text{H,H}}\mathbf{1}$  and  $^{\text{Me,H}}\mathbf{1}$  in

$\text{CD}_3\text{CN}$  with those of the synthetically isolated bis-acetonitrile complexes  $^{\text{H,H}}\mathbf{2SbF}_6$  and  $^{\text{Me,H}}\mathbf{2SbF}_6$  (Figure 4). For these two compounds the  $^1\text{H-NMR}$  spectrum was found to be identical to the corresponding bis-triflate complexes  $^{\text{H,H}}\mathbf{1}$  and  $^{\text{Me,H}}\mathbf{1}$  in  $\text{CD}_3\text{CN}$  but the signals appeared much sharper. This observation is indicative of fast competition between triflate and acetonitrile binding which gives rise to broader signals.<sup>11</sup>

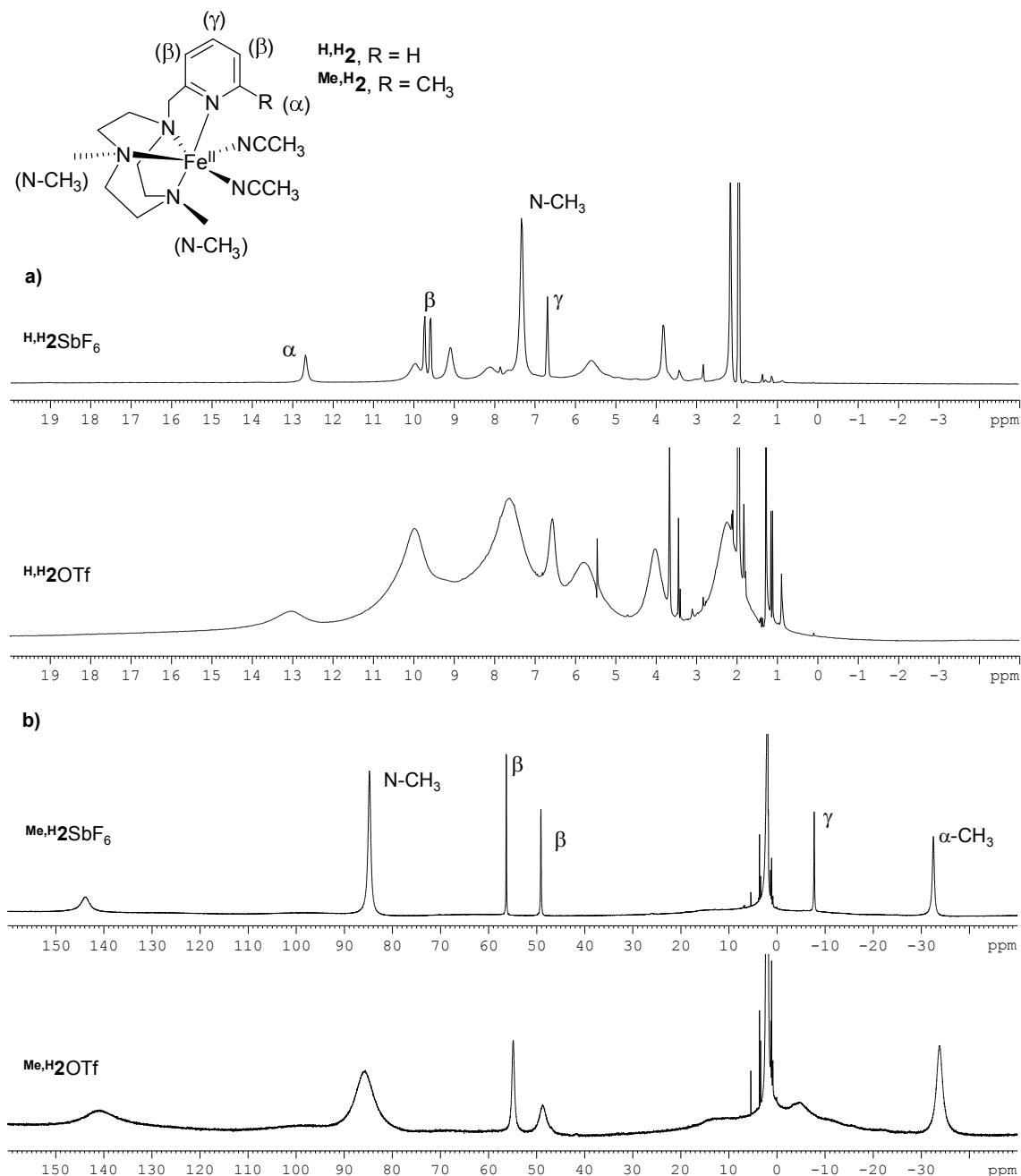


**Figure 4.** a)  $^1\text{H-NMR}$  spectra of  $^{\text{H,H}}\mathbf{2SbF}_6$  and  $^{\text{H,H}}\mathbf{1}$  in  $\text{CD}_3\text{CN}$ . The latter affords the bis-acetonitrile complex  $^{\text{H,H}}\mathbf{2}$  upon being dissolved. The partial assignment of the  $^1\text{H-NMR}$  signals for complex  $^{\text{H,H}}\mathbf{2SbF}_6$  was based on integration values and COSY experiment (Figure S7). b)  $^1\text{H-NMR}$  spectra of  $^{\text{Me,H}}\mathbf{2SbF}_6$  and  $^{\text{Me,H}}\mathbf{1}$  in  $\text{CD}_3\text{CN}$ . The latter affords the bis-acetonitrile complex  $^{\text{Me,H}}\mathbf{2}$  upon being dissolved. For complex  $^{\text{Me,H}}\mathbf{2SbF}_6$  the assignment was made by comparison with similar complexes described in the literature<sup>24,31</sup> and according to the integration values (Figure S8).

The spectral window of the  $^1\text{H}$ -NMR spectrum of each complex in  $\text{CD}_3\text{CN}$  reflects the spin-state of  $^{\text{R,R}'}\mathbf{2}$ . Important differences arise upon analysis of these NMR spectra, so that the complexes might be classified into two categories: complexes without any substituent in the  $\alpha$  position (class I) and complexes with a substituent in this position (class II).

On one hand, class I complexes, that is  $^{\text{H,R}'}\mathbf{2}$ , exhibit a compact spectral window compared to their bis-triflate counterparts ( $^{\text{H,R}'}\mathbf{1}$ ). It expands from 0-15 ppm except for  $^{\text{H,NMe}}\mathbf{2}$  which shows signals up to 45 ppm. The contraction of the spectral window is related to a modification of the electronic properties of the iron complex, which becomes mainly LS upon substitution of the triflate anions by acetonitrile ligands. This has been previously observed for other iron complexes<sup>11,19,23,32</sup> and it can be explained by simple crystal field theory because the acetonitrile ligand is a stronger ligand-field than triflate anion. Qualitative analysis of the NMR spectra allows the evaluation of the relative contribution of the HS state. It is particularly interesting to notice that complex  $^{\text{H,NO}_2}\mathbf{2}$ , with a nitro group in the  $\gamma$  position, does not show signals above 11 ppm, which indicates that in this case the compound is purely diamagnetic and it must be described as a pure LS iron(II) center (Figure 5). Instead, for  $^{\text{H,NMe}}\mathbf{2}$ , which has a strongly electron-

donating dimethylamino substituent in the  $\gamma$  position, there is an important influence of the HS state and the spectral window expands up to 45 ppm (Figure 5). Thus, it seems clear that the substituent in the *para*-position of the pyridine directly influences the electronic properties of the iron(II) center.

On the other hand, class II catalysts, that is  $^{\text{R,R}'}\mathbf{2}$  where  $\text{R} = \text{Me, Cl or F}$ , show spectral windows that expand from 0 to 150 ppm indicating a HS configuration of the iron(II) center in acetonitrile. It is worth mentioning here that the NMR spectra of  $^{\text{F,H}}\mathbf{2}$  and  $^{\text{Cl,H}}\mathbf{2}$  show broader signals. In this case, we attribute the amplitude of the signals not only to the fast dynamic exchange between OTf and acetonitrile as coordinating ligands, but also to the relatively easy breakage of the bond between the iron center and 6-R-pyridine,  $\text{R} = \text{F, Cl}$ , followed by displacement of the aromatic ligand arm. Such a fluxional phenomenon has already been reported for other iron(II) compounds.<sup>33</sup>

The different spin state of the iron(II) center in class I and class II bis-acetonitrile complexes evidenced by NMR spectroscopy could be quantified by measuring their effective magnetic moment ( $\mu_{\text{eff}}$ ) using the Evans' method (see below).

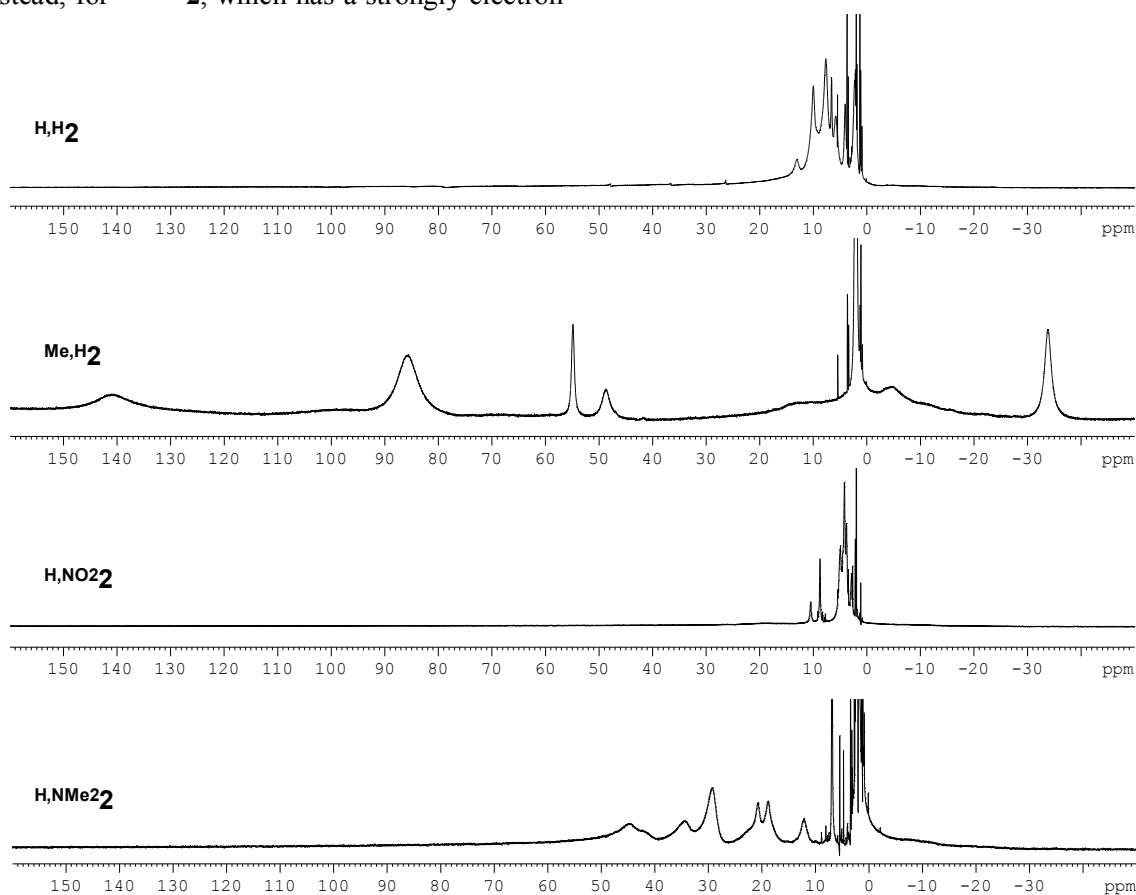


**Figure 5.**  $^1\text{H}$ -RMN spectra of  $^{\text{H,H}}\mathbf{1}$ ,  $^{\text{Me,H}}\mathbf{1}$ ,  $^{\text{H,NO}_2}\mathbf{1}$  and  $^{\text{H,NMe}}\mathbf{1}$  in  $\text{CD}_3\text{CN}$ . The triflate anions are replaced by acetonitrile molecules, thus, in solution the bis-acetonitrile complexes  $^{\text{H,H}}\mathbf{2}$ ,  $^{\text{Me,H}}\mathbf{2}$ ,  $^{\text{H,NO}_2}\mathbf{2}$  and  $^{\text{H,NMe}}\mathbf{2}$  are formed.

**Effective magnetic moment.** The measurement of the effective magnetic moment ( $\mu_{\text{eff}}$ ) allows the quantification of the contribution of the LS and HS states in iron(II) complexes. This information is specially important in the present family of complexes, for which both spin states are close in energy.  $\mu_{\text{eff}}$  values for  $\text{R,R}'\mathbf{2}$  were measured using the Evans' NMR method by dissolving  $\text{R,R}'\mathbf{1}$  in  $\text{CD}_3\text{CN}$  (Table 6).

For class I complexes, a clear correlation between the electronic properties of the group in the  $\gamma$  position and  $\mu_{\text{eff}}$  values is observed. Complex  $\text{H,NO}_2\mathbf{2}$ , which contains the strong electron-withdrawing  $\text{NO}_2$  group, has no effective magnetic moment ( $\mu_{\text{eff}} \sim 0$ ) indicative of a pure LS  $\text{Fe}^{\text{II}}$ , in agreement with its diamagnetic  $^1\text{H-NMR}$  spectrum. Compound  $\text{H,CO}_2\text{Et}\mathbf{2}$ , with an ester group in the  $\gamma$ -position of the pyridine, exhibits a low magnetic moment of  $0.78 \mu_{\text{B}}$ . Complexes  $\text{H,H}\mathbf{2}$ ,  $\text{H,Me}\mathbf{2}$  and  $\text{H,Cl}\mathbf{2}$ , which contain hydrogen, methyl and chloro substituents in the  $\gamma$  position of the pyridine ring respectively, present effective magnetic moments around  $\sim 1.3$ - $1.9 \mu_{\text{B}}$ , which accidentally approach the expected value for a single unpaired electron. However, these values must be interpreted as a small contribution of the HS state into the dominant LS state. Complexes  $\text{H,NMe}_2\mathbf{2}$  and  $\text{H,OMe}\mathbf{2}$  with a dimethylamino and a methoxy  $\gamma$ -substituent show larger  $\mu_{\text{eff}}$  values ( $2.62$  and  $2.09 \mu_{\text{B}}$ , respectively), which indicates a significant population of the HS state. The influence of the  $\gamma$ -substituents in the  $\mu_{\text{eff}}$  is clearly observed by the good correlation of this value with the corresponding Hammett  $\sigma_{\text{p}}$  constant (Figure 6a). These results fully agree with the increased spectral width of the  $^1\text{H-NMR}$  spectra upon increasing the electron-donating abilities of the *para*-substituent (Figure S9). The effect of the pyridine substitution in the  $\mu_{\text{eff}}$  values of these complexes can be understood on the basis of simple ligand field theory, by assuming that the  $\mu_{\text{eff}}$  values reflect different stages of a spin transition equilibrium. According to this theory, the magnitude of the ligand field, *i.e.* the  $t_{2g}$ - $e_g$  orbital splitting is higher when increasing the  $\pi$ -acceptor character of the ligands. Introduction of  $\text{NO}_2$  and  $\text{NMe}_2$  groups into the pyridine causes, respectively, a decrease and an increase of the energy of the pyridine  $\pi$  orbitals, with respect to the hydrogen-, methyl- or chloro-substituted ligands. Therefore, the  $\text{NO}_2$  group makes the pyridine a better  $\pi$ -acceptor, while the opposite happens with the  $\text{NMe}_2$  group. Overall, electron-withdrawing groups increase the ligand field, favoring the LS state, while the opposite occurs for electron-releasing groups, which populates the HS state.

Class I complexes exhibit an incomplete spin crossover phenomenon with the temperature, as previously observed for structurally related iron(II) complexes.<sup>28</sup> This behavior was studied for complexes  $\text{H,H}\mathbf{2}$ ,  $\text{H,NMe}_2\mathbf{2}$  and  $\text{H,NO}_2\mathbf{2}$  as representative examples of this class, bearing a hydrogen atom, an electron-donating and an electron-withdrawing group in the  $\gamma$  position of the pyridine respectively (Figure 6b). Taking 298 K as the initial temperature, it was

observed that increasing the temperature up to 338 K caused an increase in the  $\mu_{\text{eff}}$  up to  $3.2 \mu_{\text{B}}$  for  $\text{H,H}\mathbf{2}$ ,  $2.0 \mu_{\text{B}}$  for  $\text{H,NO}_2\mathbf{2}$  and  $3.5 \mu_{\text{B}}$  for  $\text{H,NMe}_2\mathbf{2}$ . The opposite behavior was observed upon cooling. As stated above,  $\text{H,NO}_2\mathbf{2}$  already has a diamagnetic behavior at room temperature, while for  $\text{H,H}\mathbf{2}$  the pure LS state was observed at 273 K. In contrast, complete conversion to the LS state does not occur for  $\text{H,NMe}_2\mathbf{2}$  in the temperature range accessible with acetonitrile, but at 233 K a small  $\mu_{\text{eff}}$  of  $0.8 \mu_{\text{B}}$  was measured, which is indicative of a major contribution of the LS state.

The situation is completely different for compounds belonging to class II, which bear a substituent in the  $\alpha$ -position of the pyridine ring. The measured  $\mu_{\text{eff}}$  values of  $4.80 \pm 0.17 \mu_{\text{B}}$  are very close to the theoretical spin-only value of  $4.90 \mu_{\text{B}}$  of a HS iron(II) center with four unpaired electrons. This result fully agrees with the paramagnetism observed by  $^1\text{H-NMR}$  for the compounds in this class, that is  $\text{R,H}\mathbf{2}$ . This is explained because the  $\alpha$ -substituent in the pyridine sterically interacts with the iron center and it disfavors the formation of the shorter Fe-N bond characteristic of the LS configuration.<sup>24</sup> However, it is interesting to notice that the value  $\mu_{\text{eff}}$  measured for  $\text{F,H}\mathbf{2}$  is slightly lower ( $4.63 \mu_{\text{B}}$ ) than what it would be expected for a pure HS center with four unpaired electrons. It was observed that the  $\mu_{\text{eff}}$  values for  $\text{F,H}\mathbf{2}$  decreased upon lowering the temperature, which is consistent with a spin transition phenomenon in solution. The  $\mu_{\text{eff}}$  values range from  $4.77 \mu_{\text{B}}$  at 320 K to  $0.92 \mu_{\text{B}}$  at 235 K (Figure 6b). The spin transition could also be followed by UV-vis spectroscopy (Figure 8). This phenomenon was not observed for the other class II complexes, that is  $\text{Me,H}\mathbf{2}$ ,  $\text{Cl,H}\mathbf{2}$  and  $\text{Me,Me}\mathbf{2}$  (with methyl or chloride groups in the  $\alpha$  position).

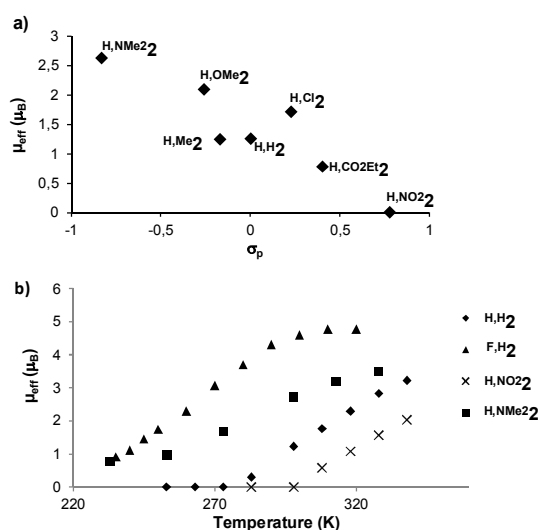


**Figure 6.** a) Representation of the effective magnetic moment of  $\text{H,R}'\mathbf{2}$  in acetonitrile- $d_3$  at 298 K in front of the Hammett constants ( $\sigma_{\text{p}}$ ). b) Representation of the effective magnetic moment of  $\text{H,H}\mathbf{2}$ ,  $\text{F,H}\mathbf{2}$ ,  $\text{H,NO}_2\mathbf{2}$  and  $\text{H,NMe}_2\mathbf{2}$  as a function of temperature.  $\text{R,R}'\mathbf{2}$  complexes were obtained by dissolving  $\text{R,R}'\mathbf{1}$  in acetonitrile- $d_3$ . The effective magnetic moment was measured in a  $\text{CD}_3\text{CN}$  solution using the Evans' method.

**UV-vis spectroscopy.** The UV-vis spectra of the bis-acetonitrile complexes  $\text{R,R}'\mathbf{2}$  formed by dissolving the corresponding bis-triflate complexes  $\text{H,R}'\mathbf{1}$  in acetonitrile were analyzed to obtain further information in the electronic structure of the complexes (Table 6 and Figure 7).

Compound  $\text{H,H}\mathbf{2}$  can be seen as a prototypical example of class I complexes. The UV-vis spectrum of this compound is characterized by intense bands at 239 nm ( $\epsilon = 13900 \text{ M}^{-1}\text{cm}^{-1}$ ), 385 nm ( $\epsilon = 3200 \text{ M}^{-1}\text{cm}^{-1}$ ) and a relatively weak band at 550 nm ( $\epsilon = 65 \text{ M}^{-1}\text{cm}^{-1}$ ), responsible for the pink-yellowish color of the solution (Figure 7, Table 6). By analogy to the UV-vis spectra of other iron(II) complexes of pyridine-alkylamino ligands,<sup>28,29</sup> the two high intensity bands in the UV region can be assigned to a ligand-centered  $\pi\text{-}\pi^*$  transition and to a metal-to-ligand charge transfer (MLCT) characteristic of the iron(II) center, respectively. This band arises from a transition between the iron(II)  $t_{2g}$  orbitals and the  $\pi^*$  pyridine orbitals,<sup>34</sup> thus being more intense for low spin iron(II) compounds. In the particular case of  $\text{H,H}\mathbf{2}$ , the intensity of the MLCT band is indicative of a LS iron(II) center. Finally, the low intensity broad band at 550 nm is assigned to a d-d transition characteristic of an octahedral LS iron(II) complex ( ${}^1\text{T}_1 \leftarrow {}^1\text{A}_1$ ).

The position of the MLCT band ( $\epsilon \approx 2400 - 6100 \text{ M}^{-1}\text{cm}^{-1}$ ) is directly related to the electronic properties of the  $\gamma$ -substituent. An increase in the electron-

withdrawing character of the  $\gamma$ -group causes a bathochromic shift (Figure 7a). For complex  $\text{H,H}\mathbf{2}$  this band is found at 385 nm and it is systematically shifted to lower wavelengths for electron-rich substituents. The methyl- and methoxy-substituted complexes  $\text{H,Me}\mathbf{2}$  and  $\text{H,OMe}\mathbf{2}$  exhibit a  $\lambda_{\text{max}}$  at 370 nm and even a more remarkable shift is observed with the dimethylamino substituted  $\text{H,NMe}_2\mathbf{2}$  with a  $\lambda_{\text{max}}$  at 327 nm. The opposite behavior is observed for electron-withdrawing substituents.  $\lambda_{\text{max}}$  is found at around 400 nm for  $\text{H,Cl}\mathbf{2}$  bearing a chloro substituent in the  $\gamma$  position, the red complex  $\text{H,CO}_2\text{Et}\mathbf{2}$  with a *para*- $\text{CO}_2\text{Et}$ -pyridine shows a  $\lambda_{\text{max}}$  at 455 nm and for the violet compound  $\text{H,NO}_2\mathbf{2}$  with a strong electron-withdrawing group ( $\text{NO}_2$ ) the MLCT band shifts to a  $\lambda_{\text{max}}$  of 526 nm. Thus, the energy of this absorption band decreases with the decrease of the electron-richness of the  $\gamma$ -substituent:  $\text{N}(\text{Me})_2 > \text{OMe} \approx \text{Me} > \text{H} > \text{Cl} > \text{CO}_2\text{Et} > \text{NO}_2$ . This phenomenon has been previously observed for other iron complexes<sup>28</sup> and it can be rationalized by the tuned  $\pi$ -acceptor character of the pyridine ring.

For class II catalysts, the UV-vis spectrum of  $\text{Me,H}\mathbf{2}$ , which is very similar to  $\text{Cl,H}\mathbf{2}$  and  $\text{Me,Me}\mathbf{2}$ , is taken as the reference. This complex exhibits a band at 267 nm ( $\epsilon \sim 5100 \text{ M}^{-1}\text{cm}^{-1}$ ) and a shoulder at 340 nm ( $\epsilon \sim 255 \text{ M}^{-1}\text{cm}^{-1}$ ), both of them characteristic of HS iron(II) complexes (Figure 7b).<sup>35</sup>

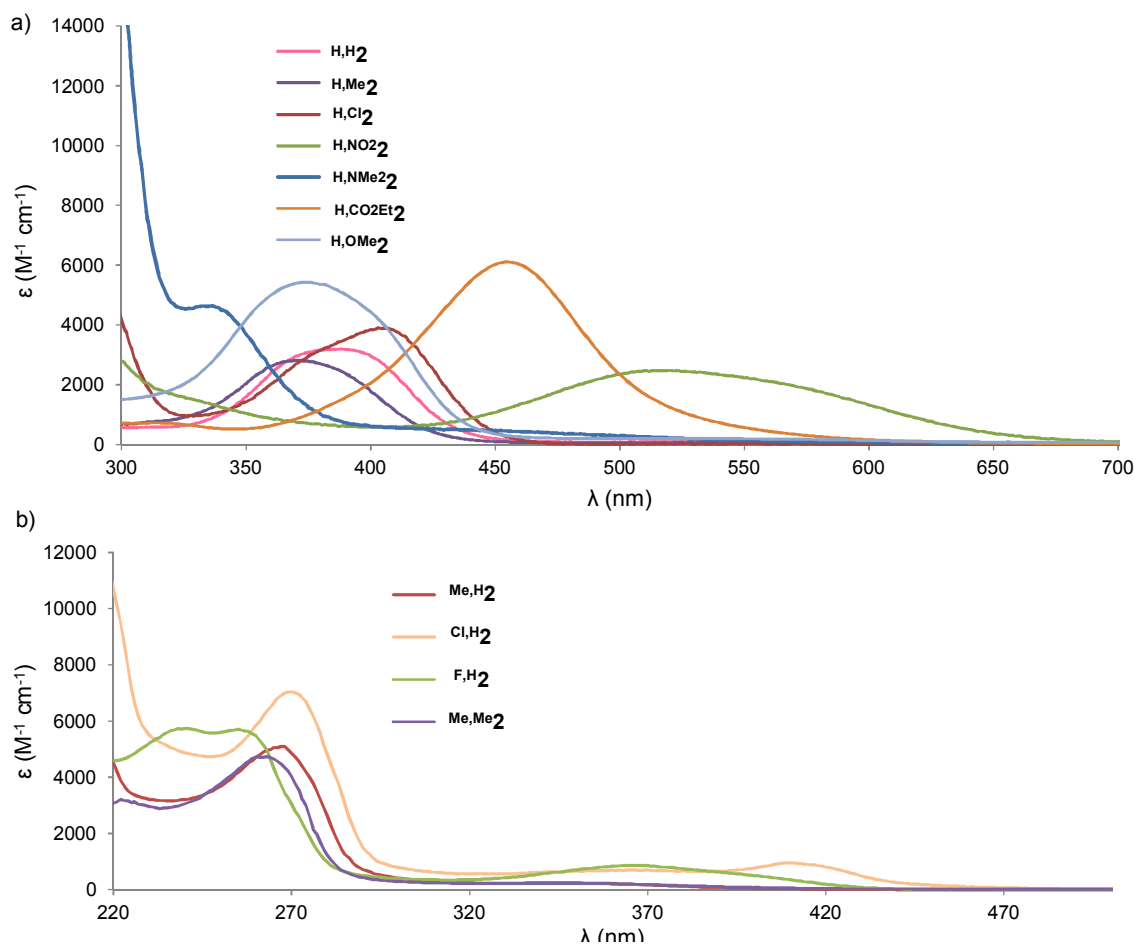


**Figure 7.** a) UV-vis spectra (298 K) in acetonitrile of complexes  $\text{H,R}'\mathbf{2}$ . b) UV-vis spectra (298 K) in acetonitrile of the complexes  $\text{R,R}'\mathbf{2}$  where  $\text{R} = \text{Me}, \text{Cl}, \text{F}$ .  $\text{R,R}'\mathbf{2}$  complexes were obtained upon dissolving  $\text{R,R}'\mathbf{1}$  in acetonitrile.

**Table 6.** Selected physical data for  $R,R'2$ .<sup>[a]</sup>

Complex	$\lambda_{\max}$ , nm ( $\epsilon$ , $M^{-1}cm^{-1}$ )			$\mu_{\text{eff}}$ ( $\mu_B$ )	$E_{1/2}$ (mV) <sup>[b]</sup>
	$\pi-\pi^*$	MLCT	d-d		
$H,H2$	239 (13900)	385 (3200)	550 (65)	1.26	138
$H,NMe22$	240 (>20000)	327 (4700)	bs: 450-550 (100)	2.62	11
$H,OMe2$	250 (13300)	370 (5400)	547 (120)	2.09	107
$H,Me2$	240 (10500)	370 (2900)	553 (70)	1.24	176
$H,Cl2$	241 (15800)	403 (3900)	552 (28)	1.71	165
$H,CO2Et2$	275 (6150)	455 (6100)		0.78	171
$H,NO22$	231 (14000)	526 (2400)		0	225
$Me,H2$	267 (5100)	340 (255)		4.95	211
$Me,Me2$	260 (4700)	344 (220)		4.75	238
$Cl,H2$	269 (7000)	410(950)		4.87	n.m. <sup>[c]</sup>
$F,H2$	237 (5600), 254 (5600)	368 (900)	578 (14)	4.63	n.m. <sup>[c]</sup>

[a] Compounds  $R,R'2$  were prepared by dissolving the bis-triflate complexes  $R,R'1$  in  $CH_3CN$  or  $CD_3CN$ .

[b]  $E_{1/2}$  values determined for  $R,R'3$  in  $CH_3CN$ . Values measured vs. SCE.

[c] Not measured.

Compound  $F,H2$  has a slight contribution of the LS state at room temperature as evidenced by the presence of low intensity bands at 237, 368 and 560 nm in its UV-vis spectrum, that strongly resemble those described above for LS iron(II) complexes (Figure 8). The intensity of these bands depends on the temperature. Lowering the temperature results in an increase of their molar absorptivity without saturation in the temperature range studied (from 20 to  $-40^\circ C$ ) (Figure 8). This behavior indicates an incomplete spin crossover phenomenon from HS to LS upon lowering the temperature which was further corroborated by measurement of the effective magnetic moment (see Figure 6b).

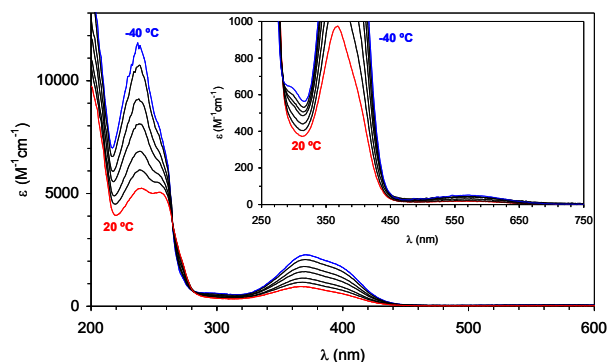


**Figure 8.** UV-vis spectra of  $F,H1$  in  $CH_3CN$  at different temperatures (from 20 to  $-40^\circ C$ ). The triflate anions are replaced by acetonitrile molecules, thus, in solution the bis-acetonitrile complex  $F,H2$  is formed.

**Electrochemistry.** A comparison between the electronic properties exerted by the different ligands can be drawn by measuring the electrochemical potential ( $E_{1/2}$ ) of the  $Fe^{III}/Fe^{II}$  redox pair of the corresponding bis-chloro complexes. Analogous analyses with bis-triflate ( $R,R'1$ ) and bis-acetonitrile complexes ( $R,R'2$ ) were precluded by their chemically irreversible redox behavior. Instead, compounds  $H,R'3$ ,  $Me,H3$  and  $Me,Me3$  exhibited a chemically reversible, electrochemically quasireversible ( $I_{pa}/I_{pc} = 1$ ,  $\Delta E \sim 100 - 200$  mV at  $100$   $mV \cdot s^{-1}$ ) redox pair that is assigned to the  $Fe^{III}/Fe^{II}$  couple (Table 6, Figure S11).

Cyclic voltammetry  $F,H3$  and  $Cl,H3$  show anodic and cathodic peaks separated by more than 300 mV, thus a clear identification of their  $E_{1/2}$  could not be registered. Such complex electrochemical behavior has also been observed for dichloro iron(II)-complexes bearing modified versions of the tpa ligand (tpa = tris-pyridylmethylamine) in which fluorine groups are introduced in the  $\alpha$  position of the pyridine rings.<sup>33,36</sup>

Within class I catalysts,  $E_{1/2}$  values follow the expected trend according to the electronic properties of the substituent in the  $\gamma$ -position of the pyridine ring. Thus, the lowest redox potential (11 mV) corresponds to complex  $H,NMe23$ , which bears an electronrich dimethylamino substituent that stabilizes  $Fe^{III}$  while the highest one (225 mV) corresponds to  $H,NO23$  with the most electron-withdrawing nitro group.  $H,Cl3$  (165 mV) and  $H,CO2Et3$  (171 mV) also present higher redox potentials with respect to  $H,H3$  (138 mV) which agrees with the slight electron-withdrawing character of their substituents (a chloride and an ester group,

respectively). The single exception to this general trend corresponds to  $^{\text{H,Me}}\mathbf{3}$ , which redox potential is increased by 38 mV with respect to the unsubstituted  $^{\text{H,H}}\mathbf{3}$ , albeit the  $\sigma$ -donor character of the  $\text{CH}_3$  should cause *a priori* a decrease in the  $\text{Fe}^{\text{III}}/\text{Fe}^{\text{II}}$  redox potential with respect to H. Currently we do not have any explanation for this unexpected behavior.

Introduction of a methyl group in the  $\alpha$ -position of the pyridine increases the redox potential by approximately 70 mV (compare  $^{\text{H,H}}\mathbf{3}$  vs  $^{\text{Me,H}}\mathbf{3}$  and  $^{\text{H,Me}}\mathbf{3}$  vs  $^{\text{Me,Me}}\mathbf{3}$ ), an increase even higher than that achieved with the introduction of a  $\text{NO}_2$  group in the  $\gamma$ -pyridine. This effect can be understood by considering that the steric clash between the  $\alpha$ -methyl group and the iron center disfavors the formation of the shorter Fe-N bonds of the iron(III) with respect to iron(II).<sup>24</sup>

**Catalytic oxidations.** In order to evaluate the electronic/steric influence imposed by the Pytacn-based ligands in the catalytic activity of the corresponding  $[\text{Fe}(\text{OTf})_2(\text{R,R-Pytacn})]$  complexes ( $^{\text{R,R}}\mathbf{1}$ ), we have tested their behavior as catalysts in oxidation reactions using  $\text{H}_2\text{O}_2$  as the oxidant. In particular, we have targeted the oxidation of cyclohexane and *cis*-cyclooctene as model substrates for C-H bond and C=C bond oxidation reactions (Table 7). In a typical experiment, 10-100 equiv  $\text{H}_2\text{O}_2$  diluted in acetonitrile were delivered via syringe pump for 30 min into an acetonitrile solution containing the iron catalyst (1 equiv) and the substrate (100-1000 equiv). The final concentrations of the reactants were 1 mM catalyst, 10-100 mM  $\text{H}_2\text{O}_2$  and 100 mM-1M substrate. Oxidant-limiting conditions were used in all the experiments in order to limit product overoxidation.

The oxidation of cyclohexane with 10 equiv  $\text{H}_2\text{O}_2$  catalyzed by complexes  $^{\text{R,R}}\mathbf{1}$  afforded excellent conversion of  $\text{H}_2\text{O}_2$  into oxidation products (cyclohexanol and cyclohexanone), that ranged from 43% to 76%. Remarkably, large alcohol/ketone ratios (A/K) between 6.7 and 12.3 were obtained, which is consistent with the involvement of a highly selective metal-centered oxidant as the active species in these reactions.<sup>37</sup> When the  $\text{H}_2\text{O}_2$  concentration was increased up to 100 equiv, the efficiency of the oxidations slightly decreased, giving yields down to 26-60%, and so did the A/K ratio (Table 7). However, these catalysts are still among the most efficient for such transformation<sup>5,38</sup> and, up to now, the catalytic results disclosed here have only been surpassed by two previously reported iron complexes under analogous conditions.<sup>39,40</sup>

Careful analysis of the catalytic results indicates that both the catalytic efficiency and the A/K ratio is essentially the same for all complexes belonging to class I ( $^{\text{H,R}}\mathbf{1}$ ), meaning that the electronic properties of the  $\gamma$  substituent in the pyridine ring does not significantly influence the catalytic activity. Instead, the introduction of a methyl substituent in the  $\alpha$  position of the pyridine ( $^{\text{Me,H}}\mathbf{1}$  and  $^{\text{Me,Me}}\mathbf{1}$ ) gives catalysts that afford minimal depletion of efficiency

when the amount of oxidant is increased. This is exemplified for catalyst  $^{\text{Me,Me}}\mathbf{1}$ , which converts hydrogen peroxide into products in 60% yield either with 10 or 100 equiv  $\text{H}_2\text{O}_2$ . Therefore, these catalysts appear to be good candidates to catalyze C-H hydroxylation under preparative scale conditions. As a matter of fact, some of us have recently demonstrated that  $^{\text{Me,H}}\mathbf{1}$  is a remarkably efficient and selective catalyst in alkane C-H hydroxylation under preparative conditions.<sup>15b</sup>

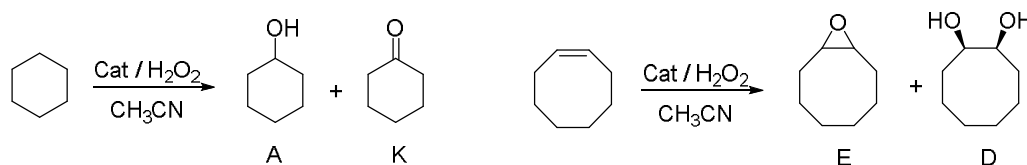
The oxidation of *cis*-cyclooctene with 10 equiv  $\text{H}_2\text{O}_2$  by complexes  $^{\text{R,R}}\mathbf{1}$  afforded high yields (between 72% and 95%) of products as a mixture of *syn*-diol (D) and epoxide (E). Even when the amount of  $\text{H}_2\text{O}_2$  was increased up to 100 equiv, the yields remained at the same level, with the single exception of  $^{\text{H,NO}_2}\mathbf{1}$  that showed modest efficiency under these conditions. Such high efficiencies in the conversion of oxidant into oxidized products indicate that the complexes described in this work could be potentially suitable for alkene oxidation for synthetic purposes. The diol:epoxide ratio (D/E) was modest for most complexes (D/E = 1 – 2), except for  $^{\text{Me,H}}\mathbf{1}$ ,  $^{\text{Cl,H}}\mathbf{1}$  and  $^{\text{Me,Me}}\mathbf{1}$  belonging to class II which exhibited D/E values up to 6.2. This observation suggests that these three complexes could be used as catalysts for the preparation of *syn*-diols. *Syn*-diols are very interesting synthons for a number of organic transformations and their preparation often entails the *cis*-dihydroxylation of olefins with osmium-based catalysts. Thus, it would be of special interest to find catalysts that could perform this chemistry under environmentally friendly conditions using less harmful metal-based catalysts such as iron.<sup>41,42</sup>

**Isotopic labeling studies in the oxidation of cyclooctene.** Isotopic labeling experiments were devised to investigate if this set of complexes operates through a common reaction mechanism. Two main mechanisms of action have been proposed for iron catalysts that mediate olefin *cis*-dihydroxylation with  $\text{H}_2\text{O}_2$  (Scheme 2). On one hand, some catalysts operate through a  $\text{Fe}^{\text{III}}/\text{Fe}^{\text{V}}$  catalytic cycle being a  $\text{Fe}^{\text{V}}(\text{O})(\text{OH})$  the active species, formed via water-assisted O-O cleavage of a  $\text{Fe}^{\text{III}}(\text{OOH})(\text{OH}_2)$ .<sup>32,43-46</sup> Consequently, the oxygen inventory in  $\text{Fe}^{\text{V}}(\text{O})(\text{OH})$  is composed by one oxygen atom that comes from the oxidant ( $\text{H}_2\text{O}_2$ ) and the second one derived from water. Rapid oxo-hydroxo tautomerism explains that oxygen atoms originally coming from water end up being incorporated as terminal oxo ligands. Initial electrophilic attack of the hydroxyl ligand of  $\text{Fe}^{\text{V}}(\text{O})(\text{OH})$  towards an olefin results in a *cis*-dihydroxylation reaction,<sup>44</sup> so that the two oxygen atoms of the  $\text{Fe}^{\text{V}}(\text{O})(\text{OH})$  species end up in the corresponding *syn*-diol product. C-H hydroxylation and olefin epoxidation by  $\text{Fe}^{\text{V}}(\text{O})(\text{OH})$  are initiated by the oxo ligand and occur with stereoretention. On the other hand, other catalysts operate via a  $\text{Fe}^{\text{II}}/\text{Fe}^{\text{IV}}$  catalytic cycle where a  $\text{Fe}^{\text{IV}}(\text{O})(\text{OH}_2)$  or  $\text{Fe}^{\text{IV}}(\text{OH})_2$  is the key oxidizing species.<sup>47,48</sup> When this mechanism is operative and in contrast to the  $\text{Fe}^{\text{III}}/\text{Fe}^{\text{V}}$  pathway,

the two oxygen atoms that end up into the *syn*-diol originate from the oxidant. Therefore, the isotopic labeling pattern observed in the *cis*-dihydroxylation of olefins contains essential information about the nature of the oxidizing species. Herein we perform isotopic labeling studies in the oxidation of cyclooctene as a

way to obtain information about the reaction mechanism operating in the present family of complexes.

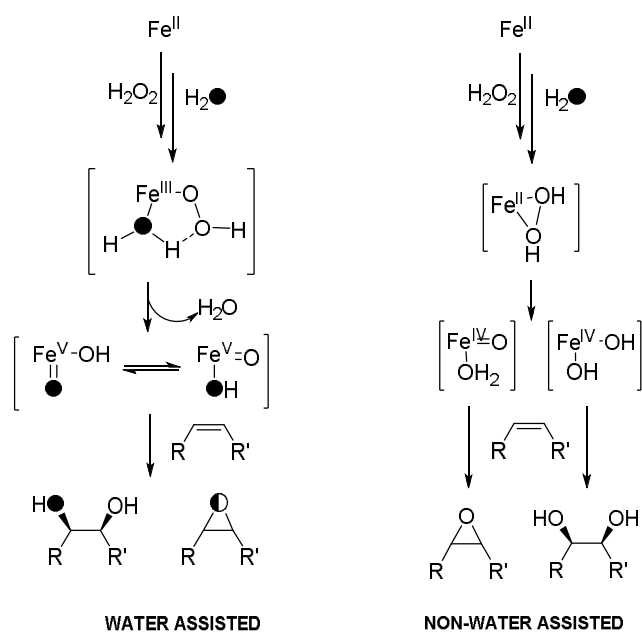
**Table 7.** Oxidation of cyclohexane and *cis*-cyclooctene with H<sub>2</sub>O<sub>2</sub> using complexes [Fe(OTf)<sub>2</sub>(<sup>R,R'</sup>Pytacn)] (<sup>R,R'</sup>**1**) as catalysts.<sup>[a]</sup>



Catalyst	H <sub>2</sub> O <sub>2</sub> (equiv)	Cyclohexane		Cyclooctene	
		A+K <sup>[b]</sup> (A/K) <sup>[c]</sup>	D+E <sup>[d]</sup> (D/E) <sup>[e]</sup>	<sup>16</sup> O <sup>18</sup> O <sup>[f]</sup>	<sup>18</sup> O <sup>[g]</sup>
H,H <sub>1</sub>	10	6.5 (12.3) <sup>15</sup>	8.1 (1.0) <sup>15</sup>	97	77
	100	39 (2.6) <sup>15</sup>	99 (1.0) <sup>15</sup>		
H,NMe <sub>2</sub> <sub>1</sub>	10	4.3 (8.9)	8.2 (2.3)	95	74
	100	31 (3.8)	69 (1.4)		
H,OMe <sub>1</sub>	10	6.2 (10.2)	7.6 (1.1)	95	71
	100	47 (2.8)	83 (1.5)		
H,Me <sub>1</sub>	10	6.5 (10.5)	9.3 (2.6)	97	72
	100	48 (2.3)	85 (1.0)		
H,Cl <sub>1</sub>	10	5.9 (8.3)	9.5 (1.5)	97	67
	100	40 (4.3)	85 (2.1)		
H,CO <sub>2</sub> Et <sub>1</sub>	10	5.7 (9.2)	8.2 (1.5)	97	63
	100	43 (3.2)	82 (1.2)		
H,NO <sub>2</sub> <sub>1</sub>	10	5.3 (8.1)	7.8 (1.5)	99	66
	100	34 (3.9)	50 (1.1)		
Me,H <sub>1</sub>	10	7.6 (10.2) <sup>15</sup>	7.1 (5.5) <sup>15</sup>	78	5
	100	64 (4.3) <sup>15</sup>	86 (6.2) <sup>15</sup>		
Me,Me <sub>1</sub>	10	6.1 (9.3)	8.6 (5.2)	80	4
	100	60 (5.1)	81 (3.5)		
Cl,H <sub>1</sub>	10	6.8 (6.7)	8.4 (2.6)	80	9
	100	28 (3.0)	63 (4.7)		
F,H <sub>1</sub>	10	5.9 (8.3)	7.5 (0.8)	89	4
	100	26 (2.7)	73 (1.0)		

[a] 1000 equiv of substrate (100 equiv for isotope labeling studies) with respect to catalyst. Final catalyst concentration = 1 mM. The reaction was performed by slow syringe pump addition over 30 min of an acetonitrile solution of H<sub>2</sub>O<sub>2</sub> (10 or 100 equiv) into a solution of catalyst and substrate at room temperature. [b] Turnover number (mols of products/mols of catalyst), A = cyclohexanol, K = Cyclohexanone. [c] A/K=mols of alcohol/mols of epoxide. [d] Turnover number (mol product/mol catalyst), D = *syn*-cyclooctane-1,2-diol, E = cyclooctene epoxide. [e] D/E = mols of diol/mols of epoxide. [f] Percentage of *syn*-diol <sup>16</sup>O<sup>18</sup>O-labeled when the oxidation of cyclooctene was carried out in the presence of 1000 equiv H<sub>2</sub><sup>18</sup>O. [g] Percentage of epoxide <sup>18</sup>O-labeled when the oxidation of cyclooctene was carried out in the presence of 1000 equiv H<sub>2</sub><sup>18</sup>O.





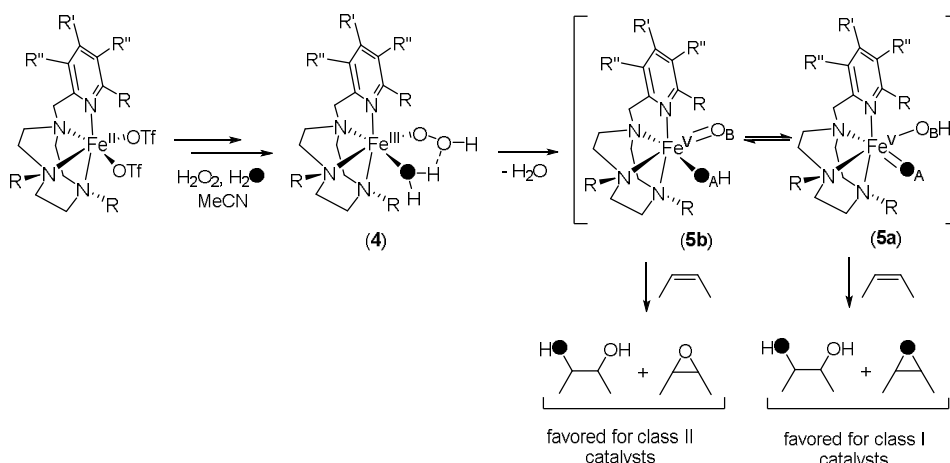
**Scheme 2.** Water assisted (Fe<sup>III</sup>/Fe<sup>V</sup>) and non-water assisted (Fe<sup>II</sup>/Fe<sup>IV</sup>) mechanisms to explain the oxidation of olefins by mononuclear non-heme iron catalysts.

Labeling experiments have been carried out by oxidizing *cis*-cyclooctene (100 equiv) in the presence of H<sub>2</sub><sup>18</sup>O (1000 equiv) using H<sub>2</sub>O<sub>2</sub> as oxidant (10 equiv) (Table 7). For all catalysts, most of the *syn*-diol product contains one oxygen atom coming from water (89±10% singly <sup>18</sup>O-labeled diol). However, it is worth highlighting that class I complexes give a higher percentage of <sup>18</sup>O-atom incorporation (95-99%) than class II (78-89%). The other oxygen atom into the *syn*-diol product originates from H<sub>2</sub>O<sub>2</sub> as previously reported for catalysts <sup>H,H</sup>1 and <sup>Me,H</sup>1 using H<sub>2</sub><sup>18</sup>O<sub>2</sub> as oxidant.<sup>15,46</sup> Clear-cut differences between class I and class II complexes arise when the labeling results for the other product of the reaction, cyclooctene oxide, are analyzed. Incorporation of water into the epoxide product is very high for class I complexes (70±7%), while for class II the amount of <sup>18</sup>O-labeled epoxide dramatically decreases to 7±3% (Table 7). A similar trend in the <sup>18</sup>O-content, *i.e.* high incorporation for class I and low for class II, has been previously observed in alcohol products obtained in the hydroxylation of alkanes in the presence of H<sub>2</sub><sup>18</sup>O.<sup>49</sup> Therefore, by analyzing the isotope labeling in *cis*-dihydroxylation and epoxidation products we conclude that class I and class II of catalysts operate via a water-assisted pathway with a common Fe<sup>V</sup>(O)(OH) oxidant. However, while the oxo ligand transferred to cyclooctene in class I catalysts mainly originates from water, it almost exclusively comes from H<sub>2</sub>O<sub>2</sub> in class II as ascertained from the labeling results in the epoxide product. Some involvement of the non-water assisted mechanism (Scheme 2, right) cannot be ruled out, particularly for class II complexes for which a lower percentage of <sup>18</sup>O-atom incorporation into the *cis*-diol is observed (78-89%) compared to class I (95-99%).

It is also important to notice that within class I catalysts the percentage of water incorporation into the epoxide is slightly tuned by the electronic properties of the  $\gamma$  substituent in the pyridine ring, though this effect is much subtler. Catalysts with no substituent (<sup>H,H</sup>1) or an electron-rich group in  $\gamma$  position (<sup>H,Me</sup>1, <sup>H,NMe2</sup>1 and <sup>H,OMe</sup>1) afford epoxide with a <sup>18</sup>O-content roughly 10% higher compared to catalysts with electron-withdrawing groups (<sup>H,Cl</sup>1, <sup>H,NO2</sup>1 and <sup>H,CO2Et</sup>1) (74±3% versus 65±2%).

In a previous mechanistic study on the olefin epoxidation reaction catalyzed by <sup>H,H</sup>1 we concluded that, since the two coordination sites where oxo and hydroxide ligand binding occur are not identical, Fe<sup>V</sup>(O)(OH) species (5) can exist as two tautomers which are related by a fast water-assisted equilibrium (Scheme 3).<sup>46</sup> The difference between these two isomers is the relative position of the oxo and the hydroxide ligand. While in the isomer Fe<sup>V</sup>(O<sub>A</sub>)(O<sub>B</sub>H) (5a) the oxo ligand binds in position A, which is *trans* to the NCH<sub>2</sub>Py unit, in isomer Fe<sup>V</sup>(O<sub>B</sub>)(O<sub>A</sub>H) (5b) the oxo group is located *trans* to one of the N-methyl groups (position B). As hydrogen peroxide binding in the preceding Fe<sup>III</sup>(OOH)(H<sub>2</sub>O) intermediate (4) takes place preferentially in B position,<sup>49</sup> water binding occurs mainly in position A. Thus, the relative reactivity of 5a and 5b determines the percentage of oxygen from water that ends up into the oxidized product. In the particular case of <sup>H,H</sup>1, this value was found to be dependent on the nature of the olefin. *Cis*-olefins were epoxidized with ~60-70% incorporation of water, while *trans* and terminal olefins incorporated substantially smaller amounts of water (~30%).<sup>46</sup>

The present analysis indicates that the relative reactivity of the two tautomers is only slightly modified when the electronic properties of the pyridine are altered by introducing electron-releasing or electron-withdrawing groups at the  $\gamma$  position. This conclusion is not surprising if it is taken into account that the pyridine ligand is disposed in a relative *cis*-position with respect to the two coordination sites occupied by the oxo and hydroxide ligands (Scheme 3). Ligands in relative *cis*-position are expected to have a smaller effect than those in *trans* because the latter facilitates electronic communication between the two ligands. Instead, the introduction of sterically more demanding groups at the  $\alpha$  position has a profound impact in the relative reactivity of 5a/5b and, in turn, in the epoxide labeling result. Indeed, a space filling analysis (Figure 1) shows that position A, which falls in the same plane as the pyridine ring, is in close proximity to the  $\alpha$ -pyridine substituent and presumably becomes less accessible to the substrate. As a consequence, isomer 5a becomes less reactive and the percentage of water incorporated into products is diminished. With these premises, we suggest that steric interactions produce a more sensitive modification of the relative reactivity of the two tautomers. However, further clarification of this point is under study.



**Scheme 3.** Proposed mechanism for alkene oxidation, where the fast equilibrium between the two tautomers 5a and 5b is represented.

## Conclusion

In the present work we have described the synthesis and the characterization of a broad family of mononuclear iron complexes containing a derivatized Pytacn ligand structure. We have demonstrated that the introduction of different substituents in the pyridine ring causes modest but systematic effects in the geometric parameters of the resulting complexes, but substantial changes in the electronic properties of the iron center. Modification of the electronic properties of the iron center are achieved by introducing different substituents in the  $\gamma$ -position of the pyridine ring (class I complexes). These modifications become important to systematically and consistently define the spin state of the iron center in this class of complexes, for which the LS and HS configurations are energetically very close. In particular, for  $^{H,R'}2$  complexes the effect of the  $\gamma$ -substituent can be understood in accordance with simple ligand field theory; the LS contribution is more important upon increasing the  $\pi$ -acceptor character of the pyridine, in turn modulated by the electron-releasing ability of the  $\gamma$ -substituent. On the other hand, the presence of substituents in the  $\alpha$ -position of the pyridine (class II compounds) introduce steric constraints that cause dramatic modifications in the properties of the iron center by favoring the HS configuration over the LS configuration. This effect also causes an increase in  $Fe^{III}/Fe^{II}$  redox potentials because the more compact ferric center becomes destabilized.

Although all complexes presented herein behave as highly efficient catalysts in the oxidation of C-H and C=C bonds using  $H_2O_2$  as the oxidant through the intermediacy of a common  $Fe^V(O)(OH)$  oxidant, there are some clear differences among them. The presence of a methyl group in the  $\alpha$  position of the pyridine ring affords catalysts that maintain their activity at higher oxidant concentrations and exhibit remarkably high D/E ratios in the oxidation of cyclooctene. These

results convert them as potentially good catalysts for the preparation of alcohols and *syn*-diols in large scale. Differences between class I and class II catalysts are evidenced in the  $^{18}O$ -content of the epoxide product for experiments carried out in the presence of  $H_2^{18}O$ . Complexes without any substituent in the  $\alpha$  position (class I) exhibit much higher levels of oxygen-incorporation from water into the oxidized products than those bearing a substituent in this position (class II). While the effect of the introduction of a substituent in the  $\alpha$  position is dramatic, the electronic properties of the group in the  $\gamma$ -position of the pyridine only induce minimal modifications. Thus, steric demands in close proximity to the iron site emerge from this study as the key structural aspect defining not only the relative reactivity of the two tautomeric active  $Fe^V(O)(OH)$  species, but also the chemoselectivity towards *cis*-dihydroxylation over epoxidation.

## Experimental Section

**Materials.** Reagents and solvents used were of commercially available reagent quality unless otherwise stated.  $H_2^{18}O_2$  (90%  $^{18}O$ -enriched, 2% solution in  $H_2O$ ) and  $H_2^{18}O$  (95%  $^{18}O$ -enriched) were received from ICON Isotopes. Solvents were purchased from SDS and Scharlab.

**Physical measurements.** IR spectra were taken in a Mattson-Galaxy Satellite FT-IR spectrophotometer using a MKII Golden Gate single reflection ATR system. UV-vis spectroscopy was performed on a Cary 50 Scan (Varian) UV-vis spectrophotometer with 1 cm quartz cells. NMR spectra were taken on Bruker DXP300 or 400MHz spectrometer using standard conditions. Elemental analyses were performed using a CHNS-O EA-2400 serie II from Perkin Elmer. The ESI-MS experiments were performed on a HPLC/MS chromatograph, HPLC from Agilent 1100 Series and MS from Bruker Daltonics, Esquire6000 Ion Trap, using acetonitrile as a mobile phase. Product analyses were performed on an Agilent 7820A gas chromatograph (HP5 column, 30m or Cyclosil-B column, 30m) and a flame ionization detector. GC-MS spectral analyses were performed on an Agilent 7890A gas chromatograph interfaced with an Agilent 5975c MS mass spectrometer. A

50% NH<sub>3</sub>/CH<sub>4</sub> mix was used as the ionization gas for chemical ionization analyses. The products were identified by comparison of their GC retention times and GC/MS with those of authentic compounds. Cyclic voltammetric (CV) experiments were performed in an IJ-Cambria IH-660 potentiostat using a three electrode cell. Glassy carbon disk electrode (3 mm diameter) from BAS were used as working electrode, platinum wire was used as auxiliary, and SCE was used as the reference electrode (all the potentials given in this work are always with regard to this reference electrode). All cyclic voltammograms were recorded at 100 mV·s<sup>-1</sup> scan rate. The complexes were dissolved in previously degassed solvents containing the necessary amount of n-Bu<sub>4</sub>NPF<sub>6</sub> as supporting electrolyte to yield a 0.1 M ionic strength solution. All E<sub>1/2</sub> values reported in this work were estimated from cyclic voltammetric experiments as the average of the oxidative and reductive peak potentials (Ep<sub>a</sub> + Ep<sub>c</sub>)/2.

Solution magnetic susceptibility measurements were measured by NMR using the Evans' method as described in the literature using special coaxial insert tubes purchased from Wilmad Glass Co..

**Synthesis of ligands.** Syntheses and full characterization of ligands <sup>R,R'</sup>Pytacn are included in the Supporting Information.

### Synthesis of complexes.

*Synthesis of bis-triflate complexes [Fe(OTf)<sub>2</sub>(<sup>R,R'</sup>Pytacn)] (<sup>R,R'</sup>1)*

[Fe(OTf)<sub>2</sub>(<sup>H,H</sup>Pytacn)] (<sup>H,H</sup>1)<sup>16</sup> and [Fe(OTf)<sub>2</sub>(<sup>Me,H</sup>Pytacn)] (<sup>Me,H</sup>1)<sup>15</sup> were synthesized as previously reported. Single crystals of compounds <sup>R,R'</sup>1 suitable for X-ray analyses were obtained by slow diethyl ether diffusion into CH<sub>2</sub>Cl<sub>2</sub> solutions of the complexes.

**[Fe(OTf)<sub>2</sub>(<sup>H,Me</sup>Pytacn)] (<sup>H,Me</sup>1).** A suspension of [Fe(OTf)<sub>2</sub>(CH<sub>3</sub>CN)<sub>2</sub>] (176 mg, 0.40 mmols) in CH<sub>2</sub>Cl<sub>2</sub> (2 mL) was added dropwise to a vigorously stirred solution of <sup>H,Me</sup>Pytacn (106 mg, 0.40 mmols) in CH<sub>2</sub>Cl<sub>2</sub> (1 mL). The iron triflate salt solubilized quickly affording a dark red solution which was stirred for 3 hours. Afterwards, the solution was filtered off and slow diethyl ether diffusion afforded 190 mg of yellow crystals (0.31 mmols, 77 %). Anal. Calcd for C<sub>17</sub>H<sub>26</sub>F<sub>6</sub>FeN<sub>4</sub>O<sub>6</sub>S<sub>2</sub>: C, 33.13; H, 4.25; N, 9.09; S, 10.40 %. Found: C, 32.79; H, 3.79; N, 8.83; S, 10.09 %. <sup>1</sup>H-NMR (CD<sub>3</sub>CN, 200 MHz, 300 K) δ, ppm: 14.66, 11.17, 7.73, 5.46. <sup>1</sup>H-NMR (CD<sub>2</sub>Cl<sub>2</sub>, 200 MHz, 300 K) δ, ppm: 145.68, 119.76, 92.89, 48.61, 35.44, -11.56. ESI-MS (m/z): 159.1 [M-2OTf]<sup>2+</sup>.

**[Fe(OTf)<sub>2</sub>(<sup>H,NMe2</sup>Pytacn)] (<sup>H,NMe2</sup>1).** Prepared in analogous manner to <sup>H,Me</sup>1. Yield = 69%. Anal. Calcd for C<sub>18</sub>H<sub>29</sub>F<sub>6</sub>FeN<sub>5</sub>O<sub>6</sub>S<sub>2</sub>·0.6 H<sub>2</sub>O: C, 32.95; H, 4.64; N, 10.67; S, 9.77 %. Found: C, 32.83; H, 4.59; N, 10.60; S, 9.80 %. FT-IR (ATR) ν, cm<sup>-1</sup>: 2916-2872 (C-H)<sub>sp3</sub>, 1298 (py), 1219, 1158, 1027, 1010, 632 (CF<sub>3</sub>SO<sub>3</sub>). <sup>1</sup>H-NMR (CD<sub>3</sub>CN, 400 MHz, 400 K) δ, ppm: 44.52, 34.32, 29.21, 20.73, 18.80, 12.11, 6.90. <sup>1</sup>H-NMR (CD<sub>2</sub>Cl<sub>2</sub>, 400 MHz, 300 K) δ, ppm: 120.50, 108.63, 83.25, 42.69, 39.49. ESI-MS (m/z): 496.0 [M-OTf]<sup>+</sup> (100), 173.5 [M-2OTf]<sup>2+</sup> (25).

**[Fe(OTf)<sub>2</sub>(<sup>H,OMe</sup>Pytacn)] (<sup>H,OMe</sup>1).** Prepared in analogous manner to <sup>H,Me</sup>1. Yield = 38%. Anal. Calcd for C<sub>19</sub>H<sub>30</sub>F<sub>6</sub>FeN<sub>4</sub>O<sub>7</sub>S<sub>2</sub>·0.25 H<sub>2</sub>O: C, 34.32; H, 4.62; N, 8.43%. Found: C, 34.04; H, 4.50; N, 8.65 %. FT-IR (ATR) ν, cm<sup>-1</sup>: 2968-2888 (C-H)<sub>sp3</sub>, 1468 (py), 1250, 1157, 1026, 635

(CF<sub>3</sub>SO<sub>3</sub>). <sup>1</sup>H-NMR (CD<sub>3</sub>CN, 400 MHz, 400 K) δ, ppm: 13.41, 11.60, 8.80, 6.49, 3.64. <sup>1</sup>H-NMR (CD<sub>2</sub>Cl<sub>2</sub>, 400 MHz, 300 K) δ, ppm: 120.38, 114.44, 94.31. ESI-MS (m/z): 511.1 [M-OTf]<sup>+</sup> (25), 181.0 [M-2OTf]<sup>2+</sup> (100).

**[Fe(OTf)<sub>2</sub>(<sup>H,Cl</sup>Pytacn)] (<sup>H,Cl</sup>1).** A solution of [Fe(OTf)<sub>2</sub>(CH<sub>3</sub>CN)<sub>2</sub>] (155 mg, 0.36 mmols) in anhydrous THF (2 mL) was added dropwise to a vigorously stirred solution of <sup>H,Cl</sup>Pytacn (101 mg, 0.36 mmols) in THF (1.5 mL). After a few seconds the solution became cloudy and a pale yellow precipitate appeared. After stirring for 2 hours the solution was filtered off and the resultant yellow solid dried under vacuum. This solid was dissolved in CH<sub>2</sub>Cl<sub>2</sub> and filtered through Celite. Slow diethyl ether diffusion over the resulting solution afforded, in a few days, 143 mg of yellow crystals (0.22 mmols, 63 %). Anal. Calcd for C<sub>16</sub>H<sub>23</sub>ClF<sub>6</sub>FeN<sub>4</sub>O<sub>6</sub>S<sub>2</sub>: C, 30.18; H, 3.64; N, 8.80; S, 10.07 %. Found: C, 30.09; H, 3.62; N, 8.88; S, 9.95 %. FT-IR (ATR) ν, cm<sup>-1</sup>: 2960-2885 (C-H)<sub>sp3</sub>, 1281 (py), 1222, 1161, 1027, 634 (CF<sub>3</sub>SO<sub>3</sub>). <sup>1</sup>H-NMR (CD<sub>3</sub>CN, 400 MHz, 300 K) δ, ppm: 12.44, 9.53, 7.07, 5.45, 3.95, 3.43, 2.18, 1.13. <sup>1</sup>H-NMR (CD<sub>2</sub>Cl<sub>2</sub>, 400 MHz, 300 K) δ, ppm: 157.29, 119.78, 100.05, 89.73, 47.813, 33.75. ESI-MS (m/z): 487.0 [M-OTf]<sup>+</sup> (100), 168.9 [M-OTf]<sup>2+</sup> (25).

**[Fe(OTf)<sub>2</sub>(<sup>H,CO2Et</sup>Pytacn)] (<sup>H,CO2Et</sup>1).** Prepared in analogous manner to <sup>H,Cl</sup>1. Yield = 43 %. Anal. Calcd for C<sub>19</sub>H<sub>28</sub>F<sub>6</sub>FeN<sub>4</sub>O<sub>8</sub>S<sub>2</sub>: C, 33.84; H, 4.18; N, 8.31%. Found: C, 33.36; H, 3.86; N, 8.52 %. FT-IR (ATR) ν, cm<sup>-1</sup>: 2982-2865 (C-H)<sub>sp3</sub>, 1732 (C=O), 1284 (py), 1284, 1224, 1164, 1026, 633 (CF<sub>3</sub>SO<sub>3</sub>). <sup>1</sup>H-NMR (CD<sub>3</sub>CN, 400 MHz, 400 K) δ, ppm: 10.84, 8.89, 5.76, 4.83, 4.36, 4.39, 3.04, 2.11, 1.97. <sup>1</sup>H-NMR (CD<sub>2</sub>Cl<sub>2</sub>, 400 MHz, 300 K) δ, ppm: 164.22, 103.84, 90.26, 49.67, 39.01. ESI-MS (m/z): 525.1 [M-OTf]<sup>+</sup> (25), 188.0 [M-2OTf]<sup>2+</sup> (100).

**[Fe(OTf)<sub>2</sub>(<sup>H,NO2</sup>Pytacn)] (<sup>H,NO2</sup>1).** Prepared in analogous manner to <sup>H,Me</sup>1. Yield = 73 %. Anal. Calcd for C<sub>16</sub>H<sub>23</sub>F<sub>6</sub>FeN<sub>5</sub>O<sub>8</sub>S<sub>2</sub>: C, 29.69; H, 3.58; N, 10.82; S, 9.91 %. Found: C, 29.87; H, 3.70; N, 10.81; S, 9.76 %. FT-IR (ATR) ν, cm<sup>-1</sup>: 2917 (C-H)<sub>sp3</sub>, 1279 (py), 1223, 1159, 1028, 633 (CF<sub>3</sub>SO<sub>3</sub>). <sup>1</sup>H-NMR (CD<sub>3</sub>CN, 400 MHz, 400 K) δ, ppm: 10.47, 8.73, 4.93, 4.17, 7.78, 2.86, 2.64, 2.14, 1.13. <sup>1</sup>H-NMR (CD<sub>2</sub>Cl<sub>2</sub>, 400 MHz, 300 K) δ, ppm: 174.18, 136.30, 108.77, 92.12, 47.82, 33.18. ESI-MS (m/z): 498.0 [M-OTf]<sup>+</sup> (100), 174.5 [M-2OTf]<sup>2+</sup> (100).

**[Fe(OTf)<sub>2</sub>(<sup>Me,Me</sup>Pytacn)] (<sup>Me,Me</sup>1).** Prepared in analogous manner to <sup>H,Me</sup>1. Yield = 59 %. Anal. Calcd for C<sub>18</sub>H<sub>28</sub>F<sub>6</sub>FeN<sub>4</sub>O<sub>6</sub>S<sub>2</sub>·1.25 CH<sub>2</sub>Cl<sub>2</sub>: C, 31.39; H, 4.17; N, 7.61; S, 8.71 %. Found: C, 31.24; H, 4.12; N, 7.90; S, 9.06 %. <sup>1</sup>H-NMR (CD<sub>3</sub>CN, 200 MHz, 300 K) δ, ppm: 138.63, 84.64, 54.02, 47.91, 42.83, 31.14, 13.71, -32.78. <sup>1</sup>H-NMR (CD<sub>2</sub>Cl<sub>2</sub>, 200 MHz, 300 K) δ, ppm: 176.16, 130.18, 101.05, 95.33, 60.52, 52.75, 38.97, -1.70, -37.25. ESI-MS (m/z): 166.1 [M-2OTf]<sup>2+</sup>, 481.12 [M-OTf]<sup>+</sup>.

**[Fe(OTf)<sub>2</sub>(<sup>Cl,H</sup>Pytacn)] (<sup>Cl,H</sup>1).** Prepared in analogous manner to <sup>H,Cl</sup>1. 80 mg of yellow crystals were obtained (0.12 mmols, 66 %). Anal. Calcd for C<sub>16</sub>H<sub>23</sub>F<sub>6</sub>ClFeN<sub>4</sub>O<sub>6</sub>S<sub>2</sub>·1.5H<sub>2</sub>O: C, 28.95; H, 3.92; N, 8.44 %. Found: C, 29.01; H, 3.76; N, 8.49. FT-IR (ATR) ν, cm<sup>-1</sup>: 3357-3262 (C-H)<sub>sp3</sub>, 1281, 1226, 1163, 1027, 630 (CF<sub>3</sub>SO<sub>3</sub>). <sup>1</sup>H-NMR (CD<sub>3</sub>CN, 200 MHz, 300 K) δ, ppm: 100.19, 60.14, 39.41. <sup>1</sup>H-NMR (400 MHz, CD<sub>2</sub>Cl<sub>2</sub>, 300 K) δ, ppm: 155.97, 121.95, 106.25, 101.89, 89.16, 75.50, 60.30, 44.68, 32.45, 18.57. ESI-MS (m/z): 169.0 [M-2OTf]<sup>2+</sup>, 487.1 [M-OTf]<sup>+</sup>.

**[Fe(OTf)<sub>2</sub>(<sup>F,H</sup>Pytacn)] (<sup>F,H</sup>1).** Prepared in analogous manner to <sup>H,Cl</sup>1. Yield = 27 %. Anal. Calcd for

C<sub>16</sub>H<sub>23</sub>F<sub>7</sub>eN<sub>4</sub>O<sub>6</sub>S<sub>2</sub>·3H<sub>2</sub>O: C, 28.50; H, 4.33; N, 8.31; S, 9.51 %. Found: C, 28.40; H, 3.70; N, 8.15; S, 9.48 %. FT-IR (ATR)  $\nu$ , cm<sup>-1</sup>: 2927 (C-H)<sub>sp3</sub>, 1309, 1213, 1158, 1015, 630 (CF<sub>3</sub>SO<sub>3</sub>). <sup>1</sup>H-NMR (CD<sub>3</sub>CN, 200 MHz, 300 K)  $\delta$ , ppm: 104.67, 84.41, 70.10, 50.59, 28.53, -2.91. <sup>1</sup>H-NMR (200 MHz, CD<sub>2</sub>Cl<sub>2</sub>, 300 K)  $\delta$ , ppm: 142.65, 122.50, 108.05, 80.16, 69.76, 29.99, 18.95. ESI-MS (m/z): 161.0 [M-2OTf]<sup>2+</sup>, 471.1 [M-OTf]<sup>+</sup>.

*Synthesis of bis-chloro complexes [FeCl<sub>2</sub>(<sup>R,R</sup>Pytacn)] (<sup>R,R</sup>3)*

Chlorocomplexes <sup>R,R</sup>3 were prepared by reaction of the particular ligand (<sup>R,R</sup>Pytacn) with equimolar amounts of FeCl<sub>2</sub> in THF as exemplified for <sup>H,H</sup>3.

**[FeCl<sub>2</sub>(<sup>H,H</sup>Pytacn)] (<sup>H,H</sup>3).** A suspension of FeCl<sub>2</sub> (22 mg, 0.17 mmols) in anhydrous THF (2 mL) was added dropwise to a vigorously stirred solution of Pytacn (41 mg, 0.17 mmols) in THF (1.5 mL). The FeCl<sub>2</sub> slowly entered into the solution and after about 10 min under vigorous stirring a yellow precipitate appeared. After stirring for 12 hours the solution was filtered off and the resulting pale yellow solid was dried under vacuum. This compound was dissolved in CH<sub>3</sub>CN and filtered through Celite. Slow diethyl ether diffusion over this solution afforded 51 mg of the desired compound (0.14 mmols, 82 %). Anal. Calcd for C<sub>14</sub>H<sub>24</sub>Cl<sub>2</sub>FeN<sub>4</sub>·1/4H<sub>2</sub>O: C, 44.29; H, 6.51; N, 14.76 %. Found: C, 44.35; H, 6.35; N, 14.51 %. FT-IR (ATR)  $\nu$ , cm<sup>-1</sup>: 2968 - 2900 (C-H)<sub>sp3</sub>, 1602, 1455, 1134, 725. <sup>1</sup>H-NMR (CD<sub>3</sub>CN, 200 MHz, 300 K)  $\delta$ , ppm: 99.48, 78.07, 47.39, 36.23, 25.74, 11.19. ESI-MS (m/z): 339 [M-Cl]<sup>+</sup>, 416 [M+CH<sub>3</sub>CN+H]<sup>+</sup>. CV (CH<sub>3</sub>CN) E<sub>1/2</sub>, mV: 138.

**[FeCl<sub>2</sub>(<sup>H,NMe2</sup>Pytacn)] (<sup>H,NMe2</sup>3).** Yield = 35 %. Anal. Calcd for C<sub>16</sub>H<sub>29</sub>Cl<sub>2</sub>FeN<sub>5</sub>·0.2 CH<sub>2</sub>Cl<sub>2</sub>: C, 44.71; H, 6.81; N, 16.09 %. Found: C, 44.71; H, 6.80; N, 15.97 %. FT-IR (ATR)  $\nu$ , cm<sup>-1</sup>: 2949 - 2851 (C-H)<sub>sp3</sub>, 1613, 1010, 810. <sup>1</sup>H-NMR (CD<sub>3</sub>CN, 400 MHz, 300 K)  $\delta$ , ppm: 110.52, 93.09, 45.00, 34.48. ESI-MS (m/z): 382.1 [M-Cl]<sup>+</sup> (100), 173.5 [M-2Cl]<sup>2+</sup> (75), 390.1 [2M-2Cl+O]<sup>2+</sup> (100). CV (CH<sub>3</sub>CN) E<sub>1/2</sub>, mV: 11.

**[FeCl<sub>2</sub>(<sup>H,OMe</sup>Pytacn)] (<sup>H,OMe</sup>3).** Yield = 60 %. Anal. Calcd for C<sub>17</sub>H<sub>30</sub>Cl<sub>2</sub>FeN<sub>4</sub>O: C, 47.13; H, 6.98; N, 12.93 %. Found: C, 47.32; H, 6.78; N, 12.78 %. FT-IR (ATR)  $\nu$ , cm<sup>-1</sup>: 2953 - 2843 (C-H)<sub>sp3</sub>, 1016, 990 (O-CH<sub>3</sub>), 1595, 1263, 804. <sup>1</sup>H-NMR (CD<sub>3</sub>CN, 400 MHz, 300 K)  $\delta$ , ppm: 132.72, 91.05, 78.63. ESI-MS (m/z): 475.1 [M-Cl]<sup>+</sup> (100), 181.1 [M-2Cl]<sup>2+</sup> (50). CV (CH<sub>3</sub>CN) E<sub>1/2</sub>, mV: 107.

**[FeCl<sub>2</sub>(<sup>H,Me</sup>Pytacn)] (<sup>H,Me</sup>3).** Yield = 65 %. Anal. Calcd for C<sub>15</sub>H<sub>26</sub>Cl<sub>2</sub>FeN<sub>4</sub>·0.5 CH<sub>2</sub>Cl<sub>2</sub>: C, 43.13; H, 6.31; N, 12.98 %. Found: C, 43.66; H, 6.33; N, 12.41 %. <sup>1</sup>H-NMR (CD<sub>3</sub>CN, 200 MHz, 300 K)  $\delta$ , ppm: 93.35, 68.86, 48.32, 34.02, -21.20. ESI-MS (m/z): 353.1 [M-Cl]<sup>+</sup>. CV (CH<sub>3</sub>CN) E<sub>1/2</sub>, mV: 176.

**[FeCl<sub>2</sub>(<sup>H,Cl</sup>Pytacn)] (<sup>H,Cl</sup>3).** Yield = 71 %. Anal. Calcd for C<sub>14</sub>H<sub>23</sub>Cl<sub>3</sub>FeN<sub>4</sub>·0.35 CH<sub>2</sub>Cl<sub>2</sub>: C, 39.24; H, 5.44; N, 12.75 %. Found: C, 39.26; H, 5.53; N, 12.92; S, 0.33 %. FT-IR (ATR)  $\nu$ , cm<sup>-1</sup>: 2961 - 2856 (C-H)<sub>sp3</sub>, 1588, 1461, 1104, 1016, 730. <sup>1</sup>H-NMR (CD<sub>3</sub>CN, 400 MHz, 300 K)  $\delta$ , ppm: 149.50, 83.17, 48.24, 35.24, 33.16. ESI-MS (m/z): 373.1 [M-Cl]<sup>+</sup> (25), 168.9 [M-2Cl]<sup>2+</sup> (100). CV (CH<sub>3</sub>CN) E<sub>1/2</sub>, mV: 165.

**[FeCl<sub>2</sub>(<sup>H,CO2Et</sup>Pytacn)] (<sup>H,CO2Et</sup>3).** Yield = 33 %. Anal. Calcd for C<sub>16</sub>H<sub>29</sub>Cl<sub>2</sub>FeN<sub>5</sub>·0.35 Et<sub>2</sub>O: C, 46.71; H, 6.71; N, 11.84 %. Found: C, 46.55; H, 6.28; N, 11.54 %. FT-IR

(ATR)  $\nu$ , cm<sup>-1</sup>: 2967 - 2855 (C-H)<sub>sp3</sub>, 1711 (C=O), 1207, 1002, 766. <sup>1</sup>H-NMR (CD<sub>3</sub>CN, 400 MHz, 300 K)  $\delta$ , ppm: 156.02, 82.55, 50.15, 34.93. ESI-MS (m/z): 411.1 [M-Cl]<sup>+</sup> (100), 188.0 [M-2Cl]<sup>2+</sup> (50). CV (CH<sub>3</sub>CN) E<sub>1/2</sub>, mV: 171.

**[FeCl<sub>2</sub>(<sup>H,NO2</sup>Pytacn)] (<sup>H,NO2</sup>3).** Yield = 65 %. Anal. Calcd for C<sub>14</sub>H<sub>23</sub>Cl<sub>2</sub>FeN<sub>5</sub>O<sub>2</sub>·1CH<sub>2</sub>Cl<sub>2</sub>: C, 35.67; H, 4.99; N, 13.87 %. Found: C, 35.80; H, 5.08; N, 13.72 %. FT-IR (ATR)  $\nu$ , cm<sup>-1</sup>: 2969 - 2859 (C-H)<sub>sp3</sub>, 2361, 1738, 1524, 1345, 731. <sup>1</sup>H-NMR (CD<sub>3</sub>CN, 400 MHz, 300 K)  $\delta$ , ppm: 167.68, 122.59, 110.33, 90.58, 84.99, 59.47, 48.56, 34.57. ESI-MS (m/z): 384.0 [M-Cl]<sup>+</sup> (100). CV (CH<sub>3</sub>CN) E<sub>1/2</sub>, mV: 225.

**[FeCl<sub>2</sub>(<sup>Me,H</sup>Pytacn)] (<sup>Me,H</sup>3).** Yield = 82 %. Anal. Calcd for C<sub>15</sub>H<sub>26</sub>Cl<sub>2</sub>FeN<sub>4</sub>·1/2H<sub>2</sub>O: C, 45.25; H, 6.84; N, 14.07 %. Found: C, 45.74; H, 7.30; N, 14.15 %. FT-IR (ATR)  $\nu$ , cm<sup>-1</sup>: 2994 - 2816 (C-H)<sub>sp3</sub>, 1601, 1462, 1020, 809. <sup>1</sup>H-NMR (CD<sub>3</sub>CN, 200 MHz, 300 K)  $\delta$ , ppm: 82.84, 74.60, 47.16, 32.07, 18.78, -28.37. ESI-MS (m/z): 353.1 [M-Cl]<sup>+</sup>. CV (CH<sub>3</sub>CN) E<sub>1/2</sub>, mV: 211.

**[FeCl<sub>2</sub>(<sup>Me,Me</sup>Pytacn)] (<sup>Me,Me</sup>3).** Yield = 82 %. Anal. Calcd for C<sub>16</sub>H<sub>28</sub>Cl<sub>2</sub>FeN<sub>4</sub>·0.25THF·0.50H<sub>2</sub>O: C, 47.46; H, 7.26; N, 13.02 %. Found: C, 47.59; H, 7.02; N, 12.85 %. <sup>1</sup>H-NMR (CD<sub>3</sub>CN, 200 MHz, 300 K)  $\delta$ , ppm: 83.61, 74.86, 46.39, 31.47, -6.65. ESI-MS (m/z): 367.1 [M-Cl]<sup>+</sup>, 408.2 [M-Cl+CH<sub>3</sub>CN]<sup>+</sup>. CV (CH<sub>3</sub>CN) E<sub>1/2</sub>, mV: 238.

**[FeCl<sub>2</sub>(<sup>F,H</sup>Pytacn)] (<sup>F,H</sup>3).** Yield = 43 %. Anal. Calcd for C<sub>14</sub>H<sub>23</sub>Cl<sub>2</sub>FFeN<sub>4</sub>·H<sub>2</sub>O: C, 40.90; H, 6.13; N, 13.63 %. Found: C, 40.21; H, 6.45; N, 13.14 %. FT-IR (ATR)  $\nu$ , cm<sup>-1</sup>: 2921 - 2854 (C-H)<sub>sp3</sub>, 1615, 1454, 1017, 816. <sup>1</sup>H-NMR (CD<sub>3</sub>CN, 200 MHz, 300 K)  $\delta$ , ppm: 87.85, 73.47, 59.58, 38.40, 27.84, 16.42. ESI-MS (m/z): 357.7 [M-Cl]<sup>+</sup>, 161.0 [M-2Cl]<sup>2+</sup>.

*Synthesis of bis-acetonitrile complexes [Fe(<sup>R,R</sup>Pytacn)(CH<sub>3</sub>CN)<sub>2</sub>]<sub>2</sub>X<sub>2</sub> (<sup>R,R</sup>2X)*

[Fe(<sup>H,H</sup>Pytacn)(CH<sub>3</sub>CN)<sub>2</sub>](PF<sub>6</sub>)<sub>2</sub> (<sup>H,H</sup>2PF<sub>6</sub>) was prepared as previously reported.<sup>16</sup>

**[Fe(<sup>H,H</sup>Pytacn)(CH<sub>3</sub>CN)<sub>2</sub>](SbF<sub>6</sub>)<sub>2</sub> (<sup>H,H</sup>2SbF<sub>6</sub>).** FeCl<sub>2</sub> (51 mg, 0.40 mmols) was added directly as a solid to a vigorously stirred solution of <sup>H,H</sup>Pytacn (100 mg, 0.40 mmols) in CH<sub>3</sub>CN. The initially pale yellow solution became gradually bright orange as the FeCl<sub>2</sub> got dissolved. After stirring for 30 minutes, AgSbF<sub>6</sub> (277 mg, 0.80 mmols) was added which caused the immediate precipitation of AgCl and an evident color change of the solution from bright orange to dark brown. After stirring for 30 minutes, the solution was filtered through Celite. Slow diethyl ether diffusion over the resulting solution afforded, in a few days, 245 mg of brown crystals (0.29 mmol, 71% yield). <sup>1</sup>H-NMR (CD<sub>3</sub>CN, 400 MHz, 300 K)  $\delta$ , ppm: 12.68, 9.73, 9.59, 9.10, 7.33, 6.70, 3.82, 2.17, 1.96. HRMS (m/z): 152.0668 [M-2CH<sub>3</sub>CN-2SbF<sub>6</sub>]<sup>2+</sup>, 161.07 [M-2CH<sub>3</sub>CN-2SbF<sub>6</sub>+H<sub>2</sub>O]<sup>2+</sup>, 539.0312 [M-2CH<sub>3</sub>CN-SbF<sub>6</sub>]<sup>+</sup>.

**[Fe(<sup>Me,H</sup>Pytacn)(CH<sub>3</sub>CN)<sub>2</sub>](SbF<sub>6</sub>)<sub>2</sub> (<sup>Me,H</sup>2SbF<sub>6</sub>).** FeCl<sub>2</sub> (11 mg, 0.09 mmols) was added directly as a solid to a vigorously stirred solution of <sup>Me,H</sup>Pytacn (21 mg, 0.09 mmols) in CH<sub>3</sub>CN. The initially pale yellow solution became gradually bright orange as the FeCl<sub>2</sub> got dissolved. After stirring for 30 minutes, AgSbF<sub>6</sub> (60 mg, 0.17 mmols) was added which caused the immediate precipitation of AgCl and an evident color change of the solution from bright orange to yellowish. After stirring for 30 minutes, the solution was filtered through Celite. Slow diethyl ether

diffusion over the resulting solution afforded, in a few days, 54 mg of white crystals (0.05 mmol, 69% yield). <sup>1</sup>H-NMR (CD<sub>3</sub>CN, 400 MHz, 300 K) δ, ppm: 143.94, 84.76, 56.30, 49.10, -7.74, -32.53. ESI-MS (m/z): 159.1 [M-2CH<sub>3</sub>CN-2SbF<sub>6</sub>]<sup>2+</sup>, 353.1 [M-2CH<sub>3</sub>CN-2SbF<sub>6</sub>+Cl]<sup>+</sup>.

**Reaction conditions for catalysis.** In a typical reaction, 0.36 mL of a 70 mM (25 μmols) or 700 mM (250 μmols) H<sub>2</sub>O<sub>2</sub> solution (diluted from a 35% H<sub>2</sub>O<sub>2</sub> aqueous solution) in CH<sub>3</sub>CN was delivered by syringe pump over 30 min at 25 °C to a vigorously stirred CH<sub>3</sub>CN solution (2.14 mL) containing the iron catalyst (2.5 μmols) and the substrate (2500 μmols). The final concentrations of reagents were 1 mM iron catalyst, 10 mM / 100 mM H<sub>2</sub>O<sub>2</sub> and 1 M substrate. After syringe pump addition, the resulting solution was stirred for another 10 min. For the oxidation of cyclohexane, biphenyl (internal standard) was added at this point and the iron complex was removed by passing the solution through a short path of basic alumina or silica followed by elution with 2 mL of AcOEt. Finally, the solution was subjected to GC analysis. The organic products were identified by comparison with authentic compounds.

For the oxidation of cyclooctene, the reaction was performed as described above but under a N<sub>2</sub> atmosphere. After syringe pump addition of the oxidant and stirring for 10 min, 1 mL of acetic anhydride together with 0.1 mL of 1-methylimidazole were added to afford the esterification of the diol product. After stirring for 15 min at room temperature, ice was added and the mixture was stirred for about 30 min. Biphenyl (internal standard) was added and the mixture was extracted with 2 mL CHCl<sub>3</sub>. The organic layer was washed with 2 mL H<sub>2</sub>SO<sub>4</sub> 1M, 2 mL sat. NaHCO<sub>3</sub> and 2 mL H<sub>2</sub>O, dried with MgSO<sub>4</sub> and subjected to GC analysis. The organic products were identified by comparison with authentic compounds.

**Isotopic labeling experiments using H<sub>2</sub><sup>18</sup>O.** The experimental procedure was similar to the one described above for a typical oxidation reaction of cyclooctene. In these experiments 50 μL H<sub>2</sub><sup>18</sup>O (2500 μmols) were delivered by syringe pump together with 0.36 mL of a 70 mM (25 μmols) H<sub>2</sub>O<sub>2</sub> solution into the catalyst (2.5 μmols) and cyclooctene (250 μmols) solution under an inert atmosphere. The incorporation of <sup>18</sup>O into the epoxide and *syn*-diol products was measured by GC-MS analyses. Specific ions corresponding to the epoxide and *syn*-diol mass spectra were computer simulated. In order to account for the isotopic purity of H<sub>2</sub><sup>18</sup>O and its dilution because of the use of aqueous H<sub>2</sub>O<sub>2</sub> solutions, corrected values were obtained by dividing the simulated percentage of <sup>18</sup>O-labeled epoxide and <sup>18</sup>O-labeled *syn*-diol by 0.94.

## ASSOCIATED CONTENT

### Supporting Information

Full description of the synthesis of <sup>R,R'</sup>Pytaen ligands, solid state characterization of <sup>H,OMe</sup>**1**, <sup>H,Me</sup>**1**, <sup>H,Cl</sup>**1**, <sup>H,CO<sub>2</sub>Et</sup>**1** and <sup>Cl,H</sup>**1**, paramagnetic <sup>1</sup>H-NMR spectra of <sup>R,R'</sup>**1** and <sup>R,R'</sup>**2**, variable-temperature paramagnetic <sup>1</sup>H-NMR of <sup>Me,H</sup>**1** and cyclic voltammograms of <sup>R,R'</sup>**3**. This material is available free of charge via the Internet at <http://pubs.acs.org>.

## Acknowledgements

Financial support for this work was provided by the Spanish Ministry of Science (Project CTQ2009-08464/BQU and Consolider Ingenio Ingenio/CSD2010-00065 to M.C. and X. R.)

and the European Research Council (ERC-2009-StG-239910 to M.C.). M. C. and X. R. acknowledge Generalitat de Catalunya for ICREA-Academia Awards and 2009-SGR637. A. C. acknowledges the European Commission for a Career Integration Grant (FP7-PEOPLE-2011-CIG-303522). The Spanish Ministry of Science is acknowledged for a FPU PhD grant to I. P. and for a Ramón y Cajal contract to A.C. We thank Catexel for a generous gift of tritosyl-1,4,7-triazacyclononane.

## References

- (1) a) *Biomimetic Oxidations Catalyzed by Transition Metal Complexes*; Imperial College Press: London, 2000. b) Arakawa, H.; Aresta, M.; Armour, J. N.; Barteau, M. A.; Beckman, E. J.; Bell, A. T.; Bercaw, J. E.; Creutz, C.; Dinjus, E.; Eckert, J.; Fujita, E.; Gibson, D. H.; Goddard, W. A.; Goodman, D. W.; Keller, J.; Kubas, G. J.; Kung, H. H.; Lyons, J. E.; Manzer, L. E.; Marks, T. J.; Morokuma, K.; Nivholas, K. M.; Periana, R.; Que, L.; Rostrup-Nielson, J.; Sachtler, W. M. H.; Schmidt, L. D.; Sen, A.; Somorjai, G. A.; Stair, P. C.; Stults, B. R.; Tumas, W. *Chem. Rev.* **2001**, *101*, 953. c) Bäckvall, J.-E. *Modern oxidation Methods*; Wiley-VCH: Weinheim, 2004. d) Shul'pin, G. B. *Minirew in Org. Chem.* **2009**, *6*(2), 95-104.
- (2) a) Enthaler, S.; Junge, K.; Beller, M. *Angew. Chem. Int. Ed.* **2008**, *47*, 3317. b) Schröder, K.; Junge, K.; Bitterlich, B.; Beller, M. *Top. Organomet. Chem.* **2010**, *33*, 83. c) Mayer, A. C.; Bolm, C. In *Iron Catalysis in Organic Chemistry*; Plietker, B., Ed.; Wiley-VCH: Weinheim, 2008, p 73. d) Liang-Xian, L. *Curr. Org. Chem.* **2010**, *14*, 1099-1126.
- (3) a) Ortiz de Montellano, P. R. *Chem. Rev.* **2010**, *110*, 932. b) Ortiz de Montellano, P. R.; De Voss, J. J. *Nat. Prod. Rep.* **2002**, *19*, 477.
- (4) a) Sazinsky, M. H.; Lippard, S. J. *Acc. Chem. Res.* **2006**, *39*, 558. b) Costas, M.; Mehn, M. P.; Jensen, M. P.; Que Jr., L. *Chem. Rev.* **2004**, *104*, 939. c) Kovaleva, E. G.; Lipscomb, J. D. *Nat. Chem. Biol.* **2008**, *4*, 186. d) Bruijninx, P. C. A.; Koten, G. v.; Gebbink, R. J. M. K. *Chem. Soc. Rev.* **2008**, *12*, 2716. e) Tshuva, E. Y.; Lippard, S. J. *Chem. Rev.* **2004**, *104*, 987.
- (5) a) Que, L.; Tolman, W. B. *Nature* **2008**, *455*, 333. b) Talsi, E. P.; Bryliakov, K. P. *Coord. Chem. Rev.* **2012**, *256*, 1418.
- (6) a) Lu, H.; Zhang, P. *Chem. Soc. Rev.* **2011**, *40*, 1899. b) Che, C.-M.; Huang, J.-S. *Chem. Commun.* **2009**, 3996. c) Costas, M. *Coord. Chem. Rev.* **2011**, *255*, 2912.
- (7) a) Gibson, D. T.; Subramanian, V. In *Microbial Degradation of Aromatic Hydrocarbons*; Gibson, D. T., Ed.; Marcel Dekker: New York, 1984, p 181. b) Gibson, D. T.; Parales, R. E. *Curr. Opin. Biotechnol.* **2000**, *11*, 236. c) Chakrabarty, S.; Austin, R. N.; Deng, D.; Groves, J. T.; Lipscomb, J. D. *J. Am. Chem. Soc.* **2007**, *129*, 3514.
- (8) For Fe-catalyzed arene oxidation see; a) Thibon, A.; Jollet, V.; Ribal, C.; Senechal-David, K.; Billon, L.; Sorokin, A. B.; Banse, F. *Chem. Eur. J.* **2012**, *18*, 2715. b) Möller, K.; Wienhöfer, G.; Schröder, K.; Join, B.; Junge, K.; Beller, M. *Chem. Eur. J.* **2010**, *16*, 10300.
- (9) Selected examples of Fe-catalyzed olefin oxidation; a) Wang, B.; Wang, S.; Xia, C.; Sun, W. *Chem. Eur. J.* **2012**, *18*, 7332. b) Mikhalyova, E. A.; Makhlynets, O. V.; Palluccio, T. D.; Filatov, A. S.; Rybak-Akimova, E.

- V. *Chem. Commun.* **2012**, 48, 687. c) Oddon, F.; Girgenti, E.; Lebrun, C.; Marchi-Delapierre, C.; Pecaut, J.; Menage, S. *Eur. J. Inorg. Chem.* **2012**, 85. d) Feng, Y.; England, J.; Que, L., Jr. *Acs Catal.* **2011**, 1, 1035. e) Wu, M.; Miao, C.-X.; Wang, S.; Hu, X.; Xia, C.; Kühn, F. E.; Sun, W. *Adv. Synth. & Catal.* **2011**, 353, 3014. f) Bruijninx, P. C. A.; Buurmans, I. L. C.; Gosiewska, S.; Moelands, M. A. H.; Lutz, M.; Spek, A. L.; van Koten, G.; Gebbink, R. J. M. K. *Chem. Eur. J.* **2008**, 14, 1228. g) Liu, P.; Wong, E. L. M.; Yuen, A. W. H.; Che, C. M. *Org. Lett.* **2008**, 10, 3275. h) Comba, P.; Rajaraman, G. *Inorg. Chem.* **2008**, 47, 78. i) Mas-Balleste, R.; Que, L., Jr. *J. Am. Chem. Soc.* **2007**, 129, 15964. j) Marchi-Delapierre, C.; Jorge-Robin, A.; Thibon, A.; Ménage, S. *Chem. Commun.* **2007**, 11, 1166. k) Taktak, S. Y., W.; Herrera, A. M.; Rybak-Akimova, E. V. *Inorg. Chem.* **2007**, 46, 2929. l) Bukowski, M. R.; Comba, P.; Lienke, A.; Limberg, C.; de Laorden, C. L.; Mas-Balleste, R.; Merz, M.; Que, L. *Angew. Chem. Int. Ed.* **2006**, 45, 3446. m) Klopstra, M.; Roelfes, G.; Hage, R.; Kellogg, R. M.; Feringa, B. L. *Eur. J. Inorg. Chem.* **2004**, 4, 846. n) Dubois, G.; Murphy, A.; Stack, T. D. P. *Org. Lett.* **2003**, 5, 2469. o) Fujita, M.; Costas, M.; Que Jr., L. *J. Am. Chem. Soc.* **2003**, 125, 9912. p) Ryu, J. Y.; Kim, J.; Costas, M.; Chen, K.; Nam, W.; Que Jr., L. *Chem. Commun.* **2002**, 12, 1288. q) Mekmouche, Y.; Ménage, S.; Toia-Duboc, C.; Fontecave, M.; Galey, J.-B.; Lebrun, C.; Pecaut, J. *Angew. Chem. Int. Ed.* **2001**, 40, 949. r) White, M. C.; Doyle, A. G.; Jacobsen, E. N. *J. Am. Chem. Soc.* **2001**, 123, 7194.
- (10) Selected examples of Fe-catalyzed C-H oxidation; a) Djernes, K. E.; Padilla, M.; Mettry, M.; Young, M. C.; Hooley, R. J. *Chem. Commun.* **2012**, 48, 11576. b) Hitomi, Y.; Arakawa, K.; Funabiki, T.; Kodera, M. *Angew. Chem. Int. Ed.* **2012**, 51, 3448. c) Djernes, K. E.; Moshe, O.; Mettry, M.; Richards, D. D.; Hooley, R. J. *Org. Lett.* **2012**, 14, 788. d) White, M. C. *Science* **2012**, 335, 807. e) He, Y.; Gorden, J. D.; Goldsmith, C. R. *Inorg. Chem.* **2011**, 50, 12651. f) Bigi, M. A.; Reed, S. A.; White, M. C. *Nat. Chem.* **2011**, 3, 216. g) Liu, P.; Liu, Y.; Wong, E. L.-M.; Xiang, S.; Che, C.-M. *Chem. Sci.* **2011**, 2, 2187. h) Bruijninx, P. C. A.; Buurmans, I. L. C.; Huang, Y.; Juhasz, G.; Viciano-Chumillas, M.; Quesada, M.; Reedijk, J.; Lutz, M.; Spek, A. L.; Muenck, E.; Bominaar, E. L.; Gebbink, R. J. M. K. *Inorg. Chem.* **2011**, 50, 9243. i) Chen, M. S.; White, M. C. *Science* **2010**, 327, 566. j) Gomez, L.; Garcia-Bosch, I.; Company, A.; Benet-Buchholz, J.; Polo, A.; Sala, X.; Ribas, X.; Costas, M. *Angew. Chem. Int. Ed.* **2009**, 48, 5720. k) Mayilmurugan, R. Stoeckli-Evans, H.; Suresh, E.; Palaniandavar, M. *Dalton Trans.* **2009**, 26, 5101. l) Comba, P.; Maurer, M.; Vadivelu, P. *Inorg. Chem.* **2009**, 48, 10389. m) Romakh, V. B.; Therrien, B.; Suss-Fink, G.; Shul'pin, G. B. *Inorg. Chem.* **2007**, 46, 3166. n) van den Berg, T. A.; de Boer, J. W.; Browne, W. R.; Roelfes, G.; Feringa, B. L. *Chem. Commun.* **2004**, 22, 2550. o) Roelfes, G.; Lubben, M.; Hage, R.; Que Jr., L.; Feringa, B. L. *Chem. Eur. J.* **2000**, 6, 2152.
- (11) England, J.; Britovsek, G. J. P.; Rabadia, N.; White, A. J. P. *Inorg. Chem.* **2007**, 46, 3752.
- (12) Mas-Ballesté, R.; Costas, M.; Berg, T. v. d.; Que, L. *J. Chem. Eur. J.* **2006**, 12, 7489.
- (13) Costas, M.; Que Jr., L. *Angew. Chem. Int. Ed.* **2002**, 12, 2179.
- (14) Chen, K.; Costas, M.; Que, L., Jr. *J. Chem. Soc., Dalton Trans.* **2002**, 672.
- (15) Fe(pytacn) systems; a) Company, A.; Gómez, L.; Fontrodona, X.; Ribas, X.; Costas, M. *Chem. Eur. J.* **2008**, 14, 5727. b) Prat, I.; Gómez, L.; Canta, M.; Ribas, X.; Costas, M. *Chem. Eur. J.* **2013**, 19, 1908. c) Garcia-Bosch, I.; Codolà, Z.; Prat, I.; Ribas, X.; Lloret-Fillol, J.; Costas, M. *Chem. Eur. J.* **2012**, 18, 13269.
- (16) Company, A.; Gómez, L.; Güell, M.; Ribas, X.; Luis, J. M.; Que, L., Jr.; Costas, M. *J. Am. Chem. Soc.* **2007**, 129, 15766.
- (17) Lloret, J.; Codolà, Z.; Garcia-Boch, I.; Gómez, L.; Pla, J. J.; Costas, M. *Nat. Chem.* **2011**, 3, 807.
- (18) Mn(pytacn) systems; a) Garcia-Bosch, I.; Company, A.; Fontrodona, X.; Ribas, X.; Costas, M. *Organic Letters* **2008**, 10, 2095. b) Garcia-Bosch, I.; Ribas, X.; Costas, M. *Adv. Synth. & Catal.* **2009**, 351, 348.
- (19) Diebold, A.; Hagen, K. S. *Inorg. Chem.* **1998**, 37, 215.
- (20) Blakesley, D. W.; Payne, S. C.; Hagen, K. S. *Inorg. Chem.* **2000**, 39, 1979.
- (21) Simaan, A. J.; Döpner, S.; Banse, F.; Bourcier, S.; Bouchoux, G.; Boussac, A.; Hildebrandt, P.; Girerd, J.-J. *Eur. J. Inorg. Chem.* **2000**, 1627.
- (22) Chen, K.; Que, L., Jr. *J. Am. Chem. Soc.* **2001**, 123, 6327.
- (23) Britovsek, G. J. P.; England, J.; White, A. J. P. *Inorg. Chem.* **2005**, 44, 8125.
- (24) a) Zang, Y.; Kim, J.; Dong, Y.; Wilkinson, E. C.; Appelman, E. H.; Que, L., Jr. *J. Am. Chem. Soc.* **1997**, 119, 4197. b) Constable, E. C.; Baum, G.; Bill, E.; Dyson, R.; Eldik, R. v.; Fenske, D.; Kaderli, S.; Morris, D.; Neubrand, A.; Neuburger, M.; Smith, D. R.; Wieghardt, K.; Zehnder, M.; Zuberbühler, A. D. *Chem. Eur. J.* **1999**, 5, 498.
- (25) Marchivie, M.; Guionneau, P.; Létard, J. F.; Chasseau, D. *Acta Cryst. Sect. B* **2003**, 479.
- (26) Mashuta, M. S.; Webb, R. J.; McCusker, J. K.; Schmitt, E. A.; Oberhausen, K. J.; Richardson, J. F.; Buchanan, R. M.; Hendrickson, D. N. *J. Am. Chem. Soc.* **1992**, 114, 3815.
- (27) Ming, L.-J. In *Physical Methods in Bioinorganic Chemistry*; Lawrence Que, J., Ed.; University Science Books: Sausalito, California, 2000, p 375.
- (28) England, J.; Gondhia, R.; Bigorra-Lopez, L.; Petersen, A. R.; White, A. J. P.; Britovsek, G. J. P. *Dalton Trans.* **2009**, 5319.
- (29) England, J.; Davies, C. R.; Banaru, M.; White, A. J. P.; Britovsek, G. J. P. *Adv. Synth. Catal.* **2008**, 350, 883.
- (30) Benhamou, L.; Thibon, A.; Brelot, L.; Lachkar, M.; Mandon, D. *Dalton Trans.* **2012**, 41, 14369.
- (31) Bryliakov, K. P.; Duban, E. A.; Talsi, E. P. *Eur. J. Inorg. Chem.* **2005**, 1, 72.
- (32) Chen, K.; Costas, M.; Kim, J.; Tipton, A. K.; Que Jr., L. *J. Am. Chem. Soc.* **2002**, 124, 3026.
- (33) Thallaj, N. K.; Rothaus, O.; Benhamou, L.; Humbert, N.; Elhabiri, M.; Lachkar, M.; Welter, R.; Albrecht-Gary, A.-M.; Mandon, D. *Chemistry – A European Journal* **2008**, 14, 6742.
- (34) Mialane, P.; Nivorojkine, A.; Pratiel, G.; Azéma, L.; Slany, M.; Godde, F.; Simaan, A.; Banse, F.; Kargar-Grisel, T.; Bouchoux, G.; Sainton, J.; Horner, O.;

Guilhem, J.; Tchertanova, L.; Meunier, B.; Girerd, J.-J. *Inorg. Chem.* **1999**, *38*, 1085.

(35) Niel, V.; Gaspar, A. B.; Muñoz, M. C.; Abarca, B.; Ballesteros, R.; Real, J. A. *Inorg. Chem.* **2003**, *42*, 4782.

(36) Mandon, D.; Machkour, A.; Goetz, S.; Welter, R. *Inorg. Chem.* **2002**, *41*, 5364.

(37) Costas, M.; Chen, K.; Que, L., Jr. *Coord. Chem. Rev.* **2000**, *200-202*, 517.

(38) Company, A.; Gomez, L.; Costas, M. In *Iron-Containing Enzymes, Versatile Catalysts of Hydroxylation Reactions in Nature*; De Visser, S. P., Kumar, D., Eds.; RSC: Cambridge, 2011.

(39) Chen, M. S.; White, M. C. *Science* **2007**, *318*, 783.

(40) Gomez, L.; Canta M.; Font, D.; Prat, I.; Ribas, X.; Costas, M. *J. Org. Chem.* DOI.org/10.1021/jo302196q

(41) Bataille, C. J. R.; Donohoe, T. J. *Chem. Soc. Rev.* **2011**, *40*, 114.

(42) Chow, T. W.-S.; Wong, E. L.-M.; Guo, Z.; Liu, Y.; Huang, J.-S.; Che, C.-M. *J. Am. Chem. Soc.* **2010**, *132*, 13229.

(43) Quinonero, D.; Morokuma, K.; Musaev, D. G.; Mas-Balleste, R.; Que, L., Jr. *J. Am. Chem. Soc.* **2005**, *127*, 6548.

(44) Bassan, A.; Blomberg, M. R. A.; Siegbahn, P. E. M.; Jr., L. Q. *Angew. Chem. Int. Ed.* **2005**, *44*, 2939.

(45) Prat, I.; Mathieson, J. S.; Ribas, X.; Güell, M.; Luis, J. M.; Cronin, L.; Costas, M. *Nat. Chem.* **2011**, *3*, 788.

(46) Company, A.; Feng, Y.; Güell, M.; Ribas, X.; Luis, J. M.; Que, L., Jr.; Costas, M. *Chem. Eur. J.* **2009**, *15*, 3359.

(47) Bautz, J.; Comba, P.; Laorden, C. L. d.; Menzel, M.; Rajaraman, G. *Angew. Chem. Int. Ed.* **2007**, *46*, 8067.

(48) Oldenburg, P. D.; Feng, Y.; Pryjomska-Ray, I.; Ness, D.; Que Jr., L. *J. Am. Chem. Soc.* **2010**, *132*, 17713.

(49) Prat, I.; Company, A.; Postils, V.; Ribas, X.; Lawrence Que, J.; Luis, J. M.; Costas, M. *Chem. Eur. J.* **2013**, DOI: 10.1002/chem.201300110.

$C_{16}H_{23}F_7eN_4O_6S_2 \cdot 3H_2O$ : C, 28.50; H, 4.33; N, 8.31; S, 9.51 %. Found: C, 28.40; H, 3.70; N, 8.15; S, 9.48 %. FT-IR (ATR)  $\nu$ ,  $cm^{-1}$ : 2927 (C-H)<sub>sp3</sub>, 1309, 1213, 1158, 1015, 630 (CF<sub>3</sub>SO<sub>3</sub>). <sup>1</sup>H-NMR (CD<sub>3</sub>CN, 200 MHz, 300 K)  $\delta$ , ppm: 104.67, 84.41, 70.10, 50.59, 28.53, -2.91. <sup>1</sup>H-NMR (200 MHz, CD<sub>2</sub>Cl<sub>2</sub>, 300 K)  $\delta$ , ppm: 142.65, 122.50, 108.05, 80.16, 69.76, 29.99, 18.95. ESI-MS (m/z): 161.0 [M-2OTf]<sup>2+</sup>, 471.1 [M-OTf]<sup>+</sup>.

*Synthesis of bis-chloro complexes [FeCl<sub>2</sub>(<sup>R,R'</sup>Pytacn)] (<sup>R,R'</sup>3)*

Chlorocomplexes <sup>R,R'</sup>3 were prepared by reaction of the particular ligand (<sup>R,R'</sup>Pytacn) with equimolar amounts of FeCl<sub>2</sub> in THF as exemplified for <sup>H,H</sup>3.

**[FeCl<sub>2</sub>(<sup>H,H</sup>Pytacn)] (<sup>H,H</sup>3)**. A suspension of FeCl<sub>2</sub> (22 mg, 0.17 mmols) in anhydrous THF (2 mL) was added dropwise to a vigorously stirred solution of Pytacn (41 mg, 0.17 mmols) in THF (1.5 mL). The FeCl<sub>2</sub> slowly entered into the solution and after about 10 min under vigorous stirring a yellow precipitate appeared. After stirring for 12 hours the solution was filtered off and the resulting pale yellow solid was dried under vacuum. This compound was dissolved in CH<sub>3</sub>CN and filtered through Celite. Slow diethyl ether diffusion over this solution afforded 51 mg of the desired compound (0.14 mmols, 82 %). Anal. Calcd for C<sub>14</sub>H<sub>24</sub>Cl<sub>2</sub>FeN<sub>4</sub>·1/4H<sub>2</sub>O: C, 44.29; H, 6.51; N, 14.76 %. Found: C, 44.35; H, 6.35; N, 14.51 %. FT-IR (ATR)  $\nu$ ,  $cm^{-1}$ : 2968 - 2900 (C-H)<sub>sp3</sub>, 1602, 1455, 1134, 725. <sup>1</sup>H-NMR (CD<sub>3</sub>CN, 200 MHz, 300 K)  $\delta$ , ppm: 99.48, 78.07, 47.39, 36.23, 25.74, 11.19. ESI-MS (m/z): 339 [M-Cl]<sup>+</sup>, 416 [M+CH<sub>3</sub>CN+H]<sup>+</sup>. CV (CH<sub>3</sub>CN) E<sub>1/2</sub>, mV: 138.

**[FeCl<sub>2</sub>(<sup>H,NMe2</sup>Pytacn)] (<sup>H,NMe2</sup>3)**. Yield = 35 %. Anal. Calcd for C<sub>16</sub>H<sub>29</sub>Cl<sub>2</sub>FeN<sub>5</sub>·0.2 CH<sub>2</sub>Cl<sub>2</sub>: C, 44.71; H, 6.81; N, 16.09 %. Found: C, 44.71; H, 6.80; N, 15.97 %. FT-IR (ATR)  $\nu$ ,  $cm^{-1}$ : 2949 - 2851 (C-H)<sub>sp3</sub>, 1613, 1010, 810. <sup>1</sup>H-NMR (CD<sub>3</sub>CN, 400 MHz, 300 K)  $\delta$ , ppm: 110.52, 93.09, 45.00, 34.48. ESI-MS (m/z): 382.1 [M-Cl]<sup>+</sup> (100), 173.5 [M-2Cl]<sup>2+</sup> (75), 390.1 [2M-2Cl+O]<sup>2+</sup> (100). CV (CH<sub>3</sub>CN) E<sub>1/2</sub>, mV: 11.

**[FeCl<sub>2</sub>(<sup>H,OMe</sup>Pytacn)] (<sup>H,OMe</sup>3)**. Yield = 60 %. Anal. Calcd for C<sub>17</sub>H<sub>30</sub>Cl<sub>2</sub>FeN<sub>4</sub>O: C, 47.13; H, 6.98; N, 12.93 %.

Found: C, 47.32; H, 6.78; N, 12.78 %. FT-IR (ATR)  $\nu$ ,  $cm^{-1}$ : 2953 - 2843 (C-H)<sub>sp3</sub>, 1016, 990 (O-CH<sub>3</sub>), 1595, 1263, 804. <sup>1</sup>H-NMR (CD<sub>3</sub>CN, 400 MHz, 300 K)  $\delta$ , ppm: 132.72,

91.05, 78.63. ESI-MS (m/z): 475.1 [M-Cl]<sup>+</sup> (100), 181.1 [M-2Cl]<sup>2+</sup> (50). CV (CH<sub>3</sub>CN) E<sub>1/2</sub>, mV: 107.

**[FeCl<sub>2</sub>(<sup>H,Me</sup>Pytacn)] (<sup>H,Me</sup>3)**. Yield = 65 %. Anal. Calcd for C<sub>15</sub>H<sub>26</sub>Cl<sub>2</sub>FeN<sub>4</sub>·0.5 CH<sub>2</sub>Cl<sub>2</sub>: C, 43.13; H, 6.31; N, 12.98 %. Found: C, 43.66; H, 6.33; N, 12.41 %. <sup>1</sup>H-NMR (CD<sub>3</sub>CN, 200 MHz, 300 K)  $\delta$ , ppm: 93.35, 68.86, 48.32, 34.02, -21.20. ESI-MS (m/z): 353.1 [M-Cl]<sup>+</sup>. CV (CH<sub>3</sub>CN) E<sub>1/2</sub>, mV: 176.

**[FeCl<sub>2</sub>(<sup>H,Cl</sup>Pytacn)] (<sup>H,Cl</sup>3)**. Yield = 71 %. Anal. Calcd for C<sub>14</sub>H<sub>23</sub>Cl<sub>3</sub>FeN<sub>4</sub>·0.35 CH<sub>2</sub>Cl<sub>2</sub>: C, 39.24; H, 5.44; N, 12.75 %. Found: C, 39.26; H, 5.53; N, 12.92; S, 0.33 %. FT-IR (ATR)  $\nu$ ,  $cm^{-1}$ : 2961 - 2856 (C-H)<sub>sp3</sub>, 1588, 1461, 1104, 1016, 730. <sup>1</sup>H-NMR (CD<sub>3</sub>CN, 400 MHz, 300 K)  $\delta$ , ppm: 149.50, 83.17, 48.24, 35.24, 33.16. ESI-MS (m/z): 373.1 [M-Cl]<sup>+</sup> (25), 168.9 [M-2Cl]<sup>2+</sup> (100). CV (CH<sub>3</sub>CN) E<sub>1/2</sub>, mV: 165.

**[FeCl<sub>2</sub>(<sup>H,COPh</sup>Pytacn)] (<sup>H,COPh</sup>3)**. Yield = 54 %. Anal.

(ATR)  $\nu$ ,  $cm^{-1}$ : 2967 - 2855 (C-H)<sub>sp3</sub>, 1711 (C=O), 1207, 1002, 766. <sup>1</sup>H-NMR (CD<sub>3</sub>CN, 400 MHz, 300 K)  $\delta$ , ppm: 156.02, 82.55, 50.15, 34.93. ESI-MS (m/z): 411.1 [M-Cl]<sup>+</sup> (100), 188.0 [M-2Cl]<sup>2+</sup> (50). CV (CH<sub>3</sub>CN) E<sub>1/2</sub>, mV: 171.

**[FeCl<sub>2</sub>(<sup>H,NO2</sup>Pytacn)] (<sup>H,NO2</sup>3)**. Yield = 65 %. Anal. Calcd for C<sub>14</sub>H<sub>23</sub>Cl<sub>2</sub>FeN<sub>5</sub>O<sub>2</sub>·1CH<sub>2</sub>Cl<sub>2</sub>: C, 35.67; H, 4.99; N, 13.87 %. Found: C, 35.80; H, 5.08; N, 13.72 %. FT-IR (ATR)  $\nu$ ,  $cm^{-1}$ : 2969 - 2859 (C-H)<sub>sp3</sub>, 2361, 1738, 1524, 1345, 731. <sup>1</sup>H-NMR (CD<sub>3</sub>CN, 400 MHz, 300 K)  $\delta$ , ppm: 167.68, 122.59, 110.33, 90.58, 84.99, 59.47, 48.56, 34.57. ESI-MS (m/z): 384.0 [M-Cl]<sup>+</sup> (100). CV (CH<sub>3</sub>CN) E<sub>1/2</sub>, mV: 225.

**[FeCl<sub>2</sub>(<sup>Me,H</sup>Pytacn)] (<sup>Me,H</sup>3)**. Yield = 82 %. Anal. Calcd for C<sub>15</sub>H<sub>26</sub>Cl<sub>2</sub>FeN<sub>4</sub>·1/2H<sub>2</sub>O: C, 45.25; H, 6.84; N, 14.07 %. Found: C, 45.74; H, 7.30; N, 14.15 %. FT-IR (ATR)  $\nu$ ,  $cm^{-1}$ : 2994 - 2816 (C-H)<sub>sp3</sub>, 1601, 1462, 1020, 809. <sup>1</sup>H-NMR (CD<sub>3</sub>CN, 200 MHz, 300 K)  $\delta$ , ppm: 82.84, 74.60, 47.16, 32.07, 18.78, -28.37. ESI-MS (m/z): 353.1 [M-Cl]<sup>+</sup>. CV (CH<sub>3</sub>CN) E<sub>1/2</sub>, mV: 211.

**[FeCl<sub>2</sub>(<sup>Me,Me</sup>Pytacn)] (<sup>Me,Me</sup>3)**. Yield = 82 %. Anal. Calcd for C<sub>16</sub>H<sub>28</sub>Cl<sub>2</sub>FeN<sub>4</sub>·0.25THF·0.50H<sub>2</sub>O: C, 47.46; H, 7.26; N, 13.02 %. Found: C, 47.59; H, 7.02; N, 12.85 %. <sup>1</sup>H-NMR (CD<sub>3</sub>CN, 200 MHz, 300 K)  $\delta$ , ppm: 83.61, 74.86, 46.39, 31.47, -6.65. ESI-MS (m/z): 367.1 [M-Cl]<sup>+</sup>, 408.2 [M-Cl+CH<sub>3</sub>CN]<sup>+</sup>. CV (CH<sub>3</sub>CN) E<sub>1/2</sub>, mV: 238.

**[FeCl<sub>2</sub>(<sup>F,H</sup>Pytacn)] (<sup>F,H</sup>3)**. Yield = 43 %. Anal. Calcd for C<sub>14</sub>H<sub>23</sub>Cl<sub>2</sub>FFeN<sub>4</sub>·H<sub>2</sub>O: C, 40.90; H, 6.13; N, 13.63 %. Found: C, 40.21; H, 6.45; N, 13.14 %. FT-IR (ATR)  $\nu$ ,  $cm^{-1}$ : 2921 - 2854 (C-H)<sub>sp3</sub>, 1615, 1454, 1017, 816. <sup>1</sup>H-NMR (CD<sub>3</sub>CN, 200 MHz, 300 K)  $\delta$ , ppm: 87.85, 73.47, 59.58, 38.40, 27.84, 16.42. ESI-MS (m/z): 357.7 [M-Cl]<sup>+</sup>, 161.0 [M-2Cl]<sup>2+</sup>.

*Synthesis of bis-acetonitrile complexes [Fe(<sup>R,R'</sup>Pytacn)(CH<sub>3</sub>CN)<sub>2</sub>]<sub>X<sub>2</sub></sub> (<sup>R,R'</sup>2X)*

[Fe(<sup>H,H</sup>Pytacn)(CH<sub>3</sub>CN)<sub>2</sub>](PF<sub>6</sub>)<sub>2</sub> (<sup>H,H</sup>2PF<sub>6</sub>) was prepared as previously reported.<sup>16</sup>

**[Fe(<sup>H,H</sup>Pytacn)(CH<sub>3</sub>CN)<sub>2</sub>](SbF<sub>6</sub>)<sub>2</sub> (<sup>H,H</sup>2SbF<sub>6</sub>)**. FeCl<sub>2</sub> (51 mg, 0.40 mmols) as directly as solid to a vigorously stirred solution of <sup>H,H</sup>Pytacn (100 mg, 0.40 mmols) in CH<sub>3</sub>CN. The initially pale yellow solution became gradually bright orange as the FeCl<sub>2</sub> got dissolved.

After stirring usually for 30 minutes, AgSbF<sub>6</sub> (277 mg, 0.80 mmols) was added which caused the immediate precipitation of AgCl and an evident color change of the solution from bright orange to dark brown. After stirring for 30 minutes, the solution was filtered through Celite. Slow diethyl ether diffusion over the resulting solution afforded, in a few days, 245 mg of brown crystals (0.29 mmol, 71% yield). <sup>1</sup>H-NMR (CD<sub>3</sub>CN, 400 MHz, 300 K)  $\delta$ , ppm: 12.68, 9.73, 9.59, 9.10, 7.33, 6.70, 3.82, 2.17, 1.96. HRMS (m/z): 152.0668 [M-2CH<sub>3</sub>CN-2SbF<sub>6</sub>]<sup>2+</sup>, 161.07 [M-2CH<sub>3</sub>CN-2SbF<sub>6</sub>+H<sub>2</sub>O]<sup>2+</sup>, 539.0312 [M-2CH<sub>3</sub>CN-SbF<sub>6</sub>]<sup>+</sup>.

**[Fe(<sup>Me,H</sup>Pytacn)(CH<sub>3</sub>CN)<sub>2</sub>](SbF<sub>6</sub>)<sub>2</sub> (<sup>Me,H</sup>2SbF<sub>6</sub>)**. FeCl<sub>2</sub> (11 mg, 0.09 mmols) was added directly as a solid to a vigorously stirred solution of <sup>Me,H</sup>Pytacn (21 mg, 0.09 mmols) in CH<sub>3</sub>CN. The initially pale yellow solution became gradually bright orange as the FeCl<sub>2</sub> got dissolved. Calcd for C<sub>16</sub>H<sub>29</sub>Cl<sub>2</sub>FeN<sub>5</sub>·0.35 Et<sub>2</sub>O: C, 46.71; H, 6.71; N,

the solution was filtered through Celite. Slow diethyl ether



© 2013 American Chemical Society

After stirring for 30 minutes,  $\text{AgSbF}_6$  (60 mg, 0.17 mmols) was added which caused the immediate precipitation of  $\text{AgCl}$  and an evident color change of the solution from bright orange to yellowish. After stirring for 30 minutes,

11.84 %. Found: C, 46.55; H, 6.28; N, 11.54 %. FT-IR the solution was filtered through Celite. Slow diethyl ether

diffusion over the resulting solution afforded, in a few days, 54 mg of white crystals (0.05 mmol, 69% yield).  $^1\text{H-NMR}$  ( $\text{CD}_3\text{CN}$ , 400 MHz, 300 K)  $\delta$ , ppm: 143.94, 84.76, 56.30, 49.10, -7.74, -32.53. ESI-MS ( $m/z$ ): 159.1  $[\text{M}-2\text{CH}_3\text{CN}-2\text{SbF}_6]^{2+}$ , 353.1  $[\text{M}-2\text{CH}_3\text{CN}-2\text{SbF}_6+\text{Cl}]^+$ .

**Reaction conditions for catalysis.** In a typical reaction, 0.36 mL of a 70 mM (25  $\mu\text{mol}$ s) or 700 mM (250  $\mu\text{mol}$ s)  $\text{H}_2\text{O}_2$  solution (diluted from a 35%  $\text{H}_2\text{O}_2$  aqueous solution) in  $\text{CH}_3\text{CN}$  was delivered by syringe pump over 30 min at 25 °C to a vigorously stirred  $\text{CH}_3\text{CN}$  solution (2.14 mL) containing the iron catalyst (2.5  $\mu\text{mol}$ s) and the substrate (2500  $\mu\text{mol}$ s). The final concentrations of reagents were 1 mM iron catalyst, 10 mM / 100 mM  $\text{H}_2\text{O}_2$  and 1 M substrate. After syringe pump addition, the resulting solution was stirred for another 10 min. For the oxidation of cyclohexane, biphenyl (internal standard) was added at this point and the iron complex was removed by passing the solution through a short path of basic alumina or silica followed by elution with 2 mL of AcOEt. Finally, the solution was subjected to GC analysis. The organic products were identified by comparison with authentic compounds.

For the oxidation of cyclooctene, the reaction was performed as described above but under a  $\text{N}_2$  atmosphere. After syringe pump addition of the oxidant and stirring for 10 min, 1 mL of acetic anhydride together with 0.1 mL of 1-methylimidazole were added to afford the esterification of the diol product. After stirring for 15 min at room temperature, ice was added and the mixture was stirred for about 30 min. Biphenyl (internal standard) was added and the mixture was extracted with 2 mL  $\text{CHCl}_3$ . The organic layer was washed with 2 mL  $\text{H}_2\text{SO}_4$  1M, 2 mL sat.  $\text{NaHCO}_3$  and 2 mL  $\text{H}_2\text{O}$ , dried with  $\text{MgSO}_4$  and subjected to GC analysis. The organic products were identified by comparison with authentic compounds.

**Isotopic labeling experiments using  $\text{H}_2^{18}\text{O}$ .** The experimental procedure was similar to the one described above for a typical oxidation reaction of cyclooctene. In these experiments 50  $\mu\text{L}$   $\text{H}_2^{18}\text{O}$  (2500  $\mu\text{mol}$ s) were delivered by syringe pump together with 0.36 mL of a 70 mM (25  $\mu\text{mol}$ s)  $\text{H}_2\text{O}_2$  solution into the catalyst (2.5  $\mu\text{mol}$ s) and cyclooctene (250  $\mu\text{mol}$ s) solution under an inert atmosphere. The incorporation of  $^{18}\text{O}$  into the epoxide and *syn*-diol products was measured by GC-MS analyses. Specific ions corresponding to the epoxide and *syn*-diol mass spectra were computer simulated. In order to account for the isotopic purity of  $\text{H}_2^{18}\text{O}$  and its dilution because of the use of aqueous  $\text{H}_2\text{O}_2$  solutions, corrected values were obtained by dividing the simulated percentage of  $^{18}\text{O}$ -labeled epoxide and  $^{18}\text{O}$ -labeled *syn*-diol by 0.94.

## ASSOCIATED CONTENT

### Supporting Information

Full description of the synthesis of  $\text{R,R'}$ Pytacn ligands, solid state characterization of  $^{\text{H,OMe}}\mathbf{1}$ ,  $^{\text{H,Me}}\mathbf{1}$ ,  $^{\text{H,Cl}}\mathbf{1}$ ,  $^{\text{H,CO}_2\text{Et}}\mathbf{1}$  and  $^{\text{Cl,H}}\mathbf{1}$ , paramagnetic  $^1\text{H-NMR}$  spectra of  $\text{R,R'}$  $\mathbf{1}$  and  $\text{R,R'}$  $\mathbf{2}$ , variable-temperature paramagnetic  $^1\text{H-NMR}$  of  $^{\text{Me,H}}\mathbf{1}$  and cyclic voltammograms of  $\text{R,R'}$  $\mathbf{3}$ . This material is available free of charge via the Internet at <http://pubs.acs.org>.

## Acknowledgements

Financial support for this work was provided by the Spanish Ministry of Science (Project CTQ2009-08464/BQU and Consolider Ingenio Ingenio/CSD2010-00065 to M.C. and X. R.)

and the European Research Council (ERC-2009-StG-239910 to M.C.). M. C. and X. R. acknowledge Generalitat de Catalunya for ICREA-Academia Awards and 2009-SGR637. A. C. acknowledges the European Commission for a Career Integration Grant (FP7-PEOPLE-2011-CIG-303522). The Spanish Ministry of Science is acknowledged for a FPU PhD grant to I. P. and for a Ramón y Cajal contract to A.C. We thank Catexel for a generous gift of tritosyl-1,4,7-triazacyclononane.

## References

- (1) a) *Biomimetic Oxidations Catalyzed by Transition Metal Complexes*; Imperial College Press: London, 2000. b) Arakawa, H.; Aresta, M.; Armour, J. N.; Barteau, M. A.; Beckman, E. J.; Bell, A. T.; Bercaw, J. E.; Creutz, C.; Dinjus, E.; Eckert, J.; Fujita, E.; Gibson, D. H.; Goddard, W. A.; Goodman, D. W.; Keller, J.; Kubas, G. J.; Kung, H. H.; Lyons, J. E.; Manzer, L. E.; Marks, T. J.; Morokuma, K.; Nivholas, K. M.; Periana, R.; Que, L.; Rostrup-Nielson, J.; Sachtler, W. M. H.; Schmidt, L. D.; Sen, A.; Somorjai, G. A.; Stair, P. C.; Stults, B. R.; Tumas, W. *Chem. Rev.* **2001**, *101*, 953. c) Bäckvall, J.-E. *Modern oxidation Methods*; Wiley-VCH: Weinheim, 2004. d) Shul'pin, G. B. *Minirew in Org. Chem.* **2009**, *6*(2), 95-104.
- (2) a) Enthaler, S.; Junge, K.; Beller, M. *Angew. Chem. Int. Ed.* **2008**, *47*, 3317. b) Schröder, K.; Junge, K.; Bitterlich, B.; Beller, M. *Top. Organomet. Chem.* **2010**, *33*, 83. c) Mayer, A. C.; Bolm, C. In *Iron Catalysis in Organic Chemistry*; Plietker, B., Ed.; Wiley-VCH: Weinheim, 2008, p 73. d) Liang-Xian, L. *Curr. Org. Chem.* **2010**, *14*, 1099-1126.
- (3) a) Ortiz de Montellano, P. R. *Chem. Rev.* **2010**, *110*, 932. b) Ortiz de Montellano, P. R.; De Voss, J. J. *Nat. Prod. Rep.* **2002**, *19*, 477.
- (4) a) Sazinsky, M. H.; Lippard, S. J. *Acc. Chem. Res.* **2006**, *39*, 558. b) Costas, M.; Mehn, M. P.; Jensen, M. P.; Que Jr., L. *Chem. Rev.* **2004**, *104*, 939. c) Kovaleva, E. G.; Lipscomb, J. D. *Nat. Chem. Biol.* **2008**, *4*, 186. d) Bruijninx, P. C. A.; Koten, G. v.; Gebbink, R. J. M. K. *Chem. Soc. Rev.* **2008**, *12*, 2716. e) Tshuva, E. Y.; Lippard, S. J. *Chem. Rev.* **2004**, *104*, 987.
- (5) a) Que, L.; Tolman, W. B. *Nature* **2008**, *455*, 333. b) Talsi, E. P.; Bryliakov, K. P. *Coord. Chem. Rev.* **2012**, *256*, 1418.
- (6) a) Lu, H.; Zhang, P. *Chem. Soc. Rev.* **2011**, *40*, 1899. b) Che, C.-M.; Huang, J.-S. *Chem. Commun.* **2009**, 3996. c) Costas, M. *Coord. Chem. Rev.* **2011**, *255*, 2912.
- (7) a) Gibson, D. T.; Subramanian, V. In *Microbial Degradation of Aromatic Hydrocarbons*; Gibson, D. T., Ed.; Marcel Dekker: New York, 1984, p 181. b) Gibson, D. T.; Parales, R. E. *Curr. Opin. Biotechnol.* **2000**, *11*, 236. c) Chakrabarty, S.; Austin, R. N.; Deng, D.; Groves, J. T.; Lipscomb, J. D. *J. Am. Chem. Soc.* **2007**, *129*, 3514.
- (8) For Fe-catalyzed arene oxidation see; a) Thibon, A.; Jollet, V.; Ribal, C.; Senechal-David, K.; Billon, L.; Sorokin, A. B.; Banse, F. *Chem. Eur. J.* **2012**, *18*, 2715. b) Möller, K.; Wienhöfer, G.; Schröder, K.; Join, B.; Junge, K.; Beller, M. *Chem. Eur. J.* **2010**, *16*, 10300.
- (9) Selected examples of Fe-catalyzed olefin oxidation; a) Wang, B.; Wang, S.; Xia, C.; Sun, W. *Chem. Eur. J.* **2012**, *18*, 7332. b) Mikhalyova, E. A.; Makhlynets, O. V.; Palluccio, T. D.; Filatov, A. S.; Rybak-Akimova, E.

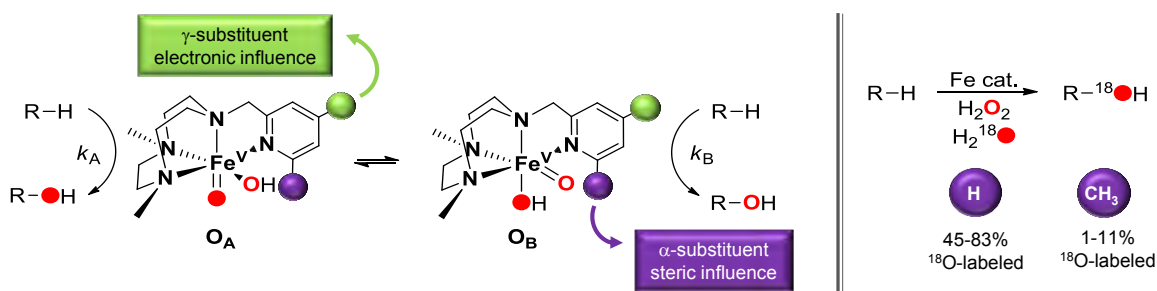
- V. *Chem. Commun.* **2012**, 48, 687. c) Oddon, F.; Girgenti, E.; Lebrun, C.; Marchi-Delapierre, C.; Pecaut, J.; Menage, S. *Eur. J. Inorg. Chem.* **2012**, 85. d) Feng, Y.; England, J.; Que, L., Jr. *Acs Catal.* **2011**, 1, 1035. e) Wu, M.; Miao, C.-X.; Wang, S.; Hu, X.; Xia, C.; Kühn, F. E.; Sun, W. *Adv. Synth. & Catal.* **2011**, 353, 3014. f) Bruijninx, P. C. A.; Buurmans, I. L. C.; Gosiewska, S.; Moelands, M. A. H.; Lutz, M.; Spek, A. L.; van Koten, G.; Gebbink, R. J. M. K. *Chem. Eur. J.* **2008**, 14, 1228. g) Liu, P.; Wong, E. L. M.; Yuen, A. W. H.; Che, C. M. *Org. Lett.* **2008**, 10, 3275. h) Comba, P.; Rajaraman, G. *Inorg. Chem.* **2008**, 47, 78. i) Mas-Balleste, R.; Que, L., Jr. *J. Am. Chem. Soc.* **2007**, 129, 15964. j) Marchi-Delapierre, C.; Jorge-Robin, A.; Thibon, A.; Ménage, S. *Chem. Commun.* **2007**, 11, 1166. k) Taktak, S. Y., W.; Herrera, A. M.; Rybak-Akimova, E. V. *Inorg. Chem.* **2007**, 46, 2929. l) Bukowski, M. R.; Comba, P.; Lienke, A.; Limberg, C.; de Laorden, C. L.; Mas-Balleste, R.; Merz, M.; Que, L. *Angew. Chem. Int. Ed.* **2006**, 45, 3446. m) Klopstra, M.; Roelfes, G.; Hage, R.; Kellogg, R. M.; Feringa, B. L. *Eur. J. Inorg. Chem.* **2004**, 4, 846. n) Dubois, G.; Murphy, A.; Stack, T. D. P. *Org. Lett.* **2003**, 5, 2469. o) Fujita, M.; Costas, M.; Que Jr., L. *J. Am. Chem. Soc.* **2003**, 125, 9912. p) Ryu, J. Y.; Kim, J.; Costas, M.; Chen, K.; Nam, W.; Que Jr., L. *Chem. Commun.* **2002**, 12, 1288. q) Mekmouche, Y.; Ménage, S.; Toia-Duboc, C.; Fontecave, M.; Galey, J.-B.; Lebrun, C.; Pecaut, J. *Angew. Chem. Int. Ed.* **2001**, 40, 949. r) White, M. C.; Doyle, A. G.; Jacobsen, E. N. *J. Am. Chem. Soc.* **2001**, 123, 7194.
- (10) Selected examples of Fe-catalyzed C-H oxidation; a) Djernes, K. E.; Padilla, M.; Mettry, M.; Young, M. C.; Hooley, R. J. *Chem. Commun.* **2012**, 48, 11576. b) Hitomi, Y.; Arakawa, K.; Funabiki, T.; Kodera, M. *Angew. Chem. Int. Ed.* **2012**, 51, 3448. c) Djernes, K. E.; Moshe, O.; Mettry, M.; Richards, D. D.; Hooley, R. J. *Org. Lett.* **2012**, 14, 788. d) White, M. C. *Science* **2012**, 335, 807. e) He, Y.; Gorden, J. D.; Goldsmith, C. R. *Inorg. Chem.* **2011**, 50, 12651. f) Bigi, M. A.; Reed, S. A.; White, M. C. *Nat. Chem.* **2011**, 3, 216. g) Liu, P.; Liu, Y.; Wong, E. L.-M.; Xiang, S.; Che, C.-M. *Chem. Sci.* **2011**, 2, 2187. h) Bruijninx, P. C. A.; Buurmans, I. L. C.; Huang, Y.; Juhasz, G.; Viciano-Chumillas, M.; Quesada, M.; Reedijk, J.; Lutz, M.; Spek, A. L.; Muenck, E.; Bominaar, E. L.; Gebbink, R. J. M. K. *Inorg. Chem.* **2011**, 50, 9243. i) Chen, M. S.; White, M. C. *Science* **2010**, 327, 566. j) Gomez, L.; Garcia-Bosch, I.; Company, A.; Benet-Buchholz, J.; Polo, A.; Sala, X.; Ribas, X.; Costas, M. *Angew. Chem. Int. Ed.* **2009**, 48, 5720. k) Mayilmurugan, R. Stoeckli-Evans, H.; Suresh, E.; Palaniandavar, M. *Dalton Trans.* **2009**, 26, 5101. l) Comba, P.; Maurer, M.; Vadivelu, P. *Inorg. Chem.* **2009**, 48, 10389. m) Romakh, V. B.; Therrien, B.; Suss-Fink, G.; Shul'pin, G. B. *Inorg. Chem.* **2007**, 46, 3166. n) van den Berg, T. A.; de Boer, J. W.; Browne, W. R.; Roelfes, G.; Feringa, B. L. *Chem. Commun.* **2004**, 22, 2550. o) Roelfes, G.; Lubben, M.; Hage, R.; Que Jr., L.; Feringa, B. L. *Chem. Eur. J.* **2000**, 6, 2152.
- (11) England, J.; Britovsek, G. J. P.; Rabadia, N.; White, A. J. P. *Inorg. Chem.* **2007**, 46, 3752.
- (12) Mas-Balleste, R.; Costas, M.; Berg, T. v. d.; Que, L. *J. Chem. Eur. J.* **2006**, 12, 7489.
- (13) Costas, M.; Que Jr., L. *Angew. Chem. Int. Ed.* **2002**, 12, 2179.
- (14) Chen, K.; Costas, M.; Que, L., Jr. *J. Chem. Soc., Dalton Trans.* **2002**, 672.
- (15) Fe(pytacn) systems; a) Company, A.; Gómez, L.; Fontrodona, X.; Ribas, X.; Costas, M. *Chem. Eur. J.* **2008**, 14, 5727. b) Prat, I.; Gómez, L.; Canta, M.; Ribas, X.; Costas, M. *Chem. Eur. J.* **2013**, 19, 1908. c) Garcia-Bosch, I.; Codolà, Z.; Prat, I.; Ribas, X.; Lloret-Fillol, J.; Costas, M. *Chem. Eur. J.* **2012**, 18, 13269.
- (16) Company, A.; Gómez, L.; Güell, M.; Ribas, X.; Luis, J. M.; Que, L., Jr.; Costas, M. *J. Am. Chem. Soc.* **2007**, 129, 15766.
- (17) Lloret, J.; Codolà, Z.; Garcia-Boch, I.; Gómez, L.; Pla, J. J.; Costas, M. *Nat. Chem.* **2011**, 3, 807.
- (18) Mn(pytacn) systems; a) Garcia-Bosch, I.; Company, A.; Fontrodona, X.; Ribas, X.; Costas, M. *Organic Letters* **2008**, 10, 2095. b) Garcia-Bosch, I.; Ribas, X.; Costas, M. *Adv. Synth. & Catal.* **2009**, 351, 348.
- (19) Diebold, A.; Hagen, K. S. *Inorg. Chem.* **1998**, 37, 215.
- (20) Blakesley, D. W.; Payne, S. C.; Hagen, K. S. *Inorg. Chem.* **2000**, 39, 1979.
- (21) Simaan, A. J.; Döpner, S.; Banse, F.; Bourcier, S.; Bouchoux, G.; Boussac, A.; Hildebrandt, P.; Girerd, J.-J. *Eur. J. Inorg. Chem.* **2000**, 1627.
- (22) Chen, K.; Que, L., Jr. *J. Am. Chem. Soc.* **2001**, 123, 6327.
- (23) Britovsek, G. J. P.; England, J.; White, A. J. P. *Inorg. Chem.* **2005**, 44, 8125.
- (24) a) Zang, Y.; Kim, J.; Dong, Y.; Wilkinson, E. C.; Appelman, E. H.; Que, L., Jr. *J. Am. Chem. Soc.* **1997**, 119, 4197. b) Constable, E. C.; Baum, G.; Bill, E.; Dyson, R.; Eldik, R. v.; Fenske, D.; Kaderli, S.; Morris, D.; Neubrand, A.; Neuburger, M.; Smith, D. R.; Wieghardt, K.; Zehnder, M.; Zuberbühler, A. D. *Chem. Eur. J.* **1999**, 5, 498.
- (25) Marchivie, M.; Guionneau, P.; Létard, J. F.; Chasseau, D. *Acta Cryst. Sect. B* **2003**, 479.
- (26) Mashuta, M. S.; Webb, R. J.; McCusker, J. K.; Schmitt, E. A.; Oberhausen, K. J.; Richardson, J. F.; Buchanan, R. M.; Hendrickson, D. N. *J. Am. Chem. Soc.* **1992**, 114, 3815.
- (27) Ming, L.-J. In *Physical Methods in Bioinorganic Chemistry*; Lawrence Que, J., Ed.; University Science Books: Sausalito, California, 2000, p 375.
- (28) England, J.; Gondhia, R.; Bigorra-Lopez, L.; Petersen, A. R.; White, A. J. P.; Britovsek, G. J. P. *Dalton Trans.* **2009**, 5319.
- (29) England, J.; Davies, C. R.; Banaru, M.; White, A. J. P.; Britovsek, G. J. P. *Adv. Synth. Catal.* **2008**, 350, 883.
- (30) Benhamou, L.; Thibon, A.; Brelot, L.; Lachkar, M.; Mandon, D. *Dalton Trans.* **2012**, 41, 14369.
- (31) Bryliakov, K. P.; Duban, E. A.; Talsi, E. P. *Eur. J. Inorg. Chem.* **2005**, 1, 72.
- (32) Chen, K.; Costas, M.; Kim, J.; Tipton, A. K.; Que Jr., L. *J. Am. Chem. Soc.* **2002**, 124, 3026.
- (33) Thallaj, N. K.; Rotthaus, O.; Benhamou, L.; Humbert, N.; Elhabiri, M.; Lachkar, M.; Welter, R.; Albrecht-Gary, A.-M.; Mandon, D. *Chemistry – A European Journal* **2008**, 14, 6742.
- (34) Mialane, P.; Nivorojkine, A.; Pratviel, G.; Azéma, L.; Slany, M.; Godde, F.; Simaan, A.; Banse, F.; Kargar-Grisel, T.; Bouchoux, G.; Sainton, J.; Horner, O.;

- Guilhem, J.; Tchertanova, L.; Meunier, B.; Girerd, J.-J. *Inorg. Chem.* **1999**, *38*, 1085.
- (35) Niel, V.; Gaspar, A. B.; Muñoz, M. C.; Abarca, B.; Ballesteros, R.; Real, J. A. *Inorg. Chem.* **2003**, *42*, 4782.
- (36) Mandon, D.; Machkour, A.; Goetz, S.; Welter, R. *Inorg. Chem.* **2002**, *41*, 5364.
- (37) Costas, M.; Chen, K.; Que, L., Jr. *Coord. Chem. Rev.* **2000**, *200-202*, 517.
- (38) Company, A.; Gomez, L.; Costas, M. In *Iron-Containing Enzymes, Versatile Catalysts of Hydroxylation Reactions in Nature*; De Visser, S. P., Kumar, D., Eds.; RSC: Cambridge, 2011.
- (39) Chen, M. S.; White, M. C. *Science* **2007**, *318*, 783.
- (40) Gomez, L.; Canta M.; Font, D.; Prat, I.; Ribas, X.; Costas, M. *J. Org. Chem.* DOI.org/10.1021/jo302196q
- (41) Bataille, C. J. R.; Donohoe, T. J. *Chem. Soc. Rev.* **2011**, *40*, 114.
- (42) Chow, T. W.-S.; Wong, E. L.-M.; Guo, Z.; Liu, Y.; Huang, J.-S.; Che, C.-M. *J. Am. Chem. Soc.* **2010**, *132*, 13229.
- (43) Quinonero, D.; Morokuma, K.; Musaev, D. G.; Mas-Balleste, R.; Que, L., Jr. *J. Am. Chem. Soc.* **2005**, *127*, 6548.
- (44) Bassan, A.; Blomberg, M. R. A.; Siegbahn, P. E. M.; Jr., L. Q. *Angew. Chem. Int. Ed.* **2005**, *44*, 2939.
- (45) Prat, I.; Mathieson, J. S.; Ribas, X.; Güell, M.; Luis, J. M.; Cronin, L.; Costas, M. *Nat. Chem.* **2011**, *3*, 788.
- (46) Company, A.; Feng, Y.; Güell, M.; Ribas, X.; Luis, J. M.; Que, L., Jr.; Costas, M. *Chem. Eur. J.* **2009**, *15*, 3359.
- (47) Bautz, J.; Comba, P.; Laorden, C. L. d.; Menzel, M.; Rajaraman, G. *Angew. Chem. Int. Ed.* **2007**, *46*, 8067.
- (48) Oldenburg, P. D.; Feng, Y.; Pryjomska-Ray, I.; Ness, D.; Que Jr., L. *J. Am. Chem. Soc.* **2010**, *132*, 17713.
- (49) Prat, I.; Company, A.; Postils, V.; Ribas, X.; Lawrence Que, J.; Luis, J. M.; Costas, M. *Chem. Eur. J.* **2013**, DOI: 10.1002/chem.201300110.



## CHAPTER IV.

# THE MECHANISM OF STEREOSPECIFIC C-H OXIDATION BY Fe(PYTACN) COMPLEXES: BIOINSPIRED NON-HEME IRON CATALYSTS CONTAINING CIS-LABILE EXCHANGEABLE SITES



This chapter corresponds to the following publications:

Irene Prat; Anna Company; Verònica Postils; Xavi Ribas; Lawrence Que, Jr.; Josep M<sup>a</sup> Luis; Miquel Costas. Accepted in Chemistry a European Journal in **2013**. DOI: 0.1002/chem.201300110.

For this publication I. P. performed the catalytic and isotopic labeling experiments. Besides I. P. was involved in the development of concepts and discussions. Contribution is approximately 50%.

I. Prat, A. Company, V. Postils, X. Ribas, L. Que, J.M. Luis, and M. Costas. "The mechanism of stereospecific CH oxidation by Fe(Pytacn) complexes: bioinspired non-heme iron catalysts containing cis-labile exchangeable sites". *Chemistry-A European Journal*. Vol. 19, issue 21 (May 17, 2013) : p. 6724–6738. doi: 10.1002/chem.201300110

<http://onlinelibrary.wiley.com/doi/10.1002/chem.201300110/full>

<http://dx.doi.org/10.1002/chem.201300110>

Article first published online: 27 MAR 2013

### Abstract

A detailed mechanistic study of the hydroxylation of alkane CH bonds using H<sub>2</sub>O<sub>2</sub> by a family of mononuclear non heme iron catalysts with the formula [FeII(CF<sub>3</sub>SO<sub>3</sub>)<sub>2</sub>(L)] is described, in which L is a tetradentate ligand containing a triazacyclononane tripod and a pyridine ring bearing different substituents at the  $\alpha$  and  $\gamma$  positions, which tune the electronic or steric properties of the corresponding iron complexes. Two inequivalent cis-labile exchangeable sites, occupied by triflate ions, complete the octahedral iron coordination sphere. The CH hydroxylation mediated by this family of complexes takes place with retention of configuration. Oxygen atoms from water are incorporated into hydroxylated products and the extent of this incorporation depends in a systematic manner on the nature of the catalyst, and the substrate. Mechanistic probes and isotopic analyses, in combination with detailed density functional theory (DFT) calculations, provide strong evidence that CH hydroxylation is performed by highly electrophilic [FeV(O)(OH)L] species through a concerted asynchronous mechanism, involving homolytic breakage of the CH bond, followed by rebound of the hydroxyl ligand. The [FeV(O)(OH)L] species can exist in two tautomeric forms, differing in the position of oxo and hydroxide ligands. Isotopic-labeling analysis shows that the relative reactivities of the two tautomeric forms are sensitively affected by the  $\alpha$  substituent of the pyridine, and this reactivity behavior is rationalized by computational methods.

### Keywords

bioinorganic chemistry; density functional calculations; non-heme iron; oxidation; reaction mechanisms



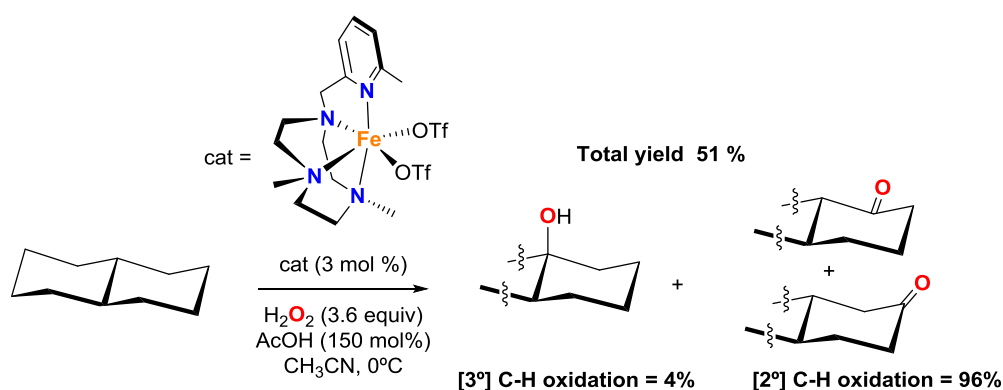


---

## CHAPTER V.

# AN IRON CATALYST FOR OXIDATION OF ALKYL C-H BONDS SHOWING ENHANCED SELECTIVITY FOR METHYLENIC SITES

---



This chapter corresponds to the following publications:

Irene Prat; Laura Gómez; Mercè Canta; Xavi Ribas; Miquel Costas. *Chemistry a European Journal* **2013**, *19(6)*, 1908-1913.

---

For this publication I. P. performed all experiments. Besides I. P. wrote the manuscript draft and was involved in the development of concepts and discussions. Contribution is approximately 80%.

I. Prat, L. Gómez, M. Canta, X. Ribas, and M. Costas. "An iron catalyst for oxidation of alkyl C-H bonds showing enhanced selectivity for methylenic sites". *Chemistry-A European Journal*. Vol. 19, issue 6 (February 4, 2013) : p. 1908–1913. doi: 10.1002/chem.201203281

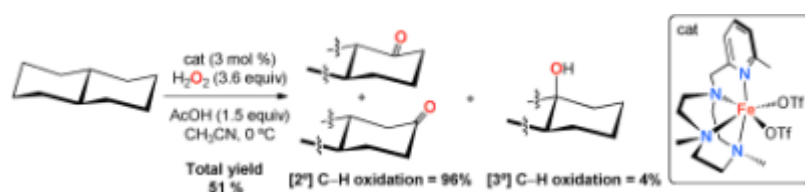
<http://onlinelibrary.wiley.com/doi/10.1002/chem.201203281/full>

<http://dx.doi.org/10.1002/chem.201203281>

Article first published online: 19 DEC 2012

### Abstract:

Many are called but few are chosen: A nonheme iron complex catalyzes the oxidation of alkyl CH bonds by using H<sub>2</sub>O<sub>2</sub> as the oxidant, showing an enhanced selectivity for secondary over tertiary CH bonds (see scheme).



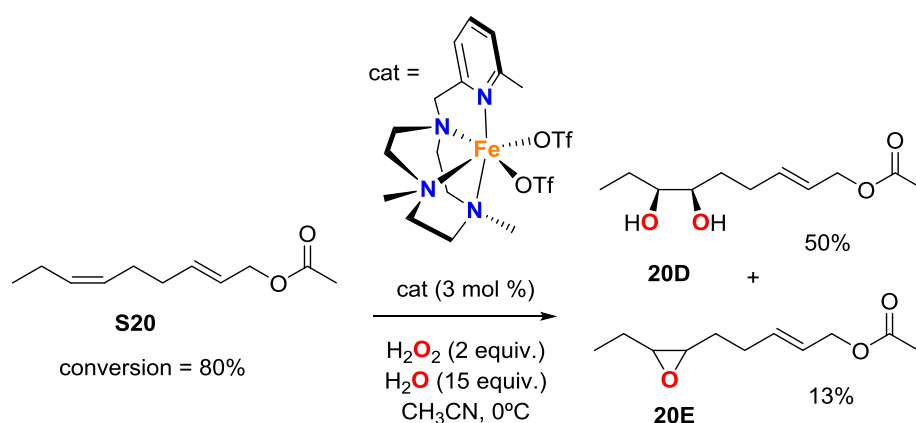
### Keywords:

bioinspired catalysis; homogeneous catalysis; hydrogen peroxide; iron; CH oxidation



## CHAPTER VI.

# Fe(PYTACN)-CATALYZED CIS-DIHYDROXYLATION OF OLEFINS WITH HYDROGEN PEROXIDE



This chapter corresponds to the following publications:

Irene Prat; David Font; Anna Company; Kathrin Junge; Xavi Ribas; Matthias Beller; Miquel Costas. *Advanced Synthesis and Catalysis* in **2013**, 355, 947-956.

For this publication I. P. performed all experiments. Besides I. P. wrote the manuscript draft and was involved in the development of concepts and discussions. Contribution is approximately 80%.

I. Prat, D. Font, A. Company, K. Junge, X. Ribas, M. Beller and M. Costas. "Fe(PyTACN)-catalyzed cis-dihydroxylation of olefins with hydrogen peroxide". *Advanced Synthesis and Catalysis*. Vol. 355, issue 5 (March 25, 2013) : p. 947-956. doi: 10.1002/adsc.201200938

<http://onlinelibrary.wiley.com/doi/10.1002/adsc.201200938/full>

<http://dx.doi.org/10.1002/adsc.201200938>

Article first published online: 15 MAR 2013

### Abstract

A family of iron complexes with general formula  $[\text{Fe}(\text{II})(^{\text{R,Y,X}}\text{PyTACN})(\text{CF}_3\text{SO}_3)_2]$ , where  $^{\text{R,Y,X}}\text{PyTACN}$ =1-[2'-(4-Y-6-X-pyridyl)methyl]-4,7-dialkyl-1,4,7-triazacyclononane, X and Y refer to the groups at positions 4 and 6 of the pyridine, respectively, and R refers to the alkyl substitution at N-4 and N-7 of the triazacyclononane ring, are shown to be catalysts for efficient and selective alkene oxidation (epoxidation and cis-dihydroxylation) employing hydrogen peroxide as oxidant. Complex  $[\text{Fe}(\text{II})(^{\text{Me,Me,H}}\text{PyTACN})(\text{CF}_3\text{SO}_3)_2]$  (7), was identified as the most efficient and selective cis-dihydroxylation catalyst among the family. The high activity of 7 allows the oxidation of alkenes to proceed rapidly (30 min) at room temperature and under conditions where the olefin is not used in large amounts but instead is the limiting reagent. In the presence of 3 mol% of 7, 2 equiv. of  $\text{H}_2\text{O}_2$  as oxidant and 15 equiv. of water, in acetonitrile solution, alkenes are cis-dihydroxylated reaching yields that might be interesting for synthetic purposes. Competition experiments show that 7 exhibits preferential selectivity towards the oxidation of *cis* olefins over the *trans* analogues, and also affords better yields and high [*syn*-diol]/[epoxide] ratios when *cis* olefins are oxidized. For aliphatic substrates, reaction yields attained with the present system compare favourably with state of the art Fe-catalyzed cis-dihydroxylation systems, and it can be regarded as an attractive complement to the iron and manganese systems described recently and which show optimum activity against electron-deficient and aromatic olefins.

### Keywords

alkenes; cis-dihydroxylation; homogeneous catalysis; hydrogen peroxide; iron

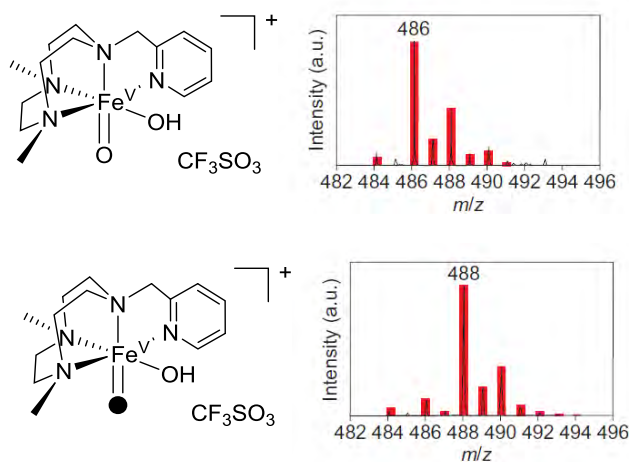


---

## CHAPTER VII.

# OBSERVATION OF $\text{Fe(V)}=\text{O}$ USING VARIABLE-TEMPERATURE MASS SPECTROMETRY AND ITS ENZYME-LIKE $\text{C-H}$ AND $\text{C}=\text{C}$ OXIDATION REACTIONS

---



This chapter corresponds to the following publications:

Irene Prat; Jennifer Mathieson; Mireia Güell; Xavi Ribas; Josep M<sup>a</sup> Luis; Leroy Cronin; Miquel Costas. *Nature Chemistry* **2011**, 3, 788-793.

---

For this publication I. P. performed all experiments together with J. M. Besides I. P. was involved in the development of concepts and discussions. Contribution is approximately 50%.

I. Prat, J. S. Mathieson, M. Güell, X. Ribas, J. M. Luis, L. Cronin and M. Costas. "Observation of Fe(V)=O using variable-temperature mass spectrometry and its enzyme-like C-H and C=C oxidation reactions". *Nature Chemistry*. Vol. 3 (October 2011) : p. 788-793. doi: 10.1038/nchem.1132

<http://www.nature.com/nchem/journal/v3/n10/full/nchem.1132.html>

<http://dx.doi.org/10.1038/nchem.1132>

Received 16 February 2011

Accepted 27 July 2011

Published online 04 September 2011

### **Abstract**

Oxo-transfer chemistry mediated by iron underpins many biological processes and today is emerging as synthetically very important for the catalytic oxidation of C–H and C=C moieties that are hard to activate conventionally. Despite the vast amount of research in this area, experimental characterization of the reactive species under catalytic conditions is very limited, although a Fe(V)=O moiety was postulated. Here we show, using variable-temperature mass spectrometry, the generation of a Fe(V)=O species within a synthetic non-haem complex at –40 °C and its reaction with an olefin. Also, with isotopic labelling we were able both to follow oxygen-atom transfer from H<sub>2</sub>O<sub>2</sub>/H<sub>2</sub>O through Fe(V)=O to the products and to probe the reactivity as a function of temperature. This study pioneers the implementation of variable-temperature mass spectrometry to investigate reactive intermediates





---

---

## **CHAPTER VIII.**

## **RESULTS AND DISCUSSION**

---

---



## VIII. RESULTS AND DISCUSSION

The oxidation of hydrocarbons are important reactions for organic chemistry and chemical industry, these reactions allow to transform inert compounds, such as alkanes or moderately reactive substrates such as alkenes, into important intermediates for more elaborate chemical synthesis.<sup>1</sup>

Traditionally the methodologies employed to perform these reactions involve oxidants with poor atom economy, high temperatures, long reactions times, and the use of expensive and toxic metals. Nowadays, different approaches are being explored to develop new methodologies that use green oxidants, mild conditions and catalysts based in first row metals, aiming at finding environmental friendly conditions operating with analogous or improved efficiency and selectivity.<sup>2</sup>

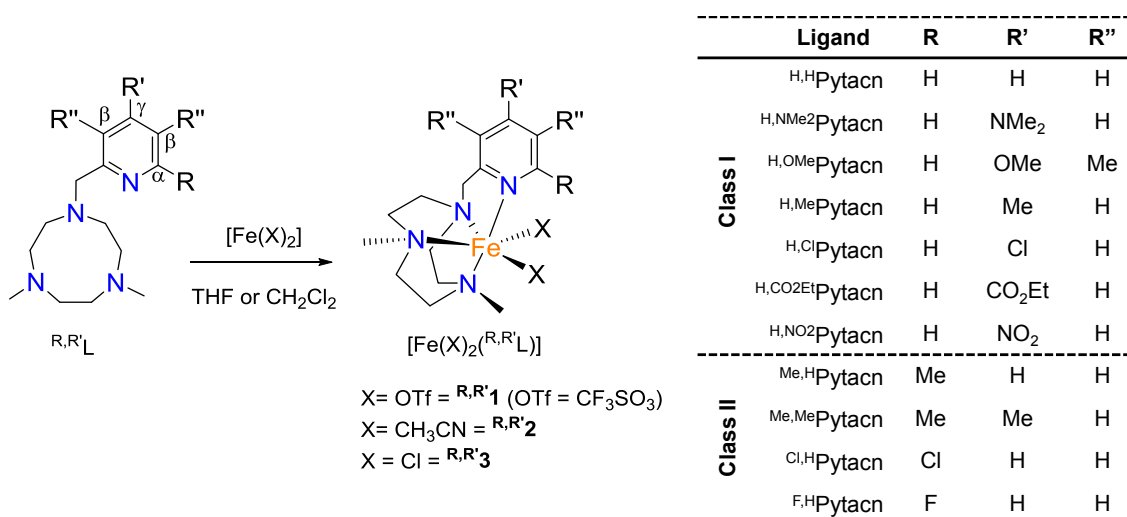
Some natural systems are capable to perform this chemistry with high efficiency and excellent selectivities, under mild conditions and using O<sub>2</sub> as oxidant. An interesting group of non-heme iron enzymes is the family of Rieske Oxygenases. These are bacterial enzymes that perform the first step in the oxidative degradation of aromatics and alkyl aromatic substrates by performing hydroxylation of C-H groups and *cis*-dihydroxylation of arenes. The active center of this family of enzymes consists of a mononuclear iron center ligated by a 2-his-1-carboxylate facial triad.<sup>3</sup>

The bioinspired approach to develop oxidation catalysts involves the design of synthetic complexes of biologically relevant metals, such as iron, and that mimic structural characteristics of the enzyme with the aim to reproduce basic aspects of its reactivity. While *a priori* one may expect that a close mimicking of the enzyme active site may be necessary to reproduce its reactivity, literature precedents indicate that this is not necessarily the case. Simple coordination complexes have already shown their ability to engage in oxidation reactions characteristic of enzymes. Therefore, an important task lays in identifying what are the minimum structural aspects that enable this reactivity, with the final goal of developing simple and synthetically useful oxidation catalysts.<sup>4</sup> Moreover, the study of these model structures can give important information about the mechanistic operation of the natural enzymes. The bioinspired approach has a long story, that may even considered to date back more than a century on the early studies on Fenton chemistry. However, even though a large amount of iron complexes have been prepared and studied as catalysts for C-H and C=C oxidation reactions, up to date only few examples have been described that can oxidize hydrocarbons with good efficiencies and selectivities, via mechanisms that do not involve Fenton type free diffusing radicals.<sup>5</sup>

In this thesis we applied this bioinspired approach to develop a family of iron complexes based on the triazacyclononane ligand with the aim of understanding the mechanistic aspects of these systems and to find catalytically active complexes that can oxidize substrates with high selectivity and efficiency, amenable for preparative purposes.

## VIII. 1. Assessing the impact of electronic tuning of the ligand in the spin state and catalytic oxidation ability of the Fe(Pytacn) family of complexes

In Chapter III a family of iron complexes based on  $N_4$ -tetradentate ligands has been described. The ligands consist in a triazacyclononane unit derivatized with a methylpyridine ring, which has been modified by introducing several substituents in the  $\alpha$  or  $\gamma$  positions of the aromatic moiety,  $[\text{Fe}^{\text{II}}(\text{CF}_3\text{SO}_3)_2(\text{R,R}'\text{Pytacn})]$ ,  $\text{R,R}'\mathbf{1}$ . These modifications aimed at tuning the electronic and steric properties of the complexes, with the objective to modulate their reactivity as catalysts in C-H and C=C oxidation reactions. Moreover, several groups with different electronic properties have been introduced in  $\gamma$  position ( $\text{R}' = \text{H}, \text{NMe}_2, \text{OMe}, \text{Me}, \text{Cl}, \text{CO}_2\text{Et}, \text{NO}_2$ ), allowing the study of the putative electronic effects. Instead, modification of the  $\alpha$  position of the pyridine ring ( $\text{R} = \text{H}, \text{Me}, \text{Cl}, \text{F}$ ) is aimed at tuning not only the electronics but also the steric crowding around the iron metal site (Scheme VIII.1). Complex  $\text{H,H}\mathbf{1}$  and  $\text{Me,H}\mathbf{1}$  were previously described by our group and exhibited high activity in C-H oxidation and C=C *cis*-dihydroxylation.<sup>6</sup>



Scheme VIII.1. Ligands and complexes employed in this thesis.

These complexes have been classified in two groups: Class I complexes are those with a hydrogen atom in the  $\alpha$  position of the pyridine, and class II are complexes with a substituent in this position. The electronic properties of the complexes have been analyzed, and their performance as C-H and C=C oxidation catalysts has been evaluated (*vide infra*).

### VIII.1.1. Structure-dependent electronic and magnetic properties

In Chapter III we study the influence of those substituents in the electronic properties of the coordinated iron center, by complete characterization of the complexes by X-ray diffraction,  $^1\text{H}$  NMR spectroscopy, UV-vis spectroscopy, magnetic susceptibility studies and measurement of the electrochemical potential ( $E_{1/2}$ ) of the  $\text{Fe}^{\text{III}}/\text{Fe}^{\text{II}}$  redox pair.

X-ray diffraction studies provide information about the molecular structure of the complexes; all of them contain an iron(II) center in a distorted octahedral coordination geometry. Four sites are occupied by nitrogen atoms of the ligand, thus leaving two sites in a relative *cis* configuration in the coordination sphere of the iron center. These two sites are accessible for binding solvent molecules, triflate anions, and reagents such as oxidants. Moreover, the distance  $\text{Fe}-\text{N}_{\text{py}}$  is an informative parameter to determine the spin state of the complex. The average distances for the  $[\text{Fe}^{\text{II}}(\text{CF}_3\text{SO}_3)_2(\text{R,R}'\text{Pytacn})]$  family of complexes range between 2.1 and 2.2 Å, characteristic of high spin  $\text{Fe}^{\text{II}}$  complexes.<sup>7, 8</sup> Even so, some differences could be observed, for instance, class II complexes show a  $\text{Fe}-\text{N}_{\text{py}}$  bond larger (2.20-2.25 Å) than class I (2.17-2.14 Å), indicating that the bulkiness of the substituent present in the  $\alpha$  position correlates with an enlargement of the  $\text{Fe}-\text{N}_{\text{py}}$  distance.

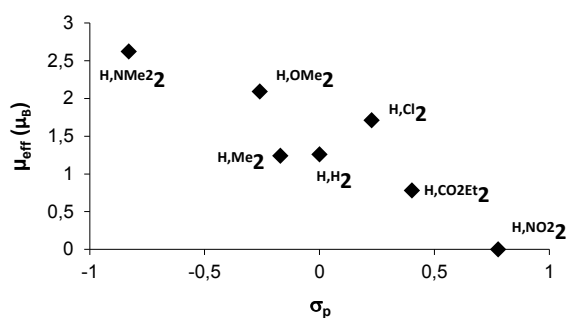
$^1\text{H}$ -NMR spectra of the  $\text{Fe}^{\text{II}}$  complexes are useful to understand the electronic properties of the complexes in solution. All the complexes exhibit a paramagnetic behavior when non-coordinated solvent, such as  $\text{CD}_2\text{Cl}_2$ , is used showing a spectral window that expands from -40 ppm to 200 ppm. This is indicative of a high spin (HS) species  $t_{2g}^4 e_g^2$ . The electronic configuration changes when a solvent that could act as strong field ligand such as  $\text{CD}_3\text{CN}$  is used. In this case, triflate anions are displaced by the solvent generating the  $[\text{Fe}^{\text{II}}(\text{R,R}'\text{Pytacn})(\text{CH}_3\text{CN})_2]^{2+}$  ( $\text{R,R}'\mathbf{2}$ ) species. The corresponding complexes that belong to class II remain as HS species, despite exchanging the triflate for  $\text{CH}_3\text{CN}$  as coordinating groups. Instead class I complexes are low spin (LS), or exist as a mixture of low and high spin species in equilibrium at room temperature. In addition in class I complexes the relative population of the high and low spin states is sensitive to the nature of the substituent in  $\gamma$  position. Complexes with electron donor groups show a spectral window that expands from 0 to 45, and denote predominant population of the HS state. In contrast, complexes with electron

withdrawing groups exhibit a much smaller spectral window, thus showing a diamagnetic behavior indicative of a LS state.<sup>9</sup>

These electronic differences could be quantified measuring the effective magnetic moments ( $\mu_{\text{eff}}$ ) by using the Evans' method. Class I catalysts exhibit a correlation between the electronic properties of the group in the  $\gamma$  position and  $\mu_{\text{eff}}$  values. Complex  $^{\text{H,NO}_2}\mathbf{2}$ , which contains the strongly electron-withdrawing  $\text{NO}_2$  group, has no effective magnetic moment, indication of a pure LS  $\text{Fe}^{\text{II}}$  ( $t_{2g}^6 e_g^0$ ). Compound  $^{\text{H,CO}_2\text{Et}}\mathbf{2}$  with an ester group exhibits a low magnetic moment of  $0.78 \mu_{\text{B}}$ . Complexes  $^{\text{H,H}}\mathbf{2}$ ,  $^{\text{H,Me}}\mathbf{2}$  and  $^{\text{H,Cl}}\mathbf{2}$ , which contain hydrogen, methyl and chloro substituents respectively, present effective magnetic moments around  $\sim 1.3$ - $1.7 \mu_{\text{B}}$ . Complexes  $^{\text{H,NMe}_2}\mathbf{2}$  and  $^{\text{H,OMe}}\mathbf{2}$  with a dimethylamino and a methoxy  $\gamma$ -substituent show larger  $\mu_{\text{eff}}$  values ( $2.62$  and  $2.09 \mu_{\text{B}}$ ), which indicates a significant population of the HS state (Scheme VIII.2). The effect of the pyridine substitution in the  $\mu_{\text{eff}}$  values of these complexes can be understood on the basis of simple ligand field theory. Electron withdrawing groups favor the  $\pi$ -acceptor character of the ligands increasing the ligand field and favoring the population of the LS state. In contrast, electron-releasing groups exhibit the opposite effect and favor the population of the HS state.

$\mu_{\text{eff}}$  values for class II complexes are  $4.80 \pm 0.17 \mu_{\text{B}}$ , very close to the theoretical spin-only value of  $4.90 \mu_{\text{B}}$  of a HS iron(II) center with four unpaired electrons. This is explained because the  $\alpha$ -substituent in the pyridine sterically interacts with the iron center and it disfavors the formation of the shorter Fe-N bond characteristic of the LS configuration.<sup>10</sup>

Complex [a]	Spin State	$\mu_{\text{eff}}$ ( $\mu_{\text{B}}$ )
$^{\text{H,H}}\mathbf{2}$	Low-Intermediate	1.26
$^{\text{H,NMe}_2}\mathbf{2}$	Intermediate	2.62
$^{\text{H,OMe}}\mathbf{2}$	Intermediate	2.09
$^{\text{H,Me}}\mathbf{2}$	Low-Intermediate	1.24
$^{\text{H,Cl}}\mathbf{2}$	Low-Intermediate	1.71
$^{\text{H,CO}_2\text{Et}}\mathbf{2}$	Low	0.78
$^{\text{H,NO}_2}\mathbf{2}$	Low	0
$^{\text{Me,H}}\mathbf{2}$	High	4.95
$^{\text{Me,Me}}\mathbf{2}$	High	4.75
$^{\text{Cl,H}}\mathbf{2}$	High	4.87
$^{\text{F,H}}\mathbf{2}$	High	4.63



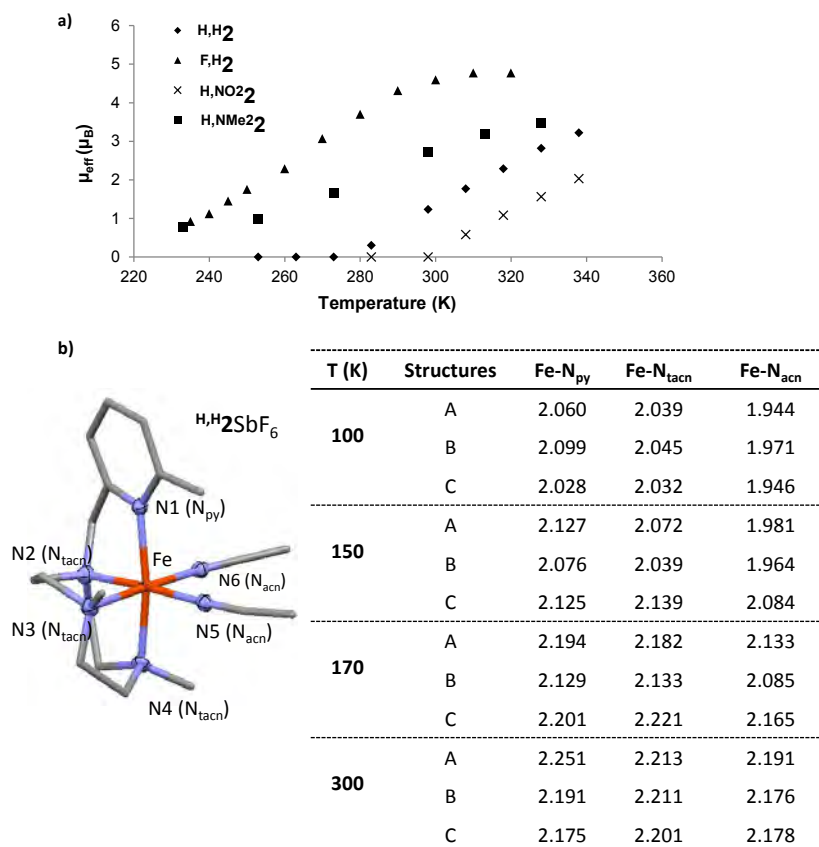
**Scheme VIII.2.** Table: Spin state and  $\mu_{\text{eff}}$  of  $^{\text{R,R'}}\mathbf{2}$  complexes at 298K in acetonitrile. Graphic:

Representation of the effective magnetic moment of  $^{\text{H,R'}}\mathbf{2}$  in front of the Hammett constants ( $\sigma_{\text{p}}$ ). [a]

Compounds  $^{\text{R,R'}}\mathbf{2}$  were prepared by dissolving the bis-triflate complexes  $^{\text{R,R'}}\mathbf{1}$  in  $\text{CH}_3\text{CN}$  or  $\text{CD}_3\text{CN}$ .

Class I complexes exhibit an incomplete spin crossover transition in the range of temperatures between 235 K and 340 K when acetonitrile is used as solvent. This is best exemplified in the correlation between the temperature and the  $\mu_{\text{eff}}$ , and also in the change of the spectral window. As the temperature is lowered, the  $\mu_{\text{eff}}$  gradually decreases and the spectral window becomes more compact, approaching that of a diamagnetic molecule. The same phenomenon is also observed with one catalyst from class II,  $^{\text{F,H}}\mathbf{2}$ , presumably because the small bulkiness of the  $\alpha\text{-F}$  does not pose important steric clash with the iron and therefore the shorter  $\text{Fe-N}_{\text{py}}$  distance of the LS state is not impeded. In this case we can observe that the  $\mu_{\text{eff}}$  values rapidly decrease upon lowering the temperature (Scheme VIII.3, a).

On the other hand, complex  $^{\text{Me,H}}\mathbf{2SbF}_6$  shows a spin crossover phenomenon in solid state evidenced by a color change, from colorless to dark blue, and by X-ray diffraction (XRD) analysis. The XRD data revealed that at 300 K the complex shows a HS state (distance  $\text{Fe-N}_{\text{py}}$  2.2Å) but it adopts a LS configuration when the crystal is measured at 100 K (distances  $\text{Fe-N}_{\text{py}}$  2.0Å) (Scheme VIII.3, b).



**Scheme VIII.3.** a) Representation of the effective magnetic moment of  $^{\text{H,H}}\mathbf{2}$ ,  $^{\text{F,H}}\mathbf{2}$ ,  $^{\text{H,NO}_2}\mathbf{2}$  and  $^{\text{H,NMe}_2}\mathbf{2}$  as a function of temperature. The effective magnetic moment was measured in a  $\text{CD}_3\text{CN}$  solution using the Evans' method. b) X-Ray structure of  $^{\text{Me,H}}\mathbf{2SbF}_6$  at 100K. The table shows the  $\text{Fe-N}_{\text{py}}$ , the average  $\text{Fe-N}_{\text{tacn}}$  and the average  $\text{Fe-N}_{\text{acn}}$  bond lengths for each of the three molecules (A, B and C) that form the unit cell at a given temperature (100 K, 150 K, 170 K and 300 K). Hydrogen atoms have been omitted for clarity.



UV-visible spectroscopy is also a good technique to determine the spin state of the complexes. Class I catalysts show bands typical of low spin complexes, one at 550 nm that corresponds to a d-d transition of the octahedral iron(II) complex and another one at 385 nm that reflects a metal-to-ligand charge transfer (MLCT).<sup>8, 11</sup> It is important to notice that the MLCT band is related to the electronic properties of the ligand and shifts bathochromically upon increasing the electronwithdrawing character of the  $\gamma$ -group. The energy of this absorption band decreases with the decrease of the electron-richness of the  $\gamma$ -substituent following the next order: NMe<sub>2</sub> > OMe  $\approx$  Me > H > Cl > CO<sub>2</sub>Et > NO<sub>2</sub> (Table VIII.1).

For class II catalysts, the UV-vis spectrum of <sup>Me,H</sup>**2**, which is very similar to <sup>Cl,H</sup>**2** and <sup>Me,Me</sup>**2**, is taken as the reference. This complex exhibits a band at 267 nm ( $\epsilon \sim 5100 \text{ M}^{-1}\text{cm}^{-1}$ ) and a shoulder at 340 nm ( $\epsilon \sim 255 \text{ M}^{-1}\text{cm}^{-1}$ ), both of them characteristic of HS iron(II) complexes.<sup>12</sup> Compound <sup>F,H</sup>**2** has a slight contribution of the LS state at room temperature as evidenced by the presence of low intensity bands at 237, 368 and 578 nm, that strongly resemble those described above for LS iron(II) complexes (Table VIII.1).

Table VIII.1. Selected physical data for <sup>R,R'</sup>**2**.<sup>[a]</sup>

Complex	$\lambda_{\text{max}}$ , nm ( $\epsilon$ , $\text{M}^{-1}\text{cm}^{-1}$ )			$E_{1/2}$ (mV) <sup>[b]</sup>
	$\pi$ - $\pi^*$	MLCT	d-d	
<sup>H,H</sup> <b>2</b>	239 (13900)	385 (3200)	550 (65)	138
<sup>H,NMe2</sup> <b>2</b>	240 (>20000)	327 (4700)	bs: 450-550 (500)	11
<sup>H,OMe</sup> <b>2</b>	250 (13300)	370 (5400)	547 (120)	107
<sup>H,Me</sup> <b>2</b>	240 (10500)	370 (2900)	553 (70)	176
<sup>H,Cl</sup> <b>2</b>	241 (15800)	403 (3900)	552 (28)	165
<sup>H,CO2Et</sup> <b>2</b>	275 (6150)	455 (6100)		171
<sup>H,NO2</sup> <b>2</b>	231 (14000)	526 (2400)		225
<sup>Me,H</sup> <b>2</b>	267 (5100)	340 (255)		211
<sup>Me,Me</sup> <b>2</b>	260 (4700)	344 (220)		238
<sup>Cl,H</sup> <b>2</b>	269 (7000)	410(950)		n.m. <sup>[c]</sup>
<sup>F,H</sup> <b>2</b>	237 (5600), 254 (5600)	368 (900)	578 (14)	n.m. <sup>[c]</sup>

[a] Compounds <sup>R,R'</sup>**2** were prepared by dissolving the bis-triflate complexes <sup>R,R'</sup>**1** in CH<sub>3</sub>CN.

[b]  $E_{1/2}$  values determined for <sup>R,R'</sup>**3** in CH<sub>3</sub>CN. Values measured vs. SCE. [c] Not measured.

Finally, a quantitative measure of the electronic properties of the resulting iron(II) complexes could be estimated by measuring the redox potential of the Fe<sup>II</sup>/Fe<sup>III</sup> pair of the corresponding chlorocomplexes [Fe<sup>II</sup>Cl<sub>2</sub>(<sup>R,R'</sup>Pytacn)], (<sup>R,R'</sup>**3**). Class I catalysts exhibit  $E_{1/2}$  values

that follow the expected trend according to the electronic properties of each ligand. The lowest redox potential is obtained by complex  ${}^{\text{H,NMe}_2}\mathbf{3}$  (11 mV), which contains an electron donating dimethylamino substituent that stabilizes  $\text{Fe}^{\text{III}}$ , instead the highest value corresponds to complex  ${}^{\text{H,NO}_2}\mathbf{3}$  (225 mV) with the most electronwithdrawing nitro group. In class II complexes the introduction of a methyl in the  $\alpha$ -position of the pyridine increases the redox potential (211-238 mV) even more than a  $\text{NO}_2$  group in the  $\gamma$ -pyridine. This effect can be understood by considering that the steric clash between the methyl group and the iron center disfavors the formation of the shorter  $\text{Fe-N}_{\text{py}}$  bonds necessary to generate the iron(III) (Table VIII.1).

### VIII.1.2. Performance in catalysis

Catalytic activity of these complexes was analyzed in order to evaluate putative electronic and steric effects in the catalytic oxidation of alkanes and alkenes mediated by these complexes. Cyclohexane was used as a model substrate for alkane oxidation, and all complexes  ${}^{\text{R,R}'}\mathbf{1}$  proved excellent catalyst for the oxidation of cyclohexane, converting 43%-76% of the oxidant into oxidized products (when 1 equiv. of catalyst, 10 equiv. of  $\text{H}_2\text{O}_2$  and 1000 equiv. of substrate are used). Moreover, a high alcohol/ketone ratio was obtained (7-12), suggesting that the active species responsible for the chemistry are metal-based oxidants. When the amount of  $\text{H}_2\text{O}_2$  was increased up to 100 equiv. the yield of class I complexes suffer a significant decrease. However, complexes that belong to class II ( ${}^{\text{Me,H}}\mathbf{1}$  and  ${}^{\text{Me,Me}}\mathbf{1}$ ) with a methyl group on  $\alpha$  position maintain the efficiency. This is indicative that these catalysts could be good candidates to catalyze C-H hydroxylation under preparative scale conditions. This is further developed in Chapter V.

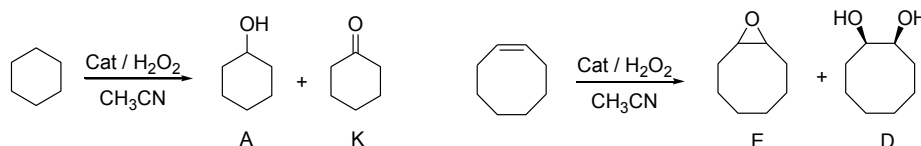
*Cis*-cyclooctene was used to evaluate the competence of the complexes in alkene oxidation employing  $\text{H}_2\text{O}_2$  as oxidant; all the complexes catalyze the oxidation giving a mixture of *syn*-diol and epoxide products with conversion of the oxidant into products that range from 71 to 95%, when 1 equiv. of catalyst, 10 equiv. of  $\text{H}_2\text{O}_2$  and 1000 equiv. of substrate are used. Moreover, the yields are maintained when 100 equiv. of  $\text{H}_2\text{O}_2$  were employed. The differences appear in the *syn*-diol/epoxide ratio. While class I complexes produce an equimolar mixture of *syn*-diol and epoxide, class II complexes favor the formation of the *syn*-diol, and best results are obtained with  $\alpha$ -methyl substituted complexes, which give a *syn*-diol/epoxide ratio around 6. This suggests that these complexes have a potential use as *cis*-dihydroxylation catalysts for preparative purposes. This was further developed in Chapter VI.

Class I complexes show similar results in the oxidation of alkanes and alkenes (see Table VIII.2, entries 1-7), similar efficiencies and selectivities, indicating that electronic

properties of the  $\gamma$  substituent in the pyridine ring does not significantly influence the catalytic activity. In contrast, the introduction of a bulky methyl group in  $\alpha$  position enhances the efficiency and the selectivity of the catalyst (Table VIII.2, entries 8-9), making it interesting for catalytic oxidative applications in synthetic scale.

**Table VIII.2.** Oxidation of cyclohexane and *cis*-cyclooctene with  $\text{H}_2\text{O}_2$  using complexes

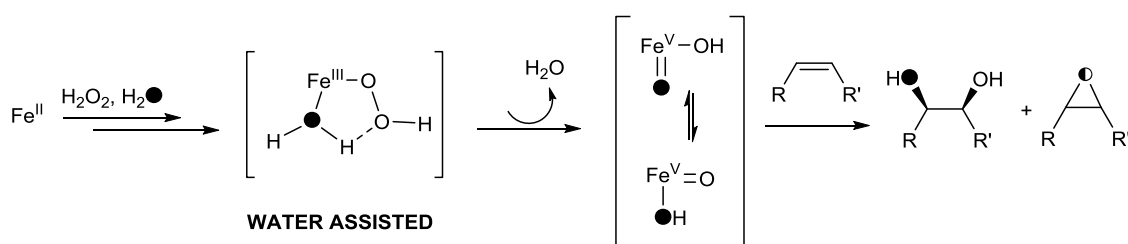
$[\text{Fe}^{\text{II}}(\text{CF}_3\text{SO}_3)_2(\text{R,R}'\text{Pytacn})]$ ,  $\text{R,R}'\mathbf{1}$ , as catalysts. [a] Results for  $\text{H,H}\mathbf{1}$  and  $\text{Me,H}\mathbf{1}$  have been previously reported.<sup>6, 13</sup>



Catalyst	$\text{H}_2\text{O}_2$ (equiv.)	Cyclohexane $\text{A}+\text{K}^{[b]}$ (A/K) <sup>[c]</sup>	Cyclooctene $\text{D}+\text{E}^{[d]}$ (D/E) <sup>[e]</sup>	Cyclooctene <i>syn</i> -diol $\text{16}_{\text{O}}^{18}\text{O}^{[f]}$	Cyclooctene epoxide $\text{18}_{\text{O}}^{[g]}$																																																																																							
$\text{H,H}\mathbf{1}$	10	6.5 (12.3)	8.1 (1.0)	97	77																																																																																							
	100	39 (2.6)	99 (1.0)			$\text{H,NMe}_2\mathbf{1}$	10	4.3 (8.9)	8.2 (2.3)	95	74	100	31 (3.8)	69 (1.4)	$\text{H,OMe}\mathbf{1}$	10	6.2 (10.2)	7.6 (1.1)	95	71	100	47 (2.8)	83 (1.5)	$\text{H,Me}\mathbf{1}$	10	6.5 (10.5)	9.3 (2.6)	97	72	100	48 (2.3)	85 (1.0)	$\text{H,Cl}\mathbf{1}$	10	5.9 (8.3)	9.5 (1.5)	97	67	100	40 (4.3)	85 (2.1)	$\text{H,CO}_2\text{Et}\mathbf{1}$	10	5.7 (9.2)	8.2 (1.5)	97	63	100	43 (3.2)	82 (1.2)	$\text{H,NO}_2\mathbf{1}$	10	5.3 (8.1)	7.8 (1.5)	99	66	100	34 (3.9)	50 (1.1)	$\text{Me,H}\mathbf{1}$	10	7.6 (10.2)	7.1 (5.5)	78	5	100	64 (4.3)	86 (6.2)	$\text{Me,Me}\mathbf{1}$	10	6.1 (9.3)	8.6 (5.2)	80	4	100	60 (5.1)	81 (3.5)	$\text{Cl,H}\mathbf{1}$	10	6.8 (6.7)	8.4 (2.6)	80	9	100	28 (3.0)	63 (4.7)	$\text{F,H}\mathbf{1}$	10	5.9 (8.3)	7.5 (0.8)	89	4
$\text{H,NMe}_2\mathbf{1}$	10	4.3 (8.9)	8.2 (2.3)	95	74																																																																																							
	100	31 (3.8)	69 (1.4)			$\text{H,OMe}\mathbf{1}$	10	6.2 (10.2)	7.6 (1.1)	95	71	100	47 (2.8)	83 (1.5)	$\text{H,Me}\mathbf{1}$	10	6.5 (10.5)	9.3 (2.6)	97	72	100	48 (2.3)	85 (1.0)	$\text{H,Cl}\mathbf{1}$	10	5.9 (8.3)	9.5 (1.5)	97	67	100	40 (4.3)	85 (2.1)	$\text{H,CO}_2\text{Et}\mathbf{1}$	10	5.7 (9.2)	8.2 (1.5)	97	63	100	43 (3.2)	82 (1.2)	$\text{H,NO}_2\mathbf{1}$	10	5.3 (8.1)	7.8 (1.5)	99	66	100	34 (3.9)	50 (1.1)	$\text{Me,H}\mathbf{1}$	10	7.6 (10.2)	7.1 (5.5)	78	5	100	64 (4.3)	86 (6.2)	$\text{Me,Me}\mathbf{1}$	10	6.1 (9.3)	8.6 (5.2)	80	4	100	60 (5.1)	81 (3.5)	$\text{Cl,H}\mathbf{1}$	10	6.8 (6.7)	8.4 (2.6)	80	9	100	28 (3.0)	63 (4.7)	$\text{F,H}\mathbf{1}$	10	5.9 (8.3)	7.5 (0.8)	89	4	100	26 (2.7)	73 (1.0)						
$\text{H,OMe}\mathbf{1}$	10	6.2 (10.2)	7.6 (1.1)	95	71																																																																																							
	100	47 (2.8)	83 (1.5)			$\text{H,Me}\mathbf{1}$	10	6.5 (10.5)	9.3 (2.6)	97	72	100	48 (2.3)	85 (1.0)	$\text{H,Cl}\mathbf{1}$	10	5.9 (8.3)	9.5 (1.5)	97	67	100	40 (4.3)	85 (2.1)	$\text{H,CO}_2\text{Et}\mathbf{1}$	10	5.7 (9.2)	8.2 (1.5)	97	63	100	43 (3.2)	82 (1.2)	$\text{H,NO}_2\mathbf{1}$	10	5.3 (8.1)	7.8 (1.5)	99	66	100	34 (3.9)	50 (1.1)	$\text{Me,H}\mathbf{1}$	10	7.6 (10.2)	7.1 (5.5)	78	5	100	64 (4.3)	86 (6.2)	$\text{Me,Me}\mathbf{1}$	10	6.1 (9.3)	8.6 (5.2)	80	4	100	60 (5.1)	81 (3.5)	$\text{Cl,H}\mathbf{1}$	10	6.8 (6.7)	8.4 (2.6)	80	9	100	28 (3.0)	63 (4.7)	$\text{F,H}\mathbf{1}$	10	5.9 (8.3)	7.5 (0.8)	89	4	100	26 (2.7)	73 (1.0)															
$\text{H,Me}\mathbf{1}$	10	6.5 (10.5)	9.3 (2.6)	97	72																																																																																							
	100	48 (2.3)	85 (1.0)			$\text{H,Cl}\mathbf{1}$	10	5.9 (8.3)	9.5 (1.5)	97	67	100	40 (4.3)	85 (2.1)	$\text{H,CO}_2\text{Et}\mathbf{1}$	10	5.7 (9.2)	8.2 (1.5)	97	63	100	43 (3.2)	82 (1.2)	$\text{H,NO}_2\mathbf{1}$	10	5.3 (8.1)	7.8 (1.5)	99	66	100	34 (3.9)	50 (1.1)	$\text{Me,H}\mathbf{1}$	10	7.6 (10.2)	7.1 (5.5)	78	5	100	64 (4.3)	86 (6.2)	$\text{Me,Me}\mathbf{1}$	10	6.1 (9.3)	8.6 (5.2)	80	4	100	60 (5.1)	81 (3.5)	$\text{Cl,H}\mathbf{1}$	10	6.8 (6.7)	8.4 (2.6)	80	9	100	28 (3.0)	63 (4.7)	$\text{F,H}\mathbf{1}$	10	5.9 (8.3)	7.5 (0.8)	89	4	100	26 (2.7)	73 (1.0)																								
$\text{H,Cl}\mathbf{1}$	10	5.9 (8.3)	9.5 (1.5)	97	67																																																																																							
	100	40 (4.3)	85 (2.1)			$\text{H,CO}_2\text{Et}\mathbf{1}$	10	5.7 (9.2)	8.2 (1.5)	97	63	100	43 (3.2)	82 (1.2)	$\text{H,NO}_2\mathbf{1}$	10	5.3 (8.1)	7.8 (1.5)	99	66	100	34 (3.9)	50 (1.1)	$\text{Me,H}\mathbf{1}$	10	7.6 (10.2)	7.1 (5.5)	78	5	100	64 (4.3)	86 (6.2)	$\text{Me,Me}\mathbf{1}$	10	6.1 (9.3)	8.6 (5.2)	80	4	100	60 (5.1)	81 (3.5)	$\text{Cl,H}\mathbf{1}$	10	6.8 (6.7)	8.4 (2.6)	80	9	100	28 (3.0)	63 (4.7)	$\text{F,H}\mathbf{1}$	10	5.9 (8.3)	7.5 (0.8)	89	4	100	26 (2.7)	73 (1.0)																																	
$\text{H,CO}_2\text{Et}\mathbf{1}$	10	5.7 (9.2)	8.2 (1.5)	97	63																																																																																							
	100	43 (3.2)	82 (1.2)			$\text{H,NO}_2\mathbf{1}$	10	5.3 (8.1)	7.8 (1.5)	99	66	100	34 (3.9)	50 (1.1)	$\text{Me,H}\mathbf{1}$	10	7.6 (10.2)	7.1 (5.5)	78	5	100	64 (4.3)	86 (6.2)	$\text{Me,Me}\mathbf{1}$	10	6.1 (9.3)	8.6 (5.2)	80	4	100	60 (5.1)	81 (3.5)	$\text{Cl,H}\mathbf{1}$	10	6.8 (6.7)	8.4 (2.6)	80	9	100	28 (3.0)	63 (4.7)	$\text{F,H}\mathbf{1}$	10	5.9 (8.3)	7.5 (0.8)	89	4	100	26 (2.7)	73 (1.0)																																										
$\text{H,NO}_2\mathbf{1}$	10	5.3 (8.1)	7.8 (1.5)	99	66																																																																																							
	100	34 (3.9)	50 (1.1)			$\text{Me,H}\mathbf{1}$	10	7.6 (10.2)	7.1 (5.5)	78	5	100	64 (4.3)	86 (6.2)	$\text{Me,Me}\mathbf{1}$	10	6.1 (9.3)	8.6 (5.2)	80	4	100	60 (5.1)	81 (3.5)	$\text{Cl,H}\mathbf{1}$	10	6.8 (6.7)	8.4 (2.6)	80	9	100	28 (3.0)	63 (4.7)	$\text{F,H}\mathbf{1}$	10	5.9 (8.3)	7.5 (0.8)	89	4	100	26 (2.7)	73 (1.0)																																																			
$\text{Me,H}\mathbf{1}$	10	7.6 (10.2)	7.1 (5.5)	78	5																																																																																							
	100	64 (4.3)	86 (6.2)			$\text{Me,Me}\mathbf{1}$	10	6.1 (9.3)	8.6 (5.2)	80	4	100	60 (5.1)	81 (3.5)	$\text{Cl,H}\mathbf{1}$	10	6.8 (6.7)	8.4 (2.6)	80	9	100	28 (3.0)	63 (4.7)	$\text{F,H}\mathbf{1}$	10	5.9 (8.3)	7.5 (0.8)	89	4	100	26 (2.7)	73 (1.0)																																																												
$\text{Me,Me}\mathbf{1}$	10	6.1 (9.3)	8.6 (5.2)	80	4																																																																																							
	100	60 (5.1)	81 (3.5)			$\text{Cl,H}\mathbf{1}$	10	6.8 (6.7)	8.4 (2.6)	80	9	100	28 (3.0)	63 (4.7)	$\text{F,H}\mathbf{1}$	10	5.9 (8.3)	7.5 (0.8)	89	4	100	26 (2.7)	73 (1.0)																																																																					
$\text{Cl,H}\mathbf{1}$	10	6.8 (6.7)	8.4 (2.6)	80	9																																																																																							
	100	28 (3.0)	63 (4.7)			$\text{F,H}\mathbf{1}$	10	5.9 (8.3)	7.5 (0.8)	89	4	100	26 (2.7)	73 (1.0)																																																																														
$\text{F,H}\mathbf{1}$	10	5.9 (8.3)	7.5 (0.8)	89	4																																																																																							
	100	26 (2.7)	73 (1.0)																																																																																									

[a] 1000 equiv. of substrate (100 equiv. for isotope labeling studies) with respect to catalyst. The reaction was performed by slow syringe pump addition over 30 min of an acetonitrile solution of  $\text{H}_2\text{O}_2$  (10 or 100 equiv.) into a solution of catalyst and substrate at room temperature. [b] Turnover number (mols of products/mols of catalyst), A = cyclohexanol, K = cyclohexanone. [c] A/K = mols of alcohol/mols of ketone. [d] Turnover number (mols product/mols catalyst), D = *syn*-cyclooctane-1,2-diol, E = cyclooctene epoxide. [e] D/E = mols of *syn*-diol/mols of epoxide. [f] Percentage of *syn*-diol  $^{16}\text{O}^{18}\text{O}$  labeled when the oxidation of *cis*-cyclooctene was carried out in the presence of 1000 equiv.  $\text{H}_2^{18}\text{O}$ . [g] Percentage of epoxide  $^{18}\text{O}$  labeled when the oxidation of *cis*-cyclooctene was carried out in the presence of 1000 equiv.  $\text{H}_2^{18}\text{O}$ .

Isotopic labeling experiments show that this family of complexes is capable of incorporating oxygen atoms from water into the oxidized products. This is indicative that a high valent iron species participate in the catalytic cycle. The mechanistic scheme proposed is extensively discussed in Chapter IV. It involves initial oxidation of the starting  $\text{Fe}^{\text{II}}$  complexes into corresponding mononuclear  $\text{Fe}^{\text{III}}$  species. Subsequent reaction of the  $\text{Fe}^{\text{III}}$  species with  $\text{H}_2\text{O}_2$  forms  $\text{Fe}^{\text{III}}(\text{OOH})$  intermediates that undergo water assisted O-O breakage leading to the formation of a  $\text{Fe}^{\text{V}}(\text{O})(\text{OH})$  species, where one oxygen comes from hydrogen peroxide and the other one from water. The fast oxo-hydroxo tautomerism allows the oxygen from water to be either in the oxo or hydroxo form (Scheme VIII.4).<sup>13</sup>

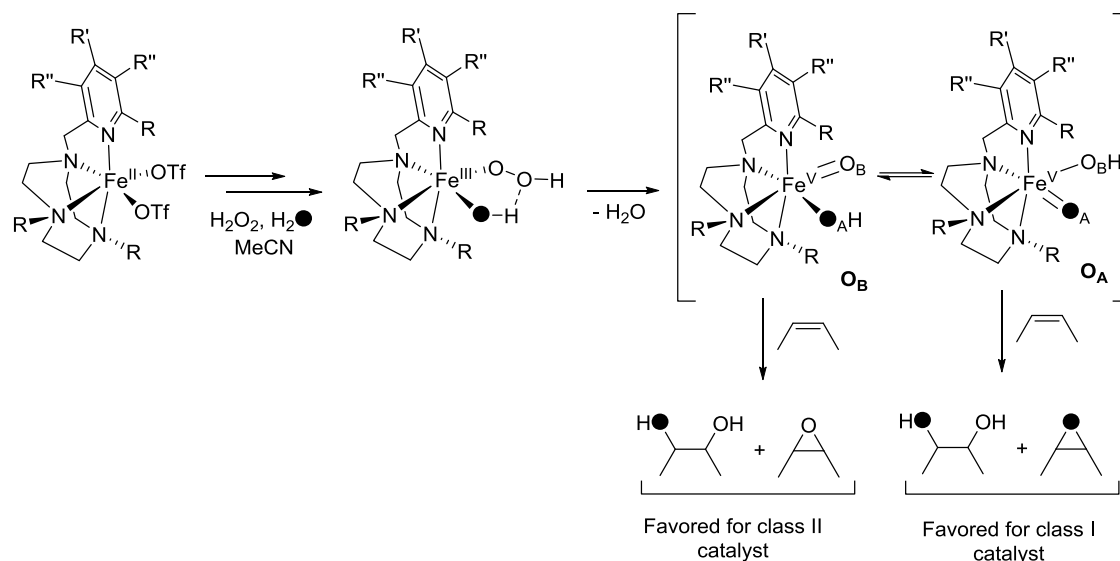


**Scheme VIII.4.** Water assisted mechanism to explain the oxidation of olefins by mononuclear non-heme iron catalysts.

The labeling experiments using *cis*-cyclooctene as substrate show that both classes of catalysts incorporated one oxygen from water and the other from hydrogen peroxide into the *syn*-diol product. Differences appeared in the formation of the epoxide, where the incorporation of water into this product was very high for class I complexes (70±7%), while for class II compounds the amount of  $^{18}\text{O}$ -labeled epoxide dramatically decreased to 7±3%.

The labeling pattern observed in the formation of the *syn*-diol strongly suggests that both classes of catalysts operated via a common iron(V)-oxo-hydroxo oxidant. The different percentage of water incorporation in epoxide product could be explained because the two iron coordination sites where the oxo and the hydroxide ligand bind are not identical, and two tautomers can exist, depending in the relative position of the oxo and the hydroxide ligand;  $\text{Fe}^{\text{V}}(\text{O}_A)(\text{O}_B\text{H})$  ( $\mathbf{O}_A$ ) and  $\text{Fe}^{\text{V}}(\text{O}_B)(\text{O}_A\text{H})$  ( $\mathbf{O}_B$ ) (Scheme VIII.5). In class II catalysts, the presence of sterically more demanding groups at position  $\alpha$  protects the position A, and presumably becomes less accessible to the substrate. On these bases, we suggest that steric interactions produce a more sensitive bias in the relative reactivity of the two tautomers. For class I catalysts the reaction of the substrate with  $\mathbf{O}_A$  is more favored and for class II catalysts is favored with  $\mathbf{O}_B$ .

In Chapter IV these studies are extended to the oxidation of alkanes by using isotopic labeling experiments, product analysis and DFT calculations.



**Scheme VIII.5.** Proposed mechanism for alkene oxidation, where the fast equilibrium between the two tautomers is represented.

## VIII.2. The mechanism of stereospecific C-H oxidation by Fe(Pytacn) complexes. Bioinspired non-heme iron centers containing *cis*-labile exchangeable sites

The  $[\text{Fe}^{\text{II}}(\text{CF}_3\text{SO}_3)_2(\text{R,R}'\text{Pytacn})]$  family of complexes was used for studying the mechanism of oxidation of C-H bonds by using isotopic labeling experiments, product analysis and detailed DFT calculations. The modification of electronic and steric properties of the ligand make this family of complexes a convenient platform to study the impact of these parameters on C-H bond oxidation, and for understanding the C-H cleavage and C-O bond formation reactions in non-heme iron complexes.<sup>6,14</sup>

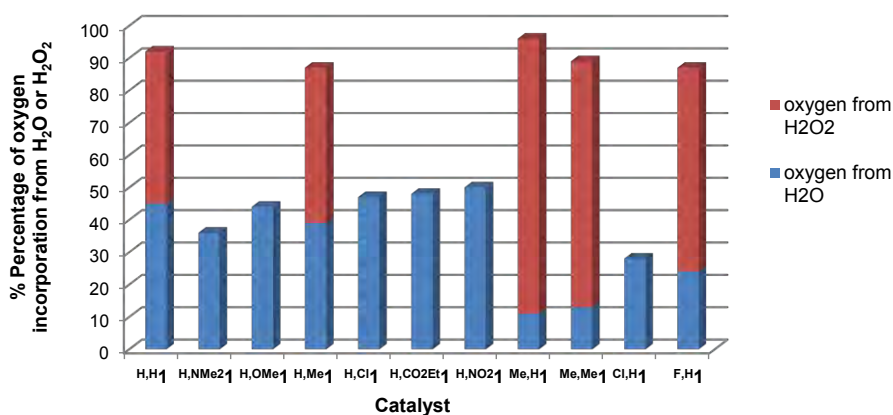
The present family of catalysts shows excellent yields in cyclohexane hydroxylation (43-76%), as previously discussed (Table VIII.2). Moreover, on the basis of the study of the reaction with mechanistic probe substrates it can be concluded that the active species responsible for the oxidation reactions must be a metal-based oxidant, as high ratios alcohol/ketone in cyclohexane oxidation (6-12), high stereoretention in *cis*-1,2-dimethyl cyclohexane (DMCH) oxidation (86-95%), large kinetic isotope effects (KIE) values on the oxidation of cyclohexane (3.3-5.0) and high normalized 3°/2° selectivities (15-30) for adamantane oxidation are observed (Table VIII. 3).<sup>15</sup>

**Table VIII. 3.** Alkane hydroxylation reactions catalyzed by  $R,R'$  **1**.<sup>[a]</sup> Results for  $H,H$  **1** and  $Me,H$  **1** have been previously reported.<sup>6, 14</sup>

catalyst	cyclohexane		adamantane	DMCH
	A+K <sup>[b]</sup> (A/K)	KIE <sup>[c]</sup>	3 <sup>o</sup> /2 <sup>o</sup> <sup>[d]</sup>	RC(%) <sup>[e]</sup>
$H,H$ <b>1</b>	6.5 (12.3)	4.3	30	93
$Me,H$ <b>1</b>	7.6 (10.2)	3.4	20	94
$H,NMe_2$ <b>1</b>	4.3 (8.9)	4.9	23	94
$H,OMe$ <b>1</b>	6.2 (10.2)	4.2	23	95
$H,Me$ <b>1</b>	6.5 (10.5)	5.0	30	88
$H,Cl$ <b>1</b>	5.9 (8.3)	4.3	30	94
$H,CO_2Et$ <b>1</b>	5.7 (9.2)	4.1	28	94
$H,NO_2$ <b>1</b>	5.3 (8.1)	4.3	29	89
$Me,Me$ <b>1</b>	6.1 (9.3)	4.0	15	95
$Cl,H$ <b>1</b>	6.8 (6.7)	3.3	28	88
$F,H$ <b>1</b>	5.9 (5.7)	4.5	19	86

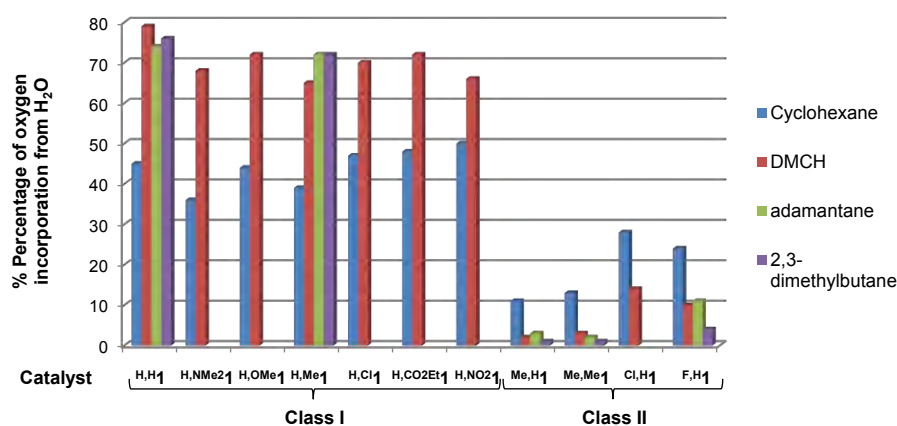
[a]  $H_2O_2$  (10 equiv.) was delivered by syringe pump to an acetonitrile solution containing the iron catalyst (1 equiv.) and the substrate (10 – 1000 equiv.). 1000 equiv. substrate for cyclohexane and DMCH. 10 equiv. for adamantane. [b] Turnover number (mols of product/mols of catalyst), A = cyclohexanol, K = cyclohexanone. [c] Kinetic Isotope Effect determined for cyclohexanol formation measured in the oxidation of a 1:3 mixture of cyclohexane: $d_{12}$ -cyclohexane. [d] 3<sup>o</sup>/2<sup>o</sup> ratio in adamantane oxidation = 3 x (1-adamantanol)/(2-adamantanol + 2-adamantanone). [e] Percentage of retention of configuration in the oxidation of the tertiary C-H bonds of *cis*-1,2-dimethylcyclohexane (DMCH) = (*cis-trans*)/(*cis+trans*)x100.

In isotopic labeling experiments, all complexes  $R,R'$  **1** were used as catalysts for alkane oxidation using 10 equiv. of  $H_2O_2$  and 1000 equiv. of  $H_2^{18}O$ . All catalysts incorporate oxygen from water into the oxidized product. Complementary experiments using  $H_2^{18}O_2$  showed that peroxide is the other source of oxygen, and consequently  $O_2$  incorporation is minimal. However, the percentage of oxygen from water incorporated is highly dependent on the specific structure of the catalyst and the substrate (Scheme VIII.6 and Scheme VIII.7).



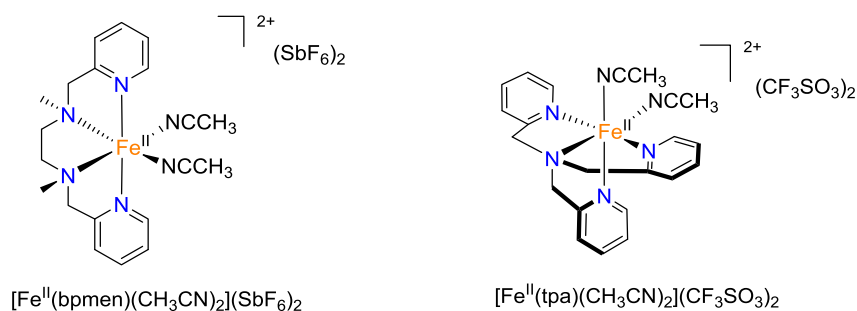
**Scheme VIII.6.** Origin of oxygen atoms in the oxidation of cyclohexane. Blue: Percentage of oxygen incorporated from water, measured for all catalysts  $R,R'$  **1**. Red: Percentage of oxygen incorporated from hydrogen peroxide, measured for catalysts:  $H,H$  **1**,  $H,Me$  **1**,  $Me,H$  **1**,  $Me,Me$  **1** and  $F,H$  **1**.

The results show the same trend as in *cis*-cyclooctene epoxidation (Table VIII.2), the catalyst with no substitution in the  $\alpha$  position of the aromatic ring (class I) afford high levels of water incorporation. An average value of  $43\pm 7\%$  of oxygen from water is incorporated into cyclohexanol ( $2^\circ$  C-H bond) and this percentage increased up to  $71\pm 8\%$  for tertiary C-H bonds. However, when a substituent is present (class II) these values dramatically decrease, and water incorporation into tertiary C-H bonds is  $7\pm 7\%$ , and  $19\pm 8\%$  for methylene sites (Scheme VIII.7). This is indicative that pure electronic modifications in the pyridine ring (by altering  $\gamma$  position) do not substantially influence neither the catalytic activity nor the isotopic patterns. However, modifications in  $\alpha$  position, which bear electronic and steric influences, have an important impact in both aspects.



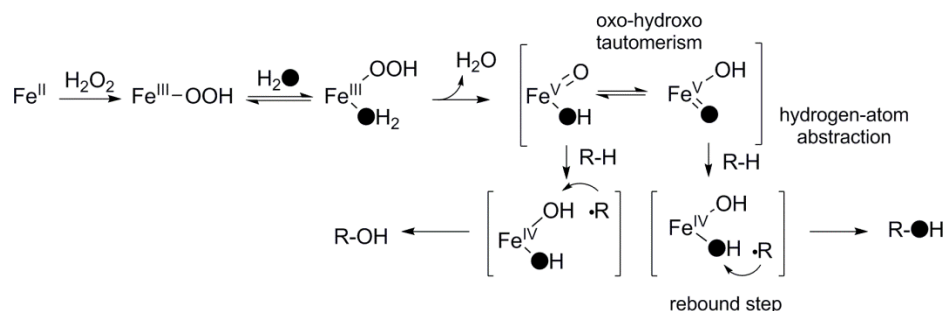
**Scheme VIII.7.** Percentage of oxygen from water incorporation into alcohol products obtained in the oxidation of alkanes catalyzed by complexes  $R,R'$  **1** in presence of 1000 equiv. of  $H_2^{18}O$ .

Previously studies performed by Que and co-workers proposed that non-heme iron complexes such as  $[Fe^{II}(bpmen)(CH_3CN)_2]^{2+}$  and  $[Fe^{II}(tpa)(CH_3CN)_2]^{2+}$  (Scheme VIII.8) incorporate water into C-H oxidation products because they engage in a oxo-hydroxo tautomerism, first described for porphyrinic systems.<sup>7, 16</sup> The  $Fe^V(O)(OH)$  tautomer is formed after O-O bond cleavage, and contains an oxo ligand originating from the oxidant that could be transferred to the substrate, and a hydroxo originating from water. However, through protopic tautomerism the initial hydroxide ligand becomes a terminal oxo ligand that can be subsequently transferred to the substrate. In these systems, the alkane oxidation takes place via "oxygen rebound" mechanism, which involve initial hydrogen-atom abstraction by the oxo group and subsequent rebound of the nascent alkyl radical with the formed  $Fe^{IV}(OH)_2$  moiety, where the same oxygen atom that abstracts the hydrogen atom ends up into the oxidized compound.<sup>7, 16</sup>



**Scheme VIII.8.** Schematic representation of complexes  $[\text{Fe}^{\text{II}}(\text{bpmen})(\text{CH}_3\text{CN})_2]^{2+}$  and  $[\text{Fe}^{\text{II}}(\text{tpa})(\text{CH}_3\text{CN})_2]^{2+}$ .

In this scenario, there is a competition between the extent of the tautomerism and the hydrogen abstraction reaction, so the level of oxygen from water incorporated into products is inversely dependent on the concentration of substrate and on its relative reactivity. Moreover, the percentage of water incorporation into the products can reach a maximum of 50% because positions bearing the oxo and the hydroxido ligands are considered equivalent (Scheme VIII.9).



**Scheme VIII.9.** A common iron(V)-oxo-hydroxo species as the active species in C-H hydroxylation and C=C *cis*-dihydroxylation as postulated for  $[\text{Fe}^{\text{II}}(\text{tpa})(\text{CH}_3\text{CN})_2]^{2+}$  and  $[\text{Fe}^{\text{II}}(\text{bpmen})(\text{CH}_3\text{CN})_2]^{2+}$  catalysts.

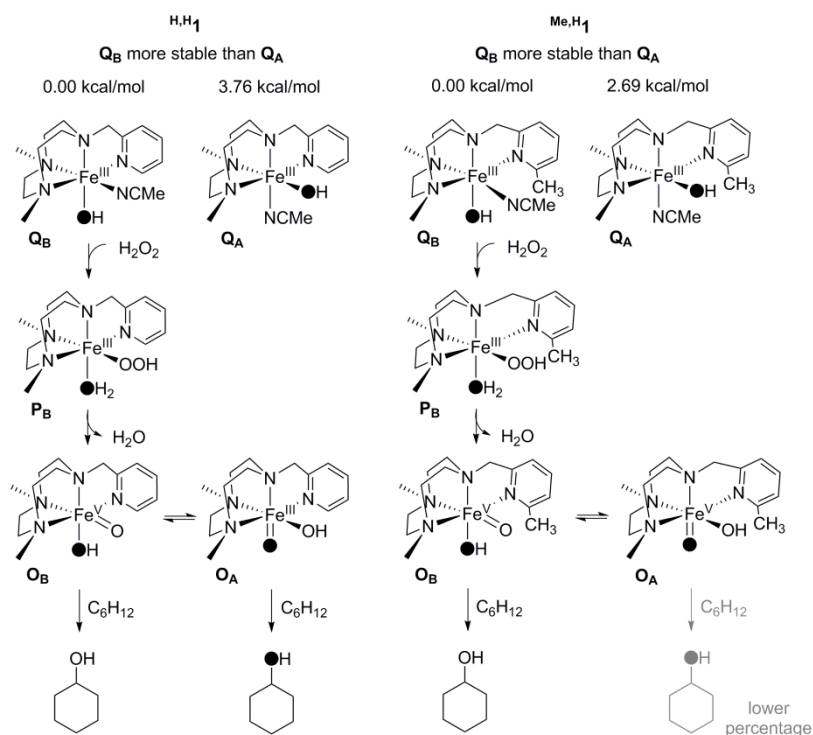
Some families of complexes such as  $[\text{Fe}^{\text{II}}(\text{tpa})(\text{CH}_3\text{CN})_2]^{2+}$  and  $[\text{Fe}^{\text{II}}(\text{bpmen})(\text{CH}_3\text{CN})_2]^{2+}$  fulfill these characteristics. However, important discrepancies appeared for  $[\text{Fe}^{\text{II}}(\text{CF}_3\text{SO}_3)_2(\text{R,R}'\text{Pytacn})]$  type of catalysts, class I complexes could incorporate a high percentage of water in the oxidation of tertiary C-H bounds ( $72 \pm 8\%$ ) by overcoming the 50% level. In addition, the extent of water incorporation is larger for substrates with weaker C-H bounds, and the level of water incorporation does not depend on the concentration of substrate. This is indicative that the  $[\text{Fe}^{\text{II}}(\text{CF}_3\text{SO}_3)_2(\text{R,R}'\text{Pytacn})]$  system must follow another mechanism.

DFT calculations were undertaken to clarify the experimental results obtained. Complex  $^{\text{H,H}}\mathbf{1}$  was taken as a reference for class I catalysts and complex  $^{\text{Me,H}}\mathbf{1}$  for class II, and cyclohexane was used as a model substrate (Scheme VIII.10).

Iron(III)-hydroxo species (**Q**) has been identified as the resting state as shown by ESI-MS monitoring of the reactions. When a hydrogen peroxide molecule coordinates to

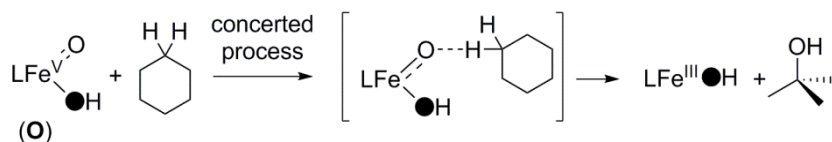


compound **Q**, followed by a proton transfer from the  $\text{H}_2\text{O}_2$  to the hydroxo ligand the species  $\text{Fe}^{\text{III}}(\text{OOH})(\text{H}_2\text{O})$  (**P**) is formed. The water assisted O-O bond cleavage result in the formation of  $\text{Fe}^{\text{V}}(\text{O})(\text{OH})$  (**O**), and this species is the responsible of the cyclohexane hydroxylation. The computational results reveal that this reaction is an asynchronous concerted process where the hydrogen abstraction and the formation of the new C-O bond take place in a single step (Scheme VIII.11). Therefore, discrete radicals are not intermediates in this mechanism, unlike in heme systems, where the “rebound mechanism” involves formation of a short lived carbon centered radical by hydrogen atom abstraction of the  $\text{Fe}^{\text{V}}=\text{O}$  oxidant.



**Scheme VIII.10.** Mechanism of cyclohexane hydroxylation that arises from DFT calculations considering the different isomers of catalyst  $^{\text{H,H}}\mathbf{1}$  (left) and  $^{\text{Me,H}}\mathbf{1}$  (right).

In a concerted process the oxo ligand that initiates the attack ends up at the oxidized product and unlike the heme type rebound mechanism, the radical species generated in the C-H bond breakage has extremely short life time (Scheme VIII.11).



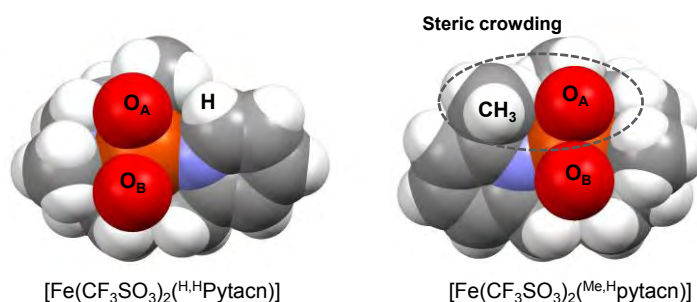
**Scheme VIII.11.** Concerted process mechanisms for the hydroxylation of cyclohexane by **O**.

To understand the isotope labeling experiments is important to notice the asymmetric nature of the complexes, and that the two oxo and hydroxo position are non-equivalent, one is

named A and the other one B. The calculations show that two isomeric forms of **Q** are accessible, Gibbs energy of isomer **Q<sub>B</sub>** is lower than **Q<sub>A</sub>** by 3.76 kcal·mol<sup>-1</sup> for complex <sup>H,H</sup>**1** and 2.69 kcal·mol<sup>-1</sup> for complex <sup>Me,H</sup>**1**, and because of that **Q<sub>B</sub>** is considered the resting state for both catalyst, and isomer **P<sub>B</sub>** (Fe<sup>III</sup>(OOH)<sub>B</sub>(H<sub>2</sub>O)<sub>A</sub>) is preferentially formed. The heterolytic cleavage of **P<sub>B</sub>** generates the isomer **O<sub>B</sub>** (Fe<sup>V</sup>(O)<sub>B</sub>(OH)<sub>A</sub>), the two **O** isomers are very similar in energy, and the barrier of the tautomerism between **O<sub>B</sub>** and **O<sub>A</sub>** is relatively small, 13.5 and 13.2 kcal·mol<sup>-1</sup> for <sup>H,H</sup>**1** and <sup>Me,H</sup>**1** respectively. It is postulated that both isomers are present in the solution. Even though the oxygen that comes from the initial water ligand (*i.e.* the labeled oxygen in Scheme VIII.10) is always in A position. This oxygen atom is the oxo ligand in **O<sub>A</sub>**, but it corresponds to the hydroxo ligand in **O<sub>B</sub>**. Up to this point, both catalyst <sup>H,H</sup>**1** and <sup>Me,H</sup>**1** behave identically, and differences in the isotopic labeling experiments arise from the reaction of **O** with the substrate.

Indeed, the relative hydroxylation reactivity of **O<sub>A</sub>/O<sub>B</sub>** isomer pairs for <sup>H,H</sup>**1** and <sup>Me,H</sup>**1** is not equivalent. For compound <sup>H,H</sup>**1**, **O<sub>A</sub>** and **O<sub>B</sub>** can be considered as equally reactive because the hydroxylation of cyclohexane presents essentially the same activation barriers for hydrogen abstraction ( $\Delta\Delta G^\ddagger = 0.25$  kcal·mol<sup>-1</sup>). Therefore, <sup>H,H</sup>**1** should lead comparable amounts of <sup>16</sup>O/<sup>18</sup>O labeled alcohols, as observed in the experimental isotopic labeling of the cyclohexanol product. Instead, for catalyst <sup>Me,H</sup>**1** the hydroxylation of cyclohexane performed by **O<sub>B</sub>** is slightly but significantly favored over **O<sub>A</sub>** ( $\Delta\Delta G^\ddagger = 2.21$  kcal·mol<sup>-1</sup>). This means that **O<sub>B</sub>**, where the oxo ligand originates from the oxidant (H<sub>2</sub>O<sub>2</sub>) dominates the C-H oxidation reaction. Again, this result agrees with the experimental labeling pattern of the cyclohexanol product obtained with catalyst <sup>Me,H</sup>**1**, which presents minimal incorporation of oxygen from water.

The different reactivity of **O<sub>A</sub>** and **O<sub>B</sub>** for complex <sup>Me,H</sup>**1** could be explained by the influence of the substituent in  $\alpha$  position of the pyridine ring in the Pytacn framework. The bulky group at  $\alpha$  position protects the Fe<sup>V</sup>=O unit of species **O<sub>A</sub>** and limit its reactivity by hindering the substrate approach. This predicts that this factor would make **O<sub>B</sub>** intrinsically more reactive than **O<sub>A</sub>**. This is indeed the scenario that emerges from DFT and isotopic labeling results (Scheme VIII.12).



**Scheme VIII.12.** Space filling diagrams for complexes  $\text{H}^{\text{H}}\mathbf{1}$  and  $\text{Me}^{\text{H}}\mathbf{1}$  showing the steric protection of the bulky group in the  $\alpha$  position of the pyridine ring. Triflate groups have been omitted for clarity.

In conclusion, we propose that all complex  $\text{R,R}'\mathbf{1}$  oxidize alkanes via an asynchronous concerted process. The catalytic active species  $\text{Fe}^{\text{V}}(\text{O})(\text{OH})$  have two different tautomeric forms due to the asymmetry of the ligand,  $\text{O}_\text{A}$  and  $\text{O}_\text{B}$ . For class I catalysts,  $\text{O}_\text{A}$  and  $\text{O}_\text{B}$  are equally reactive and this results in large percentage of water incorporation into products (45-75%). Instead,  $\text{O}_\text{B}$  dominates the reaction in class II catalysts, and therefore the extent of water incorporation is small (<10%).

It is also remarkable that this mechanistic scenario finds good agreement with that emerging from epoxidation reactions. That is, class I catalysts show large incorporation of water into the epoxide because both tautomers participate in the oxygen atom transfer reaction, but in class II catalysts tautomer  $\text{O}_\text{B}$  dominates the reaction (Chapter III).

### VIII.3. An iron catalyst for oxidation of alkyl C-H bonds showing enhanced selectivity for methylenic sites

Traditionally, the conditions employed in alkane oxidation reactions using iron complexes have involved large excess of substrate, and this excess was necessary to afford good yields and avoid over oxidation reactions.<sup>7</sup> The use of limiting amounts of substrate or higher amounts of oxidant dramatically decrease the efficiency of the catalysts. However, recently, White and Chen developed an iron(II) catalyst,  $[\text{Fe}^{\text{II}}(\text{CF}_3\text{SO}_3)_2(\text{pdp})]$  that can oxidize alkanes with limiting amounts of substrate.<sup>17</sup> Iterative additions of catalyst,  $\text{H}_2\text{O}_2$  and acetic acid were employed to afford good yields, but the main problem of this system is the use of 15-20 mol% of catalyst. More recently, Gómez *et al.* have developed a similar system  $\Lambda$ - $[\text{Fe}^{\text{II}}(\text{CF}_3\text{SO}_3)_2(\text{mcpp})]$  that incorporated bulky pinene groups attached to the pyridine rings.<sup>18</sup> These groups introduce steric protection to the iron site minimizing deactivation via oligomerization, and allowed to reduce the catalyst loading down to 1-3 mol% (Figure VIII.1).

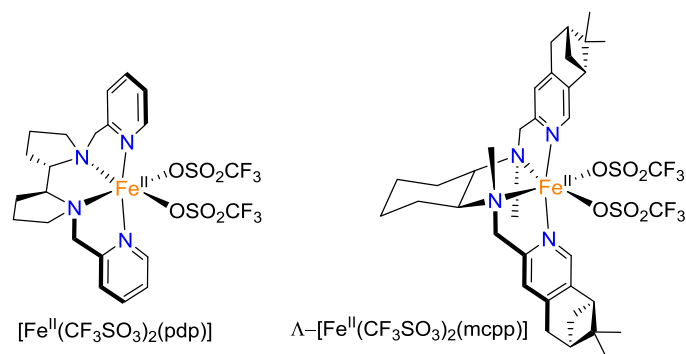


**Figure VIII.1.** Schematic representation of complex  $[\text{Fe}^{\text{II}}(\text{CF}_3\text{SO}_3)_2(\text{pdp})]$  and  $\Lambda\text{-}[\text{Fe}^{\text{II}}(\text{CF}_3\text{SO}_3)_2(\text{mcpp})]$ .

The  $[\text{Fe}^{\text{II}}(\text{CF}_3\text{SO}_3)_2(\text{R,R}'\text{Pytacn})]$  family of complexes described in this thesis shows a good activity in the oxidation of cyclohexane when 10 equiv. of  $\text{H}_2\text{O}_2$  are delivered by syringe pump to a solution that contains 1 equiv. of iron catalyst and 1000 equiv. of substrate. When the amount of oxidant increased to 100 equiv. only the two catalysts that contain a methyl in position  $\alpha$  of the pyridine,  $^{\text{Me,H}}\mathbf{1}$  and  $^{\text{Me,Me}}\mathbf{1}$ , maintain the high efficiency (Table VIII.2). This lead us to think that these catalysts could perform the oxidation of alkanes under limiting amounts of substrate, even though the structure of these catalysts differ significantly from  $[\text{Fe}^{\text{II}}(\text{CF}_3\text{SO}_3)_2(\text{pdp})]$  and  $\Lambda\text{-}[\text{Fe}^{\text{II}}(\text{CF}_3\text{SO}_3)_2(\text{mcpp})]$ .

The  $[\text{Fe}^{\text{II}}(\text{CF}_3\text{SO}_3)_2(\text{R,R}'\text{Pytacn})]$  family of catalysts was submitted to catalytic conditions similar to the ones employed with the  $\Lambda\text{-}[\text{Fe}^{\text{II}}(\text{CF}_3\text{SO}_3)_2(\text{mcpp})]$  catalyst; 3.6 equiv. of  $\text{H}_2\text{O}_2$  were added by slow syringe pump addition to a solution of 3 mol % of catalyst, 1.5 equiv. of acid acetic and 1 equiv. of substrate, the substrate used to evaluate the C-H hydroxylation activity of these catalysts was *cis*-4-methylcyclohexyl pivalate (Table VIII.4).

**Table VIII.4.** Oxidation of *cis*-4-methylcyclohexyl pivalate by the family of complexes  $^{\text{R,R}'}\mathbf{1}$ .

Cat	R	R'	[Cat(mol%)]:[Oxidant (equiv.)]:[AcOH(equiv.)]	Conversion (%)	A(%)
$^{\text{H,H}}\mathbf{1}$	H	H	3 : 3.6 : 1.5	2	2
$^{\text{H,NMe}_2}\mathbf{1}$	H	NMe <sub>2</sub>	3 : 3.6 : 1.5	6	1
$^{\text{H,Me}}\mathbf{1}$	H	Me	3 : 3.6 : 1.5	13	2
$^{\text{H,Cl}}\mathbf{1}$	H	Cl	3 : 3.6 : 1.5	9	4
$^{\text{H,NO}_2}\mathbf{1}$	H	NO <sub>2</sub>	3 : 3.6 : 1.5	8	3
$^{\text{Me,H}}\mathbf{1}$	Me	H	3 : 3.6 : 1.5	85	54
$^{\text{Me,Me}}\mathbf{1}$	Me	Me	3 : 3.6 : 1.5	84	51
$^{\text{Cl,H}}\mathbf{1}$	Cl	H	3 : 3.6 : 1.5	76	8
$^{\text{F,H}}\mathbf{1}$	F	H	3 : 3.6 : 1.5	3	3

Complexes  $^{Me,H}1$  and  $^{Me,Me}1$ , the ones with a methyl in the position  $\alpha$  of the pyridine, give a good yield of the alcohol product, similar to the ones obtained with  $[Fe^{II}(CF_3SO_3)_2(pdp)]$  and  $\Lambda-[Fe^{II}(CF_3SO_3)_2(mcpp)]$  systems.<sup>17, 18</sup> The other catalysts tested give poor yields and also poor conversions under these preparative reaction conditions. The complex chosen for the study of the oxidation of different substrates was  $^{Me,H}1$  because its preparation is relatively simple and affords the best performance among the series tested.

The comparison of our catalyst with  $[Fe^{II}(CF_3SO_3)_2(pdp)]$  and  $\Lambda-[Fe^{II}(CF_3SO_3)_2(mcpp)]$  show that  $^{Me,H}1$  gives a similar yield as  $[Fe^{II}(CF_3SO_3)_2(pdp)]$  and a bit less than  $\Lambda-[Fe^{II}(CF_3SO_3)_2(mcpp)]$ . However, while in the other two catalysts the addition of acetic acid is essential for their efficiency, for  $^{Me,H}1$  this is not strictly required (Table VIII.5).

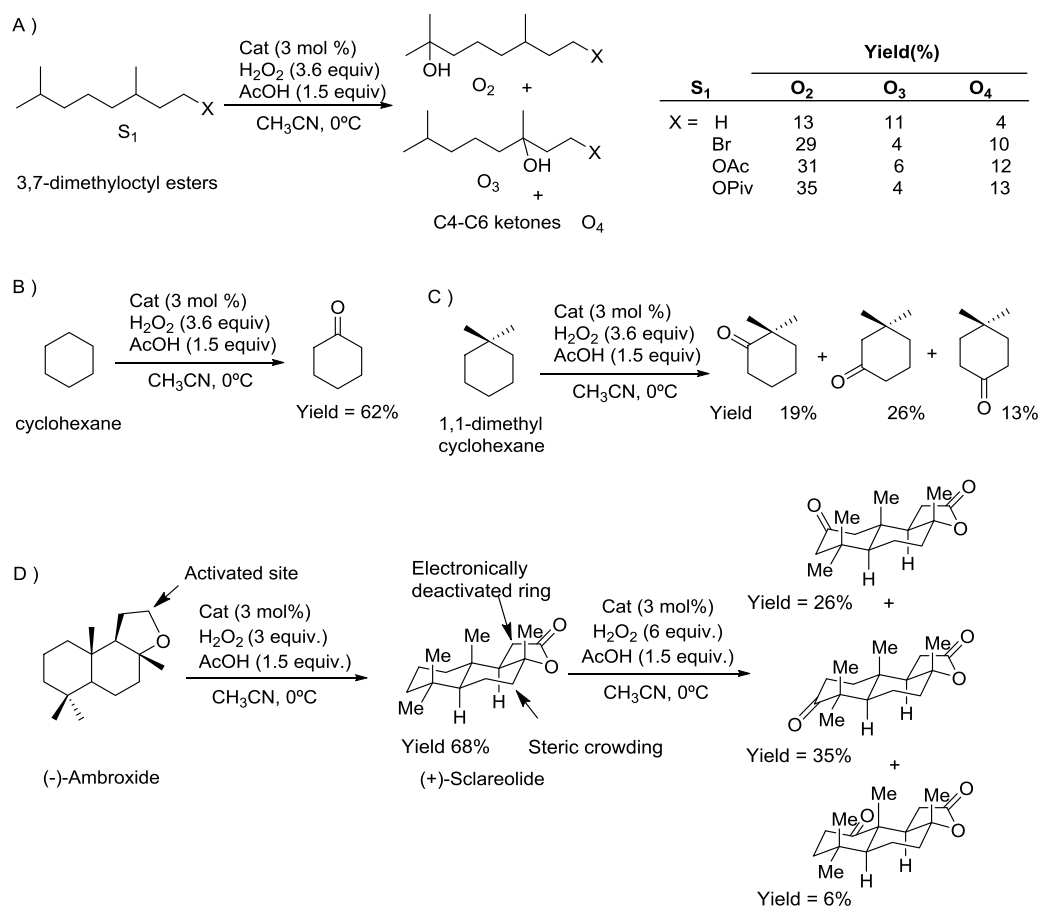
**Table VIII.5.** Oxidation of *cis*-4-methylcyclohexyl pivalate by different catalysts.<sup>[a]</sup>

Cat	[Cat(mol%)]:[H <sub>2</sub> O <sub>2</sub> : AcOH(equiv.)]	A(%) <sup>[b]</sup>
$^{Me,H}1$	<b>3:3.6:1.5</b>	<b>54</b>
<b>[Fe(pdp)]</b>	3:3.6:1.5	53
<b>[Fe(mcpp)]</b>	3:3.6:1.5	64
$^{Me,H}1$	<b>3:3.6:0</b>	<b>52</b>
<b>[Fe(pdp)]</b>	3:3.6:0	19
<b>[Fe(mcpp)]</b>	3:3.6:0	9

[a] Equiv. refer to substrate. The reaction was performed by slow syringe pump addition during 30 min, of an acetonitrile solution of H<sub>2</sub>O<sub>2</sub> into a solution of catalyst, substrate and acetic acid at 0°C. [b] GC yields.

Catalyst  $^{Me,H}1$  was used to oxidize a series of substrates, giving yields that range from 28 to 63%. The  $^{Me,H}1$  catalyst follows the same behavior as the other two catalysts (Scheme VIII.13); A) when an electron withdrawing group is present in the substrate (halide or ester) the oxidation takes place in the remote C-H bond as observed in the oxidation of 3,7-dimethyloctyl esters,<sup>17</sup> showing the electrophilic nature of the active species. B) The catalyst is capable to oxidize methylenic C-H bonds to ketones via a two-step reaction involving the first formation of the alcohol. C) The presence of bulky groups results in a lower oxidation of the C-H bonds adjacent, due to steric effects. This is observed in the oxidation of 1,1-dimethylcyclohexane, where the oxidation takes place preferably in the methylenic sites in remote positions from the bulky group gem-dimethyl.<sup>19</sup> D) The complex is capable to oxidize methylene sites in complex organic molecules; such as (-)-Ambroxide where the oxidation

takes place in the activated C-H bond adjacent to the ether moiety, and (+)-Sclareolide where the oxidation takes place preferably at the two most exposed C-H bonds (Scheme VIII.13).<sup>19</sup>

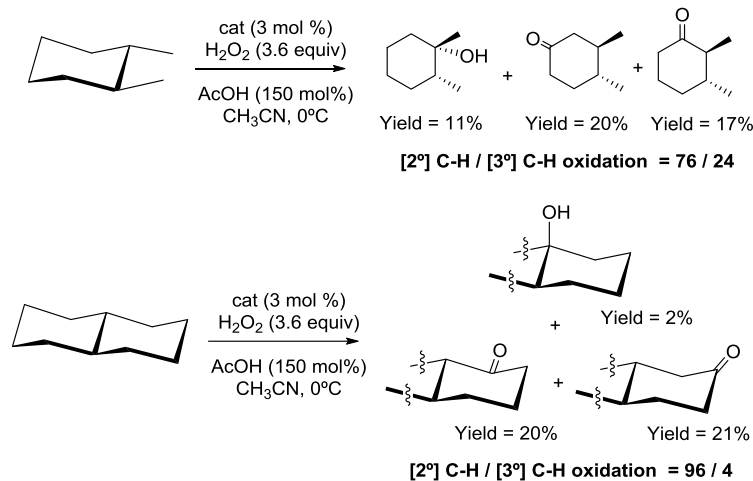


**Scheme VIII.13.** Oxidation of different substrates by complex <sup>Me,H</sup>**1** (yields measured by GC).

Even though, some differences arise between the three catalysts, [Fe<sup>II</sup>(CF<sub>3</sub>SO<sub>3</sub>)<sub>2</sub>(pdp)],  $\Lambda$ -[Fe<sup>II</sup>(CF<sub>3</sub>SO<sub>3</sub>)<sub>2</sub>(mcpp)] and <sup>Me,H</sup>**1**, when *trans*-1,2-dimethylcyclohexane and *trans*-decalines were used as substrates. Catalyst <sup>Me,H</sup>**1** shows a high preference for the oxidation of the secondary C-H bonds, giving a non normalized 3°/2° ratio ( $\Sigma[3^\circ \text{ C-H}]/\Sigma[2^\circ \text{ C-H}]$  oxidation products) of 24/76 for *trans*-1,2-dimethylcyclohexane and 4/96 for *trans*-decalin. The extent of this selectivity is extremely rare and finds very limited precedents in the literature (Scheme VIII.14).<sup>20, 21</sup>

This fact could be explained because the 3° C-H bonds are in axial position, and the breakage of these axial C-H bonds does not liberate strain in the cyclohexane ring. Because of that, they are less reactive than their equatorial counterparts.<sup>22</sup> Therefore, products arising from oxidation at the 2° site are largely dominant. However the extent of this selectivity for secondary C-H bonds is more pronounced for catalyst <sup>Me,H</sup>**1** than other oxidants. Accordingly, we conclude that the catalyst enhances this selectivity. We speculate that the methyl group in

the  $\alpha$ -position of the pyridine ligand exerts some steric demand in close proximity to the iron site where oxidation occurs, which triggers the preferential oxidation of the spatially more accessible  $2^\circ$  site with regard to the sterically more crowded  $3^\circ$  C-H bonds (Figure VIII.2).



**Scheme VIII.14.** Oxidation of *trans*-dimethylcyclohexane and *trans*-decalin by complex <sup>Me,H</sup>**1** (yields measured by GC).

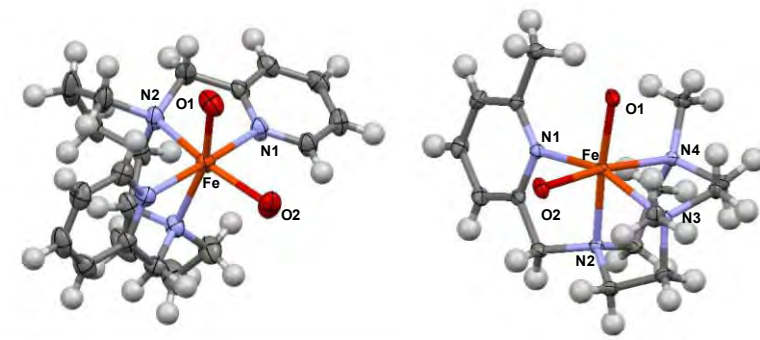
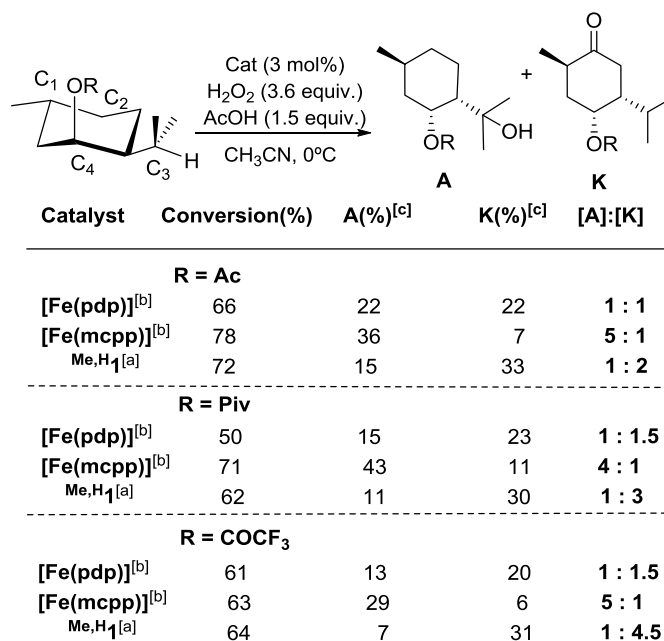


**Figure VIII.2.** Ball and stick diagram of the X-ray structures of  $[\text{Fe}^{\text{II}}(\text{CF}_3\text{SO}_3)_2(\text{pdp})]$  (left), and <sup>Me,H</sup>**1** (right). Triflate and water ligands have been omitted, leaving only the oxygen atom attached to the iron center. Color code; Iron (orange), oxygen (red), nitrogen (blue), carbon (gray) and hydrogen (white).

The importance of the selectivity for methylenic sites is illustrated in the oxidation of more complex molecules such as (+)-neomenthyl esters. In the oxidation of these substrates, the difference between the three complexes is marked (Scheme VIII.15). Oxidation of (+)-neomenthyl acetate by  $[\text{Fe}^{\text{II}}(\text{CF}_3\text{SO}_3)_2(\text{pdp})]$  provides a 1:1 mixture of alcohol and ketone, resulting from tertiary C-H oxidation at C3, and methylene oxidation at C2, respectively, in a combined 43% yield. Related selectivity and yields were obtained with pivalate and trifluoroacetate derivatives. By employing catalyst  $\Lambda$ - $[\text{Fe}^{\text{II}}(\text{CF}_3\text{SO}_3)_2(\text{mcpp})]$ , the oxidation occurs preferentially at tertiary C-H ( $3:1 < \text{A}:K < 5:1$ ). However, most remarkably the oxidation

with <sup>Me,H</sup>**1** reverses the selectivity and oxidize preferentially the methylene site (1:4.5 < A:K < 1:2) (Scheme VIII.15).



**Scheme VIII.15.** Regioselective C-H oxidation reactions catalyzed by [Fe<sup>II</sup>(CF<sub>3</sub>SO<sub>3</sub>)<sub>2</sub>(pdpp)], Λ-[Fe<sup>II</sup>(CF<sub>3</sub>SO<sub>3</sub>)<sub>2</sub>(mcpp)] and <sup>Me,H</sup>**1**. [a] Cat:H<sub>2</sub>O<sub>2</sub>:substrate:AcOH 3:360:100:150. [b] Cat:H<sub>2</sub>O<sub>2</sub>:substrate:AcOH 3:200:100:150. [c] GC yield.

In general, the reactivity of alkyl C-H bonds follows the order tertiary > secondary > primary, according to the relative strength of the C-H bond. However, the steric crowding of C-H bonds follow the inverse order primary > secondary > tertiary. Because of that we propose that the enhanced selectivity for methylene sites exhibited for <sup>Me,H</sup>**1** originates from steric discrimination. The bulky methyl group in α position of the pyridine imposes steric hindrance that favors the oxidation to take place at the most accessible secondary site.

#### VIII.4. Fe(Pytacn)-catalyzed *cis*-dihydroxylation of olefins with hydrogen peroxide

The same family of complexes was tested in olefin oxidation using *cis*-cyclooctene as model substrate. Previous studies (Chapter III) demonstrated that using a large excess of substrate (1 equiv.), a reduced amount of oxidant H<sub>2</sub>O<sub>2</sub> (10-100 equiv.) and 1 mol% of catalyst, the current family of catalysts oxidize *cis*-cyclooctene to give a mixture of cyclooctane epoxide (**E1**) and *cis*-1,2-cyclooctanediol (**D1**). The catalyst provides good to excellent yields, between 50 and 99%, and different selectivities are observed depending on the catalyst (Table VIII.2). Similar catalysts have been described that could perform the same chemistry in presence of



large amounts of substrate, such as  $[\text{Fe}^{\text{II}}(\text{tpa})(\text{CH}_3\text{CN})_2]^{2+}$ , giving modest turnover numbers and low substrate conversion, and therefore being useless for performing *cis*-dihydroxylation reactions in a more practical manner.<sup>23</sup>

The simplest catalyst  $^{\text{H,H}}\mathbf{1}$  gives an equimolar mixture of epoxide and *syn*-diol. The introduction of a substituent in the  $\gamma$  positions (class I catalysts) only causes slightly effects on the chemoselectivity between *syn*-diol and epoxide, and all of them give a mixture of both products. In contrast when a bulky group is present in the  $\alpha$  position of the pyridine (class II catalysts) the chemoselectivity towards the *syn*-diol product was substantially increased. The best yields and chemoselectivities towards *syn*-diol were obtained with catalyst  $^{\text{Me,H}}\mathbf{1}$ , that was identified as a good candidate to study the *cis*-dihydroxylation of olefins under limiting substrate conditions.

After optimizing the amount of catalyst, oxidant, temperature and the addition time of the oxidant, we found that the conditions that afford best yields and selectivities over *syn*-diol product consist of the use of 2 equiv. of  $\text{H}_2\text{O}_2$  delivered via syringe pump addition (15 min) over an acetonitrile solution that contains 3 mol% of catalyst, 15 equiv. of water and 1 equiv. substrate in acetonitrile solution at 0 °C. Some of the complexes were tested for the oxidation of *cis*-cyclooctene under these conditions. The presence of water is essential to obtain a good *syn*-diol/epoxide ratio, since in its absence, the epoxidation reaction becomes enhanced at the expenses of the *syn*-diol.

**Table VIII.6.** Oxidation of *cis*-cyclooctene with the optimization conditions for the catalysts  $^{\text{R,R'}}\mathbf{1}$ .

Catalyst	Yield <b>1D+1E</b> [%]	<b>1D/1E</b>	Conversion [%]
$^{\text{H,H}}\mathbf{1}$	46	0.56	99
$^{\text{H,Cl}}\mathbf{1}$	56	0.42	99
$^{\text{Me,H}}\mathbf{1}$	<b>71</b>	<b>3.6</b>	<b>90</b>
$^{\text{Me,Me}}\mathbf{1}$	64	3.3	91
$^{\text{Cl,H}}\mathbf{1}$	57	3.4	95
$^{\text{F,H}}\mathbf{1}$	60	0.42	95

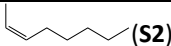
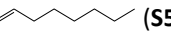
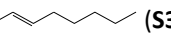
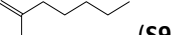
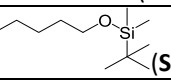
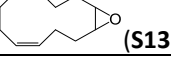
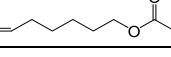
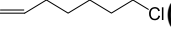
Catalyst  $^{\text{Me,H}}\mathbf{1}$  remained the most efficient for the *cis*-dihydroxylation of cyclooctene (Table VIII.6). Moreover, this screening confirmed our initial hypothesis, that the only complexes that provide high chemoselectivity towards *cis*-dihydroxylation are those that have a bulky group in the  $\alpha$  position of the pyridine; complexes  $^{\text{Cl,H}}\mathbf{1}$  and  $^{\text{Me,Me}}\mathbf{1}$  give moderate yields 57-64%, and good chemoselectivity towards *syn*-diol as shown by *syn*-diol/epoxide ratios of

3.4 and 3.3, respectively. On the other hand, complexes  $^{H,H}1$ ,  $^{H,Cl}1$  and  $^{F,H}1$  give comparable or slightly inferior yields, (46-60%), but low *syn*-diol/epoxide ratios (0.4-0.6) (Table VIII.6).

### VIII.4.1 Substrate scope

Since complex  $^{Me,H}1$  appeared to be the optimum catalyst among the series in terms of yields and chemoselectivity, the optimized conditions were used to oxidize a set of substrates to establish the substrate scope (Table VIII.7): A) Best yields were obtained when terminal or *cis* aliphatic olefins are oxidized, such as *cis*-2-octene (**S2**) and 1-octene (**S5**). In these cases the *syn*-diol product was obtained in 25-56% yield, and *syn*-diol/epoxide ratios ranging from 1.8 to 3.6. B) In the oxidation of *trans* olefins such as *trans*-2-octene (**S3**), 1,1-di-substituted olefins such as 2-methyl-heptene (**S9**) the epoxide product was obtained preferentially. C) Aromatic olefins are not suitable substrates for the system. Oxidation of *cis*- $\beta$ -methylstyrene or methyl cinnamate gives a mixture of products (not shown). D) Electronically deactivated olefins, such as dimethyl fumarate (not shown) are not oxidized by catalyst  $^{Me,H}1$ . e) Different functional groups are tolerated under catalysis conditions; olefins containing epoxide (**S13**) or siloxane (**S12**) functionalities are oxidized towards the corresponding *syn*-diol in yields close to 30%. Also, esters moieties (**S14**) are tolerated, obtaining yields of *syn*-diol around 43% when the ester group is in a remote position from the olefin. A halide moiety is reasonably tolerated (**S17**), hence 1-chloro-*cis*-non-9-ene was oxidized in 59% combined yield (37% *syn*-diol and 22% epoxide) (Table VIII.7).

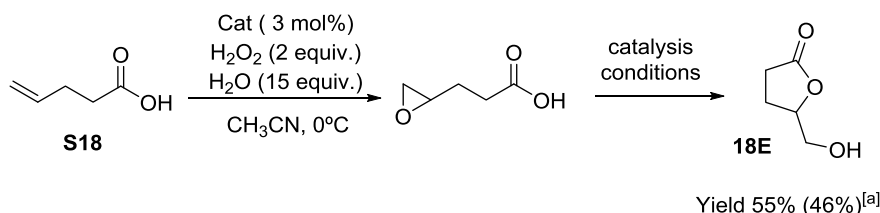
**Table VIII.7.** Substrate scope using the optimized conditions and  $^{Me,H}1$  as catalyst.<sup>[a]</sup>

Substrate	Conversion	Yield [%] <sup>[b]</sup>		D/E	Yield [%]
		D	E		
 ( <b>S2</b> )	92	56	26	2.2	82
 ( <b>S5</b> )	68	37	14	2.6	54
 ( <b>S3</b> )	80	9	25	0.4	34
 ( <b>S9</b> )	66	7	39	0.2	49
 ( <b>S12</b> )	75	25	13	1.8	38
 ( <b>S13</b> )	77	31 25 <sup>[c]</sup>	9 3 <sup>[c]</sup>	3.4	40
 ( <b>S14</b> )	80	43	23	2.0	63
 ( <b>S17</b> )	76	37 38 <sup>[c]</sup>	22 22 <sup>[c]</sup>	1.7	59

[a] 1 equiv. of substrate, 3 mol% of catalyst (1 mM). The reaction was performed by slow syringe pump addition of 2 equiv. of H<sub>2</sub>O<sub>2</sub> (700 mM solution in CH<sub>3</sub>CN) to a solution of the catalyst, substrate and 15 equiv. of water at 0°C.

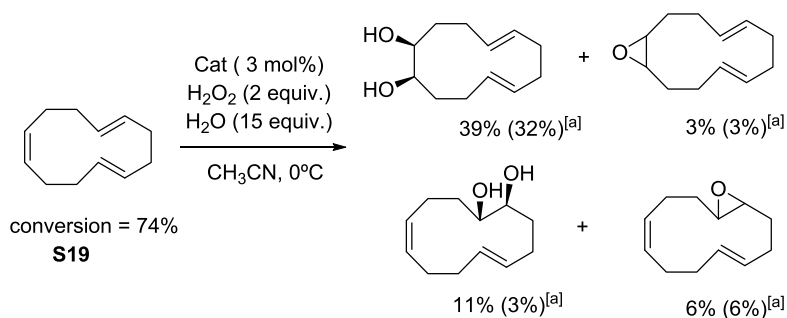
[b] CG yields. [c] Isolated yields.

Carboxylic acids are not compatible with the *cis*-dihydroxylation activity of a terminal olefin. In the oxidation of the pentanoic acid (**S18**) the formation of the *syn*-diol product was precluded, and the oxidation was diverged towards formation of the epoxide, which under the catalytic conditions provided the corresponding lactone 5-(hydroxymethyl)dihydrofuran-2(3H)-one (**18E**), in 55% yield (Scheme VIII.16).<sup>24</sup>



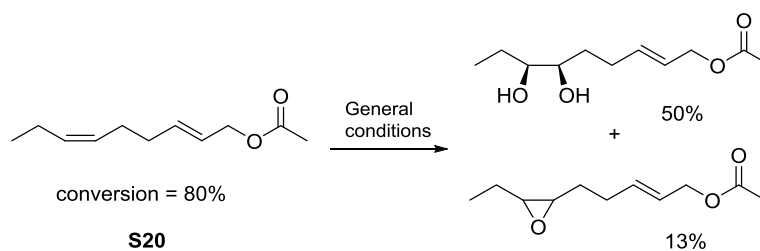
**Scheme VIII.16.** Catalytic oxidation of 3-pentenoic acid by catalyst <sup>Me,H</sup>**1**. [a] Isolated yield.

Important differences can be observed in the oxidation of *trans* and *cis* olefins by catalyst <sup>Me,H</sup>**1**, the most interesting competition experiment is the oxidation of *trans-trans-cis*-1,5,9-cyclododecatriene (**S19**). This substrate has two *trans* and one *cis* olefins sites. *Cis*-dihydroxylation took place preferentially at the *cis*-olefin, giving a 39% yield of the *syn*-diol product, and only 11% of *syn*-diol resulting from *cis*-dihydroxylation at the *trans*-olefin site. However, the epoxidation occurred with similar relative reactivity. Interestingly, oxidation of this substrate gives an excellent overall *syn*-diol/epoxide ratio of 5 (Scheme VIII.17).



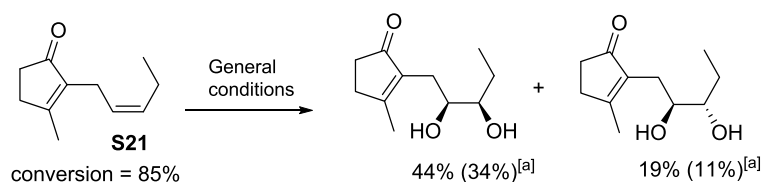
**Scheme VIII.17.** Catalytic oxidation of *trans-trans-cis*-1,5,9-cyclododecatriene. [a] Isolated yield.

As we have observed in C-H bond activation, this catalyst has an electrophilic behavior, and this fact is also observed in C=C oxidation. When we oxidize a substrate with two double bonds, such as (2*E*,6*Z*)-nona-2,6-dienyl acetate (**S20**), the oxidation only takes place in the remote *cis*-site from the electron withdrawing group, the proximal *trans*-olefinic site remains intact. The corresponding *syn*-diol resulting from selective *cis*-dihydroxylation was obtained in 50% yield and the epoxide in 13% (Scheme VIII.18).



**Scheme VIII.18.** Catalytic oxidation of (2*E*,6*Z*)-nona-2,6-dienyl acetate.

The natural product *cis*-jasmone (**S21**) is oxidized selectively to form the *syn*-diol in a relatively good yield (44%). In this case, the side product obtained was the *anti*-diol 19%, originating from the opening of the epoxide ring during work-up (Scheme VIII.19).



**Scheme VIII.19.** Catalytic oxidation of the natural product *cis*-jasmone. [a] Isolated yield.

#### VIII.4.2. *cis*-Dihydroxylation mechanism

To understand the oxidation mechanism, a time course analysis was performed using *cis*-cyclooctene as substrate. The study shows that *syn*-diol is formed with high selectivity within the first 20 minutes of the reaction, giving a ratio *syn*-diol/epoxide of 6.5. However, after these 20 minutes the reaction is slowed and the epoxidation becomes dominant giving a final ratio of 3.2. Furthermore, when we performed the oxidation of cyclooctene in the presence of different amounts of *syn*-diol product, no more *syn*-diol product was formed but instead only epoxide is generated.

These experiments indicate that the presence of *syn*-diol in the catalytic solution disfavors the catalytic activity of the complex. Our hypothesis was that *syn*-diol could reversibly bind to the iron site generating a five member chelate iron-glycolate. Since two *cis*-labile sites are required for performing the *cis*-dihydroxylation of olefins, we reasoned that an excess of *syn*-diol block the iron site, shutting down the *cis*-dihydroxylation activity and favoring the epoxidation.

Overall, we propose that the removal of *syn*-diol from the catalytic solution could allow the reaction to further proceed, and therefore the yields of *syn*-diol product could increase. Because of that, an iterative protocol was applied; the oxidation reaction was performed at substoichiometric conversion levels, and the *syn*-diol product was separated from the reaction mixture after the first peroxide addition. Then, the recovered substrate was subjected to a

second addition of catalyst and H<sub>2</sub>O<sub>2</sub>. This allows to substantially increasing the *syn*-diol product yields and in some cases also to improve the ratio of *syn*-diol/epoxide (Table VIII.8).

**Table VIII.8.** Catalysis using two iterative catalytic oxidations.

Substrate	Conversion	Yield [%]		D/E	Yield [%]
		D	E		
(S1) <sup>[a]</sup>	96	60	11	5.7	71
(S6) <sup>[a]</sup>	73	53	20	2.7	73
(S2) <sup>[a]</sup>	98	56	26	2.2	82
(S3) <sup>[a]</sup>	69	19	19	1	38
(S13) <sup>[b]</sup>	94	33	5 <sup>[a]</sup>	-	38
(S19) <sup>[b]</sup>	96	53	21	2.5	74
(S20) <sup>[b]</sup>	88	56	17	3.3	73
(S21) <sup>[b]</sup>	90	45	7 <sup>[c]</sup>	6.7	52

[a] GC yield. [b] Isolated yields. [c] *trans*-diol product originated from the ring opening of the epoxide product.

Recently, another system that can perform the *cis*-dihydroxylation under preparative scale has been described by Che and co-workers. The chemically robust complex [Fe<sup>III</sup>(Cl)<sub>2</sub>(*C*-Py<sub>2</sub>NMe<sub>2</sub>)]<sup>+</sup> in combination with <sup>®</sup>Oxone can catalyze the oxidation of a broad range of alkenes with moderate to good yields and high chemoselectivities towards the *syn*-diol formation. Surprisingly this species acts with high nucleophilic selectivity, and preferentially oxidize deactivated olefins, showing the opposite behavior of our catalyst <sup>Me,H</sup>1. In Che system, best yields were obtained in the *cis*-dihydroxylation of electron poor alkenes.<sup>25</sup> Therefore, our catalyst constitutes a complementary system to state-of-the-art Fe-catalyzed *cis*-dihydroxylation methods.

## VIII.5. Observation of Fe(V)=O using variable-temperature mass spectrometry and its enzyme-like C–H and C=C oxidation reactions

The use of non-heme iron catalysts to perform oxidation of alkanes and alkenes compounds has been intensely studied in recent years, and a large amount of mechanistic studies has been performed to clarify the catalytic cycle. Some studies have provided strong support in favor of the involvement of high valent oxo-iron species as oxidants.<sup>26, 27</sup> However, no direct experimental evidence under catalytic conditions has been found. In Chapter VII, the use of variable-temperature mass spectrometry (VT-MS) allows studying highly reactive intermediate species at very low concentrations, and the low temperature conditions are essential to minimize the decomposition pathways. Furthermore, the variation of the temperature during the experiment could give further insight in the identification of a reactive intermediate.

Our experimental approach to detect high oxidation state iron species under catalytic conditions consisted in using VT-MS to detect an intermediate under catalytic conditions (Chapter VII), by reacting complex  $^{H,H}\mathbf{1}$  with 100 equiv. of  $\text{H}_2\text{O}_2$  at  $-40\text{ }^\circ\text{C}$  in the absence of substrate. The full mass spectra show that after the mixing of the two reagents a prominent peak growth at  $m/z = 470.1$  that is assigned to  $\{[\text{Fe}^{\text{III}}(\text{OH})(^{H,H}\text{Pytacn})](\text{CF}_3\text{SO}_3)^+\}$  **Q**, a second peak assigned to  $\{[\text{Fe}^{\text{III}}(^{H,H}\text{Pytacn})](\text{CF}_3\text{SO}_3)_2\}^+$ , and a less intense peak at  $m/z = 486.1 = M$ , which could be formulated as  $\{[\text{Fe}^{\text{III}}(\text{OOH})(^{H,H}\text{Pytacn})](\text{CF}_3\text{SO}_3)^+\}$ , **P**, or  $\{[\text{Fe}^{\text{V}}(\text{O})(\text{OH})(^{H,H}\text{Pytacn})](\text{CF}_3\text{SO}_3)^+\}$ , **O** on the basis of its  $m/z$  and isotopic distribution ratio (Figure VIII.3). This second peak is not observed when reactions are performed at room temperature, and it rapidly disappears as the temperature is raised from  $-40\text{ }^\circ\text{C}$  to room temperature. This directly implies that **O/P** is a metastable reaction intermediate (Figure VIII.4).

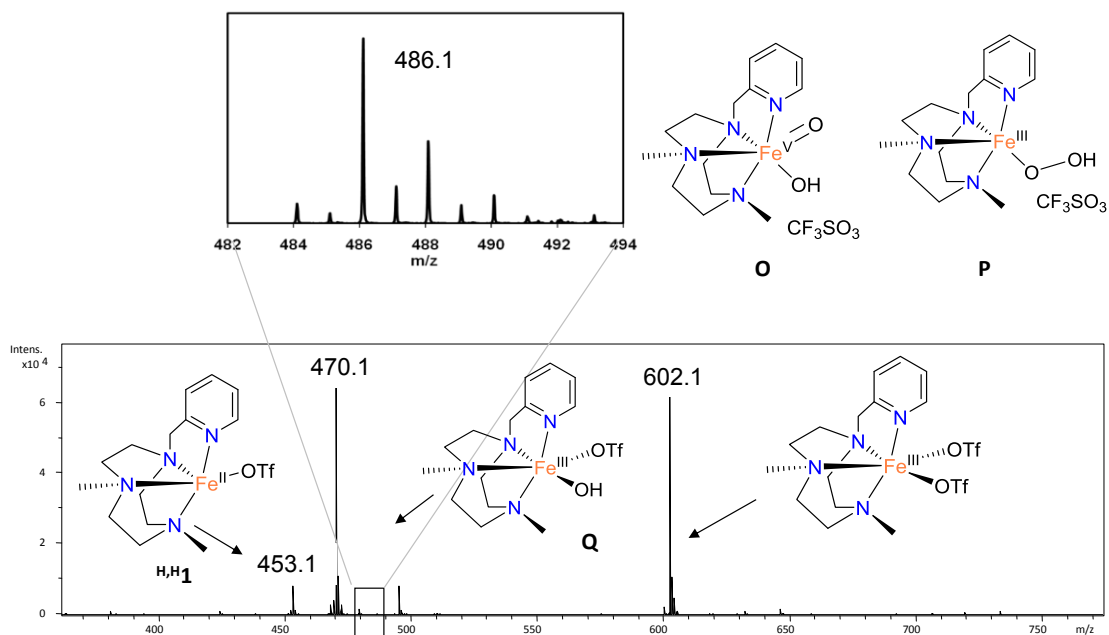


Figure VIII.3. Full mass spectra after mixing catalyst  $\text{H,H1}$  with 100 equiv. of  $\text{H}_2\text{O}_2$ .

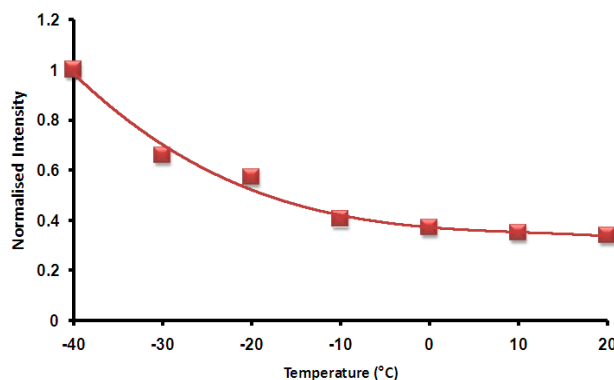
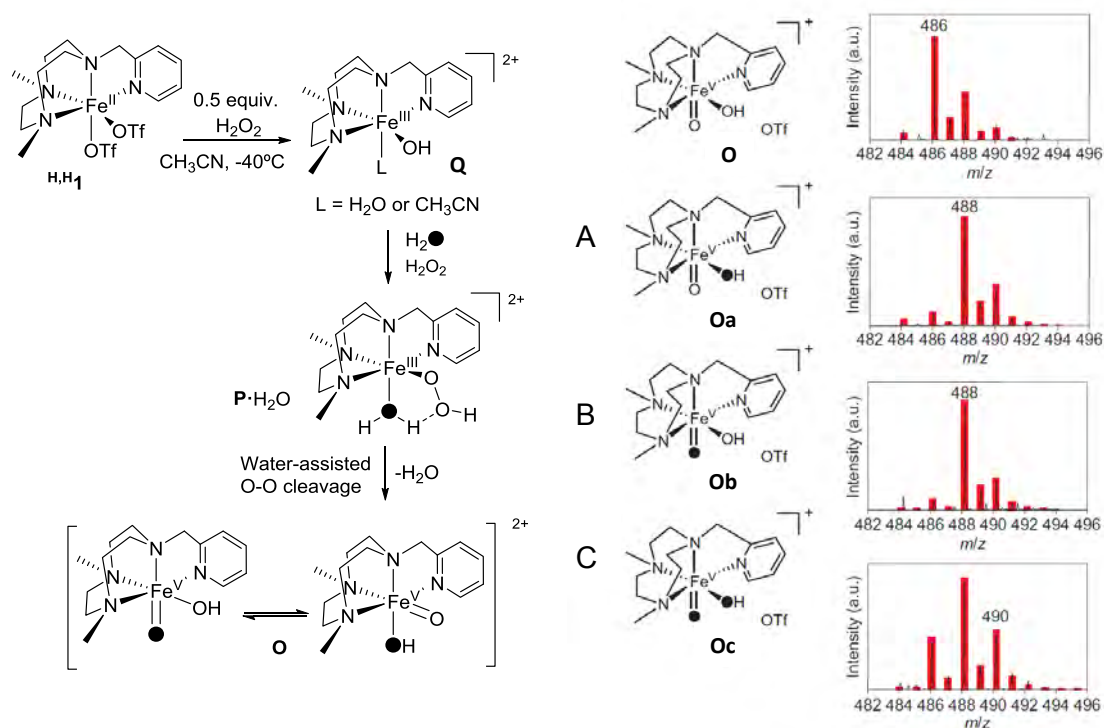


Figure VIII.4. Graph showing the decomposition of  $\text{P/O}$  species ( $486.1 m/z$ ) when the temperature is increased from  $-40^{\circ}\text{C}$  to  $20^{\circ}\text{C}$ .

In order to distinguish between the two possible formulations for the intermediate ( $\text{O/P}$ ), isotopic labeling experiments were conducted: A) The reaction of  $\text{H,H1}$  with  $\text{H}_2\text{O}_2$  (10 equiv.) in the presence of  $\text{H}_2^{18}\text{O}$  (1000 equiv.) shows a new cluster peak assigned to  $\text{O/P}$ , which is now displaced by two  $m/z$  units  $m/z = 488.1 = M+2$ . B) The complementary experiment involving the reaction of  $\text{H,H1}$  with  $\text{H}_2^{18}\text{O}_2$  (10 equiv.) in the presence of  $\text{H}_2\text{O}$  (1000 equiv.), shows the same peak centered at  $m/z = 488.1 = M+2$ . C) The reaction of  $\text{H,H1}$  with  $\text{H}_2^{18}\text{O}_2$  (10 equiv.) in the presence of  $\text{H}_2^{18}\text{O}$  (1000 equiv.), the peak at  $m/z = 488.1 = M+2$  continue to be the major species, but a peak at  $m/z = 490.1 = M+4$  appears as the second most intense component of the spectrum. However, because our  $\text{H}_2^{18}\text{O}_2$  solution is 2% in  $\text{H}_2^{16}\text{O}$ , over 300 equiv. of  $\text{H}_2^{16}\text{O}$  are also present in solution in this experiment.

Since the peroxide type species does not exchange their oxygen atoms with water,<sup>28</sup> the isotopic labeling observations appear incompatible with **P** and must be described as  $\{[\text{Fe}^{\text{V}}(\text{O})(\text{OH})(^{\text{H,H}}\text{Pytacn})](\text{CF}_3\text{SO}_3)\}^+$ , **O**, where a single oxygen atom derives from  $\text{H}_2\text{O}_2$ , and a second oxygen atom derives from  $\text{H}_2\text{O}$ , presumably *via* a water assisted heterolytic O-O breakage in a hydroperoxide  $\{[\text{Fe}^{\text{III}}(\text{OOH})(\text{OH}_2)(^{\text{H,H}}\text{Pytacn})](\text{CF}_3\text{SO}_3)\}^+$ , **P**· $\text{H}_2\text{O}$  species (Scheme VIII.20).



**Scheme VIII.20.** Mechanisms and shift of mass spectral peaks when the corresponding combination of  $\text{H}_2^{18}\text{O}$  or  $\text{H}_2^{18}\text{O}_2$  are used to form the  $\text{Fe}^{\text{V}}(\text{O})(\text{OH})$  species.

The above experimental evidence clarifies the identity of **O**, so we sought to demonstrate its reactivity as oxidant. To do this, we study the reaction of this **O** species with an olefin, aiming at forming a kinetically stable iron-(hydrogen)glycolate species. To this end, **O** was generated and then reacted with *cis*-cyclooctene (10 equiv.) at  $-40^\circ\text{C}$ . MS analysis of the reaction indicated that the cluster peak assigned to **O** disappeared, and new peaks at  $m/z = 446.3$  and  $m/z = 596.2$  emerged. The isotopic pattern of these ions could be successfully simulated as the glycolate  $[\text{Fe}^{\text{III}}(\text{C}_8\text{H}_{14}\text{O}_2)(^{\text{H,H}}\text{Pytacn})]^+$ , **G** and the hydrogenglycolate products  $\{[\text{Fe}^{\text{III}}(\text{C}_8\text{H}_{14}\text{O}_2\text{H})(^{\text{H,H}}\text{Pytacn})](\text{CF}_3\text{SO}_3)\}^+$ , **H** (Figure VIII.5).



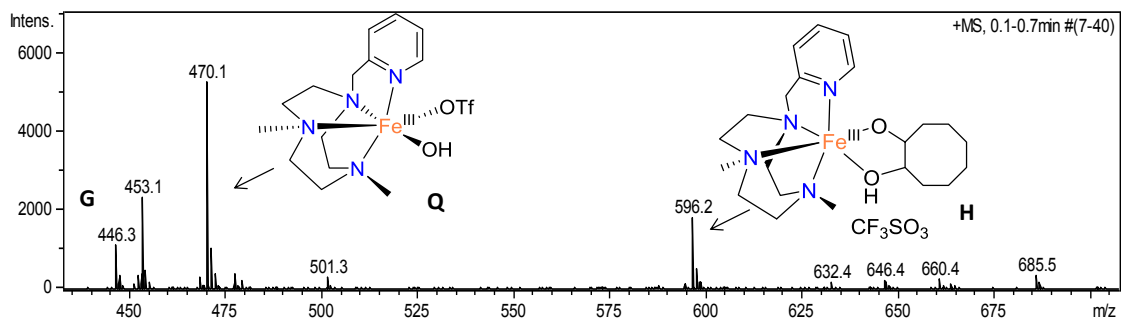
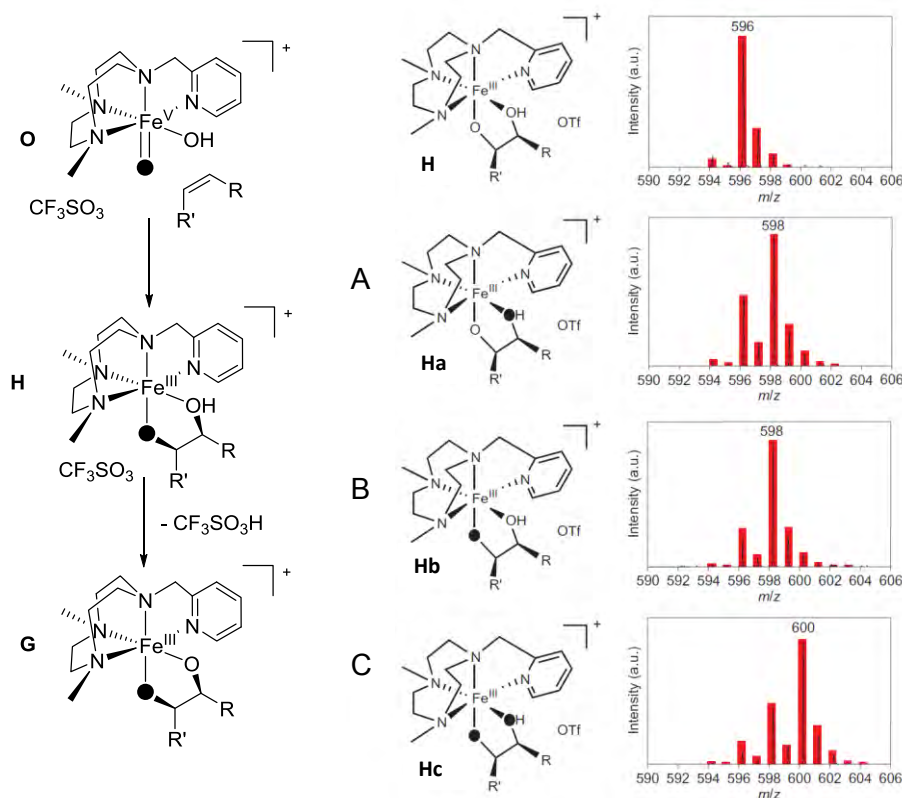


**Figure VIII.5.** Full mass spectra after mixing catalyst  $\text{H}^{\text{H}}\mathbf{1}$  with 10 equiv. of  $\text{H}_2\text{O}_2$  and adding 100 equiv. of *cis*-cyclooctene.

The same isotopic labeling experiments were performed in the presence of a substrate: A) **O** was generated with  $\text{H}_2\text{O}_2$  in the presence of  $\text{H}_2^{18}\text{O}$  and reacted with cyclooctene (100 equiv.), the cluster ion associated to **H** is displaced by 2 mass units,  $m/z = 598.2$  (Scheme VIII.20). B) When **O** was generated with  $\text{H}_2^{18}\text{O}_2$  in the presence of  $\text{H}_2\text{O}$ , the cluster is also displaced 2 mass units. C) When **O** is generated with  $\text{H}_2^{18}\text{O}_2$  in the presence of  $\text{H}_2^{18}\text{O}$ , the cluster is displaced in 4 mass units,  $m/z = 600.2$ . These observations led us to conclude that **O** constitutes a reaction intermediate that precedes formation of **G** and **H** upon reaction with an olefin (Scheme VIII.21).



**Scheme VIII.21.** Mechanisms and shift of mass spectral peaks when  $\text{H}_2^{18}\text{O}$  or  $\text{H}_2^{18}\text{O}_2$  are used to give the hydrogenglycolates **H** and the glycolates **G**.

Further support in favor of our mechanistic interpretation was provided by computational analysis. On the basis of DFT computations, water-assisted transformation of **P** into **O** is thermoneutral and has a small (Gibbs energy of activation ( $\Delta G^\ddagger$ ) = 20 kcal mol<sup>-1</sup>) activation barrier. Moreover, the reaction of **O** with *trans*-2-butene as a model substrate was computed using DFT methods, a summary of these results is given in Figure VIII.6. The *cis*-dihydroxylation is strongly exergonic, with **H** being 60.96 kcal mol<sup>-1</sup> more stable than initial reactants. In addition, the reaction proceeds with a very small energy barrier. The ground state of **O** is  $S = 3/2$ , and it is well separated in energy (11.50 kcal mol<sup>-1</sup>) with respect to the first excited state ( $S = 1/2$ ). The attack of the hydroxo ligand over the olefin leads to the formation of the first C1–O1 bond, to form the intermediate **IN**, with a small barrier of  $\Delta G^\ddagger = 3.32$  kcal mol<sup>-1</sup>. **IN** then evolves via attack of the oxo ligand over C2, with no energy barrier, which leads to the direct formation of the glycolate species **H**.

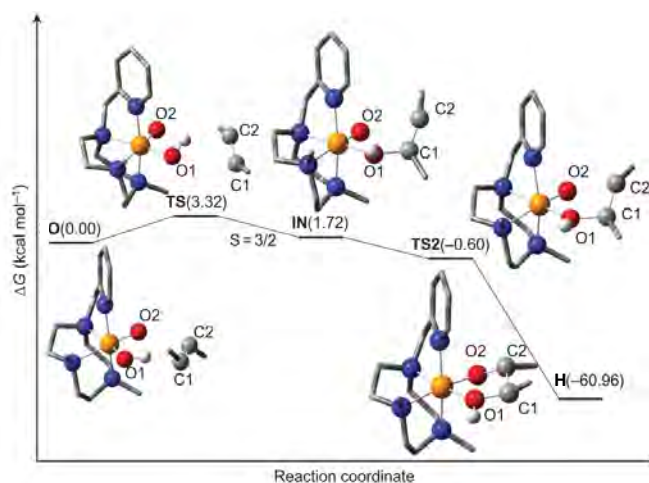


**Figure VIII.6.** DFT Gibbs energy profile of the reaction between the iron(V)-oxo-hydroxo species **O** with *trans*-2-butene to form the hydroxyglycolate species **H**. TS = transition state.

In summary, a systematic study of the family of  $[\text{Fe}^{\text{II}}(\text{CF}_3\text{SO}_3)_2(\text{R,R}'\text{Pytacn})]$  complexes as bioinspired oxidation catalysts has been developed. The family includes systematic variations of their electronic and steric properties. These complexes have been extensively characterized and their activity as C-H and C=C oxidation employing  $\text{H}_2\text{O}_2$  has been studied. The family of catalysts has proven capable of mediating the stereospecific hydroxylation of non activated alkyl C-H bonds and the *cis*-dihydroxylation of olefins. Because of that, this family of complexes constitutes a functional model of the family of Rieske Oxygenases. Mechanistic analysis of these catalytic reactions has been performed. Most remarkably, the mechanism of stereospecific C-H oxidation mediated by these catalysts has been studied, leading to the conclusion that C-H oxidation by a non-heme  $\text{Fe}^{\text{V}}=\text{O}$  species is an asynchronous concerted process.

Moreover, it has been discovered that the complex  $^{Me,H}1$  is capable to perform the selective hydroxylation of alkanes and the *cis*-dihydroxylation of alkenes under preparative scale. Finally, metastable reaction intermediates formed in the reaction of complex  $^{H,H}1$  with  $H_2O_2$  have been characterized by variable-temperature mass spectrometry. This technique has provided the first experimental evidence for a  $Fe^V(O)(OH)$  species under catalytic conditions.

## VIII.6. References

1. Punniyamurthy, T.; Velusamy, S.; Iqbal, J., *Chem. Rev.* **2005**, *105*, 2329-2364.
2. Que Jr., L.; Tolman, W. B., *Nature* **2008**, *455*, 8.
3. Costas, M.; Mehn, M. P.; Jensen, M. P.; Que Jr., L., *Chem. Rev.* **2004**, *104*, 939-986.
4. Bruijninx, P. C. A.; van Koten, G.; Klein Gebbink, R. J. M., *Chem. Soc. Rev.* **2008**, *37*, 2716-2744.
5. Sun, C.-L.; Li, B.-J.; Shi, Z.-J., *Chem. Rev.* **2011**, *111*, 1293-1314.
6. Company, A.; Gómez, L.; Fontrodona, X.; Ribas, X.; Costas, M., *Chem. Eur. J.* **2008**, *14*, 5727-5731.
7. Chen, K.; Que Jr., L., *J. Am. Chem. Soc.* **2001**, *123*, 6327-6337.
8. Britovsek, G. J. P.; England, J.; White, A. J. P., *Inorg. Chem.* **2005**, *44*, 8125-8134.
9. England, J.; Britovsek, G. J. P.; Rabadia, N.; White, A. J. P., *Inorg. Chem.* **2007**, *46*, 3752-3767.
10. Zang, Y.; Kim, J.; Dong, Y.; Wilkinson, E. C.; Appelman, E. H.; Que, L., Jr., *J. Am. Chem. Soc.* **1997**, *119*, 4197-4205.
11. Mialane, P.; Nivorojkine, A.; Pratviel, G.; Azéma, L.; Slany, M.; Godde, F.; Simaan, A.; Banse, F.; Kargar-Grisel, T.; Bouchoux, G.; Sainton, J.; Horner, O.; Guilhem, J.; Tchertanova, L.; Meunier, B.; Girerd, J.-J., *Inorg. Chem.* **1999**, *38*, 1085-1092.
12. Niel, V.; Gaspar, A. B.; Muñoz, M. C.; Abarca, B.; Ballesteros, R.; Real, J. A., *Inorg. Chem.* **2003**, *42*, 4782-4788.
13. Company, A.; Feng, Y.; Güell, M.; Ribas, X.; Luis, J. M.; Que, L.; Costas, M., *Chem. Eur. J.* **2009**, *15*, 3359.
14. Company, A.; Gómez, L.; Güell, M.; Ribas, X.; Luis, J. M.; Que Jr., L.; Costas, M., *J. Am. Chem. Soc.* **2007**, *129*, 15766-15767.
15. Costas, M.; Chen, K.; Que Jr., L., *Coord. Chem. Rev.* **2000**, *200-202*, 517-544.
16. Chen, K.; Que Jr., L., *Chem. Commun.* **1999**, 1375-1376.
17. Chen, M. S.; White, M. C., *Science* **2007**, *318*, 783-787.
18. Gomez, L.; Garcia-Bosch, I.; Company, A.; J., B.-B.; Polo, A.; Sala, X.; Ribas, X.; Costas, M., *Angew. Chem. Int. Ed. Engl.* **2009**, *48*, 5720-5723.
19. Chen, M. S.; White, M. C., *Science* **2010**, *327*, 566-571.
20. Kamata, K.; Yonehara, K.; Nakagawa, Y.; Uehara, K.; Mizuno, N., *Nat. Chem.* **2010**, *2*, 478.
21. He, Y.; Gorden, J. D.; Goldsmith, C. R., *Inorg. Chem.* **2011**, *50*, 12651.
22. Newhouse, T.; Baran, P. S., *Angew. Chem. Int. Ed.* **2011**, *50*, 3362-3374.
23. Ryu, J. Y.; Kim, J.; Costas, M.; Chen, K.; Nam, W.; Que Jr., L., *Chem. Commun.* **2002**, *12*, 1288-1289.
24. Bigi, M. A.; Reed, S. A.; White, M. C., *Nat. Chem.* **2011**, *3*, 216-222.
25. Chow, T. W.-S.; Wong, E. L.-M.; Guo, Z.; Liu, Y.; Huang, J.-S.; Che, C.-M., *J. Am. Chem. Soc.* **2010**, *132*, 13229-13239.
26. Chen, K.; Costas, M.; Kim, J.; Tipton, A. K.; Que Jr., L., *J. Am. Chem. Soc.* **2002**, *124*, 3026-3035.
27. Bassan, A.; Blomberg, R. A. M.; Siegbahn, E. M. P.; Que Jr., L., *Angew. Chem. Int. Ed.* **2005**, *44*, 2939-2941.
28. Ho, R. Y. N.; Roelfes, G.; Feringa, B. L.; Que Jr., L., *J. Am. Chem. Soc.* **1999**, *121*, 264-265.

---

---

## **CHAPTER IX.**

## **GENERAL CONCLUSIONS**

---

---



## IX. GENERAL CONCLUSIONS

- A family of mononuclear iron(II) complexes bearing a tetradentate ligand based on a triazacyclononane ring (tacn) and a pyridine arm has been prepared. These complexes contain an iron(II) center in a distorted octahedral coordination geometry giving two *cis* labile sites available for the coordination of exogenous ligands, such as substrate or oxidant. In order to modify the electronic properties of the iron(II) center, different substituents (with electron withdrawing and electron donating properties) have been incorporated in the  $\gamma$  position of the pyridine ring: H, NMe<sub>2</sub>, OMe, Me, Cl, CO<sub>2</sub>Et, NO<sub>2</sub>, and in the  $\alpha$  position: H, CH<sub>3</sub>, Cl, F.
- The complexes have been structurally and spectroscopically characterized by X-ray diffraction, <sup>1</sup>H NMR spectroscopy, UV-vis spectroscopy, magnetic susceptibility studies and measurement of the electrochemical potential ( $E_{1/2}$ ) of the Fe<sup>III</sup>/Fe<sup>II</sup> redox pair. Complexes are classified two classes: class I are those with a H atom in the  $\alpha$  position of the pyridine, and class II are complexes with a substituent in this position. The main difference of these catalysts is that class I exhibit low or intermediate spin electronic configuration in the presence of strong field ligands, such as CH<sub>3</sub>CN, while class II remain as high spin.
- All these complexes catalyze the stereospecific hydroxylation of alkanes with H<sub>2</sub>O<sub>2</sub>, when an excess of substrate is used, giving high efficiencies and high alcohol/ketone ratios. Good yields are also obtained in the epoxidation and *cis*-dihydroxylation of alkenes, and the *syn*-diol/epoxide ratio is highly dependent on the catalysts' structure; complexes with bulky groups in the  $\alpha$  position of the pyridine give high *syn*-diol/epoxide ratios, while complexes with a proton on this position give a mixture of both products.
- Mechanistic probes in combination with isotopic labelling experiments indicate that the oxidation reaction takes place via highly selective metal-centered species, and that no long lived radicals are present in the catalytic solution.
- Isotopic labeling experiments in alkene oxidation show that all catalysts incorporate one oxygen from water and the other one from hydrogen peroxide into the *syn*-diol product. This fact highly supports the implication of an Fe<sup>V</sup>(O)(OH) as the active species,

generated via a water assisted process. The incorporation of water into the epoxide product is dependent on the catalyst structure: in class I complexes the percentage of water incorporation is about  $70\pm 7\%$ , while for class II is only  $7\pm 3\%$ .

- Exhaustive studies into alkane oxidation mechanism by isotopic labeling experiments and DFT calculation have been performed. The results indicate that the incorporation of water into the alcohol product is extremely dependent on the substituent in the  $\alpha$  position of the pyridine, following the same pattern as epoxide products. These results are explained via a common catalytic active species  $\text{Fe}^{\text{V}}(\text{O})_{\text{B}}(\text{OH})_{\text{A}}$ , which could suffer a isomerization to  $\text{Fe}^{\text{V}}(\text{OH})_{\text{B}}(\text{O})_{\text{A}}$ , allowing to have the oxygen that comes from water either in the oxo or the hydroxo group. Class I complexes can equally react with both isomers and this results in large percentage of water incorporation into products (45-75%). Instead, class II catalyst have a bulky group in  $\alpha$  position that protects the isomer with the oxo group that comes from water, and the substrate preferentially reacts with the other isomer, obtaining an small percentage of water incorporation.
- DFT calculations support this mechanistic scenario and indicate that the oxidation step takes place via a concerted process, where the C-H bond breakage occurs at the same time as the C-O formation.
- The two iron catalysts with a methyl in  $\alpha$  position ( $^{\text{Me,H}}\mathbf{1}$  and  $^{\text{Me,Me}}\mathbf{1}$ ) can perform the hydroxylation of alkyl C-H bonds under preparative scale conditions, giving similar yields to the best iron catalyst described in the literature. The study has been centered within  $^{\text{Me,H}}\mathbf{1}$  catalyst, because it is the most efficient and easiest to prepare. The catalyst could perform the hydroxylation of a high number of substrates; in most cases the oxidation takes place in the weakest tertiary C-H bond. However, if the tertiary C-H bonds are sterically hindered the oxidation takes place in the secondary ones, for example in the oxidation of *trans*-1,2-dimethylcyclohexane and for *trans*-decalin, giving an extremely low  $3^{\circ}/2^{\circ}$  ratio, which has very little precedent in the literature. Moreover, this selectivity could be extended to more complex molecules such as (+)-neomenthyl acetates.
- Catalyst  $^{\text{Me,H}}\mathbf{1}$  is capable to perform the *cis*-dihydroxylation of a number of olefins giving yields up to 56%, using hydrogen peroxide as oxidant. The best yields and selectivities over the *syn*-diol product have been obtained when terminal or *cis* olefins are oxidized.

*Trans* or tri-substituted olefins give poor yields of *syn*-diol, and epoxide is the main product generated instead. Moreover, the catalyst shows an electrophilic behavior and preferentially oxidizes electron-rich double bonds. This is the second iron complex capable of performing the *cis*-dihydroxylation of olefins under preparative scale reported so far in the literature.

- Variable-temperature mass spectrometry has been applied to analyze the reaction between catalyst <sup>H,H</sup>**1** and hydrogen peroxide at -40 °C. Strikingly, this experiment led to the first experimental evidence for the identification of a metastable intermediate that could be formulated as {[Fe<sup>V</sup>(O)(OH)(<sup>H,H</sup>Pytacn)](CF<sub>3</sub>SO<sub>3</sub>)<sup>+</sup>}. Isotopic labeling experiments indicate that this species contains an oxygen atom that comes from water and the other one that comes from hydrogen peroxide. Furthermore, isotopic labeling experiments also demonstrate that this species is a competent intermediate in the *cis*-dihydroxylation reaction of olefins.





# **ANNEX**



## A.1. Supplementary Information Chapter III

1.1. Synthesis of ligands .....	183
1.1.1. Synthesis of pyridine synthons.....	183
1.1.2. Synthesis of Pytacn ligands.....	189
1.2. Solid state characterization .....	192
1.3. Paramagnetic <sup>1</sup> H-NMR.....	196
1.4. Electrochemistry .....	203
1.5. References .....	204

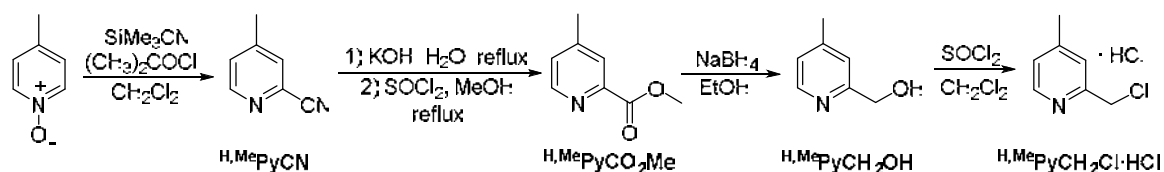
### 1.1. Synthesis of ligands

#### 1.1.1. Synthesis of pyridine synthons

Pyridine synthons 2-(chloromethyl)pyridine hydrochloride (<sup>H,H</sup>PyCH<sub>2</sub>Cl·HCl) and 2-(chloromethyl)-4-methoxy-3,5-dimethylpyridine hydrochloride (<sup>H,OMe</sup>PyCH<sub>2</sub>Cl·HCl) were purchased from Aldrich.

Synthesis of 2-chloromethyl-6-methylpyridine hydrochloride (<sup>Me,H</sup>PyCH<sub>2</sub>Cl·HCl),<sup>1</sup> 2-chloro-6-bromomethylpyridine (<sup>Cl,H</sup>PyCH<sub>2</sub>Br),<sup>2</sup> 2-fluoro-6-bromomethylpyridine (<sup>F,H</sup>PyCH<sub>2</sub>Br),<sup>2</sup> 2-chloromethyl-4-chloropyridine (<sup>H,Cl</sup>PyCH<sub>2</sub>Cl)<sup>3</sup> and 2-chloromethyl-4-dimethylaminopyridine (<sup>H,NMe<sub>2</sub></sup>PyCH<sub>2</sub>Cl)<sup>3</sup> were synthesized as previously described.

#### Synthesis of 2-chloromethyl-4-methylpyridine hydrochloride (<sup>H,Me</sup>PyCH<sub>2</sub>Cl·HCl)



**4-Methyl-pyridine-2-carbonitrile (<sup>H,Me</sup>PyCN).** 4-methylpyridine-N-oxide (7.0 g, 64 mmol) was placed in a round bottom flask, dissolved in dry dichloromethane (50 mL), and placed under a N<sub>2</sub> atmosphere. Trimethylsilyl cyanide (10.26 mL, 7.7 g, 77 mmol) was added dropwise. After 30 minutes, dimethyl carbamoyl chloride (7.1 mL, 8.22 g, 77 mmol) was added dropwise. The resulting mixture was stirred overnight. At this point, the reaction was quenched by addition of

saturated aqueous  $\text{NaHCO}_3$  (30 mL), and the organic fraction was extracted with dichloromethane (2 x 50 mL). The combined organic layers were washed with  $\text{H}_2\text{O}$  (50 mL), saturated aqueous  $\text{NaHCO}_3$  (50 mL) and  $\text{H}_2\text{SO}_4$  1M (50 mL). The resulting organic fraction was dried over  $\text{MgSO}_4$  and filtered and the solvent was removed under reduced pressure to yield the desired product as a white solid (6.7 g, 57 mmol, 89%). FT-IR (ATR)  $\nu$ ,  $\text{cm}^{-1}$ : 3505, 3049, 2233 (CN), 1598, 1506, 1408, 838.  $^1\text{H-NMR}$  ( $\text{CDCl}_3$ , 200 MHz, 300K)  $\delta$ , ppm: 8.58 (d,  $J = 5.0$  Hz, 1H, py- $\text{H}_\alpha$ ), 7.53 (m, 1H, py- $\text{H}_\beta$ ), 7.33 (m, 1H, py- $\text{H}_\beta$ ), 2.43 (s,  $\text{CH}_3$ , 3H).

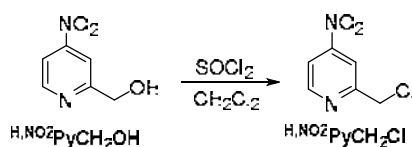
**4-Methyl-pyridine-2-carboxylic acid methyl ester ( $^{\text{H,Me}}\text{PyCO}_2\text{Me}$ ).** Potassium hydroxide (6.4 g, 114 mmol) was placed in a round bottom flask and dissolved in water (60 mL).  $^{\text{H,Me}}\text{PyCN}$  (6.7 g, 57 mmol) was then suspended in this solution and the mixture was refluxed for 1h, at which time a clear yellow-orange solution had formed. The solution was stirred at 40 °C for two days, and after cooling to room temperature,  $\text{H}_2\text{SO}_4$  cc (6.1 mL) diluted in water (20 mL) was carefully added. The solution was then neutralized to pH = 7 by careful addition of saturated aqueous  $\text{NaHCO}_3$ . The white solid that appeared was filtered off. The solvent from the filtrates was removed under reduced pressure and the resulting solid was extracted with  $\text{AcOEt}$  (2 x 50 mL) and absolute  $\text{EtOH}$  (2 x 50 mL). The filtrates were dried over  $\text{MgSO}_4$  and filtered. The solvent was removed under vacuum to obtain 3.3 g of the carboxylic acid product as an oily solid that was used without further purification. The carboxylic acid was dissolved in dry methanol (50 mL), and  $\text{SOCl}_2$  (4 mL) was added dropwise (caution, reaction is very exothermic). The resulting mixture was then refluxed for 16h. At this time, it was allowed to cool down to room temperature, and the solvent was removed under vacuum. The residue was treated with saturated aqueous  $\text{NaHCO}_3$  (75 mL) and extracted with dichloromethane (3 x 50 mL). The organic phases were combined, dried over  $\text{MgSO}_4$ , filtered and the solvent was removed under reduced pressure to obtain the product as a pale yellow oil (2.1 g, 13.6 mmol, 24%).  $^1\text{H-NMR}$  ( $\text{CDCl}_3$ , 200 MHz, 300K)  $\delta$ , ppm: 8.59 (d, 1H,  $J = 4.8$  Hz, py- $\text{H}_\alpha$ ), 7.97 (s broad, 1H, py- $\text{H}_\beta$ ), 7.29 (d,  $J = 4.8$  Hz, 1H, py- $\text{H}_\beta$ ), 4.01 (s, 3H,  $\text{CO}_2\text{CH}_3$ ), 2.44 (s, 3H, py $\text{CH}_3$ ).

**4-Methyl-2-picolylalcohol ( $^{\text{H,Me}}\text{PyCH}_2\text{OH}$ ).**  $^{\text{H,Me}}\text{PyCO}_2\text{Me}$  (2.1 g, 13.57 mmol) was placed in a round bottom flask and dissolved in dry methanol (50 mL). The mixture was placed under  $\text{N}_2$  and  $\text{NaBH}_4$  (3.0 g) was carefully added in small portions. The resulting mixture was stirred under  $\text{N}_2$  at room temperature for 24h. After this time, a second portion of  $\text{NaBH}_4$  (1.0 g) was slowly added in small portions and the mixture was stirred for further 12h under  $\text{N}_2$ . 1 M  $\text{HCl}$  (10 mL) was added and the mixture was stirred for 30 min. The solvent was removed under reduced pressure and the resulting residue was treated with saturated aqueous  $\text{NaHCO}_3$  (50

mL) and extracted with  $\text{CH}_2\text{Cl}_2$  (3 x 50 mL). The combined organic layers were dried over  $\text{MgSO}_4$ , filtered and the solvent was removed under reduced pressure to obtain a pale yellow oil (1.7 g, 13.6 mmol, 99%).  $^1\text{H-NMR}$  ( $\text{CDCl}_3$ , 200 MHz, 300K)  $\delta$ , ppm: 8.40 (d,  $J = 5.0$  Hz, 1H, py- $\text{H}_\alpha$ ), 7.04 (m, 2H, py- $\text{H}_\beta$ ), 4.72 (s, 2H,  $\text{CH}_2\text{OH}$ ), 2.36 (s, 3H,  $\text{CH}_3$ ).

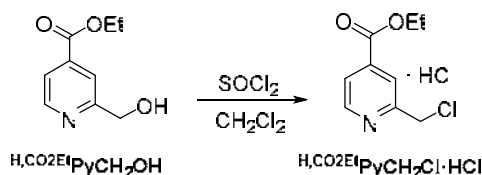
**2-Chloromethyl-4-methylpyridine hydrochloride ( $^{\text{H,Me}}\text{PyCH}_2\text{Cl}\cdot\text{HCl}$ ).**  $^{\text{H,Me}}\text{PyCH}_2\text{OH}$  (1.7 g, 13.6 mmol) was placed in a round bottom flask and dissolved in dry  $\text{CH}_2\text{Cl}_2$  (25 mL).  $\text{SOCl}_2$  (4 mL) was added dropwise and the resulting mixture was stirred under  $\text{N}_2$  overnight. After that time, methanol (10 mL) was carefully added and the resulting mixture was placed under a stream of  $\text{N}_2$  until all solvent evaporated. The oily residue was then treated with diethyl ether (70 mL) which caused the formation of a solid. This compound was filtered and the desired product was obtained as a white-cream solid (2.0 g, 11.12 mmol, 82%).  $^1\text{H-NMR}$  ( $\text{D}_2\text{O}$ , 200 MHz, 300K)  $\delta$ , ppm: 8.63 (d,  $J = 5.8$  Hz, 1H, py- $\text{H}_\alpha$ ), 8.00 (s, 1H, py- $\text{H}_\beta$ ), 7.89 (d,  $J = 5.8$  Hz, 1H, py- $\text{H}_\beta$ ), 5.00 (s,  $\text{CH}_2\text{Cl}$ , 2H), 2.71 (s, 3H,  $\text{CH}_3$ ).  $^{13}\text{C-NMR}$  ( $\text{D}_2\text{O}$ , 50 MHz, 300K)  $\delta$ , ppm: 162.34 (py $\text{C}_\alpha$ - $\text{CH}_2\text{Cl}$ ), 149.29 (py $\text{C}_\alpha$ -H), 140.68 (py $\text{C}_\gamma$ - $\text{CH}_3$ ), 127.69, 127.20 (py $\text{C}_\beta$ ), 40.04 (py- $\text{CH}_2\text{Cl}$ ), 21.65 (py- $\text{CH}_3$ ).

#### Synthesis of 2-chloromethyl-4-nitropyridine ( $^{\text{H,NO}_2}\text{PyCH}_2\text{Cl}$ )



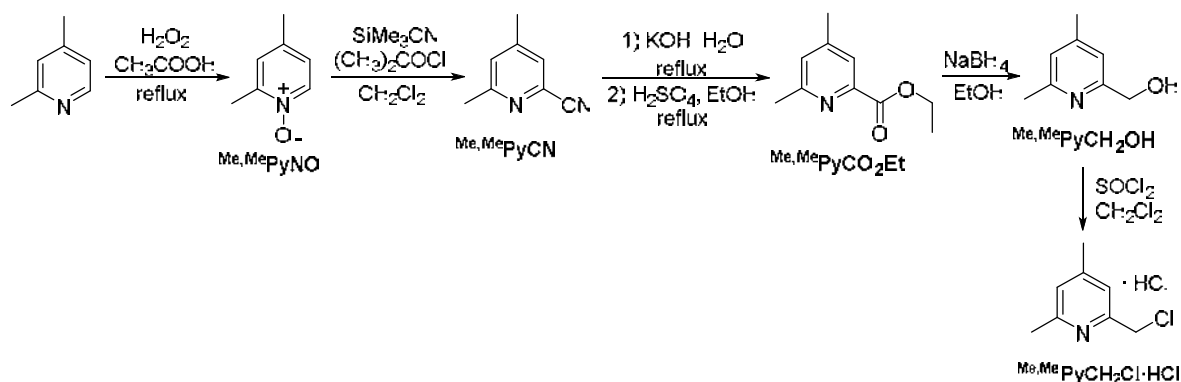
**2-Chloromethyl-4-nitropyridine ( $^{\text{H,NO}_2}\text{PyCH}_2\text{Cl}$ ).** Thionyl chloride (0.5 mL) was added dropwise to 4-nitro-2-pyridylmethanol (0.20 g, 1.30 mmol) in  $\text{CH}_2\text{Cl}_2$ . The mixture was stirred for 2 days at room temperature. The solvent was evaporated and the residue was basified with 2 M  $\text{Na}_2\text{CO}_3$  aqueous solution. The product was extracted with  $\text{CH}_2\text{Cl}_2$  (3 x 15 mL). The organic phases were combined, dried over  $\text{MgSO}_4$  and the solvent removed under reduced pressure. The residue was purified by column chromatography on silica ( $\text{CH}_2\text{Cl}_2$ ) to afford the desired product as a yellow oil (0.09 g, 0.54 mmol, 40%).  $^1\text{H-NMR}$  (400 MHz,  $\text{CDCl}_3$ ):  $\delta$  8.90 (d,  $J = 5.0$  Hz, 1H, py- $\text{H}_\alpha$ ), 8.24 (d,  $J = 2.0$  Hz, 1H, py- $\text{H}_\beta$ ), 7.96 (dd,  $J = 5.0$ ,  $J' = 2.0$  Hz, 1H, py- $\text{H}_\beta$ ), 4.77 (s, 2H). The  $^1\text{H-NMR}$  spectra agrees with the previously reported.<sup>4</sup>

### Synthesis of 2-chloromethyl-4-ethoxycarbonylpyridine hydrochloride ( ${}^{\text{H,CO}_2\text{Et}}\text{PyCH}_2\text{Cl}\cdot\text{HCl}$ )



**2-Chloromethyl-4-ethoxycarbonylpyridine hydrochloride ( ${}^{\text{H,CO}_2\text{Et}}\text{PyCH}_2\text{Cl}\cdot\text{HCl}$ ).** To a stirred solution of 4-ethoxycarbonyl-2-hydroxymethylpyridine (0.64 g, 3.5 mmol) in  $\text{CH}_2\text{Cl}_2$  (25 mL) was added thionyl chloride (1.3 mL, 17.8 mmol) dropwise. After the addition, the resulting mixture was stirred at room temperature for 16 h. The solvent was removed by bubbling  $\text{N}_2$  into the crude mixture (gaseous HCl is formed during this process and extreme cautions must be taken) and a white solid was obtained. This product was suspended in diethyl ether (20 mL) caused the formation of a solid. This compound was filtered and dried under vacuum. The desired product was obtained as a white solid (0.59 g, 2.5 mmol, 71%).  ${}^1\text{H}$  NMR (400 MHz,  $\text{CDCl}_3$ ):  $\delta$  8.78 (d,  $J = 5.5$  Hz, 1H, py- $\text{H}_\alpha$ ), 8.40 (s, 1H, py- $\text{H}_\beta$ ), 8.20 (d,  $J = 5.5$  Hz, 1H, py- $\text{H}_\beta$ ), 5.10 (s, 2H), 4.52 (q, 2H,  $J = 7.1$  Hz), 1.46 (t, 3H,  $J = 7.1$  Hz). The  ${}^1\text{H}$ -NMR spectra agrees with the previously reported.<sup>5</sup>

### Synthesis of 2-chloromethyl-4,6-dimethylpyridine hydrochloride ( ${}^{\text{Me,Me}}\text{PyCH}_2\text{Cl}\cdot\text{HCl}$ )



**2,4-Dimethylpyridine-N-oxide ( ${}^{\text{Me,Me}}\text{PyNO}$ ).** 2,4-Lutidine (30.0 g, 0.28 mol) was placed in a 250 mL round flask and acetic acid (100 mL) was carefully added.  $\text{H}_2\text{O}_2$  30% (30 mL) was carefully added to the mixture which was refluxed for 12h. After this time, a second portion of  $\text{H}_2\text{O}_2$  30% (30 mL) was added and the mixture was further refluxed for additional 12h. After this time, the acetic acid was removed under reduced pressure.  $\text{CHCl}_3$  (100 mL) and  $\text{Na}_2\text{CO}_3$  (5 g) were added over the mixture which was stirred for an hour to destroy any remaining peroxide. The solvent was removed under reduced pressure and the remaining residue was distilled

under vacuum. After initial distillation of residual acetic acid and lutidine, the desired product was collected as the fraction that distilled at 149-151°C as a pale yellow oil (24.9 g, 0.20 mol, 71%). <sup>1</sup>H-NMR (CDCl<sub>3</sub>, 200 MHz, 298K) δ, ppm: 7.99 (d, J = 6.6 Hz, 1H, py-H<sub>α</sub>), 6.92 (s, 1H, py-H<sub>β</sub>), 6.80 (dd, J = 6.6 Hz, J = 2.2 Hz, 1H, py-H<sub>β</sub>), 2.34 (s, 3H, CH<sub>3</sub>), 2.17 (s, 3H, CH<sub>3</sub>). <sup>13</sup>C-NMR (CDCl<sub>3</sub>, 50 MHz, 298K) δ, ppm: 147.91, 138.40, 136.74 (pyC<sub>q</sub> and pyC<sub>r</sub>), 126.89, 124.07 (pyC<sub>β</sub>), 19.91, 14.41 (py-CH<sub>3</sub>).

**4,6-Dimethyl-pyridine-2-carbonitrile (Me,MePyCN).** Me,MePyNO (7.0 g, 56.8 mmol) was placed in a round bottom flask, dissolved in dry dichloromethane (75 mL), and placed under a N<sub>2</sub> atmosphere. Trimethylsilyl cyanide (7.6 mL, 5.6 g, 56.7 mmol) was added dropwise. After 15 minutes, dimethyl carbamoyl chloride (5.2 mL, 6.1 g, 56.7 mmol) was carefully added and the resulting mixture was stirred overnight. At this point, the reaction was quenched by addition of saturated aqueous NaHCO<sub>3</sub>, and the organic fraction extracted with dichloromethane (2 x 50 mL). The organic phase was then washed with saturated aqueous NaHCO<sub>3</sub> (50 mL) and H<sub>2</sub>SO<sub>4</sub> 1M (50 mL). Finally, it was dried over MgSO<sub>4</sub> and filtered and the solvent was removed under reduced pressure to yield the product as a white solid (5.6 g, 42.4 mmol, 75%). <sup>1</sup>H-NMR (CDCl<sub>3</sub>, 200 MHz, 298K) δ, ppm: 7.34 (s, 1H, py-H<sub>β</sub>), 7.20 (s, 1H, py-H<sub>β</sub>), 2.56 (s, 3H, CH<sub>3</sub>), 2.38 (s, 3H, CH<sub>3</sub>). <sup>13</sup>C-NMR (CDCl<sub>3</sub>, 50 MHz, 298K) δ, ppm: 160.23 (pyC<sub>α</sub>-CH<sub>3</sub>), 148.61 (pyC<sub>r</sub>-CH<sub>3</sub>), 132.98 (pyC<sub>α</sub>-CN), 127.63, 126.63 (pyC<sub>β</sub>), 117.51 (pyCN), 24.11, 20.67 (py-CH<sub>3</sub>).

**Ethyl 4,6-dimethylpicolinate (Me,MePyCO<sub>2</sub>Et).** Potassium hydroxide (5.0 g, 89 mmol) was placed in a round bottom flask and dissolved in water (100 mL). Me,MePyCN (5.6 g, 42.4 mmol) was then suspended in this solution, and the mixture was refluxed for 4h, at which time a clear yellow-orange solution had formed. The solution was cooled down to room temperature and acidified with a mixture of H<sub>2</sub>SO<sub>4</sub> cc (5 mL) diluted in water (20 mL). The solvent was removed under vacuum, and the residue was taken in absolute ethanol (80 mL). H<sub>2</sub>SO<sub>4</sub> cc (20 mL) was then carefully added (caution, the solution becomes very hot) and the resulting suspension was refluxed for 16h. After that time, it was allowed to cool down to room temperature and it was dropped over hexanes (200 mL). The aqueous phase was taken to basic pH with a saturated aqueous solution of Na<sub>2</sub>CO<sub>3</sub>, and the organic phase collected. The aqueous layer was further extracted with hexanes (2 x 100 mL). The combined organic fractions were dried over MgSO<sub>4</sub>, filtered and the solvent was removed under reduced pressure to obtain the product as a pale yellow oil (4.1 g, 22.88 mmol, 54%). <sup>1</sup>H-NMR (CDCl<sub>3</sub>, 200 MHz, 298K) δ, ppm: 7.63 (s, 1H, py-H<sub>β</sub>), 7.15 (s, 1H, py-H<sub>β</sub>), 4.45 (q, J = 7.2 Hz, 2H, CH<sub>2</sub>CH<sub>3</sub>), 2.61 (s, 3H, CH<sub>3</sub>), 2.38 (s, 3H, CH<sub>3</sub>), 1.43 (t, J = 7.2 Hz, 3H, CH<sub>2</sub>CH<sub>3</sub>). <sup>13</sup>C-NMR (CDCl<sub>3</sub>, 50 MHz, 298K) δ, ppm: 165.64 (C=O), 158.72

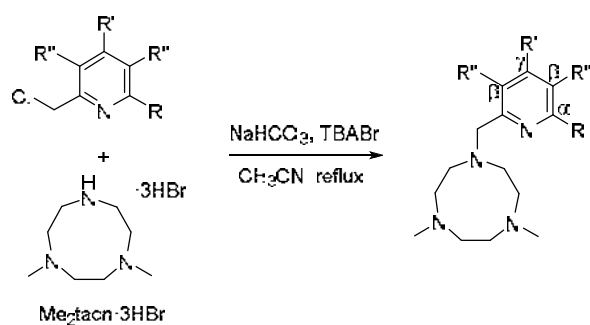


(pyC<sub>α</sub>-CH<sub>3</sub>), 148.24 (pyC<sub>γ</sub>-CH<sub>3</sub>), 147.67 (pyC<sub>α</sub>-CO<sub>2</sub>Et), 127.41, 123.33 (pyC<sub>β</sub>), 61.74 (CH<sub>2</sub>CH<sub>3</sub>), 24.39, 20.80 (py-CH<sub>3</sub>), 14.27 (CH<sub>2</sub>CH<sub>3</sub>).

**4,6-Dimethyl-2-hydroxymethylpyridine (<sup>Me,Me</sup>PyCH<sub>2</sub>OH).** <sup>Me,Me</sup>PyCO<sub>2</sub>Et (4.1 g, 22.9 mmol) was placed in a round bottom flask and dissolved in absolute ethanol (80 mL). NaBH<sub>4</sub> (5 g) was slowly added in small portions. The resulting mixture was stirred under N<sub>2</sub> at room temperature for two days. After this time, HCl cc (1 mL) was added and the mixture was stirred for 1 h. The solvent was removed under reduced pressure and the resulting residue was treated with saturated aqueous NaHCO<sub>3</sub> (50 mL) and extracted with CH<sub>2</sub>Cl<sub>2</sub> (3 x 50 mL). The organic layers were combined, dried over MgSO<sub>4</sub>, filtered and the solvent was removed under vacuum to obtain a pale yellow oil that solidified upon applying vacuum (2.9 g, 20.8 mmol, 91%). <sup>1</sup>H-NMR (CDCl<sub>3</sub>, 200 MHz, 298K) δ, ppm: 6.87 (s broad, 2H, py-H<sub>β</sub>), 4.67 (s, 2H, CH<sub>2</sub>OH), 3.27 (s broad, 1H, OH), 2.50 (s, 3H, CH<sub>3</sub>), 2.31 (s, 3H, CH<sub>3</sub>). <sup>13</sup>C-NMR (CDCl<sub>3</sub>, 50 MHz, 298K) δ, ppm: 158.11 (pyC<sub>α</sub>-CH<sub>3</sub>), 157.01 (pyC<sub>α</sub>-CH<sub>2</sub>OH), 148.15 (pyC<sub>γ</sub>-CH<sub>3</sub>), 122.82, 118.41 (pyC<sub>β</sub>), 63.91 (CH<sub>2</sub>OH), 23.84, 20.85 (py-CH<sub>3</sub>).

**2-Chloromethyl-4,6-dimethylpyridine hydrochloride (<sup>Me,Me</sup>PyCH<sub>2</sub>Cl·HCl).** <sup>Me,Me</sup>PyCH<sub>2</sub>OH (2.9 g, 20.8 mmol) was placed in a round bottom flask and dissolved in dry CH<sub>2</sub>Cl<sub>2</sub> (50 mL). SOCl<sub>2</sub> (5 mL) was added dropwise and the resulting mixture was stirred under N<sub>2</sub> overnight. After that time, methanol (15 mL) was carefully added and the resulting mixture was placed under a stream of N<sub>2</sub> until all the solvent evaporated. The oily residue was then taken in diethyl ether (100 mL) and stirred, which afforded a suspended solid. This solid was filtered and the product was isolated as a white-cream solid (3.9 g, 20.3 mmol, 98%). <sup>1</sup>H-NMR (D<sub>2</sub>O, 200 MHz, 298K) δ, ppm: 7.76 (s, 1H, py-H<sub>β</sub>), 7.67 (s, 1H, py-H<sub>β</sub>), 4.90 (s, 2H, pyCH<sub>2</sub>Cl), 2.74 (s, 3H, CH<sub>3</sub>), 2.61 (s, 3H, CH<sub>3</sub>). <sup>13</sup>C-NMR (D<sub>2</sub>O, 50 MHz, 298K) δ, ppm: 161.49, 153.72 (pyC<sub>α</sub>), 148.48 (pyC<sub>γ</sub>-CH<sub>3</sub>), 127.72, 125.12 (pyC<sub>β</sub>), 39.82 (py-CH<sub>2</sub>Cl), 21.38, 18.63 (py-CH<sub>3</sub>).

### 1.1.2. Synthesis of Pytacn ligands



ligand	R	R'	R''
H,HPytacn	H	H	H
H,NMe <sub>2</sub> Pytacn	H	NMe <sub>2</sub>	H
H,OMePytacn	H	OMe	Me
H,MePytacn	H	Me	H
H,ClPytacn	H	Cl	H
H,CO <sub>2</sub> EtPytacn	H	CO <sub>2</sub> Et	H
H,NO <sub>2</sub> Pytacn	H	NO <sub>2</sub>	H
Me,HPytacn	Me	H	H
Me,MePytacn	Me	Me	H
Cl,HPytacn	Cl	H	H
F,HPytacn	F	H	H

Me<sub>2</sub>tacn·3HBr,<sup>6</sup> H,HPytacn<sup>7</sup> and Me,HPytacn<sup>8</sup> were synthesized as previously described.

#### 1-[(4-methyl-2-pyridyl)methyl]-4,7-dimethyl-1,4,7-triazacyclononane (<sup>H,Me</sup>Pytacn).

<sup>H,Me</sup>PyCH<sub>2</sub>Cl·HCl (0.35 g, 2.0 mmol), Me<sub>2</sub>tacn·3HBr (0.79 g, 2.0 mmol) and anhydrous acetonitrile (25 mL) were mixed in a 50 mL flask. Na<sub>2</sub>CO<sub>3</sub> (1.47 g) and tetrabutylammonium bromide, TBABr (0.03 g) were added directly as solids and the resulting mixture was heated at reflux under N<sub>2</sub> for 16 hours. After cooling to room temperature, the resulting yellow mixture was filtered and the filter cake was washed with CH<sub>2</sub>Cl<sub>2</sub>. The combined filtrates were evaporated under reduced pressure. To the resulting residue, 1M NaOH (30 mL) was added and the mixture was extracted with CH<sub>2</sub>Cl<sub>2</sub> (3 x 10 mL). The combined organic layers were dried over anhydrous MgSO<sub>4</sub> and the solvent was removed under reduced pressure. The resulting residue was treated with hexane (70 mL) and stirred for 12 hours. The mixture was filtered and the solvent from the yellow filtrates was removed under reduced pressure to yield the product as a pale yellow oil (0.35 g, 1.6 mmol, 67 %). <sup>1</sup>H-NMR (CDCl<sub>3</sub>, 200 MHz, 300K) δ, ppm: 8.37 (d, J = 5.0 Hz, 1H, pyH<sub>α</sub>), 7.29 (s, 1H, pyH<sub>β</sub>), 6.96 (d, J = 5.0 Hz, 1H, pyH<sub>β</sub>), 3.81 (s, 2H, py-CH<sub>2</sub>), 2.84 – 2.79 (m, 8H, N-CH<sub>2</sub>-CH<sub>2</sub>), 2.69 – 2.67 (m, 4H, N-CH<sub>2</sub>-CH<sub>2</sub>), 2.36 (s, 6H, N-CH<sub>3</sub>), 2.35 (s, 3H, py-CH<sub>3</sub>). <sup>13</sup>C-NMR (CDCl<sub>3</sub>, 50 MHz, 300K) δ, ppm: 160.01 (pyC<sub>q</sub>), 148.62 (pyC<sub>α</sub>), 147.16 (pyC<sub>q</sub>), 124.04, 122.77 (pyC<sub>β</sub>), 64.35 (py-CH<sub>2</sub>-N), 57.11, 56.96, 55.81 (N-CH<sub>2</sub>-C), 46.55 (N-CH<sub>3</sub>), 21.06 (py-CH<sub>3</sub>). ESI-MS (m/z): 263.3 [M+H]<sup>+</sup>.

#### 1-[(4-dimethylamino-2-pyridyl)methyl]-4,7-dimethyl-1,4,7-triazacyclononane (<sup>H,NMe<sub>2</sub></sup>Pytacn).

This ligand was prepared in analogous manner to <sup>H,Me</sup>Pytacn starting with <sup>H,NMe<sub>2</sub></sup>PyCH<sub>2</sub>Cl. Yield = 73%. FT-IR (ATR) ν, cm<sup>-1</sup>: 2921 – 2791 (C-H)<sub>sp3</sub>, 1600, 1451 (py). <sup>1</sup>H-NMR (CDCl<sub>3</sub>, 400 MHz, 300K) δ, ppm: 8.13 (d, J = 6.0 Hz, 1H, pyH<sub>α</sub>), 6.81 (d, J = 2.7 Hz, 1H, pyH<sub>β</sub>), 6.37 (dd, J = 6.0 Hz, J' = 2.7

Hz, 1H, pyH<sub>β</sub>), 3.74 (s, 2H, py-CH<sub>2</sub>), 3.00 (s, 6H, py-N-(CH<sub>3</sub>)<sub>2</sub>), 2.82 – 2.79 (m, 8H, N-CH<sub>2</sub>-CH<sub>2</sub>), 2.70 – 2.68 (m, 4H, N-CH<sub>2</sub>-CH<sub>2</sub>), 2.36 (s, 6H, N-CH<sub>3</sub>). <sup>13</sup>C-NMR (CDCl<sub>3</sub>, 75 MHz, 300K) δ, ppm: 160.31 (pyC<sub>q</sub>), 154.78 (pyC<sub>γ</sub>), 148.98 (pyC<sub>α</sub>), 105.63, 105.15 (pyC<sub>β</sub>), 65.27 (py-CH<sub>2</sub>-N), 57.19, 57.06, 56.52 (N-CH<sub>2</sub>-C), 46.79 (N-CH<sub>3</sub>), 39.17 (Py-N-(CH<sub>3</sub>)<sub>2</sub>). ESI-MS (m/z): 292.2 [M+H]<sup>+</sup>.

**1-[(3,5-dimethyl-4-methoxy-2-pyridyl)methyl]-4,7-dimethyl-1,4,7-triazacyclononane**

(<sup>H,OMe</sup>Pytacn). This ligand was prepared in analogous manner to <sup>H,Me</sup>Pytacn starting with <sup>H,OMe</sup>PyCH<sub>2</sub>Cl·HCl. Yield = 66%. FT-IR (ATR) ν, cm<sup>-1</sup>: 2925 – 2808 (C-H)<sub>sp3</sub>, 1671, 1454 (py). <sup>1</sup>H-NMR (CDCl<sub>3</sub>, 400 MHz, 300K) δ, ppm: 8.15 (s, 1H, pyH<sub>α</sub>), 3.77 (s, 3H, O-CH<sub>3</sub>), 3.71 (s, 2H, py-CH<sub>2</sub>), 2.82 – 2.78 (m, 4H, N-CH<sub>2</sub>-CH<sub>2</sub>), 2.64 (s, 4H, N-CH<sub>2</sub>-CH<sub>2</sub>), 2.62 – 2.59 (m, 4H, N-CH<sub>2</sub>-CH<sub>2</sub>), 2.38 (s, 3H, py-CH<sub>3</sub>), 2.31 (s, 6H, N-CH<sub>3</sub>), 2.24 (s, 3H, py-CH<sub>3</sub>). <sup>13</sup>C-NMR (CDCl<sub>3</sub>, 75 MHz, 300K) δ, ppm: 164.10 (pyC<sub>q</sub>), 157.75 (pyC<sub>γ</sub>), 148.25 (pyC<sub>α</sub>), 126.10, 124.90 (pyC<sub>β</sub>), 63.73 (py-OCH<sub>3</sub>), 59.74 (py-CH<sub>2</sub>-N), 57.01, 56.46, 56.10 (N-CH<sub>2</sub>-C), 46.34 (N-CH<sub>3</sub>), 13.20, 11.27 (py-CH<sub>3</sub>). ESI-MS (m/z): 307.2 [M+H]<sup>+</sup>.

**1-[(4-chloro-2-pyridyl)methyl]-4,7-dimethyl-1,4,7-triazacyclononane** (<sup>H,Cl</sup>Pytacn). This ligand was prepared in analogous manner to <sup>H,Me</sup>Pytacn starting with <sup>H,Cl</sup>PyCH<sub>2</sub>Cl. Yield = 72%. FT-IR (ATR) ν, cm<sup>-1</sup>: 2924 – 2790 (C-H)<sub>sp3</sub>, 1600, 1451 (py). <sup>1</sup>H-NMR (CDCl<sub>3</sub>, 400 MHz, 300K) δ, ppm: 8.41 (dd, J = 5.4 Hz, J' = 0.5 Hz, 1H, pyH<sub>α</sub>), 7.56 (d, J = 2.0 Hz, 1H, pyH<sub>β'</sub>), 7.16 (dd, J = 5.5 Hz, J' = 2.1 Hz, 1H, pyH<sub>β</sub>), 3.84 (s, 2H, py-CH<sub>2</sub>), 2.84 – 2.82 (m, 4H, N-CH<sub>2</sub>-CH<sub>2</sub>), 2.75 (s, 4H, N-CH<sub>2</sub>-CH<sub>2</sub>), 2.68 – 2.65 (m, 4H, N-CH<sub>2</sub>-CH<sub>2</sub>), 2.36 (s, 6H, N-CH<sub>3</sub>). <sup>13</sup>C-NMR (CDCl<sub>3</sub>, 75 MHz, 300K) δ, ppm: 162.54 (pyC<sub>q</sub>), 149.81 (pyC<sub>α</sub>), 144.47 (pyC<sub>γ</sub>), 123.45, 122.24 (pyC<sub>β</sub>), 64.03 (py-CH<sub>2</sub>-N), 57.24, 57.22, 55.93 (N-CH<sub>2</sub>-C), 46.73 (N-CH<sub>3</sub>). ESI-MS (m/z): 283.1 [M+H]<sup>+</sup>.

**1-[(4-ethoxycarbonyl-2-pyridyl)methyl]-4,7-dimethyl-1,4,7-triazacyclononane** (<sup>H,CO<sub>2</sub>Et</sup>Pytacn).

This ligand was prepared in analogous manner to <sup>H,Me</sup>Pytacn starting with <sup>H,CO<sub>2</sub>Et</sup>PyCH<sub>2</sub>Cl·HCl. Yield = 77%. FT-IR (ATR) ν, cm<sup>-1</sup>: 2924 – 2785 (C-H)<sub>sp3</sub>, 1727 (C=O), 1452 (py). <sup>1</sup>H-NMR (CDCl<sub>3</sub>, 400 MHz, 300K) δ, ppm: 8.67 (dd, J = 5.1 Hz, J' = 0.9 Hz, 1H, pyH<sub>α</sub>), 8.07 (s, 1H, pyH<sub>β'</sub>), 7.70 (dd, J = 5.2 Hz, J' = 1.6 Hz, 1H, pyH<sub>β</sub>), 4.42 (q, J = 7.0 Hz, 2H, OCH<sub>2</sub>CH<sub>3</sub>), 3.91 (s, 2H, py-CH<sub>2</sub>), 2.85 – 2.83 (m, 4H, N-CH<sub>2</sub>-CH<sub>2</sub>), 2.78 (s, 4H, N-CH<sub>2</sub>-CH<sub>2</sub>), 2.69 – 2.67 (m, 4H, N-CH<sub>2</sub>-CH<sub>2</sub>), 2.36 (s, 6H, N-CH<sub>3</sub>), 1.40 (t, J = 7.0 Hz, 3H, OCH<sub>2</sub>CH<sub>3</sub>). <sup>13</sup>C-NMR (CDCl<sub>3</sub>, 75 MHz, 300K) δ, ppm: 165.45 (C=O), 161.82 (pyC<sub>q</sub>), 149.70 (pyC<sub>γ</sub>), 138.00 (pyC<sub>α</sub>), 122.49, 120.98 (pyC<sub>β</sub>), 64.47 (py-CH<sub>2</sub>-N), 61.69 (CO<sub>2</sub>CH<sub>2</sub>CH<sub>3</sub>), 57.14, 57.03, 56.12 (N-CH<sub>2</sub>-C), 46.66 (N-CH<sub>3</sub>), 14.22 (CO<sub>2</sub>CH<sub>2</sub>CH<sub>3</sub>). ESI-MS (m/z): 321.2 [M+H]<sup>+</sup>.

**1-[(4-nitro-2-pyridyl)methyl]-4,7-dimethyl-1,4,7-triazacyclononane (<sup>H,NO<sub>2</sub></sup>Pytacn).** This ligand was prepared in analogous manner to <sup>H,Me</sup>Pytacn starting with <sup>H,NO<sub>2</sub></sup>PyCH<sub>2</sub>Cl. Yield = 67%. FT-IR (ATR)  $\nu$ , cm<sup>-1</sup>: 2922 – 2791 (C-H)<sub>sp<sup>3</sup></sub>, 1571, 1453 (py), 1532, 1353 (NO<sub>2</sub>). <sup>1</sup>H-NMR (CDCl<sub>3</sub>, 400 MHz, 300K)  $\delta$ , ppm: 8.80 (dd, J = 5.2 Hz, J' = 0.5, 1H, pyH <sub>$\alpha$</sub> ), 8.41 (d, J = 2.2 Hz, 1H, pyH <sub>$\beta$</sub> ), 7.86 (dd, J = 5.4 Hz, J' = 2.3 Hz, 1H, pyH <sub>$\beta$</sub> ), 4.00 (s, 2H, py-CH<sub>2</sub>), 2.88 – 2.86 (m, 4H, N-CH<sub>2</sub>-CH<sub>2</sub>), 2.77 (s, 4H, N-CH<sub>2</sub>-CH<sub>2</sub>), 2.70 – 2.69 (m, 4H, N-CH<sub>2</sub>-CH<sub>2</sub>), 2.37 (s, 6H, N-CH<sub>3</sub>). <sup>13</sup>C-NMR (CDCl<sub>3</sub>, 75 MHz, 300K)  $\delta$ , ppm: 165.2(pyC<sub>q</sub>), 154.5(pyC <sub>$\gamma$</sub> ), 151.06 (pyC <sub>$\alpha$</sub> ), 115.54, 114.30 (pyC <sub>$\beta$</sub> ), 63.99 (py-CH<sub>2</sub>-N), 57.23, 57.21, 56.08 (N-CH<sub>2</sub>-C), 46.72 (N-CH<sub>3</sub>). ESI-MS (m/z): 294.2 [M+H]<sup>+</sup>.

**1-[(4,6-dimethyl-2-pyridyl)methyl]-4,7-dimethyl-1,4,7-triazacyclononane (<sup>Me,Me</sup>Pytacn).** This ligand was prepared in analogous manner to <sup>H,Me</sup>Pytacn starting with <sup>Me,Me</sup>PyCH<sub>2</sub>Cl·HCl. Yield = 67%. <sup>1</sup>H-NMR (CDCl<sub>3</sub>, 200 MHz, 300K)  $\delta$ , ppm: 7.05 (s, 1H, pyH <sub>$\beta$</sub> ), 6.75 (s, 1H, pyH <sub>$\beta$</sub> ), 3.71 (s, 2H, py-CH<sub>2</sub>), 2.78 – 2.71 (m, 8H, N-CH<sub>2</sub>-CH<sub>2</sub>), 2.62 – 2.57 (m, 4H, N-CH<sub>2</sub>-CH<sub>2</sub>), 2.41 (s, 3H, py-CH<sub>3</sub>), 2.29 (s, 6H, N-CH<sub>3</sub>), 2.23 (s, 3H, py-CH<sub>3</sub>). <sup>13</sup>C-NMR (CDCl<sub>3</sub>, 50 MHz, 300K)  $\delta$ , ppm: 159.61, 157.13 (pyC <sub>$\alpha$</sub> ), 147.26 (pyC <sub>$\gamma$</sub> ), 122.17, 120.85 (pyC <sub>$\beta$</sub> ), 64.47 (py-CH<sub>2</sub>-N), 57.24, 57.11, 55.98 (N-CH<sub>2</sub>-C), 46.67 (N-CH<sub>3</sub>), 24.19, 20.95 (py-CH<sub>3</sub>). ESI-MS (m/z): 277.3 [M+H]<sup>+</sup>.

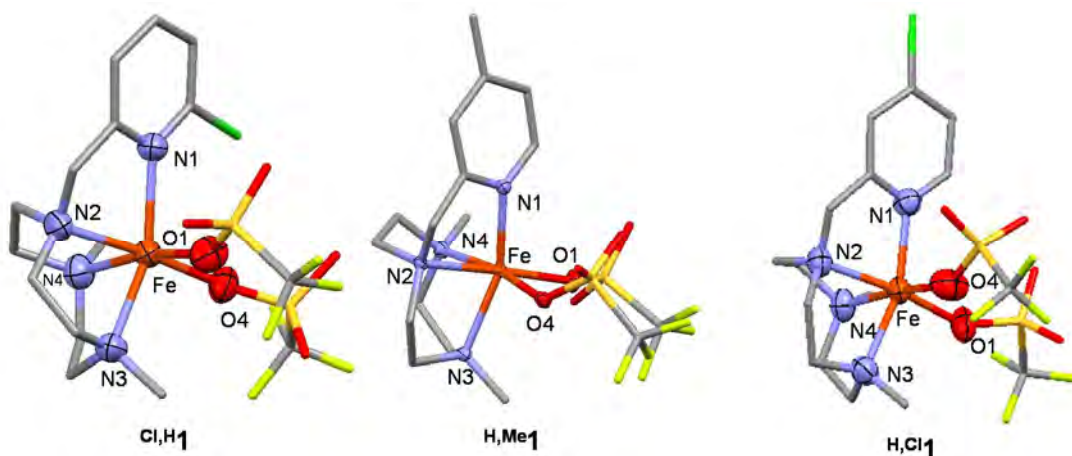
**1-[(6-chloro-2-pyridyl)methyl]-4,7-dimethyl-1,4,7-triazacyclononane (<sup>Cl,H</sup>Pytacn).** This ligand was prepared in analogous manner to <sup>H,Me</sup>Pytacn starting with <sup>Cl,H</sup>PyCH<sub>2</sub>Br. Yield = 87%. <sup>1</sup>H-NMR (CDCl<sub>3</sub>, 400 MHz, 300K)  $\delta$ , ppm: 7.63 (t, J = 7.7 Hz, 1H, py-H <sub>$\gamma$</sub> ), 7.45 (d, J = 7.7 Hz, 1H, py-H <sub>$\beta$</sub> ), 7.18 (d, J = 7.6 Hz, 1H, py-H <sub>$\beta$</sub> ), 3.83 (s, 2H, py-CH<sub>2</sub>), 2.84 – 2.82 (m, 4H, N-CH<sub>2</sub>-CH<sub>2</sub>), 2.80 (s, 4H, N-CH<sub>2</sub>-CH<sub>2</sub>), 2.68 – 2.66 (m, 4H, N-CH<sub>2</sub>-CH<sub>2</sub>), 2.36 (s, 6H, N-CH<sub>3</sub>). <sup>13</sup>C-NMR (CDCl<sub>3</sub>, 100 MHz, 300K)  $\delta$ , ppm: 161.74 (Hz, pyC<sub>q</sub>-Cl), 150.45 (pyC<sub>q</sub>-CH<sub>2</sub>), 138.90 (pyC <sub>$\gamma$</sub> ), 122.23, 121.52, (pyC <sub>$\beta$</sub> ), 64.01 (py-CH<sub>2</sub>-N), 57.07, 56.94, 56.19 (N-CH<sub>2</sub>-C), 46.60 (N-CH<sub>3</sub>). ESI-MS (m/z): 283.1 [M+H]<sup>+</sup>

**1-[(6-fluoro-2-pyridyl)methyl]-4,7-dimethyl-1,4,7-triazacyclononane (<sup>F,H</sup>Pytacn).** This ligand was prepared in analogous manner to <sup>H,Me</sup>Pytacn starting with <sup>F,H</sup>PyCH<sub>2</sub>Br. Yield = 99%. FT-IR (ATR)  $\nu$ , cm<sup>-1</sup>: 2922 – 2760 (C-H)<sub>sp<sup>3</sup></sub>, 1604, 1451, 1367 (py). <sup>1</sup>H-NMR (CDCl<sub>3</sub>, 200 MHz, 300K)  $\delta$ , ppm: 7.78 (dd, J = 7.4 Hz, J = 2.2 Hz, 1H, py-H <sub>$\gamma$</sub> ), 7.41 (dd, J = 7.4 Hz, J = 2.6 Hz, 1H, py-H <sub>$\beta$</sub> ), 6.81 (dd, J = 8.0 Hz, J = 2.8 Hz, 1H, py-H <sub>$\beta$</sub> ), 3.84 (s, 2H, py-CH<sub>2</sub>), 2.90 – 2.84 (m, 4H, N-CH<sub>2</sub>-CH<sub>2</sub>), 2.81 (s, 4H, N-CH<sub>2</sub>-CH<sub>2</sub>), 2.73 – 2.69 (m, 4H, N-CH<sub>2</sub>-CH<sub>2</sub>), 2.40 (s, 6H, N-CH<sub>3</sub>). <sup>13</sup>C-NMR (CDCl<sub>3</sub>, 50 MHz, 300K)  $\delta$ , ppm: 162.82 (d, J<sup>CF</sup> = 237.0 Hz, pyC<sub>q</sub>-F), 159.81 (d, J<sup>CF</sup> = 12.4 Hz, pyC<sub>q</sub>-CH<sub>2</sub>), 141.00 (d, J<sup>CF</sup> = 7.7 Hz, pyC <sub>$\gamma$</sub> ), 120.12 (d, J<sup>CF</sup> = 4.2 Hz, pyC <sub>$\beta$</sub> ), 107.02 (d, J<sup>CF</sup> = 36.7 Hz, pyC <sub>$\beta$</sub> ), 63.53 (py-CH<sub>2</sub>-N), 57.17, 57.04, 55.99 (N-CH<sub>2</sub>-C), 46.67 (N-CH<sub>3</sub>). ESI-MS (m/z): 267.1 [M+H]<sup>+</sup>.

## 1.2. Solid state characterization

**Crystal-Structure Determination.** The measurements were carried out on a *BRUKER SMART APEX CCD* diffractometer using graphite-monochromated Mo  $K\alpha$  radiation ( $\lambda = 0.71073 \text{ \AA}$ ) from an X-ray tube. Programs used: data collection, Smart version 5.631 (Bruker AXS 1997-02); data reduction, Saint + version 6.36A (Bruker AXS 2001); absorption correction, SADABS version 2.10 (Bruker AXS 2001). Structure solution and refinement were done using SHELXTL Version 6.14 (Bruker AXS 2000-2003). The structures were solved by direct methods and refined by full-matrix least-squares methods on  $F^2$ . The non-hydrogen atoms were refined anisotropically. The H-atoms were placed in geometrically optimized positions and forced to ride on the atom to which they are attached.

**Figure S1.** X-Ray structures of  $\text{Cl}_2\text{H}_2\mathbf{1}$ ,  $\text{H}_2\text{Me}_2\mathbf{1}$  and  $\text{H}_2\text{Cl}_2\mathbf{1}$ .

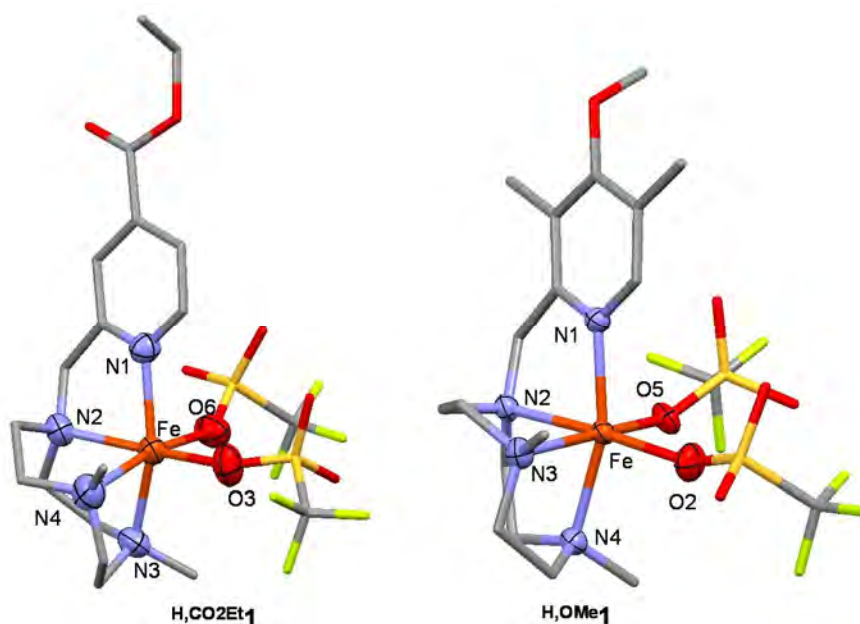


**Table S1.** Crystal data for  $^{Cl,H}1$ ,  $^{H,Me}1$  and  $^{H,Cl}1$ .

	$^{Cl,H}1$	$^{H,Me}1$	$^{H,Cl}1$
Empirical formula	$C_{17}H_{25}Cl_3F_6FeN_4O_6S_2$	$C_{17}H_{26}F_6FeN_4O_6S_2$	$C_{16}H_{23}ClF_6FeN_4O_6S_2$
Formula weight	721.73	616.39	636.80
Temperature	298(2) K	100(2) K	300(2) K
Wavelength	0.71073 Å	0.71073 Å	0.71073 Å
Crystal system	Orthorhombic	Orthorhombic	Monoclinic
Space group	P2(1)2(1)2(1)	P212121	P 21/c
Unit cell dimensions	a = 8.738(2) Å $\alpha = 90^\circ$ b = 16.228(4) Å $\beta = 90^\circ$ c = 20.412(6) Å $\gamma = 90^\circ$	a = 8.550(3) Å $\alpha = 90^\circ$ b = 13.577(5) Å $\beta = 90.00^\circ$ c = 21.298(8) Å $\gamma = 90.00^\circ$	a = 8.965(2) Å $\alpha = 90^\circ$ b = 25.125(5) Å $\beta = 123.939(11)^\circ$ c = 13.422(3) Å $\gamma = 90.00^\circ$
Volume	2894.3(13) Å <sup>3</sup>	2472.3(16) Å <sup>3</sup>	2517.8(16) Å <sup>3</sup>
Density (calculated)	1.656 g·cm <sup>-3</sup>	1.656 g·cm <sup>-3</sup>	1.680 g·cm <sup>-3</sup>
Absorption coefficient	1.020 mm <sup>-1</sup>	0.865 mm <sup>-1</sup>	0.955 mm <sup>-1</sup>
F(000)	1464	1264	1296
Cell formula units_Z	4	4	4
Crystal size	0.3 x 0.25 x 0.2 mm	0.5 x 0.2 x 0.2 mm	0.3 x 0.2 x 0.2 mm
$\Theta$ range for data collection	2.00 to 28.29°	1.78 to 28.40°	1.99 to 28.36°
Limiting indices	-11<=h<=11, -21<=k<=21, -27<=l<=27	-11<=h<=11 -18<=k<=18 -28<=l<=28	-11<=h<=11 -33<=k<=33 -17<=l<=17
Reflections collected	45303	38665	39322
Independent reflections	7156 [R(int) = 0.0558]	6147 [R(int) = 0.0529]	6201 [R(int) = 0.0245]
Completeness to $\Theta$	99.6 %	99.5 % ( $\Theta = 28.40^\circ$ )	98.9 % ( $\Theta = 28.36^\circ$ )
Refinement method	Full-matrix least-squares on F <sup>2</sup>	Full-matrix least-squares on F <sup>2</sup>	Full-matrix least-squares on F <sup>2</sup>
Data/restraints/parameters	7156 / 0 / 325	6147 / 0 / 328	6201 / 0 / 325
Goodness-of-fit on F <sup>2</sup>	0.993	1.077	1.057
Final R indices [ $I > 2\sigma(I)$ ]	R1 = 0.0460, wR2 = 0.1127	R1 = 0.0257 wR2 = 0.0582	R1 = 0.0447 wR2 = 0.1310
R indices (all data)	R1 = 0.0605, wR2 = 0.1197	R1 = 0.0299 wR2 = 0.0593	R1 = 0.0512 wR2 = 0.1355
Largest diff. peak and hole	0.320 and -0.245 e.Å <sup>-3</sup>	0.346 and -0.261 e. Å <sup>-3</sup>	0.617 and -0.447 e. Å <sup>-3</sup>

**Table S2.** Selected bond lengths (Å) and angles (°) for  $^{Cl,H}1$ ,  $^{H,Me}1$  and  $^{H,Cl}1$ .

	$^{Cl,H}1$	$^{H,Me}1$	$^{H,Cl}1$		
Fe-N1	2.258(2)	Fe-N1	2.1608(16)	Fe-N1	2.163(2)
Fe-N2	2.193(3)	Fe-N2	2.1924(15)	Fe-N2	2.2141(19)
Fe-N3	2.217(3)	Fe-N3	2.2062(15)	Fe-N3	2.193(2)
Fe-N4	2.226(3)	Fe-N4	2.2505(16)	Fe-N4	2.223(2)
Fe-O1	2.157(2)	Fe-O1	2.0610(14)	Fe-O1	2.0654(18)
Fe-O4	2.053(2)	Fe-O4	2.1604(14)	Fe-O4	2.161(2)
N2-Fe-N1	74.93(10)	N1-Fe-N2	77.61(6)	N1-Fe-N2	77.76(8)
N3-Fe-N1	153.53(11)	N1-Fe-N4	94.45(6)	N1-Fe-N4	100.52(8)
O4-Fe-N1	108.48(10)	N1-Fe-O4	90.31(5)	N1-Fe-O4	85.68(8)
O1-Fe-N1	86.52(10)	N1-Fe-O1	104.89(6)	N1-Fe-O1	107.86(8)
N2-Fe-N4	79.70(12)	N4-Fe-N2	80.08(6)	N4-Fe-N2	80.00(8)
N3-Fe-N4	80.09(11)	N4-Fe-N3	80.47(6)	N4-Fe-N3	81.27(8)
O4-Fe-N4	92.07(11)	N2-Fe-O4	91.56(5)	N2-Fe-O4	98.32(10)
O1-Fe-N4	168.71(11)	N4-Fe-O1	99.51(6)	N4-Fe-O1	89.47(8)
O1-Fe-N2	98.93(11)	N3-Fe-O1	97.41(6)	N3-Fe-O1	94.54(9)
N2-Fe-N3	80.17(10)	N2-Fe-N3	80.09(6)	N2-Fe-N3	80.53(8)
O4-Fe-N4	92.07(11)	N3-Fe-O4	91.49(5)	N3-Fe-O4	91.76(8)
O4-Fe-O1	88.93(10)	O4-Fe-O1	88.54(5)	O4-Fe-O1	91.72(10)

**Figure S2.** X-Ray structures of  $\text{H,CO}_2\text{Et}_1$  and  $\text{H,OMe}_1$ .**Table S3.** Crystal data for  $\text{H,CO}_2\text{Et}_1$  and  $\text{H,OMe}_1$ .

	$\text{H,CO}_2\text{Et}_1$	$\text{H,OMe}_1$
Empirical formula	$\text{C}_{19}\text{H}_{28}\text{F}_6\text{FeN}_4\text{O}_8\text{S}_2$	$\text{C}_{19}\text{H}_{30}\text{F}_6\text{FeN}_4\text{O}_7\text{S}_2$
Formula weight	674.42	660.44
Temperature	300(2) K	150(2) K
Wavelength	0.71073 Å	0.71073 Å
Crystal system	Monoclinic	Monoclinic
Space group	P 21/c	P 21/c
Unit cell dimensions	a = 12.949(3) Å $\alpha = 90^\circ$ b = 24.597(6) Å $\beta = 96.489(6)^\circ$ c = 8.910(2) Å $\gamma = 90^\circ$	a = 18.558 (11) Å $\alpha = 90^\circ$ b = 9.011(5) Å $\beta = 118.798(9)^\circ$ c = 19.218(11) Å $\gamma = 90.00^\circ$
Volume	2819.5(12) Å <sup>3</sup>	2816(3) Å <sup>3</sup>
Density (calculated)	1.589 g·cm <sup>-3</sup>	1.558 g·cm <sup>-3</sup>
Absorption coefficient	0.771 mm <sup>-1</sup>	0.768 mm <sup>-1</sup>
F(000)	1384	1360
Cell formula units_Z	4	4
Crystal size	0.4 x 0.15 x 0.08 mm	0.4 x 0.25 x 0.1 mm
$\Theta$ range for data collection	2.70 to 28.28°	2.12 to 28.23°
Limiting indices	-17 ≤ h ≤ 17 -32 ≤ k ≤ 32 -11 ≤ l ≤ 11	-24 ≤ h ≤ 24 -11 ≤ k ≤ 11 -25 ≤ l ≤ 25
Reflections collected	21941	42154
Independent reflections	6844 [R(int) = 0.0347]	6886 [R(int) = 0.0399]
Completeness to $\Theta$	99.1% ( $\Theta = 28.28^\circ$ )	99.1% ( $\Theta = 28.23^\circ$ )
Refinement method	Full-matrix least-squares on $F^2$	Full-matrix least-squares on $F^2$
Data/restraints/parameters	6844 / 2 / 361	6886 / 0 / 357
Goodness-of-fit on $F^2$	0.995	1.028
Final R indices [ $I > 2\sigma(I)$ ]	R1 = 0.0434 wR2 = 0.0998	R1 = 0.0409 wR2 = 0.1066
R indices (all data)	R1 = 0.0580 wR2 = 0.1093	R1 = 0.0506 wR2 = 0.1142
Largest diff. peak and hole	0.386 and -0.239 e. Å <sup>-3</sup>	0.714 and -0.459 e. Å <sup>-3</sup>

**Table S4.** Selected bond lengths (Å) and angles (°) for <sup>H,CO2Et</sup>**1** and <sup>H,OMe</sup>**1**.

<sup>H,CO2Et</sup> <b>1</b>		<sup>H,OMe</sup> <b>1</b>	
Fe-N1	2.177(3)	Fe-N1	2.1387(19)
Fe-N2	2.199(3)	Fe-N2	2.2007(19)
Fe-N3	2.188(3)	Fe-N3	2.252(2)
Fe-N4	2.226(3)	Fe-N4	2.182(2)
Fe-O3	2.208(3)	Fe-O2	2.0597(19)
Fe-O6	2.035(2)	Fe-O5	2.1813(17)
N1-Fe-N2	76.24(10)	N1-Fe-N2	77.56(7)
N1-Fe-N3	153.38(11)	N1-Fe-N4	159.25(7)
N1-Fe-O6	100.23(11)	N1-Fe-O5	87.45(7)
N1-Fe-O3	83.82(10)	N1-Fe-O2	105.82(7)
N4-Fe-N2	79.95(12)	N4-Fe-N2	81.69(7)
N4-Fe-N3	80.61(13)	N4-Fe-N3	81.05(8)
N4-Fe-O6	90.42(12)	N2-Fe-O5	89.31(7)
N4-Fe-O3	166.52(12)	N4-Fe-O2	94.92(7)
N2-Fe-O3	98.92(11)	N3-Fe-O2	97.84(8)
N2-Fe-N3	81.20(11)	N2-Fe-N3	80.36(7)
N3-Fe-O6	104.65(13)	N3-Fe-O5	168.43(6)
O4-Fe-O1	92.16(11)	O5-Fe-O2	92.17(8)



### 1.3. Paramagnetic $^1\text{H-NMR}$

Figure S3.  $^1\text{H-RMN}$  spectra of triflate complexes  $\text{H,R}'\mathbf{1}$  in  $\text{CD}_2\text{Cl}_2$ .

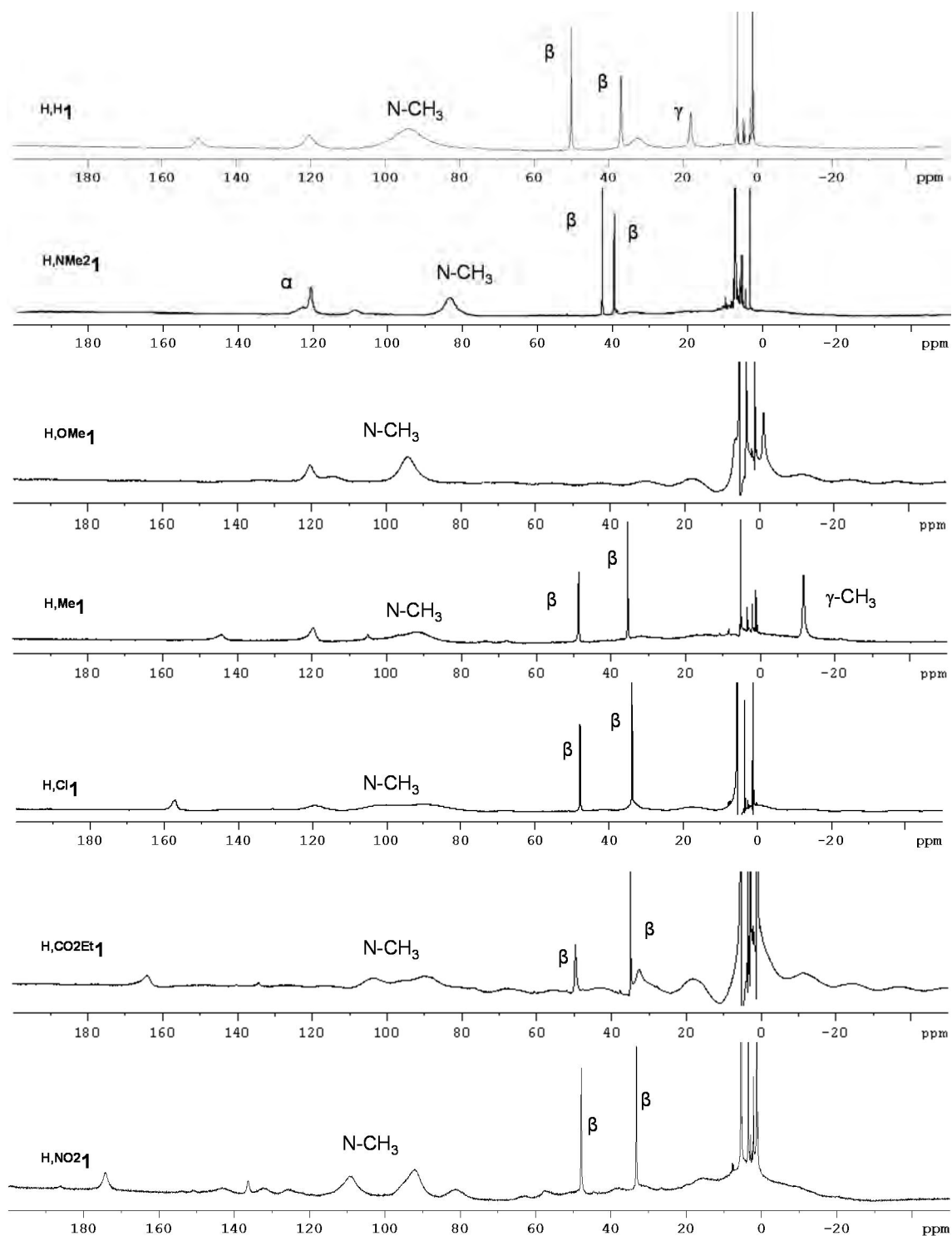
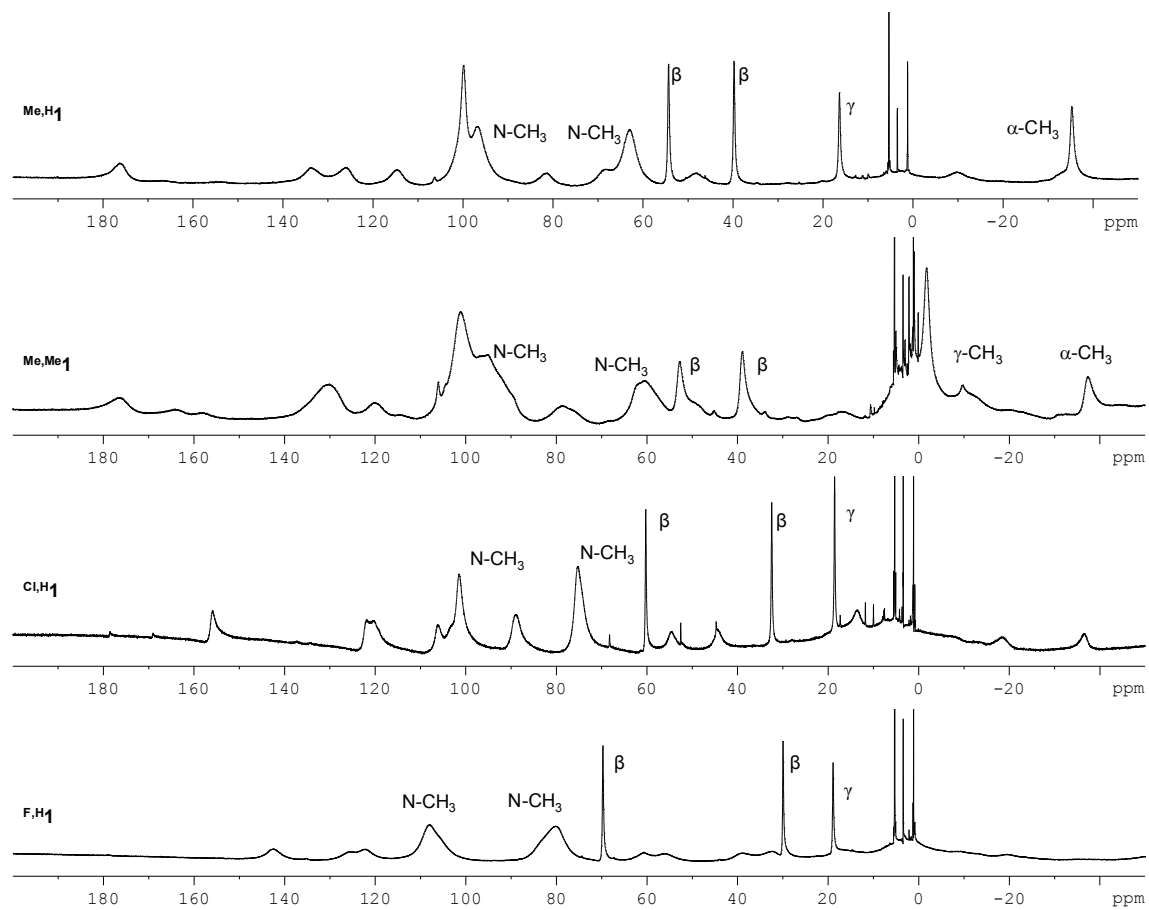
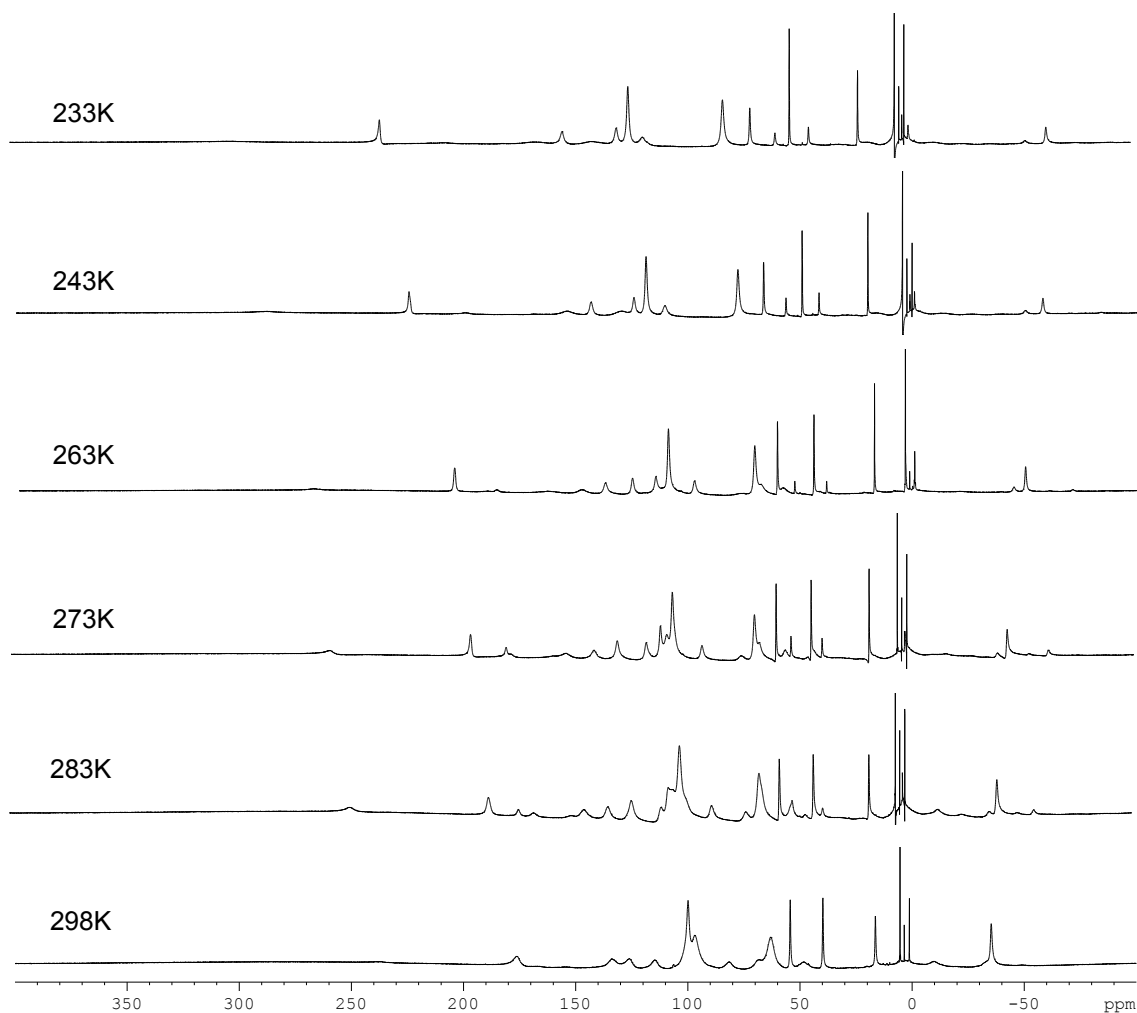
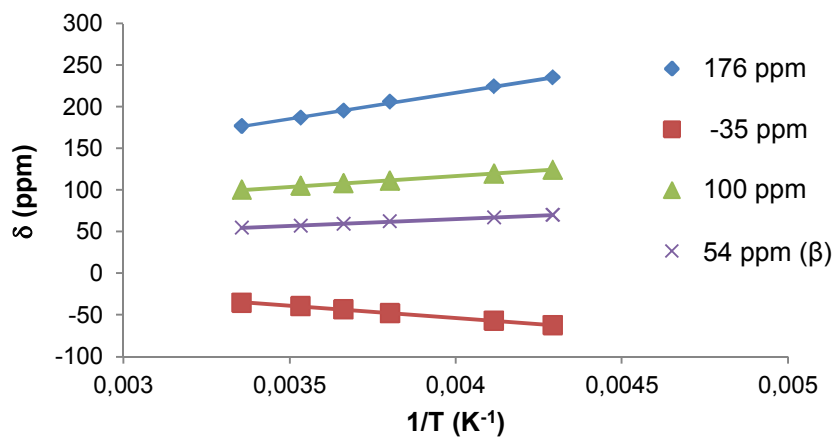
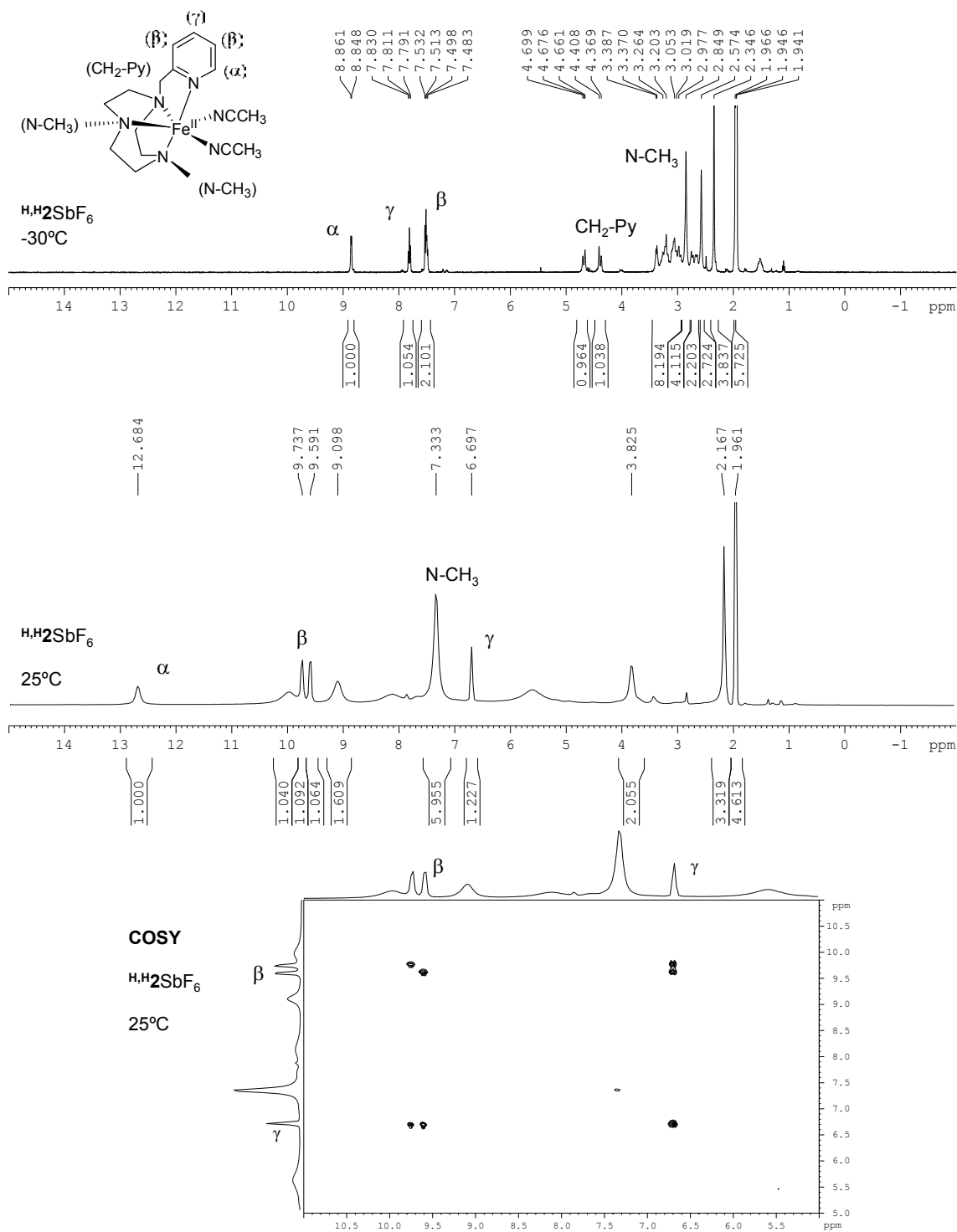


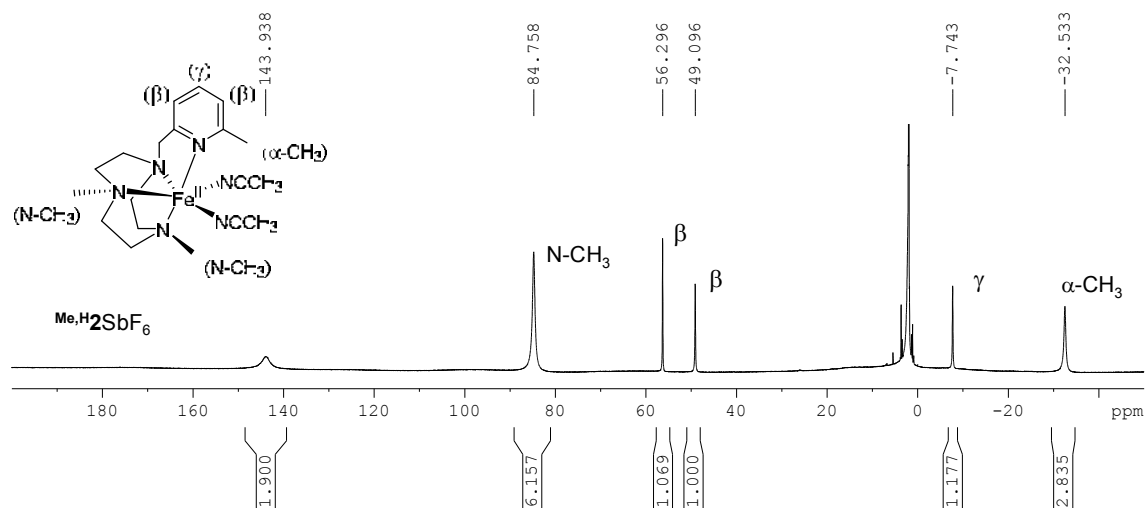
Figure S4.  $^1\text{H}$ -RMN spectra of triflate complexes  $^{\text{R,H}}\mathbf{1}$  (R = Me, Cl, F) in  $\text{CD}_2\text{Cl}_2$ .



**Figure S5.**  $^1\text{H}$ -NMR spectrum of  $^{\text{Me,H}}\mathbf{1}$  in  $\text{CD}_2\text{Cl}_2$  at different temperatures.**Figure S6.** Representation of the chemical shift in front of temperature of selected signals in the  $^1\text{H}$ -NMR spectrum of complex  $^{\text{Me,H}}\mathbf{1}$  in  $\text{CD}_2\text{Cl}_2$ . The paramagnetic shift of the protons is linearly dependent on the inverse of the temperature, which is indicative of a Curie behavior.

**Figure S7.**  $^1\text{H}$ -RMN spectrum of  $\text{H}_2\text{SbF}_6$  in  $\text{CD}_3\text{CN}$  at  $-30^\circ\text{C}$  and  $25^\circ\text{C}$  along with the aromatic region of the COSY spectrum measured at  $25^\circ\text{C}$ .



**Figure S8.**  $^1\text{H}$ -RMN spectrum of  $^{\text{Me,H}}\text{2SbF}_6$  in  $\text{CD}_3\text{CN}$  at room temperature.

**Figure S9.**  $^1\text{H}$ -RMN spectra of triflate complexes  $\text{H,R}'\mathbf{1}$  in  $\text{CD}_3\text{CN}$ . The triflate anions are replaced by acetonitrile molecules, thus, in solution the bis-acetonitrile complexes  $\text{H,R}'\mathbf{2}$  are formed.

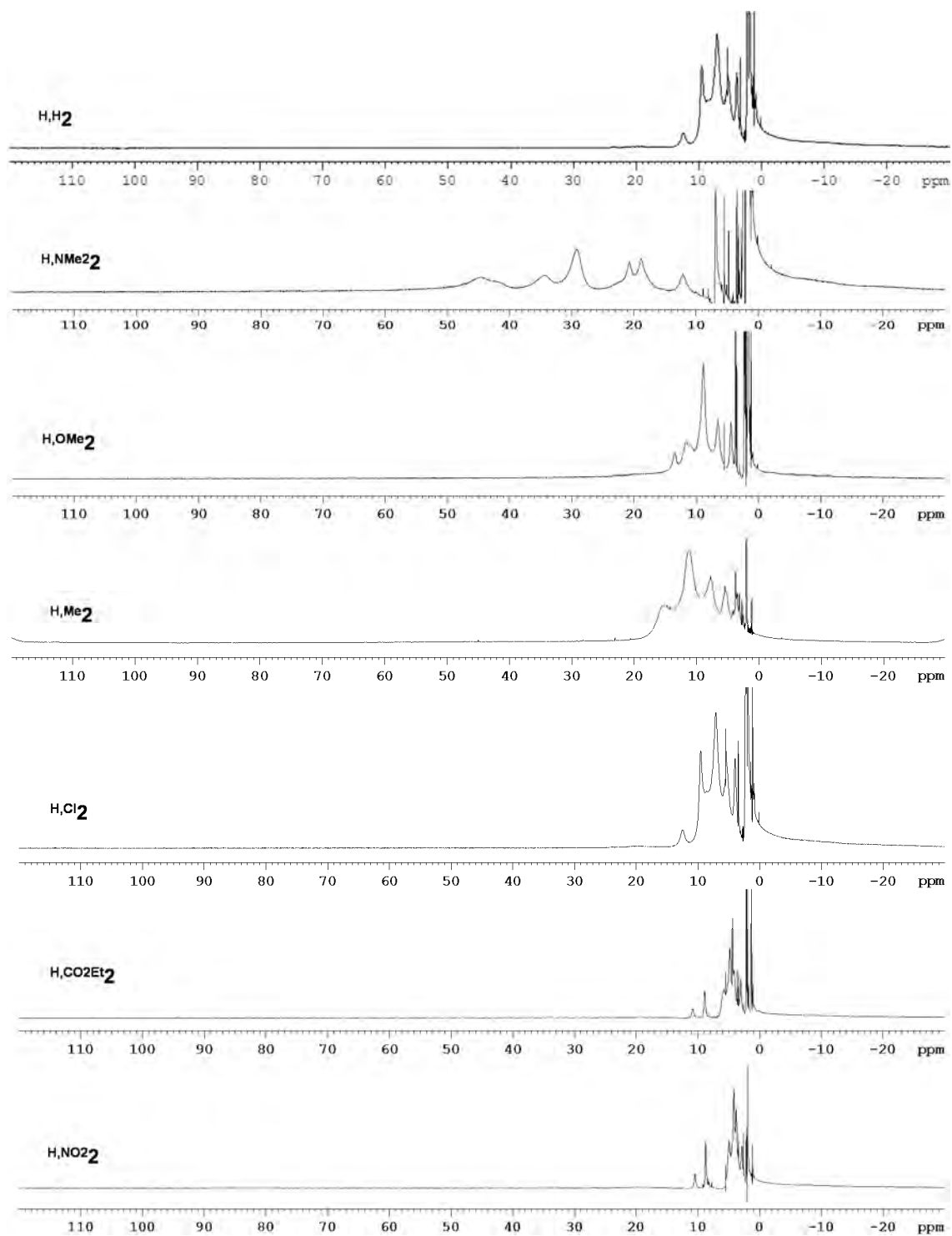
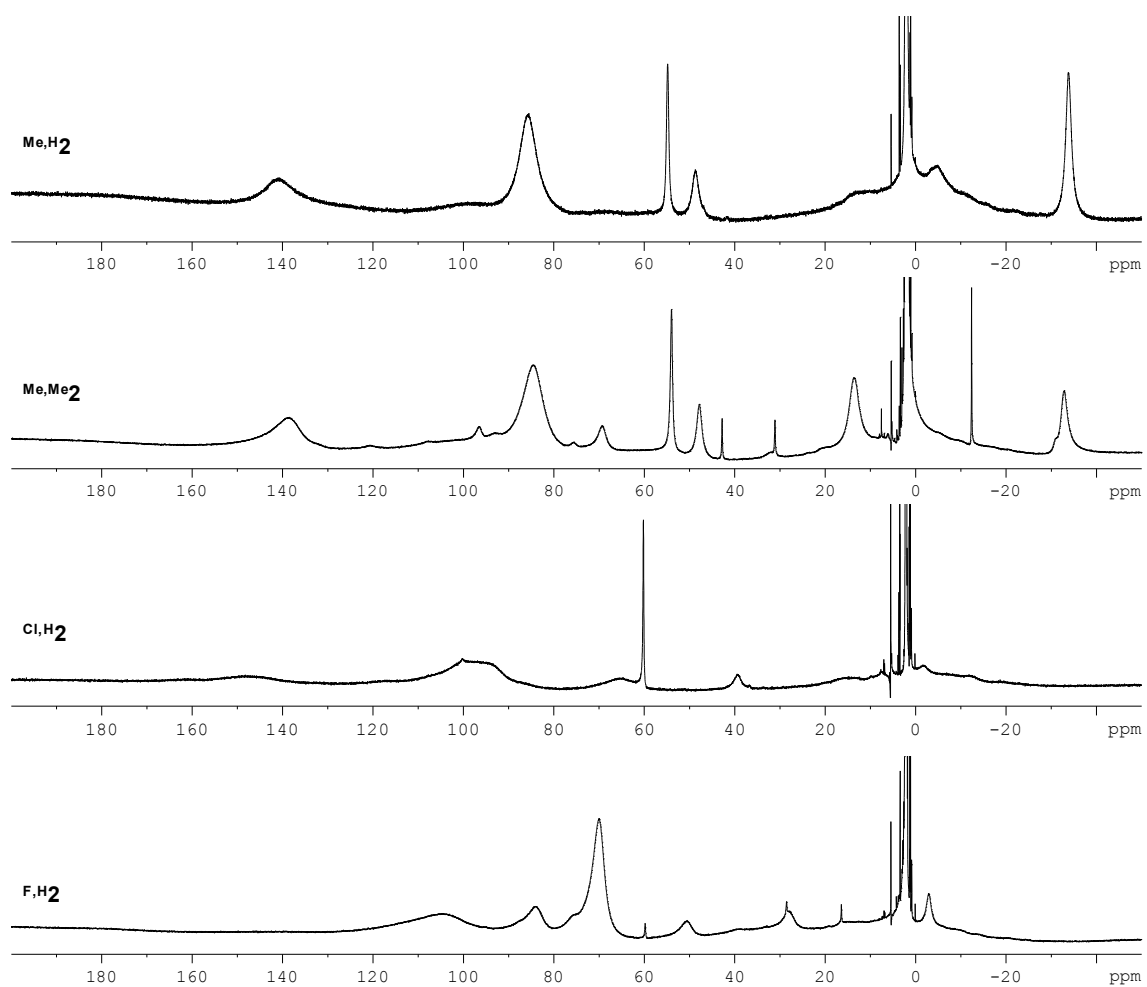


**Figure S10.**  $^1\text{H}$ -RMN spectra of triflate complexes  $\text{R}^{\text{H}}\mathbf{1}$  ( $\text{R} = \text{Me}, \text{Cl}, \text{F}$ ) in  $\text{CD}_3\text{CN}$ . The triflate anions are replaced by acetonitrile molecules, thus, in solution the bis-acetonitrile complexes  $\text{R}^{\text{H}}\mathbf{2}$  are formed.



## 1.4. Electrochemistry

**Figure S11.** a) Cyclic voltammetry for complexes  $^{\text{H,R}}\mathbf{3}$ . b) Cyclic voltammetry for complexes  $^{\text{H,H}}\mathbf{3}$ ,  $^{\text{Me,H}}\mathbf{3}$ ,  $^{\text{H,Me}}\mathbf{3}$  and  $^{\text{Me,Me}}\mathbf{3}$ . Cyclic voltammetries were measured in  $\text{CH}_3\text{CN}$  using SSCE as reference electrode.

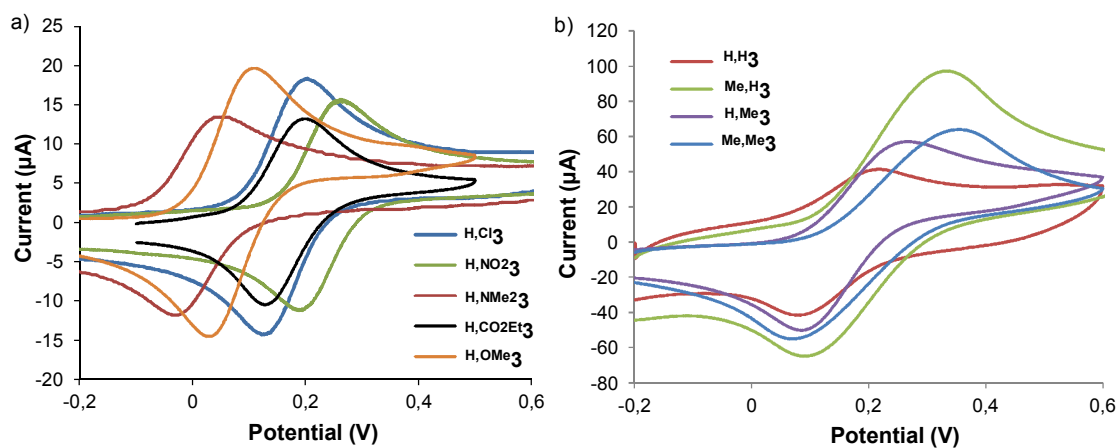
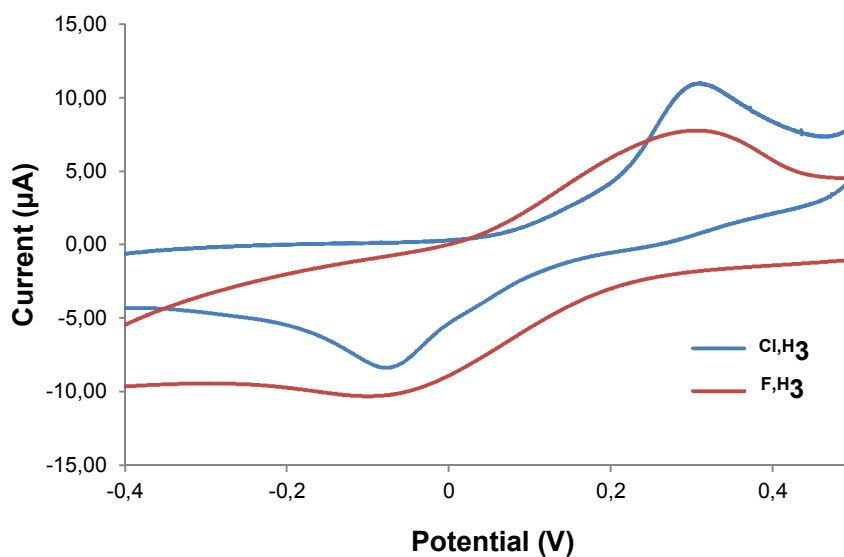


**Figure S12.** Cyclic voltammetry for complexes  $^{\text{Cl,H}}\mathbf{3}$  and  $^{\text{F,H}}\mathbf{3}$ . Cyclic voltammetries were measured in  $\text{CH}_3\text{CN}$  using SSCE as reference electrode.





## 1.5. References

1. Berreau, L. M.; Halfen, J. A.; Young, J. V. G.; Tolman, W. B., *Inorganic Chimica Acta* **2000**, *297*, 115-128.
2. Machkour, A.; Mandon, D.; Lachkar, M.; Welter, R., *Inorg. Chem.* **2004**, *43*, 1545-1550.
3. Zhang, C. X.; Kaderli, S.; Costas, M.; Kim, E.-i.; Neuhold, Y.-M.; Karlin, K. D.; Zuberbuehler, A. D., *Inorg. Chem.* **2003**, *42*, 1807-1824.
4. Tamura, M.; Urano, Y.; Kikuchi, K.; Higuchi, T.; Hirobe, M.; Nagano, T., *Chem. Pharm. Bull.* **2000**, *48*, 1514-1518.
5. Kojima, T.; Hayashi, K.-i.; Iizuka, S.-y.; Tani, F.; Naruta, Y.; Kawano, M.; Ohashi, Y.; Hirai, Y.; Ohkubo, K.; Matsuda, Y.; Fukuzumi, S., *Chem. Eur. J.* **2007**, *13*, 8212-8222.
6. Flassbeck, C.; Wieghardt, K., *Anorg. Allg. Chem.* **1992**, *608*, 60-68.
7. Company, A.; Gómez, L.; Güell, M.; Ribas, X.; Luis, J. M.; Que Jr., L.; Costas, M., *J. Am Chem. Soc.* **2007**, *129*, 15766-15767.
8. Company, A.; Gómez, L.; Fontrodona, X.; Ribas, X.; Costas, M., *Chem. Eur. J.* **2008**, *14*, 5727-5731.

## A.2. Supplementary Information Chapter IV

2.1. Experimental section.....	205
2.1.1. Materials.....	205
2.1.2. Syntheses.....	205
2.1.3. Instrumentation.....	205
2.2. Catalytic results.....	206
2.3. DFT calculations.....	207
2.4. References.....	210

### 2.1. Experimental section

#### 2.1.1. Materials

Reagents and solvents used were of commercially available reagent quality unless otherwise stated. H<sub>2</sub><sup>18</sup>O<sub>2</sub> (90% <sup>18</sup>O-enriched, 2% solution in H<sub>2</sub>O) and H<sub>2</sub><sup>18</sup>O (95% <sup>18</sup>O-enriched) were received from ICON Isotopes. Solvents were purchased from SDS and Scharlab. Solvents were purified and dried by passing through an activated alumina purification system (MBraun SPS-800). Preparation and handling of air-sensitive materials were carried out in a N<sub>2</sub> drybox (MBraun) with O<sub>2</sub> and H<sub>2</sub>O concentrations < 1 ppm.

#### 2.1.2. Syntheses

Iron complexes [Fe(OTf)<sub>2</sub>(Pytacn)] (**1**) and [Fe(OTf)<sub>2</sub>(6Me-Pytacn)] (**2**) were prepared as previously reported.<sup>1</sup> Synthesis of complexes **3-11** was performed following analogous procedures to **1** and **2** but starting from the appropriate ligand L3-L11. Preparation of chlorocomplexes [FeCl<sub>2</sub>(L)] (**1Cl-11Cl**) was carried out by direct reaction of the corresponding ligand (L1-L11) with FeCl<sub>2</sub>. Detailed syntheses and characterization of ligands L3-L11, complexes **3-11** and complexes **1Cl-11Cl** will be reported elsewhere.

#### 2.1.3. Instrumentation

Product analyses were performed on an Agilent 7820A gas chromatograph (HP5 column, 30 m) and a flame ionization detector. GC-MS spectral analyses were performed on an Agilent 7890A gas chromatograph interfaced with an Agilent 5975c MS mass spectrometer. A 50% NH<sub>3</sub>/CH<sub>4</sub> mix was used as the ionization gas for chemical ionization analyses.

ESI-MS experiments were performed and analyzed on a Bruker Daltonics Esquire 6000 spectrometer with acetonitrile as solvent.

Cyclic voltammetry (CV) experiments were performed in an IJ-Cambria HI-660 potentiostat using a three electrode cell. A glassy carbon disk electrode (3 mm diameter) from BAS was used as working electrode, platinum wire was used as auxiliary electrode and SSCE electrode as the reference.

## 2.2. Catalytic results

**Table S1.** Percentage of  $^{18}\text{O}$ -incorporation (%  $\text{R}^{18}\text{OH}$ ) into cyclohexanol in the oxidation of cyclohexane by complex **1** using different  $\text{H}_2^{18}\text{O}$  concentrations.

eq $\text{H}_2^{18}\text{O}$	$[\text{H}_2^{18}\text{O}]$ (M)	% $\text{R}^{18}\text{OH}^a$
50	0.05	21
100	0.10	29
250	0.25	40
600	0.60	45
1000	1.00	45
1200	1.20	47

Reaction catalytic conditions: 0.29 mL of a 70 mM (20  $\mu\text{mol}$ s)  $\text{H}_2\text{O}_2$  solution (diluted from a 35 %  $\text{H}_2\text{O}_2$  solution in  $\text{CH}_3\text{CN}$ ) together with the appropriate amount of  $\text{H}_2^{18}\text{O}$  (from 100 to 2400  $\mu\text{mol}$ s) was delivered by syringe pump over 30 min at 25  $^\circ\text{C}$  to a  $\text{CH}_3\text{CN}$  solution (1.71 mL) containing the iron catalyst (2.0  $\mu\text{mol}$ s) and the substrate (2000  $\mu\text{mol}$ s) under air. <sup>a</sup>Fraction of  $^{18}\text{O}$ -labeled cyclohexanol.

**Figure S1.** Fraction of  $^{18}\text{O}$ -labeled alcohol (%  $\text{R}^{18}\text{OH}$ ) obtained in cyclohexane hydroxylation catalysed by **1**/ $\text{H}_2\text{O}_2$  as a function of the concentration of  $\text{H}_2^{18}\text{O}$  ( $[\text{H}_2^{18}\text{O}]$ ). Inset: Double-reciprocal plot.

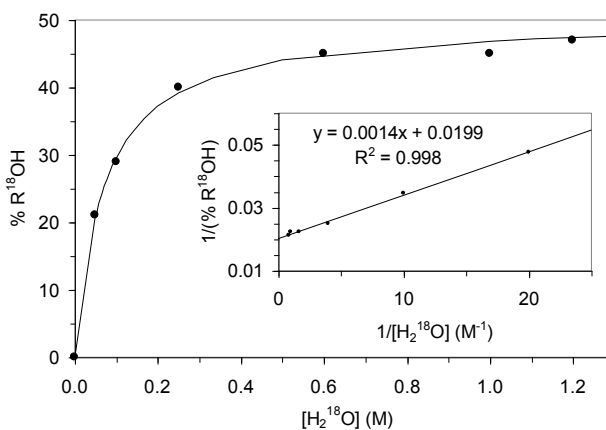


**Table S2.** Percentage of  $^{18}\text{O}$ -incorporation (%  $\text{R}^{18}\text{OH}$ ) into the alcohol in the oxidation of *cis*-1,2-dimethylcyclohexane by complex **1** using different substrate concentrations.

eq substrate	yield <sup>a</sup> (%)	% $\text{R}^{18}\text{OH}^b$
25	14	84
100	23	86
250	29	86
500	33	84
1000	35	79

Reaction catalytic conditions: 0.29 mL of a 70 mM (20  $\mu$ mol)  $\text{H}_2\text{O}_2$  solution (diluted from a 35 %  $\text{H}_2\text{O}_2$  solution in  $\text{CH}_3\text{CN}$ ) together with 40  $\mu\text{L}$  of  $\text{H}_2^{18}\text{O}$  (2000  $\mu$ mol) was delivered by syringe pump over 30 min at 25  $^\circ\text{C}$  to a  $\text{CH}_3\text{CN}$  solution (1.71 mL) containing the iron catalyst (2.0  $\mu$ mol) and the appropriate amount of substrate (from 50 to 2000  $\mu$ mol) under air. <sup>a</sup>Yield based on the oxidant. <sup>b</sup>Fraction of  $^{18}\text{O}$ -labeled (1R,2R or 1S,2S)-1,2-dimethylcyclohexanol.

**Table S3.** Percentage of  $^{18}\text{O}$ -incorporation (%  $\text{R}^{18}\text{OH}$ ) into the syn-diol product obtained in the oxidation of cyclooctene by complexes **1** and **2** using  $\text{H}_2^{18}\text{O}_2$  as oxidant.<sup>[a]</sup>

Catalyst	% $^{16}\text{O}^{18}\text{OH}^b$
<b>1</b>	96
<b>2</b>	88

[a] 0.29 mL of a 70 mM (20  $\mu$ mol)  $\text{H}_2^{18}\text{O}_2$  solution (diluted from a 2%  $\text{H}_2^{18}\text{O}_2/\text{H}_2\text{O}$  solution in  $\text{CH}_3\text{CN}$ ) was delivered by syringe pump over 30 min to an acetonitrile solution containing the iron catalyst (2.0  $\mu$ mol) and cyclooctene (2000  $\mu$ mol) under  $\text{N}_2$ . The final concentrations were 1 mM catalyst, 10 mM  $\text{H}_2^{18}\text{O}_2$ , 1 M cyclooctene and 1 M  $\text{H}_2\text{O}$ .  
[b] Percentage of  $^{16}\text{O}^{18}\text{O}$ -labeled diol determined by GC-MS.

## 2.3. DFT calculations

### Computational details

DFT geometries were optimized for each spin multiplicity at the UB3LYP level in conjunction with the SDD basis set and associated ECP for Fe, and the 6-311G(d,p) basis for the other atoms, as implemented in the Gaussian 09 program.<sup>3</sup> Then, the energies were further refined by single point calculations using cc-PVTZ basis set. The final free energies ( $\Delta\text{G}$ ) include electronic energies computed at UB3LYP in junction of the cc-PVTZ basis set ( $E_{\text{cc-PVTZ}}$ ), London dispersion effects calculated using the S. Grimme DFT-D3 method<sup>4</sup> ( $E_{\text{disp}}$ ), the free energy corrections computed at the UB3LYP/SDD&6-311G(d,p) level ( $G_{\text{corr}}$ ) and acetonitrile solvent effect corrections computed through PCM-SMD approach<sup>5</sup> at the UB3LYP/6-31G(d) level ( $G_{\text{solv}}$ ).

$$\Delta\text{G} = E_{\text{cc-PVTZ}} + E_{\text{disp}} + G_{\text{corr}} + G_{\text{solv}}$$

S. Grimme D3 London dispersion and acetonitrile PCM-SMD solvent effect corrections were calculated at the UB3LYP/SDD&6-311G(d,p) equilibrium geometries.

Spin-contaminated energies were systematically corrected when it was required (i.e. when the spin contamination was larger than 10%) using the following equation:

$$E_{\text{pure}} = \frac{E_{\text{cont}} - a \cdot E_{S+1}}{1 - a}$$

where

$$a = \frac{\langle S^2 \rangle_{\text{cont}} - S \cdot (S + 1)}{\langle S^2 \rangle_{S+1} - S \cdot (S + 1)}$$

and where  $E_{pure}$  is the B3LYP/cc-pVTZ spin corrected electronic energy, the  $E_{cont}$  and  $\langle S^2 \rangle_{cont}$  are the UB3LYP/cc-pVTZ energy and total spin angular square momentum respectively, obtained from the structure optimized at the UB3LYP/SDD&6-311G(d,p), and the  $E_{(S+1)}$  and  $\langle S^2 \rangle_{S+1}$  are the energy and total spin angular square momentum of the spin state (S+1), respectively, computed at the same level of theory and geometry.

### Thermodynamic data

**Table S4.** Free energies,  $\Delta G$  (kcal/mol), of S=1/2, S=3/2 and S=5/2 spin states of  $Q_A$  and  $Q_B$  isomers of **1**.

Catalyst 1	$\Delta G(298\text{ K})$		
	S=1/2	S=3/2	S=5/2
$Q_A$	2.95	5.51	3.76
$Q_B$	2.06	2.58	0.00

**Table S5.** Free energies,  $\Delta G$  (kcal/mol), of S=1/2, S=3/2 and S=5/2 spin states of  $Q_A$  and  $Q_B$  isomers of **2**.

Catalyst 2	$\Delta G(298\text{ K})$		
	S=1/2	S=3/2	S=5/2
$Q_A$	8.56	6.34	2.69
$Q_B$	5.21	7.42	0.00

**Table S6.** Free energies,  $\Delta G$  (kcal/mol), of S=1/2, S=3/2 and S=5/2 spin states of  $P_B$  isomer of **1**.

Catalyst 1	$\Delta G(298\text{ K})$		
	S=1/2	S=3/2	S=5/2
$P_B$	0.00	4.79	1.87

**Table S7.** Free energies,  $\Delta G$  (kcal/mol), of S=1/2, S=3/2 and S=5/2 spin states of  $P_B$  isomer of **2**.

Catalyst 2	$\Delta G(298\text{ K})$		
	S=1/2	S=3/2	S=5/2
$P_B$	2.41	3.18	0.00

**Table S8.** Free energies,  $\Delta G$  (kcal/mol), calculated for S=1/2 and S=3/2 spin states of  $O_A$ ,  $O_B$  and  $TS_{\text{oxo-hydroxo}}$  species of **oxo-hydroxo tautomerism** for **1**.

Catalyst 1	$\Delta G(298\text{ K})$	
	S=1/2	S=3/2
$O_A$	14.68	0.80
$TS_{\text{oxo-hydroxo}}$	22.34	13.50
$O_B$	15.09	0.00

**Table S9.** Free energies,  $\Delta G$  (kcal/mol), calculated for S=1/2 and S=3/2 spin states of  $\mathbf{O}_A$ ,  $\mathbf{O}_B$  and  $\mathbf{TS}_{\text{oxo-hydroxo}}$  species of **oxo-hydroxo tautomerism** for **2**.

Catalyst <b>2</b>	$\Delta G(298 \text{ K})$	
	S=1/2	S=3/2
$\mathbf{O}_A$	11.17	0.55
$\mathbf{TS}_{\text{oxo-hydroxo}}$	22.01	13.26
$\mathbf{O}_B$	11.35	0.00

**Table S10.** Free energies,  $\Delta G$  (kcal/mol), calculated for S=3/2 spin state of  $\mathbf{O}_A$ ,  $\mathbf{O}_B$  and  $\mathbf{TS}_{\text{oxo-hydroxo}}$  species of **oxo-hydroxo tautomerism not assisted by a water molecule** for **1** and **2**.

S=3/2	Catalyst <b>1</b>	Catalyst <b>2</b>
	$\Delta G(298 \text{ K})$	
$\mathbf{O}_A$	0.63	0.32
$\mathbf{TS}_{\text{oxo-hydroxo}}$	27.12	25.92
$\mathbf{O}_B$	0.00	0.00

**Table S11.** Free energies,  $\Delta G$  (kcal/mol), calculated for S=1/2 and S=3/2 spin states of  $\mathbf{O}_A$ ,  $\mathbf{TS}_A$  and  $\mathbf{Prod}_A$  involved in the cyclohexane hydroxylation concerted process for **1**. The most stable S=5/2  $\mathbf{Prod}_A$  is also included.

Catalyst <b>1</b>	$\Delta G(298 \text{ K})$		
	S=1/2	S=3/2	S=5/2
$\mathbf{O}_A$	8.61	0.00	---
$\mathbf{TS}_A$	8.61	7.66	---
$\mathbf{Prod}_A$	-52.84	-54.47	-58.20

**Table S12.** Free energies,  $\Delta G$ , (kcal/mol), calculated for S=1/2 and S=3/2 spin states of  $\mathbf{O}_B$ ,  $\mathbf{TS}_B$  and  $\mathbf{Prod}_B$  involved in the cyclohexane hydroxylation concerted process for **1**. The most stable S=5/2  $\mathbf{Prod}_B$  is also included.

Catalyst <b>1</b>	$\Delta G(298 \text{ K})$		
	S=1/2	S=3/2	S=5/2
$\mathbf{O}_B$	15.84	0.00	---
$\mathbf{TS}_B$	15.84	7.40	---
$\mathbf{Prod}_B$	-50.67	-55.31	-56.53

**Table S13.** Free energies,  $\Delta G$  (kcal/mol), calculated for  $S=1/2$  and  $S=3/2$  spin states of  $O_A$ ,  $TS_A$  and  $Prod_A$  involved in the cyclohexane hydroxylation concerted process for **2**. The most stable  $S=5/2$   $Prod_A$  is also included.

Catalyst <b>2</b>	$\Delta G(298\text{ K})$		
	$S=1/2$	$S=3/2$	$S=5/2$
$O_A$	11.62	0.00	---
$TS_A$	11.62	9.48	---
$Prod_A$	-49.16	-52.91	-59.82

**Table S14.** Free energies,  $\Delta G$  (kcal/mol), calculated for  $S=1/2$  and  $S=3/2$  spin states of  $O_B$ ,  $TS_B$  and  $Prod_B$  involved in the cyclohexane hydroxylation concerted process for **2**. The most stable  $S=5/2$   $Prod_B$  is also included.

Catalyst <b>2</b>	$\Delta G(298^\circ\text{K})$		
	$S=1/2$	$S=3/2$	$S=5/2$
$O_B$	13.52	0.00	---
$TS_B$	20.55	7.27	---
$Prod_B$	-51.48	-57.22	-62.52

## 2.4. References

1. A. Company, L. Gómez, M. Güell, X. Ribas, J. M. Luis, L. Que, Jr., M. Costas, *J. Am. Chem. Soc.* **2007**, *129*, 15766.
2. A. Company, L. Gómez, X. Fontrodona, X. Ribas, M. Costas, *Chem. Eur. J.* **2008**, *14*, 5727.
3. Gaussian 09, Revision A.02, M. J. Frisch, G. W. Trucks, H. B. Schlegel, G. E. Scuseria, M. A. Robb, J. R. Cheeseman, G. Scalmani, V. Barone, B. Mennucci, G. A. Petersson, H. Nakatsuji, M. Caricato, X. Li, H. P. Hratchian, A. F. Izmaylov, J. Bloino, G. Zheng, J. L. Sonnenberg, M. Hada, M. Ehara, K. Toyota, R. Fukuda, J. Hasegawa, M. Ishida, T. Nakajima, Y. Honda, O. Kitao, H. Nakai, T. Vreven, J. A. Montgomery, Jr., J. E. Peralta, F. Ogliaro, M. Bearpark, J. J. Heyd, E. Brothers, K. N. Kudin, V. N. Staroverov, R. Kobayashi, J. Normand, K. Raghavachari, A. Rendell, J. C. Burant, S. S. Iyengar, J. Tomasi, M. Cossi, N. Rega, J. M. Millam, M. Klene, J. E. Knox, J. B. Cross, V. Bakken, C. Adamo, J. Jaramillo, R. Gomperts, R. E. Stratmann, O. Yazyev, A. J. Austin, R. Cammi, C. Pomelli, J. W. Ochterski, R. L. Martin, K. Morokuma, V. G. Zakrzewski, G. A. Voth, P. Salvador, J. J. Dannenberg, S. Dapprich, A. D. Daniels, O. Farkas, J. B. Foresman, J. V. Ortiz, J. Cioslowski, and D. J. Fox, Gaussian, Inc., Wallingford CT, 2009.
4. Grimme, S. Antony, J. Ehrlich, S. Krieg, *H. J. Chem. Phys.*, **2010**, *132*, 154104.
5. A. V. Marenich, C. J. Cramer, and D. G. Truhlar, *J. Phys. Chem. B*, **2009**, *113*, 6378-6396.
6. J.M. Wittbrodt, H. B. Schlegel, *J. Chem. Phys.*, **1996**, *106*, 6574-6577.

## A.3. Supplementary Information Chapter V

3.1. Experimental section.....	211
3.1.1. Materials.....	211
3.1.2. Instrumentation .....	211
3.1.3 Complexes studied .....	212
3.1.4 Crystallographic data for complex $3^{\text{Me,Me}}$ .....	212
3.1.5. Synthesis of substrates.....	214
3.1.6. Reaction conditions for catalysis .....	217
3.1.6.1. Sample analysis.....	217
3.1.6.2. Reaction under catalytic conditions.....	217
3.1.6.3. Procedure for product isolation .....	217
3.2. References.....	222

### 3.1. Experimental section

#### 3.1.1. Materials

Reagents and solvents used were commercially available reagent quality unless otherwise stated. Solvents were purchased from SDS and Scharlab. Solvents were purified and dried by passing through an activated alumina purification system (MBraun SPS-800). Acetonitrile for catalysis was HPLC grade. Preparation and handling of air-sensitive materials were carried out in a N<sub>2</sub> drybox (Braun) with O<sub>2</sub> and H<sub>2</sub>O concentrations < 1 ppm. [Fe(CF<sub>3</sub>SO<sub>3</sub>)<sub>2</sub>(BPBP)],<sup>1</sup> [Fe(CF<sub>3</sub>SO<sub>3</sub>)<sub>2</sub>((S,S)-MCPD)]<sup>2</sup> and [Fe<sup>II</sup>(CF<sub>3</sub>SO<sub>3</sub>)<sub>2</sub>(<sup>Me,Me</sup>Pytacn)]<sup>3</sup> were prepared according to published procedures.

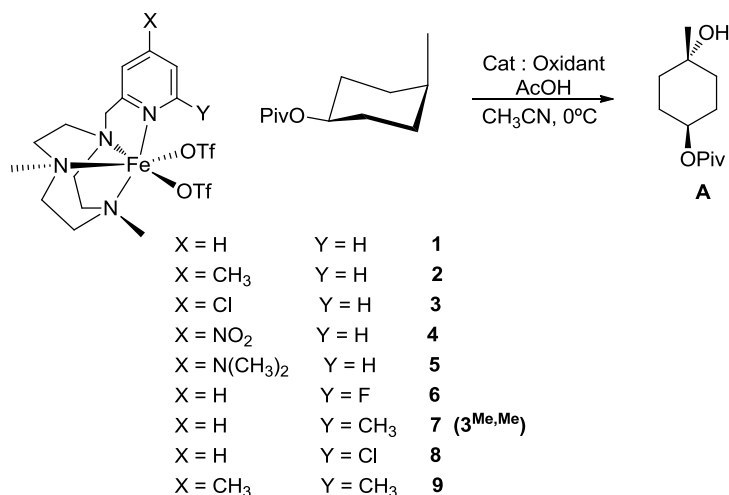
#### 3.1.2. Instrumentation

NMR spectra were taken on a Bruker DPX 300 or 400 MHz spectrometer. Spectra were referenced to the residual proto solvents peaks or TMS (tetramethylsilane) for <sup>1</sup>H. Product analyses were performed on an Agilent 7820A gas chromatograph (HP5 column, 30m or Cyclosil-B column, 30m) and a flame ionization detector. GC-MS spectral analyses were performed on an Agilent 7890A gas chromatograph interfaced with an Agilent 5975c MS mass spectrometer. A 50% NH<sub>3</sub>/CH<sub>4</sub> mix was used as the ionization gas for chemical ionization analyses.



### 3.1.3 Complexes studied

We developed a new family of complexes based on the triazacyclononane ligand,  $[\text{Fe}^{\text{II}}(\text{CF}_3\text{SO}_3)_2(\text{X},\text{Y-PyTACN})]$  (Scheme 1), with modifications in the positions 4th and 6th of the pyridine. Groups with different electronic properties were inserted in the 4th position of the pyridine and bulky groups in the position 6th.



**Scheme S1.** Oxidation of cis-4-methylcyclohexyl pivalate by different catalysts based on the triazacyclononane ring.

Cat	[Cat(mol%)]:[Oxidant (equiv.)]:[AcOH(equiv.)]	Conversion (%)	A(%)
1	3 : 3.6 : 1.5	2	2
2	3 : 3.6 : 1.5	13	2
3	3 : 3.6 : 1.5	9	4
4	3 : 3.6 : 1.5	8	3
5	3 : 3.6 : 1.5	6	1
6	3 : 3.6 : 1.5	3	3
7	3 : 3.6 : 1.5	85	54
8	3 : 3.6 : 1.5	76	8
9	3 : 3.6 : 1.5	84	51

The results show that the only complexes that give a good yield of the alcohol product were the ones with a methyl in the position 6 of the pyridine, 7 and 9. The other ones give poor yields and also poor conversions. The complex chosen is 7 because give better yields and it's easier to synthesize.

### 3.1.4 Crystallographic data for complex $\mathbf{3}^{\text{Me,Me}}$

Crystals of  $\mathbf{3}^{\text{Me,Me}}$  (CCDC 894663) were grown by slow diffusion of diethyl ether into a  $\text{CH}_2\text{Cl}_2$  solution of the corresponding compound, and used X-ray structure determination. The

measurement was carried out on a *BRUKER SMART APEX CCD* diffractometer using graphite-monochromated Mo  $K\alpha$  radiation ( $\lambda = 0.71073 \text{ \AA}$ ) from an X-ray tube.

Compound  $\mathbf{3}^{\text{Me,Me'}}$ OTf crystallizes out as very thin needles, which were not suitable for X-Ray diffraction. In this case, only the spontaneously formed crystals of the iron(II) bis-aquo complex  $[\text{Fe}^{\text{II}}(\text{Me,Me'Pytacn})(\text{H}_2\text{O})_2](\text{OTf})_2$  ( $[\mathbf{3}^{\text{Me,Me'}}[\text{H}_2\text{O}]\text{OTf}$ ) could be analyzed by X-ray diffraction.

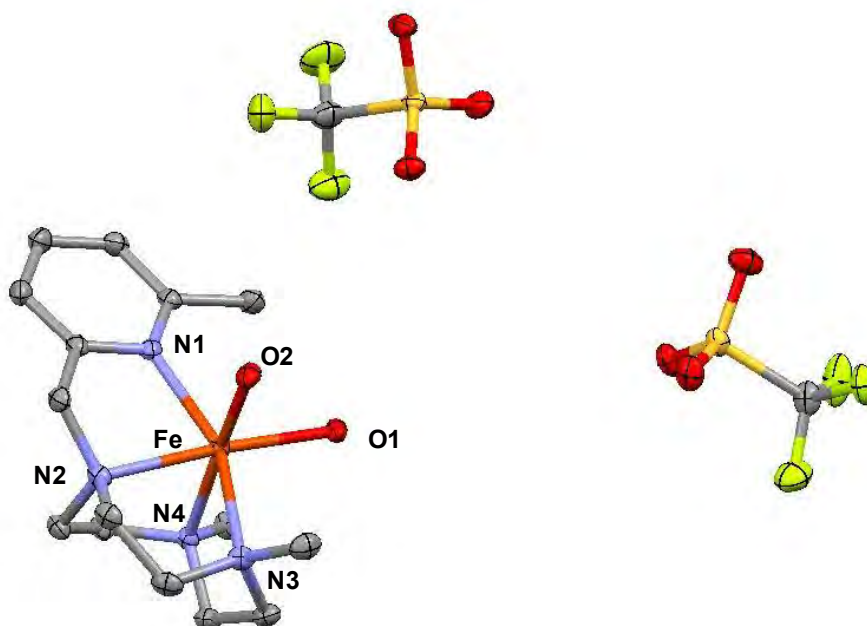


**Figure S1.** X-Ray structures  $\mathbf{3}^{\text{Me,Me'}}[\text{H}_2\text{O}]\text{OTf}$ . Hydrogen atoms were omitted for clarity.

**Table S1.** Crystal data and structure refinement  $\mathbf{3}^{\text{Me,Me'}}[\text{H}_2\text{O}]\text{OTf}$ .

	$\mathbf{3}^{\text{Me,Me'}}[\text{H}_2\text{O}]\text{OTf}$
Empirical formula	$\text{C}_{17}\text{H}_{30}\text{F}_6\text{FeN}_4\text{O}_8\text{S}_2$
Formula weight	652.42
Temperature	100(2) K
Wavelength	0.71073 $\text{\AA}$
Crystal system	Monoclinic
Space group	P 21/c
Unit cell dimensions	$a = 10.3127(15) \text{ \AA}$ $\alpha = 90^\circ$ $b = 13.910(2) \text{ \AA}$ $\beta = 100.115(2)^\circ$ $c = 18.679(3) \text{ \AA}$ $\gamma = 90^\circ$
Volume	$2637.5(7) \text{ \AA}^3$
Density (calculated)	$1.643 \text{ g}\cdot\text{cm}^{-3}$
Absorption coefficient	$0.821 \text{ mm}^{-1}$
F(000)	1344
Cell formula units_Z	4
Crystal size	$0.5 \times 0.2 \times 0.08 \text{ mm}$
$\Theta$ range for data collection	2.01 to $28.28^\circ$

Limiting indices	-13<=h<=13 -18<=k<=18 -24<=l<=24
Reflections collected	36957
Independent reflections	6504 [R(int) = 0.0245]
Completeness to $\Theta$	99.4 % ( $\Theta = 28.28^\circ$ )
Refinement method	Full-matrix least-squares on $F^2$
Data/restraints/parameters	6504 / 0 / 362
Goodness-of-fit on $F^2$	1.024
Final R indices [ $I > 2\sigma(I)$ ]	R1 = 0.0282 wR2 = 0.0664
R indices (all data)	R1 = 0.0394 wR2 = 0.0703
Largest diff. peak and hole	0.429 and -0.271 e. $\text{\AA}^{-3}$

**Table S2.** Selected bond lengths [ $\text{\AA}$ ] and angles [ $^\circ$ ] for  $\mathbf{3}^{\text{Me,Me}}[\text{H}_2\text{O}]\text{OTf}$ .

$\mathbf{3}^{\text{Me,Me}}[\text{H}_2\text{O}]\text{OTf}$	
Fe-N1	2.2278(13)
Fe-N2	2.1967(13)
Fe-N3	2.2347(13)
Fe-N4	2.2325(12)
Fe-O1	2.0771(12)
Fe-O4	2.1222(12)
N1-Fe-N2	78.03(8)
N1-Fe-N4	96.37(5)
N1-Fe-O4	90.09(5)
N1-Fe-O1	106.18(5)
N4-Fe-N2	80.38(5)
N4-Fe-N3	80.09(5)
N2-Fe-O4	95.94(5)
N4-Fe-O1	97.60(5)
N3-Fe-O1	96.73(5)
N2-Fe-N3	79.06(5)
N3-Fe-O2	91.94(5)
O4-Fe-O1	85.55(10)

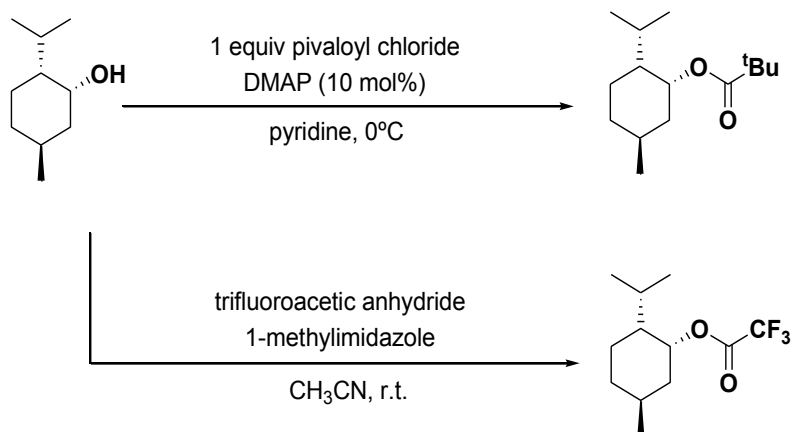
### 3.1.5. Synthesis of substrates

(1*R*)-(-)-menthyl acetate, cyclohexane, cyclooctane, 2,6-dimethyloctane, 1-bromo-3,7-dimethyloctane, n-hexane, methyl hexanoate, *cis*-1,2-dimethylcyclohexane (*cis*-DMCH), *trans*-1,2-dimethylcyclohexane (*trans*-DMCH), *cis*-decalin, *trans*-decalin, gem-dimethylcyclohexane, (1*R*)-(-)-neomenthyl acetate, (-)-ambroxide, (3*aR*)-(+)-sclareolide, and 4-methylvaleric acid were purchased from Aldrich or TCI America.

*cis*-4-methylcyclohexanol, *trans*-4-methylcyclohexanol, 3,7-dimethyl-1-octanol, (1*S*,2*S*,5*R*)-(+)-neomenthol were purchased from Aldrich and TCI America.

*cis*-4-methylcyclohexyl pivalate, *trans*-4-methylcyclohexyl pivalate and 3,7-dimethyloctyl acetate were synthesized as described in by Costas and co-workers.<sup>2</sup>

All liquid substrates were passed through an alumina plug before being used.



**Scheme S2.** Synthesis of neomenthyl derivatives.

(+)-neomenthyl pivalate was prepared by reaction of pivaloyl chloride with the commercially available (+)-neomenthol, following the procedure described below (Scheme S1):

(+)-neomenthol (5g, 30.7 mmol) and 4-dimethylaminopyridine (0.36g, 3 mmol) was dissolved in pyridine (50 mL). The mixture was cooled in an ice-bath and a solution of pivaloyl chloride (4.2 mL, 33.5 mmol) in pyridine (30 mL) was added dropwise. After stirring for 24 hours, the solvent was removed under reduced pressure and the resulting residue was treated with  $\text{CHCl}_3$  (250 mL) and washed with water (100 mL), saturated  $\text{NaHCO}_3$  aqueous solution (100 mL) and saturated  $\text{NaCl}$  aqueous solution (100 mL). The organic phase was dried over  $\text{MgSO}_4$ , filtered and the solvent was removed under reduced pressure to yield a colorless liquid.

(+)-Neomenthyl pivalate

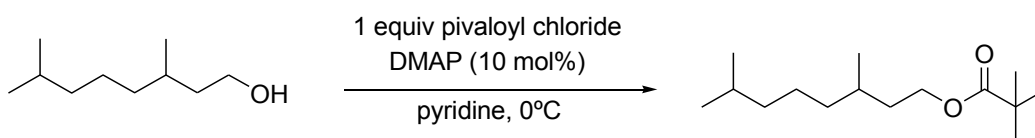
Purification by flash chromatography over silica (hexane 100%). 75% yield.  $^1\text{H-NMR}$  (400 MHz,  $\text{CDCl}_3$ , 300 K)  $\delta$ , ppm: 5.15-5.12 (m, 1H), 1.96-1.89 (m, 1H), 1.80-1.72 (m, 2H) 1.65-1.52 (m, 1H), 1.47-1.25 (m, 2H), 1.20 (s, 9H), 1.65-0.91 (m, 3H), 0.89 (d,  $J = 6.7$  Hz, 3H), 0.85 (d,  $J = 6.5$  Hz, 3H), 0.84 (d,  $J = 6.6$  Hz, 3H). GC-MS ( $m/z$ ): 258.3 [ $\text{M}+\text{NH}_4$ ] $^+$ .

(+)-neomenthyl trifluoroacetate was prepared by acetylating the commercially available (+)-neomenthol, following the procedure described below (Scheme S1):

(+)-neomenthol (2.5g, 16.0 mmol), 1-methylimidazole (1.5 mL) and trifluoroacetic anhydride (15 mL) were dissolved in CH<sub>3</sub>CN (30 mL) and stirred for 24 hours at room temperature. Ice (25 mL) was added at this point. After stirring for 15 min, CHCl<sub>3</sub> (60 mL) was added. The organic layer was washed with H<sub>2</sub>SO<sub>4</sub> 1 M (25 mL) and a mixture of water (23 mL) and saturated NaHCO<sub>3</sub> solution (2 mL) (four times, until neutral pH), dried over MgSO<sub>4</sub> and the solvent was removed under reduced pressure.

(+)-Neomenthylfluoroacetate

Purification over silica (hexane ethyl acetate 95:5). 73% yield. <sup>1</sup>H-NMR (400 MHz, CDCl<sub>3</sub>, 300 K) δ, ppm: 5.41-5.40 (m, 1H), 2.05-2.00 (m, 1H), 1.81-1.77 (m, 2H), 1.65-1.59 (m, 1H), 1.48-1.33 (m, 2H), 1.2-1.04 (m, 2H), 1.12-0.95 (m, 1H), 0.92 (d, J = 6.7 Hz, 3H), 0.89 (d, J = 6.6 Hz, 3H), 0.88 (d, J = 6.7 Hz, 3H). GC-MS (m/z): 270.1 [M+NH<sub>4</sub>]<sup>+</sup>.



**Scheme S3.** Synthesis of 3,7-dimethyloctyl pivalate.

3,7-dimethyloctyl pivalate was prepared by reaction of pivaloyl chloride with the commercially available 3,7-dimethyl-1-octanol, following the procedure described below (Scheme S2):

3,7-dimethyl-1-octanol (3.5g, 21.7 mmol) and 4-dimethylaminopyridine (0.24g, 2 mmol) was dissolved in pyridine (35 mL). The mixture was cooled in an ice-bath and a solution of pivaloyl chloride (3 mL, 24.4 mmol) in pyridine (30 mL) was added dropwise. After stirring for 24 hours, the solvent was removed under reduced pressure and the resulting residue was treated with CHCl<sub>3</sub> (250 mL) and washed with water (100 mL), saturated NaHCO<sub>3</sub> aqueous solution (100 mL) and saturated NaCl aqueous solution (100 mL). The organic phase was dried over MgSO<sub>4</sub>, filtered and the solvent was removed under reduced pressure to yield a colorless liquid.

3,7-dimethyloctyl pivalate

Purification by flash chromatography over silica (hexane 100%). 72% yield. <sup>1</sup>H-NMR (400 MHz, CDCl<sub>3</sub>, 300 K) δ, ppm: 4.10-5.06 (m, 2H), 1.67-1.63 (m, 1H), 1.55-1.50 (m, 2H) 1.45-1.42 (m, 1H), 1.29-1.27 (m, 2H), 1.19(s, 9H), 1.16-1.11 (m, 4H), 0.89 (d, J = 6.5 Hz, 3H), 0.85 (d, J = 6.6 Hz, 6H). GC-MS (m/z): 260.1 [M+NH<sub>4</sub>]<sup>+</sup>.

### **3.1.6. Reaction conditions for catalysis**

#### **3.1.6.1. Sample analysis**

GC analysis of the catalysis provided substrate conversions and product yields relative to the internal standard integration. Calibration curves were obtained from commercial products when available or from pure isolated products obtained from a catalytic reaction (see below).

Cyclohexanone, cyclohexanol, cyclooctanone, cyclooctanol, tetrahydrolinalool, tetrahydromyrcenol, n-hexanones, 1-decalone, 2-decalone, gem-dimethylcyclohexanones were purchased from Aldrich or TCI America.

For non-commercially available products, pure samples were synthesized, isolated and characterized following the experimental procedure described below or in the literature.<sup>2</sup>

In the oxidation of 4-methylvaleric acid product yields were determined by <sup>1</sup>H-NMR using mesitylene as internal standard: The internal standard was added to the crude mixture and the solvent was removed under reduced pressure. CDCl<sub>3</sub> was added and the sample was analyzed by <sup>1</sup>H-NMR.<sup>4</sup>

The ketones obtained from the oxidation of 1-bromo-3,7-dimethyloctane, 3,7-dimethyloctyl acetate and 3,7-dimethyloctyl pivalate were characterized by GC-MS.

#### **3.1.6.2. Reaction under catalytic conditions**

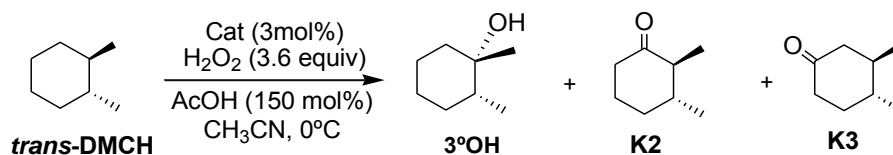
A 15 mL vial was charged with: Catalyst (1.5 μmol, 3 mol%), *cis*-4-methylcyclohexyl pivalate (50 μmol, 1 equiv), CH<sub>3</sub>CN (1 mL) and a magnetic stir bar. The vial was placed on an ice bath and stirred. A 1.74 M CH<sub>3</sub>CO<sub>2</sub>H solution in CH<sub>3</sub>CN was added (44 μL, 75 μmol, 150 mol%) and 120 μL of a 1.5 M (180 μmols, 3.6 equiv) H<sub>2</sub>O<sub>2</sub> solution (diluted from a 35% H<sub>2</sub>O<sub>2</sub> aqueous solution) were delivered by syringe pump over 30min at 0°C. After syringe pump addition, the solution was stirred for 10 min at 0°C.

An internal standard was added at this point. The iron complex was removed by passing the solution through a short path of silica followed by elution with 2 mL of AcOEt. Finally, the solution was subjected to GC analysis.

#### **3.1.6.3. Procedure for product isolation**

A 25 mL round bottom flask was charged with: catalyst (12 μmols, 3 mol%), alkane (0.4 mmol, 1 equiv), CH<sub>3</sub>CN (8 mL) and a magnetic stir bar. The mixture was placed on an ice bath and stirred. A 1.74 M CH<sub>3</sub>CO<sub>2</sub>H solution in CH<sub>3</sub>CN was added (0.35 mL, 0.6 mmol, 150 mol%) and 0.96 mL of a 1.5 M (1.4 mmols, 3.6 equiv.) H<sub>2</sub>O<sub>2</sub> solution (diluted from a 35% H<sub>2</sub>O<sub>2</sub> aqueous solution) was delivered by syringe pump over 30 min at 0°C. After syringe pump addition, the solution was stirred for 10 min at 0°C. The iron complex was removed by passing the solution

through a short path of silica followed by elution with 2 mL of AcOEt. Solvent was removed under reduced pressure and the resulting residue was purified by flash chromatography on silica gel.



**Scheme S4.** Catalytic oxidation of *trans*-dimethylcyclohexane.

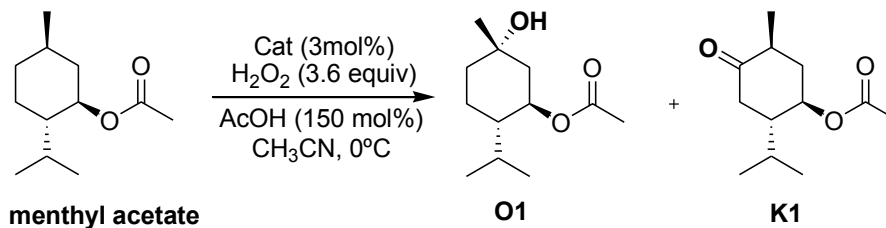
*trans*-dimethylcyclohexane (*trans*-DMCH):

Purification by flash chromatography over silica (hexane 100%).

**3°OH.**  $^1\text{H-NMR}$  (400 MHz,  $\text{CDCl}_3$ , 300 K)  $\delta$ , ppm: 1.69-1.63 (m, 2H), 1.54-1.48 (m, 2H) 1.46-1.20 (m, 5H), 1.18 (s, 3H), 0.90 (d,  $J = 6.5$  Hz, 3H). GC-MS ( $m/z$ ): 146.1  $[\text{M}+\text{NH}_4]^+$ .

**K2.**  $^1\text{H-NMR}$  (400 MHz,  $\text{CDCl}_3$ , 300 K)  $\delta$ , ppm: 2.42-2.36 (m, 1H), 2.29 (ddt,  $J_1 = 1.2$ ,  $J_2 = 5.9$ ,  $J_3 = 13.2$  Hz; 1H) 2.08-1.99 (m, 2H), 1.86-1.81 (m, 1H), 1.71-1.59 (m, 1H), 1.53-1.40 (m, 2H), 1.06 (d,  $J = 6.1$  Hz, 3H), 1.03 (d,  $J = 6.6$  Hz, 3H). GC-MS ( $m/z$ ): 144.1  $[\text{M}+\text{NH}_4]^+$ .

**K3.**  $^1\text{H-NMR}$  (400 MHz,  $\text{CDCl}_3$ , 300 K)  $\delta$ , ppm: 2.36-2.31 (m, 3H), 2.09-1.96 (m, 2H) 1.54-1.35 (m, 3H), 1.01 (d,  $J = 5.8$  Hz, 3H), 1.00 (d,  $J = 6.1$  Hz, 3H). GC-MS ( $m/z$ ): 144.1  $[\text{M}+\text{NH}_4]^+$ .



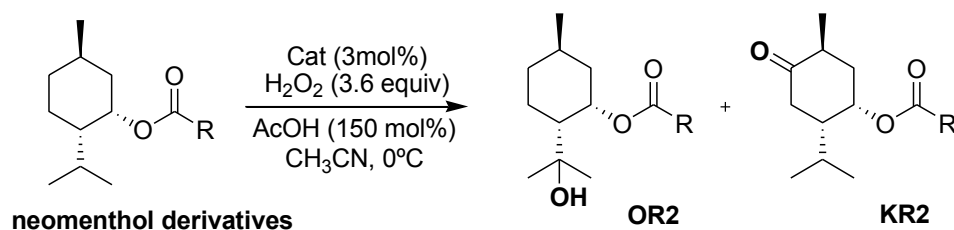
**Scheme S5.** Catalytic oxidation of menthol derivatives.

menthyl acetate:

Purification by flash chromatography over silica (hexane 100%).

**O1.**  $^1\text{H-NMR}$  (400 MHz,  $\text{CDCl}_3$ , 300 K)  $\delta$ , ppm: 5.03-4.96 (m, 1H), 2.07-2.00 (m, 1H) 2.03 (s, 3H), 1.93-1.85 (m, 1H), 1.71-1.65 (m, 1H), 1.55-1.32 (m, 5H), 1.24 (s, 3H), 0.92 (d,  $J = 7.0$  Hz, 3H), 0.80 (d,  $J = 7.1$  Hz, 3H). GC-MS ( $m/z$ ): 232.2  $[\text{M}+\text{NH}_4]^+$ .

**K1.**  $^1\text{H-NMR}$  (400 MHz,  $\text{CDCl}_3$ , 300 K)  $\delta$ , ppm: 5.11-5.03 (m, 1H), 2.58-2.47 (m, 1H) 2.39-2.30 (m, 2H), 2.21-2.11 (m, 1H), 2.08 (s, 3H), 1.99-1.87 (m, 2H), 1.47-1.36 (m, 1H), 1.03 (d,  $J = 6.6$  Hz, 3H), 0.89 (d,  $J = 6.7$  Hz, 3H), 0.83 (d,  $J = 6.7$  Hz, 3H). GC-MS ( $m/z$ ): 230.2  $[\text{M}+\text{NH}_4]^+$ .



**Scheme S6.** Catalytic oxidation of neomenthol derivatives.

neomenthyl acetate:

Purification by flash chromatography over silica (hexane 100%).

**OCH<sub>3</sub>2.** <sup>1</sup>H-NMR (400 MHz, CDCl<sub>3</sub>, 300 K) δ, ppm: 5.39-5.35 (m, 1H), 2.07 (s, 3H), 2.00-1.92 (m, 1H) 1.86-1.79 (m, 1H), 1.77-1.57 (m, 3H), 1.42-1.37 (m, 1H), 1.20 (s, 3H), 1.16 (s, 3H), 1.11-0.91 (m, 2H), 0.87 (d, J = 6.7 Hz, 3H). GC-MS (m/z): 232.1 [M+NH<sub>4</sub>]<sup>+</sup>.

**KCH<sub>3</sub>2.** <sup>1</sup>H-NMR (400 MHz, CDCl<sub>3</sub>, 300 K) δ, ppm: 5.34-3.32 (m, 1H), 2.70-2.59 (m, 1H), 2.54-2.40 (m, 2H), 2.38-2.30 (m, 1H), 2.13 (s, 3H), 1.69-1.46 (m, 3H), 1.01 (d, J = 6.4 Hz, 3H), 0.93 (d, J = 6.4 Hz, 3H), 0.89 (d, J = 6.5 Hz, 3H). GC-MS (m/z): 230.2 [M+NH<sub>4</sub>]<sup>+</sup>.

neomenthyl trifluoroacetate:

Purification by flash chromatography over silica (dichloromethane 100%).

**OCF<sub>3</sub>2.** <sup>1</sup>H-NMR (400 MHz, CDCl<sub>3</sub>, 300 K) δ, ppm: 5.62-5.59 (m, 1H), 2.08-2.02 (m, 1H) 1.90-1.84 (m, 1H), 1.79-1.61 (m, 3H), 1.53-1.48 (m, 1H), 1.22 (s, 3H), 1.19 (s, 3H), 1.07-0.90 (m, 2H), 0.90 (d, J = 6.6 Hz, 3H). GC-MS (m/z): 286.1 [M+NH<sub>4</sub>]<sup>+</sup>.

**KCF<sub>3</sub>2.** <sup>1</sup>H-NMR (400 MHz, CDCl<sub>3</sub>, 300 K) δ, ppm: 5.54 (m, 1H), 2.68-2.54 (m, 2H), 2.49-2.39 (m, 2H), 1.71-1.58 (m, 3H), 1.05 (d, J = 6.5 Hz, 3H), 0.95 (d, J = 6.4 Hz, 3H), 0.93 (d, J = 6.5 Hz, 3H). GC-MS (m/z): 284.1 [M+NH<sub>4</sub>]<sup>+</sup>.

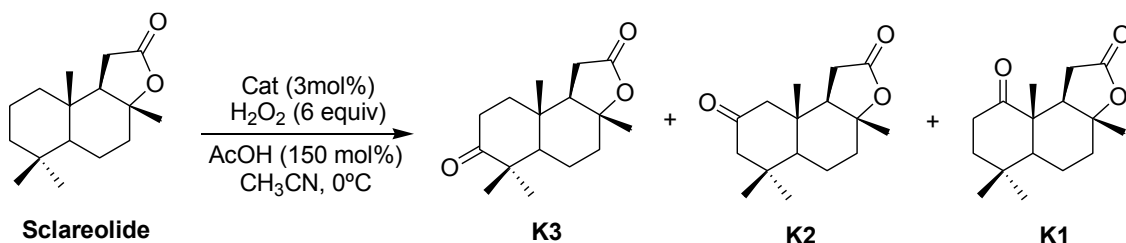
Neomenthyl pivalate:

Purification by flash chromatography over silica (hexane 100%).

**O<sup>t</sup>Bu2.** <sup>1</sup>H-NMR (400 MHz, CDCl<sub>3</sub>, 300 K) δ, ppm: 5.36-5.35 (m, 1H), 1.95-1.89 (m, 1H), 1.87-1.81 (m, 1H), 1.78-1.60 (m, 3H), 1.22 (s, 9H), 1.2 (s, 3H), 1.16 (s, 3H), 1.11-0.91 (m, 2H), 0.88 (d, J = 6.6 Hz, 3H). GC-MS (m/z): 274.3 [M+NH<sub>4</sub>]<sup>+</sup>.



**K<sup>t</sup>Bu2.** <sup>1</sup>H-NMR (400 MHz, CDCl<sub>3</sub>, 300 K) δ, ppm: 5.27 (m, 1H), 2.62-2.49 (m, 2H), 2.44-2.30 (m, 2H), 1.60-1.50 (m, 3H), 1.25 (s, 9H), 1.01 (d, J = 6.6 Hz, 3H), 0.92 (d, J = 6.9 Hz, 3H), 0.88 (d, J = 6.5 Hz, 3H). GC-MS (m/z): 272.3 [M+NH<sub>4</sub>]<sup>+</sup>.



**Scheme S7.** Catalytic oxidation of sclareolide.

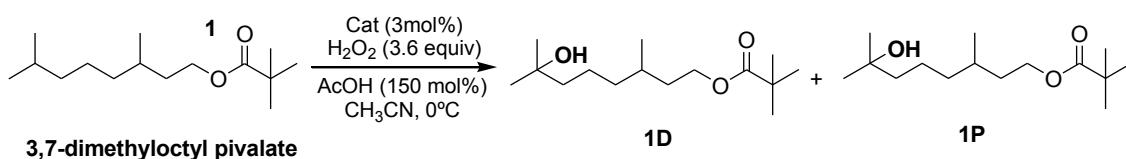
Sclareolide:

Purification by flash chromatography over silica (5% acetone/hexane).

**K1:** <sup>1</sup>H-NMR (400 MHz, CDCl<sub>3</sub>, 300 K) δ, ppm: 2.97 (dd, J = 17.0, 6.5 Hz, 1H), 2.68 (ddd, J = 15.7, 9.2, 5.1 Hz, 1H), 2.54 (dd, J = 17.0, 14.2 Hz, 1H), 2.29 (ddd, J = 15.7, 8.4, 5.0 Hz, 1H), 2.15 (dd, J = 14.2, 6.6 Hz, 1H), 2.09 (dd, J = 11.1, 2.7 Hz, 1H), 1.93-1.88 (m, 1H), 1.87-1.81 (m, 1H), 1.69 (dd, J = 9.2, 5.0 Hz, 1H), 1.66-1.62 (m, 1H), 1.58 (dd, J = 13.2, 3.1 Hz, 1H), 1.54-1.49 (m, 1H), 1.35 (s, 3H), 1.19 (s, 3H), 1.06 (s, 3H), 1.02 (s, 3H). In agreement with that reported in the literature.<sup>1</sup> GC-MS (m/z): 282.2 [M+NH<sub>4</sub>]<sup>+</sup>

**K2:** <sup>1</sup>H-NMR (400 MHz, CDCl<sub>3</sub>, 300 K) δ, ppm: 2.48-2.41 (m, 1H), 2.32-2.11 (m, 7H), 2.06-1.98 (m, 1H), 1.85-1.44 (m, 3H), 1.35 (s, 3H), 1.09 (s, 3H), 0.93 (s, 6H). In agreement with that reported in the literature.<sup>6</sup> GC-MS (m/z): 282.2 [M+NH<sub>4</sub>]<sup>+</sup>

**K3:** <sup>1</sup>H-NMR (400 MHz, CDCl<sub>3</sub>, 300 K) δ, ppm: 2.63-2.40 (m, 3H), 2.29 (ddd, J = 16.2, 6.5, 0.4 Hz, 1H), 2.14 (dt, J = 11.6, 3.0 Hz, 1H), 2.01 (dd, J = 14.7, 6.5 Hz, 1H), 1.87-1.82 (m, 1H), 1.78-1.70 (m, 2H), 1.65-1.53 (m, 3H), 1.39 (s, 3H), 1.13 (s, 3H), 1.06 (s, 3H), 1.03 (s, 3H). In agreement with that reported in the literature.<sup>6</sup> GC-MS (m/z): 282.2 [M+NH<sub>4</sub>]<sup>+</sup>



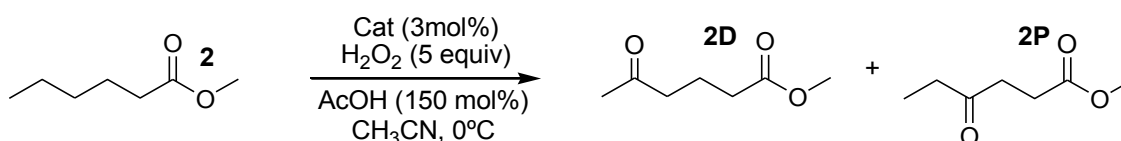
**Scheme S8.** Catalytic oxidation of 3,7-dimethyloctyl pivalate.

3,7-dimethyloctyl pivalate:

Purification by flash chromatography over silica (100% hexane).

**1D:**  $^1\text{H-NMR}$  (400 MHz,  $\text{CDCl}_3$ , 300 K)  $\delta$ , ppm: 4.12-4.06 (m, 2H), 1.70-1.64 (m, 2H), 1.58-1.40 (m, 7H), 1.22 (s, 6H), 1.19 (s, 9H), 0,92 (d,  $J = 6.5$  Hz, 3H). GC-MS (m/z): 276.1  $[\text{M}+\text{NH}_4]^+$ .

**1P:**  $^1\text{H-NMR}$  (400 MHz,  $\text{CDCl}_3$ , 300 K)  $\delta$ , ppm: 4.22 (t,  $J = 6.8$  Hz, 2H), 1.82 (tt,  $J = 6.8$  Hz,  $J' = 2.9$  Hz, 2H), 1.46-1.33 (m, 7H), 1.21 (s, 3H), 1.19 (s, 9H), 0,88 (d,  $J = 6.5$  Hz, 6H). GC-MS (m/z): 276.1  $[\text{M}+\text{NH}_4]^+$ .



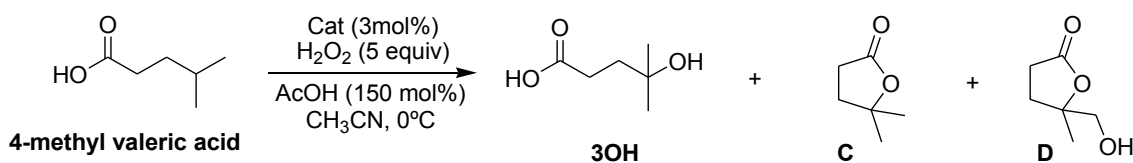
**Scheme S9.** Catalytic oxidation of methyl hexanoate.

Methylhexanoate:

Purification by flash chromatography over silica (100% hexane).

**2D:**  $^1\text{H-NMR}$  (400 MHz,  $\text{CDCl}_3$ , 300 K)  $\delta$ , ppm: 3.67 (s, 3H), 2.51 (t,  $J = 7.2$  Hz, 2H), 2.35 (t,  $J = 7.2$  Hz, 2H), 2.14 (s, 3H), 1.90 (p,  $J = 7.3$  Hz, 2H). In agreement with that reported in the literature.<sup>6</sup> GC-MS (m/z): 162.1  $[\text{M}+\text{NH}_4]^+$

**2P:**  $^1\text{H-NMR}$  (400 MHz,  $\text{CDCl}_3$ , 300 K)  $\delta$ , ppm: 3.68 (s, 3H), 2.73 (t,  $J = 6.5$  Hz, 2H), 2.60 (t,  $J = 6.6$  Hz, 2H), 2.48 (q,  $J = 7.2$  Hz, 2H), 1.08 (t,  $J = 7.2$  Hz, 3H). In agreement with that reported in the literature.<sup>6</sup> GC-MS (m/z): 162.1  $[\text{M}+\text{NH}_4]^+$ .



**Scheme S10.** Catalytic oxidation of 4-methyl valeric acid.

4-methylvaleric acid:

Purification by flash chromatography over silica (CH<sub>2</sub>Cl<sub>2</sub>:ethyl acetate 20:1 to ethyl acetate 100%).

**3OH:** <sup>1</sup>H-NMR (400 MHz, CDCl<sub>3</sub>, 300 K) δ, ppm: 2.50 (t, *J* = 7.6 Hz, 2H), 1.84 (t, *J* = 7.6 Hz, 2H), 1.25 (s, 6H). GC-MS (*m/z*): 150.1 [M+NH<sub>4</sub>]<sup>+</sup>

**C:** <sup>1</sup>H-NMR (400 MHz, CDCl<sub>3</sub>, 300 K) δ, ppm: 2.62 (t, *J* = 8.2 Hz, 2H), 2.06 (t, *J* = 8.2 Hz, 2H), 1.43 (s, 6H). In agreement with that reported in the literature.<sup>4</sup> GC-MS (*m/z*): 132.1 [M+NH<sub>4</sub>]<sup>+</sup>

**D:** <sup>1</sup>H-NMR (400 MHz, CDCl<sub>3</sub>, 300 K) δ, ppm: 3.72 (d, *J* = 12.1 Hz, 1H), 3.53 (d, *J* = 12.1 Hz, 1H), 2.76-2.52 (m, 3H), 2.40-2.31 (m, 1H), 1.93-1.89 (m, 1H), 1.37 (s, 3H). In agreement with that reported in the literature.<sup>4</sup> GC-MS (*m/z*): 148.1 [M+NH<sub>4</sub>]<sup>+</sup>

### 3.2. References

1. K. O. Suzuki, P. D.; Que Jr., L., *Angew. Chem. Int. Ed.* **2008**, *47*, 1887-1889.
2. L. Gomez, I. Garcia-Bosch, A. Company, B.-B. J., A. Polo, X. Sala, X. Ribas, M. Costas, *Angew. Chem. Int. Ed. Engl.* **2009**, *48*, 5720-5723.
3. A. Company, L. Gómez, X. Fontrodona, X. Ribas, M. Costas, *Chem. Eur. J.* **2008**, *14*, 5727-5731.
4. M. A. Bigi, S. A. Reed, M. C. White, *Nature Chemistry* **2011**, *3*, 216-222.
5. A. Cano, M. T. Ramirez-Apan, M. Delgado, *J. Braz. Chem. Soc.* **2011**, *22*, 1177-1182.
6. M. S. Chen, M. C. White, *Science* **2010**, *327*, 566-571.

## A.4. Supplementary Information Chapter VI

4.1. Experimental section.....	223
4.1.1. Materials .....	223
4.1.2. Instrumentation.....	223
4.1.3. Synthesis of substrates .....	223
4.1.4. Reaction conditions for catalysis .....	226
4.1.4.1. Sample analysis.....	226
4.1.4.2. Reaction catalytic conditions.....	227
4.1.4.3. Procedure for product isolation .....	227
4.1.4.4 Iterative addition protocol .....	237
4.2. References.....	239

### 4.1. Experimental section

#### 4.1.1. Materials

Reagents and solvents used were commercially available reagent quality unless otherwise stated. Solvents were purified and dried by passing through an activated alumina purification system. Acetonitrile for catalysis was HPLC grade. Preparation and handling of air-sensitive materials were carried out in a N<sub>2</sub> drybox with O<sub>2</sub> and H<sub>2</sub>O concentrations < 1 ppm. The preparation of the complexes **1**, **7**, **10**, **11** was previously described.<sup>1,2</sup>

#### 4.1.2. Instrumentation

NMR spectra were taken on a Bruker DPX 300 or 400 MHz spectrometer. Spectra were referenced to the residual proto solvents peaks or TMS (tetramethylsilane) for <sup>1</sup>H. Product analyses were performed on an Agilent 7820A gas chromatograph (HP5 column, 30m or Cyclosil-B column, 30 m) and a flame ionization detector. GC-MS spectral analyses were performed on an Agilent 7890A gas chromatograph interfaced with an Agilent 5975c MS mass spectrometer. A 50% NH<sub>3</sub>/CH<sub>4</sub> mix was used as the ionization gas for chemical ionization analyses. A Bruker microTOFQ Spectrometer was used for ESI-MS.

#### 4.1.3. Synthesis of substrates

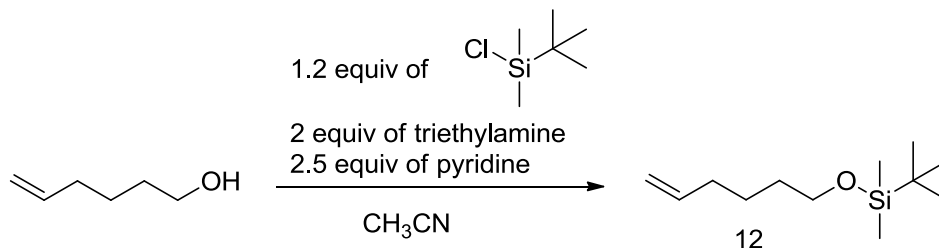
*cis*-ciclooctene (**1**), *cis*-2-octene (**2**), *trans*-2-octene (**3**), *trans*-4-octene (**4**), 1-hexene (**5**), 1-octene (**6**), 1-decene (**7**), 1-dodecene (**8**), 2-methyl-1-heptene (**9**), vinylcyclohexane (**10**), 2,3-dimethyl-2-butene (**11**), 1,5-cyclododecadiene-9,10-oxide (**13**), 5-norborene-2-yl (**16**), (2E,6Z)-

nona-2,6-dienyl (**20**), *cis,trans,trans*-1,5,9-cyclododecatriene (**19**), *cis*-jasmone (**21**) and pentenoic acid (**18**) were purchased from commercial resources.

5-hexene-1-ol, *cis*-6-nonen-1-ol and *cis*-3-nonen-1-ol were purchased from commercial resources.

1-*tert*-butyldimethylsilyloxy-5-hexene (**12**), *cis*-non-6-en-1-yl acetate (**14**), *cis*-non-3-en-1-yl acetate (**15**), *cis*-9-chloronon-3-ene (**17**) were synthesized as described below.

All liquid substrates were passed through an alumina plug before being used.



**Scheme S1.** Synthesis of 1-*tert*-butyldimethylsilyloxy-5-hexene (**12**).

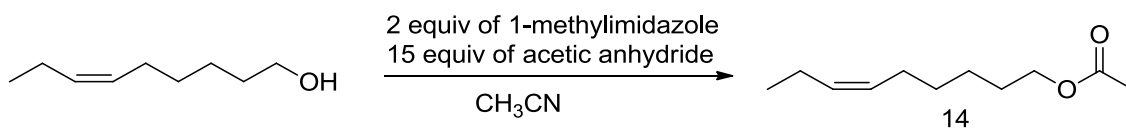
1-*tert*-butyldimethylsilyloxy-5-hexene (**12**) was prepared by reaction of *tert*-butylchlorodimethylsilane with the commercially available 5-hexene-1-ol, following the procedure described below (Scheme S1):

5-hexene-1-ol (2g, 19.6 mmol) was dissolved in 10 mL of acetonitrile, 4 mL of pyridine (50 mmol) and 6 mL of triethylamine were added and the solution was stirred during 5 min at room temperature. 1-*tert*-butyldimethylsilyloxy-5-hexene was added in small portions as a solid the mixture was stirred for 1 hour at room temperature and at 60°C overnight. The resulting residue was treated with  $\text{CHCl}_3$  (50 mL) and washed with water (30 mL), saturated  $\text{NaHCO}_3$  aqueous solution (30 mL) and saturated  $\text{NaCl}$  aqueous solution (30 mL). The organic phase was dried over  $\text{MgSO}_4$ , filtered and the solvent was removed under reduced pressure to yield a colorless liquid.

Purification by flash chromatography over silica (hexane : ethyl acetate (70% : 30%). 70% yield.

$^1\text{H-NMR}$  (400 MHz,  $\text{CDCl}_3$ , 300 K)  $\delta$ , ppm: 5.86-5.76 (m, 1H), 5.03-4.93 (m, 2H), 3.63-3.60 (t,  $J = 6.3$  Hz, 2H), 2.09-2.03 (m, 2H), 1.56-1.51 (m, 2H), 1.45-1.43 (m, 2H), 0.89 (s, 9H), 0.05 (s, 6H).

$^{13}\text{C-NMR}$  (75 MHz,  $\text{CDCl}_3$ , 300K)  $\delta$ , ppm: 138.93, 114.35, 63.07, 33.54, 32.30, 25.97, 25.15, 18.36, -5.29. HRMS TOF ( $m/z$ ) calcd for  $\text{C}_{12}\text{H}_{26}\text{OSi}+\text{H}$ , 215.1826; found, 215.1818. HRMS TOF ( $m/z$ ) calcd for  $\text{C}_{12}\text{H}_{26}\text{OSi}+\text{Na}$ , 237.1645; found, 237.1640.

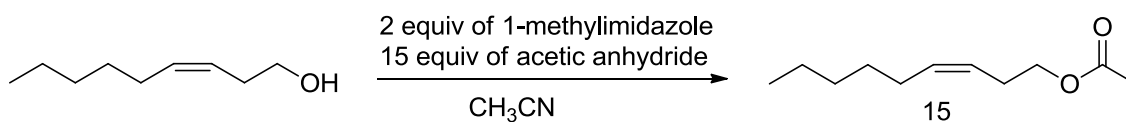


**Scheme S2.** Synthesis of *cis*-non-6-en-1-yl acetate (**14**).

*cis*-non-6-en-1-yl acetate (**14**) was prepared by acetylating the commercially available *cis*-6-nonen-1-ol, following the procedure described below (Scheme S2):

*cis*-6-nonen-1-ol (1.5g, 9.5 mmol), 1-methylimidazole (1.4 mL) and acetic anhydride (14 mL) were dissolved in CH<sub>3</sub>CN (25 mL) and stirred for 24 hours at room temperature. Ice (15 mL) was added at this point. After stirring for 15 min, CHCl<sub>3</sub> (40 mL) was added. The organic layer was washed with H<sub>2</sub>SO<sub>4</sub> 1 M (25 mL), saturated NaHCO<sub>3</sub> solution (25 mL) and a mixture of water (25 mL), dried over MgSO<sub>4</sub> and the solvent was removed under reduced pressure.

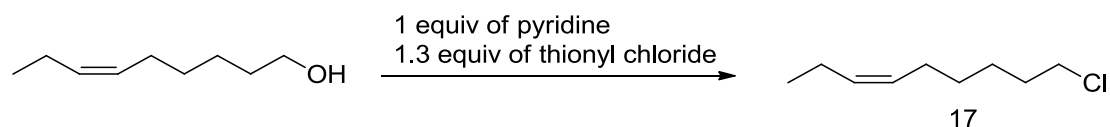
Purification over silica (hexane 100%). 57% yield. <sup>1</sup>H-NMR (400 MHz, CDCl<sub>3</sub>, 300 K) δ, ppm: 5.39-5.30 (m, 2H), 4.07-4.04 (t, J = 6.8 Hz, 2H), 2.05 (s, 3H), 2.04-2.01 (m, 4H), 1.65-1.61 (m, 2H), 1.38-1.35 (m, 4H), 0.98-0.94 (t, J = 7.5 Hz, 3H). <sup>13</sup>C-NMR (75 MHz, CDCl<sub>3</sub>, 300K) δ, ppm: 171.12, 133.01, 124.22, 63.99, 31.46, 29.25, 27.25, 26.79, 22.55, 20.98, 14.05. HRMS TOF (m/z) calcd for C<sub>11</sub>H<sub>20</sub>O<sub>2</sub>Na, 207.1356; found, 207.1360.



**Scheme S3.** Synthesis of *cis*-non-3-en-1-yl acetate (**15**).

*cis*-non-3-en-1-yl acetate (**15**) was prepared by acetylating the commercially available *cis*-3-nonen-1-ol, following the same procedure described before (Scheme S3)

Purification over silica (hexane 100%). 84% yield. <sup>1</sup>H-NMR (400 MHz, CDCl<sub>3</sub>, 300 K) δ, ppm: 5.54-5.48 (m, 1H), 5.37-5.31 (m, 1H), 4.08-4.04 (t, J = 7.0 Hz, 2H), 2.40-2.35 (m, 2H) 2.06-2.01 (m, 2H), 2.05 (s, 3H), 1.37-2.26 (m, 6H), 0.91-0.87 (t, J = 7.0 Hz, 3H). <sup>13</sup>C-NMR (75 MHz, CDCl<sub>3</sub>, 300K) δ, ppm: 171.12, 133.01, 124.22, 63.98, 31.46, 29.25, 27.25, 26.79, 22.55, 20.97, 14.04. HRMS TOF (m/z) calcd for C<sub>11</sub>H<sub>20</sub>O<sub>2</sub>Na, 207.1356; found, 207.1374.



**Scheme S4.** Synthesis of *cis*-9-chloronon-3-ene (**17**).

*cis*-9-chloronon-3-ene (**17**) was prepared by chlorination of the commercially available *cis*-6-nonen-1-ol, following the procedure described below (Scheme S4):

*cis*-6-nonen-1-ol (0.5g, 3.5 mmol) were dissolved in pyridine (0.3 mL), 0.33 mL of thionyl chloride (4.5 mmol) were added dropwise, the solution was stirred for 20 minutes at room temperature and then heated at 60°C for 5 hours. CHCl<sub>3</sub> (15 mL) was added. The organic layer was washed with HCl 2 M (10 mL), saturated NaHCO<sub>3</sub> solution (10 mL) and a mixture of water (10 mL), dried over MgSO<sub>4</sub> and the solvent was removed under reduced pressure.

Purification over silica (hexane 100%). 51% yield. <sup>1</sup>H-NMR (400 MHz, CDCl<sub>3</sub>, 300 K) δ, ppm: 5.41-5.30 (m, 2H), 3.55-3.52 (t, J = 6.8 Hz, 2H), 2.06-2.02 (m, 4H), 1.80-1.76 (m, 2H), 1.47-1.37 (m, 4H), 0.98-0.94 (t, J = 7.5 Hz, 3H). <sup>13</sup>C-NMR (75 MHz, CDCl<sub>3</sub>, 300K) δ, ppm: 131.97, 128.73, 45.12, 32.56, 29.00, 26.88, 26.51, 20.53, 14.37. GC-MS (m/z): 178.1 [M+NH<sub>4</sub>]<sup>+</sup>.

#### **4.1.4. Reaction conditions for catalysis**

##### **4.1.4.1. Sample analysis**

GC analysis of the catalysis provided substrate conversions and product yields relative to the internal standard integration. Calibration curves were obtained from commercial products when available or from pure isolated products obtained from a catalytic reaction (see below).

Cyclooctene oxide, *cis*-1,2-cyclooctandiol, 1,2-epoxyoctane, 1,2-octanediol, 1,2-epoxihexane, 1,2-hexanediol, 2,3-dimethylbutane-2,3-diol and 2,2,3,3-tetramethyloxirane were purchased from Aldrich or TCI America.

For non-commercially available products, pure samples were synthesized, isolated and characterized following the experimental procedure described below.

The epoxides and *syn*-diols products obtained from the oxidation of *cis*-2-octene, *trans*-2-octene, *trans*-4-octene, 2-methyl-1-heptene and vinylcyclohexane were characterized by GC-MS. The calibration curves used for these products were taken from those of 1,2-epoxyoctane and 1,2-octanediol, because they have the same empirical formula.

The calibration curves used for *syn*-diols products obtained from the oxidation of *cis*-non-6-en-1-yl acetate and *cis*-3-en-1-yl acetate were the obtained for (E)-6,7-dihydroxynon-2-ene-1-yl acetate products, because of the close similarity on their respective empirical formula.

#### 4.1.4.2. Reaction catalytic conditions

A 15 mL vial was charged with: Catalyst (1.5  $\mu\text{mol}$ , 3 mol%), alkene (50  $\mu\text{mol}$ , 1 equiv),  $\text{CH}_3\text{CN}$  (1.5 mL) and a magnetic stir bar. The vial was placed on an ice bath and stirred. 13.5  $\mu\text{L}$  of water were added (750  $\mu\text{mol}$ , 1500 mol%) and 143  $\mu\text{L}$  of a 700 mM (100  $\mu\text{mol}$ s, 2 equiv)  $\text{H}_2\text{O}_2$  solution (diluted from a 35%  $\text{H}_2\text{O}_2$  aqueous solution) were delivered by syringe pump over 15min at 0°C. After syringe pump addition, the solution was stirred for 30 min at 0°C.

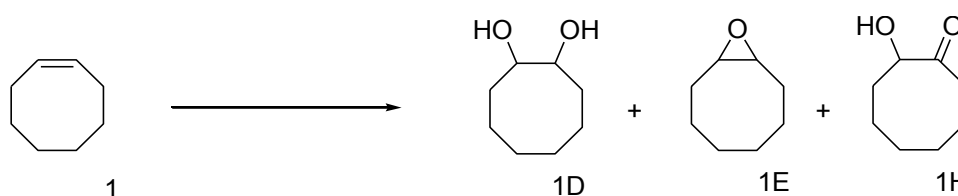
An internal standard was added at this point. The iron complex was removed by passing the solution through a short path of silica followed by elution with 2 mL of AcOEt. Finally, the solution was subjected to GC analysis.

The remaining sample was treated with acetic anhydride (1mL) together with 1-methylimidazole (0.1 mL), stirred for 15 minutes at r.t. to esterify the *syn*-diol product. Then 3 mL of ice were added and stirred for 10 minutes. Organic products were extracted with  $\text{CHCl}_3$  (2 mL). The organic layer was extracted and washed with  $\text{H}_2\text{SO}_4$  (2 mL, 1M), saturated aq.  $\text{Na}_2\text{CO}_3$  (2 mL) and water (2 mL). The organic layer was dried over  $\text{MgSO}_4$ , filtered and subjected to GC-MS analysis.

#### 4.1.4.3. Procedure for product isolation

A 25 mL round bottom flask was charged with: catalyst (12  $\mu\text{mol}$ s, 3 mol%), alkene (0.4 mmol, 1 equiv),  $\text{CH}_3\text{CN}$  (12 mL) and a magnetic stir bar. The mixture was placed on an ice bath and stirred. 110  $\mu\text{L}$  of water were added (6 mmol, 1500 mol%) and 1.14 mL of a 700 mM (0.8 mmols, 2 equiv.)  $\text{H}_2\text{O}_2$  solution (diluted from a 35%  $\text{H}_2\text{O}_2$  aqueous solution) was delivered by syringe pump over 15 min at 0°C. After syringe pump addition, the solution was stirred for 30 min at 0°C. The iron complex was removed by passing the solution through a short path of silica followed by elution with 2 mL of AcOEt. Solvent was removed under reduced pressure and the resulting residue was purified by flash chromatography on silica gel.

Purity of obtained products was checked by  $^1\text{H-NMR}$  and GC, and yields corrected based on this results.

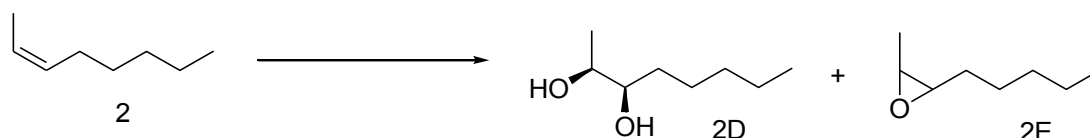


Scheme S5. Oxidation of *cis*-cyclooctene (2).



Cis-cyclooctene

**1H.**  $^1\text{H-NMR}$  (400 MHz,  $\text{CDCl}_3$ , 300 K)  $\delta$ , ppm: 4.20-4.17 (dd,  $J = 6.6$  Hz,  $J' = 2.8$  Hz, 1H), 2.75-2.68 (td,  $J = 12.2$  Hz,  $J' = 3.8$  Hz, 1H), 2.38-2.34 (m, 1H), 2.06-1.95 (m, 2H), 1.82-1.64 (m, 6H), 1.40-1.39 (m, 2H).  $^{13}\text{C-NMR}$  (100 MHz,  $\text{CDCl}_3$ , 300K)  $\delta$ , ppm: 217.52, 76.17, 37.26, 29.26, 28.61, 25.47, 24.45, 22.08. HRMS TOF ( $m/z$ ) calcd for  $\text{C}_8\text{H}_{14}\text{O}_2\text{Na}$ , 165.0886; found, 165.0895.

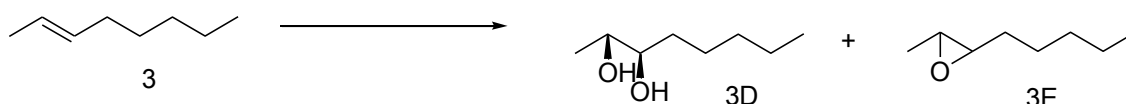


**Scheme S6.** Oxidation of *cis*-2-octene (**2**).

cis-2-octene

**2D.**  $^1\text{H-NMR}$  (400 MHz,  $\text{CDCl}_3$ , 300 K)  $\delta$ , ppm: 3.78-3.77 (m, 1H), 3.61 (m, 1H), 2.64-2.59 (m, 1H), 1.52-1.28 (m, 8H), 1.14-1.13 (d,  $J = 6.5$  Hz, 3H), 0.91-0.88 (t,  $J = 6.8$  Hz, 3H).  $^{13}\text{C-NMR}$  (100 MHz,  $\text{CDCl}_3$ , 300K)  $\delta$ , ppm: 74.95, 70.44, 31.87, 31.76, 25.73, 22.59, 16.47, 14.02. HRMS TOF ( $m/z$ ) calcd for  $\text{C}_8\text{H}_{18}\text{O}_2\text{Na}$ , 169.1199; found, 169.1208.

**2E.**  $^1\text{H-NMR}$  (400 MHz,  $\text{CDCl}_3$ , 300 K)  $\delta$ , ppm: 3.07-3.02 (m, 1H), 2.92-2.88 (m, 1H), 1.54-1.43 (m, 4H), 1.34-1.33 (d,  $J = 5.5$  Hz, 3H), 0.92-0.89 (t,  $J = 7.1$  Hz, 3H).  $^{13}\text{C-NMR}$  (100 MHz,  $\text{CDCl}_3$ , 300K)  $\delta$ , ppm: 57.14, 52.63, 31.68, 27.47, 26.11, 22.59, 13.97, 13.18. HRMS TOF ( $m/z$ ) calcd for  $\text{C}_8\text{H}_{16}\text{ONa}$ , 151.1093; found, 151.1116.



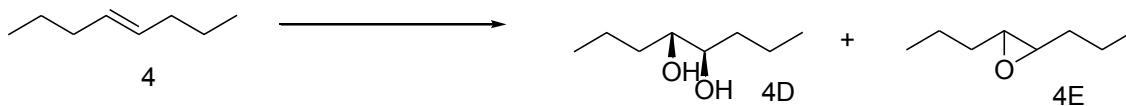
**Scheme S7.** Oxidation of *trans*-2-octene (**3**).

trans-2-octene

**3D.**  $^1\text{H-NMR}$  (400 MHz,  $\text{CDCl}_3$ , 300 K)  $\delta$ , ppm: 3.59-3.55 (m, 1H), 3.32-3.30 (m, 1H), 3.01 (bs, 2H), 1.50-1.47 (m, 2H), 1.39-1.30 (m, 6H), 1.18-1.17 (d,  $J = 6.9$  Hz, 3H), 0.91-0.88 (t,  $J = 6.9$  Hz, 3H).  $^{13}\text{C-NMR}$  (100 MHz,  $\text{CDCl}_3$ , 300K)  $\delta$ , ppm: 76.20, 70.88, 33.26, 31.87, 25.26, 22.59, 19.44, 14.01. HRMS TOF ( $m/z$ ) calcd for  $\text{C}_8\text{H}_{18}\text{O}_2\text{Na}$ , 169.1199; found, 169.1208. HRMS TOF ( $m/z$ ) calcd for  $(\text{C}_8\text{H}_{18}\text{O}_2)_2\text{Na}$ , 315.2506; found, 315.2505.

**3E.**  $^1\text{H-NMR}$  (400 MHz,  $\text{CDCl}_3$ , 300 K)  $\delta$ , ppm: 2.75-2.71 (m, 1H), 2.64-2.60 (m, 1H), 1.52-1.40 (m, 4H), 1.33-1.28 (m, 7H), 0.91-0.88 (t,  $J = 7.0$  Hz, 3H).  $^{13}\text{C-NMR}$  (100 MHz,  $\text{CDCl}_3$ , 300K)  $\delta$ , ppm: 59.79, 54.53, 31.97, 31.61, 25.64, 22.54, 17.63, 13.93. HRMS TOF ( $m/z$ ) calcd for

$C_8H_{16}ONa$ , 151.1093; found, 151.1111. HRMS TOF ( $m/z$ ) calcd for  $(C_8H_{16}O)_2Na$ , 315.2506; found, 315.2505.

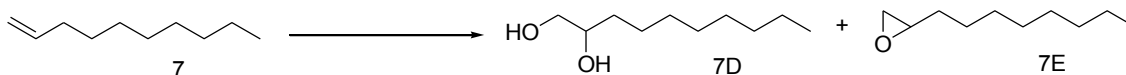


**Scheme S8.** Oxidation of *trans*-4-octene (4).

#### *trans*-4-octene

**4D.**  $^1H$ -NMR (400 MHz,  $CDCl_3$ , 300 K)  $\delta$ , ppm: 3.40-3.38 (m, 2H), 2.81 (bs, 2H), 1.52-1.38 (m, 8H), (t,  $J = 6.7$  Hz, 3H).  $^{13}C$ -NMR (100 MHz,  $CDCl_3$ , 300K)  $\delta$ , ppm: 74.25, 35.68, 18.85, 14.06. HRMS TOF ( $m/z$ ) calcd for  $C_8H_{18}O_2Na$ , 169.1199; found, 169.1208.

**4E.**  $^1H$ -NMR (400 MHz,  $CDCl_3$ , 300 K)  $\delta$ , ppm: 2.67-2.65 (m, 2H), 1.51-1.45 (m, 8H), 0.98-0.94 (t,  $J = 7.6$  Hz, 6H).  $^{13}C$ -NMR (75 MHz,  $CDCl_3$ , 300K)  $\delta$ , ppm: 58.58, 34.15, 19.31, 18.89. HRMS TOF ( $m/z$ ) calcd for  $C_8H_{16}ONa$ , 151.1093; found, 151.1104.



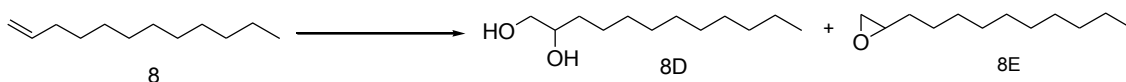
**Scheme S9.** Oxidation of 1-decene (7).

#### 1-decene

Purification by flash chromatography over silica (hexane : ethyl acetate (80% : 20%)).

**7D.**  $^1H$ -NMR (400 MHz,  $CDCl_3$ , 300 K)  $\delta$ , ppm: 3.72-3.71 (m, 1H), 3.68-3.65 (dd,  $J = 11.0$  Hz,  $J' = 3.0$  Hz, 1H), 3.46-3.42 (dd,  $J = 11.0$  Hz,  $J' = 7.5$  Hz, 1H), 1.44-1.43 (m, 2H), 1.28-1.26 (m, 12H), 0.90-0.86 (t,  $J = 6.7$  Hz, 3H).  $^{13}C$ -NMR (75 MHz,  $CDCl_3$ , 300K)  $\delta$ , ppm: 72.33, 66.87, 33.23, 31.86, 29.64, 29.50, 29.24, 25.53, 22.66, 14.1. HRMS TOF ( $m/z$ ) calcd for  $C_{10}H_{22}O_2Na$ , 197.1512; found, 197.1526.

**7E.**  $^1H$ -NMR (300 MHz,  $CDCl_3$ , 300 K)  $\delta$ , ppm: 2.93-2.89 (m, 1H), 2.76-2.73 (m, 1H), 2.48-2.45 (m, 1H), 1.54-1.44 (m, 4H), 1.36-1.27 (m, 10H), 0.90-0.86 (t,  $J = 6.5$  Hz, 3H).  $^{13}C$ -NMR (75 MHz,  $CDCl_3$ , 300K)  $\delta$ , ppm: 52.41, 47.13, 32.50, 31.85, 29.51, 29.44, 29.21, 25.97, 22.66, 14.09. HRMS TOF ( $m/z$ ) calcd for  $C_{10}H_{20}ONa$ , 179.1406; found, 179.1422. <sup>3</sup>



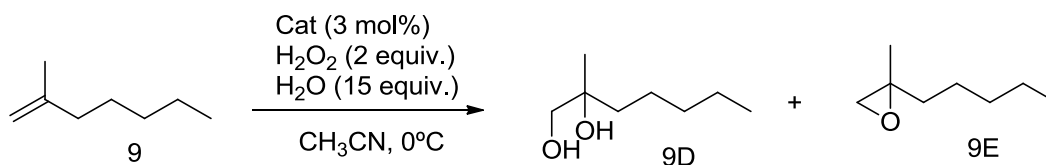
**Scheme S10.** Oxidation of 1-dodecene (8).

1-dodecene

Purification by flash chromatography over silica (hexane : ethyl acetate (80% : 20%)).

**8D.**  $^1\text{H-NMR}$  (400 MHz,  $\text{CDCl}_3$ , 300 K)  $\delta$ , ppm: 3.72-3.70 (m, 1H), 3.68-3.65 (dd,  $J = 11.0$  Hz,  $J' = 3.0$  Hz, 1H), 3.46-3.42 (dd,  $J = 11.0$  Hz,  $J' = 7.5$  Hz, 1H), 1.44-1.43 (m, 2H), 1.28-1.26 (m, 14H), 0.90-0.86 (t,  $J = 6.7$  Hz, 3H).  $^{13}\text{C-NMR}$  (75 MHz,  $\text{CDCl}_3$ , 300K)  $\delta$ , ppm: 72.33, 66.86, 33.21, 31.90, 29.64, 29.60, 29.58, 29.54, 29.32, 25.53, 22.68, 14.11. HRMS TOF ( $m/z$ ) calcd for  $\text{C}_{12}\text{H}_{26}\text{O}_2\text{Na}$ , 225.1825; found, 225.1831.

**8E.**  $^1\text{H-NMR}$  (300 MHz,  $\text{CDCl}_3$ , 300 K)  $\delta$ , ppm: 2.93-2.88 (m, 1H), 2.76-2.73 (m, 1H), 2.48-2.45 (m, 1H), 1.53-1.43 (m, 4H), 1.26 (s, 14H), 0.90-0.86 (t,  $J = 6.5$  Hz, 3H).  $^{13}\text{C-NMR}$  (75 MHz,  $\text{CDCl}_3$ , 300K)  $\delta$ , ppm: 52.43, 47.15, 32.50, 31.90, 29.60, 29.58, 29.56, 29.45, 29.33, 25.98, 22.68, 14.11. HRMS TOF ( $m/z$ ) calcd for  $\text{C}_{12}\text{H}_{26}\text{O}_2\text{Na}$ , 207.1719; found, 207.1723.<sup>3</sup>

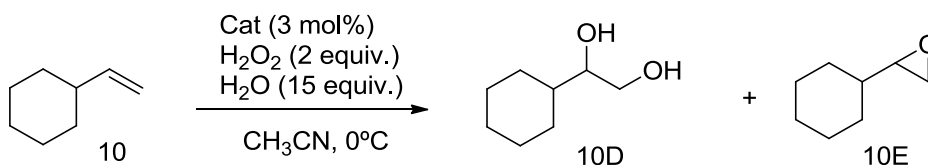


**Scheme S11.** Catalytic oxidation of 2-methyl-1-heptene (**9**).

2-methyl-1-heptene

**9D.**  $^1\text{H-NMR}$  (400 MHz,  $\text{CDCl}_3$ , 300 K)  $\delta$ , ppm: 3.49-3.45 (d,  $J = 10.8$ , 1H), 3.42-3.38 (d,  $J = 10.8$ , 1H), 1.48-1.45 (m, 2H), 1.33-1.29 (m, 6H), 1.16 (s, 3H), 0.92-0.87 (t,  $J = 6.5$  Hz, 3H).  $^{13}\text{C-NMR}$  (75 MHz,  $\text{CDCl}_3$ , 100K)  $\delta$ , ppm: 73.05, 69.74, 38.68, 32.41, 23.41, 23.17, 22.61, 14.03. HRMS TOF ( $m/z$ ) calcd for  $\text{C}_8\text{H}_{18}\text{O}_2\text{Na}$ , 169.1199; found, 169.1205.

**9E.**  $^1\text{H-NMR}$  (400 MHz,  $\text{CDCl}_3$ , 300 K)  $\delta$ , ppm: 2.54-2.52 (d,  $J = 5.1$  Hz, 1H), 2.50-2.48 (d,  $J = 5.1$  Hz, 1H), 1.53-1.29 (m, 4H), 0.84-0.82 (t,  $J = 6.6$ , 3H).  $^{13}\text{C-NMR}$  (75 MHz,  $\text{CDCl}_3$ , 100K)  $\delta$ , ppm: 56.97, 53.85, 36.68, 31.81, 24.88, 22.54, 20.83, 13.93. GC-MS ( $m/z$ ): 146.2  $[\text{M}+\text{NH}_4]^+$ .<sup>3</sup>

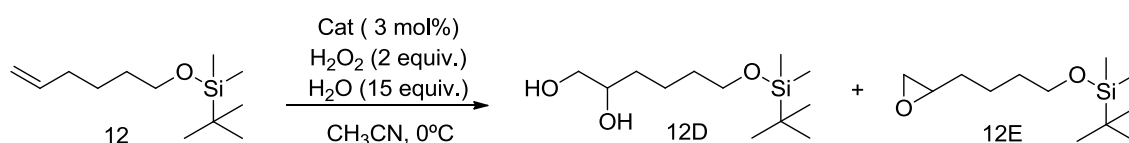


**Scheme S12.** Catalytic oxidation of vinylcyclohexane (**10**).

vinylcyclohexane

**10D.**  $^1\text{H-NMR}$  (400 MHz,  $\text{CDCl}_3$ , 300 K)  $\delta$ , ppm: 3.69-3.66 (m, 1H), 3.52-3.48 (m, 1H), 3.42 (sb, 1H), 1.88-1.84 (m, 1H), 1.77-1.72 (m, 2H), 1.68-1.62 (m, 2H), 1.40-1.01 (m, 6H).  $^{13}\text{C-NMR}$  (100 MHz,  $\text{CDCl}_3$ , 100K)  $\delta$ , ppm: 76.50, 64.75, 40.70, 28.98, 28.68, 26.38, 26.09, 26.00. HRMS TOF (m/z) calcd for  $\text{C}_8\text{H}_{16}\text{O}_2\text{Na}$ , 167.1043; found, 167.1047.

**10E.**  $^1\text{H-NMR}$  (400 MHz,  $\text{CDCl}_3$ , 300 K)  $\delta$ , ppm: 2.70-2.69 (m, 2H), 2.52-2.50 (m, 1H), 1.88-1.86 (m, 1H), 1.75-1.73 (m, 2H), 1.67-1.66 (m, 2H), 1.28-1.14 (m, 6H).  $^{13}\text{C-NMR}$  (100 MHz,  $\text{CDCl}_3$ , 100K)  $\delta$ , ppm: 56.60, 45.93, 40.35, 29.67, 28.78, 26.29, 25.67, 25.51. HRMS TOF (m/z) calcd for  $\text{C}_8\text{H}_{14}\text{ONa}$ , 149.0937; found, 149.0939.



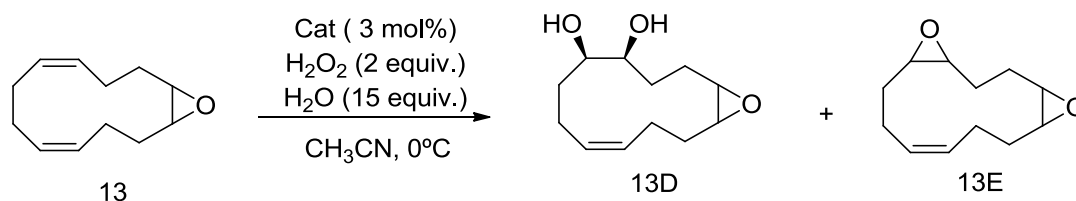
**Scheme S13.** Catalytic oxidation of 1-tert-butyltrimethylsilyloxy-5-hexene (**12**).

1-tert-butyltrimethylsilyloxy-5-hexene

Purification by flash chromatography over silica (hexane : ethyl acetate (80% : 20%).

**12D.**  $^1\text{H-NMR}$  (400 MHz,  $\text{CDCl}_3$ , 300 K)  $\delta$ , ppm: 3.75-3.70 (m, 2H), 3.64-3.61 (t,  $J = 6.2$  Hz, 2H), 3.47-3.42 (m, 1H), 1.57-1.52 (m, 2H), 1.49-1.45 (m, 4H), 0.89 (s, 9H), 0.05 (s, 6H).  $^{13}\text{C-NMR}$  (100 MHz,  $\text{CDCl}_3$ , 75K)  $\delta$ , ppm: 72.21, 66.81, 63.04, 32.85, 32.57, 25.97, 21.86, 18.37, -5.28. HRMS TOF (m/z) calcd for  $\text{C}_{12}\text{H}_{28}\text{O}_3\text{SiNa}$ , 271.1700; found, 271.1704. HRMS TOF (m/z) calcd for  $\text{C}_{12}\text{H}_{28}\text{O}_3\text{SiNa}_2$ , 519.3568; found, 519.3492.

**12E.**  $^1\text{H-NMR}$  (400 MHz,  $\text{CDCl}_3$ , 300 K)  $\delta$ , ppm: 3.64-3.60 (t,  $J = 6.1$  Hz, 2H), 2.93-2.90 (m, 1H), 2.77-2.74 (m, 1H), 2.48-2.46 (m, 1H), 1.57-1.53 (m, 6H), 0.89 (s, 9H), 0.05 (s, 6H).  $^{13}\text{C-NMR}$  (100 MHz,  $\text{CDCl}_3$ , 75K)  $\delta$ , ppm: 62.95, 52.34, 47.12, 32.56, 32.28, 25.98, 22.34, 18.37, -5.29. HRMS TOF (m/z) calcd for  $\text{C}_{12}\text{H}_{26}\text{O}_2\text{SiNa}$ , 253.1594; found, 253.1599.<sup>3</sup>



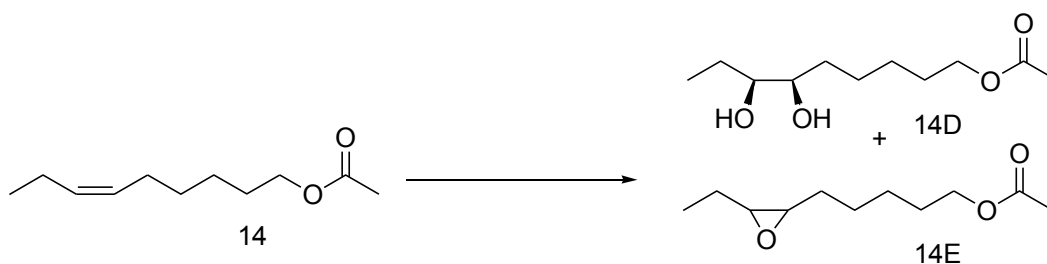
**Scheme S14.** Catalytic oxidation of dodecatriene epoxide (**13**).

dodecatriene epoxide

Purification by flash chromatography over silica (hexane 100%) and then (hexane : ethyl acetate (70% : 30%)).

**13D.**  $^1\text{H-NMR}$  (400 MHz,  $\text{CDCl}_3$ , 300 K)  $\delta$ , ppm: 5.37-5.27 (m, 2H), 3.89-3.84 (m, 2H), 2.81-2.77 (m, 1H), 2.51-2.49 (m, 1H), 2.37-2.31 (m, 2H), 2.18-1.87 (m, 6H), 1.61-1.56 (m, 2H), 1.45-1.39 (m, 2H), 1.05-0.99 (m, 2H).  $^{13}\text{C-NMR}$  (100 MHz,  $\text{CDCl}_3$ , 300K)  $\delta$ , ppm: 132.9, 129.9, 76.5, 69.3, 59.1, 58.3, 31.2, 30.9, 29.8, 28.0, 27.1, 23.6. HRMS TOF (m/z) calcd for  $\text{C}_{12}\text{H}_{20}\text{O}_3\text{Na}$ , 235.1305; found, 235.1307. HRMS TOF (m/z) calcd for  $(\text{C}_{12}\text{H}_{20}\text{O}_3)_2\text{Na}$ , 447.2717; found, 447.2694.

**13E.**  $^1\text{H-NMR}$  (400 MHz,  $\text{CDCl}_3$ , 300 K)  $\delta$ , ppm: 5.41-5.39 (m, 2H), 3.00-2.93 (m, 2H), 2.72-2.69 (d,  $J = 10.0$  Hz, 1H), 2.60-2.56 (d,  $J = 8.0$  Hz, 1H), 2.34-2.07 (m, 6H), 1.85-1.65 (m, 2H), 1.28-1.20 (m, 4H).  $^{13}\text{C-NMR}$  (100 MHz,  $\text{CDCl}_3$ , 300K)  $\delta$ , ppm: 130.09, 130.02, 77.37, 77.05, 76.74, 58.80, 58.73, 58.45, 57.83, 31.01, 29.22, 28.77, 27.59, 27.33, 22.22. HRMS TOF (m/z) calcd for  $\text{C}_{12}\text{H}_{18}\text{O}_2\text{Na}$ , 217.1199; found, 217.1208.

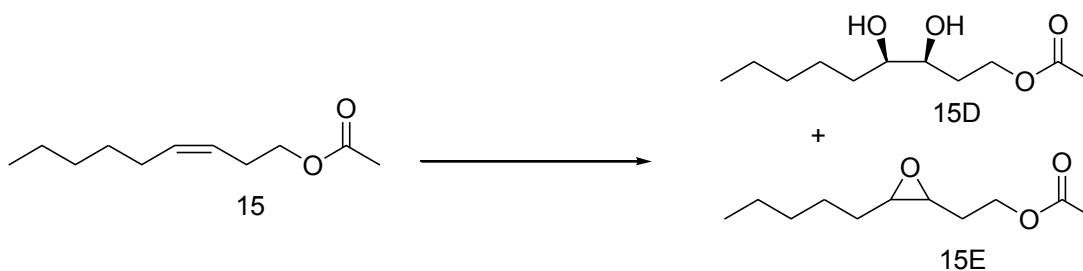


**Scheme S15.** Catalytic oxidation of *cis*-non-6-en-1-yl acetate (**14**).

*cis*-non-6-en-1-yl acetate

**14D.**  $^1\text{H-NMR}$  (300 MHz,  $\text{CDCl}_3$ , 300 K)  $\delta$ , ppm: 4.09-4.04 (t,  $J = 6.8$  Hz, 2H), 3.60 (m, 1H), 3.53-3.50 (m, 1H), 2.41 (bs, 2H), 2.05 (s, 3H), 1.67-1.62 (m, 2H), 1.48-1.38 (m, 8H), 1.02-0.97 (t,  $J = 7.6$  Hz, 3H).  $^{13}\text{C-NMR}$  (75 MHz,  $\text{CDCl}_3$ , 75K)  $\delta$ , ppm: 171.38, 76.23, 74.28, 64.49, 30.98, 28.52, 25.93, 25.64, 24.23, 21.00, 10.44. HRMS TOF (m/z) calcd for  $\text{C}_{11}\text{H}_{22}\text{O}_4\text{Na}$ , 241.1410; found, 241.1408.

**14E.**  $^1\text{H-NMR}$  (300 MHz,  $\text{CDCl}_3$ , 300 K)  $\delta$ , ppm: 4.09-4.05 (t,  $J = 6.6$  Hz, 2H), 2.91-2.85 (m, 2H), 2.05 (s, 3H), 1.68-1.47 (m, 10H), 1.07-1.02 (t,  $J = 7.6$  Hz, 3H).  $^{13}\text{C-NMR}$  (75 MHz,  $\text{CDCl}_3$ , 300K)  $\delta$ , ppm: 171.20, 64.39, 58.32, 57.14, 28.54, 27.58, 26.31, 25.86, 21.09, 20.99, 10.58. HRMS TOF (m/z) calcd for  $\text{C}_{11}\text{H}_{20}\text{O}_3\text{Na}$ , 223.1305; found, 223.1317. HRMS TOF (m/z) calcd for  $(\text{C}_{11}\text{H}_{20}\text{O}_3)_2\text{Na}$ , 423.2717; found, 423.2726.

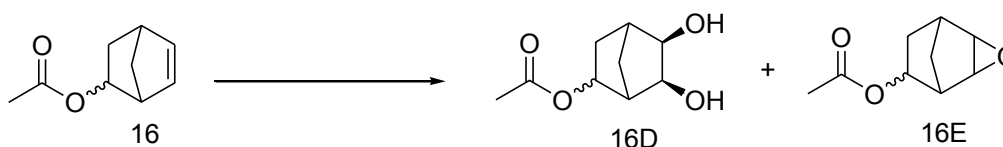


**Scheme S16.** Catalytic oxidation of *cis*-non-3-en-1-yl acetate (**15**).

#### *cis*-non-3-en-1-yl acetate

**15D.**  $^1\text{H-NMR}$  (300 MHz,  $\text{CDCl}_3$ , 300 K)  $\delta$ , ppm: 4.39-4.31 (m, 1H), 4.24-4.17 (m, 1H), 3.68-3.63 (m, 2H), 2.72 (bs, 1H), 2.28 (bs, 1H), 2.70 (s, 3H), 1.80-1.76 (m, 2H), 1.44-1.42 (m, 2H), 1.32-1.31 (m, 6H), 0.92-0.87 (t,  $J = 6.8$  Hz, 3H).  $^{13}\text{C-NMR}$  (75 MHz,  $\text{CDCl}_3$ , 300K)  $\delta$ , ppm: 171.60, 74.49, 71.24, 61.88, 31.82, 31.69, 30.14, 25.63, 22.57, 20.99, 14.01. HRMS TOF ( $m/z$ ) calcd for  $\text{C}_{11}\text{H}_{22}\text{O}_4\text{Na}$ , 241.1410; found, 241.1408. HRMS TOF ( $m/z$ ) calcd for  $(\text{C}_{11}\text{H}_{22}\text{O}_4)_2\text{Na}$ , 459.2928; found, 459.2939.

**15E.**  $^1\text{H-NMR}$  (300 MHz,  $\text{CDCl}_3$ , 300 K)  $\delta$ , ppm: 4.27-4.21 (m, 2H), 3.03-2.94 (m, 2H), 2.07 (s, 3H), 1.92-1.77 (m, 2H), 1.52-1.49 (m, 2H), 1.34-1.33 (m, 2H), 0.93-0.88 (t,  $J = 6.7$  Hz, 3H).  $^{13}\text{C-NMR}$  (75 MHz,  $\text{CDCl}_3$ , 300K)  $\delta$ , ppm: 170.93, 61.86, 56.83, 54.11, 31.64, 27.77, 27.46, 26.14, 22.54, 20.88, 13.94. HRMS TOF ( $m/z$ ) calcd for  $\text{C}_{11}\text{H}_{20}\text{O}_3\text{Na}$ , 223.1305; found, 223.1296. HRMS TOF ( $m/z$ ) calcd for  $(\text{C}_{11}\text{H}_{20}\text{O}_3)_2\text{Na}$ , 423.2717; found, 423.2718.



**Scheme S17.** Catalytic oxidation of 5-norbornene-2-yl acetate (**16**).

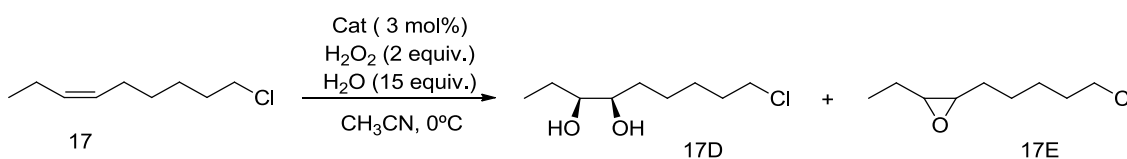
#### 5-norbornene-2-yl acetate

The substrate 5-norbornene-2-yl acetate is a mixture of endo and exo forms. The diol and epoxide products are obtained also as a mixture of endo and exo forms, and only the main product was described.

**16D.**  $^1\text{H-NMR}$  (400 MHz,  $\text{CDCl}_3$ , 400 K)  $\delta$ , ppm: 4.96-4.91 (m, 1H), 4.26-2.25 (m, 1H), 3.85-3.84 (m, 1H), 2.45-2.44 (m, 1H), 2.19-2.18 (m, 1H), 2.04 (s, 3H), 1.86-1.84 (m, 1H), 1.28-

1.24 (m, 1H), 0.93-0.87 (m, 2H).  $^{13}\text{C-NMR}$  (75 MHz,  $\text{CDCl}_3$ , 100K)  $\delta$ , ppm: 170.88, 74.16, 72.82, 68.56, 47.17, 43.41, 32.64, 30.85, 21.03. GC-MS (m/z), of the esterified diol: 288.1  $[\text{M}+\text{NH}_4]^+$ .

**16E.**  $^1\text{H-NMR}$  (400 MHz,  $\text{CDCl}_3$ , 400 K)  $\delta$ , ppm: 5.08-5.04 (m, 1H), 3.36-2.35 (m, 1H), 3.26-3.25 (m, 1H), 2.78-2.77 (m, 1H), 2.51-2.50 (m, 1H), 2.12-2.06 (m, 1H), 2.04 (s, 3H), 1.38-1.34 (m, 1H), 1.12-1.08 (m, 1H), 0.82-0.79 (m, 1H).  $^{13}\text{C-NMR}$  (75 MHz,  $\text{CDCl}_3$ , 100K)  $\delta$ , ppm: 170.97, 76.39, 50.95, 48.26, 40.35, 36.78, 32.96, 24.68, 20.99. HRMS TOF (m/z) calcd for  $\text{C}_9\text{H}_{12}\text{O}_3\text{Na}$ , 191.0679; found, 119.0685. HRMS TOF (m/z) calcd for  $\text{C}_9\text{H}_{12}\text{O}_3\text{H}_2\text{ONa}$ , 209.0784; found, 209.0792.



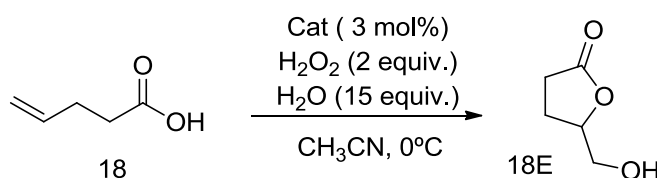
**Scheme S18.** Catalytic oxidation of *cis*-non-6-en-1-yl acetate (**17**).

#### *cis*-non-6-en-1-yl acetate

Purification by flash chromatography over silica (hexane 100%) and then (hexane : ethyl acetate (70% : 30%)).

**17D.**  $^1\text{H-NMR}$  (400 MHz,  $\text{CDCl}_3$ , 300 K)  $\delta$ , ppm: 3.63-3.59 (m, 1H), 3.56-3.53 (t,  $J = 6.7$  Hz, 2H), 3.53-3.50 (m, 1H), 1.81-1.78 (m, 2H), 1.56-1.44 (m, 8H), 1.01-0.97 (t,  $J = 7.5$  Hz, 3H).  $^{13}\text{C-NMR}$  (75 MHz,  $\text{CDCl}_3$ , 300K)  $\delta$ , ppm: 76.29, 74.31, 45.05, 32.51, 30.89, 26.89, 25.36, 24.20, 10.48. HRMS TOF (m/z) calcd for  $\text{C}_9\text{H}_{19}\text{O}_2\text{ClNa}$ , 217.0997; found, 217.0970.

**17E.**  $^1\text{H-NMR}$  (400 MHz,  $\text{CDCl}_3$ , 300 K)  $\delta$ , ppm: 3.56-5.53 (t,  $J = 6.7$  Hz, 2H), 2.92-2.86 (m, 2H), 1.82-1.79 (m, 2H), 1.60-1.48 (m, 8H), 1.06-1.03 (t,  $J = 7.5$  Hz, 3H).  $^{13}\text{C-NMR}$  (75 MHz,  $\text{CDCl}_3$ , 300K)  $\delta$ , ppm: 58.35, 57.13, 44.94, 32.50, 27.56, 26.78, 25.99, 21.11, 10.60. HRMS TOF (m/z) calcd for  $\text{C}_9\text{H}_{19}\text{O}_2\text{ClNa}$ , 217.0997; found, 217.0970. GC-MS (m/z): 194.1  $[\text{M}+\text{NH}_4]^+$ .

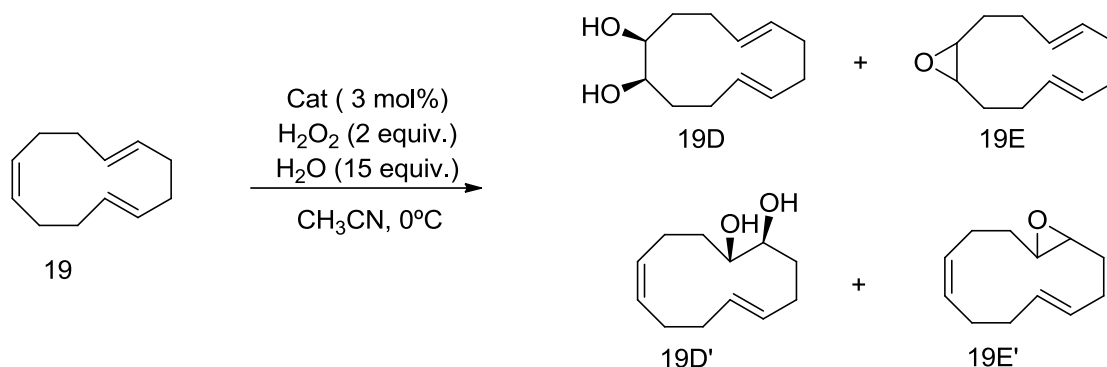


**Scheme S19.** Catalytic oxidation of pentenoic acid (**18**).

#### Pentenoic acid:

**18E.**  $^1\text{H-NMR}$  (400 MHz,  $\text{CDCl}_3$ , 300 K)  $\delta$ , ppm: 4.66-4.64 (m, 1H), 3.92-3.33 (dd,  $J = 12.6$  Hz,  $J' = 2.9$  Hz, 1H), 3.68-3.63 (dd,  $J = 12.6$  Hz,  $J' = 4.6$  Hz, 1H), 2.68-2.50 (m, 2H), 2.32-2.23 (m,

1H), 2.20-2.13 (m, 1H).  $^{13}\text{C-NMR}$  (100 MHz,  $\text{CDCl}_3$ , 300 K)  $\delta$ , ppm: 178.03, 80.98, 64.02, 28.71, 23.14. HRMS TOF (m/z) calcd for  $\text{C}_5\text{H}_8\text{O}_3\text{Na}$ , 139.0366; found, 139.0391.



**Scheme S20.** Catalytic oxidation of *trans-trans-cis*-dodecatriene (**19**).

*trans-trans-cis*-dodecatriene:

Purification by flash chromatography over silica (hexane 100%) and then (hexane : ethyl acetate (70% : 30%)).

**19D.**  $^1\text{H-NMR}$  (400 MHz,  $\text{CDCl}_3$ , 300 K)  $\delta$ , ppm: 5.25-5.19(m, 4H), 3.91-3.88 (m, 2H), 2.27-2.24 (m, 2H), 2.10-1.09 (m, 4H), 2.03-1.99 (m, 2H), 1.49-1.41 (m, 2H), 1.28-1.124 (m, 2H).  $^{13}\text{C-NMR}$  (75 MHz,  $\text{CDCl}_3$ , 300K)  $\delta$ , ppm: 133.00, 130.75, 31.64, 28.13. HRMS TOF (m/z) calcd for  $\text{C}_{12}\text{H}_{20}\text{O}_2\text{Na}$ , 219.1356; found, 219.1366. calcd for  $\text{C}_{12}\text{H}_{20}\text{O}_2\text{Na}_2$ , 415.2819; found, 415.2815.

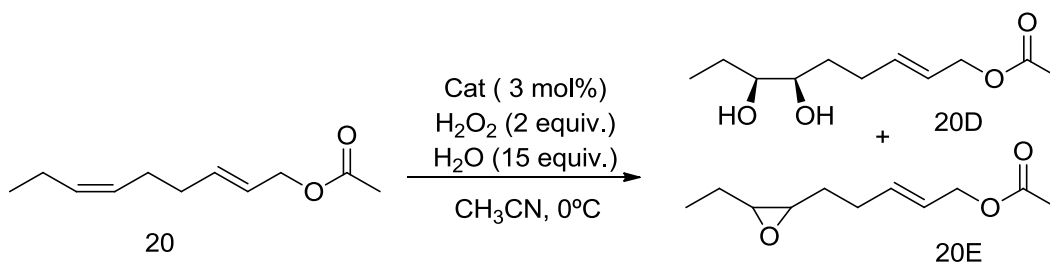
**19D'.**  $^1\text{H-NMR}$  (300 MHz,  $\text{CDCl}_3$ , 300 K)  $\delta$ , ppm: 5.39-5.22(m, 4H), 3.88-3.83 (m, 1H), 3.70-3.66 (m, 1H), 2.24-1.94 (m, 8H), 1.78-1.66 (m, 4H).  $^{13}\text{C-NMR}$  (75 MHz,  $\text{CDCl}_3$ , 300K)  $\delta$ , ppm: 132.34, 131.04, 129.1, 129.0, 68.76, 68.64, 32.80, 30.63, 28.97. HRMS TOF (m/z) calcd for  $\text{C}_{12}\text{H}_{20}\text{O}_2\text{Na}$ , 219.1356; found, 219.1366. calcd for  $\text{C}_{12}\text{H}_{20}\text{O}_2\text{Na}_2$ , 415.2819; found, 415.2814.

**19E'.**  $^1\text{H-NMR}$  (400 MHz,  $\text{CDCl}_3$ , 300 K)  $\delta$ , ppm: 5.38-5.26 (m, 4H), 2.77-2.74 (m, 1H), 2.54-2.51 (m, 1H), 2.24-2.04 (m, 10H), 1.19-1.10 (m, 2H).  $^{13}\text{C-NMR}$  (75 MHz,  $\text{CDCl}_3$ , 300K)  $\delta$ , ppm: 130.16, 130.112, 129.87, 128.90, 59.60, 58.89, 31.96, 31.93, 30.03, 28.31, 26.84, 23.52. HRMS TOF (m/z) calcd for  $\text{C}_{12}\text{H}_{18}\text{ONa}$ , 201.1250; found, 201.1254. HRMS TOF (m/z) calcd for  $(\text{C}_{12}\text{H}_{18}\text{O})_2\text{Na}$ , 379.2608; found, 379.2601.<sup>4</sup>

Epoxide **19E** was obtained as an unseparable mixture of epoxides, 19E : 19E' (1:1).

**19E.**  $^1\text{H-NMR}$  (400 MHz,  $\text{CDCl}_3$ , 300 K)  $\delta$ , ppm: 5.21-5.19 (m, 4H), 2.93-2.90 (m, 2H), 2.34-2.04 (m, 10H), 1.37-1.27 (m, 2H).  $^{13}\text{C-NMR}$  (75 MHz,  $\text{CDCl}_3$ , 300K)  $\delta$ , ppm: 132.81, 130.11, 129.87, 128.22, 59.61, 59.38, 31.93, 29.93, 29.88, 28.31, 26.96, 23.51. HRMS TOF (m/z) calcd for  $(\text{C}_{12}\text{H}_{18}\text{O})_2\text{Na}$ , 379.2608; found, 379.2601.<sup>4</sup>





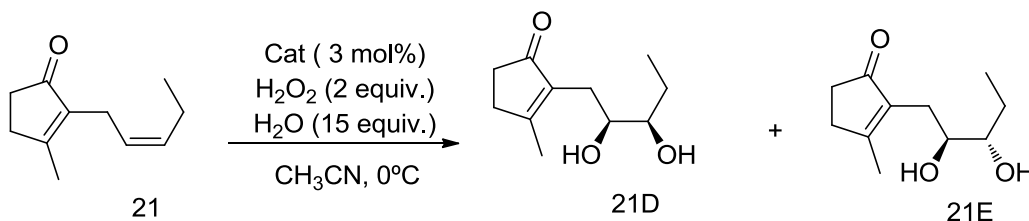
**Scheme S21.** Catalytic oxidation of (2E,6Z)-nona-2,6-dienyl acetate (**20**).

(2E,6Z)-nona-2,6-dienyl acetate

Purification by flash chromatography over silica (hexane : ethyl acetate 70% : 30%).

**20D.**  $^1\text{H-NMR}$  (300 MHz,  $\text{CDCl}_3$ , 300 K)  $\delta$ , ppm: 5.85-5.75 (m, 1H), 5.66-3.56 (m, 1H), 5.52-2.50 (d,  $J = 6.4$  Hz, 2H), 3.62-3.57 (m, 1H), 3.54-3.49 (m, 1H), 2.70 (bs, 2H), 2.34-2.25 (m, 1H), 2.19-2.12 (m, 1H), 2.06 (s, 3H), 1.58-1.42 (m, 4H), 1.01-0.96 (t,  $J = 7.3$  Hz, 3H).  $^{13}\text{C-NMR}$  (75 MHz,  $\text{CDCl}_3$ , 300K)  $\delta$ , ppm: 171.09, 135.81, 124.33, 76.66, 73.72, 65.20, 30.19, 28.73, 24.34, 21.02, 10.46. HRMS TOF ( $m/z$ ) calcd for  $\text{C}_{11}\text{H}_{20}\text{O}_4\text{Na}$ , 239.1254; found, 239.1269.

**20E.**  $^1\text{H-NMR}$  (300 MHz,  $\text{CDCl}_3$ , 300 K)  $\delta$ , ppm: 5.84-5.78 (m, 1H), 5.68-5.59 (m, 1H), 4.53-4.51 (d,  $J = 6.4$  Hz, 2H), 2.97-2.86 (m, 2H), 2.28-2.20 (m, 3H), 2.07 (s, 3H), 1.66-1.50 (m, 4H), 1.07-1.02 (t,  $J = 7.5$  Hz, 3H).  $^{13}\text{C-NMR}$  (75 MHz,  $\text{CDCl}_3$ , 300K)  $\delta$ , ppm: 170.86, 134.96, 124.68, 65.02, 58.41, 56.65, 29.31, 27.12, 21.11, 21.02, 10.59. HRMS TOF ( $m/z$ ) calcd for  $\text{C}_{11}\text{H}_{18}\text{O}_3\text{Na}$ , 221.1148; found, 221.1148.



**Scheme S22.** Catalytic oxidation of *cis*-jasmone (**21**).

*cis*-Jasmone:

Purification by flash chromatography over silica (hexane : ethyl acetate 70% : 30%).  
Diol products obtained as a mix of *trans* and *cis* diol (1:2).

**21D.**  $^1\text{H-NMR}$  (400 MHz,  $\text{CDCl}_3$ , 300 K)  $\delta$ , ppm: 3.59-3.58(m, 1H), 3.40-3.6 (m, 1H), 2.59-2.57 (m, 2H), 2.47-2.43 (m, 4H), 2.10 (s, 3H), 1.62-1.53 (m, 2H), 1.01-0.97 (t,  $J = 7.4$  Hz, 3H).  $^{13}\text{C-NMR}$  (100 MHz,  $\text{CDCl}_3$ , 300 K)  $\delta$ , ppm: 212.59, 174.79, 137.82, 75.33, 73.83, 34.17, 32.32, 26.07, 25.43, 17.56, 10.27. HRMS TOF ( $m/z$ ) calcd for  $\text{C}_{11}\text{H}_{18}\text{O}_3\text{Na}$ , 221.1148; found, 221.1165.

**21E.**  $^1\text{H-NMR}$  (400 MHz,  $\text{CDCl}_3$ , 300 K)  $\delta$ , ppm: 3.47-3.46 (m, 1H), 3.22-3.18 (m, 1H), 2.59-2.57 (m, 2H), 2.47-2.43 (m, 4H), 2.10 (s, 3H), 1.62-1.53 (m, 2H), 0.97-0.95 (t,  $J = 7.4$  Hz, 3H).  $^{13}\text{C-NMR}$  (100 MHz,  $\text{CDCl}_3$ , 300 K)  $\delta$ , ppm: 212.59, 174.79, 137.82, 74.57, 72.66, 34.17, 32.21, 26.21, 25.43, 17.46, 10.27. HRMS TOF ( $m/z$ ) calcd for  $\text{C}_{11}\text{H}_{18}\text{O}_3\text{Na}$ , 221.1148; found, 221.1165.

#### 4.1.4.4 Iterative addition protocol

Volatile substrates: *cis*-cyclohexene, 1-octene, *cis*-2-octene, *trans*-2-octene, 1-decene (2 additions).

A 5 mL vial was charged with: Catalyst (1.5  $\mu\text{mol}$ , 3 mol%), alkene (50  $\mu\text{mol}$ , 1 equiv),  $\text{CH}_3\text{CN}$  (1.5 mL) and a magnetic stir bar. The vial was placed on an ice bath and stirred. 13.5  $\mu\text{L}$  of water were added (750  $\mu\text{mol}$ , 1500 mol%) and 72  $\mu\text{L}$  of a 700 mM (100  $\mu\text{mol}$ s, 1 equiv)  $\text{H}_2\text{O}_2$  solution (diluted from a 35%  $\text{H}_2\text{O}_2$  aqueous solution) were delivered by syringe pump over 15 min at  $0^\circ\text{C}$ . After syringe pump addition, the solution was stirred for 10 min at  $0^\circ\text{C}$ . The solution was filtrate off through a plug of basic aluminum to remove the catalyst and the diol product and washed with 1 mL of  $\text{CH}_3\text{CN}$ . A new batch of catalyst (1.5  $\mu\text{mol}$ , 3 mol%) and 13.5  $\mu\text{L}$  of water were added to the eluent solution (which contains the substrate and the epoxide product), 72  $\mu\text{L}$  of a 700 mM (100  $\mu\text{mol}$ s, 1 equiv)  $\text{H}_2\text{O}_2$  solution were delivered via syringe pump over 15 min. After syringe pump addition the resulting solution was stirred for another 10 min.

An internal standard was added at this point. The iron complex was removed by passing the solution through a short path of silica followed by elution with 2 mL of  $\text{AcOEt}$ . Finally, the solution was subjected to GC analysis.

The basic aluminum plug which contains the syn-diol product formed in the first addition was treated with 2 mL of acid tartaric 1M solution to remove the syn-diol product. The aqueous phase was extracted several times with acetyl acetate, the standard was added at this point and the solution was subjected to GC analysis.

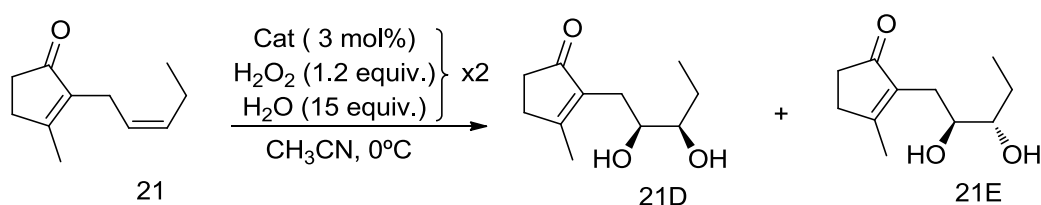
#### High molecular weight substrates:

A 25 mL round bottom flask was charged with: catalyst (12  $\mu\text{mol}$ s, 3 mol%), alkene (0.4 mmol, 1 equiv),  $\text{CH}_3\text{CN}$  (12 mL) and a magnetic stir bar. The mixture was placed on an ice bath and stirred. 110  $\mu\text{L}$  of water were added (6 mmol, 1500 mol%) and 0.69 mL of a 700 mM (0.45 mmols, 1.2 equiv.)  $\text{H}_2\text{O}_2$  solution (diluted from a 35%  $\text{H}_2\text{O}_2$  aqueous solution) was delivered by syringe over 15 min. After the syringe pump addition, the solution was stirred for 30 min at  $0^\circ\text{C}$ . At this point the solvent was removed and the substrate and products were purified by

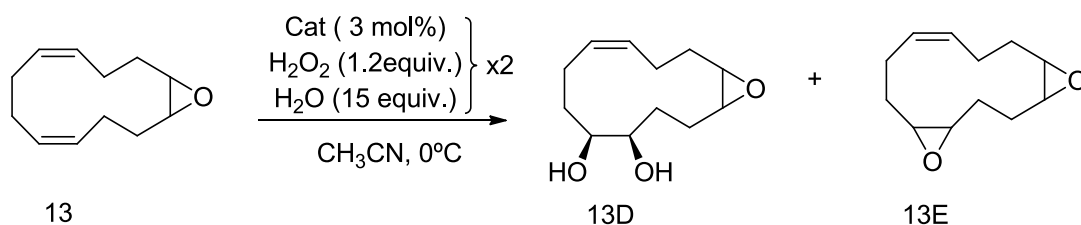
flash chromatography over silica. The products were quantified and the remained substrate was oxidized using the same catalytic conditions.

A solution of catalyst (3 mol%), CH<sub>3</sub>CN, H<sub>2</sub>O (15 equiv.) and the remained substrate (1 equiv.) was placed on an ice bath and stirred. 1.2 equiv. of a 700 mM H<sub>2</sub>O<sub>2</sub> solution (diluted from a 35% H<sub>2</sub>O<sub>2</sub> aqueous solution) was delivered by syringe over 15min. After the syringe pump addition, the solution was stirred for 30 min at 0°C. At this point the solvent was removed and the substrate and products were purified by chromatography over silica. The substrate and products were quantified as isolated yields. Purity of obtained products was checked by <sup>1</sup>H-NMR and GC, and yields corrected based on this results.

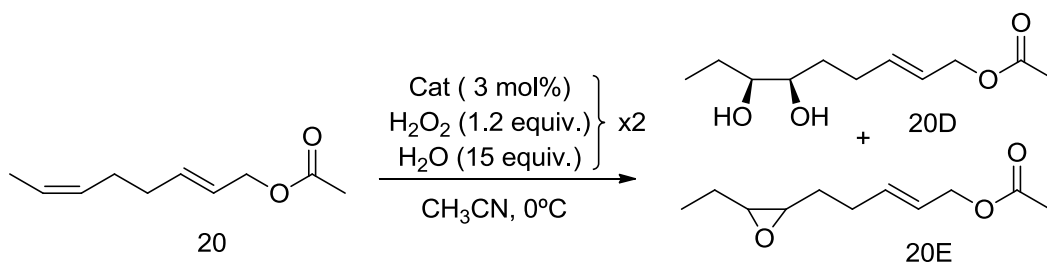
Isolated yields were obtained by 2 iterative additions.



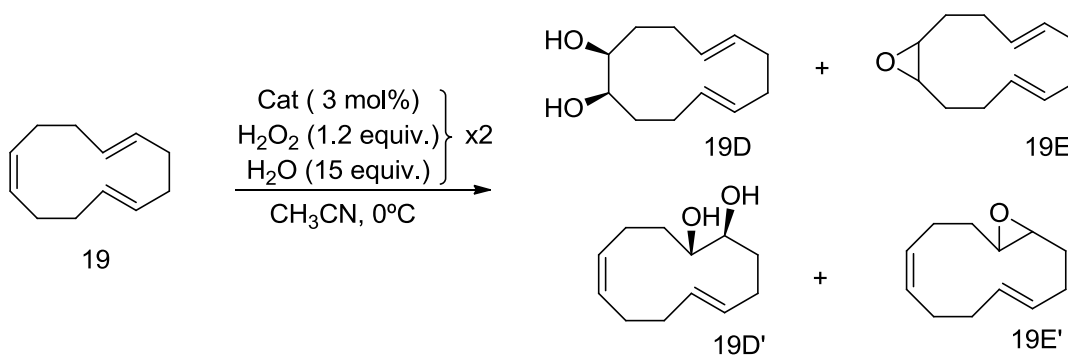
Addition	Conversion %	Yield D %	Yield E %	D/E	Total yield
First	65	35	4	8.1	39
Second	71	30	7	4.0	37
<b>Total</b>	<b>90</b>	<b>45</b>	<b>7</b>	<b>6.7</b>	<b>52</b>



Addition	Conversion %	Yield D %	Yield E %	D/E	Total yield
First	57	24	5		24
Second	86	29	5		29
<b>Total</b>	<b>94</b>	<b>36</b>	<b>5</b>		<b>36</b>



Addition	Conversion %	Yield D %	Yield E %	D/E	Total yield
First	69	44	13	3.4	57
Second	61	39	14	2.8	53
<b>Total</b>	<b>88</b>	<b>56</b>	<b>17</b>	<b>3.3</b>	<b>73</b>



Addition	Conversion %	Yield D %	Yield D' %	Yield E %	D/E	Total yield
First	72	30	9	16	2.4	55
Second	85	43	9	17	3.1	69
<b>Total</b>	<b>96</b>	<b>41</b>	<b>11</b>	<b>21</b>	<b>2.5</b>	<b>73</b>

## 4.2. References

- Company, A.; Gómez, L.; Fontrodona, X.; Ribas, X.; Costas, M., *Chem. Eur. J.* **2008**, *14*, 5727-5731.
- Company, A.; Gómez, L.; Güell, M.; Ribas, X.; Luis, J. M.; Que Jr., L.; Costas, M., *J. Am. Chem. Soc.* **2007**, *129*, 15766-15767.
- White, M. C.; Doyle, A. G.; Jacobsen, E. N., *J. Am. Chem. Soc.* **2001**, *123*, 7194-7195.
- Feng, Q.; Yuan, D.; Wang, D.; X., L.; Zhang, J.; Wu, J.; Chen, F., *Green and Sustainable Chemistry* **2011**, *1*, 63-69.



## A.5. Supplementary Information Chapter VII

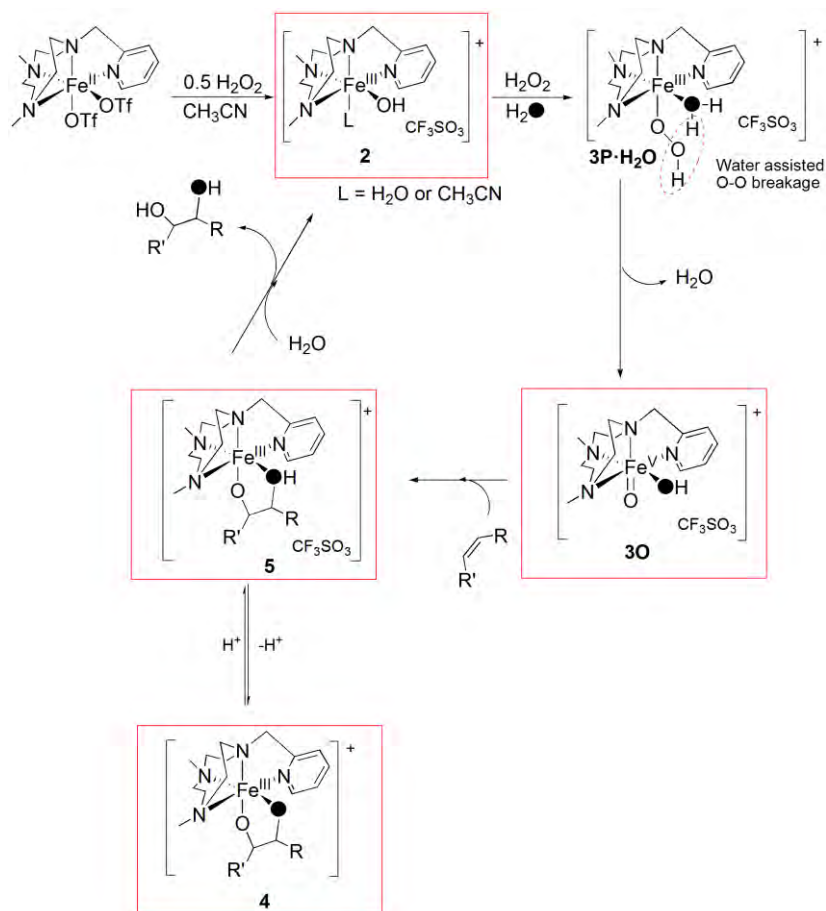
5.1. Instrumentation and synthetic details .....	241
5.2. Reaction scheme of the formation of $\{[\text{Fe}^{\text{V}}(\text{O})(\text{OH})(^{\text{Me,H}}\text{Pytacn})](\text{CF}_3\text{SO}_3)^+\}$ , 3O. ....	242
5.3. Mass spectral scheme of the formation of $\{[\text{Fe}^{\text{V}}(\text{O})(\text{OH})(^{\text{Me,H}}\text{Pytacn})](\text{CF}_3\text{SO}_3)^+\}$ , 3O.....	243
5.4. Explanation of calculated isotopic envelope patterns .....	243
5.5. VT-MS analysis of $\{[\text{Fe}^{\text{V}}(\text{O})(\text{OH})(^{\text{Me,H}}\text{Pytacn})](\text{CF}_3\text{SO}_3)^+\}$ , 3O, generated with $\text{H}_2\text{O}_2/\text{H}_2\text{O}$ from -40 °C to 20 °C.....	247
5.6. Full analysis of the isotopic envelope for dihydroxylation reaction with cyclooctene .....	250
5.7. Observation of $\{[\text{Fe}^{\text{III}}(\text{Cl})(\text{CF}_3\text{SO}_3)(^{\text{Me,H}}\text{Pytacn})]^+\}$ in the isotope distribution .....	251
5.8. Computational Details.....	252
5.9. References .....	261

### 5.1. Instrumentation and synthetic details

A Bruker microTOFQ Spectrometer with a cryospray attachment was used for ESI-MS and VT-MS. Samples were diluted to a maximum concentration of  $5 \times 10^{-5}$  M in acetonitrile and samples were injected at a rate of 180  $\mu\text{L}$  per hour.

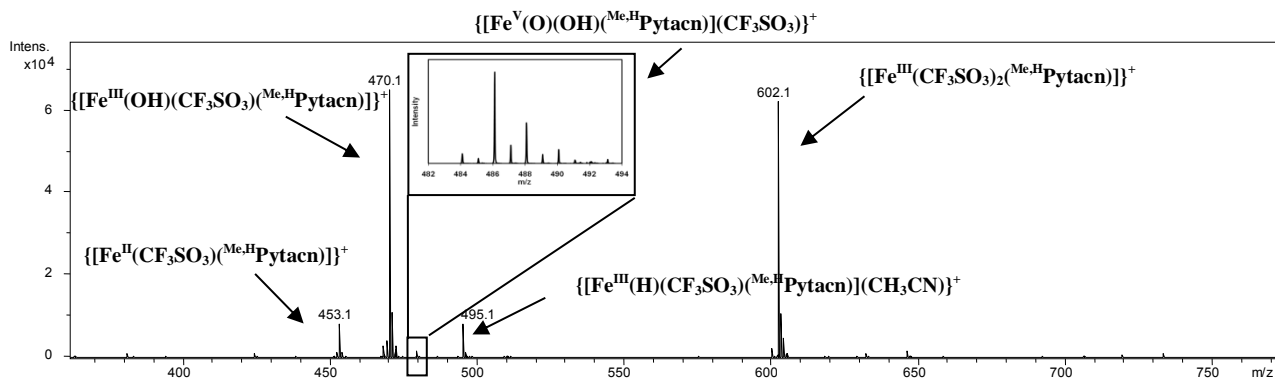
$[\text{Fe}(\text{CF}_3\text{SO}_3)_2(^{\text{Me,H}}\text{Pytacn})]$  (**1**) was prepared as previously described.<sup>1</sup>

## 5.2. Reaction scheme of the formation of

 $\{[\text{Fe}^{\text{V}}(\text{O})(\text{OH})(^{\text{Me,H}}\text{Pytacn})](\text{CF}_3\text{SO}_3)\}^+$ , **30**.


Supporting information **Figure S1**. Representation of the mechanistic scheme for the formation of the  $\text{Fe}^{\text{V}}=\text{O}$  compound  $\{[\text{Fe}^{\text{V}}(\text{O})(\text{OH})(^{\text{Me,H}}\text{Pytacn})](\text{CF}_3\text{SO}_3)\}^+$ , **30**, and the dihydroxylation reaction with cyclooctene. The boxed structures represent the species found in the mass spectrometry experiments.

## Full mass spectrum of the experimental reaction



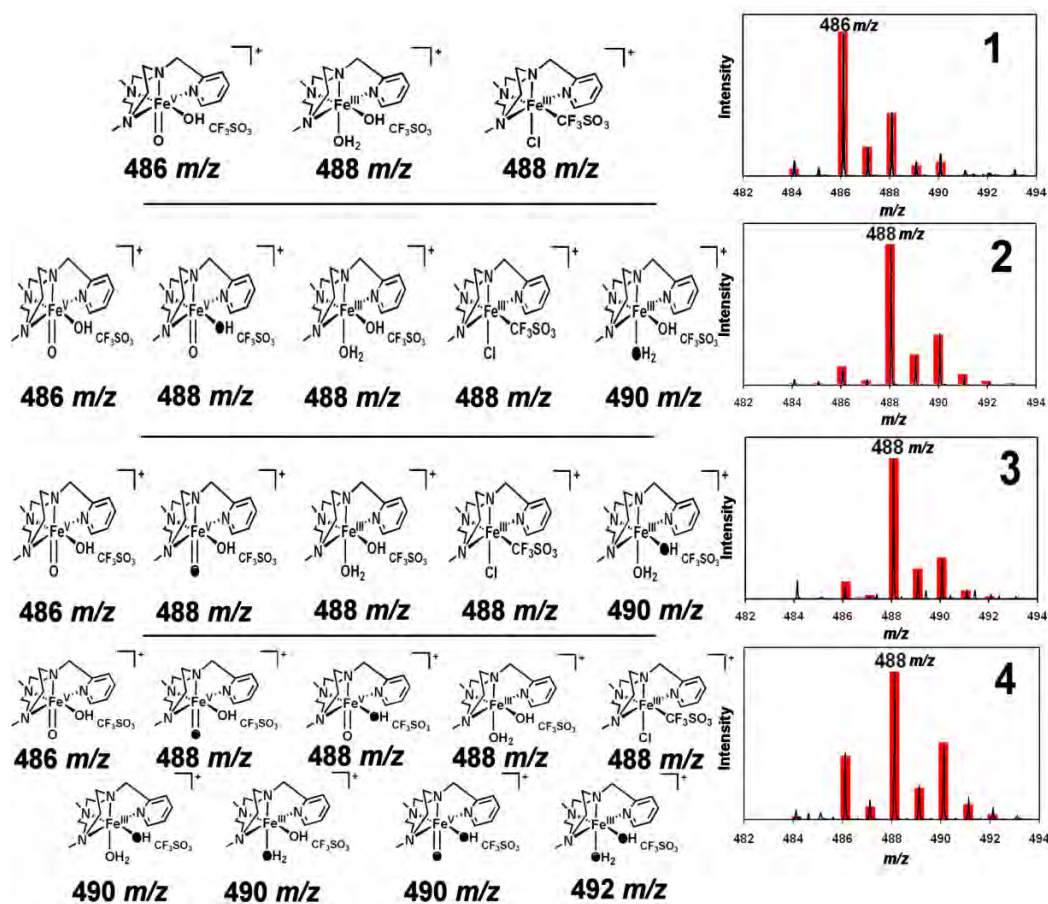
Supporting information **Figure S2**. Full VT-MS spectrum of the reaction mixture ( $[\text{Fe}(\text{CF}_3\text{SO}_3)_2(^{\text{Me,H}}\text{Pytacn})]$ , **1**, +  $\text{H}_2\text{O}$  (1000 equiv) +  $\text{H}_2\text{O}_2$  (100 equiv) in acetonitrile at  $-40^\circ\text{C}$ .



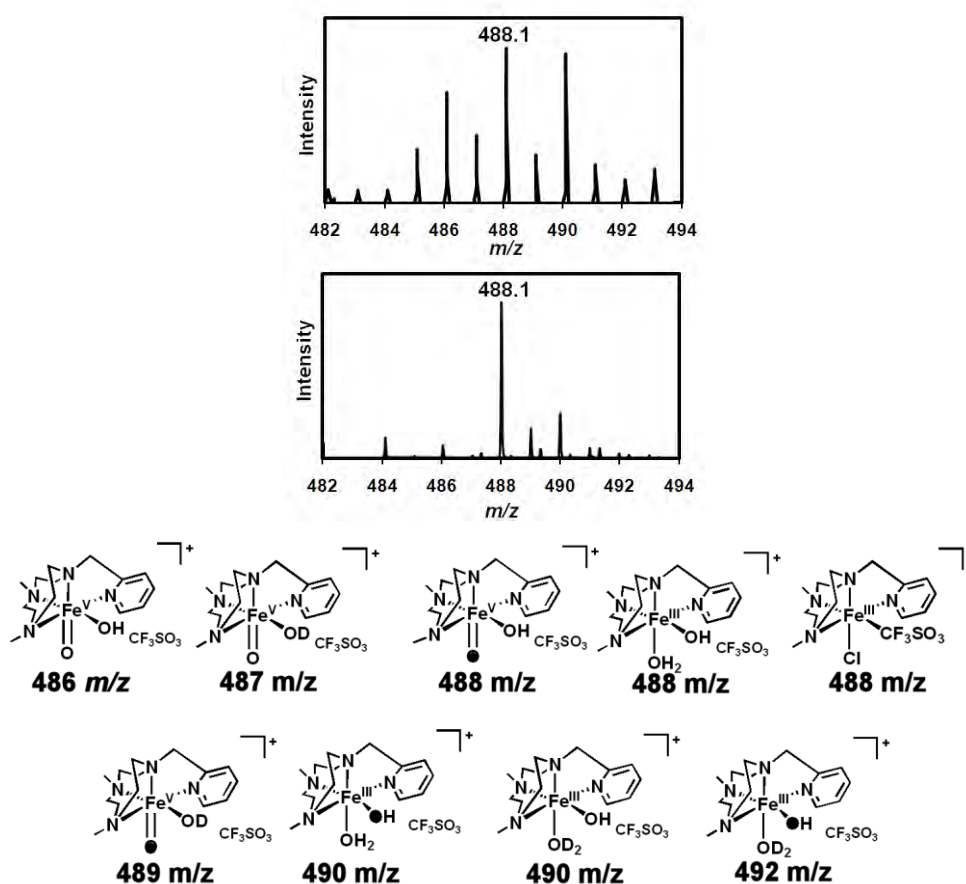


$\{[\text{Fe}^{\text{III}}(\text{OH})(\text{OH}_2)(^{\text{Me,H}}\text{Pytacn})](\text{CF}_3\text{SO}_3)\}^+$  (488  $m/z$ , 10 %) with an impurity of  $\{[\text{Fe}^{\text{III}}(\text{Cl})(\text{CF}_3\text{SO}_3)(^{\text{Me,H}}\text{Pytacn})]\}^+$  (488  $m/z$ , 27 %). This gives rise to the peak at 486  $m/z$  being the most intense as the peak at 486  $m/z$  was of the higher percentage (63 % overall). When  $\text{H}_2^{18}\text{O}$  was added (figure S4.2), the isotope envelope shifted by 2  $m/z$  units as expected but, as before, did not contain only one species. The envelope was made up from four different species: the unlabelled  $\{[\text{Fe}^{\text{V}}(\text{O})(\text{OH})(^{\text{Me,H}}\text{Pytacn})](\text{CF}_3\text{SO}_3)\}^+$  (486  $m/z$ , 5 %), the singly labelled  $\{[\text{Fe}^{\text{V}}(\text{O})(^{18}\text{OH})(^{\text{Me,H}}\text{Pytacn})](\text{CF}_3\text{SO}_3)\}^+$  (488  $m/z$ , 48 %), the unlabelled  $\{[\text{Fe}^{\text{III}}(\text{OH})(\text{OH}_2)(^{\text{Me,H}}\text{Pytacn})](\text{CF}_3\text{SO}_3)\}^+$  (488  $m/z$ , 8 %),  $\{[\text{Fe}^{\text{III}}(\text{Cl})(\text{CF}_3\text{SO}_3)(^{\text{Me,H}}\text{Pytacn})]\}^+$  (488  $m/z$ , 24 %) and the singly labelled  $\{[\text{Fe}^{\text{III}}(\text{OH})(^{18}\text{OH}_2)(^{\text{Me,H}}\text{Pytacn})](\text{CF}_3\text{SO}_3)\}^+$  (490  $m/z$ , 15 %). Statistics depict that since three out of five species (overall 80 %) have a  $m/z$  of 488 whilst one of five (5 %) has a  $m/z$  of 486 and the other one species (15%) has a  $m/z$  of 490 then the peak of highest intensity will be at 488  $m/z$  as it had the highest intensity percentage. Please note that the percentages given here are only estimated representations to show what peak should be of the highest intensity and not the exact amounts that are present in the actual envelope; the percentage of the peaks with the same  $m/z$  can be any percentage up to the total percentage for all 488  $m/z$  peaks i.e. it could be any combination of percentages that make up the overall percentage for that  $m/z$  value. When  $\text{H}_2^{18}\text{O}_2$  was added (figure S4.3) the isotopic envelope also shifted by 2  $m/z$  as with  $\text{H}_2^{18}\text{O}$  and also contains four species as before. The species present were the unlabelled  $\{[\text{Fe}^{\text{V}}(\text{O})(\text{OH})(^{\text{Me,H}}\text{Pytacn})](\text{CF}_3\text{SO}_3)\}^+$  (486  $m/z$ , 5 %), the singly labelled  $\{[\text{Fe}^{\text{V}}(^{18}\text{O})(\text{OH})(^{\text{Me,H}}\text{Pytacn})](\text{CF}_3\text{SO}_3)\}^+$  (488  $m/z$ , 50 %), the unlabelled  $\{[\text{Fe}^{\text{III}}(\text{OH})(\text{OH}_2)(^{\text{Me,H}}\text{Pytacn})](\text{CF}_3\text{SO}_3)\}^+$  (488  $m/z$ , 8 %),  $\{[\text{Fe}^{\text{III}}(\text{Cl})(\text{CF}_3\text{SO}_3)(^{\text{Me,H}}\text{Pytacn})]\}^+$  (488  $m/z$ , 27 %) and the singly labelled  $\{[\text{Fe}^{\text{III}}(^{18}\text{OH})(\text{OH}_2)(^{\text{Me,H}}\text{Pytacn})](\text{CF}_3\text{SO}_3)\}^+$  (490  $m/z$ , 10 %). As with  $\text{H}_2^{18}\text{O}$ , peak at 488  $m/z$  will have the highest intensity due to three of five species (85 %) having a  $m/z$  of 488 whilst one of five (5 %) has a  $m/z$  of 486 and the other one species (10 %) a  $m/z$  of 490. The peak of highest intensity will be at 488  $m/z$  in this case. When both  $\text{H}_2^{18}\text{O}$  and  $\text{H}_2^{18}\text{O}_2$  are added (figure S4.4) the peak should shift by 4  $m/z$  units with the peak of highest intensity being at 490  $m/z$ . This was not that case here though due to the higher percentage of peaks present in the envelope having a  $m/z$  of 488. The peaks present are the unlabelled  $\{[\text{Fe}^{\text{V}}(\text{O})(\text{OH})(^{\text{Me,H}}\text{Pytacn})](\text{CF}_3\text{SO}_3)\}^+$  (486  $m/z$ , 20 %), the singly labelled  $\{[\text{Fe}^{\text{V}}(^{18}\text{O})(\text{OH})(^{\text{Me,H}}\text{Pytacn})](\text{CF}_3\text{SO}_3)\}^+$  (488  $m/z$ , 17 %), the singly labelled  $\{[\text{Fe}^{\text{V}}(\text{O})(^{18}\text{OH})(^{\text{Me,H}}\text{Pytacn})](\text{CF}_3\text{SO}_3)\}^+$  (488  $m/z$ , 17 %), the unlabelled  $\{[\text{Fe}^{\text{III}}(\text{OH})(\text{OH}_2)(^{\text{Me,H}}\text{Pytacn})](\text{CF}_3\text{SO}_3)\}^+$  (488  $m/z$ , 17 %),  $\{[\text{Fe}^{\text{III}}(\text{Cl})(\text{CF}_3\text{SO}_3)(^{\text{Me,H}}\text{Pytacn})]\}^+$  (488  $m/z$ , 5 %), the singly labelled  $\{[\text{Fe}^{\text{III}}(\text{OH})(^{18}\text{OH}_2)(^{\text{Me,H}}\text{Pytacn})](\text{CF}_3\text{SO}_3)\}^+$  (490  $m/z$ , 1 %), the singly labelled  $\{[\text{Fe}^{\text{III}}(^{18}\text{OH})(\text{OH}_2)(^{\text{Me,H}}\text{Pytacn})](\text{CF}_3\text{SO}_3)\}^+$  (490  $m/z$ , 1 %), the doubly labelled  $\{[\text{Fe}^{\text{V}}(^{18}\text{O})(^{18}\text{OH})(^{\text{Me,H}}\text{Pytacn})](\text{CF}_3\text{SO}_3)\}^+$  (490  $m/z$ , 21 %), and the doubly labelled

$\{[\text{Fe}^{\text{III}}(^{18}\text{OH})(^{18}\text{OH}_2)(^{\text{Me,H}}\text{Pytacn})](\text{CF}_3\text{SO}_3)^+\}$  (492  $m/z$ , 1 %). The peak of highest intensity was that of 488  $m/z$  and not that of 490  $m/z$  was due to four out of nine species (56 % overall) has an  $m/z$  of 488 whilst one out of nine (20 %) has a  $m/z$  of 486, three out of nine (23 %) has a  $m/z$  of 490 and one out of nine (1 %) has a  $m/z$  of 492. Therefore the peak of highest intensity came at 488  $m/z$  and not 490  $m/z$  as calculated (see figure S4.4).



Supporting information **Figure S4**. Statistical representation of the species present in each isotopic envelope. (All calculated peaks fit the statistical treatment of experimental error).



Supporting information **Figure S5**. Top – Mass spectrum of  $[\text{Fe}(\text{CF}_3\text{SO}_3)_2(\text{Me,H})\text{Pytacn}]$  reacted with  $\text{D}_2\text{O}$  and  $\text{H}_2^{18}\text{O}_2$ ; Bottom: Mass spectrum of  $[\text{Fe}(\text{CF}_3\text{SO}_3)_2(\text{Me,H})\text{Pytacn}]$  reacted with  $\text{H}_2^{18}\text{O}_2$  and  $\text{H}_2^{18}\text{O}$ ; representation of the species present in the isotope envelop for  $[\text{Fe}(\text{CF}_3\text{SO}_3)_2(\text{Me,H})\text{Pytacn}]$  reacted with  $\text{D}_2\text{O}$  and  $\text{H}_2^{18}\text{O}_2$ .

Comparison between the two spectra shows that the envelope has changed shape with regards to the intensity of the peaks. When  $\text{D}_2\text{O} + \text{H}_2^{18}\text{O}_2$  were used the peak of highest intensity remained at 488  $m/z$  but this peak has decreased in intensity with respect to the other peaks in the envelope (figure S5, top). Consistent with the inclusion of D atoms in the molecular structure of the compounds, peaks at 487  $m/z$ , 489  $m/z$  and 490  $m/z$ , gain relative intensity, but straightforward analysis of the precise contribution of the multiple species that can be present, because of the multiple isotopic possibilities of this experiment, can not be done. Comparison of these spectra with these obtained with  $\text{H}_2\text{O}_2/\text{H}_2\text{O}$  (figure S4.1),  $\text{H}_2\text{O}_2/\text{H}_2^{18}\text{O}$  (figure S4.2), and  $\text{H}_2^{18}\text{O}_2/\text{H}_2\text{O}$  (figure S4.3) also indicates that the former experiments provide much more complex spectra, indicative of multiple ion content in the 482-492  $m/z$ . This most likely reflects that the peaks corresponding to the  $\text{Fe}^{\text{V}}$  species contribute in substantially smaller proportion to the overall shape of the spectra. A possible reason is that the use of  $\text{H}_2^{18}\text{O}_2$  (2% in  $\text{H}_2^{16}\text{O}$ ), implies that a substantially larger content of  $\text{H}_2\text{O}$  (with multiple isomers) is present in mixed labelling ( $\text{H}_2^{18}\text{O}_2 + \text{D}_2\text{O}$ , or  $\text{H}_2^{18}\text{O}_2 + \text{H}_2^{18}\text{O}$ ) experiments than in reactions where  $\text{H}_2^{16}\text{O}_2$  is used

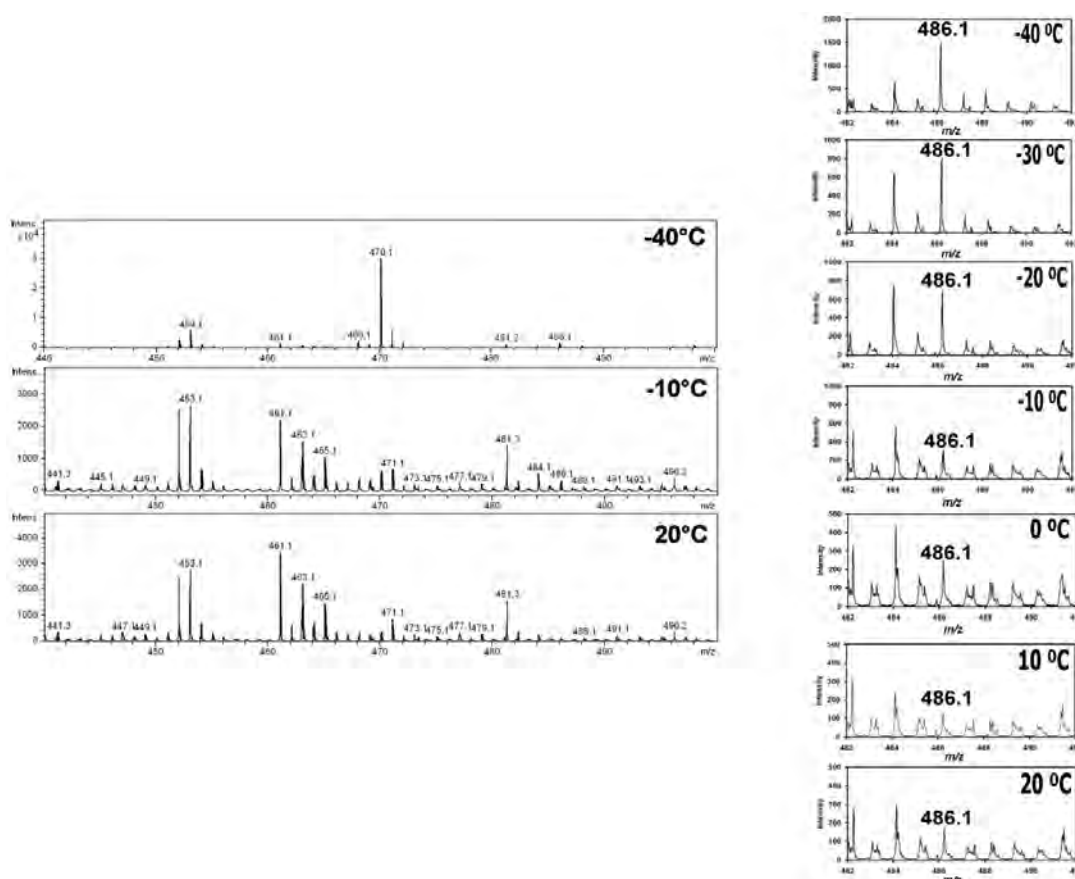
(H<sub>2</sub><sup>16</sup>O<sub>2</sub>+H<sub>2</sub><sup>18</sup>O), and this can have an impact on the chemistry and the relative stability of the species contributing to the spectra.

### 5.5. VT-MS analysis of $\{[\text{Fe}^{\text{V}}(\text{O})(\text{OH})(^{\text{Me,H}}\text{Pytacn})](\text{CF}_3\text{SO}_3)\}^+$ , **30**, generated with H<sub>2</sub>O<sub>2</sub>/H<sub>2</sub>O from -40 °C to 20 °C.

This experiment shows that the species at 486 *m/z* (Fe<sup>V</sup>=O) disappears as the time and temperature increase. (Figure S6).

#### Experimental: Procedure for mass spectrometry with isotopically abundant reagents.

[Fe(CF<sub>3</sub>SO<sub>3</sub>)<sub>2</sub>(<sup>Me,H</sup>Pytacn)] (**1**) (0.5 mg, 8 × 10<sup>-4</sup> mmols) was dissolved in MeCN (~ 7 ml) and the solution cooled to 4 °C. A solution of H<sub>2</sub>O<sub>2</sub> (10 mM in 10 ml MeCN) was made up and also cooled to 4 °C. The solution of **1** (300 μl) was added to a vial that was cooled in a dry ice/MeCN bath and H<sub>2</sub>O (15 μl, 0.83 mmols) added. To this stirring solution H<sub>2</sub>O<sub>2</sub> (300 μl, 3 × 10<sup>-3</sup> mmols) was added and the solution injected directly into the mass spectrometer (CSI-MS -40°C). The spectrum was collected immediately for 20 minutes. MS (CSI-MS) *m/z* 486.1.



Supporting information **Figure S6**. Observed chromatographs showing the 486 *m/z* ( $\{[\text{Fe}^{\text{V}}(\text{O})(\text{OH})(^{\text{Me,H}}\text{Pytacn})](\text{CF}_3\text{SO}_3)\}^+$ , **30**) species disappear with increasing temperature from -40 °C to 20 °C showing the intensity decrease from ca. 1500 in the top panel at -40 to ca. 200 in the bottom panel at 20 °C.

Time resolved mass spectrometry was also carried out with H<sub>2</sub><sup>18</sup>O and H<sub>2</sub><sup>16</sup>O<sub>2</sub> with this experiment showing the same trend as with the H<sub>2</sub><sup>16</sup>O and H<sub>2</sub><sup>16</sup>O<sub>2</sub> experiment where the peak  $\{[\text{Fe}^{\text{V}}(\text{O})(^{18}\text{OH})(^{\text{Me,H}}\text{Pytacn})](\text{CF}_3\text{SO}_3)\}^+$  (488.1 *m/z*) disappears with increasing time and temperature.

#### Procedure for mass spectrometry with isotopically labelled reagents.

$\{[\text{Fe}^{\text{V}}(\text{O})(^{18}\text{OH})(^{\text{Me,H}}\text{Pytacn})](\text{CF}_3\text{SO}_3)\}^+$  (**30a**).  $[\text{Fe}(\text{CF}_3\text{SO}_3)_2(^{\text{Me,H}}\text{Pytacn})]$  (**1**) (0.5 mg,  $8 \times 10^{-4}$  mmol) was dissolved in MeCN (~ 7 ml) and the solution cooled to 4 °C. A solution of H<sub>2</sub>O<sub>2</sub> (10 mM in 10 ml MeCN) was made up and also cooled to 4 °C. A solution of H<sub>2</sub>O<sub>2</sub> (650 mM in 10 ml MeCN) was made up and also cooled to 4 °C. The solution of **1** (300 µl) was added to a vial that was cooled in a dry ice/MeCN bath and H<sub>2</sub><sup>18</sup>O (15 µl, 0.83 mmol) added. To this stirring solution H<sub>2</sub>O<sub>2</sub> (300 µl,  $3 \times 10^{-3}$  mmol) was added and the solution injected directly into the mass spectrometer (CSI-MS -40°C). The spectrum was collected immediately for 2 minutes. MS (CSI-MS) *m/z* 488.1 (**30a**).

$\{[\text{Fe}^{\text{V}}(^{18}\text{O})(\text{OH})(^{\text{Me,H}}\text{Pytacn})](\text{CF}_3\text{SO}_3)\}^+$  (**30b**).  $[\text{Fe}(\text{CF}_3\text{SO}_3)_2(^{\text{Me,H}}\text{Pytacn})]$  (**1**) (0.5 mg,  $8 \times 10^{-4}$  mmol) was dissolved in MeCN (~ 7 ml) and the solution cooled to 4 °C. A solution of H<sub>2</sub><sup>18</sup>O<sub>2</sub> (10 mM in 10 ml MeCN) was made up and also cooled to 4 °C. The solution of **1** (300 µl) was added to a vial that was cooled in a dry ice/MeCN bath and H<sub>2</sub>O (15 µl, 0.83 mmol) added. To this stirring solution H<sub>2</sub><sup>18</sup>O<sub>2</sub> (300 µl,  $3 \times 10^{-3}$  mmol) was added and the solution injected directly into the mass spectrometer (CSI-MS -40°C). The spectrum was collected immediately for 2 minutes. MS (CSI-MS) *m/z* 488.1 (**30b**).

$\{[\text{Fe}^{\text{V}}(^{18}\text{O})(^{18}\text{OH})(^{\text{Me,H}}\text{Pytacn})](\text{CF}_3\text{SO}_3)\}^+$  (**30c**).  $[\text{Fe}(\text{CF}_3\text{SO}_3)_2(^{\text{Me,H}}\text{Pytacn})]$  (**1**) (0.5 mg,  $8 \times 10^{-4}$  mmol) was dissolved in MeCN (~ 7 ml) and the solution cooled to 4 °C. A solution of H<sub>2</sub><sup>18</sup>O<sub>2</sub> (10 mM in 10 ml MeCN) was made up and also cooled to 4 °C. The solution of **1** (300 µl) was added to a vial that was cooled in a dry ice/MeCN bath and H<sub>2</sub><sup>18</sup>O (15 µl, 0.83 mmol) added. To this stirring solution H<sub>2</sub><sup>18</sup>O<sub>2</sub> (300 µl,  $3 \times 10^{-3}$  mmol) was added and the solution injected directly into the mass spectrometer (CSI-MS -40°C). The spectrum was collected immediately for 2 minutes. MS (CSI(idem)-MS) *m/z* 490.1 (**30c**).

$[\text{Fe}^{\text{III}}(\text{C}_8\text{H}_{14}\text{O}_2)(^{\text{Me,H}}\text{Pytacn})]^+$  (**4**),  $\{[\text{Fe}^{\text{III}}(\text{C}_8\text{H}_{14}(\text{O})(\text{OH}))(^{\text{Me,H}}\text{Pytacn})](\text{CF}_3\text{SO}_3)\}^+$  (**5**) (where **5** stands for **(4)+H<sup>+</sup>+CF<sub>3</sub>SO<sub>3</sub>**).

$[\text{Fe}(\text{CF}_3\text{SO}_3)_2(^{\text{Me,H}}\text{Pytacn})]$  (**1**) (0.5 mg,  $8 \times 10^{-4}$  mmol) was dissolved in MeCN (~ 7 ml) and the solution cooled to 4 °C. A solution of H<sub>2</sub>O<sub>2</sub> (10 mM on 10 ml MeCN) was made up and also

cooled to 4 °C. The solution of **1** (300 µl) was added to a vial that was cooled in a dry ice/MeCN bath and H<sub>2</sub>O (15 µl, 0.83 mmol) added. To this stirring solution H<sub>2</sub>O<sub>2</sub> (300 µl, 3 x 10<sup>-3</sup> mmol) and cyclooctene (10 µl, 0.08 mmol) were added and the solution injected directly into the mass spectrometer (ESI-MS). The spectrum was collected for 2 mins. MS (ESI(idem)-MS) *m/z* 446.2 (**4**), 596.2 (**5**).

**[Fe<sup>III</sup>(C<sub>8</sub>H<sub>14</sub>O(<sup>18</sup>O))(<sup>Me,H</sup>Pytacn)]<sup>+</sup> (**4a**), {[Fe<sup>III</sup>(C<sub>8</sub>H<sub>14</sub>(O)(<sup>18</sup>OH))(<sup>Me,H</sup>Pytacn)](CF<sub>3</sub>SO<sub>3</sub>)<sup>+</sup> (**5a**)** (where **5a** stands for **(4a)+H<sup>+</sup>+CF<sub>3</sub>SO<sub>3</sub>**).

[Fe(CF<sub>3</sub>SO<sub>3</sub>)<sub>2</sub>(<sup>Me,H</sup>Pytacn)] (**1**) (0.5 mg, 8 x 10<sup>-4</sup> mmol) was dissolved in MeCN (~ 7 ml) and the solution cooled to 4 °C. A solution of H<sub>2</sub>O<sub>2</sub> (10 mM on 10 ml MeCN) was made up and also cooled to 4 °C. The solution of **1** (300 µl) was added to a vial that was cooled in a dry ice/MeCN bath and H<sub>2</sub><sup>18</sup>O (15 µl, 0.83 mmol) added. To this stirring solution H<sub>2</sub>O<sub>2</sub> (300 µl, 3 x 10<sup>-3</sup> mmol) and cyclooctene (10 µl, 0.08 mmol) were added and the solution injected directly into the mass spectrometer (ESI-MS). The spectrum was collected for 2 mins. MS (ESI(idem)-MS) *m/z* 448.2 (**4a**), 598.2 (**5a**).

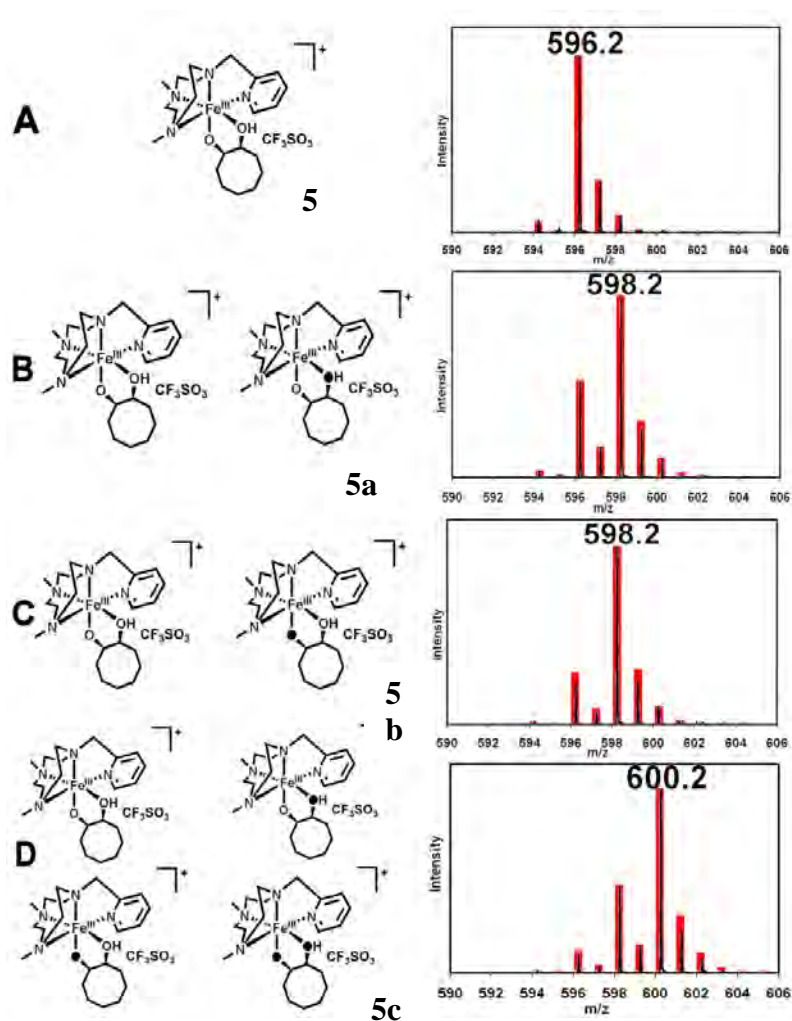
**[Fe<sup>III</sup>(C<sub>8</sub>H<sub>14</sub><sup>18</sup>O(O))(<sup>Me,H</sup>Pytacn)]<sup>+</sup> (**4b**), {[Fe<sup>III</sup>(C<sub>8</sub>H<sub>14</sub>(<sup>18</sup>O)(OH))(<sup>Me,H</sup>Pytacn)](CF<sub>3</sub>SO<sub>3</sub>)<sup>+</sup> (**5b**)** (where **5b** stands for **(4b)+H<sup>+</sup>+CF<sub>3</sub>SO<sub>3</sub>**).

[Fe(CF<sub>3</sub>SO<sub>3</sub>)<sub>2</sub>(<sup>Me,H</sup>Pytacn)] (**1**) (0.5 mg, 8 x 10<sup>-4</sup> mmol) was dissolved in MeCN (~ 7 ml) and the solution cooled to 4 °C. A solution of H<sub>2</sub><sup>18</sup>O<sub>2</sub> (10 mM on 10 ml MeCN) was made up and also cooled to 4 °C. The solution of **1** (300 µl) was added to a vial that was cooled in a dry ice/MeCN bath and H<sub>2</sub>O (15 µl, 0.83 mmol) added. To this stirring solution H<sub>2</sub><sup>18</sup>O<sub>2</sub> (300 µl, 3 x 10<sup>-3</sup> mmol) and cyclooctene (10 µl, 0.08 mmol) were added and the solution injected directly into the mass spectrometer (ESI-MS). The spectrum was collected for 2 mins. MS (ESI(idem)-MS) *m/z* 448.2 (**4b**), 598.2 (**5b**).

**[Fe<sup>III</sup>(C<sub>8</sub>H<sub>14</sub><sup>18</sup>O(<sup>18</sup>O))(<sup>Me,H</sup>Pytacn)]<sup>+</sup> (**4c**), {[Fe<sup>III</sup>(C<sub>8</sub>H<sub>14</sub>(<sup>18</sup>O)(<sup>18</sup>OH))(<sup>Me,H</sup>Pytacn)](CF<sub>3</sub>SO<sub>3</sub>)<sup>+</sup> (**5c**)** (where **5c** stands for **(4c)+H<sup>+</sup>+CF<sub>3</sub>SO<sub>3</sub>**).

[Fe(CF<sub>3</sub>SO<sub>3</sub>)<sub>2</sub>(<sup>Me,H</sup>Pytacn)] (**1**) (0.5 mg, 8 x 10<sup>-4</sup> mmol) was dissolved in MeCN (~ 7 ml) and the solution cooled to 4 °C. A solution of H<sub>2</sub><sup>18</sup>O<sub>2</sub> (10 mM on 10 ml MeCN) was made up and also cooled to 4 °C. The solution of **1** (300 µl) was added to a vial that was cooled in a dry ice/MeCN bath and H<sub>2</sub><sup>18</sup>O (15 µl, 0.83 mmol) added. To this stirring solution H<sub>2</sub><sup>18</sup>O<sub>2</sub> (300 µl, 3 x 10<sup>-3</sup> mmol) and cyclooctene (10 µl, 0.08 mmol) were added and the solution injected directly into the mass spectrometer (ESI(idem)-MS). The spectrum was collected for 2 mins. MS (ESI(idem)-MS) *m/z* 450.2 (**4c**), 600.2 (**5c**).

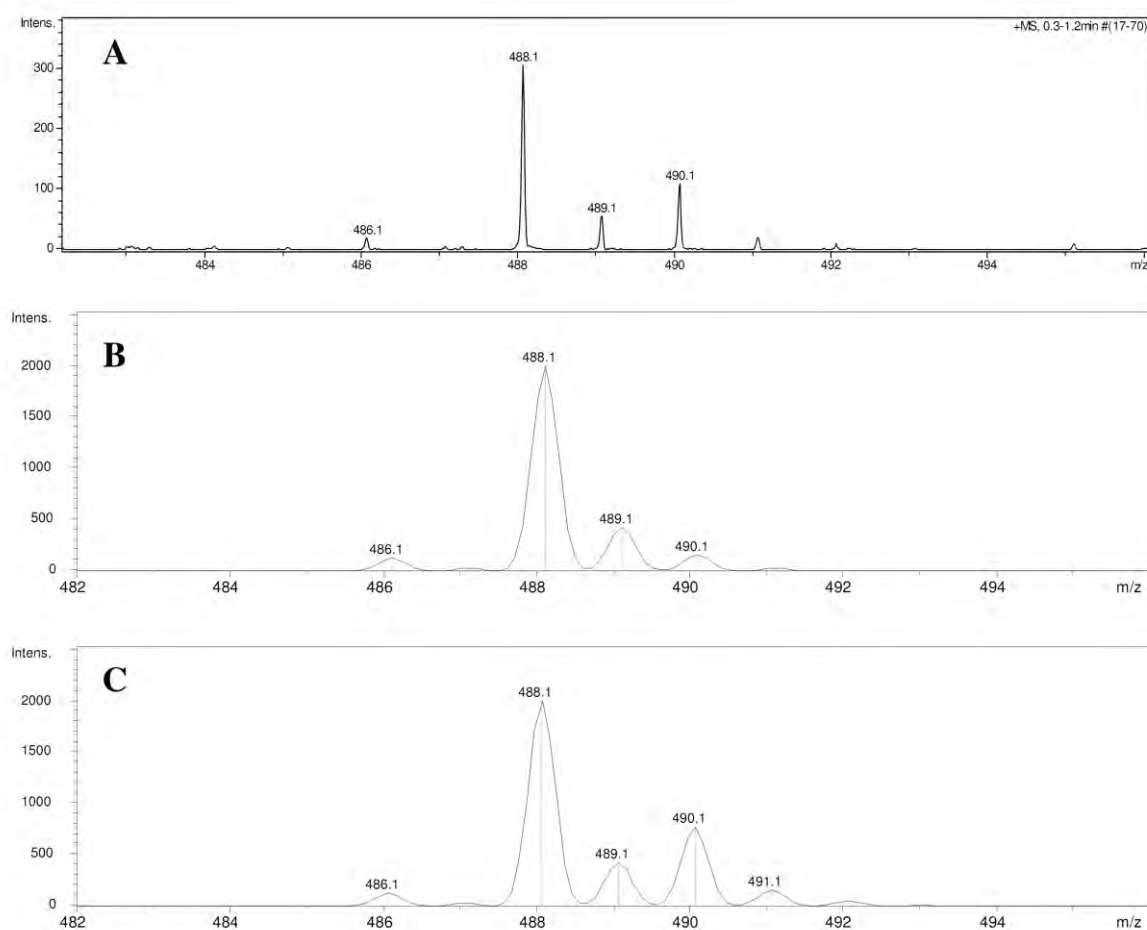
## 5.6. Full analysis of the isotopic envelope for dihydroxylation reaction with cyclooctene



Supporting Information **Figure S7**. Representation of the species **5**, **5a**, **5b** and **5c** formed in the dihydroxylation present in each isotopic envelope. The percentages for each species present in each isotopic envelope are: **A**.  $[\text{Fe}^{\text{III}}(\text{C}_8\text{H}_{14}\text{O}_2)(^{\text{Me,H}}\text{Pytacn})]^+$  100 %; **B**.  $[\text{Fe}^{\text{III}}(\text{C}_8\text{H}_{14}\text{O}_2)(^{\text{Me,H}}\text{Pytacn})]^+$  23 %,  $[\text{Fe}^{\text{III}}(\text{C}_8\text{H}_{14}^{16}\text{O}^{18}\text{O})(^{\text{Me,H}}\text{Pytacn})]^+$  77 %; **C**.  $[\text{Fe}^{\text{III}}(\text{C}_8\text{H}_{14}\text{O}_2)(^{\text{Me,H}}\text{Pytacn})]^+$  20 %,  $[\text{Fe}^{\text{III}}(\text{C}_8\text{H}_{14}^{18}\text{O}^{16}\text{O})(^{\text{Me,H}}\text{Pytacn})]^+$  80 %; **D**.  $[\text{Fe}^{\text{III}}(\text{C}_8\text{H}_{14}\text{O}_2)(^{\text{Me,H}}\text{Pytacn})]^+$  6 %,  $[\text{Fe}^{\text{III}}(\text{C}_8\text{H}_{14}^{18}\text{O}^{16}\text{O})(^{\text{Me,H}}\text{Pytacn})]^+$  13 %,  $[\text{Fe}^{\text{III}}(\text{C}_8\text{H}_{14}^{16}\text{O}^{18}\text{O})(^{\text{Me,H}}\text{Pytacn})]^+$  15 %,  $[\text{Fe}^{\text{III}}(\text{C}_8\text{H}_{14}^{18}\text{O}^{18}\text{O})(^{\text{Me,H}}\text{Pytacn})]^+$  66 %. (All calculated peaks fit the statistical treatment of experimental error).

## 5.7. Observation of $\{[\text{Fe}^{\text{III}}(\text{Cl})(\text{CF}_3\text{SO}_3)(^{\text{Me,H}}\text{Pytacn})]\}^+$ in the isotope distribution

When the  $[\text{Fe}^{\text{II}}(\text{CF}_3\text{SO}_3)_2(^{\text{Me,H}}\text{Pytacn})] + \text{H}_2\text{O}$  in acetonitrile were infused into the mass spectrometer (before addition of the oxidant) a peak at 488  $m/z$  was observed which can be assigned as being  $\{[\text{Fe}^{\text{III}}(\text{OH})(\text{OH}_2)(^{\text{Me,H}}\text{Pytacn})](\text{CF}_3\text{SO}_3)\}^+$  species (see Scheme S2). Since the synthesis of this compound derives from a chloride containing species, then the presence of chloride is not unexpected.



Supporting information **Figure S10**. **A** is the 488  $m/z$  peak taken from the  $[\text{Fe}^{\text{II}}(\text{CF}_3\text{SO}_3)_2(^{\text{Me,H}}\text{Pytacn})] + \text{H}_2\text{O}$  in acetonitrile; **B** is the calculated isotope pattern for the species  $\{[\text{Fe}^{\text{III}}(\text{OH})(\text{OH}_2)(^{\text{Me,H}}\text{Pytacn})](\text{CF}_3\text{SO}_3)\}^+$ ; **C** is the calculated isotope pattern for the species  $\{[\text{Fe}^{\text{III}}(\text{Cl})(\text{CF}_3\text{SO}_3)(^{\text{Me,H}}\text{Pytacn})]\}^+$ . Note that the peak at 490.1  $m/z$  in the observed spectrum is higher than it is in the calculated.

When the two calculated spectrum for the  $\{[\text{Fe}^{\text{III}}(\text{OH})(\text{OH}_2)(^{\text{Me,H}}\text{Pytacn})](\text{CF}_3\text{SO}_3)\}^+$  and  $\{[\text{Fe}^{\text{III}}(\text{Cl})(\text{CF}_3\text{SO}_3)(^{\text{Me,H}}\text{Pytacn})]\}^+$  are overlaid, this accounts for the observed envelope allowing the conclusion that the species  $\{[\text{Fe}^{\text{III}}(\text{Cl})(\text{CF}_3\text{SO}_3)(^{\text{Me,H}}\text{Pytacn})]\}^+$  is present, and this should be taken into account when the data is examined.



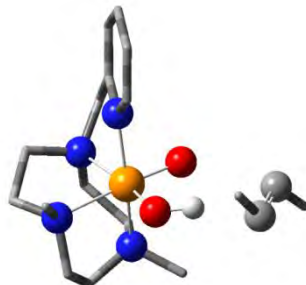
## 5.8. Computational Details

### Computational methods

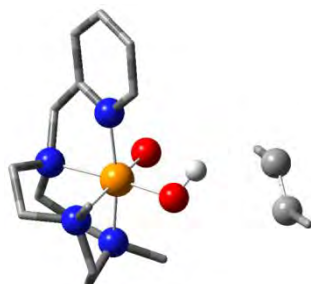
DFT geometries were optimized at the B3LYP level in conjunction with the LANL2DZ basis set and associated ECP for Fe, and D95V basis set for the other atoms, as implemented in the Gaussian 09 program. The energies were further refined by single-point calculations with the SDD basis set and associated ECP for Fe, and the 6-311G(d,p) basis for the other atoms. Final free energies include energies computed at the B3LYP/SDD&6-311G(d,p)//B3LYP/LANL2DZ&D95V level of theory together with enthalpic and free energy corrections at the B3LYP/LANL2DZ&D95V level.<sup>2</sup>

Supporting information figures **S11-S15** show the optimized structures studied in this work calculated at the B3LYP level in conjunction with the LANL2DZ basis set and associated ECP for Fe, and D95V basis set for the other atoms.

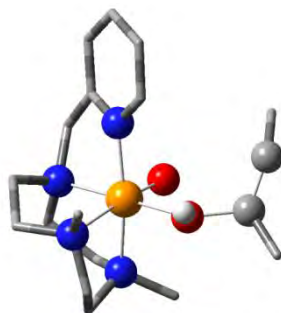
Supporting information **Figure S11**: Structure of **30** calculated at the B3LYP level in conjunction with the LANL2DZ basis set and associated ECP for Fe, and D95V basis set for the other atoms.



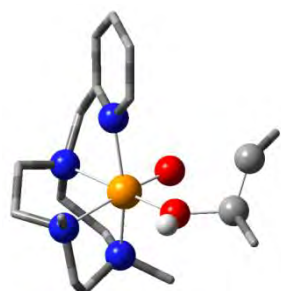
Supporting information **Figure S12**: Structure of **TS** calculated at the B3LYP level in conjunction with the LANL2DZ basis set and associated ECP for Fe, and D95V basis set for the other atoms.



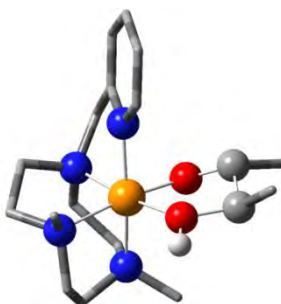
Supporting information **Figure S13**: Structure of **IN** calculated at the B3LYP level in conjunction with the LANL2DZ basis set and associated ECP for Fe, and D95V basis set for the other atoms.



Supporting information **Figure S14**: Structure of **TS2** calculated at the B3LYP level in conjunction with the LANL2DZ basis set and associated ECP for Fe, and D95V basis set for the other atoms.



Supporting information **Figure S15**: Structure of **5** calculated at the B3LYP level in conjunction with the LANL2DZ basis set and associated ECP for Fe, and D95V basis set for the other atoms.



Supporting information **Tables S1-S5** show the optimized Cartesian xyz coordinates in Ångstroms for all structures studied in this work at the B3LYP level in conjunction with the LANL2DZ basis set and associated ECP for Fe, and D95V basis set for the other atoms.

Supporting information **table S1**: Optimized Cartesian xyz coordinates of **30** calculated at the B3LYP level in conjunction with the LANL2DZ basis set and associated ECP for Fe, and D95V basis set for the other atoms.

H	-3.203256	0.181649	2.450201
H	-1.776352	-2.455031	2.775818
H	-3.362994	-1.185090	1.363882
C	-2.794610	-0.268608	1.538796
H	-2.550849	-2.836305	0.455442
H	-3.993980	0.766142	0.042189
C	-1.140777	-2.098625	1.953327

## ANNEX

---

H	-3.520933	-1.289687	-0.949547
H	-1.175432	-3.892509	0.739944
C	-0.768686	0.141560	2.921559
C	-1.477434	-2.843153	0.659587
N	-1.328655	-0.610626	1.740445
C	-2.948001	0.703344	0.369752
H	-0.095904	-2.253828	2.231903
H	-2.633248	1.705065	0.668975
C	-2.673286	-0.923859	-1.534777
H	-3.071640	-0.599196	-2.502398
H	-2.131796	-2.985698	-1.978760
N	-2.070630	0.264308	-0.792645
N	-0.750312	-2.200448	-0.517593
C	-1.632303	-2.034847	-1.750033
H	-2.705544	1.981296	-1.943095
C	0.468078	-3.028455	-0.875680
C	-1.776958	1.461909	-1.675969
H	-0.968053	-1.790502	-2.581848
Fe	-0.222273	-0.281643	-0.056921
H	-1.298638	1.105915	-2.594391
C	-0.828789	2.363157	-0.909190
N	-0.063858	1.718981	0.028319
H	-1.312578	4.243068	-1.853340
C	-0.697803	3.740359	-1.113292
C	0.850497	2.397270	0.768911
H	1.437337	1.820335	1.472805
C	0.244546	4.459179	-0.349157
C	1.023187	3.779374	0.606187
H	0.366025	5.527858	-0.497331
H	1.756211	4.302215	1.210842
H	1.060014	-2.507150	-1.629181
H	0.142669	-3.999958	-1.268341
H	1.074362	-3.179416	0.019199
H	-0.969517	1.209982	2.809552
H	0.307636	-0.027554	2.971770
H	-1.238780	-0.208991	3.849721
O	0.542623	-0.182876	-1.551024
O	1.220212	-0.651201	0.889525
H	2.120640	-0.674307	0.429239
H	3.910722	0.592812	-1.072860
C	3.984142	-0.467652	-0.816553
C	4.248988	-0.805776	0.477919
H	4.385675	-1.862687	0.721635

---

C	4.507632	0.172069	1.602302
H	3.905486	-0.055730	2.492714
H	5.558691	0.105480	1.915369
H	4.322722	1.209095	1.294933
C	3.921848	-1.435176	-1.975720
H	3.933324	-2.479988	-1.642168
H	3.039203	-1.259830	-2.604795
H	4.797741	-1.290074	-2.623639

Supporting information **Table S2**: Optimized Cartesian xyz coordinates of of **TS** calculated at the B3LYP level in conjunction with the LANL2DZ basis set and associated ECP for Fe, and D95V basis set for the other atoms.

H	-2.844908	-1.627431	2.378655
H	-0.223481	-3.122943	2.581510
H	-2.270279	-2.782592	1.191762
C	-2.267124	-1.721768	1.452069
H	-0.735271	-3.688555	0.215044
H	-3.845331	-1.351809	-0.005969
C	0.106981	-2.433056	1.791830
H	-2.399430	-2.754771	-1.147075
H	0.988329	-3.901142	0.467859
C	-0.747420	-0.418281	2.920369
C	0.189237	-3.152477	0.445890
N	-0.839683	-1.258888	1.675807
C	-2.917769	-0.884814	0.350450
H	1.083055	-2.027026	2.069641
H	-3.172900	0.104565	0.736113
C	-1.850443	-1.959496	-1.659062
H	-2.346205	-1.804171	-2.623781
H	-0.335675	-3.426134	-2.198790
N	-1.951843	-0.699541	-0.809648
N	0.465374	-2.140533	-0.655883
C	-0.383919	-2.370917	-1.896615
H	-3.397942	0.539241	-1.837181
C	1.925236	-2.195251	-1.027343
C	-2.332455	0.550111	-1.574325
H	0.055057	-1.764653	-2.690885
Fe	-0.110745	-0.259938	-0.074707
H	-1.741511	0.582411	-2.494994
C	-1.991555	1.743605	-0.698563
N	-1.002111	1.526632	0.226479
H	-3.406094	3.142408	-1.537708
C	-2.620721	2.989806	-0.804003

---

C	-0.623928	2.527542	1.063506
H	0.147022	2.300509	1.790878
C	-2.221941	4.035965	0.050790
C	-1.213885	3.798058	1.004212
H	-2.694375	5.010932	-0.019714
H	-0.891906	4.575152	1.688926
H	2.132244	-1.428993	-1.774456
H	2.170815	-3.185637	-1.432833
H	2.522849	-1.996491	-0.136318
H	-1.462050	0.406567	2.866064
H	0.266467	-0.021806	3.003304
H	-0.974882	-1.021919	3.809232
O	0.448458	0.324918	-1.552911
O	1.466931	0.098180	0.877415
H	1.756476	1.034957	0.834120
H	3.634667	2.580199	-0.201456
C	3.812349	1.608924	-0.670668
C	4.541060	0.663302	0.057356
H	4.737472	-0.302560	-0.412180
C	5.131303	0.897288	1.405107
H	4.817782	0.111476	2.110097
H	6.229538	0.809335	1.352092
H	4.884020	1.878762	1.819969
C	3.279825	1.400624	-2.034879
H	3.771096	0.580097	-2.568795
H	2.189984	1.139236	-1.965120
H	3.320495	2.317704	-2.635667

Supporting information **Table S3**: Optimized Cartesian xyz coordinates of **IN** calculated at the B3LYP level in conjunction with the LANL2DZ basis set and associated ECP for Fe, and D95V basis set for the other atoms.

H	1.818421	-3.031012	1.811520
H	3.494976	-0.581928	2.327354
H	2.914733	-2.279481	0.670040
C	1.873676	-2.297880	0.998955
H	3.809730	-0.637985	-0.137195
H	1.392090	-3.594188	-0.669781
C	2.761845	-0.064876	1.692428
H	2.733587	-1.920101	-1.648577
H	4.167853	0.981356	0.426575
C	0.816851	-1.054557	2.873670
C	3.359876	0.248915	0.315691

---

N	1.508064	-0.914344	1.541119
C	0.951788	-2.732742	-0.147362
H	2.476419	0.861237	2.204615
H	-0.011064	-3.056156	0.253382
C	1.894617	-1.303729	-1.986580
H	1.686621	-1.609779	-3.019179
H	3.262811	0.313662	-2.459439
N	0.706703	-1.592199	-1.101356
N	2.280874	0.792243	-0.597897
C	2.277543	0.190734	-1.986394
H	-0.627028	-2.736911	-2.355390
C	2.402331	2.289325	-0.705605
C	-0.588879	-1.769704	-1.834704
H	1.546598	0.764931	-2.561070
Fe	0.356128	0.154351	0.151906
H	-0.668094	-0.971139	-2.580668
C	-1.739036	-1.653278	-0.845202
N	-1.493660	-0.915259	0.280164
H	-3.160698	-2.844747	-1.953997
C	-2.987030	-2.257207	-1.057639
C	-2.472152	-0.758417	1.213598
H	-2.229749	-0.156464	2.082004
C	-4.002517	-2.096555	-0.095736
C	-3.739052	-1.338753	1.062361
H	-4.974562	-2.557472	-0.242867
H	-4.493704	-1.201105	1.829241
H	1.563392	2.674452	-1.285578
H	3.342857	2.561354	-1.203181
H	2.393249	2.736140	0.293143
H	-0.062268	-1.693720	2.765853
H	0.502321	-0.072985	3.239549
H	1.491140	-1.501937	3.615622
O	-0.398474	1.182352	-1.155178
O	-0.278376	1.769637	1.339219
H	-0.137355	2.043917	2.267951
H	-2.349973	1.562493	-0.489430
C	-1.439779	2.126982	-0.740125
C	-0.953344	2.868787	0.522241
H	-0.158341	3.579041	0.266449
C	-2.048669	3.538136	1.345872
H	-2.837509	2.829364	1.623563
H	-1.647058	3.999835	2.257383
H	-2.509513	4.345361	0.765001

---

C	-1.729008	3.073720	-1.913627
H	-0.845913	3.667860	-2.176180
H	-2.025359	2.493445	-2.792946
H	-2.551378	3.757117	-1.670927

Supporting information **Table S4**: Optimized Cartesian xyz coordinates of **TS2** calculated at the B3LYP level in conjunction with the LANL2DZ basis set and associated ECP for Fe, and D95V basis set for the other atoms.

H	2.094150	-2.234547	2.493392
H	3.399926	0.483684	2.335655
H	3.134197	-1.675794	1.200389
C	2.090027	-1.746922	1.512007
H	3.863832	-0.207916	0.006265
H	1.843307	-3.516811	0.285509
C	2.636277	0.691322	1.572366
H	3.059390	-2.028418	-1.089784
H	3.957578	1.540279	0.086379
C	0.799737	-0.223139	2.966955
C	3.268461	0.692577	0.175003
N	1.518315	-0.335105	1.646400
C	1.286864	-2.599547	0.526583
H	2.202878	1.672241	1.793758
H	0.341634	-2.901956	0.981565
C	2.180918	-1.648059	-1.620260
H	2.077827	-2.260478	-2.524062
H	3.402939	-0.063052	-2.462758
N	0.975721	-1.820640	-0.726515
N	2.193123	0.784769	-0.890786
C	2.394031	-0.178836	-2.041717
H	-0.104487	-3.461371	-1.617752
C	2.107663	2.193754	-1.421638
C	-0.231627	-2.388461	-1.417069
H	1.670528	0.103486	-2.810476
Fe	0.304632	0.154580	-0.070173
H	-0.353080	-1.871633	-2.375704
C	-1.459456	-2.148495	-0.552299
N	-1.386115	-1.095680	0.315403
H	-2.650870	-3.776734	-1.325726
C	-2.613187	-2.940356	-0.634491
C	-2.446581	-0.796638	1.111004
H	-2.342668	0.056835	1.770329
C	-3.715202	-2.636520	0.187390
C	-3.628248	-1.550327	1.079436

---

H	-4.618551	-3.236710	0.136552
H	-4.453609	-1.291462	1.733860
H	1.266054	2.269182	-2.112437
H	3.034829	2.457222	-1.947503
H	1.961578	2.890021	-0.591560
H	-0.024630	-0.939381	3.002020
H	0.404472	0.786897	3.108154
H	1.484286	-0.430310	3.809500
O	-0.406879	0.574381	-1.501406
O	-0.410429	1.889792	0.803160
H	-0.396707	2.096535	1.761065
H	-3.276039	2.429458	0.453608
C	-2.546278	2.572936	-0.346957
C	-1.203327	3.059351	0.047610
H	-0.566302	3.235947	-0.819035
C	-1.198530	4.248064	1.017897
H	-1.803831	4.046987	1.912404
H	-0.179784	4.523823	1.317974
H	-1.638977	5.121821	0.524276
C	-3.018603	2.465352	-1.764039
H	-2.195278	2.500743	-2.483738
H	-3.581716	1.535677	-1.928243
H	-3.719794	3.283539	-2.002210

Supporting information **Table S5**: Optimized Cartesian xyz coordinates of **5** calculated at the B3LYP level in conjunction with the LANL2DZ basis set and associated ECP for Fe, and D95V basis set for the other atoms.

H	1.831699	-3.137405	1.581876
H	3.425765	-0.695570	2.350435
H	2.942706	-2.257908	0.551316
C	1.893849	-2.326863	0.847317
H	3.773962	-0.517707	-0.096148
H	1.468269	-3.424549	-0.983313
C	2.683053	-0.146062	1.755063
H	2.766730	-1.692760	-1.776568
H	4.058419	1.064045	0.601078
C	0.741101	-1.283231	2.783014
C	3.284204	0.309266	0.423927
N	1.465821	-1.010995	1.490489
C	1.005246	-2.653108	-0.354786
H	2.361024	0.716352	2.349305
H	0.044100	-3.041090	-0.012555



## ANNEX

---

C	1.929619	-1.047397	-2.058382
H	1.701879	-1.267107	-3.107341
H	3.308206	0.620993	-2.290811
N	0.740268	-1.401199	-1.178646
N	2.187040	0.881084	-0.457910
C	2.294660	0.436887	-1.908302
H	-0.553485	-2.510399	-2.513045
C	2.260275	2.386624	-0.415426
C	-0.559398	-1.575660	-1.938030
H	1.590230	1.056054	-2.466322
Fe	0.353101	0.089626	0.087594
H	-0.662244	-0.729577	-2.623987
C	-1.686150	-1.552859	-0.922039
N	-1.410528	-0.865030	0.233761
H	-3.126147	-2.711779	-2.039456
C	-2.927396	-2.169619	-1.120222
C	-2.354423	-0.773950	1.208207
H	-2.090721	-0.203360	2.089477
C	-3.907884	-2.077876	-0.112329
C	-3.614119	-1.374021	1.071395
H	-4.876980	-2.548697	-0.246942
H	-4.343139	-1.287183	1.869774
H	1.435409	2.800362	-0.993283
H	3.211149	2.728347	-0.844239
H	2.199616	2.732109	0.620263
H	-0.095585	-1.961556	2.603636
H	0.353880	-0.350238	3.202101
H	1.415767	-1.743208	3.516959
O	-0.391491	1.175119	-1.177758
O	-0.294770	1.552782	1.339981
H	0.062552	1.831773	2.205960
H	-2.362658	1.490139	-0.542067
C	-1.447213	2.076913	-0.713006
C	-1.005643	2.700449	0.629757
H	-0.243043	3.468767	0.456460
C	-2.129597	3.238887	1.508868
H	-2.886990	2.472694	1.709358
H	-1.749541	3.619981	2.465391
H	-2.620242	4.080966	1.007460
C	-1.717034	3.135650	-1.789800
H	-0.829399	3.751782	-1.977334
H	-1.995271	2.645705	-2.728195
H	-2.543542	3.795340	-1.499697

## 5.9. References

1. Company, A.; Gómez, L.; Fontrodona, X.; Ribas, X.; Costas, M., *Chem. Eur. J.* **2008**, *14*, 5727-5731.
2. Frisch, M. J.; Trucks, G. W.; Schlegel, H. B.; Scuseria, G. E.; Robb, M. A.; Cheeseman, J. R.; Scalmani, G.; Barone, V.; Mennucci, B.; Petersson, G. A.; Nakatsuji, H.; Caricato, M.; Li, X.; Hratchian, H. P.; Izmaylov, A. F.; Bloino, J.; Zheng, G.; Sonnenberg, J. L.; Hada, M.; Ehara, M.; Toyota, K.; Fukuda, R.; Hasegawa, J.; Ishida, M.; Nakajima, T.; Honda, Y.; Kitao, O.; Nakai, H.; Vreven, T.; J. A. Montgomery, J.; Peralta, J. E.; Ogliaro, F.; Bearpark, M.; Heyd, J. J.; Brothers, E.; Kudin, K. N.; Staroverov, V. N.; Kobayashi, R.; Normand, J.; Raghavachari, K.; Rendell, A.; Burant, J. C.; Iyengar, S. S.; Tomasi, J.; Cossi, M.; Rega, N.; Millam, J. M.; Klene, M.; Knox, J. E.; Cross, J. B.; Bakken, V.; Adamo, C.; Jaramillo, J.; Gomperts, R.; Stratmann, R. E.; Yazyev, O.; Austin, A. J.; Cammi, R.; Pomelli, C.; Ochterski, J. W.; Martin, R. L.; Morokuma, K.; Zakrzewski, V. G.; Voth, G. A.; Salvador, P.; Dannenberg, J. J.; Dapprich, S.; Daniels, A. D.; Farkas, Ö.; Foresman, J. B.; Ortiz, J. V.; Cioslowski, J.; Fox, D. J. *Gaussian 09, Revision A.1*, Wallingford CT, 2009.

